CISM International Centre for Mechanical Sciences 604
Courses and Lectures

Dimitri Breda *Editor*

Controlling Delayed Dynamics

Advances in Theory, Methods and Applications

International Centre for Mechanical Sciences

Springer

CISM International Centre for Mechanical Sciences

Courses and Lectures

Volume 604

For more than 40 years the book series edited by CISM, “International Centre for Mechanical Sciences: Courses and Lectures”, has presented groundbreaking developments in mechanics and computational engineering methods. It covers such fields as solid and fluid mechanics, mechanics of materials, micro- and nanomechanics, biomechanics, and mechatronics. The papers are written by international authorities in the field. The books are at graduate level but may include some introductory material.

Dimitri Breda
Editor

Controlling Delayed Dynamics

Advances in Theory, Methods and Applications

Springer

Editor
Dimitri Breda
CDLab - Computational Dynamics
Laboratory
University of Udine
Udine, Italy

ISSN 0254-1971 ISSN 2309-3706 (electronic)
CISM International Centre for Mechanical Sciences
ISBN 978-3-031-00981-5 ISBN 978-3-031-01129-0 (eBook)
https://doi.org/10.1007/978-3-031-01129-0

This Springer imprint is published by the registered company Springer Nature Switzerland AG
The registered company address is: Gewerbestrasse 11, 6330 Cham, Switzerland

Preface

Delays are ubiquitous in engineering and natural sciences: communication delays in control devices or the incubation period during an epidemic spread are just a couple of noteworthy examples. The inclusion of past history in the time evolution adds nontrivial complexities with respect to ordinary systems, balancing the advantage of dealing with more realistic models. Equations involving delays generate infinite-dimensional dynamical systems, asking for advanced tools and methods in the background mathematical analysis, the numerical treatment and the development, design and optimization of control strategies. Eventually, understanding fundamental issues like stability is crucial, especially for varying or uncertain parameters.

These premises motivated the organization of an international course at CISM in 2019, and this book collects contributions of the lecturers about analytical, numerical and application aspects of time-delay systems, under the paradigm of control theory. The aim is at discussing recent advances in these different contexts, also highlighting the interdisciplinary connections.

Chapter "The Twin Semigroup Approach Towards Periodic Neutral Delay Equations" deals with twin semigroups and norming dual pairs for neutral delay equations, including time-dependent perturbations in view of periodic problems. Then in chapter "Characteristic Matrix Functions and Periodic Delay Equations", characteristic matrix functions are introduced to analyze spectral properties, focusing on monodromy operators of neutral periodic delay equations.

Chapters "Pseudospectral Methods for the Stability Analysis of Delay Equations. Part I: The Infinitesimal Generator Approach and "Pseudospectral Methods for the Stability Analysis of Delay Equations. Part II: The Solution Operator Approach" concern the use of pseudospectral collocation techniques to reduce to finite dimension the dynamical analysis of both delay differential and renewal equations. Discretizations of the infinitesimal generator of the relevant semigroup (Chapter "Pseudospectral Methods for the Stability Analysis of Delay Equations. Part I: The Infinitesimal Generator Approach") and of the semigroup itself (Chapter "Pseudospectral Methods for the Stability Analysis of Delay Equations. Part II: The Solution Operator Approach") are described in view of analyzing local stability and performing bifurcation analysis.

The focus moves then to the characteristic roots of linear time-invariant time-delay systems in view of stability. Frequency-sweeping techniques are illustrated in chapter "Counting Characteristic Roots of Linear Delay Differential Equations. Part I: Frequency-Sweeping Stability Tests and Applications", while frequency-domain approaches are presented in chapter "Counting Characteristic Roots of Linear Delay Differential Equations. Part II: From Argument Principle to Rightmost Root Assignment Methods", linking maximal multiplicity to dominancy, also in view of low-complexity controllers.

Chapter "Bifurcation Analysis of Systems With Delays: Methods and Their Use in Applications" presents a dynamical systems point of view to study problems with possibly state-dependent delays. By using the most recent release of DDE-BIFTOOL, the numerical continuation of steady states and periodic orbits, their bifurcations and relevant normal forms are addressed, also through the analysis of two longer case studies.

Chapters "Design of Structured Controllers for Linear Time-Delay Systems" gives an overview of control design methods, grounded in matrix theory and numerical linear algebra and relying on a direct optimization of stability, robustness and performance indicators as a function of controller or design parameters. Then Chapter "A Scalable Controller Synthesis Method for the Robust Control of Networked Systems" concentrates on a scalable controller synthesis method in the framework of $\mathcal{H}_\infty$-norm control for networked systems.

Finally, chapters "Regenerative Machine Tool Vibrations" and "Dynamics of Human Balancing" discuss models of, respectively, machine tool vibrations and human balancing tasks. In the former, the phenomenon called surface regeneration is analyzed in terms of the delay differential equations governing the vibrations, and stability diagrams are constructed. In the latter, the central role played by the reaction time is addressed by discussing stabilizability issues in terms of the critical delay for different feedback concepts.

After two years of the global pandemic, the time has eventually come to put an end to this volume: after all, some delay is not completely out of place given the subject. Once more, let me thank the lecturers: I am sure that their stimulating contributions to the course have been much appreciated by the 46 attendees from 13 different countries, to which I gratefully add myself. The priceless help and kind presence of CISM administrative staff are also acknowledged with true pleasure.

This book is the result of the lecturers' effort, Sjoerd Verduyn Lunel, Silviu-Iulian Niculescu, Bernd Krauskopf, Wim Michiels and Tamás Insperger (and of that of their co-authors, whom I thank as well). I am tremendously grateful to them, as well as to many other colleagues for all I could learn about delay systems. Since the list would be excessively long, let me just give credit to Gabor Stépán for having inspired the course behind this volume, and to Rossana Vermiglio and Stefano Maset for having patiently introduced me to this research field, for which I trust this volume will be a valid resource.

Udine, Italy Dimitri Breda

Contents

The Twin Semigroup Approach Towards Periodic Neutral Delay Equations

Sjoerd Verduyn Lunel

Abstract In the first part of this chapter we review the recently developed theory of twin semigroups and norming dual pairs in the light of neutral delay equations. In the second part we extend the perturbation theory for twin semigroups to include time-dependent perturbations. Finally we apply this newly developed theory to neutral periodic delay equations.

1 Introduction

Consider a function x defined on the half-line $[0, \infty)$ with values in $\mathbb{R}^n$ and assume that the derivative $\dot{x}$ depends on the history of x and $\dot{x}$. More precisely, we assume that there exists $h > 0$ such that $\dot{x}(t)$ depends on $x(\tau)$ and $\dot{x}(\tau)$ for $t - h \leq \tau \leq t$. Given these restrictions we would like to consider a general linear differential equation.

To formulate precisely what type of equations we consider, we first define the segment $x_t : [-h, 0] \to \mathbb{R}^n$ by

$$x_t(\theta) := x(t + \theta), \qquad \text{for } -h \leq \theta \leq 0. \tag{1}$$

Let η and ζ be $n \times n$-matrix-valued functions of bounded variation defined on $[0, \infty)$ such that $\eta(0) = \zeta(0) = 0$, η and ζ are continuous from the right on $(0, h)$, $\eta(t) = \eta(h)$ and $\zeta(t) = \zeta(h)$ for $t \geq h$. We call such functions η and ζ of normalized bounded variation. Furthermore assume that $\eta(t)$ is continuous at $t = 0$. (See Appendix A for the precise definition and basic properties of such functions.)

The class of equations that we will study can now be written as

$$\frac{\mathrm{d}}{\mathrm{d}t}\left[x(t) - \int_0^h \mathrm{d}\eta(\theta)x(t-\theta)\right] = \int_0^h \mathrm{d}\zeta(\theta)x(t-\theta). \tag{2}$$

S. Verduyn Lunel (✉)
Mathematical Institute, Utrecht University, Utrecht, The Netherlands
e-mail: S.M.VerduynLunel@uu.nl

D. Breda (ed.), *Controlling Delayed Dynamics*, CISM International Centre for Mechanical Sciences 604, https://doi.org/10.1007/978-3-031-01129-0_1

To single out a unique solution we have to provide an initial condition at a certain time s. The initial condition should specify the values of x on the interval of length h preceding time s. Let y satisfy (2) for $t \geq s$ and the initial condition

$$y(s+\theta) = \varphi(\theta), \qquad -h \leq \theta \leq 0,$$

where $\varphi \in B([-h, 0]; \mathbb{R}^n)$, the Banach space of bounded Borel measurable functions provided with the supremum norm (see Sect. A for the precise definition and basic properties). Then x defined for $t \geq 0$ by $x(t) = y(s+t)$, satisfies (2) for $t \geq 0$ and the initial condition

$$x(\theta) = \varphi(\theta), \qquad -h \leq \theta \leq 0. \tag{3}$$

Equation (2) is time invariant and called autonomous. So we can, without loss of generality, restrict our attention to an initial condition imposed at time zero. This in contrast to time periodic equations which we will consider in Sect. 8.

Equation (2) is called a neutral functional differential equation (NFDE). A solution of the initial-value problem (2)–(3) on the half-line $[0, \infty)$ is a function $x \in B([0, \infty); \mathbb{R}^n)$ such that

(i) (3) holds;
(ii) on $(0, \infty)$, the function x is absolutely continuous and (2) holds;
(iii) the following limit exists

$$\lim_{t \downarrow 0} \frac{1}{t} \left[x(t) - \int_0^h \mathrm{d}\eta(\theta) x(t-\theta) - \varphi(0) - \int_0^h \mathrm{d}\eta(\theta)\, \varphi(-\theta) \right]$$

and equals $\int_0^h \mathrm{d}\zeta(\theta)\, \varphi(-\theta)$.

We end the introduction with an outline of this chapter. In Sect. 2 we derive a representation of the solution of a NFDE by direct methods. The main result is given in Theorem 2.4. In Sect. 3 we introduce the notions of norming dual pair and twin semigroup following Diekmann and Verduyn Lunel (2021). In Sect. 4 we introduce a concrete norming dual pair that will be used in Sect. 5 to represent the solution semigroup corresponding to a NFDE as a twin semigroup. In Sect. 6 we use the twin semigroup approach towards NFDE to prove a variation-of-constants formula, see Theorem 6.4. In Sect. 7 we develop the perturbation theory for bounded time-dependent perturbations of twin semigroups. The main result is given in Theorem 7.5. In Sect. 8 we consider periodic NFDE as an application of the perturbation theory developed in Sect. 7 and prove that periodic NFDE define a twin evolutionary system. Finally in Appendix A we review some basic properties of functions of bounded variations and complex Borel measures.

2 Introduction to NFDE

This section is concerned with the existence, uniqueness and representation of a solution of the initial-value problem (2)–(3). For $0 \le t \le h$, we can combine the two separate pieces of information given in (2) and (3) and write

$$\frac{\mathrm{d}}{\mathrm{d}t}\left[x(t) - \int_0^h \mathrm{d}\eta(\theta)x(t-\theta)\right] = \int_0^t \mathrm{d}\zeta(\theta)x(t-\theta) + \int_t^h \mathrm{d}\zeta(\theta)\varphi(t-\theta). \quad (4)$$

By integration and changing the order of integration we can write (4) as

$$x(t) - \int_0^h \mathrm{d}\eta(\theta)x(t-\theta) = \int_0^t \zeta(\theta)x(t-\theta)\,\mathrm{d}\theta + g(t), \quad (5)$$

where

$$g(t) := \varphi(0) - \int_0^h \mathrm{d}\eta(\theta)\varphi(-\theta) + \int_0^t \left(\int_s^h \mathrm{d}\zeta(\theta)\varphi(s-\theta)\right)\mathrm{d}s. \quad (6)$$

Next we write (5) as follows

$$x(t) = \int_0^t \mathrm{d}\eta(\theta)x(t-\theta) + \int_0^t \zeta(\theta)x(t-\theta)\,\mathrm{d}\theta + f(t), \quad (7)$$

where, using (6),

$$\begin{aligned} f(t) &:= g(t) + \int_t^h \mathrm{d}\eta(\theta)\varphi(t-\theta) \\ &= \varphi(0) + \int_0^h [\zeta(t+\sigma) - \zeta(\sigma)]\,\varphi(-\sigma)\,\mathrm{d}\sigma \\ &\qquad + \int_0^h \mathrm{d}\,[\eta(t+\sigma) - \eta(\sigma)]\,\varphi(-\sigma). \end{aligned} \quad (8)$$

Here we have used that

$$\int_0^t \left(\int_s^h \mathrm{d}\zeta(\theta)\varphi(s-\theta)\right)\mathrm{d}s = \int_0^h [\zeta(t+\sigma) - \zeta(\sigma)]\,\varphi(-\sigma)\,\mathrm{d}\sigma$$

and that

$$\int_t^h \mathrm{d}\eta(\theta)\varphi(t-\theta) = \int_0^h \mathrm{d}\eta(t+\sigma)\varphi(-\sigma).$$

It follows from Theorem A.2 that the function f defined by (8) is a bounded Borel measurable function on $[0, \infty)$ that is constant on $[h, \infty)$.

Define the function μ by

$$\mu(\theta) := \eta(\theta) + \int_0^\theta \zeta(s)\,\mathrm{d}s, \qquad 0 \le \theta \le h, \tag{9}$$

and $\mu(\theta) = \mu(h)$ for $\theta \ge h$, then μ is a $n \times n$-matrix-valued function of normalized bounded variation. Note that, since $\eta(\theta)$ is continuous at $\theta = 0$, we have that $\mu(\theta)$ is continuous at $\theta = 0$.

The convolution product of a $n \times n$-matrix-valued function of normalized bounded variation μ and a bounded Borel measurable function f is defined by

$$(\mu * f)(t) := \int_0^t \mathrm{d}\mu(\theta) f(t-\theta), \qquad t \ge 0. \tag{10}$$

From Theorem A.1, it follows that $\mu * f$ is a bounded Borel measurable function on $[0, \infty)$.

Using the convolution product defined by (10), the initial-value problem (2)–(3), i.e., (7), can be rewritten as a renewal equation for x

$$x = \mu * x + f, \tag{11}$$

where μ is given by (9) and f, given by (8), can be rewritten as

$$f(t) = \varphi(0) + \int_0^h \mathrm{d}\left[\mu(t+\sigma) - \mu(\sigma)\right]\varphi(-\sigma). \tag{12}$$

Therefore to prove existence and uniqueness of solutions of the initial-value problem (2)–(3), it suffices to prove existence and uniqueness of solutions of the renewal equation (11).

The convolution product of two $n \times n$-matrix-valued functions of normalized bounded variation μ and ν, defined by

$$(\mu * \nu)(t) := \int_0^t \mathrm{d}\mu(\theta)\nu(t-\theta), \qquad t \ge 0, \tag{13}$$

is again a function of bounded variation (see Appendix A and, in particular, Theorem A.3).

The resolvent kernel ρ of a renewal equation (11) with kernel μ and convolution product (13) is defined as the matrix solution of the resolvent equation

$$\rho = \rho * \mu + \mu = \mu * \rho + \mu. \tag{14}$$

The key property of the resolvent concerns the representation of the solution of the renewal equation (11) as

$$x = f + \rho * f. \tag{15}$$

Indeed taking to convolution with ρ on the left and right of (11) yields

$$\rho * x = (\rho * \mu) * x + \rho * f = (\rho - \mu) * x + \rho * f.$$

Hence $\mu * x = \rho * f$ and substituting this relation into (11) yields (15).

We now discuss the existence and uniqueness of the solution of (14) under the assumption that μ is a $n \times n$-matrix-valued function of normalized bounded variation. It follows from Appendix A and in particular Theorem A.1 that functions of normalized bounded variation are in one-to-one correspondence to complex Borel measures. This allows us to use measure theory to prove existence and uniqueness of the solution of (14). We start with some preparations.

Let $\mathcal{E}$ denote the Borel σ-algebra on $[0, \infty)$. The Banach space of complex Borel measures of bounded total variation is denoted by $M([0, \infty))$ (see (82)). Let $M_{loc}([0, \infty))$ denote the vector space of local measures, i.e., set functions that are defined on relatively compact Borel measurable subsets of $[0, \infty)$ and that locally behave like bounded measures: for every $T > 0$ the set function μ_T defined by

$$\mu_T(E) := \mu(E \cap [0, T]), \qquad E \in \mathcal{E},$$

belongs to $M([0, \infty))$. The elements of $M_{loc}([0, \infty))$ are called Radon measures. Since the restriction to $[0, T]$ of $\mu * \nu$ depends only on the restrictions of μ and ν to $[0, T]$, we can unambiguously extend the convolution product to $M_{loc}([0, \infty))$ (see (84)).

We continue with the existence of the resolvent ρ of a complex Borel measure μ supported on $[0, \infty)$. For details see Diekmann and Verduyn Lunel (2021, Theorem A.7) and for further information and details see Grippenberg et. al. (1990).

Theorem 2.1 *Suppose that $\mu \in M_{loc}\left([0, \infty); \mathbb{R}^{n\times n}\right)$. There exists a unique measure $\rho \in M_{loc}\left([0, \infty); \mathbb{R}^{n\times n}\right)$ satisfying either one of the following identities*

$$\rho - \mu * \rho = \mu = \rho - \rho * \mu \tag{16}$$

if and only if $\det[I - \mu(\{0\})] \neq 0$. *Furthermore, if $\mu((0, t])$ is continuous as $t = 0$, then $\rho((0, t])$ is continuous at $t = 0$ as well.*

The following theorem summarizes some relevant results for renewal equations (Diekmann and Verduyn Lunel 2021, Theorem A.9).

Theorem 2.2 *Let $\mu \in M_{loc}\left([0, \infty), \mathbb{R}^{n\times n}\right)$ with* $\det[I - \mu(\{0\}] \neq 0$.

(i) For every $f \in B_{loc}([0, \infty), \mathbb{R}^n)$, the renewal equation (15) has a unique solution $x \in B_{loc}([0, \infty), \mathbb{R}^n)$ given by

$$x = f + \rho * f,$$

where ρ satisfies (16). Furthermore, if f is locally absolutely continuous, then the solution x is locally absolutely continuous as well.

(ii) If the kernel μ has no discrete part and if $f \in C([0,\infty),\mathbb{R}^n)$, then $x \in C([0,\infty),\mathbb{R}^n)$.

We now summarize the conclusions obtained so far in this section in the following theorem.

Theorem 2.3 *Let η and ζ be of normalized bounded variation. Let $\varphi \in B([-h,0];\mathbb{R}^n)$ be given. Define μ by (9). If $\det[I-\mu(0)] \neq 0$, then the NFDE (2) provided with the initial condition (3) admits a unique solution. For $t \geq 0$ this solution coincides with the unique solution of the renewal equation (11) and the solution has the representation (15) where ρ satisfies the resolvent equation (14) and f is given by (8).*

Representation (15) will be used to derive a representation of the solution of (2)–(3) directly in terms of the initial data $x_0 = \varphi$. We first need a definition. The *fundamental solution* of the delay equation (2)–(3) on $[-h,\infty)$ is defined by the $n \times n$-matrix-valued function

$$X(t) := \begin{cases} I + \rho((0,t]) & \text{for } t \geq 0, \\ 0 & \text{for } -h \leq t < 0, \end{cases} \tag{17}$$

where ρ is the resolvent of μ given by Theorem 2.1. Since $t \mapsto \mu((0,t])$ is continuous at $t = 0$, it follows from Theorem 2.1 that $\rho((0,t])$ is continuous at $t = 0$. Therefore we can conclude that $X(t)$ has a jump at $t = 0$.

By construction, the fundamental matrix solution $X(t)$ satisfies (2) with initial data

$$X_0(\theta) = \begin{cases} I & \text{for } \theta = 0, \\ 0 & \text{for } -h \leq \theta < 0. \end{cases} \tag{18}$$

Using the fundamental matrix solution $X(t)$ given by (17) and Fubini's theorem, we can rewrite the representation formula (15) in terms of the forcing function f given by (8) directly in terms of the initial condition φ.

We summarize the result in a theorem.

Theorem 2.4 *The solution of (2)–(3) is given explicitly by*

$$x(t;\varphi) = X(t)\varphi(0) + \int_0^h \mathrm{d}\left[\int_{-h}^t \mathrm{d}X(\tau)\,(\mu(t-\tau+\sigma)-\mu(\sigma))\right]\varphi(-\sigma). \tag{19}$$

Or, equivalently, in terms of the resolvent ρ we have

$$\begin{aligned} x(t;\varphi) = {} & (I+\rho((0,t]))\,\varphi(0) + \int_0^h \mathrm{d}\,[\mu(t+\sigma)-\mu(\sigma)]\varphi(-\sigma) \\ & + \int_0^h \mathrm{d}\left[\int_0^t \rho(\mathrm{d}\tau)\,(\mu(t-\tau+\sigma)-\mu(\sigma))\right]\varphi(-\sigma). \end{aligned} \tag{20}$$

Here μ is given by (9).

3 Norming Dual Pairs and Twin Semigroups

The system of equations (2)–(3) defines an infinite-dimensional dynamical system on the state space $B([-h, 0]; \mathbb{R}^n)$, but for the qualitative study of such a dynamical system we need an adjoint theory in place (see Hale and Verduyn Lunel 1993). In the classical theory of delay equations this is the main reason to work with the state space $C([-h, 0]; \mathbb{R}^n)$ despite the fact that the initial data of the fundamental solution (see (18)) does not belong to this space. From the Riesz representation theorem it follows that the dual space of $C([-h, 0]; \mathbb{R}^n)$ has a nice characterization as the space of functions of normalized bounded variation.

The state space $B([-h, 0]; \mathbb{R}^n)$ includes the initial data of the fundamental solution but its dual space does not have a nice characterization. So although the state space $B([-h, 0]; \mathbb{R}^n)$ is a more natural space to consider, it has not yet been used because its dual space is too large to provide a useful adjoint theory. A beautiful idea to repair this discrepancy is to use the notion of a dual pair (see Aliprantis and Border 2006) made precise in Kunze (2011) for infinite-dimensional dynamical systems in the following way.

Two Banach spaces Y and $Y^\diamond$ are called a *norming dual pair* (cf. Kunze (2011)) if a bilinear map

$$\langle \cdot, \cdot \rangle : Y^\diamond \times Y \to \mathbb{R}$$

exists such that, for some $M \in [1, \infty)$,

$$|\langle y^\diamond, y \rangle| \leq M \|y^\diamond\| \|y\|$$

and, moreover,

$$\begin{aligned} \|y\| &:= \sup \left\{ |\langle y^\diamond, y \rangle| \mid y^\diamond \in Y^\diamond, \ \|y^\diamond\| \leq 1 \right\} \\ \|y^\diamond\| &:= \sup \left\{ |\langle y^\diamond, y \rangle| \mid y \in Y, \ \|y\| \leq 1 \right\}. \end{aligned}$$

So we can consider Y as a closed subspace of $Y^{\diamond *}$, the dual of $Y^\diamond$, and $Y^\diamond$ as a closed subspace of Y^* and both subspaces are necessarily weak* dense since they separate points.

The collection of linear functionals $Y^\diamond$ defines a weak topology on Y, denoted by $\sigma(Y, Y^\diamond)$. The corresponding locally convex topological vector space is denoted by $(Y, \sigma(Y, Y^\diamond))$. A crucial point in our approach is that the dual space $(Y, \sigma(Y, Y^\diamond))'$ is (isometrically isomorphic to) $Y^\diamond$ (Rudin 1991, Theorem 3.10). So if a linear functional on Y is continuous with respect to the topology induced by $Y^\diamond$, it can be (uniquely) represented by an element of $Y^\diamond$.

The next key idea to study infinite-dimensional dynamical systems on a norming dual pair is the notion of a twin operator introduced in Diekmann and Verduyn Lunel (2021).

A *twin operator* L on a norming dual pair $(Y, Y^\diamond)$ is a bounded bilinear map from $Y^\diamond \times Y$ to $\mathbb{R}$ that defines both a bounded linear map from Y to Y and a bounded linear map from $Y^\diamond$ to $Y^\diamond$. More precisely,

$$L : Y^\diamond \times Y \to \mathbb{R} \qquad (y^\diamond, y) \mapsto y^\diamond L y$$

is such that

(i) for some $C > 0$ the inequality

$$|y^\diamond L y| \leq C \|y^\diamond\| \|y\|$$

holds for all $y \in Y$ and $y^\diamond \in Y^\diamond$;

(ii) for given $y \in Y$ the map $y^\diamond \mapsto y^\diamond L y$ is continuous as a map from $(Y^\diamond, \sigma(Y^\diamond, Y))$ to $\mathbb{R}$ and hence there exists $Ly \in Y$ such that

$$\langle y^\diamond, Ly \rangle = y^\diamond L y$$

for all $y^\diamond \in Y^\diamond$;

(iii) for given $y^\diamond \in Y^\diamond$ the map $y \mapsto y^\diamond L y$ is continuous as a map from $(Y, \sigma(Y, Y^\diamond))$ to $\mathbb{R}$ and hence there exists $y^\diamond L \in Y^\diamond$ such that

$$\langle y^\diamond L, y \rangle = y^\diamond L y$$

for all $y \in Y$.

So all three maps are denoted by the symbol L, but to indicate on which space L acts we write, inspired by Feller (1953) which, in turn, is inspired by matrix notation, either $y^\diamond Ly$, Ly or $y^\diamond L$. As a concrete example, consider the identity operator. It maps $(y^\diamond, y)$ to $\langle y^\diamond, y \rangle$, y to y and $y^\diamond$ to $y^\diamond$.

If our starting point is a bounded linear operator $L : Y \to Y$ then there exists an associated twin operator if and only if the adjoint of L leaves the embedding of $Y^\diamond$ into Y^* invariant. We express this in words by saying that L extends to a twin operator. Likewise, if our starting point is an operator $L : Y^\diamond \to Y^\diamond$ then L extends to a twin operator if and only if the adjoint of L leaves the embedding of Y into $Y^{\diamond *}$ invariant. So a twin operator on a norming dual pair is reminiscent of the combination of a bounded linear operator on a reflexive Banach space and its adjoint, whence the adjective "twin".

The composition of bounded bilinear maps is, in general, not defined. But for twin operators it is! Indeed, if L_1 and L_2 are both twin operators on the norming dual pair $(Y, Y^\diamond)$, we define the composition $L_1 L_2$ by

$$y^\diamond L_1 L_2 y := \langle y^\diamond L_1, L_2 y \rangle.$$

Note that this definition entails that $L_1 L_2$ acts on Y by first applying L_2 and next L_1, whereas $L_1 L_2$ acts on $Y^\diamond$ by first applying L_1 and next L_2.

Definition 3.1 A family $\{S(t)\}_{t\geq 0}$ of twin operators on a norming dual pair $(Y, Y^\diamond)$ is called a *twin semigroup* if

(i) $S(0) = I$, and $S(t+s) = S(t)S(s) \quad$ for $t, s \geq 0$;
(ii) there exist constants $M \geq 1$ and $\omega \in \mathbb{R}$ such that

$$|y^\diamond S(t)y| \leq Me^{\omega t}\|y\|\,\|y^\diamond\|;$$

(iii) for all $y \in Y$, $y^\diamond \in Y^\diamond$ the function

$$t \mapsto y^\diamond S(t)y$$

is measurable;
(iv) for $\operatorname{Re}\lambda > \omega$ (with ω as introduced in ii)) there exists a twin operator $\overline{S}(\lambda)$ such that

$$y^\diamond \overline{S}(\lambda)y = \int_0^\infty e^{-\lambda t} y^\diamond S(t)y \,\mathrm{d}t. \tag{21}$$

Note that the combination of $ii)$ and $iii)$ allows us to conclude that the right hand side of (21) defines a bounded bilinear map, but not that it defines a twin operator. Hence $iv)$ is indeed an additional assumption.

We call $\overline{S}(\lambda)$ defined on $\{\lambda \mid \operatorname{Re}\lambda > \omega\}$ the *Laplace transform* of $\{S(t)\}$. It actually suffices to assume that the assertion of iv) holds for $\lambda = \lambda_0$ with $\operatorname{Re}\lambda_0 > \omega$. This assumption allows us to introduce the multi-valued operator

$$C = \lambda_0 I - \overline{S}(\lambda_0)^{-1} \tag{22}$$

on Y and next define the function $\lambda \mapsto \overline{S}(\lambda)$ by

$$\overline{S}(\lambda) = (\lambda I - C)^{-1} \tag{23}$$

on an open neighbourhood of λ_0.

In Definition 2.6 of Kunze (2009) an operator C is called the *generator* of the semigroup provided the Laplace transform is injective and hence C is single-valued. In Diekmann and Verduyn Lunel (2021) we adopted a more pliant position and call C the generator even when it is multi-valued and we refer to this paper for additional information.

Focusing on $\{S(t)\}_{t\geq 0}$ as a semigroup of bounded linear operators on Y, we now list some basic results from Kunze (2011).

Lemma 3.2 *The following statements are equivalent*

1. $y \in \mathcal{D}(C)$ *and* $z \in Cy$;
2. *there exist* $\lambda \in \mathbb{C}$ *with* $\operatorname{Re}\lambda > \omega$, *here* ω *is as introduced in ii) of Definition 3.1, and* $y, z \in Y$ *such that*

$$y = \overline{S}(\lambda)(\lambda y - z)$$

3. $y, z \in Y$ *and for all* $t > 0$

$$\int_0^t S(\tau)z \, \mathrm{d}\tau = S(t)y - y.$$

Here it should be noted that item 3. includes the assertions

- *the integral* $\int_0^t S(\tau)z \, \mathrm{d}\tau$ *defines an element of* Y *(even though at first it only defines an element of* $Y^{\diamond *}$*);*
- *the integral* $\int_0^t S(\tau)z \, \mathrm{d}\tau$ *does not depend on the choice of* $z \in Cy$ *in case* C *is multi-valued.*

Lemma 3.3 *For all* $t > 0$ *and* $y \in Y$*, we have* $\int_0^t S(\tau)y \, \mathrm{d}\tau \in \mathcal{D}(C)$ *and*

$$S(t)y - y \in C \int_0^t S(\tau)y \, \mathrm{d}\tau.$$

4 The Norming Dual Pair (B, NBV)

In the study of delay differential equations, the natural dual pair is given by

$$Y = B\left([-1, 0], \mathbb{R}^n\right) \quad \text{and} \quad Y^{\diamond} = NBV\left([0, 1], \mathbb{R}^n\right) \tag{24}$$

with the pairing

$$\langle y^{\diamond}, y \rangle = \int_{[0,1]} y^{\diamond}(\mathrm{d}\sigma) \cdot y(-\sigma) \tag{25}$$

(see Appendix A for the definition of NBV). Here Y is provided with the supremum norm and $Y^{\diamond}$ with the total variation norm (see (83)). See Diekmann and Verduyn Lunel 2021.

In the study of renewal equations, the natural dual pair is given by

$$Y = NBV\left([-1, 0], \mathbb{R}^n\right) \quad \text{and} \quad Y^{\diamond} = B\left([0, 1], \mathbb{R}^n\right)$$

with the pairing

$$\langle y^{\diamond}, y \rangle = \int_{[-1,0]} y(\mathrm{d}\sigma) \cdot y^{\diamond}(-\sigma).$$

Returning to (24)–(25), we first make two trivial, yet useful, observations: fix $1 \leq i \leq n$ and $-1 \leq \theta \leq 0$,

$$\int_{[0,1]} y^\diamond(\mathrm{d}\sigma)\cdot y(-\sigma) = y_i(\theta),$$

if $y_j^\diamond(\sigma) = 0$, $0 \le \sigma \le 1$, $j \ne i$, and $y_i^\diamond(\sigma) = 0$ for $0 \le \sigma < -\theta$ and $y_i^\diamond(\sigma) = 1$ for $\sigma \ge -\theta$, and similarly

$$\int_{[0,1]} y^\diamond(\mathrm{d}\sigma)\cdot y(-\sigma) = y_i^\diamond(-\theta),$$

if $y_j(-\sigma) = 0$, $0 \le \sigma \le 1$, $j \ne i$, and $y_i(-\sigma) = 1$ for $0 \le \sigma \le -\theta$ and $y_i(-\sigma) = 0$ for $\sigma > -\theta$.

The point is that, consequently, in case of (24)–(25), convergence in both $(Y, \sigma(Y, Y^\diamond))$ and $(Y^\diamond, \sigma(Y^\diamond, Y))$ entails pointwise convergence (in, respectively, $B([-1, 0], \mathbb{R}^n)$ and $NBV([0, 1], \mathbb{R}^n)$).

In the first case, the dominated convergence theorem implies that, conversely, a bounded pointwise convergent sequence in $B([-1, 0], \mathbb{R}^n)$ converges in $(Y, \sigma(Y, Y^\diamond))$. For $NBV([0, 1], \mathbb{R}^n)$, this is not so clear. It is true that the pointwise limit of a sequence of functions of bounded variation is again of bounded variation (Helly's theorem), but there is no dominated convergence theorem for measures.

The following theorem is proved in Diekmann and Verduyn Lunel (2021, Theorem B.1).

Theorem 4.1 *The dual pair given by* (24) *and* (25) *is a norming dual pair, i.e.,*

$$\|y\| = \sup\left\{|\langle y^\diamond, y\rangle| \mid y^\diamond \in Y^\diamond,\ \|y^\diamond\| \le 1\right\}$$
$$\|y^\diamond\| = \sup\left\{|\langle y^\diamond, y\rangle| \mid y \in Y,\ \|y\| \le 1\right\}.$$

Furthermore

(*i*) $(Y, \sigma(Y, Y^\diamond))$ *is sequentially complete;*
(*ii*) *a linear map* $(Y, \sigma(Y, Y^\diamond)) \to \mathbb{R}$ *is continuous if it is sequentially continuous.*

5 The Twin Semigroup Approach to NFDE

Consider the norming dual pair $(Y, Y^\diamond)$ with Y and $Y^\diamond$ as given in Sect. 4 by (24).

By solving (2)–(3), see Theorem 2.3, we can define a Y-valued function $u : [0, \infty) \to Y$ by

$$u(t; \varphi) := x_t(\cdot\,; \varphi), \qquad t \ge 0, \tag{26}$$

where x_t is defined by (1), and bounded linear operators $S(t) : Y \to Y$ by

$$S(t)\varphi = u(t; \varphi). \tag{27}$$

The initial condition (2) translates into

$$S(0)\varphi = u(0;\varphi) = \varphi$$

and (27) reflects that we define a dynamical system on Y by translating along the function φ extended according to (2). Below we show that $\{S(t)\}$ is a twin semigroup and we characterize its generator C. But first we present some heuristics.

In order to motivate an abstract ODE for the Y-valued function u, we first observe that the infinitesimal formulation of the translation rule (26) amounts to the PDE

$$\frac{\partial u}{\partial t} - \frac{\partial u}{\partial \theta} = 0.$$

We need to combine this with (2), in terms of $u(t)(0) = x(t)$, and we have to specify the domain of definition of the derivative with respect to θ. The latter is actually rather subtle. An absolutely continuous function has almost everywhere a derivative and when the function is Lipschitz continuous this derivative is bounded. Thus a Lipschitz function specifies a unique L^∞-equivalence class by the process of differentiation. But *not* a unique element of Y. In fact the set

$$C\psi = \Big\{\psi' \in Y \mid \psi(\theta) = \psi(-1) + \int_{-1}^{\theta} \psi'(\sigma)\, d\sigma, \\ \psi'(0) - \int_0^h \mathrm{d}\eta(\theta)\psi'(-\theta) = \int_0^h \mathrm{d}\zeta(\theta)\psi(-\theta)\Big\} \tag{28}$$

is, for a given Lipschitz continuous function ψ, very large indeed. Note that the boundary condition

$$\psi'(0) - \int_0^h \mathrm{d}\eta(\theta)\psi'(-\theta) = \int_0^h \mathrm{d}\zeta(\theta)\psi(-\theta)$$

takes care of (2). We define C as a multi-valued, unbounded, operator on Y by (28) with domain given by

$$\mathcal{D}(C) = Lip\left([-1,0],\mathbb{R}^n\right). \tag{29}$$

We claim that (2)–(3) and (26) correspond to an abstract differential equation

$$\frac{\mathrm{d}u}{\mathrm{d}t} \in Cu.$$

To substantiate this claim, we shall verify that $\{S(t)\}_{t\geq 0}$ defined by (27) is a twin semigroup and, finally, that C is the corresponding generator in the sense of (23) where $\overline{S}(\lambda)$ is given by (21).

From the representation (19) of the solution of (2)–(3) we can derive an explicit representation of the semigroup $\{S(t)\}_{t\geq 0}$ defined by (27).

Theorem 5.1 *The semigroup $\{S(t)\}_{t\geq 0}$ defined by (27) is given by*

$$(S(t)\varphi)(\theta) = \int_0^h K_t(\theta, \mathrm{d}\sigma)\,\varphi(-\sigma) \tag{30}$$

with for $\sigma > 0$ and $-h \leq \theta \leq 0$ the kernel $K_t(\theta, \sigma)$ defined by

$$\begin{aligned} K_t(\theta,\sigma) := {} & H(\sigma + t + \theta) + H(t+\theta)\rho(t+\theta) \\ & + H(t+\theta)\int_0^{t+\theta} \mathrm{d}X(\xi)\,(\mu(t+\theta+\sigma-\xi) - \mu(\sigma))\,, \end{aligned} \tag{31}$$

and $K_t(\theta, 0) = 0$. Here ρ denotes the resolvent of μ with μ defined in (9), X denotes the fundamental solution given by (17), and H is the standard Heaviside function.

Proof For $t + \theta < 0$ the second and third terms in the expression for K_t do not contribute, and the first term yields

$$(S(t)\varphi)(\theta) = \varphi(t+\theta)$$

which is in accordance with (27) because of (3).

Now assume that $t + \theta \geq 0$. Clearly the first term contributes a unit jump at $\sigma = 0$ and $H(t+\theta) = 1$. The second term has, as a function of σ, a jump of magnitude $\rho(t+\theta)$ at $\sigma = 0$, an absolutely continuous part with derivative given by

$$\int_0^{t+\theta} \mathrm{d}X(\xi)\,(\zeta(t+\theta+\sigma-\xi) - \zeta(\sigma))\,,$$

and a part of bounded variation given by

$$\int_0^{t+\theta} \mathrm{d}X(\xi)\,(\eta(t+\theta+\sigma-\xi) - \eta(\sigma))\,.$$

The jumps yield the first term at the right hand side of (19) (see also (20)) evaluated at $t + \theta$, the absolutely continuous part yields the second, and the bounded variation part the third term. □

Note that K_t is *bounded*, in the sense (cf. Kunze 2009, Definition 3.2) that for fixed θ in $[-1, 0]$ the function $\sigma \mapsto K_t(\theta, \sigma)$ is of normalized bounded variation, while for fixed $\sigma \in [0, 1]$ the function $\theta \mapsto K_t(\theta, \sigma)$ is bounded and measurable.

The next corollary is a general property of kernel operators.

Corollary 5.2 *The operator $S(t)$ extends to a twin operator.*

Proof The proof directly follows from the observation that we can represent the action of $y^\diamond S(t)$ explicitly as

$$\left(y^{\diamond} S(t)\right)(\sigma) = \int_0^h y^{\diamond}(\mathrm{d}\tau)\, K_t(-\tau, \sigma).$$

□

Theorem 5.3 *The semigroup* $\{S(t)\}_{t\geq 0}$ *defined by* (30) *is a twin semigroup.*

Proof With reference to Definition 3.1 we note that $S(0) = I$ follows directly from (30)–(31), while the semigroup property follows from the uniqueness of solutions to (2)–(3) and the fact that $S(t)$ corresponds to translation along the solution.

The exponential estimates (ii) are well-established in the theory of NFDE, see Sect. 9.3 of Hale and Verduyn Lunel (1993) or the proof of Proposition 7.3 below.

Property (iii), the measurability of $t \mapsto y^{\diamond} S(t) y$, is a direct consequence of the way $K_t(\theta, \sigma)$, defined in (31), depends on t.

It remains to verify that the Laplace transform defines a twin operator. By Fubini's Theorem, the Laplace transform is a kernel operator with kernel

$$\int_0^{\infty} e^{-\lambda t} K_t(\theta, \sigma)\, \mathrm{d}t.$$

□

Theorem 5.4 *The operator* C *defined by* (28) *and* (29) *is the generator (in the sense of* (23)*) of* $\{S(t)\}_{t\geq 0}$ *defined by* (30).

Proof Assume $\varphi \in (\lambda I - C)\psi$. Then there exists $\psi' \in Y$ which is a.e. a derivative of ψ such that

$$\lambda\psi - \psi' = \varphi, \qquad -1 \leq \theta < 0,$$

satisfying the boundary condition

$$\lambda\psi(0) - \int_0^h \mathrm{d}\eta(\theta)\psi'(-\theta) - \int_0^h \mathrm{d}\zeta(\theta)\psi(-\theta) = \varphi(0).$$

Solving the differential equation yields that

$$\psi(\theta) = e^{\lambda\theta}\psi(0) + e^{\lambda\theta} \int_{\theta}^0 e^{-\lambda\sigma}\varphi(\sigma)\, \mathrm{d}\sigma \tag{32}$$

and accordingly the boundary condition for $\theta = 0$ boils down to

$$\psi(0) = \Delta(\lambda)^{-1} H(\lambda; \varphi), \tag{33}$$

where

$$H(\lambda;\varphi) := \varphi(0) + \lambda \int_0^h \mathrm{d}\eta(\sigma) e^{-\lambda\sigma} \int_{-\sigma}^0 e^{-\lambda\tau}\varphi(\tau)\,\mathrm{d}\tau + \int_0^h \mathrm{d}\zeta(\sigma) e^{-\lambda\sigma} \int_{-\sigma}^0 e^{-\lambda\tau}\varphi(\tau)\,\mathrm{d}\tau.$$

This requires that $\det \Delta(\lambda) \neq 0$ with

$$\Delta(\lambda) = \lambda\left[I - \int_0^h \mathrm{d}\eta(\sigma)e^{-\lambda\sigma}\right] + \int_0^h \mathrm{d}\zeta(\sigma)e^{-\lambda\sigma}.$$

Our claim is that the identity

$$(\lambda I - C)^{-1}\varphi = \int_0^\infty e^{-\lambda t} S(t)\varphi\,\mathrm{d}t \tag{34}$$

or, equivalently,

$$\psi(\theta) = \int_0^\infty e^{-\lambda t}\,(S(t)\varphi)\,(\theta)\,\mathrm{d}t$$

holds. To verify this, we first note that

$$\begin{aligned}\int_0^\infty e^{-\lambda t}\,(S(t)\varphi)\,(\theta)\,\mathrm{d}t &= \int_0^\infty e^{-\lambda t} x(t+\theta;\varphi)\,\mathrm{d}t \\ &= \int_0^{-\theta} e^{-\lambda t}\varphi(t+\theta)\,\mathrm{d}t + \int_{-\theta}^\infty e^{-\lambda t} x(t+\theta)\,\mathrm{d}t \\ &= e^{\lambda\theta}\int_\theta^0 e^{-\lambda\sigma}\varphi(\sigma)\,\mathrm{d}\sigma + e^{\lambda\theta}\bar{x}(\lambda;\varphi),\end{aligned}$$

where $\bar{x}(\lambda;\varphi) := \int_0^\infty e^{-\lambda t}x(t;\varphi)\,\mathrm{d}t$, with $x(t;\varphi)$ the solution of (2)–(3) given by (19). So, since (32) holds, to prove (34) it remains to check that

$$\psi(0) = \bar{x}(\lambda;\varphi).$$

By taking the Laplace transform on both sides of (11) we deduce that

$$\begin{aligned}\bar{x}(\lambda;\varphi) &= \left(1 - \int_0^\infty e^{-\lambda t}\,\mathrm{d}\mu(t)\right)^{-1}\bar{f}(\lambda) \\ &= \Delta(\lambda)^{-1}\lambda\bar{f}(\lambda),\end{aligned}$$

where $\bar{f}(\lambda) := \int_0^\infty e^{-\lambda t} f(t)\,\mathrm{d}t$. Therefore, using the representation of f in (12), it follows that

$$\begin{aligned}
\lambda\bar{f}(\lambda) &= \varphi(0) + \int_0^\infty \lambda e^{-\lambda t} \int_0^t \left(\int_s^h \mathrm{d}\zeta(\theta)\varphi(s-\theta)\,\mathrm{d}s \right) \mathrm{d}t \\
&\quad + \lambda \int_0^\infty e^{-\lambda t} \int_t^h \mathrm{d}\eta(\theta)\varphi(t-\theta)\,\mathrm{d}t \\
&= \varphi(0) + \int_0^\infty e^{-\lambda t} \int_t^h \mathrm{d}\zeta(\theta)\varphi(t-\theta)\,\mathrm{d}t \\
&\quad + \lambda \int_0^\infty e^{-\lambda t} \int_t^h \mathrm{d}\eta(\theta)\varphi(t-\theta)\,\mathrm{d}t \\
&= \varphi(0) + \int_0^h \mathrm{d}\zeta(\theta) \int_0^\theta e^{-\lambda t}\varphi(t-\theta)\,\mathrm{d}t \\
&\quad + \lambda \int_0^h \mathrm{d}\eta(\theta) \int_0^\theta e^{-\lambda t}\varphi(t-\theta)\,\mathrm{d}t \\
&= \varphi(0) + \int_0^h \mathrm{d}\zeta(\theta) e^{-\lambda\theta} \int_{-\theta}^0 e^{-\lambda\sigma}\varphi(\sigma)\,\mathrm{d}\sigma \\
&\quad \lambda \int_0^h \mathrm{d}\eta(\theta) e^{-\lambda\theta} \int_{-\theta}^0 e^{-\lambda\sigma}\varphi(\sigma)\,\mathrm{d}\sigma \\
&= H(\lambda;\varphi).
\end{aligned}$$

Therefore it follows from (33) that indeed $\psi(0) = \bar{x}(\lambda;\varphi)$ and this completes the proof of the identity (34). □

In Diekmann and Verduyn Lunel (2021), we proved Theorems 5.1, 5.3 and 5.4 for retarded functional differential equations, and gave an alternative proof of Theorem 5.3 in the neutral case using a relative bounded perturbation argument, see Diekmann and Verduyn Lunel (2021, Theorem 11.1).

6 The Variation-of-Constants Formula for NFDE

It is a direct consequence of (29) that

$$X = \overline{\mathcal{D}(C)} = C\left([-1,0],\mathbb{R}^n\right).$$

Clearly $C\psi \cap X$ is either empty or a singleton, cf. (28), and for the set to be nonempty we need that $\psi \in C^1$ and

$$\psi'(0) - \int_0^h \mathrm{d}\eta(\theta)\psi'(-\theta) = \int_0^h \mathrm{d}\zeta(\theta)\psi(-\theta).$$

So the generator A of the restriction $\{T(t)\}_{t\geq 0}$ of $\{S(t)\}_{t\geq 0}$ to X is given by

$$\mathcal{D}(A) = \left\{ \psi \in C^1 \mid \psi'(0) - \int_0^h \mathrm{d}\eta(\theta)\psi'(-\theta) = \int_0^h \mathrm{d}\zeta(\theta)\psi(-\theta) \right\}$$
$$A\psi = \psi'$$

in complete agreement with the standard theory.

As $S(t)$ maps Y into X for $t \geq 1$, one might wonder whether we gained anything at all by the extension from X to Y? Already in the pioneering work of Jack Hale he emphasized that if one adds a forcing term to (2), one needs

$$q(\theta) := \begin{cases} 1 & \text{for } \theta = 0, \\ 0 & \text{for } -1 \leq \theta < 0, \end{cases}$$

to describe the solution by way of the variation-of-constants formula.

Indeed, the solution of

$$\begin{aligned} \frac{\mathrm{d}}{\mathrm{d}t}\left[x(t) - \int_0^h \mathrm{d}\eta(\theta)x(t-\theta) \right] &= \int_0^h \mathrm{d}\zeta(\theta)x(t-\theta) + f(t), \qquad t \geq 0, \\ x(\theta) &= \varphi(\theta), \qquad -1 \leq \theta \leq 0, \end{aligned} \tag{35}$$

is explicitly given by

$$x_t = S(t)\varphi + \int_0^t S(t-\tau)qf(\tau)\,\mathrm{d}\tau, \tag{36}$$

where $S(t)$ is given by (30) and x_t is as defined in (1). This formally follows directly from the fact that the inhomogeneous NFDE (35) corresponds to the initial value problem

$$\frac{\mathrm{d}u}{\mathrm{d}t} \in Cu + qf, \qquad u(0) = \varphi,$$

where as before $u(t) = x_t$. Note that the solution with initial condition q is the so-called fundamental solution, cf. (18) and (17).

The integration theory presented next provides a precise underpinning of the integral in (36) and the remainder of this section is devoted to a proof of (36). In the original approach of Hale, the hidden argument θ in (36) is inserted and thus the integral reduces to the integration of an $\mathbb{R}^n$-valued function. Note that evaluation in a point corresponds to the application of a Dirac functional, so our approach yields, in a sense, a theoretical underpinning of Hale's approach.

As a final remark, we emphasize that the variation-of-constants formula (36) is the key first step towards a local stability and bifurcation theory for nonlinear problems, as shown in detail in Diekmann et. al. (1995) for retarded functional differential equations. For neutral functional differential equations this is work in progress.

Motivated by (36), we want to define an element $u(t)$ of Y by way of the action on $Y^\diamond$ expressed in the formula

$$\langle y^\diamond, u(t)\rangle = y^\diamond S(t)u_0 + \int_0^t y^\diamond S(t-\tau)q\ f(\tau)\,\mathrm{d}\tau, \tag{37}$$

where the standard assumptions are

(i) $(Y, Y^\diamond)$ is a norming dual pair;
(ii) $q \in Y$;
(iii) $f : [0, T] \to \mathbb{R}$ is bounded and measurable;
(iv) $\{S(t)\}$ is a twin semigroup,

and where u_0 (corresponding to φ in (36)) is an arbitrary element of Y.

The definition of the first term at the right hand side of (37) is no problem at all, it contributes $S(t)u_0$ to $u(t)$. The second term defines an element of $Y^{\diamond *}$, but it is not clear that this element is, without additional assumptions, represented by an element of Y. The following lemma provides a sufficient condition.

Lemma 6.1 *In addition to (i)–(iv) assume that*

$$\big(Y, \sigma(Y, Y^\diamond)\big) \quad \textit{is sequentially complete.} \tag{38}$$

Then

$$y^\diamond \mapsto \int_0^t y^\diamond S(t-\tau)q\ f(\tau)\,\mathrm{d}\tau \tag{39}$$

is represented by an element of Y, to be denoted as $\int_0^t S(t-\tau)q\ f(\tau)\,\mathrm{d}\tau$.

Proof There exists a sequence of step functions f_m such that $|f_m| \le |f|$ and $f_m \to f$ pointwise. Lemma 3.3 shows that

$$\int_0^t S(t-\tau)q\ f_m(\tau)\,\mathrm{d}\tau$$

belongs to Y (in fact even to $\mathcal{D}(C)$). Since (see Definition 3.1(ii))

$$\big|y^\diamond S(t-\tau)q f_m(\tau)\big| \le M e^{\omega(t-\tau)}\|q\|\|y^\diamond\| \sup_\sigma |f(\sigma)|,$$

the dominated convergence theorem implies that for every $y^\diamond \in Y^\diamond$

$$\lim_{m\to\infty} \int_0^t y^\diamond S(t-\tau)q\ f_m(\tau)\,\mathrm{d}\tau = \int_0^t y^\diamond S(t-\tau)q\ f(\tau)\,\mathrm{d}\tau.$$

The sequential completeness next guarantees that the limit too is represented by an element of Y. □

In Diekmann and Verduyn Lunel (2021) we have developed a perturbation theory to study neutral equations directly as an unbounded perturbation of a retarted equation. In order to do this, we have to replace $f(\tau)\,\mathrm{d}\tau$ by $F(\mathrm{d}\tau)$ with F of bounded

variation. In this setting the approximation by step functions used in the proof of Lemma 6.1 no longer works. This observation motivates to look for an alternative sufficient condition to replace (38). This is taken care of in the following lemma.

Lemma 6.2 *In addition to (i)–(iv) assume that*

$$\begin{aligned} &\text{a linear map } \left(Y^\diamond, \sigma(Y^\diamond, Y)\right) \to \mathbb{R} \text{ is continuous} \\ &\text{if it is sequentially continuous.} \end{aligned} \tag{40}$$

Then the assertion of Lemma 6.1 holds.

Proof Again we are going to make use of the dominated convergence theorem. Consider a sequence $\{y_m^\diamond\}$ in $Y^\diamond$ such that for every $y \in Y$ the sequence $\langle y_m^\diamond, y\rangle$ converges to zero in $\mathbb{R}$. Then for all relevant t and τ we have

$$\lim_{m\to\infty} y_m^\diamond S(t-\tau)q = 0$$

and consequently

$$\lim_{m\to\infty} \int_0^t y_m^\diamond S(t-\tau)q\ f(\tau)\,\mathrm{d}\tau = 0.$$

So the linear map (39) is, in the sense described in (40), sequentially continuous and therefore, by the assumption, continuous. Since

$$\left(Y^\diamond, \sigma(Y^\diamond, Y)\right)' = Y,$$

we conclude that (39) is represented by an element of Y. □

We are going to use the above results to show that a certain type of perturbation of a twin semigroup $\{S(t)\}$ yields again a *twin* semigroup. In order to do this we need a dual version of (37), i.e., we want to define an element $u^\diamond(t)$ of $Y^\diamond$ by way of the action on Y expressed in the formula

$$\langle u^\diamond(t), y\rangle = u_0^\diamond S(t)y + \int_0^t q^\diamond S(t-\tau)y\ f(\tau)\,\mathrm{d}\tau, \tag{41}$$

where the standard assumptions are as before with (ii) replaced by (ii)′, i.e.,

(i) $(Y, Y^\diamond)$ is a norming dual pair;
(ii)′ $q^\diamond \in Y^\diamond$;
(iii) $f : [0, T] \to \mathbb{R}$ is bounded and measurable;
(iv) $\{S(t)\}$ is a twin semigroup,

and where $u_0^\diamond$ is an arbitrary element of $Y^\diamond$. This implies that

$$y \mapsto \int_0^t q^\diamond S(t-\tau)y\ f(\tau)\,\mathrm{d}\tau \tag{42}$$

is represented by an element of $Y^\diamond$, to be denoted as $\int_0^t q^\diamond S(t-\tau)\, f(\tau)\, \mathrm{d}\tau$.

Applying the two lemmas above, with the role of Y and $Y^\diamond$ interchanged, we find that this is indeed the case if either

$$\big(Y^\diamond, \sigma(Y^\diamond, Y)\big) \quad \text{is sequentially complete} \tag{43}$$

or

$$\begin{aligned} &\text{a linear map } \big(Y, \sigma(Y, Y^\diamond)\big) \to \mathbb{R} \text{ is continuous} \\ &\text{if it is sequentially continuous.} \end{aligned} \tag{44}$$

Therefore to develop a perturbation theory for twin semigroups we need both (39) and (42) to be represented by elements from, respectively, Y and $Y^\diamond$. This motivates the following definition.

Definition 6.3 We say that a norming dual pair $(Y, Y^\diamond)$ is *suitable for twin perturbation* if

(a) at least one of (38) and (40) holds; and
(b) at least one of (43) and (44) holds

Recall from Theorem 4.1 that for the norming dual pair (B, NBV) introduced in Sect. 4 we have that (38) and (44) are satisfied. This shows that the norming dual pair (B, NBV) is suitable for twin perturbation.

We are now ready to give a rigorous proof of the variation-of-constants formula for NFDE.

Theorem 6.4 *The solution of the inhomogeneous NFDE* (35) *can be represented by the variation-of-constants formula* (36)*, i.e.,*

$$x_t = S(t)\varphi + \int_0^t S(t-\tau) q f(\tau)\, \mathrm{d}\tau,$$

where $S(t)$ *is the twin semigroup given by* (30)*.*

Proof It follows from Theorem 4.1 that

$$Y = B([-1, 0]; \mathbb{R}^n) \quad \text{and} \quad Y^\diamond = NBV([0, 1]; \mathbb{R}^n)$$

is a norming dual pair suitable for twin perturbation. Therefore the claim follows by applying Lemma 6.1 with respect to the norming dual pair (B, NBV) and Lemma 6.2 with respect to the norming dual pair (NBV, B). □

In the treatment of renewal equations in Diekmann and Verduyn Lunel (2021) we assumed (43) and (40). In fact for delay differential equations we take as normal dual pair $(Y, Y^\diamond)$ with $Y = B([-1, 0])$ and $Y^\diamond = NBV([0, 1])$, while for renewal equations we take $(Y, Y^\diamond)$ with $Y = NBV([-1, 0])$ and $Y^\diamond = B([0, 1])$.

7 Bounded Time-Dependent Perturbation of a Twin Semigroup

In this section we assume

- $(Y, Y^\diamond)$ is a norming dual pair that is suitable for twin perturbation, cf. Definition 6.3;
- $\{S_0(t)\}$ is a twin semigroup on $(Y, Y^\diamond)$ with generator C_0;
- For $j = 1, \ldots, n$ the elements $q_j \in Y$ and $t \mapsto q_j^\diamond(t) \in Y^\diamond$ are given.

Definition 7.1 A two-parameter family $U = \{U(t,s)\}_{t \geq s}$ of twin operators on a norming dual pair $(Y, Y^\diamond)$ is called a *twin evolutionary system* if

(i) $U(s,s) = I$ and $U(t,s) = U(t,r)U(r,s)$ for $s \leq r \leq t$
(ii) there exist constants $M \geq 1$ and $\omega_0 \in \mathbb{R}$ such that for all $y \in Y$, $y^\diamond \in Y^\diamond$

$$|y^\diamond U(t,s)y| \leq Me^{\omega_0(t-s)}\|y\|\,\|y^\diamond\|, \qquad t \geq s;$$

(iii) Let the set $\triangle \subset \mathbb{R}^2$ be defined by $\triangle = \{(t,s) \mid -\infty < s \leq t < \infty\}$. For all $y \in Y$, $y^\diamond \in Y^\diamond$ the function

$$\triangle \ni (t,s) \mapsto y^\diamond U(t,s)y \in \mathbb{R}$$

is measurable.

Our aim is to define constructively a twin evolutionary system $\{U(t,s)\}$ corresponding to the abstract multi-valued differential equation

$$\frac{\mathrm{d}u}{\mathrm{d}t} \in C(t)u, \qquad t \geq s, \qquad u(s) \text{ given}, \tag{45}$$

with

$$\mathcal{D}(C(t)) = \mathcal{D}(C_0), \qquad C(t)y = C_0 y + \sum_{j=1}^{n} \langle q_j^\diamond(t), y\rangle q_j. \tag{46}$$

The first step is to introduce a $n \times n$-matrix-valued function $k(t,s)$ on $\mathbb{R} \times \mathbb{R}$ via $k(t,s) = 0$ for $-\infty < t \leq s < \infty$ and

$$k_{ij}(t,s) := q_i^\diamond(t) S_0(t-s) q_j, \qquad -\infty < s \leq t < \infty. \tag{47}$$

Note that for each pair c_1, c_2 with $-\infty < c_1 < c_2 < \infty$ and for each $f \in L^1([c_1, c_2]; \mathbb{R}^n)$, we have

$$\sup_{\|f\| \leq 1} \int_{c_1}^{c_2} \left(\int_{c_1}^{c_2} \|k(t,s)f(s)\|\,\mathrm{d}s \right) \mathrm{d}t < \infty.$$

Here $\|f\|$ denotes the norm of f as function belonging to $L^1([c_1, c_2]; \mathbb{R}^n)$ and the map

$$f \mapsto \int_{c_1}^{t} k(t,s) f(s)\, \mathrm{d}s, \quad c_1 \le t \le c_2,$$

defines a bounded linear operator on $L^1([c_1, c_2]; \mathbb{R}^n)$ which we shall denote by K.

The linear space of lower triangular kernel functions on $[c_1, c_2] \times [c_1, c_2]$ of type L^1_{loc} endowed with the norm

$$\begin{aligned} \|k\|_1 &:= \sup_{\|f\| \le 1} \int_{c_1}^{c_2} \left(\int_{c_1}^{c_2} \|k(t,s) f(s)\| \, \mathrm{d}s \right) \mathrm{d}t \\ &= \operatorname*{ess\,sup}_{s \in [c_1, c_2]} \int_{c_1}^{c_2} \|k(t,s)\| \, \mathrm{d}t \end{aligned} \tag{48}$$

is a Banach space (see Theorem 9.2.4 and Proposition 9.2.7 of Grippenberg et. al. 1990) which we will denote by $L^1_+\left([c_1, c_2] \times [c_1, c_2]; \mathbb{R}^{n \times n}\right)$.

Now let k be a lower triangular kernel function of type L^1_{loc}. We call an $n \times n$-matrix-function $r(t,s)$ a *resolvent kernel function of* k if $r(t,s)$ is a lower triangular kernel function of type L^1_{loc} and

$$r(t,s) = k(t,s) + \int_s^t r(t,a) k(a,s)\, \mathrm{d}a, \qquad -\infty < s \le t < \infty, \tag{49}$$

$$= k(t,s) + \int_s^t k(t,a) r(a,s)\, \mathrm{d}a, \qquad -\infty < s \le t < \infty. \tag{50}$$

Define the integral operator R similar as the operator K but with the kernel $k(t,s)$ replaced by $r(t,s)$, i.e.,

$$(Rf)(t) := \int_{c_1}^{t} r(t,s) f(s)\, \mathrm{d}s, \qquad c_1 \le t \le c_2.$$

Using the integral operators K and R, it follows from the identity (50) that for $c_1 < t < c_2$ we have

$$\begin{aligned} (KRf)(t) &= \int_{c_1}^{t} k(t,s)(Rf)(s)\, \mathrm{d}s \\ &= \int_{c_1}^{t} k(t,s) \left(\int_0^s r(s,\tau) f(\tau)\, \mathrm{d}\tau \right) \mathrm{d}s \\ &= \int_{c_1}^{t} \left(\int_\tau^t k(t,s) r(s,\tau)\, \mathrm{d}s \right) f(\tau)\, \mathrm{d}\tau \\ &= \int_{c_1}^{t} \left(r(t,\tau) - k(t,\tau) \right) f(\tau)\, \mathrm{d}\tau \\ &= (Rf)(t) - (Kf)(t), \quad c_1 \le t \le c_2. \end{aligned}$$

It follows that $KR = R - K$. Similarly, using (49), we have $RK = R - K$. This yields $KR = RK$ and

$$(I - K)(I + R) = (I + R)(I - K) = I, \tag{51}$$

where I is the identity operator on $L^1([c_1, c_2]; \mathbb{R}^n)$. Thus $I - K$ is an invertible operator on $L^1([c_1, c_2]; \mathbb{R}^n)$, and its inverse is given by $I + R$.

Theorem 7.2 *If $k(t, s)$ is a lower triangular kernel function of type L^1_{loc}, then $k(t, s)$ has a unique resolvent kernel function $r(t, s)$ of type L^1_{loc}. In particular, the integral equation $x = Kx + f$ has a unique solution given by $x = f + Rf$.*

Proof The proof will be done in three steps. Throughout $k(t, s)$ is a lower triangular kernel function of type L^1_{loc}.

STEP 1. First note that if k_1 and k_2 are lower triangular kernel functions on $\mathbb{R} \times \mathbb{R}$, then the same holds true for the functions

$$(t, s) \mapsto \int_s^t k_1(t, a)k_2(a, s)\, da \quad \text{and} \quad (t, s) \mapsto \int_s^t k_2(t, a)k_1(a, s)\, da.$$

Furthermore, from the discussion in the paragraph preceding the present theorem it follows that a resolvent kernel function of type L^1_{loc} is unique whenever it exists.

STEP 2. Because of uniqueness of the resolvent kernel of type L^1_{loc}, it suffices to prove existence of a resolvent kernel on $[c_1, c_2]$ for every $c_1, c_2 \in (0, \infty)$ with $c_1 < c_2$. Assume first that $\|k\|_1 \leq 1$ with $\|k\|_1$ given by (48), then the map

$$r(t, s) \mapsto \int_s^t k(t, a)r(a, s)\, \mathrm{d}a + k(t, s)$$

is a contraction on $L^1_+\big([c_1, c_2] \times [c_1, c_2]; \mathbb{R}^{n\times n}\big)$. This shows that (50) (and, using (51), similarly (49)) has a unique solution, and this solution is a resolvent kernel of type L^1_{loc}.

STEP 3. Since $k(t, s)$ is a lower triangular kernel function of type L^1_{loc}, we define a scaled lower triangular kernel function of type L^1_{loc} by

$$\widehat{k}(t, s) := e^{-\gamma(t-s)}k(t, s).$$

Since the norm of $\widehat{k}$ is defined by (see (48))

$$\|\widehat{k}\|_1 := \operatorname*{ess\,sup}_{s\in[c_1,c_2]} \int_{c_1}^{c_2} \|\widehat{k}(t, s)\|\, \mathrm{d}t = \operatorname*{ess\,sup}_{s\in[c_1,c_2]} \int_{c_1}^{c_2} e^{-\gamma(t-s)}\|k(t, s)\|\, \mathrm{d}t,$$

we can choose γ so large that $\|\widehat{k}\|_1 < 1$. From Step 2, it follows that the equation

$$\widehat{r}(t, s) = \widehat{k}(t, s) + \int_s^t \widehat{k}(t, a)\widehat{r}(a, s)\, \mathrm{d}a$$

has a unique solution $\widehat{r} \in L^1_+\left([c_1, c_2] \times [c_1, c_2]; \mathbb{R}^{n\times n}\right)$. Therefore, we have

$$\widehat{r}(t,s) = e^{-\gamma(t-s)}k(t,s) + \int_s^t e^{-\gamma(t-a)}k(t,a)\widehat{r}(a,s)\,\mathrm{d}a,$$

and hence

$$e^{\gamma(t-s)}\widehat{r}(t,s) = k(t,s) + \int_s^t k(t,a)e^{\gamma(a-s)}\widehat{r}(a,s)\,\mathrm{d}a.$$

Thus

$$r(t,s) = k(t,s) + \int_s^t k(t,a)r(a,s)\,\mathrm{d}a,$$

where $r(t,s) = e^{\gamma(t-s)}\widehat{r}(t,s)$. This completes the proof. □

Proposition 7.3 *If $k(t,s)$ is a lower triangular kernel function that satisfies the estimate $\|k(t,s)\| \le m(t)$ for $0 \le s \le t$ and $r(t,s)$ denotes the corresponding resolvent kernel function, then*

$$\|r(t,s)\| \le m(t)\exp\left[\int_s^t m(\sigma)\,\mathrm{d}\sigma\right], \quad 0 \le s \le t < \infty.$$

Proof From the estimate $\|k(t,s)\| \le m(t)$ for $0 \le s \le t$ we obtain the following integral inequality for the function $u(t,s) := \|r(t,s)\|$ on $0 \le s \le t$:

$$u(t,s) \le m(t) + m(t)\int_s^t u(a,s)\,\mathrm{d}a, \quad 0 \le s \le t < \infty. \tag{52}$$

Now fix $s \in [0,\infty)$, and put

$$q(t) := \exp\left[-\int_s^t m(\sigma)\,d\sigma\right]\int_s^t u(a,s)\,\mathrm{d}a. \quad t \ge s. \tag{53}$$

Differentiation of q with respect to t yields

$$\begin{aligned}\frac{\mathrm{d}q}{\mathrm{d}t}(t) &= -m(t)q(t) + \exp\left[-\int_s^t m(\sigma)\,\mathrm{d}\sigma\right]u(t,s)\\ &= \left(u(t,s) - m(t)\int_s^t u(a,s)\,\mathrm{d}a\right)\exp\left[-\int_s^t m(\sigma)\,\mathrm{d}\sigma\right]\\ &\le m(t)\exp\left[-\int_s^t m(\sigma)\,\mathrm{d}\sigma\right],\end{aligned}$$

where we have used (52). Integration from s to t yields the inequality

$$q(t) \le \int_s^t m(a) \exp\left[-\int_s^a m(\sigma)\,\mathrm{d}\sigma\right]\mathrm{d}a = 1 - \exp\left[-\int_s^t m(\sigma)\,\mathrm{d}\sigma\right].$$

Together with the definition of q in (53) we arrive at

$$\begin{aligned} m(t)\int_s^t u(a,s)\,\mathrm{d}a &= m(t)\exp\left[\int_s^t m(\sigma)\,\mathrm{d}\sigma\right] q(t) \\ &\le -m(t) + m(t)\exp\left[\int_s^t m(\sigma)\,\mathrm{d}\sigma\right]. \end{aligned}$$

Substitution into (52) yields

$$u(t,s) \le m(t)\exp\left[\int_s^t m(\sigma)\,\mathrm{d}\sigma\right], \quad 0 \le s \le t < \infty,$$

which completes the proof. □

In the context of the variation-of-constants spirit (46) motivates us to presuppose that $U(t,s)$ and $S_0(t)$ should be related to each other by the equation

$$U(t,s) = S_0(t-s) + \int_s^t S_0(t-\tau)B(\tau)U(\tau,s)\,\mathrm{d}\tau, \qquad t \ge s, \tag{54}$$

where

$$B(t)y := \sum_{j=1}^{n} \langle q_j^{\diamond}(t), y\rangle q_j, \qquad t \ge s. \tag{55}$$

By letting $B(t)$ act on (54) we obtain, for a given initial point $y \in Y$, a finite dimensional renewal equation.

To derive this renewal equation, we first write (55) as

$$B(t)y = \langle q^{\diamond}(t), y\rangle \cdot q, \qquad t \ge s, \tag{56}$$

where $t \mapsto q^{\diamond}(t)$ is the n-vector-valued function with $Y^{\diamond}$-valued components $q_j^{\diamond}(t)$ and q is the n-vector-valued with Y-valued components q_j. Here we use $\cdot$ to denote the inner product in $\mathbb{R}^n$.

We can factor (a rank factorization) B as $B = B_2B_1$ with $B_1 : Y \to \mathbb{R}^n$ and $B_2 : \mathbb{R}^n \to Y$ defined by

$$B_1(t)y := \langle q^{\diamond}(t), y\rangle, \qquad B_2 x := \sum_{j=1}^{n} x_j q_j, \qquad t \ge s. \tag{57}$$

Now let (54) act on $y \in Y$ and use (56) to obtain

$$U(t,s)y = S_0(t-s)y + \int_s^t S_0(t-\tau)q^\diamond(\tau)U(\tau,s)y \cdot q \, \mathrm{d}\tau, \quad t \geq s. \tag{58}$$

Next act on both sides of (58) with the operator $B_1(t)$ as defined in (57) to arrive at

$$v(t,s)y = q^\diamond(t)S_0(t-s)y + \int_s^t k(t,\tau)v(\tau,s)y \, \mathrm{d}\tau, \qquad t \geq s, \tag{59}$$

where

$$v(t,s)y := B_1(t)U(t,s)y = q^\diamond(t)U(t,s)y, \qquad t \geq s,$$

and the lower triangular kernel function $k(t,s)$ is given by (47). Using Theorem 7.2 we can express the solution of (59) in terms of the resolvent $r(t,s)$ of the kernel $k(t,s)$ and the forcing function $t \mapsto q^\diamond(t)S_0(t-s)y$ by the formula

$$v(t,s)y = q^\diamond(t)S_0(t-s)y + \int_s^t r(t,\tau)q^\diamond(\tau)S_0(\tau-s)y \, \mathrm{d}\tau, \quad t \geq s. \tag{60}$$

And now that the function $v(t,s)y$, representing $q^\diamond(t)U(t,s)y$, can be considered as known, Eq. (54) becomes an explicit formula for $U(t,s)$:

$$U(t,s) = S_0(t-s) + \int_s^t S_0(t-\tau)q \cdot v(\tau,s) \, \mathrm{d}\tau, \qquad t \geq s. \tag{61}$$

Please note that, with this definition of $U(t,s)$, we do indeed have that

$$v(t,s)y = q^\diamond(t)U(t,s)y$$

(compare (61) to (59)).

Formula (61) is well suited for proving, on the basis of Lemma 6.1 or Lemma 6.2, that $U(t,s)$ maps Y into Y. But not for proving that $U(t,s)$ maps $Y^\diamond$ into $Y^\diamond$. So even though this may seem superfluous, we now provide an alternative dual constructive definition starting from the following equation

$$U(t,s) = S_0(t-s) + \int_s^t U(t,\tau)B(\tau)S_0(\tau-s) \, \mathrm{d}\tau, \qquad t \geq s, \tag{62}$$

which is the variant of (54) in which the roles of $U(t,s)$ and $S_0(t)$ are interchanged. Let (62) act (from the right) on $y^\diamond \in Y^\diamond$ and next let the resulting identity act on the vector q. Using (56) this yields the equation

$$y^\diamond w(t,s) = y^\diamond S_0(t-s)q + \int_s^t y^\diamond w(t,\tau)k(\tau,s) \, \mathrm{d}\tau, \qquad t \geq s, \tag{63}$$

where $y^\diamond w(t,s) := y^\diamond U(t,s)q$ and $k(t,s)$ is given by (47). The formula

$$y^\diamond w(t,s) = y^\diamond S_0(t-s)q + \int_s^t y^\diamond S_0(t-\tau)q\, r(\tau,s)\,\mathrm{d}\tau, \quad t \geq s, \tag{64}$$

expresses the solution of (63) in terms of the forcing function in (63) and the resolvent $r(t,s)$ of the kernel $k(t,s)$. Next use (56) to rewrite (62) in the form

$$U(t,s) = S_0(t-s) + \int_s^t w(t,\tau)\cdot q^\diamond S_0(\tau-s)\,\mathrm{d}\tau, \qquad t \geq s. \tag{65}$$

Please note that indeed $y^\diamond w(t,s) = y^\diamond U(t,s)q$ (compare (65) to (63)).

Of course we should now verify that the integrals in (61) and (65) do indeed define the same object. Writing the integral in (61) as $w_0 * v$ and the integral in (65) as $w * v_0$, equality follows from (60) written in the form

$$v = v_0 + r * v_0$$

and (64) written in the form

$$w = w_0 + w_0 * r$$

since

$$\begin{aligned} w_0 * v &= w_0 * (v_0 + r * v_0) = w_0 * v_0 + w_0 * r * v_0 \\ &= (w_0 + w_0 * r) * v_0 = w * v_0. \end{aligned}$$

Before we can prove Theorem 7.5 below we first need an auxiliary result.

Lemma 7.4 *The solution $v(t,s)y$ of (59) has the property*

$$v(t,s)y = v(t,r)U(r,s)y, \qquad t \geq r \geq s. \tag{66}$$

Proof From (59) it follows that

$$\begin{aligned} v(t,s)y = q^\diamond(t)S_0(t-r)S_0(r-s)y + \int_s^r k(t,\tau)v(\tau,s)y\,\mathrm{d}\tau \\ + \int_r^t k(t,\tau)v(\tau,s)y\,\mathrm{d}\sigma, \qquad t \geq r \geq s, \end{aligned}$$

and, by uniqueness, (66) follows provided the following identity holds

$$q^\diamond(t)S_0(t-r)S_0(r-s)y + \int_s^r k(t,\tau)v(\tau,s)y\,\mathrm{d}\tau = q^\diamond(t)S_0(t-r)U(r,s)y.$$

Recall from (47) that

$$k(t,s) = q^\diamond S_0(t-s)q = q^\diamond S_0(t-r)S_0(r-s)q, \qquad t \geq r \geq s,$$

so we conclude from (61) that this identity does indeed hold. □

Theorem 7.5 *Equation* (61) *in combination with* (60)*, or Eq.* (65) *in combination with* (64)*, defines a twin evolutionary system* $\{U(t,s)\}$ *corresponding to the abstract differential equation* (45)*.*

Proof Fix $t \geq s$. Since $(Y, Y^\diamond)$ is suitable for twin perturbation, we can use (61) and either Lemma 6.1 or Lemma 6.2 to deduce that $U(t,s)$ maps Y into Y. Similarly we can use (65) and the observation concerning (42) to deduce that $U(t,s)$ maps $Y^\diamond$ into $Y^\diamond$. So $U(t,s)$ is a twin operator.

Next we use Lemma 7.4 to derive the property

$$U(t,s) = U(t,r)U(r,s), \qquad t \geq r \geq s, \tag{67}$$

To verify (67), we start from (61) and use Lemma 7.4 to write

$$\begin{aligned} U(t,s)y &= S_0(t-r)\left[S_0(r-s)y + \int_s^r S_0(r-\tau)q \cdot v(\tau,s)y\,d\tau\right] \\ &\quad + \int_r^t S_0(t-\tau)q \cdot v(\tau,r)U(r,s)y\,d\tau \\ &= S_0(t-r)U(r,s)y + \int_r^t S_0(t-\tau)q \cdot v(\tau,r)U(r,s)y\,d\tau \\ &= U(t,r)U(r,s)y. \end{aligned}$$

Both the property $S(s,s) = I$ and the measurability, for all $y \in Y$, $y^\diamond \in Y^\diamond$, of $t \mapsto y^\diamond S(t)y$ follow from (61) and the corresponding properties of $\{S_0(t)\}$.

Finally, the exponential estimate for $y^\diamond S_0(t)y$ yields exponential estimates for both the kernel $k(t,s)$ and the forcing function $t \mapsto q^\diamond(t)S_0(t-s)y$, $t \geq s$, in the renewal equation (59). Therefore, using Proposition 7.3 we obtain an exponential estimate for the resolvent $r(t,s)$ and hence via (60) an exponential bound for $v(t,s)y$. Finally, using (61) we obtain an exponential bound for $y^\diamond U(t,s)y$ for $t \geq s$.

This completes the proof of Theorem 7.5. □

8 A Perturbation Approach Towards Periodic NFDE

We shall be dealing with linear periodic neutral functional differential equations of the following type:

$$\begin{cases} \dfrac{\mathrm{d}}{\mathrm{d}t}\left[x(t) - \displaystyle\int_0^h [\mathrm{d}\eta(\tau)]x(t-\tau)\right] = \displaystyle\int_0^h [\mathrm{d}_\tau\zeta(t,\tau)]x(t-\tau), \ t \geq s, \\ x(s+\theta) = \varphi(\theta), \qquad -h \leq \theta \leq 0. \end{cases} \tag{68}$$

Here d_τ denotes integration with respect to the τ variable and φ is a given function in $B([-h,0],\mathbb{R}^n)$. Throughout we assume that for each $t\in\mathbb{R}$ the functions η and $\zeta(t,\cdot)$ are $n\times n$ matrices of which the entries are real functions of bounded variation on $[0,h]$ and continuous from the left on $(0,h)$, and $\eta(0)=\zeta(t,0)=0$. Moreover, it is assumed that there is a nondecreasing bounded function $m\in L^1_{\mathrm{loc}}[-h,\infty)$ such that

$$\mathrm{Var}_{[-h,0]}\,\zeta(t,\cdot)\le m(t),\qquad t\ge 0.$$

Theorem 8.1 *Under the above conditions, Eq.* (68) *defines a well-posed dynamical system, that is, Eq.* (68) *has a unique solution x on $[0,\infty)$ such that $x_t\in B([-h,0],\mathbb{R}^n)$ for $t\ge 0$.*

The above theorem is an extension of Theorem 6.1.1 in Hale and Verduyn Lunel (1993) to the neutral case. In this section we shall derive Theorem 8.1 as a corollary of Theorem 7.5 using the perturbation approach developed in the previous section.

Consider as the unperturbed problem the special case $\zeta=0$ in (68). Let y denote the solution of the autonomous NFDE

$$\begin{cases}\dfrac{\mathrm{d}}{\mathrm{d}t}\left[y(t)-\displaystyle\int_0^h[\mathrm{d}\eta(\tau)]y(t-\tau)\right]=0, & t\ge 0,\\ y(\theta)=\varphi(\theta), & -h\le\theta\le 0.\end{cases}\tag{69}$$

From the theory developed in Sect. 2, it follows that the solution y of (69) satisfies the autonomous renewal equation

$$y(t)-\int_0^t \mathrm{d}\eta(\theta)y(t-\theta)=f_0(t),\quad t\ge s,\tag{70}$$

where

$$f_0(t):=\varphi(0)-\int_0^h \mathrm{d}\eta(\theta)\varphi(-\theta)+\int_t^h \mathrm{d}\eta(\theta)\varphi(t-\theta),\quad t\ge s.\tag{71}$$

The solution of (70) is given by

$$y(t)=f_0(t)+\int_0^t \mathrm{d}\rho_0(\theta)\,f_0(t-\theta),\quad t\ge 0,\tag{72}$$

where ρ_0 denotes the resolvent of η, i.e., it satisfies the resolvent equation

$$\rho_0=\eta*\rho_0+\eta,\tag{73}$$

see Theorem 2.2. Denote by $X(t)=I+\rho_0(t)$ the fundamental matrix solution of (69) so that we can write the solution y given by (72) as

$$y(t) = \int_0^t \mathrm{d}X(\tau) f_0(t-\tau), \quad t \geq 0. \tag{74}$$

It follows from Theorem 5.3 that the semigroup $\{S_0(t)\}$ defined by translation along the solution of (69), i.e.,

$$(S_0(t)\varphi)(\theta) = y(t+\theta;\varphi), \quad -h \leq \theta \leq 0, \quad t \geq 0,$$

is a twin semigroup.

Define for $i = 1, \ldots, n$ elements $q_i \in Y$ and functions $t \mapsto q_i^\diamond(t) \in Y^\diamond$ by

$$q_i(\theta) := \begin{cases} 0 & \text{for } -h \leq \theta < 0, \\ e_i & \text{for } \theta = 0, \end{cases} \tag{75}$$

where e_i is the i-th unit vector in $\mathbb{R}^n$ and the maps $t \mapsto q_i^\diamond(t)$ are defined by

$$\left(q_i^\diamond(t)\right)(\theta) := \zeta_i(t,\theta), \quad -h \leq \theta \leq 0, \quad t \geq 0, \tag{76}$$

where ζ_i is the i-th row of the $n \times n$-matrix-valued function ζ.

For the matrix kernel $k(t,s)$ introduced in (47) we have, using (75) and (76), the representation

$$\begin{aligned} k_{ij}(t,s) &= q_i^\diamond(t) S_0(t-s) q_j \\ &= \int_0^{t-s} \mathrm{d}_\tau \zeta_i(t,\tau) X_j(t-s-\theta), \quad t \geq s, \end{aligned} \tag{77}$$

where $X_j(t)$ is the j-th column of the fundamental matrix solution $X(t)$. Furthermore for $\varphi \in Y$, using (76),

$$\begin{aligned} q^\diamond(t) S_0(t-s)\varphi &= q^\diamond(t) y(t-s;\varphi) \\ &= \int_0^h \mathrm{d}\zeta(t,\theta) y(t-s-\theta;\varphi), \quad t \geq s. \end{aligned}$$

Let $v(t,s)\varphi$ be the solution to the renewal equation (59), i.e.,

$$v(t,s)\varphi = q^\diamond(t) S_0(t-s)\varphi + \int_s^t k(t,\tau) v(\tau,s)\varphi \, \mathrm{d}\tau, \quad t \geq s,$$

where the kernel $k(t,s)$ is given by (77). We claim that the solution $v(t,s)\varphi$ is given by

$$v(t,s)\varphi = \int_0^h \mathrm{d}\zeta(t,\theta) x(t-\theta;\varphi), \quad t \geq s, \tag{78}$$

where $x(\cdot;\varphi)$ is the solution of (68).

Define

$$\bar{v}(t,s)\varphi := \int_0^h \mathrm{d}\zeta(t,\theta)x(t-\theta;\varphi). \tag{79}$$

To prove that $v(t,s) = \bar{v}(t,s)$ it suffices to show that $\bar{v}(t,s)\varphi$ is also a solution of the renewal equation (59).

Let $x(\cdot;\varphi)$ be the solution of (68). Similar as before we can rewrite equation (68) to obtain that x is a solution of the renewal equation

$$x(t) - \int_0^t \mathrm{d}\eta(\theta)x(t-\theta) = \int_s^t \bar{v}(\sigma,s)\varphi\,\mathrm{d}\sigma + f_0(t), \tag{80}$$

where f_0 is given by (71). Note that the left hand side of (80) can be written as $x - \eta * x$. Using the resolvent equation (73) we obtain

$$\begin{aligned}(1+\rho_0)*(x-\eta*x) &= x - \eta*x + \rho_0*x - \rho_0*\eta*x\\ &= x - \eta*x + \rho_0*x - (\rho_0-\eta)*x\\ &= x.\end{aligned}$$

Thus if we take on both sides of (80) the convolution with the fundamental solution $X(t) = I + \rho_0(t)$ of (69) then

$$\begin{aligned}x(t) &= y(t;\varphi) + \int_s^t \mathrm{d}X(t-\tau)\int_s^\tau \bar{v}(\sigma,s)\varphi\,\mathrm{d}\sigma\\ &= y(t;\varphi) + \int_s^t X(t-\tau)\bar{v}(\tau,s)\varphi\,\mathrm{d}\tau,\end{aligned} \tag{81}$$

where y is given by (74). Finally take the convolution with $q^\diamond(t)$ on both sides of (81) to arrive at

$$\begin{aligned}\bar{v}(t,s)\varphi &= q^\diamond(t)y(t;\varphi) + \int_s^t q^\diamond(t)X(t-\tau)\bar{v}(\tau,s)\varphi\,\mathrm{d}\tau\\ &= q^\diamond(t)S_0(t-s)\varphi + \int_s^t \left[\int_0^h \mathrm{d}\zeta(t,\theta)X(t-\tau-\theta)\right]\bar{v}(\tau,s)\varphi\,\mathrm{d}\tau\\ &= q^\diamond(t)S_0(t-s)\varphi + \int_s^t k(t,\tau)\bar{v}(\tau,s)\varphi\,\mathrm{d}\tau,\end{aligned}$$

where we have used (77) and (78). Therefore $\bar{v}(t,s)\varphi$ given by (79) satisfies the identity

$$\bar{v}(t,s)\varphi = q^\diamond(t)S_0(t-s)\varphi + \int_s^t k(t,\tau)\bar{v}(\tau,s)\varphi\,\mathrm{d}\tau.$$

This shows that $\bar{v}(t,s)\varphi$ is a solution to the renewal equation (59) and completes the proof of the claim (78).

Finally apply to (61) the element of $Y^\diamond$ that corresponds to the Dirac measure in $-\theta \in [0, 1]$ to obtain

$$\begin{aligned}(U(t,s)\varphi)(\theta) &= y(t-s+\theta) + \int_s^t X(t-\tau+\theta)\cdot v(\tau,s)\varphi\,\mathrm{d}\tau \\ &= x(t-s+\theta;\varphi),\end{aligned}$$

where in the last identity we have used (81).

Thus we conclude that the the perturbation approach based on the abstract variation-of-constants formula developed in the previous section precisely yields the twin evolutionary system defined by translation along the solution of (68).

We summarize this result in a theorem.

Theorem 8.2 *Under the above conditions, translation along the solution of equation* (68) *defines a twin evolutionary system* $\{U(t,s)\}_{t\geq s}$ *given by* (61).

A Review of Functions of Bounded Variation

In this appendix $\mathcal{E}$ denotes the Borel σ-algebra on $[0,\infty)$. For $E \in \mathcal{E}$, we call a sequence of disjoint sets $\{E_j\}$ in $\mathcal{E}$ a *partition* of E if $\cup_{j=1}^\infty E_j = E$. A complex Borel measure is a map $\mu : \mathcal{E} \to \mathbb{C}$ such that $\mu(\emptyset) = 0$ and

$$\mu(E) = \sum_{j=1}^\infty \mu(E_j),$$

for every partition $\{E_j\}$ of E with the series converging absolutely. In the following we will often omit the adjective 'bounded'. The *total variation* measure $|\mu|$ of a complex Borel measure μ is given by

$$|\mu|(E) = \sup\left\{\sum_{j=0}^n |\mu(E_j)| \mid n\in\mathbb{N},\ \{E_j\} \text{ a partition of } E \text{ in } \mathcal{E}\right\}.$$

The vector space of complex Borel measures of bounded total variation is denoted by $M([0,\infty))$. Provided with the total variation norm given by

$$\|\mu\|_{TV} = |\mu|([0,\infty)), \tag{82}$$

the vector space $M([0,\infty))$ becomes a Banach space.

Let $f : [0,\infty) \to \mathbb{C}$ be a given function. For a partition $\{E_j\}$ of $[0,t]$ with $E_j = [t_{j-1}, t_j)$ and $0 = t_0 < t_1 < \cdots < t_n = t$ we define the function $T_f : [0,\infty) \to [0,\infty]$ by

$$T_f(t) := \sup \sum_{j=1}^{n} |f(t_j) - f(t_{j-1})|,$$

where the supremum is taken over $n \in \mathbb{N}$ and all such partitions of $[0, t]$. The extended real function T_f is called the *total variation function* of f. Note that if $0 \leq a < b$, then $T_f(b) - T_f(a) \geq 0$ and hence T_f is an increasing function.

If $\lim_{t\to\infty} T_f(t)$ is finite, then we call f a function of bounded variation. We denote the space of all such functions by BV. The space $NBV([0, \infty))$ of *normalized* functions of bounded variation is defined by

$$NBV([0, \infty)) := \{f \in BV \mid f \text{ is continuous from the right on } (0, \infty) \text{ and } f(0) = 0\}.$$

Provided with the norm

$$\|f\|_{TV} := \lim_{t\to\infty} T_f(t) \tag{83}$$

the space $NBV([0, \infty))$ becomes a Banach space. More generally, we define for $-\infty < a < b < \infty$, the vector space $NBV([a, b])$ to be the space of functions $f : [a, b] \to \mathbb{C}$ such that $f(a) = 0$, f is continuous from the right on the open interval (a, b), and whose total variation on $[a, b]$, given by $T_f(b) - T_f(a) = T_f(b)$, is finite. Provided with the norm $\|f\|_{TV} := T_f(b)$, the space $NBV([a, b])$ becomes a Banach space. We extend the domain of definition of a function of bounded variation by defining $f(t) = 0$ for $t < 0$ if $f \in NBV([0, \infty))$ and $f(t) = 0$ for $t < a$ and $f(t) = f(b)$ for $t > b$ if $f \in NBV([a, b])$.

The following fundamental result (see Folland 1999, Theorem 3.29) provides the correspondence between functions of bounded variation and complex Borel measures.

Theorem A.1 *Let μ be a complex Borel measure on $\mathbb{R}$. If $f : [0, \infty) \to \mathbb{C}$ is defined by $f(t) = \mu((0, t])$, then $f \in NBV([0, \infty))$. Conversely, if $f \in NBV([0, \infty))$ is given, then there is a unique complex Borel measure μ_f such that $\mu_f((0, t]) = f(t)$. Moreover $|\mu_f| = \mu_{T_f}$.*

Given a function $f \in NBV([a, b])$ with corresponding measure μ_f, we define the Lebesgue-Stieltjes integral $\int g \, \mathrm{d}f$ or $\int g(x) \, f(\mathrm{d}x)$ to be $\int g \, \mathrm{d}\mu_f$. Thus, a Lebesgue-Stieltjes integral is a special Lebesgue integral and the theory for the Lebesgue integral applies to the Lebesgue-Stieltjes integral. We embed $L^1([0, \infty))$ into $M([0, \infty))$ by identifying $f \in L^1([0, \infty))$ with the measure μ defined by

$$\mu(E) = \int_E f(x) \, \mathrm{d}x \quad \text{or, in short,} \quad \mu(\mathrm{d}x) = f(x) \, \mathrm{d}x.$$

In this section we collect some results about the convolution of a measure and a function and the convolution of two measures needed to study renewal equations.

For details we refer to Appendix A of Diekmann and Verduyn Lunel (2021) and for further results we refer to Folland (1999); Grippenberg et. al. (1990).

Let $B([0,\infty))$ denote the vector space of all bounded, Borel measurable functions $f : [0,\infty) \to \mathbb{R}$. Provided with the supremum norm (denoted by $\|\cdot\|$), the space $B([0,\infty))$ becomes a Banach space. With $B([a,b])$ we denote the Banach space of all bounded, Borel measurable functions $f : [a,b] \to \mathbb{R}$ provided with the supremum norm.

The half-line convolution $\mu * f$ of a measure $\mu \in M([0,\infty))$ and a Borel measurable function $f \in B([0,\infty))$ is the function

$$(\mu * f)(t) := \int_{[0,t]} \mu(\mathrm{d}s) f(t-s)$$

defined for those values of t for which $[0,t] \ni s \mapsto f(t-s)$ is $|\mu|$-integrable.

The following result can be found in Grippenberg et. al. (1990, Theorem 3.6.1(ii)).

Theorem A.2 *If $f \in B([0,\infty))$ and $\mu \in M([0,\infty))$, then the convolution of f and μ satisfies $\mu * f \in B([0,\infty))$ and*

$$\|\mu * f\| \leq \|\mu\|_{TV} \|f\|.$$

The half-line convolution $\mu * \nu$ of two measures $\mu, \nu \in M([0,\infty))$ is defined by the complex Borel measure that to each Borel set $E \in \mathcal{E}$ assigns the value

$$(\mu * \nu)(E) := \int_{[0,\infty)} \mu(\mathrm{d}s) \nu\left((E-s)_+\right), \tag{84}$$

where $(E-s)_+ := \{e - s \mid e \in E\} \cap [0,\infty)$ (cf. Grippenberg et. al. 1990, Definition 4.1.1)).

If χ_E is the characteristic function of the set E, then

$$\nu((E-s)_+) = \int_{[0,\infty)} \chi_E(\sigma + s) \nu(\mathrm{d}\sigma),$$

where $[0,\infty) \ni \sigma \mapsto \chi_E(\sigma + s)$ is the characteristic function of $(E-s)_+$. It follows from Theorem A.2 that $s \mapsto \nu(E-s)_+)$ belongs to $B([0,\infty))$ and hence the definition of the convolution of two measures $\mu * \nu : \mathcal{E} \to \mathbb{C}$ given in (84) makes sense. Furthermore, using Fubini's Theorem, we have the following useful identity

$$\begin{aligned}\mu * \nu(E) &= \int_{[0,\infty)} \mu(\mathrm{d}s)\nu\left((E-s)_+\right) \\ &= \int_{[0,\infty)} \int_{[0,\infty)} \chi_E(\sigma+s)\mu(\mathrm{d}s)\nu(\mathrm{d}\sigma) \\ &= \int_{[0,\infty)} \mu\left((E-s)_+\right)\nu(\mathrm{d}s).\end{aligned}$$

The following result can be found in Grippenberg et. al. (1990, Theorem 4.1.2(ii)).

Theorem A.3 *Let $\mu, \nu \in M([0,\infty))$ and let the convolution $\mu * \nu$ be defined by (84).*

(i) The convolution $\mu * \nu$ belongs to $M([0,\infty))$ and

$$\|\mu * \nu\|_{TV} \leq \|\mu\|_{TV}\|\nu\|_{TV}.$$

(ii) For any bounded Borel function $h \in B([0,\infty))$, we have

$$\int_{[0,\infty)} h(t)\,(\mu * \nu)\,(\mathrm{d}t) = \int_{[0,\infty)} \int_{[0,\infty)} h(t+s)\,\mu(\mathrm{d}t)\nu(\mathrm{d}s).$$

Using the one-to-one correspondence between complex Borel measures and functions of bounded variation, see Theorem A.1, we can combine the above results to obtain the following theorem (see Diekmann and Verduyn Lunel 2021, Theorem A.5).

Theorem A.4 *If $f \in NBV([0,\infty))$ and $\mu \in M([0,\infty))$, then the convolution of μ and f satisfies $\mu * f \in NBV([0,\infty))$ and*

$$\|\mu * f\|_{TV} \leq \|\mu\|_{TV}\|f\|_{TV}.$$

We also need the following result (see Diekmann and Verduyn Lunel 2021, Theorem A.6).

Theorem A.5 *Let $\mu \in M([0,\infty))$ and let $f : [0,\infty) \to \mathbb{C}$ be a bounded continuous function. If μ has no discrete part, then $\mu * f$ is a bounded continuous function and*

$$\|\mu * f\| \leq \|\mu\|_{TV}\|f\|.$$

References

Aliprantis, C. D., & Border, K. C. (2006). *Infinite Dimensional Analysis. A Hitchhiker's Guide*, 3rd Edn. Berlin: Springer.

Diekmann, O., van Gils, S. A., Verduyn Lunel, S. M., & Walther, H. O. (1995). *Delay Equations: Functional-, Complex-, and Nonlinear Analysis*. New York: Springer.

Diekmann, O., & Verduyn Lunel, S. M. (2021). Twin semigroups and delay equations. *Journal of Differential Equations,* **286**, 332–410.

Feller, W. (1953). Semigroups of transformations in general weak topologies. *Annals of Mathematics, 57,* 287–308.

Hale, J. K., & Verduyn Lunel, S. M. (1993). *Introduction to Functional Differential Equations*. New York: Springer.

Folland, G. B. (1999). *Real Analysis*, 2nd Edn. Wiley-Interscience.

Gripenberg, G., Londen, S.-O., & Staffans, O. (1990). *Volterra Integral and Functional Equations*. Cambridge: Cambridge University Press.

Kunze, M. (2009). Continuity and equicontinuity of semigroups on norming dual pairs. *Semigroup Forum, 79*, 540–560.

Kunze, M. (2011). A Pettis-type integral and applications to transition semigroups. *Czechoslovak Mathematical Journal, 61,* 437–459.

Rudin, W. (1991). *Functional Analysis* (2nd ed.). New York: McGraw-Hill.

Characteristic Matrix Functions and Periodic Delay Equations

Sjoerd Verduyn Lunel

Abstract In the first part of this chapter we recall the notion of a characteristic matrix function for classes of operators as introduced in Kaashoek and Verduyn Lunel (2023). The characteristic matrix function completely describes the spectral properties of the corresponding operator. In the second part we show that the period map or monodromy operator associated with a periodic neutral delay equation has a characteristic matrix function. We end this chapter with a number of illustrative examples of periodic neutral delay equations for which we can compute the characteristic matrix function explicitly.

1 Introduction

Let X denote a complex Banach space, and let $A : \mathcal{D}(A) \to X$ be a linear operator with domain $\mathcal{D}(A)$ a subspace of X. A complex number λ belongs to the resolvent set $\rho(A)$ of A if and only if the resolvent $(zI - A)^{-1}$ exists and is bounded, i.e.,

(i) $\lambda I - A$ is one-to-one;

(ii) $\text{Im}\, \lambda I - A = X$;

(iii) $(zI - A)^{-1}$ is bounded.

Note that for closed operators, (iii) is superfluous, since it is a direct consequence of the other assumptions by the closed graph theorem. The spectrum $\sigma(A)$ is by definition the complement of $\rho(A)$ in $\mathbb{C}$. The point spectrum $\sigma_p(A)$ is the set of those $\lambda \in \mathbb{C}$ for which $\lambda I - A$ is not one-to-one, i.e., $A\varphi = \lambda\varphi$ for some $\varphi \neq 0$. One then calls λ an eigenvalue and φ an eigenvector corresponding to λ.

The null space Ker $(\lambda I - A)$ is called the eigenspace and its dimension the *geometric multiplicity* of λ. The generalized eigenspace $\mathcal{M}_\lambda = \mathcal{M}_\lambda(A)$ is the smallest closed linear subspace that contains all Ker $(\lambda I - A)^j$ for $j = 1, 2, \ldots$ and its dimension $M(A; \lambda)$ is called the *algebraic multiplicity* of λ. If, in addition, λ is an isolated

S. Verduyn Lunel (✉)
Mathematical Institute, Utrecht University, Utrecht, The Netherlands
e-mail: S.M.VerduynLunel@uu.nl

D. Breda (ed.), *Controlling Delayed Dynamics*, CISM International Centre for Mechanical Sciences 604, https://doi.org/10.1007/978-3-031-01129-0_2

point in $\sigma(T)$ and $M(A;\lambda)$ is finite, then λ is called an *eigenvalue of finite type*. When $M(A;\lambda) = 1$ we say that λ is a *simple* eigenvalue. A class of operators for which the eigenvalues are of finite type is formed by the compact operators. Other classes appear later in this chapter.

If λ is an eigenvalue of finite type, the operator $T = A\mid_{\mathcal{M}_\lambda}$ is a bounded operator from a finite dimensional space into itself. So the situation is reduced to the finite dimensional case, which we shall, therefore, discuss first.

Let $T : \mathbb{C}^m \to \mathbb{C}^m$ be a bounded linear operator. The eigenvalues of T are precisely given by the roots of the characteristic polynomial

$$C(z) := \det(zI - T).$$

Over the scalar field $\mathbb{C}$ the characteristic polynomial can be factorized into a product of m linear factors

$$C(z) = \prod_{j=1}^{m}(z - \lambda_j),$$

where $\lambda_j \in \sigma(T)$. Define the multiplicity $m(\lambda_j, zI - T)$ of λ_j to be the number of times the factor $(z - \lambda_j)$ appears, or, in other words, the order of λ_j as a zero of the characteristic polynomial C. The characteristic polynomial is an annihilating polynomial of T, i.e., $C(T) = 0$. The *minimal polynomial* C_m of T is defined to be an annihilating polynomial of T that divides any other annihilating polynomial. Necessarily, C_m is of the form

$$C_m(z) = \prod_{j=1}^{l}(z - \lambda_j)^{k_j},$$

where $\sigma(T) = \{\lambda_1, \ldots, \lambda_l\}$, and for $j = 1, \ldots, l$, the number k_j is positive and called the *ascent* of λ_j.

Define

$$\mathcal{M}_j := \operatorname{Ker}(\lambda_j I - T)^{k_j}.$$

This is a T-invariant subspace, i.e., $T\mathcal{M}_j \subseteq \mathcal{M}_j$, and we can define the part of T in $\mathcal{M}_j$, i.e., $T_j = T\mid_{\mathcal{M}_j} : \mathcal{M}_j \to \mathcal{M}_j$. This yields $\mathbb{C}^m = \mathcal{M}_1 \oplus \cdots \oplus \mathcal{M}_l$. The operator T decomposes accordingly

$$T = \bigoplus_{j=1}^{l} T_j.$$

This decomposition is unique (up to the order of summands). The action of T can be broken down to the study of the action of T_j. To continue the decomposition one first studies the structure of the subspaces $\mathcal{M}_j$ more closely.

Let $\lambda \in \sigma(T)$. A vector x is called a generalized eigenvector of order r if

$$(\lambda I - T)^r x = 0 \qquad \text{while} \quad (\lambda I - T)^{r-1} x \neq 0.$$

Suppose x_{r-1} is a generalized eigenvector of order r; then there are vectors $(x_{r-2}, \ldots, x_1, x_0)$ for which $x_0 \neq 0$ and

$$\begin{aligned} Tx_0 &= \lambda x_0, \\ Tx_1 &= \lambda x_1 + x_0, \\ &\vdots \\ Tx_{r-1} &= \lambda x_{r-1} + x_{r-2} \end{aligned}$$

and hence $x_j \in \operatorname{Ker}(\lambda I - T)^{j+1}$. Such a sequence is called a *Jordan chain*. Obviously, the length of the Jordan chain is less than or equal to k_λ, the ascent of λ, and a Jordan chain consists of linearly independent elements. As a consequence of this construction, the matrix representation of T_j with respect to the basis $(x_{r-2}, \ldots, x_1, x_0)$ is given by a Jordan block of order r corresponding to λ. See Diekmann et al. (1995, Chap. IV) and the next section for more information about Jordan chains for analytic matrix-valued functions.

Next consider the case that T is an operator defined on an infinite dimensional complex Banach space X, then, in general, T no longer has a matrix representation and we cannot define the characteristic polynomial of T by $\det(zI - T)$. Nevertheless there is a large class of operators for which one has a characteristic function whose zeros determine the spectrum of the corresponding operator. For example, this is true for the infinitestimal generator of solution semigroup corresponding to autonomous delay equations, see Diekmann et al. (1995, Chap. I). As it turned out the abstract notion of a characteristic matrix function, introduced in Kaashoek and Verduyn Lunel (1992) for unbounded operators, can be used to explain this connection. As a consequence it was possible to extend the finite dimensional theory to specific classes of unbounded operators. To briefly explain the connection between unbounded operators $A : \mathcal{D}(A) \to X$ and analytic matrix functions, as developed in Kaashoek and Verduyn Lunel (1992), let $\Delta : \Omega \to \mathcal{L}(\mathbb{C}^n)$ be an analytic $n \times n$ matrix function with $\Omega \subset \mathbb{C}$.

We call Δ a characteristic matrix function for A on Ω if there exist analytic operator functions E and F, $E : \Omega \to \mathcal{L}(\mathbb{C}^n \oplus X)$ and $F : \Omega \to \mathcal{L}(\mathbb{C}^n \oplus X)$, whose values are invertible operators, such that

$$\begin{bmatrix} \Delta(z) & 0 \\ 0 & I \end{bmatrix} = F(z) \begin{bmatrix} I_{\mathbb{C}^n} & 0 \\ 0 & zI - A \end{bmatrix} E(z), \qquad z \in \Omega.$$

The characteristic matrix function Δ completely determines the spectral properties of the unbounded operator A. See Kaashoek and Verduyn Lunel (1992) and Diekmann et al. (1995, Chap. IV) for details.

In this chapter we will follow recent work, Kaashoek and Verduyn Lunel (2023), and extend the notion of a characteristic matrix function to classes of bounded

operators, and show that the period map of a periodic neutral delay equation has a characteristic matrix function.

We end the introduction with an outline of this chapter. In Sect. 2 we introduce and discuss the basic properties of Jordan chains. In Sect. 3 we introduce the notion of a characteristic matrix function for a class of bounded operators, and prove that the characteristic matrix function completely determines the spectral properties of the associated bounded operator. In Sect. 4 we show that the period map associated with a periodic neutral delay equation has a characteristic matrix function. In Sect. 5 we show that in case the period is equal to the delay, then we can compute the characteristic matrix function rather explicitly. Finally, in Sect. 6, we consider a class of periodic delay equations for which the period is two times the delay. We construct new examples for which we can compute the characteristic matrix function explicitly. In particular, we construct an example for which the period map has a finite spectrum. In the literature such examples are only known in case the period is equal to the delay, and were unknown in case the period is two times the delay.

2 Equivalence and Jordan Chains

Let X, Y, X', Y' be complex Banach spaces, and suppose that $L : \mathcal{U} \to \mathcal{L}(X, Y)$ and $M : \mathcal{U} \to \mathcal{L}(X', Y')$ are operator-valued functions, analytic on the open subset $\mathcal{U} \subset \mathbb{C}$. The two operator-valued functions L and M are called *equivalent* on $\mathcal{U}$ (see Sect. 2.4 in Bart et al. (1979)) if there exist analytic operator-valued functions $E : \mathcal{U} \to \mathcal{L}(X', X)$ and $F : \mathcal{U} \to \mathcal{L}(Y, Y')$, whose values are invertible operators, such that,

$$M(z) = F(z)L(z)E(z), \quad z \in \mathcal{U}. \tag{1}$$

Let $L : \mathcal{U} \to \mathcal{L}(X, Y)$ be an analytic operator-valued function. A point $\lambda_0 \in \mathcal{U}$ is called a *root* of L if there exists a vector $x_0 \in X$, $x_0 \neq 0$, such that,

$$L(\lambda_0)x_0 = 0.$$

An ordered set $(x_0, x_1, \ldots, x_{k-1})$ of vectors in X is called a *Jordan chain* for L at λ_0 if $x_0 \neq 0$ and

$$L(z)[x_0 + (z - \lambda_0)x_1 + \cdots + (z - \lambda_0)^{k-1}x_{k-1}] = O((z - \lambda_0)^k). \tag{2}$$

The number k is called the *length* of the chain and the maximal length of the chain starting with x_0 is called the *rank* of x_0. The analytic function

$$\sum_{l=0}^{k-1}(z - \lambda_0)^l x_l$$

in (2) is called a *root function* of L corresponding to λ_0.

Proposition 2.1 *If two analytic operator functions L and M are equivalent on $\mathcal{U}$, then there is a one-to-one correspondence between their Jordan chains.*

Proof The equivalence relation (1) is symmetric, and thus it suffices to show that Jordan chains for L yield Jordan chains for M. If $(x_0, \ldots, x_{k-1})$ is a Jordan chain for L at λ_0, then

$$\begin{aligned} &E(z)^{-1}(x_0 + (z-\lambda_0)x_1 + \cdots + (z-\lambda_0)^{k-1}x_{k-1}) \\ &\quad = y_0 + (z-\lambda_0)y_1 + \cdots + (z-\lambda_0)^{k-1}y_{k-1} + \text{h.o.t.} \end{aligned}$$

and $(y_0, \ldots, y_{k-1})$ is a Jordan chain for M at λ_0. Here h.o.t. stands for the higher order terms. Furthermore, the equivalence yields that the null spaces Ker $L(\lambda_0)$ and Ker $M(\lambda_0)$ are isomorphic and this proves the proposition. □

Let $\Omega \subset \mathbb{C}$ and $\Delta : \Omega \to \mathcal{L}(\mathbb{C}^n)$ denote an entire $n \times n$ matrix function. If the determinant of Δ is not identically zero, then we define $m(\lambda, \Delta)$ to be the order of λ as a zero of $\det \Delta$ and $k(\lambda, \Delta)$ is the order of λ as pole of the matrix function $\Delta(\cdot)^{-1}$.

Let λ_0 be an isolated root of Δ, then the Jordan chains for Δ at λ_0 have finite length, and we can organize the chains as follows. Choose an eigenvector, say $x_{1,0}$, with maximal rank, say r_1. Next, choose a Jordan chain

$$(x_{1,0}, \ldots, x_{1,r_1-1})$$

of length r_1 and let N_1 be the complement in Ker $\Delta(\lambda_0)$ of the subspace spanned by $x_{1,0}$. In N_1 we choose an eigenvector $x_{2,0}$ of maximal rank, say r_2, and let

$$(x_{2,0}, \ldots, x_{2,r_2-1})$$

be a corresponding Jordan chain of length r_2. We continue as follows, let N_2 be the complement in N_1 of the subspace spanned by $x_{2,0}$ and replace N_1 by N_2 in the above described procedure.

In this way, we obtain a basis $\{x_{1,0}, \ldots, x_{p,0}\}$ of Ker $\Delta(\lambda_0)$ and a corresponding *canonical system* of Jordan chains

$$x_{1,0}, \ldots, x_{1,r_1-1}, x_{2,0}, \ldots, x_{2,r_2-1}, x_{p,0}, \ldots, x_{p,r_p-1}$$

for Δ at λ_0.

It is easy to see that the rank of any eigenvector x_0 corresponding to the root λ_0 is always equal to one of the r_j for $1 \le j \le p$. Thus, the integers $r_1, \ldots, r_p$ do not depend on the particular choices made in the procedure described above and are called the *zero-multiplicities* of Δ at λ_0. Their sum $r_1 + \cdots + r_p$ is called the *algebraic multiplicity* of Δ at λ_0 and will be denoted by $M(\Delta(\lambda_0))$.

To illustrate this procedure, recall the case that $\Delta = zI - A$ is a linear matrix function with A an $n \times n$ matrix as discussed in the Introduction. The Jordan chain $(x_0, \ldots, x_{k-1})$ for Δ at λ_0 satisfies

$$(A - \lambda_0)x_0 = 0, \quad (A - \lambda_0)x_1 = x_0, \ \ldots, \ (A - \lambda_0)x_{k-1} = x_{k-2},$$

and hence

$$\{(x_{i,0}, \ldots, x_{i,r_i-1}) \mid i = 1, 2, \ldots, p\}$$

is a canonical basis of eigenvectors and generalized eigenvectors for A at λ_0.

Next we recall the connection between the Jordan chains and the local Smith form for an analytic $n \times n$ matrix function $\Delta : \Omega \to \mathcal{L}(\mathbb{C}^n)$ with $\det \Delta \not\equiv 0$. Let $\lambda_0 \in \mathbb{C}$. The *local Smith form* states there exist a neighborhood $\mathcal{U}$ of λ_0 and analytic matrix functions E and F on $\mathcal{U}$ whose values are invertibe operators such that

$$\Delta(z) = F(z)D(z)E(z), \quad z \in \mathcal{U}, \tag{3}$$

where

$$D(z) = \operatorname{diag}\left[(z - \lambda_0)^{\nu_1}, \ldots, (z - \lambda_0)^{\nu_n}\right], \qquad z \in \mathcal{U}. \tag{4}$$

The integers $\{\nu_1, \ldots, \nu_n\}$ are uniquely determined by Δ and the diagonal matrix D in (4) is called the local Smith form for Δ at λ_0. See Gohberg et al. (1993, Theorems 1.2 and 1.3) for a proof of (3)–(4), or see Diekmann et al. (1995, Chap. IV).

The Jordan chains for the local Smith form D are easily determined, and it follows that the set of zero multiplicities is given by $\{\nu_1, \ldots, \nu_n\}$. Hence, the equivalence (3) and Proposition 2.1 show that the algebraic multiplicity of Δ at λ is given by

$$M(\Delta(\lambda)) = \sum_{l=1}^{n} \nu_l.$$

On the other hand the equivalence (3) yields

$$\det \Delta(z) = \det F(z)(z - \lambda_0)^{\sum_{l=1}^{n} \nu_l} \det E(z)$$

with $\det E(\lambda_0) \neq 0$ and $\det F(\lambda_0) \neq 0$. So, $m(\lambda_0, \Delta)$ the multiplicity of λ_0 as zero of $\det \Delta$ equals

$$m(\lambda_0, \Delta) = \sum_{l=1}^{n} \nu_l$$

as well. This shows that the algebraic multiplicity of Δ at λ equals the multiplicity of λ as zero of $\det \Delta$, i.e., $m(\lambda, \Delta) = M(\Delta(\lambda))$.

The following application of the local Smith form will be used in the proof of Theorem 3.1 below. The identity in (5) below can be viewed as a matrix-valued

version of the Cauchy multiplicity theorem and is due to Gohberg and Sigal, see Kaashoek and Verduyn Lunel (2023, Theorem 5.1.2).

Theorem 2.2 *Let $\Delta : \Omega \to \mathcal{L}(\mathbb{C}^n)$ be an analytic $n \times n$ matrix function on $\Omega \subset \mathbb{C}$ with* $\det \Delta \not\equiv 0$. *If $\lambda_0 \in \Omega$ is an isolated zero of* $\det \Delta$, *then*

$$m(\lambda_0, \Delta) = \operatorname{Tr}\Big(\frac{1}{2\pi \mathrm{i}} \int_{\Gamma_{\lambda_0}} \Delta(z)^{-1} \frac{\mathrm{d}}{\mathrm{d}z} \Delta(z)\, \mathrm{d}z\Big), \tag{5}$$

where Γ_{λ_0} is a small circle surrounding λ_0 and no other zeros of $\det \Delta$. *Here* $\operatorname{Tr}(A)$ *denotes the trace of an $n \times n$ matrix A.*

3 Introduction to the Theory of Characteristic Matrix Functions

Let $T : X \to X$ be a bounded operator, and let $\Delta : \Omega \to \mathcal{L}(\mathbb{C}^n)$ be an analytic $n \times n$ matrix function with $\Omega \subset \mathbb{C}$. We call Δ a *characteristic matrix function* for T on Ω if there exist analytic operator functions E and F, $E : \Omega \to \mathcal{L}(\mathbb{C}^n \oplus X)$ and $F : \Omega \to \mathcal{L}(\mathbb{C}^n \oplus X)$, whose values are invertible operators, such that

$$\begin{bmatrix} \Delta(z) & 0 \\ 0 & I \end{bmatrix} = F(z) \begin{bmatrix} I_{\mathbb{C}^n} & 0 \\ 0 & I - zT \end{bmatrix} E(z), \qquad z \in \Omega. \tag{6}$$

The operator function appearing in the left hand side of (6) is called the *X-extension* of Δ.

We call Δ *nondegenerate* if $\det \Delta(z)$ does not vanish identically. In this case, $I - zT$ is invertible for $z \in \Omega$ if and only if $\det \Delta(z)$ is non-zero, and in that case

$$E(z) \begin{bmatrix} \Delta(z)^{-1} & 0 \\ 0 & I \end{bmatrix} F(z) = \begin{bmatrix} I_{\mathbb{C}^n} & 0 \\ 0 & (I - zT)^{-1} \end{bmatrix}, \quad \det \Delta(z) \neq 0. \tag{7}$$

Note that if $\Omega = \mathbb{C}$, then Δ is always nondegenerate (take $z = 0$ in (6)). The operator functions F and E appearing in (6) can also be described by 2×2 matrix functions with entries that are analytic operator functions on Ω. For instance, for F we have

$$F(z) \begin{pmatrix} c \\ x \end{pmatrix} = \begin{bmatrix} F_{11}(z) & F_{12}(z) \\ F_{21}(z) & F_{22}(z) \end{bmatrix} \begin{pmatrix} c \\ x \end{pmatrix} = \begin{pmatrix} F_{11}(z)c + F_{12}(z)x \\ F_{21}(z)c + F_{22}(z)x \end{pmatrix}.$$

Using these partitioning of $E(z)$ and $F(z)$, the equivalence relation (7) yields a useful representation for the resolvent operator $(I - zT)^{-1}$ of T on Ω, namely

$$(I - zT)^{-1} = E_{21}(z)\Delta(z)^{-1}F_{12}(z) + E_{22}(z)F_{22}(z), \qquad z \in \Omega. \tag{8}$$

If $Q(z) := E(z)^{-1}$ and $R(z) := F(z)^{-1}$, then it follows from (8) that

$$Q_{12}(z)(I - zT)^{-1} = \Delta(z)^{-1}F_{12}(z), \qquad z \in \Omega,$$
$$(I - zT)^{-1}R_{21}(z) = E_{21}(z)\Delta(z)^{-1}, \qquad z \in \Omega.$$

Since the zeros of $\det \Delta(z)$ do not have an accumulation point in Ω, we see from (8) that the non-zero part of the spectrum of T inside Ω consists of eigenvalues of finite type only.

In this section we introduce an important class of operators T that have a characteristic matrix function Δ, i.e., there exist functions E and F such that (6) holds. Before we do this, we present a spectral resolution theorem that justifies the terminology introduced above.

The next theorem is an adapted version of Theorem 2.1 of Kaashoek and Verduyn Lunel (1992) for bounded operators and justifies the terminology introduced above. See Kaashoek and Verduyn Lunel (2023, Theorem 5.2.6) for a complete proof.

Theorem 3.1 *Let T be a bounded linear operator on a Banach space X, and let Δ be a nondegenerate characteristic matrix function for T on Ω. Then*

(i) *the set $\Omega \cap \sigma(T) \setminus \{0\}$ consists of eigenvalues of finite type and*

$$\Omega \cap \sigma(T) \setminus \{0\} = \{\lambda^{-1} \in \Omega \mid \det \Delta(\lambda) = 0\};$$

(ii) *for $\lambda_0^{-1} \in \Omega \cap \sigma(T) \setminus \{0\}$, the partial multiplicities of λ_0^{-1} as an eigenvalue of T are equal to the zero-multiplicities of Δ at λ_0;*

(iii) *for $\lambda_0^{-1} \in \Omega \cap \sigma(T) \setminus \{0\}$, the algebraic multiplicity $m(T, \lambda_0^{-1})$ of λ_0^{-1} as an eigenvalue of T equals $m(\lambda_0, \Delta)$, the order of λ_0 as a zero of* det Δ*;*

(iv) *for $\lambda_0^{-1} \in \Omega \cap \sigma(T) \setminus \{0\}$, the ascent $k(T, \lambda_0^{-1})$ of λ_0^{-1} equals $k(\lambda_0, \Delta)$, the order of λ_0 as a pole of Δ^{-1} and* dim Ker $(I - \lambda_0 T)^k = m$ *where $k = k(\lambda_0, \Delta)$ and $m = m(\lambda_0, \Delta)$.*

Next we introduce a class of operators T that have a characteristic matrix function Δ in the sense of (6). Consider an operator $T : X \to X$ that is a finite rank perturbation of a given operator, i.e., admits a representation of the form

$$T := W + R, \tag{9}$$

where $W : X \to X$ is a bounded operator and $R : X \to X$ is an operator of finite rank. Define $\Omega \subset \mathbb{C}$ such that for every $x \in X$

$$z \mapsto (I - zW)^{-1}x \text{ is analytic on } \Omega. \tag{10}$$

A specific example of such an operator W is given by a the operator of integration, i.e., for $x \in C([0, 1]; \mathbb{C}^n)$ define

$$(Wx)(t) := \int_0^t x(s)\,\mathrm{d}s, \quad 0 \le t \le 1. \tag{11}$$

The resolvent of the operator W defined in (11) can be computed explicitly and is given by

$$\left((I - zW)^{-1}x\right)(t) = x(t) + z\int_0^t e^{z(t-s)}x(s)\,\mathrm{d}s, \quad 0 \le t \le 1. \tag{12}$$

This shows that (10) is defined for all $z \in \mathbb{C}$ and we can take $\Omega = \mathbb{C}$ in this specific case.

The fact that R has finite rank allows us to factor R as $R = BC$, where $B : \mathbb{C}^n \to X$ and $C : X \to \mathbb{C}^n$, with $n \ge \operatorname{rank} R$. If n is equal to the rank of R we call $R = BC$ a *minimal rank factorization*.

To a pair W and R with factorization $R = BC$ we associate the $n \times n$ matrix function

$$\Delta(z) := I_{\mathbb{C}^n} - zC(I - zW)^{-1}B, \quad z \in \Omega. \tag{13}$$

The next theorem tells us that Δ defined by (13) satisfies (6) with the operator T defined by (9) on Ω. Note that in case W is given by (11) we have $\Omega = \mathbb{C}$. Hence the operator W is *quasi-nilpotent*, i.e., for every $x \in X$ we have that $z \mapsto (I - zW)^{-1}x$ is an entire function, and hence in this case Δ defined by (13) is an entire matrix function as well.

The following theorem is an adapted version of Kaashoek and Verduyn Lunel (2023, Theorem 6.1.1) and the proof is given for the convenience of the reader.

Theorem 3.2 *Let $W : X \to X$ be a bounded operator. Define $\Omega \subset \mathbb{C}$ such that (10) holds. The $n \times n$ entire matrix function Δ defined by (13) is a characteristic matrix function for the operator T defined by (9) on Ω. In particular, the identity (6) is satisfied with Δ given by (13) and where the analytic operator-valued functions $E(z) : \mathbb{C}^n \oplus X \to \mathbb{C}^n \oplus X$ and $F(z) : \mathbb{C}^n \oplus X \to \mathbb{C}^n \oplus X$ are given by*

$$E(z) := \begin{bmatrix} \Delta(z) & C(I - zW)^{-1} \\ -z(I - zW)^{-1}B & (I - zW)^{-1} \end{bmatrix}, \quad z \in \Omega,$$

$$F(z) := \begin{bmatrix} \Delta(z) & -C(I - zW)^{-1} \\ zB & I_X \end{bmatrix}, \quad z \in \Omega.$$

The inverses $E(z)^{-1} : \mathbb{C}^n \oplus X \to \mathbb{C}^n \oplus X$ and $F(z)^{-1} : \mathbb{C}^n \oplus X \to \mathbb{C}^n \oplus X$ are the operator-valued functions given by

$$E(z)^{-1} = \begin{bmatrix} I_{\mathbb{C}^n} & -C \\ zB & I - zT \end{bmatrix}, \qquad z \in \Omega,$$
$$F(z)^{-1} = \begin{bmatrix} I_{\mathbb{C}^n} & C(I - zW)^{-1} \\ -zB & I - zBC(I - zW)^{-1} \end{bmatrix}, \qquad z \in \Omega.$$

Proof Take $z \in \Omega$ fixed and apply Theorem 4.7 in Bart et al. (2008) with

$$M = \begin{bmatrix} M_{11} & M_{12} \\ M_{21} & M_{22} \end{bmatrix} := \begin{bmatrix} I - zW & zB \\ C & I_{\mathbb{C}^n} \end{bmatrix} : X \oplus \mathbb{C}^n \to X \oplus \mathbb{C}^n.$$

Note that both M_{11} and M_{22} are invertible operators. Hence the Schur complements of M_{11} and M_{22} in M are well defined and are given by

$$\begin{aligned} \Lambda_1 &:= M_{22} - M_{21}M_{11}^{-1}M_{12} \\ &= I_{\mathbb{C}^n} - zC(I - zW)^{-1}B = \Delta(z); \end{aligned} \tag{14}$$
$$\begin{aligned} \Lambda_2 &:= M_{11} - M_{12}M_{22}^{-1}M_{21} \\ &= I - zW - zBC = I - zT. \end{aligned} \tag{15}$$

Put

$$\begin{aligned} E_1(z) &:= \begin{bmatrix} -M_{21}M_{11}^{-1} & \Lambda_1 \\ M_{11}^{-1} & M_{11}^{-1}M_{21} \end{bmatrix} \\ &= \begin{bmatrix} -C(I - zW)^{-1} & \Delta(z) \\ (I - zW)^{-1} & z(I - zW)^{-1}B \end{bmatrix}, \\ F_1(z) &:= \begin{bmatrix} -M_{11}^{-1}M_{12} & I \\ I_{\mathbb{C}^n} - M_{22}^{-1}M_{21}M_{11}^{-1}M_{12} & M_{22}^{-1}M_{21} \end{bmatrix} \\ &= \begin{bmatrix} -z(I - zW)^{-1}B & I \\ \Delta(z) & C \end{bmatrix}. \end{aligned}$$

Then, using the identities (14) and (15), Theorem 4.7 in Bart et al. (2008) tells us that

$$\begin{bmatrix} \Delta(z) & 0 \\ 0 & I_X \end{bmatrix} = E_1(z) \begin{bmatrix} I - zT & 0 \\ 0 & I_{\mathbb{C}^n} \end{bmatrix} F_1(z). \tag{16}$$

Note that the identify (16) can be verified directly using the definitions.

Moreover, the operators $E_1(z)$ and $F_1(z)$ are invertible and

$$E_1(z)^{-1} = \begin{bmatrix} -M_{12}M_{22}^{-1} & \Lambda_2 \\ M_{22}^{-1} & M_{22}^{-1}M_{21} \end{bmatrix}$$
$$= \begin{bmatrix} -zB & I - zT \\ I_{\mathbb{C}^n} & C \end{bmatrix}, \tag{17}$$
$$F_1(z)^{-1} = \begin{bmatrix} -M_{22}^{-1}M_{21} & I_{\mathbb{C}^n} \\ I - M_{11}^{-1}M_{12}M_{22}^{-1}M_{21} & M_{11}^{-1}M_{12} \end{bmatrix}$$
$$= \begin{bmatrix} -C & I_{\mathbb{C}^n} \\ I - z(I - zW)^{-1}BC & z(I - zW)^{-1}B \end{bmatrix}. \tag{18}$$

Finally put

$$E(z) := \begin{bmatrix} 0 & I_{\mathbb{C}^n} \\ I & 0 \end{bmatrix} F_1(z) \begin{bmatrix} I_{\mathbb{C}^n} & 0 \\ 0 & (I - zW)^{-1} \end{bmatrix},$$
$$F(z) := \begin{bmatrix} I_{\mathbb{C}^n} & 0 \\ 0 & I - zW \end{bmatrix} E_1(z) \begin{bmatrix} 0 & I \\ I_{\mathbb{C}^n} & 0 \end{bmatrix}.$$

Then the identities for $E(z)$ and $F(z)$ given in the statement of the theorem hold. For example, the identity (16) yields (6):

$$F(z) \begin{bmatrix} I_{\mathbb{C}^n} & 0 \\ 0 & I - zT \end{bmatrix} E(z) =$$
$$= \begin{bmatrix} I_{\mathbb{C}^n} & 0 \\ 0 & I - zW \end{bmatrix} E_1(z) \begin{bmatrix} 0 & I \\ I_{\mathbb{C}^n} & 0 \end{bmatrix} \begin{bmatrix} I_{\mathbb{C}^n} & 0 \\ 0 & I - zT \end{bmatrix} E(z)$$
$$= \begin{bmatrix} I_{\mathbb{C}^n} & 0 \\ 0 & I - zW \end{bmatrix} E_1(z) \begin{bmatrix} I - zT & 0 \\ 0 & I_{\mathbb{C}^n} \end{bmatrix} F_1(z) \begin{bmatrix} I_{\mathbb{C}^n} & 0 \\ 0 & (I - zW)^{-1} \end{bmatrix}$$
$$= \begin{bmatrix} I_{\mathbb{C}^n} & 0 \\ 0 & I - zW \end{bmatrix} \begin{bmatrix} \Delta(z) & 0 \\ 0 & I_X \end{bmatrix} \begin{bmatrix} I_{\mathbb{C}^n} & 0 \\ 0 & (I - zW)^{-1} \end{bmatrix}$$
$$= \begin{bmatrix} \Delta(z) & 0 \\ 0 & I_X \end{bmatrix}.$$

Furthermore, using (17) and (18), we see that $E(z)$ and $F(z)$ are invertible with inverses as given in the statement of the theorem. □

As a corollary to Theorem 3.2 we have the following identities involving the resolvent operator $(I - zT)^{-1}$ that will be useful in the future.

$$(I - zT)^{-1} = z(I - zW)^{-1}B\Delta(z)^{-1}C(I - zW)^{-1} + (I - zW)^{-1},$$
$$\Delta(z)C(I - zT)^{-1} = C(I - zW)^{-1},$$
$$(I - zT)^{-1}B\Delta(z) = (I - zW)^{-1}B.$$

As a first illustration of Theorem 3.2 we compute the characteristic matrix function of a rank one perturbation of the operator of integration on $C[0, 1]$, i.e., the operator

W is given by (11). More precisely, take $X = C[0, 1]$ and define $T : X \to X$ by

$$(Tx)(t) := \int_0^t x(s)\,\mathrm{d}s + \int_0^1 x(s)\,\mathrm{d}\eta(s), \quad x \in C[0, 1], \quad 0 \le t \le 1. \tag{19}$$

Here η is a function of bounded variation (see Appendix A of Verduyn Lunel (2023) for more information about functions of bounded variation). The operator T can be written as $T = W + R$, where W and R are operators on X defined by

$$(Wx)(t) := \int_0^t x(s)\,\mathrm{d}s, \quad (Rx)(t) := \int_0^1 x(s)\,\mathrm{d}\eta(s), \quad 0 \le t \le 1.$$

From (12) it follows that we can take $\Omega = \mathbb{C}$. It follows that T given by (19) is a finite rank perturbation of a quasi-nilpotent operator. Thus we can apply Theorem 3.2 with $\Omega = \mathbb{C}$, and $C : X \to \mathbb{C}$ and $B : \mathbb{C} \to X$ given by

$$Cx := \int_0^1 x(s)\,\mathrm{d}\eta(s), \quad x \in X, \qquad (Bc)(t) := c, \quad 0 \le t \le 1. \tag{20}$$

Then $R = BC$ is a minimal rank factorization. It follows from (12) and (20) that

$$\left((I - zW)^{-1}Bc\right)(t) = c + z\int_0^t e^{z\tau}c\,\mathrm{d}\tau = e^{zt}c, \qquad 0 \le t \le 1.$$

Using this together with (13) and (20) we derive that the corresponding characteristic matrix function Δ is the scalar function given by

$$\begin{aligned}\Delta(z) &:= I - zC(I - zW)^{-1}B \\ &= 1 - z\int_0^1 e^{zs}\,\mathrm{d}\eta(s).\end{aligned}$$

In particular, the characteristic matrix function Δ of the operator T defined by

$$(Tx)(t) := \int_0^t x(s)\,\mathrm{d}s + x(1), \quad x \in C[0, 1], \tag{21}$$

is given by

$$\Delta(z) = 1 - ze^z. \tag{22}$$

Thus an application of Theorem 3.1 now yields that Δ given by (22) completely characterizes the nonzero spectrum of the operator T given by (21). In fact, the nonzero spectrum of T consists of simple eigenvalues only, and e^μ is an eigenvalue of T if and only if

$$\mu - e^{-\mu} = 0. \tag{23}$$

The asymptotic behavior of the roots of Equation (23) is well-known, see Diekmann et al. (1995, Sect. XI.2), and this information can be used to derive detailed estimates on the nonzero spectrum of the operator T given by (21).

4 The Period Map of a Neutral Periodic Delay Equation

In this section we consider linear periodic functional differential equations of the following type:

$$\begin{cases} \dfrac{\mathrm{d}}{\mathrm{d}t}\left[x(t) - \displaystyle\int_0^h \mathrm{d}\eta(\tau)x(t-\tau)\right] = \displaystyle\int_0^h \mathrm{d}_\tau\zeta(t,\tau)x(t-\tau), \quad t \geq s, \\ x(s+\theta) = \varphi(\theta), \qquad -h \leq \theta \leq 0. \end{cases} \tag{24}$$

Here d_τ denotes integration with respect to the τ variable and φ is a given function in $B([-h,0],\mathbb{C}^n)$, the complex Banach space of bounded Borel measurable functions provided with the supremum norm. Throughout we assume that for each $t \in \mathbb{R}$ the functions η and $\zeta(t,\cdot)$ are $n \times n$ matrices of which the entries are real functions of bounded variation on $[0,h]$ and continuous from the left on $(0,h)$, and $\eta(0) = \zeta(t,0) = 0$. See Appendix A of Verduyn Lunel (2023) for more information about functions of bounded variation. Finally, we assume periodicity of the kernel ζ, i.e., there is a non negative real number ω such that

$$\zeta(t+\omega,\cdot) = \zeta(t,\cdot), \qquad t \geq 0.$$

In Sect. 8 of Verduyn Lunel (2023) we have proved the following theorem regarding system (24).

Theorem 4.1 *Under the above conditions, equation* (24) *has a unique solution* $x = x(\cdot;s;\varphi)$ *on* $[s,\infty)$. *Furthermore the family of solution operators* $U(t,s)$, $t \geq s$, *defined by translation along the solution of* (24) *and given by*

$$\big(U(t,s)\varphi\big)(\theta) := x(t+\theta;s,\varphi), \quad -h \leq \theta \leq 0, \quad \varphi \in B\left([-h,0];\mathbb{C}^n\right),$$

is a twin evolutionary system of operators and has the following properties:

(i) $U(s,s)$ *is the identity operator for all* $s \in \mathbb{R}$,
(ii) $U(t,s)U(s,\sigma) = U(t,\sigma)$ *for all* $t \geq s \geq \sigma$.

The period map T associated with (24) is defined by $T := U(\omega,0)$. Using the results from Sect. 8 of Verduyn Lunel (2023), we have an explicit representation of the period map in terms of the fundamental matrix solution $X(t)$.

The main purpose of this section is to show that the period map T admits a characteristic matrix function Δ in the sense of (6). Before we prove this, we briefly

recall the importance of the spectral properties of the period map in the study of the qualitative behaviour of the solutions of (24). See Hale and Verduyn Lunel (1993, Chap. 11) for the general qualitative theory for periodic functional differential equations.

The first result relates all period maps $U(\omega + s, s)$, $s \in \mathbb{R}$, to the operator T. For a proof of the next theorem and more information about the period maps we refer to Diekmann et al. (1995, Sect. XIV.3).

Theorem 4.2 *Assume that $\lambda \neq 0$ is an isolated eigenvalue of finite type of the operator $U(t + \omega, t)$ for each $t \geq 0$. Let $\mathcal{M}_{\lambda,t}$ denote the generalized eigenspace at λ of the operator $U(t + \omega, t)$. If $t \geq s$ then*

(i) $\lambda \in \sigma(U(t + \omega, t))$ *if and only if* $\lambda \in \sigma(U(s + \omega, s))$;
(ii) *if $\lambda \in \sigma(U(t + \omega, t))$, then $U(t, s)$ maps $\mathcal{M}_{\lambda,s}$ in a one-to-one way onto $\mathcal{M}_{\lambda,t}$.*

We continue with some more notation and terminology. If μ belongs to the nonzero point spectrum of T, then μ is called a *characteristic multiplier* of (24), and λ for which $\mu = \exp(\lambda\omega)$ (unique up to multiples of $2\pi i$) is called a *characteristic exponent* of (24).

Let $\mu \neq 0$ be an eigenvalue of finite type and let m_μ denote the algebraic multiplicity of μ. Assume that $\varphi_1, \ldots, \varphi_{m_\mu}$ in $B([-h, 0]; \mathbb{C}^n)$ is a basis of eigenvectors and generalized eigenvectors of T at μ, and let $\mathcal{M}_\mu = \operatorname{span}\{\varphi_1, \ldots, \varphi_{m_\mu}\}$ be the corresponding generalized eigenspace. Furthermore, let Φ_0 be the m_μ-row vector defined by $\Phi_0 := [\varphi_1, \ldots, \varphi_{m_\mu}]$, viewed as a linear operator from $\mathbb{C}^{m_\mu}$ into $B([-h, 0]; \mathbb{C}^n)$. Since $\mathcal{M}_\mu$ is invariant under T, there exists a $m_\mu \times m_\mu$ matrix L with scalar entries such that

$$T\Phi_0 = \Phi_0 L,$$

and the only eigenvalue of L is $\mu \neq 0$. But then, there is an $m_\mu \times m_\mu$ matrix $\mathbb{B}$ with scalar entries such that $L = \exp(\omega\mathbb{B})$, and thus $L \exp(-\omega\mathbb{B})$ is the $m_\mu \times m_\mu$ identity matrix. Moreover, the unique eigenvalue λ of $\mathbb{B}$ satisfies the identity $\mu = \exp(\omega\lambda)$. From Theorem 4.2 it follows that if

$$\Phi(t) = \left[U(t, 0)\varphi_1 \cdots U(t, 0)\varphi_{m_\mu}\right], \qquad t \geq 0,$$

then

$$(T\Phi_0)(t) = \Phi(t)L, \quad t \geq 0.$$

Next, let $\mathbb{P}(t)$, $t \geq 0$, be the block m_μ-row vector given by

$$\mathbb{P}(t) = U(t, 0)\Phi_0 \exp(-t\mathbb{B}) = \Phi(t) \exp(-t\mathbb{B}), \quad t \geq 0.$$

Thus $\mathbb{P}(t)$ has size $1 \times m_\mu$ and its entries are in $B([-h, 0]; \mathbb{C}^n)$.

Lemma 4.3 *The function $\mathbb{P}(t)$, $t \geq 0$, is periodic with period ω. Furthermore, we have*

$$U(t, 0)\Phi_0 = \mathbb{P}(t) \exp(t\mathbb{B}), \quad t \geq 0. \tag{25}$$

Proof From item (ii) in Theorem 4.1 we know that $U(t+\omega,0) = U(t,0)T$ for $t \geq 0$. Using the latter identity we see that

$$\begin{aligned}\mathbb{P}(t+\omega) &= U(t+\omega,0)\Phi_0 e^{-(t+\omega)\mathbb{B}} \\ &= U(t,0)T\Phi_0 e^{-\omega\mathbb{B}}e^{-t\mathbb{B}} = U(t,0)\Phi_0 L e^{-\omega\mathbb{B}}e^{-t\mathbb{B}} \\ &= U(t,0)\Phi_0 e^{-t\mathbb{B}} = \mathbb{P}(t), \quad t \geq 0. \end{aligned} \tag{26}$$

Thus $\mathbb{P}(t)$ is periodic with period ω, and the final equality in (26) yields (25). □

The solution of (24) with initial value $\varphi \in \mathcal{M}_\mu$ is of *Floquet type*, i.e., of the form

$$x(t;\varphi) = p(t)\exp(t\mathbb{B})c, \tag{27}$$

where $c \in \mathbb{C}^{m_\mu}$ is such that $\varphi = \Phi_0 c$, the matrix $\mathbb{B}$ has size $m_\mu \times m_\mu$ and only one eigenvalue at λ with $\mu = e^{\lambda\omega}$, and $p(t) = p(t+\omega)$ is a periodic function. Indeed, from Lemma 4.3 it follows that

$$x(t;\varphi) = (U(t,0)\Phi_0 c)(0) = (\mathbb{P}(t))(0)\exp(t\mathbb{B})c.$$

Put $p(t) := (\mathbb{P}(t))(0)$, then $p(t) = p(t+\omega)$ and this shows (27). Furthermore, since λ is the only eigenvalue of $\mathbb{B}$, it follows from the Jordan decomposition of $\mathbb{B}$ that we can write

$$e^{t\mathbb{B}}c = q(t)e^{\lambda t},$$

where q is a polynomial of degree at most m_μ, and hence

$$x(t;\varphi) = p(t)q(t)\exp(\lambda t).$$

Next we prove that the period map T admits a characteristic matrix function Δ in the sense of (6). In order to apply Theorem 3.2 we have to show that T satisfies (9). In the case that $\eta = 0$ and $\omega = h$ in equation (24), we have a general result with $\Omega = \mathbb{C}$. This is the contents of the next theorem.

Theorem 4.4 *Consider equation* (24) *with* $\eta = 0$ *and period* $\omega = h$ *and let* T *on* $B([-h,0];\mathbb{C}^n)$ *be the corresponding period map. The period map* T *satisfies* (9)*, where* W *is quasi-nilpotent and* R *is an operator of finite rank. The operators* W *and* R *are operators on* $B([-h,0];\mathbb{C}^n)$ *given by*

$$(W\varphi)(\theta) := x(h+\theta,0;\varphi) - X(s+h+\theta,0)\varphi(0), \quad -h \leq \theta \leq 0, \tag{28}$$

$$(R\varphi)(\theta) := X(h+\theta,0)\varphi(0), \quad -h \leq \theta \leq 0, \tag{29}$$

where $x(t,s;\varphi)$ *denotes the solution of* (24) *with initial data* φ*, and* $X(t,s)$ *denotes the fundamental matrix solution of* (24)*, i.e., the matrix solution with initial data*

$$X_0(\theta) = \begin{cases} I & \text{for } \theta = 0, \\ 0 & \text{for } -h \leq \theta < 0. \end{cases}$$

Proof To prove that W is quasi-nilpotent, we have to show that given ψ the equation

$$\varphi - zW\varphi = \psi. \tag{30}$$

has a unique solution φ for each $z \in \mathbb{C}$.

We will use a contraction mapping principle in a weighted norm to prove that (30) has a unique solution for each $z \in \mathbb{C}$. Define for $\gamma \in \mathbb{R}$ the weighted norm $\| \cdot \|_\gamma$ on $B[-h, 0]$ by

$$\|\varphi\|_\gamma := \max_{-h \leq \theta \leq 0} \|e^{\gamma(\theta - h)}\varphi(\theta)\|. \tag{31}$$

From (30) and the definition of W given in (28) it follows that

$$\psi = \varphi - z\left(x(h + \cdot, 0; \varphi) - X(h + \cdot, 0)\varphi(0)\right). \tag{32}$$

Hence $\varphi(-h) = \psi(-h)$ and φ satisfies the differential equation

$$\dot{\psi} = \dot{\varphi} - z\left(\dot{x}(h + \cdot, 0; \varphi) - \dot{X}(h + \cdot, 0)\varphi(0)\right).$$

Using (24) with $\eta = 0$ and recalling that $\zeta(h + \cdot) = \zeta(\cdot)$ we obtain

$$\begin{aligned} \dot{\psi}(\sigma) = \dot{\varphi}(\sigma) &- z\int_0^h \mathrm{d}\zeta(\sigma, \theta)x(h + \sigma - \theta, 0; \varphi) \\ &- z\int_0^{h+\sigma} \mathrm{d}\zeta(\sigma, \theta)X(h + \sigma - \theta, 0)\varphi(0). \end{aligned}$$

Using (32) we can rewrite this equation as follows:

$$\begin{aligned} \dot{\psi}(\sigma) = \dot{\varphi}(\sigma) &- \int_0^{h+\sigma} \mathrm{d}\zeta(\sigma, \theta)\left(\varphi(\sigma - \theta) - \psi(\sigma - \theta)\right) \\ &- z\int_{h+\sigma}^h \mathrm{d}\zeta(\sigma, \theta)\varphi(h + \sigma - \theta). \end{aligned} \tag{33}$$

To show that given ψ the equation (33) has a unique solution φ for each $z \in \mathbb{C}$, we first write the convolution part for φ (and similarly for ψ) in (33) which is given by

$$\dot{\varphi}(\sigma) - \int_0^{h+\sigma} \mathrm{d}\zeta(\sigma, \theta)\varphi(\sigma - \theta),$$

as follows:

$$\dot{\varphi}(\sigma) - \zeta(\sigma, h+\sigma)\varphi(-1) - \int_{-h}^{\sigma} \zeta(\sigma, \sigma-\tau)\dot{\varphi}(\tau)\,\mathrm{d}\tau.$$

Put $k(\sigma,\tau) := \zeta(\sigma, \sigma-\tau)$ and rewrite equation (33) now as follows:

$$\dot{\varphi}(\sigma) - \int_{-h}^{\sigma} k(\sigma,\tau)\dot{\varphi}(\tau)\,\mathrm{d}\tau = F(\sigma;\psi), \tag{34}$$

where

$$F(z,\sigma;\varphi,\psi) := \dot{\psi}(\sigma) - \int_{h}^{\sigma} k(\sigma,\tau)\psi(\tau)\,\mathrm{d}\tau + z\int_{h+\sigma}^{h} \mathrm{d}\zeta(\sigma,\theta)\varphi(h+\sigma-\theta).$$

Solving equation (34) yields

$$\dot{\varphi}(\sigma) = F(z,\sigma;\varphi,\psi) + \int_{s}^{\sigma} r(\sigma,\tau)F(z,\tau;\varphi,\psi)\,\mathrm{d}\tau, \tag{35}$$

where $r(t,s)$ denotes the resolvent of $k(t,s)$, see Theorem 7.2 of Verduyn Lunel (2023). Integration of equation (35) yields

$$\varphi(\sigma) = G(z,\sigma;\varphi,\psi), \tag{36}$$

where

$$\begin{aligned} G(z,\sigma;\varphi,\psi) := \psi(-1) &+ \int_{-1}^{\sigma} F(z,\xi;\varphi,\psi)\,\mathrm{d}\xi \\ &+ \int_{-1}^{\sigma}\int_{s}^{\xi} r(\xi,\tau)F(z,\tau;\varphi,\psi)\,\mathrm{d}\tau\,\mathrm{d}\xi. \end{aligned}$$

Using the exponential estimate for the resolvent $r(t,s)$, see Proposition 7.3 of Verduyn Lunel (2023) and the weighted norm (31), we can estimate

$$\|G(z,\sigma;\varphi_1,\psi) - G(z,\sigma;\varphi_2,\psi)\|_\gamma \le \frac{C}{|\gamma|}\|\varphi_1-\varphi_2\|_\gamma,$$

where $C>0$ and $\gamma>0$ is sufficiently large. So the map $\varphi \mapsto G(z,\sigma;\varphi,\psi)$ is a contraction for $\gamma>0$ sufficiently large. This shows that equation (36) has a unique solution. Therefore equation (33) has a unique solution and this completes the proof that (30) has a unique solution for every $z\in\mathbb{C}$ and $\psi\in B([-h,0],\mathbb{C}^n)$. □

In case $\eta\neq 0$, it turns out that $\Omega\subset\mathbb{C}$ with $\Omega\neq\mathbb{C}$. See the examples in Sect. 5. By choosing Ω appropriately, we can extend the proof of Theorem 4.4 to include the case that $\eta\neq 0$ and $\omega = h$ using a time-dependent version of Theorem 2.1 of Verduyn Lunel (2023) (instead of using Theorem 7.2 of Verduyn Lunel (2023) as we did in the proof of Theorem 4.4). The theory of Grippenberg et al. (1990) can be

used to prove a time-dependent version of Theorem 2.1 of Verduyn Lunel (2023). To make the present work self-contained we have decided to focus on the examples in Sect. 5 and not to aim for a general abstract result.

It is also possible to extend the proof of Theorem 4.4 to include the case that the period ω is an integer multiple of the delay. The construction however becomes more involved, see Kaashoek and Verduyn Lunel (2023, Chap. 11). Again in the present work we have decided to focus on the examples in Sect. 6 and not to aim for a general abstract result.

As an application of Theorem 3.2 we can, in case $\eta = 0$ and $\omega = h$, compute the characteristic matrix function Δ of the period map T associated with (24) explicitly in terms of the fundamental matrix solution.

Corollary 4.5 *Consider equation* (24) *with* $\eta = 0$ *and period* $\omega = h$ *and let* T *on* $B[-h, 0]$ *be the corresponding period map. The characteristic matrix function* $\Delta(z)$ *of the period map* T *is given by*

$$\Delta(z) = I - zC(I - zW)^{-1}B,$$

where the operator W *is given by* (28) *and the operators* $B : \mathbb{C}^n \to B[-h, 0]$ *and* $C : B[-h, 0]\mathbb{C}^n$ *are defined by*

$$(Bu)(\theta) := X(h + \theta, 0)u, \quad -h \le \theta \le 0, \quad \text{and} \quad C\varphi := \varphi(0). \tag{37}$$

Proof From the definitions of B and C in (37) we see that, using (29),

$$(BC\varphi)(\theta) = (B\varphi(0)(\theta) = X(h + \theta, 0)\varphi(0) = (R\varphi)(\theta), \quad -h \le \theta \le 0.$$

Thus $R = BC$, and Theorem 3.2 yields that $\Delta(z)$ is a characteristic matrix function for T. □

As a first illustration of the results of this section we consider the delay equation

$$\dot{x}(t) = b(t)x(t - 1),$$

where $b(t) = b(t + 1)$. The period map T on $B([-1, 0]; \mathbb{C}^n)$ is given by

$$(T\varphi)(\theta) = \varphi(0) + \int_{-1}^{\theta} b(\sigma)\varphi(\sigma)\, \mathrm{d}\sigma, \qquad -1 \le \theta \le 0.$$

The operator W on $B([-1, 0]; \mathbb{C}^n)$, defined in (28), is given by

$$(W\varphi)(\theta) = \int_{-1}^{\theta} b(\sigma)\varphi(\sigma)\, \mathrm{d}\sigma, \qquad -1 \le \theta \le 0. \tag{38}$$

and the resolvent of W defined by (38) is given by

$$\left((I - zW)^{-1}\varphi\right)(\theta) = \varphi(\theta) + z\int_{-1}^{\theta} G(\theta - s; z)b(s)\varphi(s)\,\mathrm{d}s,\ -1 \le \theta \le 0.$$

Here $G(t; z)$ is the fundamental solution of the homogeneous ordinary differential equation

$$\dot{x}(t) = zb(t)x(t), \qquad t \ge -1,$$

normalized to 1 at $t = -1$. Therefore $G(t; z)$ is given by

$$G(t; z) = \exp\left(\int_{-1}^{t} zb(s)\,\mathrm{d}s\right), \quad t \ge -1.$$

Moreover, $B : \mathbb{C}^n \to B([-1, 0]; \mathbb{C}^n)$ and $C : B([-1, 0]; \mathbb{C}^n) \to \mathbb{C}^n$ are defined by

$$(Bu)(\theta) := u, \quad -1 \le \theta \le 0, \quad \text{and} \quad C\varphi := \varphi(0).$$

Furthermore

$$\left((I - zW)^{-1}B\right)(\theta) = G(\theta; z), \quad -1 \le \theta \le 0,$$

and hence

$$\begin{aligned}\Delta(z) &:= 1 - zC_0(I - zW)^{-1}B \\ &= 1 - zG(0; z) = 1 - ze^{zm(b)},\end{aligned}$$

where

$$m(b) := \int_{-1}^{0} b(s)\,\mathrm{d}s.$$

An application of Theorem 3.1 now yields that all nonzero eigenvalues of T are algebraically simple eigenvalues. Furthermore, if b is such that $m(b) = 0$, then the nonzero spectrum of T consists of the single point $\{1\}$ only.

5 Scalar Periodic Delay Equations of Period One

Consider the scalar periodic delay equation

$$\begin{cases} \dfrac{\mathrm{d}}{\mathrm{d}t}\left[x(t) - cx(t-1)\right] = b(t)x(t-1), & t \ge s, \\ x(\theta) = \varphi(\theta), & -1 \le \theta \le 0. \end{cases} \tag{39}$$

Here b is a complex-valued continuous periodic function of period one defined on the full real line, $c \in \mathbb{C}$, and $\varphi \in B([-1,0];\mathbb{C}^n)$.

The period map T on $B([-1,0];\mathbb{C}^n)$ defined by the periodic delay equation (39) is given by

$$(T\varphi)(\theta) = \varphi(0) - c\varphi(-1) + c\varphi(\theta) + \int_{-1}^{\theta} b(s)\varphi(s)\,\mathrm{d}s, \quad -1 \le \theta \le 0.$$

The operator T consists of two parts: a finite rank operator R defined by

$$R\varphi := \varphi(0), \qquad \varphi \in B\left([-1,0];\mathbb{C}^n\right), \tag{40}$$

and an operator W on $B([-1,0];\mathbb{C}^n)$ defined by

$$(W\varphi)(\theta) := c\varphi(\theta) - c\varphi(-1) + \int_{-1}^{\theta} b(s)\varphi(s)\,\mathrm{d}s, \quad -1 \le \theta \le 0. \tag{41}$$

The minimal rank factorization of R is given by $R = BC$ with B and C, for each $u \in \mathbb{C}$ and $\varphi \in B([-1,0];\mathbb{C}^n)$, defined by

$$(Bu)(\theta) := u, \quad -1 \le \theta \le 0, \quad \text{and} \quad (C\varphi) := \varphi(0).$$

The resolvent $(I - zW)^{-1}$ of the operator W defined by (41) is analytic for $z \in \Omega$ with $\Omega = \{z \in \mathbb{C} \mid 1 - cz \neq 0\}$ and explicitly given by

$$\left((I - zW)^{-1}\varphi\right)(\theta) = \varphi(\theta) + z\int_{-1}^{\theta} G(\theta - s; z)b(s)\varphi(s)\,\mathrm{d}s, \quad -1 \le \theta \le 0.$$

Here $G(t;z)$ is the fundamental solution of the ordinary differential equation

$$(1 - cz)\dot{x}(t) = zb(t)x(t), \qquad t \ge -1,$$

normalized to 1 at $t = -1$. So $G(t;z)$ is given by

$$G(t;z) = \frac{1}{1-cz}\exp\left(\int_{-1}^{t}\frac{z}{1-cz}b(\sigma)\,\mathrm{d}\sigma\right), \quad t \ge -1.$$

Moreover,

$$\left((I - zW)^{-1}B\right)(\theta) = (1 - cz)G(\theta; z), \quad -1 \le \theta \le 0,$$

and hence according to Theorem 3.2, the characteristic function Δ defined by (13) is given by

$$\begin{aligned}\Delta(z) &:= 1 - zC(I - zW)^{-1}B \\ &= 1 - z(1 - cz)G(0; z).\end{aligned}$$

Summarizing we have proved the following result.

Theorem 5.1 *Let W and R be the operators given by (41) and (40), respectively. Then $T = W + R$ is the period map associated with (39), and T has a characteristic matrix function on $\Omega = \{z \in \mathbb{C} \mid 1 - cz \neq 0\}$, namely the function $\Delta(z)$ given by*

$$\Delta(z) = 1 - z \exp\left(\frac{z}{1 - cz} \int_{-1}^{0} b(s)\, \mathrm{d}s\right)$$

Furthermore $\lambda = 1/c$ belongs to the essential spectrum of T.

Note that in the retarded case ($c = 0$), the set Ω defined in Theorem 5.1 equals $\mathbb{C}$, and the operator W is a quasi-nilpotent operator. See also the example at the end of the previous section.

6 Scalar Periodic Delay Equations (Two Periodic)

In this section we consider the special class of scalar periodic delay equations

$$\begin{cases} \dot{x}(t) = b(t)x(t-1), & t \geq s, \\ x(t) = \varphi(t), & -1 \leq t \leq 0, \end{cases}$$

where b is of the form

$$b(t) := \begin{cases} b_0(t) & 0 \leq t \bmod 2 < 1 \\ \alpha b_0(t) & 1 \leq t \bmod 2 < 2, \end{cases} \tag{42}$$

where $\alpha \in \mathbb{R} \setminus \{0\}$ and b_0 is a complex-valued continuous periodic function of period 1. So b is a complex-valued continuous periodic function of period two for $\alpha \neq 1$. The situation is similar to the one periodic case considered in the previous section, but the computations of the period map become more involved. The special class of equations considered in this section present a rich class of new examples.

The period two map $T : B([-1, 0]; \mathbb{C}^n) \to B([-1, 0]; \mathbb{C}^n)$ for the periodic delay equation $\dot{x}(t) = b(t)x(t-1)$ with b given by (42) becomes

$$
\begin{aligned}
(T\varphi)(\theta) &= \varphi(0) + \int_{-1}^{0} b_0(s)\varphi(s)\,\mathrm{d}s \\
&\qquad + \alpha \int_{-1}^{\theta} b_0(s)\left(\varphi(0) + \int_{-1}^{s} b_0(\sigma)\varphi(\sigma)\,\mathrm{d}\sigma\right)\mathrm{d}s \\
&= \varphi(0) + \int_{-1}^{0} b_0(s)\varphi(s)\,\mathrm{d}s + \alpha\varphi(0)\int_{-1}^{\theta} b_0(s)\,\mathrm{d}s \\
&\qquad + \alpha \int_{-1}^{\theta} b_0(s)\int_{-1}^{s} b_0(\sigma)\varphi(\sigma)\,\mathrm{d}\sigma\,\mathrm{d}s. \qquad (43)
\end{aligned}
$$

From the representation (43) for T we conclude that T satisfies (9), where W and R are operators acting on $C[-1,0]$ given by

$$
\begin{aligned}
(W\varphi)(\theta) &:= \alpha \int_{-1}^{\theta} b_0(s)\int_{-1}^{s} b_0(\sigma)\varphi(\sigma)\,\mathrm{d}\sigma\,\mathrm{d}s, \qquad (44)\\
(R\varphi)(\theta) &:= \varphi(0) + \int_{-1}^{0} b_0(s)\varphi(s)\,\mathrm{d}s + \alpha\varphi(0)\int_{-1}^{\theta} b_0(s)\,\mathrm{d}s.
\end{aligned}
$$

Furthermore, the rank two operator R admits a minimal rank factorization $R = BC$, where

$$
B : \mathbb{C}^2 \to B\left([-1,0];\mathbb{C}^n\right), \qquad B\begin{pmatrix} c_1 \\ c_2 \end{pmatrix}(\theta) := c_1 + c_2\int_{-1}^{\theta} b_0(s)\,ds, \qquad (45)
$$

$$
C : B\left([-1,0];\mathbb{C}^n\right) \to \mathbb{C}^2, \qquad C\varphi := \begin{pmatrix} \varphi(0) + \int_{-1}^{0} b_0(s)\varphi(s)\,ds \\ \alpha\varphi(0) \end{pmatrix}. \qquad (46)
$$

Lemma 6.1 *The operator W defined by (44) is a quasi-nilpotent operator, and the resolvent of W is given by*

$$
\left((I - zW)^{-1}\varphi\right)(\theta) = \varphi(\theta) + \int_{-1}^{\theta} \frac{\partial g}{\partial s}(\alpha, z; \theta, s)\varphi(s)\,ds, \quad -1 \le \theta \le 0,
$$

where

$$
\begin{aligned}
g(\alpha, z; \theta, s) &:= \frac{1}{2}\exp\left(\sqrt{\alpha z}\int_{s}^{\theta} b_0(\sigma)\,\mathrm{d}\sigma\right) + \\
&\qquad + \frac{1}{2}\exp\left(-\sqrt{\alpha z}\int_{s}^{\theta} b_0(\sigma)\,\mathrm{d}\sigma\right), \quad -1 \le s \le \theta \le 0. \qquad (47)
\end{aligned}
$$

Proof Put $\psi = (I - zW)^{-1}\varphi$, then we need to solve the equation

$$
\psi - zW\psi = \varphi \qquad (48)
$$

with φ given and ψ as the unknown. By differentiating (48) we arrive at the following initial value problem

$$\psi'(\theta) - \alpha z b_0(\theta) \int_{-1}^{\theta} b_0(\sigma)\psi(\sigma)\,\mathrm{d}\sigma = \varphi'(\theta), \quad -1 \le \theta \le 0 \tag{49}$$

with initial condition $\psi(-1) = \varphi(-1)$. The general solution of the homogeneous part of the differential integral equation in (49) is given by

$$\psi(\theta) = g(\alpha, z; \theta, -1)\varphi(-1), \qquad -1 \le \theta \le 0,$$

where $g(\alpha, z; \theta, -1)$ is given by (47) with $s = -1$. A particular solution of the differential equation in (49) with $\psi(-1) = 0$ is given by

$$\psi_p(\theta) = \int_{-1}^{\theta} g(\alpha, z; \theta, s)\varphi'(s)\,\mathrm{d}s,$$

where $g(\alpha, z; \theta, s)$ is given by (47) and we have used that $g(\alpha, z; \theta, \theta) = 1$ and $g'(\alpha, z; s, s) = 0$.

This shows that the solution of the initial value problem (49) with initial condition $\psi(-1) = \varphi(-1)$ is given by

$$\begin{aligned}\psi(\theta) &= g(\alpha, z; \theta, -1)\varphi(-1) + \int_{-1}^{\theta} g(\alpha, z; \theta, s)\varphi'(s)\,ds \\ &= \varphi(\theta) + \int_{-1}^{\theta} \frac{\partial g}{\partial s}(\alpha, z; \theta, s)\varphi(s)\,ds,\end{aligned} \tag{50}$$

where we have used integration by parts in the last identity. This completes the proof of the lemma. □

An application of Theorem 3.2 now yields that the period map T given by (43) has a characteristic matrix function Δ given by (13). In the next theorem we will compute Δ explicitly.

Theorem 6.2 *The characteristic matrix function* $\Delta(z) : \mathbb{C}^2 \to \mathbb{C}^2$ *associated with the operator* T *defined by* (43) *is given by*

$$\Delta(z) = \begin{bmatrix} 1 - z\gamma_1(z) - \frac{1}{\alpha}\gamma_2(z) & -\frac{1}{\alpha}\left(\gamma_1(z) + \gamma_2(z) - 1\right) \\ -z\alpha\gamma_1(z) & 1 - \gamma_2(z) \end{bmatrix}, \tag{51}$$

where

$$\gamma_1(z) := \frac{1}{2}\left(\exp\left(\sqrt{\alpha z}m(b_0)\right) + \exp\left(-\sqrt{\alpha z}m(b_0)\right)\right), \qquad -1 \le \theta \le 0.$$

$$\gamma_2(z) := \frac{\sqrt{\alpha z}}{2}\left(\exp\left(\sqrt{\alpha z}m(b_0)\right) - \exp\left(-\sqrt{\alpha z}m(b_0)\right)\right), \qquad -1 \le \theta \le 0,$$

where $m(b_0) := \int_{-1}^{0} b_0(\sigma)\,\mathrm{d}\sigma$. *Moreover,*

$$\det \Delta(z) = 1 - \left(\frac{1+\alpha}{\alpha}\right)\gamma_2(z) - z.$$

Proof Observe using (45) and (50) that

$$\left((I - zW)^{-1}B\begin{pmatrix} c_1 \\ c_2 \end{pmatrix}\right)(\theta) = g(\alpha, z; \theta, -1)c_1 + c_2\int_{-1}^{\theta} b_0(s)g(\alpha, z; \theta, s)\,\mathrm{d}s. \tag{52}$$

Using (47) we can rewrite the last term in (52) as follows

$$\int_{-1}^{\theta} b_0(s)g(\alpha, z; \theta, s)\,\mathrm{d}s = \frac{1}{2}x + \frac{1}{2}y, \tag{53}$$

where

$$x := \int_{-1}^{\theta} b_0(s)\exp\left(\sqrt{\alpha z}\int_{s}^{\theta} b_0(\sigma)\,\mathrm{d}\sigma\right)\mathrm{d}s,$$
$$y := \int_{-1}^{\theta} b_0(s)\exp\left(-\sqrt{\alpha z}\int_{s}^{\theta} b_0(\sigma)\,\mathrm{d}\sigma\right)\mathrm{d}s.$$

Now put $k(s) := \int_s^{\theta} b_0(\sigma)\,\mathrm{d}\sigma$, $c := \sqrt{\alpha z}$, and $\varphi(s) := ck(s)$. Note that both $k(\theta)$ and $\varphi(\theta)$ are zero. Furthermore, we have

$$\begin{aligned} x &= -\int_{-1}^{\theta} k'(s)\exp\left(ck(s)\right)\mathrm{d}s = -\frac{1}{c}\int_{-1}^{\theta}\varphi'(s)\exp\left(\varphi(s)\right)\mathrm{d}s \\ &= -\frac{1}{c}\exp(\varphi(s))\Big|_{-1}^{\theta} = -\frac{1}{c} + \frac{1}{c}\exp\left(ck(-1)\right). \end{aligned}$$

Similarly

$$\begin{aligned} y &= \int_{-1}^{\theta} k'(s)\exp\big(-ck(s)\big)\,\mathrm{d}s = \frac{1}{c}\int_{-1}^{\theta} -\varphi'(s)\exp\big(-\varphi(s)\big)\,\mathrm{d}s \\ &= \frac{1}{c}\exp(-\varphi(s))\Big|_{-1}^{\theta} = \frac{1}{c} - \frac{1}{c}\big(v - ck(-1)\big). \end{aligned}$$

Summarizing and using (53) we have

$$\int_{-1}^{\theta} b_0(s)g(\alpha, z; \theta, s)\,\mathrm{d}s = \frac{1}{2c}\exp\left(ck(-1)\right) - \frac{1}{2c}\exp\left(-ck(-1)\right)$$
$$= \frac{1}{2\sqrt{\alpha z}}\left(\exp\left(\sqrt{\alpha z}\int_{-1}^{\theta} b_0(\sigma)\,\mathrm{d}\sigma\right)\right.$$
$$\left. - \exp\left(-\sqrt{\alpha z}\int_{-1}^{\theta} b_0(\sigma)\,\mathrm{d}\sigma\right)\right).$$

In particular,

$$\int_{-1}^{0} b_0(s)g(\alpha, z; 0, s)\,\mathrm{d}s = \frac{1}{\alpha z}\gamma_2(z).$$

Since $g(\alpha, z; 0, -1) = \gamma_1(z)$ this shows that

$$\left((I - zW)^{-1}B\begin{pmatrix} c_1 \\ c_2 \end{pmatrix}\right)(0) = \gamma_1(z)c_1 + \frac{1}{\alpha z}\gamma_2(z)c_2.$$

Similarly using (47) with $\theta = t$ and $s = -1$ we obtain

$$\int_{-1}^{0} b_0(t)g(\alpha, z; t, -1)\,dt = \frac{1}{2}\tilde{x} + \frac{1}{2}\tilde{y},$$

where

$$\tilde{x} := \int_{-1}^{0} b_0(t)\exp\left(\sqrt{\alpha z}\int_{-1}^{t} b_0(\sigma)\,\mathrm{d}\sigma\right)\mathrm{d}t,$$
$$\tilde{y} := \int_{-1}^{0} b_0(t)\exp\left(-\sqrt{\alpha z}\int_{-1}^{t} b_0(\sigma)\,\mathrm{d}\sigma\right)\mathrm{d}t.$$

Now put $\ell(t) := \int_{-1}^{t} b_0(\sigma)\,\mathrm{d}\sigma$, and let $c := \sqrt{\alpha z}$. Then $\ell'(t) = b_0(t)$, and hence

$$\tilde{x} = \int_{-1}^{0} \ell'(t)\exp\left(cl(t)\right)dt = \frac{1}{c}\exp\left(c\ell(t)\right)\Big|_{-1}^{0}$$
$$= \frac{1}{c}\exp\left(c\int_{-1}^{0} b_0(\sigma)\,\mathrm{d}\sigma\right) - \frac{1}{c}.$$

An analogous calculation with $\tilde{y}$ in place of $\tilde{x}$ yields

$$\tilde{y} = \int_{-1}^{0} \ell'(t)\exp\left(-cl(t)\right)\mathrm{d}t = -\frac{1}{c}\exp\left(-c\ell(t)\right)\Big|_{-1}^{0}$$
$$= -\frac{1}{c}\exp\left(-c\int_{-1}^{0} b_0(\sigma)\,\mathrm{d}\sigma\right) + \frac{1}{c}.$$

It follows that

$$\begin{aligned}\int_{-1}^{0} b_0(t)g(\alpha,z;t,-1)\,\mathrm{d}t &= \\ &= \frac{1}{2\sqrt{\alpha z}}\left(\exp\left(\sqrt{\alpha z}\int_{-1}^{0} b_0(\sigma)\,\mathrm{d}\sigma\right)-\exp\left(-\sqrt{\alpha z}\int_{-1}^{0} b_0(\sigma)\,\mathrm{d}\sigma\right)\right)\\ &= \frac{1}{\alpha z}\gamma_2(z).\end{aligned}$$

Furthermore

$$\int_{-1}^{0} b_0(t)\int_{-1}^{s} b_0(\sigma)g(\alpha,z;t,\sigma)\,\mathrm{d}\sigma\,\mathrm{d}t = \frac{1}{\alpha z}\left(\gamma_1(z)-1\right).$$

Thus using (46) it follows that $C(I-zW)^{-1}B$ can be written as

$$C(I-zW)^{-1}B = \begin{pmatrix}\gamma_1(z)+\frac{1}{\alpha z}\gamma_2(z) & \frac{1}{\alpha z}\left(\gamma_1(z)+\gamma_2(z)-1\right)\\ \alpha\gamma_1(z) & \frac{1}{z}\gamma_2(z)\end{pmatrix}.$$

This proves that $\Delta(z)$ is given by (51). Moreover

$$\begin{aligned}\det\Delta(z) &= \left(1-z\gamma_1(z)-\alpha^{-1}\gamma_2(z)\right)\left(1-\gamma_2(z)\right)\\ &\qquad -z\gamma_1(z)\left(\gamma_1(z)+\gamma_2(z)-1\right)\\ &= 1-\alpha^{-1}\gamma_2(z)-\gamma_2(z)+\alpha^{-1}\gamma_2^2-z\gamma_1^2.\end{aligned}$$

Next observe that

$$\begin{aligned}\alpha^{-1}\gamma_2^2-z\gamma_1^2 &= \alpha^{-1}\left(\frac{\sqrt{\alpha z}}{2}\left(e^{\sqrt{\alpha z}m(b_0)}-e^{-\sqrt{\alpha z}m(b_0)}\right)\right)^2\\ &\qquad -z\left(\frac{1}{2}\left(e^{\sqrt{\alpha z}m(b_0)}+e^{-\sqrt{\alpha z}m(b_0)}\right)\right)^2\\ &= -z\end{aligned}$$

Thus

$$\det\Delta(z) = 1-\left(\frac{1+\alpha}{\alpha}\right)\gamma_2(z)-z,$$

and this completes the proof of the theorem. □

To illustrate the applications of Theorem 6.2, we first consider the case $\alpha=1$ and $b_0\equiv 1$ and the case $\alpha=-1$ and $b_0\equiv 1$.

In case $\alpha=1$ and $b_0\equiv 1$, the operator T defined by (43) can be written as $T=T_1^2$, where $T_1: B([-1,0];\mathbb{C}^n)\to B([-1,0];\mathbb{C}^n)$ is given by

$$(T_1\varphi)(\theta) := \varphi(0) + \int_{-1}^{\theta} \varphi(s)\, ds.$$

It follows from Theorem 5.1 that the operator T_1 admits a characteristic matrix function Δ_1 defined by $\Delta_1(z) := 1 - ze^{-z}$. Furthermore, it follows from Theorem 6.2 that the characteristic matrix function Δ corresponding to period map T defined by (43) satisfies

$$\begin{aligned}\det \Delta(z) &= 1 - \sqrt{z}\left(e^{\sqrt{z}} - e^{-\sqrt{z}}\right) - z \\ &= \left(1 - \sqrt{z}e^{\sqrt{z}}\right)\left(1 + \sqrt{z}e^{-\sqrt{z}}\right) \\ &= \Delta_1(\sqrt{z})\Delta_1(-\sqrt{z}).\end{aligned}$$

Since $T = T_1^2$, this result is in agreement with the fact that

$$\lambda \in \sigma(T) \setminus \{0\} \text{ if and only if } \sqrt{\lambda} \text{ or } -\sqrt{\lambda} \text{ belongs to } \sigma(T_0) \setminus \{0\}.$$

In general, if we define the operator $T_\alpha : B([-1, 0]; \mathbb{C}^n) \to B([-1, 0]; \mathbb{C}^n)$ by

$$(T_\alpha\varphi)(\theta) := \varphi(0) + \alpha \int_{-1}^{\theta} b_0(s)\varphi(s)\, \mathrm{d}s, \qquad \alpha \neq 0,$$

then the operator T defined by (43) can be written as

$$T = T_\alpha T_1.$$

In case $\alpha = -1$ and $b_0 \equiv 1$, the operator T becomes $T = T_{-1}T_1$. In this case

$$\det \Delta(z) = 1 - z \quad \text{and} \quad \sigma(T_{-1}T_1) \setminus \{0\} = \{1\}.$$

As a next example consider the 2-periodic delay equation

$$\dot{x}(t) = \cos(\pi t)x(t - 1). \tag{54}$$

Define

$$b_0(t) := \begin{cases} \cos(\pi t) & 0 \leq t \bmod 2 < 1, \\ -\cos(\pi t) & 1 \leq t \bmod 2 < 2. \end{cases} \tag{55}$$

Then b_0 is 1-periodic and

$$m(b_0) = -\int_{-1}^{0} \cos(\pi s)\, ds = 0.$$

Furthermore

$$\cos(\pi t) = \begin{cases} b_0(t) & 0 \leq t \bmod 2 < 1, \\ -b_0(t) & 1 \leq t \bmod 2 < 2. \end{cases}$$

Thus it follows that $b(t) = \cos(\pi t)$ satisfies (42) with $b_0(t)$ defined by (55) and $\alpha = -1$. Consequently, the spectrum of the period map associated with (54) consists of a single point only.

Examples of periodic delay equations with period a multiple of the delay for which the spectrum of the period map is finite was a open problem in the literature. With the class of equations considered in this section, we can now construct many periodic delay equations for which one still can compute the characteristic matrix function rather explicitly.

References

Bart, H., Gohberg, I., & Kaashoek, M. A. (1979). *Minimal Factorization of Matrix and Operator Functions*. Basel: Birkhäuser Verlag.

Bart, H., Gohberg, I., Kaashoek, M. A., & Ran, A. C. M. (2008). *Factorization of Matrix and Operator Functions: the State Space Method*. Basel: Birkhäuser Verlag.

Diekmann, O., van Gils, S. A., Verduyn Lunel, S. M., & Walther, H. O. (1995). *Delay Equations: Functional-, Complex-, and Nonlinear Analysis*. New York: Springer.

Gohberg, I., Kaashoek, M. A., & van Schagen, F. (1993). On the local theory of regular analytic matrix functions. *Linear Algebra and Its Applications, 182*, 9–25.

Gripenberg, G., Londen, S.-O., & Staffans, O. (1990). *Volterra Integral and Functional Equations*. Cambridge: Cambridge University Press.

Hale, J. K., & Verduyn Lunel, S. M. (1993). *Introduction to Functional Differential Equations*. New York: Springer.

Kaashoek, M. A., & Verduyn Lunel, S. M. (1992). Characteristic matrices and spectral properties of evolutionary systems. *Transactions of the American Mathematical Society, 334*, 479–517.

Kaashoek, M. A., & Verduyn Lunel, S. M. (2023). *Completeness theorems, characteristic matrices and applications to integral and differential operators, Operator Theory: Advances and Applications* (Vol. 288). Birkäuser.

Verduyn Lunel, S. M. (2023). The twin semigroup approach towards periodic neutral delay equations. In D. Breda, (Ed.), *Controlling Delayed Dynamics: Advances in Theory, Methods and Applications*, *CISM Lecture Notes* (pp. 1–36). Wien-New York: Springer.

Pseudospectral Methods for the Stability Analysis of Delay Equations. Part I: The Infinitesimal Generator Approach

Dimitri Breda

Abstract Delay equations generate dynamical systems on infinite-dimensional state spaces. Their stability analysis is not immediate and reduction to finite dimension is often the only chance. Numerical collocation via pseudospectral techniques recently emerged as an efficient solution. In this part we analyze the application of these methods to discretize the infinitesimal generator of the semigroup of solution operators associated to the system. The focus is on both local stability of equilibria and general bifurcation analysis of nonlinear problems, for either delay differential and renewal equations.

1 Introduction

We are interested in *delay equations*, by which term we mean equations where the evolution of an unknown function of time depends on both the present and the past. They can be of either differential or renewal (integral) type, or systems of both, and they represent a fundamental tool in modeling several phenomena with particular relevance in the fields of population dynamics and control engineering (see, e.g., Inaba 2017; Michiels and Niculescu 2014 as starting references). The dependence on the history generically leads to dynamical systems on infinite-dimensional state spaces, typically Banach spaces of functions defined on some interval of the real line (Hale 1977; Hale and Verduyn Lunel 1993; Diekmann et al. 1995 are cornerstone monographs on the subject). Exactly this infinite dimension is the major motivation for resorting to numerical methods, in order to either simulate solutions of Initial Value Problms (IVPs, see Bellen and Zennaro 2003 or Bellen et al. 2009) or address

Dimitri Breda is member of INdAM Research group GNCS and of UMI Research group "Modellistica socio-epidemiologica". His work was partially supported by the Italian Ministry of University and Research (MUR) through the PRIN 2020 project (No. 2020JLWP23) "Integrated Mathematical Approaches to Socio-Epidemiological Dynamics" (CUP: E15F21005420006).

D. Breda (✉)
CDLab - Computational Dynamics Laboratory, Department of Mathematics, Computer Science and Physics, University of Udine, Udine, Italy
e-mail: dimitri.breda@uniud.it

D. Breda (ed.), *Controlling Delayed Dynamics*, CISM International Centre for Mechanical Sciences 604, https://doi.org/10.1007/978-3-031-01129-0_3

crucial issues like stability and bifurcations in presence of varying parameters (see Breda et al. 2015b; Insperger and Stépán 2011 to name a couple).

In this chapter we focus our attention first on the local stability analysis of equilibria, as it represents the typical entrance to the dynamical analysis. A well-established theory of strongly continuous semigroups (see, e.g., Engel and Nagel 1999; Batkai and Piazzera 2005; Pazy 1983) furnishes the essential tools at the base of the *principle of linearized stability*, by which the local stability of an equilibrium of an autonomous nonlinear system can be inferred from the stability of the system obtained by linearizing the original system at such equilibrium (at least in the *hyperbolic* case, see below). The stability of the linearized system is determined by the position of the so-called *characteristic roots* with respect to the imaginary axis in the complex plane. These roots can be conveniently seen as eigenvalues of a differential operator acting on a subspace of the state space, viz. the *infinitesimal generator* of the underlying semigroup of solution operators. Discretizing this operator allows to approximate (part of) its spectrum, thus providing reliable numerical tools to address the stability of equilibria.

Among several other discretization techniques (see, e.g., Breda et al. 2015b; Lehotzky and Insperger 2016 as sources of recent references), the use of *pseudospectral collocation* has revealed particularly efficient (see (Andò et al.) for a self-contained account of). Here we aim at discussing the essential elements of its use in addressing the local stability of equilibria of delay equations. Then, we also illustrate how this technique can be conveniently extended to the case of *nonlinear* equations, giving rise to a particularly flexible approach to bifurcation analysis. The latter, originally presented in Breda et al. (2016a) (but see also Breda et al. 2016b; Getto et al. 2019; Gyllenberg et al. 2018; Scarabel et al. 2020), consists in reducing the delay equation to a system of Ordinary Differential Equations (ODEs), which can then be treated with standard tools for continuation and bifurcation (e.g., `Auto` Doedel 1981, 2007, `MatCont` Dhooge et al. 2003, 2008 or `XPPaut` Ermentrout 2002 to recall the main ones).

The chapter is organized as follows. Section 2 deals with the basics of the theory of strongly continuous semigroups of bounded linear operators and their infinitesimal generators, first in general and then specializing to delay differential (Sect. 2.1), renewal (Sect. 2.2) and coupled (Sect. 2.3) equations. A brief account of the related principle of linearized stability is given in Sect. 2.4. Section 3 collects the main aspects of polynomial interpolation and pseudospectral collocation. The latter is then applied to discretize the infinitesimal generator of linear(ized) systems in Sect. 4, particularizing to delay differential (Sect. 4.1), renewal (Sect. 4.2) and coupled (Sect. 4.3) equations, with an overview on convergence and related questions in Sect. 4.4. Section 5 treats the extension of the pseudospectral approach to nonlinear systems of coupled equations. Some illustrative computations on examples from applications are presented in Sect. 6, after discussing some implementation issues. Relevant codes are also provided. Finally, some closing remarks are given in Sect. 7. Note that the introductory expositions in Sect. 2 and Sect. 3 serve both this chapter and Breda (2023).

We conclude this introduction by presenting the prototypical delay equation we are concerned with. To this aim, let $\tau > 0$ be the (maximum bounded) delay of the

system and let X and Y be spaces of (real, possibly vector-valued) functions defined on $[-\tau, 0]$. We consider systems of the form

$$\begin{cases} x(t) = F(x_t, y_t) \\ y'(t) = G(x_t, y_t), \end{cases} \tag{1}$$

where t denotes time and $F : X \times Y \to \mathbb{R}^{d_X}$ and $G : X \times Y \to \mathbb{R}^{d_Y}$ are smooth, autonomous, in general nonlinear functions defined on a state space $X \times Y$. In this respect we use the standard notation

$$x_t(\theta) := x(t + \theta), \quad y_t(\theta) := y(t + \theta), \qquad \theta \in [-\tau, 0],$$

defining the state (x_t, y_t) at time t through time translation. Above, F is assumed to be integral in the X-component, while d_X and d_Y are positive integers denoting the number of, respectively, renewal (the X-component) and differential (the Y-component) equations. Concerning the state space, we consider the classical choices of Banach spaces of functions

$$X := L^1([-\tau, 0]; \mathbb{R}^{d_X}), \qquad \|\varphi\|_X := \int_{-\tau}^{0} |\varphi(\theta)| \, \mathrm{d}\theta \tag{2}$$

and

$$Y := C([-\tau, 0]; \mathbb{R}^{d_Y}), \qquad \|\psi\|_Y := \max_{\theta \in [-\tau, 0]} |\psi(\theta)| \tag{3}$$

for $|\cdot|$ a norm in either $\mathbb{R}^{d_X}$ or $\mathbb{R}^{d_Y}$ (see, e.g., Diekmann et al. 2008). Eventually, we call (1) a *coupled* equation. In the sequel we also treat separately the cases of Renewal Equations (REs), viz.

$$x(t) = F(x_t)$$

and Delay Differential Equations (DDEs), viz.

$$y'(t) = G(y_t),$$

with the definitions of F and G adapted accordingly. Let us remark that the well-posedness of the IVP for (1), obtained by imposing $(x_0, y_0) = (\varphi, \psi)$ for some $(\varphi, \psi) \in X \times Y$, is ensured by assuming Lipschitz conditions on F and G (see Diekmann et al. 2008, 1995). Note that it is not restrictive to set the initial time to 0 as we deal with autonomous problems.

2 Semigroups of Solution Operators and Infinitesimal Generator

This section summarizes standard definitions, concepts and results from the theory of strongly continuous semigroups of bounded linear operators and their infinitesimal generators, the relevant implications with respect to the stability of linear systems to arrive, eventually, at formulating the principle of linearized stability. Readers may refer to Engel and Nagel (1999); Batkai and Piazzera (2005); Pazy (1983) for a full treatment and relevant proofs.

Let $(X, \|\cdot\|_X)$ be a Banach space. A one parameter family $\{T(t)\}_{t\geq 0}$ of bounded linear operators $T(t) : X \to X$ is called a semigroup of bounded linear operators on X if $T(0) = I_X$ and $T(t+s) = T(t)T(s)$ for every $t, s \geq 0$. A semigroup of bounded linear operators is called strongly continuous (or $\mathcal{C}_0$-semigroup) if $T(t)x \to x$ as $t \downarrow 0$ for all $x \in X$. In the sequel, for brevity, the world *semigroup* implicitly refers to a strongly continuous semigroup of bounded linear operators. The operator $\mathcal{A} : \mathcal{D}(\mathcal{A}) \subseteq X \to X$ defined by

$$\mathcal{A}x := T'(0)x = \lim_{t\downarrow 0} \frac{T(t)x - x}{t}$$

for every $x \in \mathcal{D}(\mathcal{A})$ with

$$\mathcal{D}(\mathcal{A}) := \left\{ x \in X \ : \ \lim_{t\downarrow 0} \frac{T(t)x - x}{t} \text{ exists} \right\}$$

is called the *infinitesimal generator* of the semigroup $\{T(t)\}_{t\geq 0}$. $\mathcal{D}(\mathcal{A})$ is dense in X, $\mathcal{A}$ is a closed linear operator and it determines the semigroup uniquely. The set of $\lambda \in \mathbb{C}$ such that $\lambda I_X - \mathcal{A}$ is bijective is called the resolvent set of $\mathcal{A}$. The complement of the resolvent set is called spectrum, denoted by $\sigma(\mathcal{A})$. An important part of $\sigma(\mathcal{A})$ is the point spectrum, $\sigma_p(\mathcal{A})$, i.e., values λ such that $\lambda I_X - \mathcal{A}$ is not injective. The elements $\lambda \in \sigma_p(\mathcal{A})$ are called eigenvalues of $\mathcal{A}$ and any $x \in \mathcal{D}(\mathcal{A}) \setminus \{0\}$ such that $\mathcal{A}x = \lambda x$ is called an eigenvector (or eigenfunction if X is a space of functions). The null space $\mathcal{N}(\lambda I_X - \mathcal{A})$ is called the eigenspace of λ and its dimension $g(\lambda)$ the geometric multiplicity. The smallest closed linear subspace $M(\lambda)$ that contains all $\mathcal{N}(\lambda I_X - \mathcal{A})^j$ for $j \geq 1$ is called the generalized eigenspace of λ and its dimension $m(\lambda)$ the algebraic multiplicity. If λ is an isolated point of $\sigma_p(\mathcal{A})$ and $m(\lambda) < +\infty$, then λ is called an eigenvalue of finite type, simple if $m(\lambda) = 1$. Finally, the quantities $\rho(\mathcal{A}) := \sup\{|\lambda| \ : \ \lambda \in \sigma(\mathcal{A})\}$ and $\alpha(\mathcal{A}) := \sup\{\Re(\lambda) \ : \ \lambda \in \sigma(\mathcal{A})\}$ are called, respectively, spectral radius and spectral abscissa of $\mathcal{A}$.

Going back to the semigroup, there exist constants $\omega \in \mathbb{R}$ and $M \geq 1$ such that $\|T(t)\| \leq Me^{\omega t}$ for all $t \geq 0$. The quantity

$$\omega_0 := \inf\{\omega \in \mathbb{R} \ : \ \text{exists } M_\omega \geq 1 \text{ such that } \|T(t)\| \leq M_\omega e^{\omega t} \text{ for all } t \geq 0\}$$

is called the growth bound of the semigroup. It holds $-\infty \leq \alpha(\mathcal{A}) \leq \omega_0 < +\infty$ as well as $\rho(T(t)) = e^{\omega_0 t}$ for every $t \geq 0$. These properties suggest an exponential relation between the semigroup and its generator, which becomes concrete thanks to the spectral mapping theorem for point spectra. Indeed, $\sigma_p(T(t)) \setminus \{0\} = e^{t\sigma_p(\mathcal{A})}$ and, more precisely, if $\lambda \in \sigma_p(\mathcal{A})$ then $e^{\lambda t} \in \sigma_p(T(t))$ while if $e^{\lambda t} \in \sigma_p(T(t))$, then there exists $k \in \mathbb{Z}$ such that $\lambda_k := \lambda + \mathrm{i}2\pi k/t \in \sigma_p(\mathcal{A})$. Unfortunately, the equality $\alpha(\mathcal{A}) = \omega_0$ need not be true in general, but it is so if some compactness is available. In this respect, a semigroup is called eventually compact if there exists $t_0 > 0$ such that $T(t_0)$ is compact[1] (and then it is compact for all $t \geq t_0$ since $T(t) = T(t - t_0)T(t_0)$). If the semigroup is eventually compact then $\sigma(\mathcal{A}) = \sigma_p(\mathcal{A})$, $e^{\alpha(\mathcal{A})t} = \rho(T(t))$ for every $t \geq 0$ and, finally, $\alpha(\mathcal{A}) = \omega_0$.

Typically, a semigroup $\{T(t)\}_{t\geq 0}$ is a fundamental tool in describing the time evolution of a linear dynamical system on a state space X. It arises in the implicit definition of the state x_t at time t of the system originating from an initial state x_0 given at time 0:

$$T(t)x_0 = x_t, \quad t \geq 0. \tag{4}$$

This implicit definition is well posed as soon as existence and uniqueness of the related IVP are available. If so, it is clear that the knowledge of the growth bound ω_0 becomes crucial in assessing the long-time behavior. But being the semigroup defined only implicitly, it is easier to look at the spectral abscissa $\alpha(\mathcal{A})$ of the relevant infinitesimal generator. Indeed, it will be clear in the following sections that $\mathcal{A}$ can be defined explicitly. Nevertheless, the equality $\alpha(\mathcal{A}) = \omega_0$ is not necessarily true but, as anticipated, it becomes so if the semigroup is eventually compact. Therefore, well-posedness of the underlying IVP and eventual compactness of the associated semigroup are the two properties we shall be equipped with in order to be able to declare the stability character of the linear system. In fact, $\alpha(\mathcal{A}) < 0$ would imply asymptotic stability, while $\alpha(\mathcal{A}) > 0$ would give instability. Given then that $\sigma(\mathcal{A}) = \sigma_p(\mathcal{A})$, the stability issue is finally reduced to the determination of the rightmost eigenvalue(s) of $\mathcal{A}$. Then the principle of linearized stability possibly transfers the stability of the linearized system to the stability of the equilibrium around which the linearization of the original nonlinear equation has been performed, see Sect. 2.4 below. First we deal separately with DDEs, REs and coupled equations, reporting on the related IVP, the associated semigroup and its generator, and giving references concerning the issues of well-posedeness and eventual compactness.[2]

[1] Recall that a compact linear operator $K : X \to X$ satisfies $\sigma(K) = \{0\} \cup \sigma_p(K)$ and either $\sigma_p(K)$ has finitely-many points or they accumulate at 0.

[2] We treat first DDEs for their longer tradition with respect to REs. Then, when dealing with coupled equations, we put REs first as in (1) following the convention in, e.g., Diekmann et al. (2008), due to the relative importance of REs with respect to DDEs in describing several models in population dynamics.

2.1 Delay Differential Equations

Given $\psi \in Y$, consider the IVP

$$\begin{cases} y'(t) = G(y_t), & t \geq 0, \\ y_0 = \psi. \end{cases}$$

If $G : Y \to \mathbb{R}^{d_Y}$ is Lipschitz continuous then existence and uniqueness of a solution y forward in time are granted, see, e.g., (Hale (1977), Sect. 2.2), or (Bellen et al. (2009), Sect. 4) for a modern account. Assume that there exists an equilibrium, i.e., a function $\bar{y} \in Y$ satisfying $G(\bar{y}) = 0$. Linearization leads to

$$y'(t) = L_G y_t \tag{5}$$

for $L_G := DG(\bar{y})$ the Fréchet differential[3] of G at $\bar{y}$. The associated solution operator

$$T_G(t)y_0 = y_t, \quad t \geq 0,$$

is well defined and eventually compact (Hale 1977, Sect. 7.1). In particular, $T_G(t)$ is compact for every $t \geq \tau$. Eventually, it is not difficult to recover the infinitesimal generator

$$\mathcal{A}_G\psi = \psi', \quad \psi \in \mathcal{D}(\mathcal{A}_G), \tag{6}$$

with

$$\mathcal{D}(\mathcal{A}_G) := \left\{\psi \in Y \ : \ \psi' \in Y \text{ and } \psi'(0) = L_G\psi\right\}, \tag{7}$$

see again (Hale (1977), Sect. 7.1). Note that the action of $\mathcal{A}$ is differentiation independently of (5), while the latter, viz. L_G, characterizes $\mathcal{D}(\mathcal{A}_G)$ through the nonlocal boundary condition $\psi'(0) = L_G\psi$. To remark that this form of the generator follows the choice (3). Other choices are possible, even though less frequent. Among these, it is worth mentioning $Y = \mathbb{R}^{d_Y} \times L^2([-\tau, 0], \mathbb{R}^{d_Y})$, which is not uncommon in the field of control engineering (see, e.g., Breda 2010 and the references therein or Michiels 2023).

Finally, note that the general instance of (5) can be described through the Lebesgue-Stieltjes integral

$$y'(t) = \int_{-\tau}^{0} \mathrm{d}\eta(\theta)y(t+\theta)$$

for some function η of bounded variation, see, e.g., (Section I.1 Diekmann et al. (1995)) or Verudyn Lunel (2023).

[3] For a primer on Fréchet derivatives see (Ambrosetti and Prodi (1995), Chap. 1).

2.2 Renewal Equations

Given $\varphi \in X$, consider the IVP

$$\begin{cases} x(t) = F(x_t), & t \geq 0, \\ x_0 = \varphi. \end{cases}$$

If $F : X \to \mathbb{R}^{d_X}$ is Lipschitz continuous then existence and uniqueness of a solution x forward in time are granted, see, e.g., (Diekmann et al. (2008), Theorem 3.8). Assume that there exists an equilibrium, i.e., a function $\bar{x} \in X$ satisfying $\bar{x} = F(\bar{x})$. Linearization leads to

$$x(t) = L_F x_t \tag{8}$$

for $L_F := DF(\bar{x})$ the Fréchet differential of F at $\bar{x}$. The associated solution operator

$$T_F(t)x_0 = x_t, \quad t \geq 0,$$

is well defined and eventually compact (Diekmann et al. (2008), Theorem 2.8). In particular, $T_F(t)$ is compact for every $t \geq \tau$. Eventually, it is not difficult to recover the infinitesimal generator

$$\mathcal{A}_F \varphi = \varphi', \quad \varphi \in \mathcal{D}(\mathcal{A}_F), \tag{9}$$

with

$$\mathcal{D}(\mathcal{A}_F) := \left\{ \varphi \in X \ : \ \varphi' \in X \text{ and } \varphi(0) = L_F \varphi \right\}. \tag{10}$$

Note again that the action of $\mathcal{A}_F$ is differentiation independently of (8), while the latter, viz. L_F, characterizes $\mathcal{D}(\mathcal{A}_F)$ through the nonlocal boundary condition $\varphi(0) = L_F \varphi$. Let us stress the difference with respect to DDEs, where the boundary condition regards the value of the derivative at zero rather than the value of the function itself.

Finally, note that the Riesz representation Theorem allows to express (8) in the integral form

$$x(t) = \int_{-\tau}^{0} K(\theta) x(t+\theta) \, \mathrm{d}\theta$$

for some kernel K, see, e.g., (Breda and Liessi (2020), Appendix B).

2.3 Coupled Equations

Given $(\varphi, \psi) \in X \times Y$, consider the IVP for (1). By joining the results in Diekmann et al. (2008) together with those in Diekmann et al. (1995) it is possible to recover all the necessary ingredients already seen in the preceding sections. In particular, we

are mainly interested in the infinitesimal generator of the linearized problem

$$\begin{cases} x(t) = L_F(x_t, y_t) \\ y'(t) = L_G(x_t, y_t), \end{cases} \tag{11}$$

which reads

$$\mathcal{A}_{F,G}(\varphi, \psi) = (\varphi', \psi'), \quad (\varphi, \psi) \in \mathcal{D}(\mathcal{A}_{F,G}), \tag{12}$$

with

$$\begin{aligned} \mathcal{D}(\mathcal{A}_{F,G}) := \{(\varphi, \psi) \in X \times Y \ : \ (\varphi, \psi) \in X \times Y \text{ and} \\ (\varphi(0), \psi'(0)) = (L_F(\varphi, \psi), L_G(\varphi, \psi))\}. \end{aligned} \tag{13}$$

2.4 Principle of Linearized Stability

We limit ourselves to describe the principle in a very general fashion, avoiding to give precise statements in view of this or that specific class of equations. For a starting reference on delay equations see anyway (Diekmann et al. (2008), Theorem 2.18) and the related bibliographical sources.

Consider a dynamical system generated by a nonlinear equation and assume it has an equilibrium, i.e., a fixed point of the related solution operator. Note that the notion of semigroup introduced in Sect. 2 through (4) is unchanged if the underlying problem is nonlinear (yet well-posed). Let $\mathcal{A}$ be the infinitesimal generator of the semigroup associated to the equation obtained by linearizing the original nonlinear problem around the given equilibrium. Then, in its most generality, the principle of lienarized stability states that if $\Re(\lambda) < 0$ for all $\lambda \in \sigma(\mathcal{A})$ then the equilibrium is asymptotically (exponentially) stable, whereas if $\Re(\lambda) > 0$ for some $\lambda \in \sigma(\mathcal{A})$ then the equilibrium is unstable. To remark that this principle concerns *local* stability and its validity ceases to hold when $\mathcal{A}$ has eigenvalues along the imaginary axis, in which case we talk about *non-hyperbolic* equilibria (for a treatment of which see, e.g., (Diekmann et al. (1995), Chapter IX)).

3 Basics of Polynomial Interpolation and Pseudospectral Methods

Several mathematical problems concern functions, and most of them are not solvable exactly. We can tackle the issue in the context of approximation in Banach spaces. As general references for the results in this section let us advise Rivlin (1981); Trefethen (2013).

To fix some notation (independently of the one used in the other sections), let $a, b \in \mathbb{R}$ with $a < b$ and consider a Banach space $(X, \|\cdot\|_X)$ of functions $[a, b] \to$

$\mathbb{R}$ with $\dim X = \infty$. Restriction to the scalar case does not preclude generality as extension to vector-valued functions is straightforward. The goal is to find a suitable finite-dimensional approximation of a given $f \in X$.

To this aim, let us represent this approximation as a vector in some finite-dimensional space X_n, where the positive integer n is an indication of this finite dimension. By defining a restriction operator $R_n : X \to X_n$ and a prolongation operator $P_n : X_n \to X$, we can formalize the approximation process by the two steps

$$F := R_n f, \qquad f_n := P_n F \approx f.$$

Above, F is the finite-dimensional representation of the finite-dimensional approximation f_n of f: note, in fact, that $F \in X_n$ is a vector, while $f_n \in X$ is a function.[4] Let us observe that even though it is reasonable to assume that $R_n P_n = I_{X_n}$, in general we have $P_n R_n \neq I_X$. Therefore, measuring $e_n := P_n R_n - I_X$ is crucial and several aspects should be taken into consideration, e.g., whether considering $|e_n(t)|$ for $t \in [a, b]$ or $\|e_n\|_X$; if the latter are bounded (possibly uniformly in n) or they even vanish as $n \to \infty$; if these properties hold in all X or just in some subspace. Nor other computational issues should be neglected, such as how the choice of the representation affects conditioning and stability, or the computational cost and similar ones.

A quite natural (and indeed widely followed) way to find a reasonable approximation is that of substituting the function with its interpolating polynomial at a given set of nodes discretizing the domain of definition. We assume henceforth that the functions in X are regular enough for point-wise evaluation to make sense. Consider the discretization of $[a, b]$ through $n + 1$ distinct points, say

$$a \leq t_{n,0} < t_{n,1} < \cdots < t_{n,n} \leq b. \tag{14}$$

Correspondingly, define $X_n := \mathbb{R}^{n+1}$,

$$R_n f := (f(t_{n,0}), f(t_{n,1}), \ldots, f(t_{n,n}))^T \tag{15}$$

and

$$P_n F := p_n \tag{16}$$

for p_n the polynomial of degree at most n interpolating the components of $F = (F_0, F_1, \ldots, F_n)^T \in X_n$ at the points (14), i.e., the one satisfying

$$p_n(t_{n,i}) = F_i, \quad i = 0, 1, \ldots, n. \tag{17}$$

While p_n uniquely exists, its representation in X_n needs not be unique. The standard Lagrange representation

[4] In what follows we use lower case letters for functions and upper case letters for their finite-dimensional counterparts, i.e., the vectors of their representation.

$$p_n(t) = \sum_{j=0}^{n} \ell_{n,j}(t) F_j, \quad t \in [a,b], \tag{18}$$

for the Lagrange basis polynomials

$$\ell_{n,j}(t) := \prod_{\substack{k=0 \\ k \neq j}}^{n} \frac{t - t_{n,k}}{t_{n,j} - t_{n,k}}, \quad j = 0, 1, \ldots, n, \tag{19}$$

is theoretically convenient, as, e.g., (17) follows immediately from the cardinal property $\ell_{n,j}(t_{n,i}) = \delta_{i,j}$ for $\delta_{i,j}$ the Kronecker's delta. From the numerical standpoint, it becomes equally convenient when considered in its barycentric form (see Berrut and Trefethen 2004), i.e.,

$$p_n(t) = \pi_{n+1}(t) \sum_{j=0}^{n} \frac{w_j}{t - t_j} F_j$$

for the nodal polynomial

$$\pi_{n+1}(t) := \prod_{k=0}^{n} (t - t_k)$$

and the barycentric weights

$$w_j := \prod_{\substack{k=0 \\ k \neq j}}^{n} \frac{1}{t_j - t_k}, \quad j = 0, 1, \ldots, n.$$

Note that the weights are independent of the evaluation point t and thus can be computed in advance once for all evaluation points, in $O(n^2)$ operations.

Polynomial interpolation is an excellent technique when f is smooth and the interpolation nodes t_j are suitably chosen. For instance, when $X = C([a,b], \mathbb{R})$ and $\|\cdot\|_X = \|\cdot\|_\infty$, a classical result in uniform approximation theory gives

$$\|p_n - f\|_\infty \leq (1 + \Lambda_n) E_n(f) \tag{20}$$

for

$$\Lambda_n := \max_{t \in [a,b]} \sum_{j=0}^{n} |\ell_j(t)|$$

the so-called Lebesgue constant and

$$E_n(f) := \min_{p_n \in \Pi_n} \|f - p_n\|_\infty$$

the best uniform approximation error (Π_n denotes the set of algebraic polynomials of degree at most n). The independent roles of the interpolation nodes and of the interpolated function emerge clear from (20). As for the former, it is well-known that Λ_n grows *at least* as $O(\log n)$ for any choice of nodes, but also *at most* with the same order when Chebyshev nodes are chosen, either zeros (left) or extrema (right):

$$t_i = \cos\left(\frac{(2i+1)\pi}{2n+2}\right) \in (-1,1), \qquad t_i = \cos\left(\frac{i\pi}{n}\right) \in [-1,1].$$

As for the latter, the Weierstrass approximation Theorem ensures that $E_n(f)$ vanishes as $n \to \infty$ for every continuous function f. More regularity is required to know about the rate of decay, and results of the Jackson's type guarantee an order $O(n^{-k})$ for f of class C^k, or $O(n^{-k})$ for every $k \in \mathbb{N}$ for f of class C^∞, or even $O(e^{-\gamma n})$ for some positive γ for f analytic. The latter two are known as *convergence of infinite order* or *spectral accuracy* (see, e.g., Trefethen 2000).[5]

Having recalled the basics of polynomial interpolation, it is not difficult now to understand what a *pseudospectral*[6] approach is: nothing else then replacing the (unknown) function in the problem of interest with the interpolating polynomial of a(n unknown) vector. Assume to reformulate the problem as $H(f) = 0$ for some operator $H : X \to X$. Of course, in general, we cannot demand a polynomial to solve this problem exactly, rather we can ask for something weaker as, e.g., to satisfy the problem at given points (possibly different from the interpolation points). The latter choice undergoes the name of *collocation*, thus leading to *pseudospectral collocation*.[7] A classic example is finding $F \in X_n$ such that $R_n H(P_n F) = 0$, i.e., the collocation nodes coincide with the interpolation nodes, even though the general approach is much more flexible.[8]

A first crucial question in the analysis of a pseudospectral collocation approach is whether the finite-dimensional problem is well posed, i.e., existence and uniqueness of $F \in X_n$. Once this is granted, the next issue is to estimate the error. In this respect, note that F and f leave in different spaces, so that $P_n F$ is used to compare with

[5] Anyway, let us also recall that Faber's Theorem tells us that for any chosen set of nodes there is always a continuous function f for which $\|p_n - f\|_\infty$ does not vanish, Faber (1914).

[6] For an explanation of the term *pseudospectral* see (Brunner (2004), Sect. 1.7).

[7] Note that pseudospacetral collocation is an alternative among many other ones, as, e.g., Galerkin-type or weighted-residuals approaches and series truncation. All these correspond in some sense to different choices of R_n and P_n and different strategies to obtain F. Note, however, that any choice must be suitably related to the features of X: e.g., there is no much sense in using Fourier series in $C([a,b],\mathbb{R})$ or interpolation in $L^2([a,b],\mathbb{R})$. Finally, let us remark that the choices above potentially lead to discretization approaches different from the one described in the rest of this chapter or in Breda (2023) when dealing with delay equations, see, e.g., Lehotzky and Insperger (2016) to name some examples.

[8] For instance, if H acts on a domain $\mathcal{D}(H) \subset X$ characterized by some given constraints (e.g., smoothness or boundary conditions), then the latter should be suitably taken into account in the discretization process, e.g., by explicitly replacing an equal number of collocation conditions (as, e.g., in Sect. 4.1) or by implicitly imposing such constraints in the construction of P_n (as, e.g., in Sect. 4.2).

f and thus one can define the collocation error $e_n := P_n F - f$ with the aim at measuring $\|e_n\|_X$. Assuming to prove convergence in a further step of the analysis, a final issue is how to choose n in order to ensure an error below some desired tolerance. Unsurprisingly, pseudospectral collocation usually enjoys the property of spectral accuracy above recalled when based on certain nodes and f is smooth. The price to pay is often represented by complicated theoretical proofs of convergence (due to working on Banach spaces and to the need of some level of smoothness), or by the difficulty of estimating n for a given tolerance (possibly due to the infinite order of convergence, see related comments in Sect. 4.4 below).

Let us note that the operator H describing above the infinite-dimensional problem at hands often involves differentiation and/or integration. In this respect, we illustrate in Fig. 1 the good behavior of the pseudospectral approach by comparing with classical methods of finite order.[9] In the left panel, the derivative of an analytic function is approximated with both (first order) finite differences and pseudospectral differentiation. The latter corresponds to approximate the derivative of a (smooth) function f at a point $t \in (a, b)$ as

$$f'(t) \approx (P_n R_n f)'(t).$$

If we let $F := (f(t_{n,0}), f(t_{n,1}), \ldots, f(t_{n,n}))^T$ and evaluate the approximated derivative at the same interpolation nodes, the resulting vector of derivative values is $D_n F$ where $D_n := [\ell_{n,j}(t_{n,i})]_{i,j=0,1,\ldots,n}$ is the so-called *differentiation matrix* associated to the nodes $t_{n,i}$, see, e.g., Weideman and Reddy (2000) and the references therein. In the right panel of Fig. 1, instead, the definite integral is approximated both with the trapezoid rule (second order) and pseudospectral (interpolatory) quadrature, i.e.,

$$\int_a^b f(t)\,\mathrm{d}t \approx \int_a^b (P_n R_n f)(t)\,\mathrm{d}t.$$

Note that the resulting approximation is $w^T F$ for the same F above and w the vector of quadrature weights

$$w_i = \int_a^b \ell_{n,i}(t)\,\mathrm{d}t, \quad i = 0, 1, \ldots, n.$$

For the problems of interest in this chapter the nodes can be freely selected. As we approximate mainly spectral values of linear operators, the concerned functions are eigenfunctions, and they are in general smooth under reasonable regularity conditions on the original problem. So the use of pseudospectral collocation is largely motivated. Nevertheless, rather then the high accuracy they can perform, we take more profit of the low dimension of the approximation required for a given tolerance. The latter translates indeed into a lighter computational load. This is an advantage when dealing

[9] Recall that in general a method of finite order, say m, applied to a function f of class C^k with $k > m$ gives an error decaying as $O(n^{-m})$ independently of k.

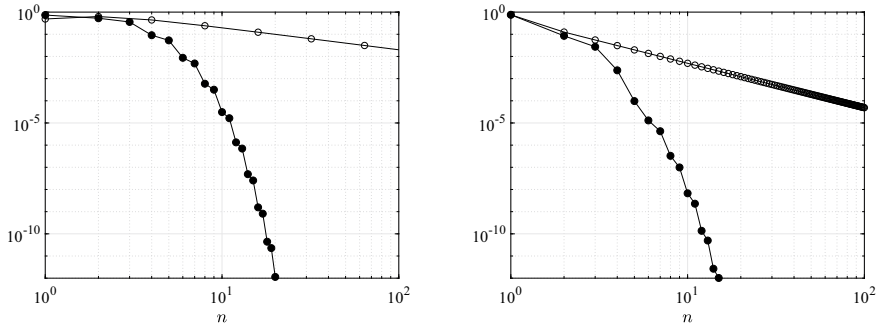

Fig. 1 Errors of the pseudospectral approach based on Chebyshev extrema (•) and of finite-order methods (○) for approximating $f'(0)$ (left) and $\int_{-1}^{1} f(t)\,\mathrm{d}t$ (right) for $f(t) = e^{-t^2}$; see text for more details

with continuation and bifurcation as it is typical in a dynamical analysis, where many instances of the same problem are solved repeatedly.

Let us finally highlight that the proposed pseudospectral approach is not meant for simulation (i.e., time integration of IVPs): solutions need not be necessarily smooth in fact, as due in general to the presence of *breaking points* (see Bellen and Zennaro 2003 for an exhaustive treatment of the subject).

4 Pseudospectral Discretization of the Infinitesimal Generator

The main idea behind the concerned numerical approach is that of replacing the derivative action of the infinitesimal generator $\mathcal{A}$ by differentiating at given nodes a polynomial interpolating a function in the domain $\mathcal{D}(\mathcal{A})$ and simultaneously satisfying or being close to satisfy the boundary condition characterizing the latter. We recall that this boundary condition is the only link to the given linear(ized) equation[10] and we stress that its treatment is the main difference among DDEs and REs from the numerical standpoint (see also Remark 1 below). This and other aspects related to the specific class of equations are treated separately in the forthcoming Sects. 4.1, 4.2 and 4.3. Then we summarize in Sect. 4.4 the main aspects concerning the related convergence, together with other impotrant issues.

Prior to start we introduce a common ingredient. Let M be a positive integer and let

$$\theta_{M,i} = \frac{\tau}{2}\left[\cos\left(\frac{i\pi}{M}\right) - 1\right], \quad i = 0, 1, \ldots, M, \tag{21}$$

be the Chebyshev extremal nodes in $[-\tau, 0]$. Note that $\theta_{M,0} = 0$ and $\theta_{M,M} = -\tau$.

[10] One can always rescale time to set $\tau = 1$ and hence fix the state space independently of the equation.

4.1 Delay Differential Equations

Consider (5) and recall (6) and (7). Consider (21) and let R_M and P_M be the corresponding restriction and prolongation operators as introduced respectively in (15) and (16), operating between Y and $Y_M := \mathbb{R}^{d_Y(M+1)}$. Given $\Psi \in Y_M$, define the linear finite-dimensional operator $\mathcal{A}_{G,M} : Y_M \to Y_M$ as

$$\begin{cases} [\mathcal{A}_{G,M}\Psi]_0 = L_G P_M \Psi \\ [\mathcal{A}_{G,M}\Psi]_i = (P_M\Psi)'(\theta_{M,i}), \quad i = 1, \dots, M. \end{cases}$$

The component of index 0 mimics the derivative action (6) at $\theta_{M,0} = 0$: it is given through the boundary condition characterizing (7) as applied to the collocation polynomial $P_M\Psi$. The components of index $i = 1, \dots, M$ mimic the general derivative action (6) at $\theta_{M,i} \neq 0$: they are given by the exact derivative of the collocation polynomial at the relevant nodes. Observe that $\mathcal{A}_{G,M} = R_M \mathcal{A}_G P_M$ needs not be true in general,[11] even though it well explains the underlying idea of the pseudospectral collocation approach in view of approximating (the spectrum of) $\mathcal{A}_G$ with (the spectrum of) $\mathcal{A}_{G,M}$.

For the sake of implementation one needs a matrix representation of $\mathcal{A}_{G,M}$, which asks in turn to express the collocation polynomial $P_M\Psi$ in some basis. The Lagrange one (19) provides the block form

$$\mathcal{A}_{G,M} = \begin{pmatrix} L_{G,M} \\ D_{Y,M} \otimes I_{d_Y} \end{pmatrix} \in \mathbb{R}^{d_Y(M+1)\times d_Y(M+1)} \tag{22}$$

through (18), with[12]

$$L_{G,M} := \begin{pmatrix} L_G\ell_{M,0} & L_G\ell_{M,1} & \cdots & L_G\ell_{M,M} \end{pmatrix} \in \mathbb{R}^{d_Y\times d_Y(M+1)}, \tag{23}$$

$$D_{Y,M} := \begin{pmatrix} d_{M,1,0} & d_{M,1,1} & \cdots & d_{M,1,M} \\ \vdots & \vdots & \ddots & \vdots \\ d_{M,M,0} & d_{M,M,1} & \cdots & d_{M,M,M} \end{pmatrix} \in \mathbb{R}^{M\times(M+1)} \tag{24}$$

for

$$d_{M,i,j} := \ell'_{M,j}(\theta_{M,i}), \quad i = 1, \dots, M, \ \ j = 0, 1, \dots, M, \tag{25}$$

and $\otimes$ denoting the Kronecker's product. In particular, (23) accounts for the discrete version of the boundary condition in $\mathcal{D}(\mathcal{A}_G)$, while (24) is the Chebyshev differentiation matrix (see, e.g., Trefethen 2000) without the first row. This representation

[11] In fact, the range of P_M is not contained in $\mathcal{D}(\mathcal{A}_G)$, i.e., $(P_M\Psi)'(0) = L_G P_M \Psi$ does not hold for all $\Psi \in Y_M$.

[12] Let $g \in C([-\tau, 0]; \mathbb{R})$ and $\{e_1, \dots, e_{d_Y}\}$ be the canonical basis of $\mathbb{R}^{d_Y}$. Then $L_G g$ is a shorthand notation for the matrix $(L_G g e_1 | \cdots | L_G g e_{d_Y}) \in \mathbb{R}^{d_Y\times d_Y}$.

highlights the fact that $\mathcal{A}_{G,M}$ is a differentiation matrix perturbed along the first (block-) row, as the infinitesimal generator $\mathcal{A}_G$ is a derivative operator perturbed with the boundary condition at $\theta_{M,0} = 0$ characterizing $\mathcal{D}(\mathcal{A}_G)$.

4.2 Renewal Equations

Consider (8) and recall (9) and (10). Consider (21) *without* $\theta_{M,0} = 0$ and let R_M be the corresponding restriction operator as introduced in (15), operating between X and $X_M := \mathbb{R}^{d_X M}$. Note that R_M is not defined on all X as chosen in (2), so we implicitly assume that it acts on a suitable subspace $\tilde{X}$ where point-wise evaluation makes sense: this is indeed the case as shown below. Given $\Phi \in X_M$, define the prolongation operator P_M such that $P_M\Phi$ is the unique polynomial of degree at most M satisfying

$$\begin{cases} (P_M\Phi)(\theta_{M,0}) = L_F P_M \Phi \\ (P_M\Phi)(\theta_{M,i}) = \Phi_i, \quad i = 1, \dots, M. \end{cases} \tag{26}$$

Note that the boundary condition characterizing (10) is imposed directly to construct the collocation polynomial $P_M\Phi$. Then, in the spirit of the pseudospectral approach, define the linear finite-dimensional operator $\mathcal{A}_{F,M} : X_M \to X_M$ as

$$[\mathcal{A}_{F,M}\Phi]_i = (P_M\Phi)'(\theta_i), \quad i = 1, \dots, M.$$

These components mimic the general derivative action (9) at $\theta_{M,i} \neq 0, i = 1, \dots, M$. Observe now that differently from the case of DDEs $\mathcal{A}_{F,M} = R_M \mathcal{A}_F P_M$ holds true.[13] Moreover, the range of $\mathcal{A}_F P_M$ is surely contained in $\tilde{X}$ (given that it contains only polynomials).

Remark 1 The approach of including the boundary condition in the definition of P_M and hence only implicitly in the construction of $\mathcal{A}_{\cdot,M}$ is possible also for DDEs, yet less natural. In this case it is in fact more convenient to apply the boundary condition explicitly when defining $\mathcal{A}_{G,M}$, being the latter a condition on $\psi'(0) = (\mathcal{A}_G\psi)(0)$ and having chosen the nodes such that $\theta_{M,0} = 0$.

Constructing a matrix representation of $\mathcal{A}_{F,M}$ is slightly more involved than what illustrated in Sect. 4.1. By using always (18), we can express the collocation polynomial $P_M\Phi$ as

$$(P_M\Phi)(\theta) = \sum_{j=0}^{M} \ell_{M,j}(\theta)\Phi_j, \quad \theta \in [-\tau, 0],$$

[13] In fact, the range of P_M is now contained in $\mathcal{D}(\mathcal{A}_F)$ thanks to the first of (26).

where we implicitly introduced $\Phi_0 := (P_M\Phi)(0)$. The latter quantity is unknown but it can be recovered from the first of (26) as

$$\Phi_0 = (I_{d_X} - L_F\ell_{M,0})^{-1}\sum_{j=1}^{M} L_F\ell_{M,j}\Phi_j$$

by recalling that L_F is linear (recall also note 12, which equally applies to L_F with obvious modifications). Observe that the inverse above is well-defined for M sufficiently large otherwise the term $x(t)$ would cancel out from (8). Then we get

$$\mathcal{A}_{F,M} = D_{X,M}\otimes I_{d_X} + (d_{X,M}\otimes I_{d_X})L_{F,M} \in \mathbb{R}^{d_X M\times d_X M} \tag{27}$$

with

$$L_{F,M} := (I_{d_X} - L_F\ell_{M,0})^{-1}\left(L_F\ell_{M,1}\cdots L_F\ell_{M,M}\right) \in \mathbb{R}^{d_X\times d_X M}, \tag{28}$$

$$D_{X,M} := \begin{pmatrix} d_{M,1,1} & \cdots & d_{M,1,M}\\ \vdots & \ddots & \vdots\\ d_{M,M,1} & \cdots & d_{M,M,M}\end{pmatrix} \in \mathbb{R}^{M\times M} \tag{29}$$

and

$$d_{X,M} := \begin{pmatrix} d_{M,1,0}\\ \vdots\\ d_{M,M,0}\end{pmatrix} \in \mathbb{R}^{M\times 1} \tag{30}$$

for the same $d_{M,i,j}$ defined in (25). In particular, the term (28) in the second addend at the right-hand side of (27) accounts for the discrete version of the boundary condition in $\mathcal{D}(\mathcal{A}_G)$ as imposed implicitly, while (29) and (30) account for the derivative action (9).

4.3 Coupled Equations

Consider (11) and recall (12) and (13). To tackle the case of coupled equations we combine the pseudospectral approaches described separately in Sect. 4.1 for DDEs and in Sect. 4.2 for REs. Recall that $X_M = \mathbb{R}^{d_X M}$ and $Y_M = \mathbb{R}^{d_Y(M+1)}$. Based on (21), define the prolongation operator $P_M : X_M \times Y_M \to X \times Y$ such that $P_M(\Phi, \Psi)$ is the unique polynomial of degree at most M satisfying

$$\begin{cases} P_M(\Phi,\Psi)(\theta_{M,0}) = (L_F P_M(\Phi,\Psi), \Psi_0)\\ P_M(\Phi,\Psi)(\theta_{M,i}) = (\Phi_i, \Psi_i), \quad i = 1,\ldots,M.\end{cases} \tag{31}$$

In the sequel let us denote by $P_{M,X}$ the X-component of P_M and by $P_{M,Y}$ the Y-component of P_M. Similarly, let us also represent a vector $v \in X_M \times Y_M$ by its block-components listed as $v_{X,1}, \ldots, v_{X,M}, v_{Y,0}, v_{Y,1}, \ldots, v_{Y,M}$, observing that $v_{X,i} \in \mathbb{R}^{d_X}$ for every $i = 1, \ldots, M$ while $v_{Y,i} \in \mathbb{R}^{d_Y}$ for every $i = 0, 1, \ldots, M$. An approximation to the infinitesimal generator (12) is then represented by the linear finite-dimensional operator $\mathcal{A}_{F,G,M} : X_M \times Y_M \to X_M \times Y_M$ defined as

$$\begin{cases} [\mathcal{A}_{F,G,M}(\Phi, \Psi)]_{X,i} = (P_{M,X}(\Phi, \Psi))'(\theta_{M,i}), & i = 1, \ldots, M, \\ [\mathcal{A}_{F,G,M}(\Phi, \Psi)]_{Y,0} = L_G P_M(\Phi, \Psi) \\ [\mathcal{A}_{F,G,M}(\Phi, \Psi)]_{Y,i} = (P_{M,Y}(\Phi, \Psi))'(\theta_{M,i}), & i = 1, \ldots, M. \end{cases} \tag{32}$$

Above we can recognize the derivative action (12) in the first and third rows. The boundary condition in (13) is imposed in the construction of P_M as far as the X-component is concerned (first row of (31)), while it appears explicitly in the definition of $\mathcal{A}_{F,G,M}$ as far as the Y-component is concerned (second row of (32)).

To get a matrix representation of $\mathcal{A}_{F,G,M}$ let us express the collocation polynomial $P_M(\Phi, \Psi)$ in the Lagrange basis (19), i.e.,

$$P_M(\Phi, \Psi)(\theta) = \sum_{j=0}^{M} \ell_{M,j}(\theta)(\Phi_j, \Psi_j), \quad \theta \in [-\tau, 0],$$

where $\Phi_0 = P_{M,X}(\Phi, \Psi)(0)$ is recovered from the first of (31) as

$$\Phi_0 = (I_{d_X} - L_{F,X}\ell_{M,0})^{-1} \left(\sum_{j=1}^{M} L_{F,X}\ell_{M,j}\Phi_j + \sum_{j=0}^{M} L_{F,Y}\ell_{M,j}\Psi_j \right).$$

Note that above we used $L_F\ell_{M,j}(\Phi_j, \Psi_j) = L_{F,X}\ell_{M,j}\Phi_j + L_{F,Y}\ell_{M,j}\Psi_j$ for suitable linear functions $L_{F,X} : X \to \mathbb{R}^{d_X}$ and $L_{F,Y} : Y \to \mathbb{R}^{d_X}$ and any $j = 0, 1, \ldots, M$ by virtue of the linearity of L_F.[14] Then the resulting matrix $\mathcal{A}_{F,G,M}$ is made of an X-block (i.e., the first $d_X M$ rows) given by

$$\mathcal{A}_{F,G,M,X} = D_{X,M,0} \otimes I_{d_X} + (d_{X,M} \otimes I_{d_X}) L_{F,M} \in \mathbb{R}^{d_X M \times d_X M}$$

with $D_{X,M,0} \in \mathbb{R}^{d_X M \times [d_X M + d_Y (M+1)]}$ the matrix whose first $d_X M$ columns coincide with $D_{X,M}$ in (29) and the rest of the entries are zeros, $d_{X,M}$ in (30) and

$$\begin{aligned} L_{F,M} := (I_{d_X} - L_{F,X}\ell_{M,0})^{-1} \\ \begin{pmatrix} L_{F,X}\ell_{M,1} & \cdots & L_{F,X}\ell_{M,M} \\ L_{F,Y}\ell_{M,0} & L_{F,Y}\ell_{M,1} & \cdots & L_{F,Y}\ell_{M,M} \end{pmatrix} \end{aligned} \tag{33}$$

[14] A similar decompoistion is used below for L_G and note 12 applies to all $L_{F,X}$, $L_{F,Y}$, $L_{G,Y}$ and $L_{G,Y}$ with obvious modifications.

in $\mathbb{R}^{d_X\times[d_XM+d_Y(M+1)]}$, and a Y-block (the last $d_Y(M+1)$ rows) given by

$$\mathcal{A}_{F,G,M,Y}=\begin{pmatrix}L_{G,M}\\ D_{Y,M,0}\otimes I_{d_Y}\end{pmatrix}\in\mathbb{R}^{d_Y(M+1)\times[d_XM+d_Y(M+1)]}$$

with

$$\begin{aligned}L_{G,M}:=\big(&L_{G,X}\ell_{M,1} & \cdots & & L_{G,X}\ell_{M,M}\\ &L_{G,Y}\ell_{M,0} & L_{G,Y}\ell_{M,1} & \cdots & L_{G,Y}\ell_{M,M}\big)\end{aligned}\tag{34}$$

in $\mathbb{R}^{d_Y\times[d_XM+d_Y(M+1)]}$ and $D_{Y,M,0}\in\mathbb{R}^{d_YM\times[d_XM+d_Y(M+1)]}$ the matrix whose last $d_Y(M+1)$ columns coincide with $D_{Y,M}$ in (24) and the rest of the entries are zeros.

4.4 Convergence and Other Issues

A complete error analysis for the case of DDEs has been developed in Breda et al. (2005). The general proof relies on translating the eigenvalue problem for $\mathcal{A}_G$ into an IVP for an ODE whose solution is exponential. In parallel, the eigenvalue problem for $\mathcal{A}_{G,M}$ relates to the collocation of the above IVP at the nodes (21). Then the first key step is to measure the error in approximating the exponential solution with the collocation polynomial. It is here that spectral accuracy takes place, as the exponential solution is analytic, and indeed it represents the generic eigenfunction of $\mathcal{A}_G$ (see (Diekmann et al., 1995)). The second step regards the characteristic equations associated to the eigenvalue problems, exact and discrete. Their difference can be linked to the above collocation error and a relevant bound is thus obtained. The last step exploits this bound in the framework of Rouché's Theorem (see, e.g., (Priestley 1990, Theorem 7.7)), which provides a final bound on the distance between an eigenvalue of $\mathcal{A}_G$ and its approximation through eigenvalues of $\mathcal{A}_{G,M}$. The same arguments have been extended to coupled equations in Breda et al. (2015a). A softened version of the final result in the latter case follows, which includes of course the separate cases of DDEs and REs.

Theorem 1 *Let $\lambda\in\sigma(\mathcal{A}_{F,G})$ have algebraic multiplicity ν. There exists $M\in\mathbb{N}$ sufficiently large such that $\mathcal{A}_{F,G,M}$ has ν eigenvalues $\lambda_{M,1},\ldots,\lambda_{M,\nu}$ counted with multiplicities satisfying*

$$\max_{i=1,\ldots,\nu}|\lambda_{M,i}-\lambda|\leq C_2\left(\frac{C_1}{M!}\right)^{M/\nu}\tag{35}$$

for C_1 and C_2 constants depending on λ but independent of M.

The bound (35) ensures a convergence of infinite order[15] from the theoretical standpoint. From the practical one, it is commonly verified that M of the order of few tens

[15] Indeed, Stirling's formula for the factorial shows that the error decays as $O(M^{-M})$.

is enough to get machine accuracy for simple roots, unless the relevant eigenfunction(s) were highly oscillatory. Nevertheless, a couple of delicate issues deserve some attention. On the one hand, the constant C_1 in (35) is proportional to $|\lambda|$, leading to better approximations for eigenvalues of smaller magnitude.[16] This may represent a drawback in some cases since one is rather interested in rightmost roots in view of assessing stability.[17] On the other hand, it is not immediate to accurately estimate the value of M needed to ensure a certain tolerance, as this would lead to solve a nonlinear equation for M which may require more effort than what actually devoted to the approximation itself of the eigenvalues.[18]

We conclude this section by mentioning two other questions one should be aware of when applying a pseudospectral approach as presented in the previous sections in its basic formulation. First of all, the construction of the approximation matrices always requires to evaluate the right-hand side of the relevant class of equations at the Lagrange basis polynomials: see the terms of the form $L_\cdot \ell_{M,\cdot}$ in (23), (28), (33) or (34). In general, it might happen that this evaluation itself asks for numerical approximation, in which case we rather compute $\tilde{L}_\cdot \ell_{M,\cdot}$ and introduce a relevant error $(\tilde{L}_\cdot - L_\cdot)\ell_{M,\cdot}$. A typical case is that of equations involving distributed delays, for which an integral must be treated through a suitable quadrature. As discussed in detail in (Breda et al. (2015b), Sect. 5.3.3), the additional error appears inside the parentheses in (35), so that spectral accuracy takes place down to a barrier determined by the quadrature error. A second question is that of treating efficiently also the presence of multiple delays, in which case a piecewise approach is advisable. The latter simply consists in extending restriction and prolongation operators in order to allow for piecewise polynomials based on a mesh in $[-\tau, 0]$ whose pieces are defined through the multiple delays (or the integration limits of the possible distributed delays). This extension is treated in (Breda et al. (2015b), Sects. 5.2 and 5.4) for DDEs, and in Breda et al. (2015a) for coupled equations in view, e.g., of population dynamics structured by age and thus with individuals divided into, e.g., juveniles and adults cohorts.

5 Extension to Nonlinear Problems

The content of this section is a summary of what illustrated in detail in Breda et al. (2016a). To understand why such an extension is possible, and furthermore natural, it is enough to apply the general idea of the pseudospectral approach as described at the beginning of Sect. 4 to the infinitesimal generator of the semigroup describing the original *nonlinear* delay equation. As recalled in Sect. 2.4, indeed, the notions of semigroup and generator extend straightforwardly to the nonlinear case. As antici-

[16] Here "better" means that smaller values of M are required to reach a given tolerance.

[17] Some work in this direction for DDEs can be found in Wu and Michiels (2012).

[18] Although some indications are given in Breda et al. (2005), these may appear a little conservative and however a precise answer to the issue of choosing M is not available yet.

pated in the introduction, the final goal is that of obtaining a finite-dimensional system of ODEs approximating (1) in order to perform a potentially complete dynamical analysis through existing continuation and bifurcation software.

Consider then (1) and assume that F and G guarantee the IVP with $(x_0, y_0) = (\varphi, \psi)$ for some $(\varphi, \psi) \in X \times Y$ to be well posed. Let $T(t) : X \times Y \to X \times Y$ be the solution operator defined as

$$T(t)(x_0, y_0) = (x_t, y_t), \quad t \geq 0,$$

and let

$$\mathcal{A}(\varphi, \psi) = (\varphi', \psi'), \quad (\varphi, \psi) \in \mathcal{D}(\mathcal{A}),$$

be the infinitesimal generator of the relevant semigroup, with domain

$$\begin{aligned} \mathcal{D}(\mathcal{A}) := \{(\varphi, \psi) \in X \times Y \ : \ & (\varphi, \psi) \in X \times Y \text{ and} \\ & (\varphi(0), \psi'(0)) = (F(\varphi, \psi), G(\varphi, \psi))\}. \end{aligned} \tag{36}$$

Note that $\mathcal{A}$ has linear (derivative) action but nonlinear domain. Through $\mathcal{A}$ we can equivalently describe the IVP in the abstract ordinary form

$$\begin{cases} \frac{\mathrm{d}}{\mathrm{d}t}(u(t), v(t)) = \mathcal{A}(u(t), v(t)), & t \geq 0, \\ (u(0), v(0) = (\varphi, \psi), \end{cases} \tag{37}$$

the correspondence relying on $(u(t), v(t)) = (x_t, y_t)$, which holds strictly when $(\varphi, \psi) \in \mathcal{D}(\mathcal{A})$, otherwise in a mild sense being $\mathcal{D}(\mathcal{A})$ dense in $X \times Y$ Engel and Nagel (1999).

The pseudospectral reduction of the abstract[19] ODE in (37) to a finite-dimensional system of ODEs is based on adapting the discretization procedure illustrated in Sect. 4.3, in particular by considering (31) and (32) with the nonlinear functions F and G replacing the linear(ized) versions L_F and L_G. This leads to a discrete version of $\mathcal{A}$ and, consequently, to the system of $d_X M + d_Y(M + 1)$ ODEs

$$\begin{cases} U'(t) = D_{X,M} U(t) + d_{X,M} U_0(t) \\ V_0'(t) = G(P_M(U(t), V(t)) \\ V'(t) = D_{Y,M} V(t), \end{cases} \tag{38}$$

where U_0 is obtained from

$$U_0(t) = F(P_M(U(t), V(t)) \tag{39}$$

as a function of the unknowns $U(t) := (U_1(t), \ldots, U_M(t))^T \in \mathbb{R}^{d_X M}$ and $V(t) := (V_0(t), V_1(t), \ldots, V_M(t))^T \in \mathbb{R}^{d_Y(M+1)}$. Above, $D_{X,M}$, $d_{X,M}$ and $D_{Y,M}$ are given

[19] Here the term "abstract" refers to the infinite-dimensional state space on which the ODE is posed.

respectively by (29), (30) and (24). In the spirit of the pseudospectral approach, the components $U_i(t)$ and $V_i(t)$ for all $i = 0, 1, \ldots, M$ are meant as approximations to $x(t + \theta_i) = x_t(\theta_i) = u(t)(\theta_i)$ and $y(t + \theta_i) = y_t(\theta_i) = v(t)(\theta_i)$, respectively. Again, as in the linear case of Sect. 4, the boundary condition characterizing $\mathcal{D}(\mathcal{A})$ in (36) is imposed implicitly through (39) for the X-component and explicitly through the second of (38) for the Y-component. Note that most of (38) can be written (and hence implemented) independently of the specific right-hand sides F and G, highlighting once more the different roles of the derivative action of $\mathcal{A}$ and of the boundary condition describing $\mathcal{D}(\mathcal{A})$. Finally, observe that (39) can be solved explicitly[20] for U_0 if the dependence of F from the X-component of the state is linear: this is the case, e.g., of several models from population dynamics (Diekmann et al. 2010).

6 Implementation and Results

In the following sections we provide four examples of applications of the pseudospectral collocation presented in this chapter, respectively about a DDE in Sect. 6.1, an RE in Sect. 6.2, a coupled equation in Sect. 6.3 and a last DDE in Sect. 6.4 concerning the nonlinear approach. In each section we describe some relevant implementation issues. All the following computations are performed on a MacBook Pro 2.3GHz Intel Core i7 16GB by using Matlab R2019a. A demo (`demo`) including scripts to run the codes relevant to the following tests is freely available at http://cdlab.uniud.it/software.

6.1 Example 1: A Delay Differential Equation.

Consider the celebrated Mackey-Glass equation (Mackey and Glass 1977)

$$y'(t) = \frac{\beta y(t-\tau)}{1 + y(t-\tau)^\alpha} - \gamma y(t) \tag{40}$$

with $\alpha, \beta, \gamma \geq 0$ and $\tau > 0$. It is not difficult to recover the nontrivial equilibrium

$$\bar{y} := \left(\frac{\beta}{\gamma} - 1\right)^{1/\alpha},$$

which exists for $\beta \geq \gamma$ and $\alpha > 0$. Linearization leads to

[20] Recall in fact that P_M (and hence U_0) is defined only implicitly through the first of (31) (with F replacing L_F).

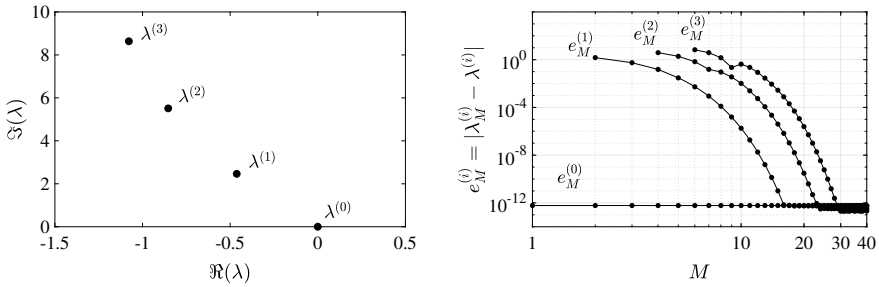

Fig. 2 Results on Example 1 with $\alpha = 0$, description in the text

$$y'(t) = ay(t) + by(t - \tau)$$

with

$$a = -\gamma, \qquad b = \beta \cdot \frac{1 + (1 - \alpha)\bar{y}^{\alpha}}{(1 + \bar{y}^{\alpha})^2}.$$

The discretized generator takes the form (22) with first row

$$L_{G,M} := \begin{pmatrix} a & 0 & \cdots & 0 & b \end{pmatrix} \in \mathbb{R}^{1\times(M+1)}$$

according to (23). All is implemented in three lines of code, namely lines 37-39 in the code `example1`, where the matrix $D_{Y,M}$ in (24) is obtained with the auxiliary function `cheb` taken from Trefethen (2000). The rest of `example1` concerns the computation of the eigenvalues of $\mathcal{A}_{G,M}$ through `eig` and the ordering of the eigenvalues by decreasing real part (lines 42-44).

Let us choose $\beta = 2, \gamma = 1$ and $\tau = 2$. We get $\bar{y} = 1, a := -1$ and $b := 1 - \alpha/2$. The relevant characteristic equation reads[21]

$$\lambda - a - be^{-\lambda\tau} = \lambda + 1 - \left(1 - \frac{\alpha}{2}\right) e^{-2\lambda} = 0.$$

As $\bar{y} = 1$, we can consider also the limit case $\alpha = 0$, for which it is not difficult to show that $\lambda = 0$ is the rightmost characteristic root. Figure 2 confirms the result: a few rightmost eigenvalues are shown in the left panel, computed with $M = 40$, with relevant errors shown in the right panel for increasing M.[22] Observe the spectral accuracy taking place in the right panel, with the role played by the constant C_1 in (35) as described in Sect. 4.4. In particular, the rightmost root $\lambda = 0$ is computed at very high accuracy already with $M = 1$.

[21] Just replace formally $y(t)$ in (40) with $e^{\lambda t}$.

[22] Apart from the rightmost root $\lambda = 0$, we use as reference values for the other roots those computed with a very large value of M, viz. $M = 1000$. The same comment holds also for the other examples.

A second rapid test is then executed by choosing $\alpha = 2$. This is a special choice as the linearized DDE reduces to the ODE $y'(t) = ay(t)$, and so the only eigenvalue is $\lambda = a = -1$. Indeed, we get $\lambda_M = -1$ at machine precision already with $M = 5$.

6.2 Example 2: A Renewal Equation

Consider the nonlinear RE

$$x(t) = \frac{\gamma}{2} \int_{-3}^{-1} x(t+\theta)[1 - x(t+\theta)]\, \mathrm{d}\theta$$

taken from (Breda et al. (2016b), Appendix A). Assume $\gamma > 0$. It is not difficult to recover the nontrivial equilibrium $\bar{x} := 1 - 1/\gamma$, which exists positive only for $\gamma > 1$ and vanishes at $\gamma = \gamma_T := 1$, the latter value representing a transcritical bifurcation. It is shown in (Breda et al. (2016b), Appendix A) that $\bar{x}$ exists stable until $\gamma = \gamma_H := 2(1 + \pi/4)$, value at which a Hopf bifurcation takes place and a periodic solution arises. Let us confirm these two bifurcations by the pseudospectral collocation of the infinitesimal generator of the linearized equation. The latter reads[23]

$$x(t) = c \int_{-3}^{-1} x(t+\theta)\, \mathrm{d}\theta$$

for $c := 1 - \gamma/2$. As the delay is distributed on the interval $[-3, -1]$, it is convenient to adopt a piecewise discretization based on a mesh of nodes $\Omega_{M_1} \cup \Omega_{M_2}$ with Ω_{M_1} made of the Chebyshev extrema in $[-1, 0]$ and Ω_{M_2} made of the Chebyshev extrema in $[-3, -1]$. In the code `example2` we choose M_1 and M_2 proportional to the lengths of the relevant intervals (lines 36-37), even though other choices are possible (e.g., proportional to the error bounds from (35)). The relevant differentiation matrices are computed again through the auxiliary function `cheb` (lines 38-39), while a second auxiliary function, namely `clencurt` again from Trefethen (2000), provides the quadrature weights (line 40) based on the Clenshaw-Curtis formula, i.e., the one using the Chebyshev extrema as quadrature nodes. Note that only the weights on the second delay interval $[-3, -1]$ are needed, where the distributed delay term is defined. We avoid to give full details of the piecewise approach,[24] rather we limit ourselves to describe the case of this specific example, as we believe it contains all the main ingredients. Indeed, it is enough to realize that the boundary condition characterizing $\mathcal{D}(\mathcal{A})$ in (10) affects only the polynomial in the first delay interval $[-1, 0]$ (the one containing 0), so that the first of (26) gives rise to $L_{F,M}$ in (28) where the application of L_F vanishes on $[-1, 0]$ and takes place only on $[-3, -1]$. In the latter, the integral

[23] Concerning linerization of REs see ((Diekmann et al., 2008), Sect. 3.5).

[24] For a complete treatment see Breda et al. (2015a).

$$L_F \ell^{(2)}_{M_2,j} = c \int_{-3}^{-1} \ell^{(2)}_{M_2,j}(\theta)\,\mathrm{d}\theta$$

is approximated by the Clenshaw-Curtis formula[25] as

$$\tilde{L}_F \ell^{(2)}_{M_2,j} = c \sum_{k=0}^{M_2} w^{(2)}_{M_2,k} \ell^{(2)}_{M_2,j}(\theta^{(2)}_{M_2,k}) = c w^{(2)}_{M_2,j}$$

thanks to the cardinal properties of the Lagrange basis. This corresponds to lines 41 and 44 in the code. The rest (lines 42, 43 and 45) implements the differentiation part of $\mathcal{A}_{F,M}$ in (27), which has a block-diagonal structure due to the piecewise strategy.

Running the code `example2` with $\gamma = \gamma_T$ and $M = 20$ gives back a rightmost root which is 0 to machine precision, confirming the transcritical bifurcation. By using $\gamma = \gamma_H$ and again $M = 20$ we obtain a rightmost couple $0.000000049143744 \pm 1.570796291925258\mathrm{i}$, with an error of about 6×10^{-8} with respect to the exact couple $\pm\mathrm{i}\pi/2$.[26] Eventually, by increasing M to 40 the rightmost couple is approximated to machine precision. We avoid to report on convergence as the relevant figures would not differ from Fig. 2 (right) given that spectral accuracy takes place again.[27]

6.3 *Example 3: A Coupled Equation.*

Consider from (Breda et al. (2013), Sect. 5.2) the age-structured coupled equation

$$\begin{cases} x(t) = \beta y(t) \displaystyle\int_{\bar{a}}^{a_{\max}} x(t-a)\,\mathrm{d}a \\ y'(t) = r y(t) \left(1 - \dfrac{y(t)}{K}\right) - \gamma y(t) \displaystyle\int_{\bar{a}}^{a_{\max}} x(t-a)\,\mathrm{d}a, \end{cases}$$

which models the birth rate x of a consumer species feeding on a resource y, the latter evolving according to a logistic growth in absence of the former. Let all the parameters be non-negative and assume $a_{\max} > \bar{a} \geq 0$, denoting respectively the maximum and maturation ages of the consumer individuals. It is not difficult to recover the nontrivial equilibrium

$$(\bar{x}, \bar{y}) := \left(\frac{r}{\gamma(a_{\max} - \bar{a})} \left(1 - \frac{1}{K\beta(a_{\max} - \bar{a})}\right), \frac{1}{\beta(a_{\max} - \bar{a})} \right)$$

[25] Formally, a coefficient $(\tau_2 - \tau_1)/2 = 1$ (for $\tau_1 = 1$ and $\tau_2 = 3$) should appear in front of the sum as the weights are referred to the normalized integration interval $[-1, 1]$.

[26] It is left as an exercise to verify that this is indeed the rightmost couple (hint: write the characteristic equation and split it into real and imaginary parts).

[27] For the smoothness of eigenfunctions of $\mathcal{A}_F$ see ((Breda and Liessi, 2020), Sect. 5).

beyond the trivial one $(0, 0)$ and the single-species one $(0, K)$. Note that $(\bar{x}, \bar{y})$ exists positive only for $\beta > 1/[K(a_{\max} - \bar{a})]$ and it reduces to $(0, K)$ when $\beta = \beta_T := 1/[K(a_{\max} - \bar{a})]$. The latter represents a transcritical bifurcation. In (Breda et al. (2013), Sect. 5.2) it is also shown that $(\bar{x}, \bar{y})$ exists stable until $\beta = \beta_H \approx 3.0162$,[28] value at which a Hopf bifurcation takes place and a periodic solution arises. As for Example 2, let us numerically confirm these two bifurcations. The linearization leads to

$$\begin{cases} x(t) = a_x y(t) + c_x \displaystyle\int_{-\tau_2}^{-\tau_1} x(t+\theta)\,\mathrm{d}\theta \\ y'(t) = a_y y(t) + c_y \displaystyle\int_{-\tau_2}^{-\tau_1} x(t+\theta)\,\mathrm{d}\theta \end{cases}$$

for

$$a_x := \beta(a_{\max} - \bar{a})\bar{x}, \qquad c_x := \beta\bar{y},$$

$$a_y := r(1 - 2\bar{y}/K) - \gamma(a_{\max} - \bar{a})\bar{x}, \qquad c_y := -\gamma\bar{y},$$

$\tau_2 := a_{\max}$ and $\tau_1 := \bar{a}$. Given the distributed delay term acting only on $[-\tau_2, -\tau_1]$, we adopt the same piecewise approach used for the RE in Example 2. In this respect, the structure of the code `example3` should be self-explanatory. It is enough to consider properly the terms (33) (lines 48-49 and 54) and (34) (lines 50-51 and 56) relevant to the boundary condition characterizing (13). Then the block-diagonal structure relevant to the differentiation part already seen in the code `example2` for the RE (lines 53 and 55) is replicated also for the DDE (with M_2 replacing M_1, lines 57-58).

Let us fix $r = \gamma = K = 1$, $a_{\max} = 4$ and $\bar{a} = 3$. Running the code `example3` with $\beta = \beta_T = 1$ and $M = 20$ gives back a rightmost root which is 0 to machine precision, confirming the transcritical bifurcation. By using $\beta = \beta_H = 3.01619677726\,1349$ and again $M = 20$ we obtain a rightmost couple $-0.000000002223957 \pm 0.398673660634495$i. Eventually, by increasing M to 200 the rightmost couple becomes $0.000000000000041 \pm 0.398673660102389$i, confirming a Hopf bifurcation within an accuracy of about 13 digits.

6.4 Example 4: The Nonlinear Approach for a Delay Differential Equation

Consider the delay logistic equation

$$y'(t) = ry(t)[1 - y(t-1)],$$

[28] This value is approximated in Breda et al. (2013) by a pseudospectral approach slightly different from the one proposed here, difference due to an alternative treatment of the boundary condition in (10).

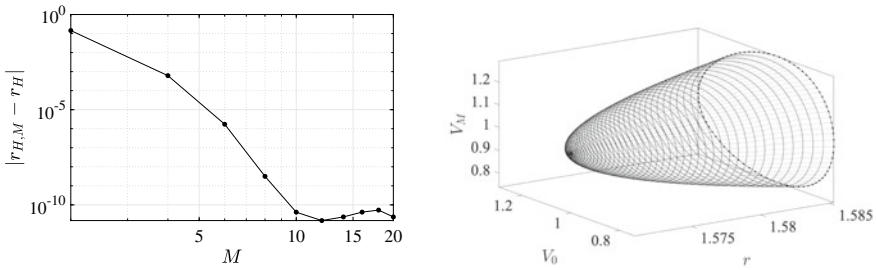

Fig. 3 Results on Example 4, description in the text

known also as the Hutchinson's equation Hutchinson 1948. It has the nontrivial equilibrium $\bar{y} := 1$ independently of the growth parameter r, which we assume to be positive. It is not difficult to prove that $\bar{y}$ is (locally) asymptotically stable for $r \in (0, \pi/2)$ via linearization. At $r = r_H = \pi/2$ a Hopf bifurcation arises. Here we want to confirm the result without resorting to linearization, neither analytically nor numerically, but rather applying the pseudospectral approach of Sect. 5 directly to the nonlinear equation. The resulting approximating system of $M + 1$ ODEs reads

$$\begin{cases} V_0'(t) = r V_0(t)[1 - V_M(t)] \\ V'(t) = D_{Y,M} V(t), \end{cases} \tag{41}$$

for $D_{Y,M}$ as in (24). The code `example4` contains the definition of the right-hand side of (41) in view of using it within `MatCont` Dhooge et al. (2008). This right-hand side depends on the numerical parameter M, as well as on the growth rate r, with respect to which we want to perform the bifurcation analysis. The demo file `demo` contains all the necessary instructions to run the continuation for a given value of M, including the initialization of `MatCont` and the setting of its options, among which we fix all the tolerances to 10^{-10}. In Fig. 3 (left) we plot the error $|r_{H,M} - r_H|$ with respect to increasing $M = 2, 4, \ldots, 20$, with $r_{H,M}$ representing the Hopf bifurcation value returned by MatCont for the chosen value of M. Note, once more, the expected spectrally accurate behavior, at least down to 10^{-10}, a barrier indeed imposed by the tolerances set for `MatCont`. In Fig. 3 (right) we show also an initial continuation of the limit cycle arising from the Hopf point (obtained with $M = 5$ and 50 continuation points). The relevant instructions are always contained in the demo file `demo`. Note that the represented coordinates (V_0, V_M) refer to (41) and give an approximated representation of the true cycle in the projected state space $(\psi(0), \psi(-1))$ for $\psi \in Y$ (recall indeed that $V_0(t) \approx y(t)$ and $V_M(t) \approx y(t-1)$). To give just a reference, running all Example 4 with $M = 5$ requires less than 1 s to continue the equilibrium and about 16 s to continue the limit cycle.[29]

[29] We did not report on the CPU time for the preceding examples as the computation of the eigenvalues is practically instantaneous.

7 Conclusions

A general pseudospectral collocation approach to approximate the infinitesimal generator of the semigroup of delay equations has been illustrated. The technique can be used for the local stability analysis of equilibria of DDEs, REs and systems of coupled REs and DDEs through the principle of linearized stability, as well as to perform a bifurcation analysis through continuation directly on the nonlinear instances of the same classes of equations. Independently of which case or class, the approach has been described from the points of view of discretization, convergence, implementation and application. Where not all the details have been included (as, e.g., the proofs of convergence), suitable references have been provided for those interested in deepen their study of the subject. Eventually, relevant codes are made freely available at http://cdlab.uniud.it/software.

Pseudospectral collocation is not new of course, dating back to pioneering works on Partial Differential Equations (PDEs) (see, e.g., Gottlieb and Orszag 1977 and the references therein). Its application to delay equations has revealed rather robust and flexible in the last 15 years starting from Breda (2004) or Butcher et al. (2004). Beyond the (autonomous) cases treated here, it is worthy to mention more recent studies that have not found room in this chapter, concerning in particular the case of infinite delay Gyllenberg et al. 2018, that of state-dependent delays Getto et al. 2019 or still the case of models with multiple structuring variables formulated as PDEs Scarabel et al. 2020. A last class of problems, that of time-dependent (and especially time-periodic) delay equations, is adequately treated in Breda (2023), where the pseudospectral collocation is used to approximate directly the semigroup rather than its generator. This alternative approach appears perhaps less immediate, but it is certainly more general as far as the linearized analysis is concerned, as it goes well beyond the case of equilibria.

Finally, we remark once more that by no way the pseudospectral approach represents the only solution to the numerical stability analysis of delay equations, nor the most efficient one, or at least it is not so in view of the generality of cases it can deal with.[30] In the end, the great advantage it offers is precisely its flexibility in front of this generality, beyond the fact that, as any other spectral method, it is able to fully exploit the (potentially infinite) smoothness made available when solving eigenvalue problems.

[30] Starting references to other techniques (and there are quite many of them nowadays) have been given in the introduction.

References

Ambrosetti, A., & Prodi, G. (1995). *A Primer of Nonlinear Analysis*. Cambridge Studies in Advanced Mathematics (Vol. 34). New York: Cambridge University Press.

Andò, A., Breda, D., Liessi, D., Maset, S., Scarabel, F., & Vermiglio, R. (2022) 15 years or so of pseudospectral collocation methods for stability and bifurcation of delay equations. In G. Valmorbida, W. Michiels, & P. Pepe (Eds.), *Incorporating constraints on the Analysis of Delay and Distributed Parameter Systems, Advaced Delays Dynamic Series* (pp. 127–323). Springer. https://link.springer.com/chapter/10.1007/978-3-030-89014-8_7

Batkai, A., & Piazzera, S. (2005). *Semigroups for Delay Equations*. Number 10 in Research Notes in Mathematics. Canada: A K Peters Ltd.

Bellen, A., Guglielmi, A., Maset, S., & Zennaro, M. (2009). Recent trends in the numerical solution of retarded functional differential equations. *Acta Numerica, 18*, 1–110.

Bellen, A., & Zennaro, M. (2003). *Numerical Methods for Delay Differential Equations*. Numerical Mathemathics and Scientifing Computing Series. Oxford University Press.

Berrut, J. P., & Trefethen, L. N. (2004). Barycentric Lagrange interpolation. *SIAM Review, 46*(3), 501–517.

Breda, D. (2004). *Numerical Computation of Characteristic Roots for Delay Differential Equations*. Ph.D. thesis, Ph.D. in Computational Mathematics, Università di Padova.

Breda, D. (2010). Nonautonomous delay differential equations in Hilbert spaces and Lyapunov exponents. *Differential and Integral Equations, 23*(9–10), 935–956.

Breda, D. (2023). Pseudospectral methods for the stability analysis of delay equations. Part II: the solution operator approach. In D. Breda (Ed.), *Controlling Delayed Dynamics: Advances in Theory Methods and Applications, CISM Lecture Notes* (pp. 95–116). Wien-New York: Springer.

Breda, D., & Liessi, D. (2020). Floquet theory and stability of periodic solutions of renewal equations. *Journal of Dynamics and Differential Equations*. https://doi.org/10.1007/s10884-020-09826-7.

Breda, D., Maset, S., & Vermiglio, R. (2005). Pseudospectral differencing methods for characteristic roots of delay differential equations. *Journal on Scientific Computing, 27*(2), 482–495.

Breda, D., Diekmann, O., Maset, S., & Vermiglio, R. (2013). A numerical approach for investigating the stability of equilibria for structured population models. *Journal of Biological Dynamics, 7*(1), 4–20.

Breda, D., Getto, P., Sánchez Sanz, J., & Vermiglio, R. (2015a). Computing the eigenvalues of realistic Daphnia models by pseudospectral methods. *SIAM Journal on Scientific Computing, 37*(6), 2607–2629.

Breda, D., Maset, S., & Vermiglio, R. (2015b). *Stability of Linear Delay Differential Equations—A Numerical Approach with MATLAB*. SpringerBriefs in Control, Automation and Robotics. New York: Springer.

Breda, D., Diekmann, O., Gyllenberg, M., Scarabel, F., & Vermiglio, R. (2016). Pseudospectral discretization of nonlinear delay equations: New prospects for numerical bifurcation analysis. *SIAM Journal on Applied Dynamical Systems, 15*(1), 1–23.

Breda, D., Diekmann, O., Liessi, D., & Scarabel, F. (2016). Numerical bifurcation analysis of a class of nonlinear renewal equations. *Electronic Journal of Qualitative Theory of Differential Equations, 65*, 1–24.

Brunner, H. (2004). *Collocation Methods for Volterra Integral and Related Functional Differential Equations*. Number 15 in Cambridge monographs on applied and computational mathematics. Cambridge: Cambridge University Press.

Butcher, E. A., Ma, H. T., Bueler, E., Averina, V., & Szabo, Z. (2004). Stability of linear time-periodic delay-differential equations via Chebyshev polynomials. *International Journal for Numerical Methods in Engineering, 59*, 895–922.

Dhooge, A., Govaerts, W. J. F., & Kuznetsov, Y. A. (2003). MatCont: A MATLAB package for numerical bifurcation analysis of ODEs. *ACM Transactions on Mathematical Software, 29*(2), 141–164.

Dhooge, A., Govaerts, W. J. F., Kuznetsov, Y. A., Meijer, H. G. E., & Sautois, B. (2008). New features of the software MatCont for bifurcation analysis of dynamical systems. *Mathematical and Computer Modelling of Dynamical Systems, 14*(2), 147–175.

Diekmann, O., van Gils, S.A., Verduyn Lunel, S.M., Walther, H.O. (1995). *Delay Equations—Functional, Complex and Nonlinear Analysis*. Number 110 in Applied Mathematical Sciences. New York: Springer.

Diekmann, O., Getto, P., & Gyllenberg, M. (2008). Stability and bifurcation analysis of Volterra functional equations in the light of suns and stars. *Journal on Mathematical Analysis, 39*(4), 1023–1069.

Diekmann, O., Gyllenberg, M., Metz, J. A. J., Nakaoka, S., & de Roos, A. M. (2010). Daphnia revisited: Local stability and bifurcation theory for physiologically structured population models explained by way of an example. *Journal of Mathematical Biology, 61*(2), 277–318.

Doedel, E. (1981). AUTO: a program for the automatic bifurcation analysis of autonomous systems. In *Proceedings of the Tenth Manitoba Conference on Numerical Mathematics and Computing* (vol. I, pp. 265–284), Winnipeg, Man.

Doedel, E. (2007). Lecture notes on numerical analysis of nonlinear equations. In H.M. Osinga, B. Krauskopf, & J. Galán-Vioque, (Eds.), *Numerical Continuation Methods for Dynamical Systems*, Understanding Complex Systems (pp. 1–49). Springer.

Engel, K., & Nagel, R. (1999). *One-Parameter Semigroups for Linear Evolution Equations*. Number 194 in Graduate Texts in Mathematics. New York: Springer.

Ermentrout, B. (2002). *Simulating, Analyzing, and Animating Dynamical Systems-A Guide to XPPAUT for Researchers and Students*. Software—Environment—Tools seriesPhiladelphia: SIAM.

Faber, George. (1914). Über die interpolatorische darstellung stetiger funktionen. *Jahresber. Deut. Math. Verein., 23*, 192–210.

Getto, P., Gyllenberg, M., Nakata, Y., & Scarabel, F. (2019). Stability analysis of a state-dependent delay differential equation for cell maturation: Analytical and numerical methods. *Journal of Mathematical Biology, 79*(1), 281–328.

Gottlieb, D., & Orszag, S. (1977). *Numerical Analysis of Spectral Methods: Theory and Applications*. CBMS-NSF Regional Conference Series in Applied Mathematics (Vol. 26). Philadelphia: SIAM.

Gyllenberg, M., Scarabel, F., & Vermiglio, R. (2018). Equations with infinite delay: numerical bifurcation analysis via pseudospectral discretization. *Applied Mathematics and Computation, 333*, 490–505.

Halem, J.K. (1977). *Theory of Functional Differential Equations*. Number 99 in Applied Mathematical Sciences, 1st edn. New York: Springer.

Hale, J.K., & Verduyn Lunel, S.M. (1993). *Introduction to Functional Differential Equations*. Number 99 in Applied Mathematical Sciences, 2nd edn. New York: Springer.

Hutchinson, G. E. (1948). Circular causal systems in ecology. *Annals of the New York Academy of Sciences, 50*, 221–246.

Inaba, H. (2017). *Age-Structured Population Dynamics in Demography and Epidemiology*. New York: Springer.

Insperger, T., & Stépán, G. (2011). *Semi-Discretization for Time-Delay Systems—Stability and Engineering Applications*. Number 178 in Applied Mathematical Sciences. New York: Springer.

Lehotzky, D., & Insperger, T. (2016). A pseudospectral tau approximation for time delay systems and its comparison with other weighted-residual-type methods. *International Journal for Numerical Methods in Engineering, 108*(6), 588–613.

Mackey, M. C., & Glass, L. (1977). Oscillations and chaos in physiological control systems. *Science, 197*, 287–289.

Michiels, W. (2023). Design of structured controllers for linear time-delay systems. In D. Breda (Ed.), *Controlling Delayed Dynamics: Advances in Theory, Methods and Applications, CISM Lecture Notes* (pp. 247–288). Wien-New York: Springer.

Michiels, W., & Niculescu, S. I. (2014). *Stability, Control, and Computation for Time-Delay Systems. An Eigenvalue Based Approach*. Number 27 in Advances in Design and Control. Philadelphia: SIAM.

Pazy, A. (1983). *Semigroups of Linear Operators and Applications to Partial Differential Equations*. Number 44 in Applied Mathematical Sciences. New York: Springer.

Priestley, H. A. (1990). *Introduction to Complex Analysis*. New York: Oxford University Press.

Rivlin, T. (1981). *An Introduction to the Approximation of Functions*. New York: Dover.

Scarabel, F., Breda, D., Diekmann, O., Gyllenberg, M., & Vermiglio, R. (2020). Numerical bifurcation analysis of physiologically structured population models via pseudospectral approximation. *Vietnam Journal of Mathematic, 2020*. To appear.

Trefethen, L. N. (2000). *Spectral Methods in MATLAB*. Software—Environment—Tools SeriesPhiladelphia: SIAM.

Trefethen, L. N. (2013). *Approximation Theory and Approximation Practice*. Number 128 in Other Titles in Applied Mathematics. Philadelphia: SIAM.

Verudyn Lunel, S. M. (2023). The twin semigroup approach towards periodic neutral delay equations. In D. Breda (Ed.), *Controlling Delayed Dynamics: Advances in Theory, Methods and Applications*, *CISM Lecture Notes* (pp. 1–36). Wien-New York: Springer.

Weideman, J. A., & Reddy, S. C. (2000). A MATLAB differentiation matrix suite. *ACM Transactions on Mathematical Software, 26*(4), 465–519.

Wu, Z., & Michiels, W. (2012). Reliably computing all characteristic roots of delay differential equations in a given right half plane using a spectral method. *Journal of Computational and Applied Mathematics, 236*, 2499–2514.

Pseudospectral Methods for the Stability Analysis of Delay Equations. Part II: The Solution Operator Approach

Dimitri Breda

Abstract Delay equations generate dynamical systems on infinite-dimensional state spaces. Their stability analysis is not immediate and reduction to finite dimension is often the only chance. Numerical collocation via pseudospectral techniques recently emerged as an efficient solution. In this part we analyze the application of these methods to discretize the evolution family associated to linear problems. The focus is on local stability of either equilibria and periodic orbits as well as on generic nonautonomous systems, for either delay differential and renewal equations.

1 Introduction

In this chapter we deal again with *delay equations*, for an introduction of which we refer to Breda (2023, Sect. 1) to avoid repetitions. Here we limit ourselves to recall the general instance we are concerned with. Let X and Y be spaces of real, possibly vector-valued functions defined on $[-\tau, 0]$, $\tau > 0$ being the maximum and bounded delay of the system. The classical choices we consider are the Banach spaces of functions

$$X := L^1([-\tau, 0]; \mathbb{R}^{d_X}), \qquad \|\varphi\|_X := \int_{-\tau}^{0} |\varphi(\theta)| \, \mathrm{d}\theta \tag{1}$$

and

$$Y := C([-\tau, 0]; \mathbb{R}^{d_Y}), \qquad \|\psi\|_Y := \max_{\theta \in [-\tau, 0]} |\psi(\theta)|, \tag{2}$$

Dimitri Breda is member of INdAM Research group GNCS and of UMI Research group "Modellistica socio-epidemiologica". His work was partially supported by the Italian Ministry of University and Research (MUR) through the PRIN 2020 project (No. 2020JLWP23) "Integrated Mathematical Approaches to Socio-Epidemiological Dynamics" (CUP: E15F21005420006).

D. Breda (✉)
CDLab - Computational Dynamics Laboratory, Department of Mathematics, Computer Science and Physics, University of Udine, Udine, Italy
e-mail: dimitri.breda@uniud.it

D. Breda (ed.), *Controlling Delayed Dynamics*, CISM International Centre for Mechanical Sciences 604, https://doi.org/10.1007/978-3-031-01129-0_4

where $|\cdot|$ is a norm in either $\mathbb{R}^{d_X}$ or $\mathbb{R}^{d_Y}$ (see, e.g., Diekmann et al. 2008), with d_X and d_Y positive integers counting the number of renewal and differential equations, respectively the X- and Y-components. The general form of so-called *coupled* equation we have in mind reads

$$\begin{cases} x(t) = F(x_t, y_t) \\ y'(t) = G(x_t, y_t) \end{cases} \tag{3}$$

for t denoting time and $F : X \times Y \to \mathbb{R}^{d_X}$ and $G : X \times Y \to \mathbb{R}^{d_Y}$ being smooth, autonomous, in general nonlinear functions defined on a state space $X \times Y$, according to the time translation

$$x_t(\theta) := x(t+\theta), \quad y_t(\theta) := y(t+\theta), \qquad \theta \in [-\tau, 0], \tag{4}$$

defining the state (x_t, y_t) at time t. We assume F to be integral in the X-component. In the sequel we mostly treat in detail the case of Delay Differential Equations (DDEs), viz.

$$y'(t) = G(y_t), \tag{5}$$

commenting then on the extension to Renewal Equations (REs), viz.

$$x(t) = F(x_t), \tag{6}$$

and to coupled equations (3). In (5) and (6) the definitions of F and G are suitably adapted.

The original motivation behind the solution operator approach we discuss in this chapter is to be found in the local stability analysis of periodic orbits of nonlinear equations, whose existence is given as granted. The stability analysis of periodic orbits is a natural task following the stability analysis of equilibria and their bifurcation (see, e.g., Krauskopf and Sieber 2023 for an illustration of the natural path of dynamical analysis also beyond this single step). Determining the local stability of equilibria is the focus of Breda (2023), for which the infinitesimal generator approach illustrated therein has been developed. In view again of the principle of linearized stability, we deal with linear problems with time periodic coefficients. As far as the latter are concerned, Floquet theory suggests to focus on the so-called *monodromy operator*, i.e., the operator advancing the evolution of the system of one period. Then the asymptotic stability of the zero solution of the liner periodic system is dictated by the position with respect to the unit circle of the eigenvalues of this operator, the so-called *Floquet multipliers*. Discretizing the monodromy operator is therefore crucial in view of approximating (part of) its spectrum, thus furnishing suitable numerical schemes to address the stability of periodic orbits of the original nonlinear problem (at least in the *hyperbolic* case, see below). Floquet theory is available since long for DDEs, together with the principle of linearized stability for periodic orbits based on relevant Poincaré sections and maps (see, e.g., Diekmann et al. 1995, Chaps. XIII

and XIV). The same tools have been provided for REs only recently (Breda and Liessi 2020a). Instead, rigorous proofs for coupled problems are still lacking, yet under investigation (by D. Liessi and the author himself), even though it is fairly reasonable to expect that similar results hold true (as we assume in the following).

In this chapter we describe the discretization based on the use of *pseudospectral collocation*. Originally proposed for DDEs first in Breda et al. (2006) and then fully developed in Breda et al. (2012), it has been extended to REs in Breda and Liessi (2018) and further to coupled equations in Breda and Liessi (2020b). All the resulting techniques rely on a preliminary reformulation of the monodromy operator, which holds unchanged also for any other element of the relevant *evolution family*, i.e., for the general evolution operator $T(t, s)$ advancing at time $t \geq s$ the state given at any initial time s. If the monodromy operator reads indeed $T(\omega, 0)$ for ω the period of the concerned periodic orbit, the discretization of $T(h, 0)$ for any stepsize h relevant to autonomous problems leads to a class of methods to address the local stability of equilibria, hence an alternative to the infinitesimal generator approach discussed in Breda (2023). Finally, the discretization of the elements of the sequence $\{T(n\tau, (n-1)\tau)\}_{n\in\mathbb{N}}$ reveals to be essential in computing Lyapunov exponents, thus addressing the generic nonautonomous case, where with the term "generic" we identify time-dependent problems explicitly excluding the constant and periodic cases. Results on the numerical computation of Lyapunov exponents appear in Breda and Van Vleck (2014) for DDEs and only marginally in Breda et al. (2016b) for REs. In fact, a systematic approach to tackle both REs and coupled equations has not been fully developed yet. Finally, by no means the pseudospectral collocation technique is meant to be the only choice for discretizing evolution operators. Other more or less similar approaches have been proposed in the literature, among which we mention the recent work Borgioli et al. (2020), in which one can find also a reference bibliography on the subject. In particular, we refer the interested reader to Krauskopf and Sieber (2023) to fully appreciate some of these methods in action as part of DDE-BIFTOOL (Engelborghs et al. 2001, 2002; Sieber et al. 2022), the most advanced and complete software package for bifurcation analysis of DDEs (including state-dependent and neutral problems), based on the framework of numerical continuation Doedel (2007).

The chapter is organized as follows. Section 2 deals with the basics of the theory of evolution families associated to linear(ized) nonautonomous DDEs, first in general and then specializing to the constant (Sect. 2.1), periodic (Sect. 2.2) and generic (Sect. 2.3) cases. The discretization of a general evolution operator is illustrated in Sect. 3, particularizing to the computation of characteristic roots for the stability of equilibria (constant case, Sect. 3.1), Floquet multipliers for the stability of periodic orbits (periodic case, Sect. 3.2) and Lyapunov exponents of attractors (the generic case, Sect. 3.3). Section 4 contains some guidelines on the extension of the pseudospectral approach to both REs and coupled equations. Some illustrative computations are presented in Sect. 5, where we report on experiments about both convergence and bifurcation analysis in view of applications. Relevant codes are also provided. Some concluding remarks are collected in Sect. 6. Finally, we refer the

reader to the introductory expositions in Breda (2023, Sects. 2 and 3) for general overviews on the theory of semigroups and on the basics of polynomial interpolation and pseudospectral collocation.

2 Evolution Families

Consider a given solution $\bar{y}$ of (5). Linearization leads to

$$y'(t) = A(t)y_t \tag{7}$$

for $A(t) := DG(\bar{y}_t)$ with DG the Fréchet differential[1] of G at $\bar{y}_t$. Well-posedness of the relevant Initial Value Problem (IVP) allows to define the solution operator $T(t,s) : Y \to Y$ associating to an initial function $y_0 = \psi$ for some $\psi \in Y$ given at time s the state y_t at time $t \geq s$ as

$$T(t,s)y_0 = y_t.$$

It is not difficult to show that the collection $\{T(t,s)\}_{t \geq s}$ defines a so-called *evolution family*, i.e., it satisfies $T(s,s) = I_Y$ for any s, $T(t,s) = T(t,r)T(r,s)$ for any $t \geq r \geq s$ and, for each $\psi \in Y$, the map $(t,s) \mapsto T(t,s)\psi$ is continuous (see, e.g., Chicone and Latushkin 1999, Chap. 3).

As an evident difference with respect to the autonomous case and to the relevant semigroup of solution operators (see Breda 2023), here we deal with a family of operators depending on two parameters, namely the current and starting times, the latter inevitably playing a role in nonautonomous problems as (7) is in general. The possibility of linking the evolution family to an abstract ODE in Y is tempting, but the resulting equation would be nonautonomous. Correspondingly, a similar notion of infinitesimal generator would be time-dependent and, in particular, with a time-dependent domain if the state space is chosen as in (2) (as it is assumed here for the time being). Although other choices can lead to better posed definitions of a generator, as it is the case, e.g., for $Y = \mathbb{R}^{d_Y} \times L^2([-\tau, 0], \mathbb{R}^{d_Y})$ (see, e.g., Breda 2010 and the references therein or Curtain and Zwart 1995; Michiels 2023), it is not difficult to argue that the spectrum of this "generator" is not the right place where to look for if one is interested in the stability of the null solution of (7), or eventually in the local stability of $\bar{y}$. Indeed, this is a well-known fact already in the finite-dimensional case of Ordinary Differential Equations (ODEs). Consequently, the focus is headed directly towards the spectrum of $T(t,s)$, or of related quantities. In particular, in the following sections we consider three separate cases, which are those of interest in this chapter, distinguished depending on $\bar{y}$ being an equilibrium of (5), a periodic solution or none of the two (what we call a *generic* solution henceforth).

[1] For a primer on Fréchet derivatives see Ambrosetti and Prodi (1995, Chap. 1).

2.1 Autonomous Problems and Stability of Equilibria

When $\bar{y}$ is an equilibrium, $A(t) \equiv A$ holds independently of t in (7). In this case it is not difficult to see that $T(t, s)$ depends only on the difference $t - s$ (the amount of time spanned during the evolution) rather than on t and s separately. Therefore, $T(t, s) = T(t + r, s + r)$ for any r and, by taking $r = -s$, we get $T(t, s) = T(t - s, 0)$. As a consequence, by defining $S(t) := T(t, 0)$ for any $t \geq 0$, we get back to the standard semigroup of solution operators for the autonomous case (see Breda 2023, Sect. 2). In fact, $S(0) = T(0, 0) = I_Y$ and $S(t + s) = T(t + s, 0) = T(t, -s) = T(t, 0)T(0, -s) = T(t, 0)T(s, 0) = S(t)S(s)$.

From the above considerations it follows that the spectrum of $T(h, 0) = S(h)$ for any $h > 0$ gives information on the stability of the zero solution of (7) with constant A and, in the hyperbolic case of absence of eigenvalues on the unit circle, also on the local stability of $\bar{y}$. Indeed, if $\mu \in \sigma(T(h, 0)$ then $\lambda := (\log \mu + \mathrm{i}2\pi k)/h$ is a characteristic root for some $k \in \mathbb{Z}$, i.e., an eigenvalue of the infinitesimal generator of the semigroup $\{S(t)\}_{t \geq 0}$. Eventually, the interest is thus in discretizing $T(h, 0)$ to get approximations to its (dominant) eigenvalues by computing the eigenvalues of the resulting approximating matrix, see Sect. 3.1.

2.2 Periodic Problems and Stability of Periodic Orbits

When $\bar{y}$ is periodic of period ω, $A(t + \omega) = A(t)$ holds independently of t in (7). In this case, $T(s + \omega, s)$ becomes the so-called *monodromy operator* at s. Then Floquet theory shows that all the monodromy operators share the same spectrum independently of s, which is moreover a point spectrum possibly accumulating only at 0 (see, e.g., Diekmann et al. 1995, Chap. XIII). The elements of this spectrum are the so-called *Floquet multipliers* and, without loss of generality, they can be thought as eigenvalues of $T(\omega, 0)$.

The stability of the null solution of (7) depends on whether the associated Floquet multipliers are inside (all of them: asymptotic stability) or outside (at least one of them: instability) the unit circle. Then, through the use of Poincaré sections and maps (see, e.g., Diekmann et al. 1995, Chap. XIV), the stability of the null solution can be translated into the local stability of $\bar{y}$, but only if the so-called *trivial* multiplier $\mu = 1$, which is always present due to linearization, is simple and is the only multiplier on the unit circle (i.e., the so-called *hyperbolic* case). Eventually, the interest is thus in discretizing $T(\omega, 0)$ to get approximations to the (dominant) Floquet multipliers by computing the eigenvalues of the resulting approximating matrix, see Sect. 3.2.

2.3 Generic Problems and Detection of Chaos

When $\bar{y}$ is generic, one can no longer refer to a single element of the evolution family associated to (7) in order to address the question of stability. Rather, the focus is on the long-time behavior of $\{T(t,s)\}_{t\geq s}$ as it provides information on the average exponential growth in the long time of the solutions of (5) through the so-called *Lyapunov exponents*. Without entering into much detail, for which we refer the interested reader to Breda (2010, Sect. 6) and to the references therein, the exponent of a single solution y is defined as

$$\alpha(y) := \limsup_{t\to+\infty} \frac{1}{t} \log|y(t)|,$$

following the original definition of Lyapunov in his Ph.D. thesis Lyapunov (1892). For reasons that will be clarified later on in Sect. 3.3 when dealing with the computation of the exponents, it is common (if not mandatory) to resort to the use of a norm induced by a inner product, in order to have a proper notion of orthogonality at disposal. For the single exponent $\alpha(y)$ this is not a real concern, as it can be proved that the latter is independent of the particular norm $|\cdot|$ used in $\mathbb{R}^{d_Y}$. But when it comes to consider all the possible exponents of solutions of (7), which are unsurprisingly infinitely-many due to the infinite dimension of the underlying state space Y, it becomes necessary to resort to orthogonality. Consequently, the classical space Y defined in (2) adopted so far is no longer appropriate and must be suitably replaced, e.g., by

$$Y = \mathbb{R}^{d_Y} \times L^2([-\tau,0],\mathbb{R}^{d_Y}), \tag{8}$$

with norm $\|(v,\psi)\|_Y := \sqrt{|v|^2 + \|\psi\|_2^2}$ for $\|\cdot\|_2$ the standard norm in L^2. Given these premises, the Lyapunov exponents of (7) are defined to be the eigenvalues of the limit operator

$$\Lambda(s) := \limsup_{n\to\infty} \frac{1}{n} \log\|T(s+n\tau,s)\|_{Y\leftarrow Y}. \tag{9}$$

It can be shown that the above operator and hence the relevant exponents are independent of s, yet another matter is to see whether it exists as an exact limit. When this happens one usually talks about *regular* systems, but not all systems are regular (already in the case of ODEs). So, in general, one can talk about *upper* and *lower* Lyapunov exponents, referring them respectively to lim sup and lim inf. In any case, the main outcome is that a positive (upper) Lyapunov exponent is a signature of chaos. Therefore, the interest is thus in discretizing the elements of the sequence $\{T(s+n\tau,s)\}_{n\in\mathbb{N}}$ for some s to get approximations to the (dominant) Lyapunov exponents. How to exploit this discrete sequence in view of their computation is left to Sect. 3.3, a procedure which will also clarify why orthogonality is necessary.

3 Pseudospectral Discretization of the Evolution Family

In view of what illustrated in the previous sections, we aim at discretizing a general element of the evolution family, say $T(s+h, s)$ for a given starting time s and a given advancing step $h > 0$. Then, the choice $s = 0$ and any $h > 0$ in the autonomous case refers to Sect. 2.1 and to Sect. 3.1 below, the choice $s = 0$ and $h = \omega$ in the ω-periodic case refers to Sect. 2.2 and to Sect. 3.2 below, while the choice $s = n\tau$ for $n \in \mathbb{N}$ and $h = \tau$ turns out to be useful in the generic case of Sect. 2.3, as treated in Sect. 3.3 below.

The approach we are going to discuss, named *solution operator approach* in relation to the *infinitesimal generator approach* described in Breda (2023), is based again on the use of pseudospectral collocation. Concerning the latter technique, as already said, we refer to Breda (2023, Sect. 3) for an introductory exposition. Prior to discretize the problem, it is useful to adopt the following reformulation, where we use $T := T(s+h, s)$ for brevity and introduce the auxiliary spaces

$$Y^+ := C([0, h]; \mathbb{R}^{d_Y}), \qquad Y^\pm := C([-\tau, h]; \mathbb{R}^{d_Y}) \tag{10}$$

beyond the state space Y of functions defined in $[-\tau, 0]$.[2] Moreover, let us define the operator $V : Y \times Y^+ \to Y^\pm$ given by

$$[V(\psi, w)](t) := \begin{cases} \psi(0) + \int_0^t w(s)\,\mathrm{d}s, & t \in [0, h], \\ \psi(t), & t \in [-\tau, 0], \end{cases} \tag{11}$$

and the operator $\mathcal{F}_s : Y^\pm \to Y^+$ given by

$$(\mathcal{F}_s v)(t) := A(t+s)v_t, \quad t \in [0, h].$$

Then, the action of the evolution operator T on $\psi \in Y$ can be expressed as

$$T\psi = V(\psi, w^*)_h$$

for w^* the[3] solution of the fixed point equation

$$w = \mathcal{F}_s V(\psi, w) \tag{12}$$

in Y^+. Note, indeed, that the action of $\mathcal{F}_s$ is that of applying the right-hand side of (7), just shifting the starting time from s to 0. On the other hand, the action of V is that of reconstructing the solution in $[-\tau, h]$ of the IVP for (5) with initial

[2] For ease of presentation, we restrict to the case $h \geq \tau$. For the case $h < \tau$ we refer the interested reader to Breda et al. (2012), Breda and Liessi (2018) and Breda and Liessi (2020b) concerning, respectively, DDEs, REs and coupled equations. The case $h < \tau$ is usually tackled by a piecewise version of the method for the case $h \geq \tau$, introducing just technicalities but no conceptual novelties.

[3] Uniqueness follows since we assume the relevant IVP to be well-posed.

function ψ. This solution obviously coincides with ψ in $[-\tau, 0]$, while it is obtained by basically integrating the derivative in $[0, h]$, derivative whose role is played by the second input w of V. Then the fixed-point equation (12) emerges naturally by observing that the derivative of the solution is given by the right-hand side of (7) as applied to the solution itself described in terms of the operator V. Finally, the action of T is that of extracting the state at time h from the whole solution generated again through V, according to (4).

Now, the problem of approximating T translates into replacing both $\psi \in Y$ and $w \in Y^+$ by suitable polynomials, which can be determined through relevant collocation equations imposed on two distinct meshes, respectively in $[-\tau, 0]$ and in $[0, h]$.

Let us then fix two positive integers M and N and define two meshes relevant to Y and Y^+ respectively as

$$\Omega_M := \{\theta_{M,m},\ m = 0, 1, \ldots, M\ :\ -\tau =: \theta_{M,M} < \cdots < \theta_{M,1} < \theta_{M,0} := 0\}$$

and

$$\Omega_N^+ := \{t_{N,n},\ n = 1, \ldots, N\ :\ 0 < t_{N,1} < \cdots < t_{N,N} < h\}.$$

Correspondingly, let us set $X_M := \mathbb{R}^{d_Y(M+1)}$ and $X_N^+ := \mathbb{R}^{d_Y N}$ for the discrete counterparts of X and Y^+, respectively, and introduce the restriction and prolongation operators R_M, P_M, R_N^+ and P_N^+ according to Breda (2023, Sect. 3). Then the action of $T : X \to X$ on $\psi \in Y$ reformulated as explained above, i.e.,

$$\begin{cases} T\psi = V(\psi, w^*)_h \\ w^* = \mathcal{F}_s V(\psi, w^*), \end{cases} \tag{13}$$

is approximated by the action of the finite-dimensional operator $T_{M,N} : X_M \to X_M$ on $\Psi \in X_M$ given as

$$\begin{cases} T_{M,N}\Psi = R_M V(P_M\Psi, P_N^+ W^*)_h \\ W^* = R_N^+ \mathcal{F}_s V(P_M\Psi, P_N^+ W^*). \end{cases} \tag{14}$$

In practice, the input function ψ and the fixed point w^* are replaced, respectively, by the polynomials $P_M\Psi$ and $P_N^+ W^*$ constructed by interpolating the given input vector $\Psi \in X_M$ and the vector $W^* \in X_N^+$. The latter is a fixed point of the second equation, determined by collocation on the nodes of Ω_N^+ through the restriction R_N^+.[4] Eventually, the action of $T_{M,N}$ is obtained by restricting the exact action of V on the named polynomials to the nodes of Ω_M through the restriction R_M, thus giving back a vector in X_M.

A matrix representation of $T_{M,N}$ is needed in view of implementation. Details are elaborated in Breda et al. (2012) by choosing for Ω_M and Ω_N^+ respectively Chebyshev

[4] The fixed point is actually unique for sufficiently large N (Breda et al. 2012, Sect. 3.4).

extrema and zeros, viz.

$$\theta_{M,m} = \frac{\tau}{2}\left[\cos\left(\frac{m\pi}{M}\right) - 1\right], \qquad t_{N,n} = \frac{h}{2}\left[1 - \cos\left(\frac{(2n-1)\pi}{2N}\right)\right].$$

These choices also allow for a complete error analysis as developed in Breda et al. (2012), based on comparing T with a finite-rank infinite-dimensional version of $T_{M,N}$ which shares the same nontrivial eigenvalues together with their multiplicities. Convergence in norm of the latter to T guarantees the convergence of the relevant multipliers and (generalized) eigenspaces thanks to the general results in Chatelin (1983). A softened version of the final result follows from Breda et al. (2012).

Theorem 3.1 *Let $\mu \in \sigma(T)$ have algebraic multiplicity ν and ascent l, with (generalized) eigenfunctions of class C^p. Then there exists $N \in \mathbb{N}$ sufficiently large such that, for $M \geq N$, $T_{M,N}$ has ν eigenvalues $\mu_{M,N,i}$, $i = 1, \ldots, \nu$, counted with multiplicities satisfying*

$$\max_{i=1,\ldots,\nu} |\mu_{M,N,i} - \mu| = o\left(N^{\frac{1-p}{l}}\right).$$

Note that the relevant eigenfunctions are known to be analytic functions for DDEs with smooth right-hand side, so that the resulting scheme performs the so-called *spectral accuracy* (Trefethen 2000), as expected from pseudospectral methods.[5]

3.1 Computation of Characteristic Roots

We have already shown in Sect. 2.1 that $\{S(t)\}_{t\geq 0}$ for $S(t) := T(t, 0)$ is the semigroup of solution operators of the linear DDE obtained by linearizing (5) around an equilibrium $\bar{y}$, i.e., (7) with $A(t) \equiv A := DG(\bar{y})$ constant. This semigroup is eventually compact, so it has only point spectrum. Let $\mathcal{A}$ be its infinitesimal generator. Given any $h > 0$, if $\mu \in \sigma(S(h))$ then there exists $k \in \mathbb{Z}$ such that $\lambda = (\log \mu + \mathrm{i}2\pi k)/h \in \sigma(\mathcal{A})$. Conversely, if λ is a characteristic root, i.e., $\lambda \in \sigma(\mathcal{A})$, then $\mu = e^{\lambda h} \in \sigma(S(h))$. This relation is enough to address the local stability of $\bar{y}$ through the knowledge of the eigenvalues μ of $S(h)$, although it is not enough if one wants to recover, e.g., information about the frequency at Hopf points, given that the imaginary part of the characteristic root λ is known in terms of μ only modulo periodicity. In conclusion, the solution operator approach previously described is a valid (yet not necessarily better nor worse) alternative to the infinitesimal generator approach described in Breda (2023) if one is interested in the local stability of equilibria.

[5] For relevant comments on the feature of spectral accuracy see Breda (2023).

3.2 Computation of Floquet Multipliers

In the periodic case of (7) obtained by linearizing (5) around a given ω-periodic solution, we have seen that $T(\omega, 0)$ represents the reference monodromy operator. Therefore, the solution operator approach applied with $h = \omega$ and $s = 0$ provides us with accurate approximations to the Floquet multipliers, hence a numerical tool to address the local stability of the concerned periodic orbit (in the hyperbolic case).

3.3 Computation of Lyapunov Exponents

In order to present the main concepts behind the computation of Lyapunov exponents we start from the case of ODEs. In this context, Adrianova (1995) is among the main references from a theoretical point of view, beyond the original thesis of Lyapunov (1892). Concerning computation see Dieci and Van Vleck (2002), Dieci et al. (2010) and the references therein.

Let us consider then linear and nonautonomous systems

$$y'(t) = A(t)y(t) \tag{15}$$

for $A : [0, +\infty) \to \mathbb{R}^{n\times n}$ continuous and bounded.[6,7] By first reducing (15) to triangular form through orthogonalization, Lyapunov exponents can be extracted as a limit for $t \to +\infty$ from the diagonal elements of the matrix of coefficients of the reduced system. The key observation is that the orthogonalization process cannot be performed directly (and exclusively) in the long time, but rather along every step of a sequence of not too-distant time instants. This in order to avoid alignment along the direction of highest growth, i.e., the one corresponding to the largest exponent. From the computational standpoint, this process leads to the family of QR methods, perhaps the most used class of computational techniques. We summarize below the discrete version of the QR method for computing the Lyapunov exponents of (15), taking inspiration from Dieci et al. (2010), yet giving credits also to the pioneering works Benettin et al. (1980a, b) and to Dieci and Van Vleck (2002). Let us remark the the name "QR" comes from the celebrated QR scheme to factorize a matrix into the product of an orthogonal matrix Q and a triangular matrix R. Here we point out that we refer to the unique such factorization of nonsingular matrices by requiring that R has positive diagonal elements.

Let then $Y(t)$ be a fundamental matrix solution of (15) such that $Y(t_0) = Y_0$ is assigned for some nonsingular matrix Y_0 prescribed at time $t_0 = 0$ without loss of generality. Let also $\{t_k\}_{k\in\mathbb{N}}$ be a strictly increasing sequence of time instants and

[6] The choice of 0 as starting time is not restrictive at all given that Lyapunov exponents concern the long-time behavior.

[7] If interested in attractors of nonlinear problems, one usually linearizes around a reference (generic) trajectory.

construct the iterative QR factorization

$$Y(t_k) = Q_k R_k \tag{16}$$

of the sequence $\{Y(t_k)\}_{k\in\mathbb{N}}$ starting from $Y_0 = Q_0 R_0$ as follows. First, at each step $j = 1, \ldots, k$ solve the IVP

$$\begin{cases} \Psi'(t, t_{j-1}) = A(t)\Psi(t, t_{j-1}), \quad t \in [t_{j-1}, t_j], \\ \Psi(t_{j-1}, t_{j-1}) = Q_{j-1} \end{cases} \tag{17}$$

for the matrix solution $\Psi(t, t_{j-1})$. Second, take the QR factorization of the solution at t_j as

$$\Psi(t_j, t_{j-1}) = Q_j R_{j,j-1}. \tag{18}$$

In view of (9), consider now the evolution matrix $T(t, s) = Y(t)Y(s)^{-1}$. Then

$$\begin{aligned} Y(t_k) &= T(t_k, t_0)Y_0 \\ &= T(t_k, t_{k-1}) \cdots T(t_2, t_1)T(t_1, t_0)Q_0 R_0 \\ &= T(t_k, t_{k-1}) \cdots T(t_2, t_1)\Psi(t_1, t_0)R_0 \\ &= T(t_k, t_{k-1}) \cdots T(t_2, t_1)Q_1 R_{1,0} R_0 \\ &= T(t_k, t_{k-1}) \cdots \Psi(t_2, t_1)R_{1,0} R_0 \\ &= T(t_k, t_{k-1}) \cdots Q_2 R_{2,1} R_{1,0} R_0 \\ &\cdots \\ &= Q_k R_{k,k-1} \cdots R_{1,0} R_0. \end{aligned}$$

Then

$$R_k = \left(\prod_{j=1}^{k} R_{j,j-1} \right) R_0$$

follows from (16) by uniqueness of the QR factorization. Eventually, by denoting with $[R_{j,j-1}]_{i,i}$ the i-th diagonal entry of the j-th triangular factor $R_{j,j-1}$, we recover the (upper[8]) Lyapunov exponents as

$$\alpha_i = \limsup_{k\to\infty} \frac{1}{t_k} \sum_{j=1}^{k} \log[R_{j,j-1}]_{i,i}, \quad i = 1, \ldots, n.$$

Going back now to DDEs, if we assume to choose (8) as a state space in order to guarantee a notion of orthogonality, there is no conceptual change in the scheme

[8] Lower exponents come either as lim inf or as upper exponents of the adjoint system. If (15) is regular both upper and lower exponents coincide and exist as exact limit.

described above if not for the infinite dimension of the state space.[9] If this observation lay the theoretical basis for the determination of the exponents, for a practical computation one has to go back to finite-dimension through discretization. This translates into replacing the evolution operator T in the infinite-dimensional QR factorization (18) seen as

$$T(t_j, t_{j-1})Q_{j-1} = \Psi_{t_j,t_{j-1}} = Q_j R_{j,j-1}$$

with its finite-dimensional counterpart $T_{M,N}$. This is the methodology first proposed in Breda and Van Vleck (2014), where a rigorous convergence analysis is also provided. The main (yet only) difference with respect to what described in Sect. 3 is that the discretization $T_{M,N}$, for obvious reasons, is constructed through generalized Fourier projection rather than through pseudospectral collocation, the latter being based on the choice (2) where orthogonality has no sense. Eventually, let us note that with respect to ODEs, where one does not usually compute evolution matrices but rather solve related IVPs (i.e., (17)), for DDEs one directly approximates the evolution family thanks to the solution operator approach. And indeed, the method proposed in Breda and Van Vleck (2014) was mainly inspired by that of Breda et al. (2012), where the original solution operator approach was first fully developed and rigorously analyzed.

To conclude, let us remark that a valid alternative has been proposed more recently (Breda and Della Schiava 2018), inspired by the perspective originally presented in Breda et al. (2016a). Indeed, one can first reduce (7) to a system of ODEs through the nonlinear (pseudospectral) approach discussed in Breda (2023, Sect. 5), and then compute the Lyapunov exponents of the resulting ODE as approximations to (part of) those of the original DDE by using standard techniques for ODEs. Of course, the discrete QR method above illustrated is one of these techniques. To highlight that going this way there is no need to change the state space from the classical (2) to (8). Finally, it is worth mentioning that most of the computational techniques available in the literature for computing Lyapunov exponents of DDEs are indeed based on first reducing to ODEs (see, e.g., Farmer 1982; Sprott 2007).[10]

4 Extension to Renewal and Coupled Equations

The reformulation (13) of the evolution operator T is advantageous not only from the point of view of computation through numerical discretization via (14), but also in view of applying the same strategy to classes of equations other than DDEs. Indeed, let us note that the action of T is described by two separate contributions, namely the action of the right-hand side of the concerned equation through the operator $\mathcal{F}_s$ on the one hand and, on the other hand, the way one reconstructs the solution through

[9] The latter, of course, is responsible for infinitely-many Lyapunov exponents as already mentioned, yet they all accumulate at $-\infty$ Breda (2010).

[10] Krauskopf and Sieber (2023, Sect. 4) is an example of application of Farmer (1982).

the operator V given an initial function (necessary since it is a problem with delay) and the output of the right-hand side of the concerned equation. In the specific case of DDEs, the right-hand side of (5) prescribes the derivative of the solution, so that the operator V integrates the latter to get the solution forward in time. If we now consider the class (6) of renewal equations, where the right-hand side gives the solution itself, the operator V becomes simply

$$[V(\varphi, u)](t) := \begin{cases} u(t), & t \in (0, h], \\ \varphi(t), & t \in [-\tau, 0], \end{cases} \tag{19}$$

where the point-wise definition is intended in the sense of equivalence classes in L^1 given the choice (1) for the state space X and for the relevant spaces X^+ and $X^\pm$ defined similarly to Y^+ and $Y^\pm$ in (10). With this new definition of V, the discretization (14) remains unchanged, with the attention that now u represents the solution forward in time and not its derivative as it is the case for DDEs. Of course, the change in V leads to obvious differences in the construction of the discrete matrices involved in the implementation of the method. All the details can be found in Breda and Liessi (2018), where also a rigorous convergence analysis is reported. The latter follows the main ideas of that in Breda et al. (2012), yet with nontrivial modifications due to the different spaces, i.e., (1) instead of (2).[11] The final result on the error in computing the eigenvalues of T is unchanged with respect to Theorem 3.1, as far as the stability of equilibria and periodic orbits[12] is concerned. We reserve to comment on the computation of Lyapunov exponents at the end of this section, for both REs and coupled equations together.

The solution operator approach has been recently extended also to coupled equations (3), see Breda and Liessi (2020b). The same, as anticipated in the Introduction, cannot be said yet for the relevant Floquet theory, although we give as reasonably granted that results similar to that for DDEs and REs hold also for this class of systems. The principle guiding the extension is the same one above described for REs: separating the action of the right-hand side of (3) from the way one reconstructs the solution. This amounts to new definitions of the operators V and $\mathcal{F}_s$ which unsurprisingly combine (11) with (19) taking in due account the presence of crossing terms, i.e., those relevant to y in the equation for x and the other way around. Indeed, the state space for (3) is the cross-product $X \times Y$, which "mixes" L^1 functions with continuous ones, requiring a certain ability in treating all the elements mainly in view of the relevant analysis of convergence, fully developed in Breda and Liessi (2020b). Nevertheless, and once more, Theorem 3.1 holds unchanged. Unfortunately, the "mixing" of the state spaces causes major difficulties in tackling the extension of the Floquet theory, which is in fact still in progress (by D. Liessi and the author).

[11] To note that, in any case, in (14) the operator V acts on polynomials.

[12] The relevant theoretical background including Floquet theory, Poincaré sections and maps as well as the principle of linearized stability for periodic orbits has been developed only recently and can be found in Breda and Liessi (2020a).

Finally, let us briefly comment on the extension of the solution operator approach in view of computing Lyapunov exponents for REs and for coupled equations. As previously illustrated, this approach has been first proposed for DDEs in Breda and Van Vleck (2014), changing the state space from (2) to (8) in view of the necessary orthogonality. For basically the same reason, the pseudospectral collocation approach based on interpolating polynomials on family of Chebyshev nodes has been substituted by a more appropriate truncation of generalized Fourier series. In particular, the latter is based on the family of orthogonal Legendre polynomials as far as the L^2 component of (8) is concerned. The same strategy has not been fully developed yet for REs, nor for coupled problems. Let us anyway remark that at a first sight we cannot see any particular obstacle in view of pursuing this extension. Instead, the approach developed for DDEs in Breda and Della Schiava (2018) has been successfully applied also to REs in Breda et al. (2016b), and being based on the prior reduction of the delay equation to ODEs, it is expected to work properly for coupled problems, too. The results concerning Lyapunov exponents reported in Sect. 5 are indeed obtained by following the latter approach.

5 Results and Applications

All the following computations are performed on a MacBook Pro 2.3GHz Intel Core i7 16GB by using Matlab R2019a. Two demos including scripts to run the codes relevant to the following tests are freely available at http://cdlab.uniud.it/software. The first one, `demo_DDE_mackeyglass`, refers to the experiments described in Sect. 5.1 about a DDE. The second one, `demo_RE_logistic`, refers to the experiments described in Sect. 5.2 about an RE.[13]

5.1 Tests on the Mackey-Glass Equation

As in Breda (2023, Sect. 6.1), we consider again the celebrated Mackey-Glass equation (Mackey and Glass 1977)

$$y'(t) = \frac{\beta y(t-\tau)}{1+y(t-\tau)^\alpha} - \gamma y(t) \tag{20}$$

with $\alpha, \beta, \gamma \geq 0$ and $\tau > 0$. In particular, we fix $\beta = 2, \gamma = 1$ and $\tau = 2$, so that the nontrivial equilibrium

$$\bar{y} := \left(\frac{\beta}{\gamma} - 1\right)^{1/\alpha}$$

[13] The auxiliary codes `clencurt`, `mybarint` and `mybarwei` are also included, whose implementation follows Berrut and Trefethen (2004), Trefethen (2000).

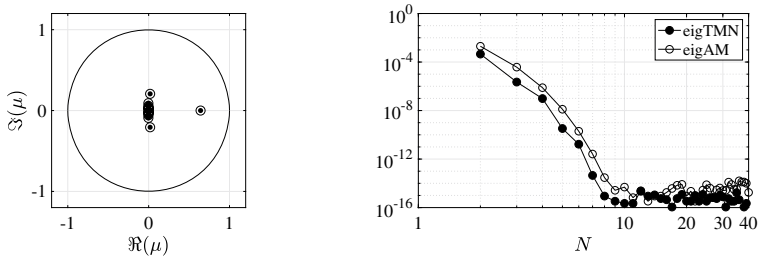

Fig. 1 Results on (20) with $\alpha = 1$, $\beta = 2$, $\gamma = 1$ and $\tau = 2$: (left) dominant eigenvalues of $T(2, 0)$ computed with `eigTMN` (•'s) and with `eigAM` (∘'s); (right) convergence of the error on the dominant multiplier; further details in the text

becomes simply $\bar{y} = 1$ independently of α. The latter is either kept fixed or made varying in view of bifurcation analysis. Linearization leads to

$$y'(t) = ay(t) + by(t - \tau)$$

with

$$a = -\gamma = -1, \qquad b = \beta \cdot \frac{1 + (1 - \alpha)\bar{y}^{\alpha}}{(1 + \bar{y}^{\alpha})^2} = 1 - \frac{\alpha}{2}.$$

As a first experiment we fix $\alpha = 1$ and compute the approximations to the eigenvalues μ of $T(2, 0)$, •'s in Fig. 1 (left), by using the solution operator approach with $M = N = 40$. We also compare them with $e^{2\lambda}$, ∘'s in Fig. 1 (left), for λ the eigenvalues computed by using the infinitesimal generator approach described in Breda (2023) with $M = 40$ (i.e., the same N used above). They are obtained respectively through the codes `eigTMN` (for μ) and `eigAM` (for λ) from Breda et al. (2015). The first 21 dominant eigenvalues are plotted, with no visible difference between •'s and ∘'s. Then, in Fig. 1 (right) and with respect to the dominant eigenvalue, we test the convergence of both approaches by increasing N. The reference value $\mu = 0.642200704059874$ for the dominant eigenvalue is computed to machine accuracy by `eigTMN` with $M = N = 100$. To note that spectral accuracy takes place as expected for both methods, with the solution operator approach showing slightly better error constants.

As a second test we search for bifurcations of the nontrivial equilibrium by computing the dominant eigenvalue(s) of $T(2, 0)$ for α increasing from 1, using the solution operator approach implemented in `eigTMN` with $M = N = 40$ again. This can be easily done via Matlab's `fzero` as described in `demo_DDE_mackeyglass`, which returns a Hopf bifurcation at $\alpha = \bar{\alpha} := 5.039605122412380$ to machine accuracy. Figure 2 (left) shows the dominant pair crossing the unit circle outwards when increasing α from $\bar{\alpha} - 1$ (∘) through $\bar{\alpha}$ (•) to $\bar{\alpha} + 1$ (□). The dominant pair at $\alpha = \bar{\alpha}$ is $\mu = 0.413533430035905 \pm 0.910488935815664\mathrm{i}$, computed to machine accuracy again by `eigTMN` with $M = N = 100$. The emergence of a branch of stable periodic solutions at the Hopf bifurcation at $\alpha = \bar{\alpha}$ is confirmed experimentally. In fact, in

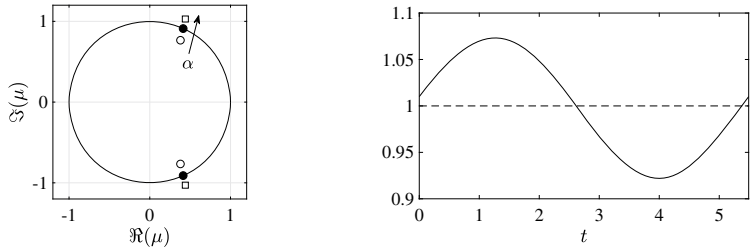

Fig. 2 Results on (20) with $\beta = 2, \gamma = 1$ and $\tau = 2$: (left) crossing of the dominant pair of $T(2, 0)$ corresponding to a Hopf bifurcation at $\alpha = \bar{\alpha}$, computed with `eigTMN` for increasing α from $\bar{\alpha} - 1$ ($\circ$) through $\bar{\alpha}$ ($\bullet$) to $\bar{\alpha} + 1$ ($\square$); (right) periodic solution (solid line) for $\alpha = 5.1$, soon after the Hopf bifurcation of the nontrivial equilibrium (dashed line) at $\alpha = \bar{\alpha}$; further details in the text

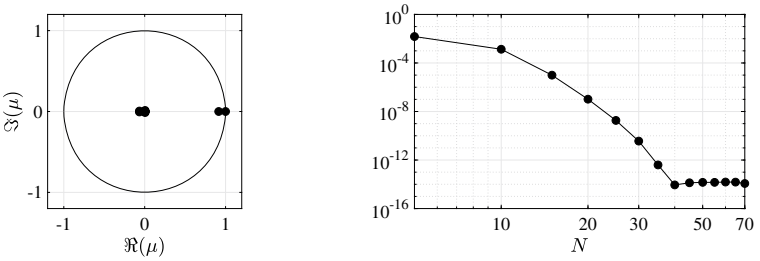

Fig. 3 Results on (20) with $\alpha = 5.1$, $\beta = 2$, $\gamma = 1$ and $\tau = 2$: (left) dominant eigenvalues of $T(\omega, 0)$; (right) convergence of the error on the trivial Floquet multiplier; further details in the text

Fig. 2 (right) the periodic solution at $\alpha = 5.1$ soon after the Hopf point is shown. The trajectory is obtained through collocation of a boundary value problem as explained in Krauskopf and Sieber (2023, Sect. 3.6). The relevant data, taken from Breda et al. (2016b), are contained in the file `periodic_51.mat` provided together with `demo_DDE_mackeyglass`.

To test further the solution operator approach, we show in Fig. 3 (left) the dominant eigenvalues of the monodromy operator $T(\omega, 0)$ of the linearization around the periodic solution previously computed at $\alpha = 5.1$, whose period is $\omega = 5.490522200153110$ to machine accuracy. These Floquet multipliers are computed again through the solution operator approach, but the relevant code `example1per` is a version of `eigTMN` adapted to the necessity of linearizing the DDE around a solution computed numerically. Apart from this, we always use $M = N = 40$. To note anyway the correct presence of the trivial Floquet multiplier 1 due to linearization. Finally, Fig. 3 (right) shows the spectrally accurate behavior of the error on this trivial multiplier, the latter being indeed a "true" error. Let us observe that a lower barrier around 10^{-14} is reached instead of the usual machine precision: this is actually the tolerance at which the periodic solution is numerically computed, given that the relevant Newton's iteration was stopped when the error fell below 10^{-12}.

5.2 Tests on a Logistic RE

We consider the RE

$$x(t) = \frac{\gamma}{2} \int_{-3}^{-1} x(t+\theta)[1 - x(t+\theta)]\,\mathrm{d}\theta \tag{21}$$

with $\gamma > 0$ a varying parameter in view of bifurcation analysis. Equation (21) represents the logistic instance of a family of REs treated in Breda et al. (2016b). In this section we repeat some of the experiments run therein, following the bifurcation diagram represented in Fig. 4 (top-left), which can be reconstructed by using `demo_RE_logistic` and the data from Breda et al. (2016b) provided with the related files. By increasing γ beyond 0, the trivial equilibrium looses its stability in favor of the nontrivial one

$$\bar{x} := 1 - \frac{1}{\gamma}, \tag{22}$$

which exists positive for $\gamma > 1$. At $\gamma_{BP} := 1$, indeed, a transcritical bifurcation (colloquially, a "brancing point") takes place. This is confirmed experimentally by computing the characteristic roots of (21) linearized around (22) as eigenvalues of the infinitesimal generator. In particular, in Fig. 4 (top-right) we show the transition of the rightmost real root through the imaginary axis from left to right for γ increasing

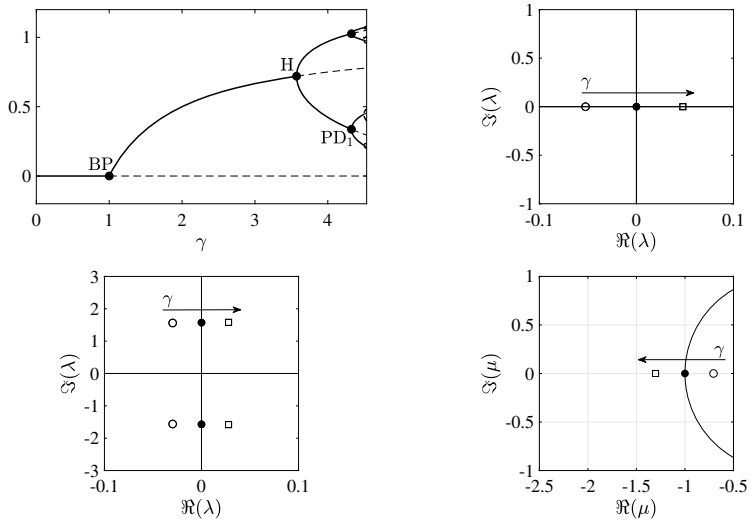

Fig. 4 Results on (21) for varying γ: (top-left) bifurcation diagram; (top-right) transcritical bifurcation of the trivial equilibrium; (bottom-left) Hopf bifurcation of the nontrivial equilibrium; (bottom-right) period doubling bifurcation of the branch of periodic solution rising from the Hopf bifurcation; description in the text

from $\gamma = 0.9$ ($\circ$) through γ_{BP} ($\bullet$) to $\gamma = 1.1$ ($\square$). The roots are approximated by the infinitesimal generator approach implemented in `eigAM_RE` and described in Breda (2023, Sect. 6.2), which is based on a piecewise discretization given that the integral right-hand side of (21) has a kernel which is nontrivial only on $[-3, -1]$, while it vanishes on $[-1, 0]$.

The same approach is used to correctly detect the Hopf bifurcation of the nontrivial equilibrium, which can be shown to occur at $\gamma_H := 2 + \pi/2 \simeq 3.571$, Breda et al. (2016b). Indeed, Fig. 4 (bottom-left) refers to the rightmost pair of roots crossing the imaginary axis from left to right for γ increasing from $\gamma = 3.471$ ($\circ$) through γ_H ($\bullet$) to $\gamma = 3.670$ ($\square$). At γ_H a branch of stable periodic solution emerges. The elements of this branch can be obtained explicitly and, moreover, they all share the same period $\omega = 4$, see Breda et al. (2016b, Appendix A), at least until the first period doubling bifurcation occurs. Till this point, we are thus able to linearize (21) around the exact periodic solution, in order to compute the eigenvalues of $T(\omega, 0)$ and detect the relevant local stability. To this aim, we switch to the solution operator approach described in this chapter. Then, following the branch, we find a first period doubling at $\gamma_{PD1} := 4.324731218522237$ computed to machine accuracy. Correspondingly, the transition of the dominant nontrivial Floquet multiplier through the unit circle at -1 in the outward direction is shown in Fig. 4 (bottom-right), for γ increasing from $\gamma = 4.225$ ($\circ$) through γ_{PD1} ($\bullet$) to $\gamma = 4.424$ ($\square$).

As far as the convergence is concerned, we avoid to report on the results relevant to the above experiments as they are qualitative the same as those presented in Sect. 5.1 for the Mackey-Glass equation. Indeed, as already remarked, Theorem 3.1 is unchanged passing from DDEs to REs and even to coupled equations. With regards to the latter class, tests similar to those illustrated above can be found in Breda and Liessi (2020b), whose relevant codes are freely available always at http://cdlab.uniud.it/software.

Finally, at least other two period doubling bifurcations are found with clear distinction after γ_{PD1} in Breda et al. (2016b), see Fig. 2.1a. Chaotic dynamics can be found soon after the last detected period doubling by simulating the IVP for the ODE obtained by approximating (21) with the nonlinear pseudospectral approach described in Breda (2023, Sect. 5). In order to confirm experimentally the presence of a potential period doubling cascade, (21) is first linearized around a reference trajectory computed by the nonlinear approach just mentioned. Then we approximate the relevant Lyapunov exponents via the solution operator approach applied to the linearized equation, embedded into the discrete QR scheme as illustrated in Sect. 3.3. The results are illustrated in Fig. 5, where the onset of chaos corresponds to the transition of the dominant nontrivial[14] Lyapunov exponent from negative to positive, which occurs around $\gamma \simeq 4.54$. From the computed exponents, other islands of stability are found beyond the onset of chaos, the most evident of which corresponds

[14] A trivial exponent is always present due to linearization.

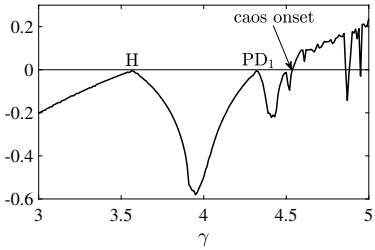

Fig. 5 Results on (21) for varying γ: dominant nontrivial Lyapunov exponent

to a "period 6 cascade", approximately in the range $\gamma \in [4.85, 4.89]$. The data concerning the Lyapunov exponents, contained in the file `LE.mat`, are produced with the codes used in Breda et al. (2016b).[15]

6 Conclusions

A general pseudospectral collocation approach to approximate the evolution family of delay equations has been illustrated. The technique can be used for either DDEs, REs and systems of coupled REs and DDEs, and it enables one to investigate the local stability of equilibria and periodic orbits through the principle of linearized stability, as well as to detect chaotic dynamics by computing Lyapunov exponents. Independently of which target or class of equations, the approach has been described from the points of view of discretization, convergence and application. Where not all the details have been included (as, e.g., the proofs of convergence or the details of implementation), suitable references have been provided for those interested in deepen their study of the subject. Eventually, relevant codes are made freely available at http://cdlab.uniud.it/software.

The approach has been described mostly for DDEs. The extension to REs and coupled equations has been summarized, providing relevant references. Nevertheless, there are still open direction with regards to potential extensions, beyond those described in Sect. 4 concerning the computation of Lyapunov exponents. Indeed, important classes of equations including neutral problems or equations with state-dependent delays have not been addressed yet. Let us refer the interested reader to Krauskopf and Sieber (2023) where effective computational solutions are provided through the package DDE-BIFTOOL. Instead, we mention Borgioli et al. (2020) for a versatile approach aimed also to equations with discontinuous right-hand side.

Finally, repeating from Breda (2023), we remark again that the pseudospectral approach is clearly not the only solution to the numerical stability analysis of delay equations, even if restricted to periodic problems. An interesting experimental comparison is carried out in Lehotzky and Insperger (2016), where it turns out that other choices may reveal more efficient in this or that case. Nevertheless, the reformula-

[15] Available by the author upon request.

tion of the solution operator on which the presented approach is based allows for a uniform view concerning the plethora of discretization schemes that one can resort to. Which, in turn, hopefully open the doors to tackle the theoretical convergence analysis that more than once leaves the place to an experimental validation. Eventually, we remark once more that the great advantage offered by the pseudospectral approach resides in its ability to fully exploit the (potentially infinite) smoothness made available when solving eigenvalue problems.

References

Adrianova, L. Ya. (1995). *Introduction to linear systems of differential equations*. Number 146 in Translations of Mathematical Monographs. Providence: American Mathematical Society.

Ambrosetti, A., & Prodi, G. (1995). *A primer of nonlinear analysis* Cambridge Studies in Advanced Mathematics (Vol. 34). New York: Cambridge University Press.

Benettin, G., Galgani, L., Giorgilli, A., & Strelcyn, J. M. (1980a). Lyapunov exponents for smooth dynamical systems and for hamiltonian systems; a method for computing all of them. Part 1: Theory. *Meccanica, 15,* 9–20.

Benettin, G., Galgani, L., Giorgilli, A., & Strelcyn, J. M. (1980b). Lyapunov exponents for smooth dynamical systems and for hamiltonian systems; a method for computing all of them. Part 2: Numerical applications. *Meccanica, 15,* 21–30.

Berrut, J. P., & Trefethen, L. N. (2004). Barycentric Lagrange interpolation. *SIAM Review, 46*(3), 501–517.

Borgioli, F., Hajdu, D., Insperger, T., Stepán, G., & Michiels, W. (2020). Pseudospectral method for assessing stability robustness for linear time-periodic delayed dynamical systems. *International Journal for Numerical Methods in Engineering, 121*, 3505–3528.

Breda, D. (2010). Nonautonomous delay differential equations in Hilbert spaces and Lyapunov exponents. *Differential and Integral Equations, 23*(9–10), 935–956.

Breda, D. (2023). Pseudospectral methods for the stability analysis of delay equations. Part I: The infinitesimal generator approach. In D. Breda (Ed.), *Controlling Delayed Dynamics: Advances in Theory, Methods and Applications, CISM Lecture Notes* (pp. 65–94). Wien-New York: Springer.

Breda, D., & Della Schiava, S. (2018). Pseudospectral reduction to compute Lyapunov exponents of delay differential equations. *Discrete and Continuous Dynamical Systems - B, 23*(7), 2727–2741.

Breda, D., & Liessi, D. (2018). Approximation of eigenvalues of evolution operators for linear renewal equations. *SIAM Journal on Numerical Analysis, 56*(3), 1456–1481.

Breda, D., & Liessi, D. (2020a). Floquet theory and stability of periodic solutions of renewal equations. *Journal of Dynamics and Differential Equations*. https://doi.org/10.1007/s10884-020-09826-7.

Breda, D., & Liessi, D. (2020b). Approximation of eigenvalues of evolution operators for linear coupled renewal and retarded functional differential equations. *Ricerche di Matematica*. https://doi.org/10.1007/s11587-020-00513-9.

Breda, D., & Van Vleck, E. S. (2014). Approximating Lyapunov exponents and Sacker-Sell spectrum for retarded functional differential equations. *Numerische Mathematik, 126*, 225–257.

Breda, D., Maset, S., & Vermiglio, R. (2006). Numerical computation of characteristic multipliers for linear time periodic delay differential equations. IFAC Proceedings Volumes. In C. Manes & P. Pepe (Eds.), *Time Delay Systems 2006* (Vol. 6). Elsevier.

Breda, D., Maset, S., & Vermiglio, R. (2012). Approximation of eigenvalues of evolution operators for linear retarded functional differential equations. *SIAM Journal on Numerical Analysis, 50*(3), 1456–1483.

Breda, D., Maset, S., & Vermiglio, R. (2015). *Stability of linear delay differential equations – A numerical approach with MATLAB*. SpringerBriefs in Control, Automation and RoboticsNew York: Springer.

Breda, D., Diekmann, O., Gyllenberg, M., Scarabel, F., & Vermiglio, R. (2016a). Pseudospectral discretization of nonlinear delay equations: New prospects for numerical bifurcation analysis. *SIAM Journal on Applied Dynamical Systems, 15*(1), 1–23.

Breda, D., Diekmann, O., Liessi, D., & Scarabel, F. (2016b). Numerical bifurcation analysis of a class of nonlinear renewal equations. *Electronic Journal of Qualitative Theory of Differential Equations, 65*, 1–24.

Chatelin, F. (1983). *Spectral approximation of linear operators*. New York: Academic Press.

Chicone, C., & Latushkin, Y. (1999). *Evolution semigroups in dynamical systems and differential equations*. Number 70 in Mathematical Surveys and Monographs. Providence: American Mathematical Society.

Curtain, F., & Zwart, H. (1995). *An Introduction to Infinite-Dimensional Linear Systems Theory* Texts in Applied Mathematics (Vol. 21). New York: Springer.

Dieci, L., & Van Vleck, E. S. (2002). Lyapunov spectral intervals: Theory and computation. *SIAM Journal on Numerical Analysis, 40*(2), 516–542.

Dieci, L., Jolly, M. S., & Van Vleck, E. S. (2010). Numerical techniques for approximating Lyapunov exponents and their implementation. *Journal of Computational and Nonlinear Dynamics, 6*(1), 011003-1–7.

Diekmann, O., van Gils, S. A., Verduyn Lunel, S. M., & Walther, H. O. (1995). *Delay equations – functional, complex and nonlinear analysis*. Number 110 in Applied Mathematical Sciences. New York: Springer.

Diekmann, O., Getto, P., & Gyllenberg, M. (2008). Stability and bifurcation analysis of Volterra functional equations in the light of suns and stars. *SIAM Journal on Mathematical Analysis, 39*(4), 1023–1069.

Doedel, E. (2007). Lecture notes on numerical analysis of nonlinear equations. Understanding Complex Systems. In H. M. Osinga, B. Krauskopf, & J. Galán-Vioque (Eds.), *Numerical continuation methods for dynamical systems* (pp. 1–49). Springer.

Engelborghs, K., Luzyanina, T., & Samaey, G. (2001). DDE-BIFTOOL v. 2.00: a Matlab package for bifurcation analysis of delay differential equations. Technical Report TW330, Department of Computer Science, K. U. Leuven, Belgium.

Engelborghs, K., Luzyanina, T., & Roose, D. (2002). Numerical bifurcation analysis of delay differential equations using DDE-BIFTOOL. *ACM Transactions on Mathematical Software, 28*(1), 1–21.

Farmer, D. (1982). Chaotic attractors of an infinite-dimensional dynamical system. *Physica D, 4*, 605–617.

Krauskopf, B., & Sieber, J. (2023). Bifurcation analysis of systems with delays: Methods and their use in applications. In D. Breda (Ed.), *Controlling Delayed Dynamics: Advances in Theory, Methods and Applications, CISM Lecture Notes* (pp. 195–246). Wien-New York: Springer.

Lehotzky, D., & Insperger, T. (2016). A pseudospectral tau approximation for time delay systems and its comparison with other weighted-residual-type methods. *International Journal for Numerical Methods in Engineering, 108*(6), 588–613.

Lyapunov, A. M. (1892). *The general problem of the stability of motion*. Number 7 in Collected Works II (in Russian). Kharkov Mathematical Society. Republished by the University of Tolouse 1908 and Princeton University Press 1949 (in French), in International Journal of Control 55, 531-773 and as a book by Taylor & Francis, London, 1992 (in English).

Mackey, M. C., & Glass, L. (1977). Oscillations and chaos in physiological control systems. *Science, 197*, 287–289.

Michiels, W. (2023). Design of structured controllers for linear time-delay systems. In D. Breda (Ed.), *Controlling Delayed Dynamics: Advances in Theory, Methods and Applications, CISM Lecture Notes* (pp. 277–323). Wien-New York: Springer.

Sieber, J., Engelborghs, K., Luzyanina, T., Samaey, G., & Roose, D. (2022). Dde-biftool manual - bifurcation analysis of delay differential equations. arXiv:1406.7144. https://sourceforge.net/projects/ddebiftool.

Sprott, J. C. (2007). A simple chaotic delay differential equation. *Physics Letters A, 366*, 397–402.

Trefethen, L. N. (2000). *Spectral methods in MATLAB*. Software - Environment - Tools series. Philadelphia: SIAM.

Counting Characteristic Roots of Linear Delay Differential Equations. Part I: Frequency-Sweeping Stability Tests and Applications

Silviu-Iulian Niculescu, Xu-Guang Li and Arben Çela

Abstract This chapter addresses the stability analysis of linear dynamical systems represented by delay differential equations with a focus on the effects induced by the delay, seen as a *parameter*, on the dynamical behavior. More precisely, we propose a *frequency-sweeping framework* for treating the problem, and the stability problem is reformulated in terms of properties of frequency-sweeping curves. The presentation is teaching-oriented and focuses more on discussing the main ideas of the method and their illustration through appropriate examples and less on explicit proofs of the results. Some applications from Life Sciences complete the presentation.

1 Introduction

One of the important problems in the analysis of dynamical systems is to understand how changes in the systems' parameters may affect the qualitative and quantitative behavior of the systems. Such a problem becomes challenging when the system is infinite-dimensional. This chapter is devoted to such issues in the case of linear time-delay systems represented by Delay Differential Equations (DDEs). More precisely, we focus on the analysis of the *effects* induced by the *delay parameters* on the (exponential) stability of the corresponding system.

Roughly speaking, to better capture the heterogeneity of the temporal phenomena in systems' dynamics the knowledge of "past" may appear as being essential in deriving appropriate models, and there exists a large variety of processes in nature

S.-I. Niculescu (✉)
Laboratory of Signals and Systems (L2S), University Paris-Saclay, CNRS, CentraleSupélec, Inria, Gif-sur-Yvette, France
e-mail: silviu.niculescu@l2s.centralesupelec.fr

X.-G. Li
School of Information Science and Engineering, Northeastern University, Shenyang, Liaoning, China

A. Çela
Department of Embedded Systems, University Paris-Est, ESIEE Paris, Noisy-Le-Grand, France

D. Breda (ed.), *Controlling Delayed Dynamics*, CISM International Centre for Mechanical Sciences 604, https://doi.org/10.1007/978-3-031-01129-0_5

having such characteristics. In these cases, the use of *delays*[1] in representing such phenomena may help in a better understanding of the underlying mechanisms or of the interactions/coupling with other (eventually spatial) phenomena. For instance, in Physics and Engineering, the delay may be used to model transport and propagation in interconnected cyber-physical systems or to represent the effect induced by the presence of humans in traffic flow models. In Life Sciences, the delays may appear as good approximations for incubation periods, maturation times or age structure in epidemic dynamics or they may be used to represent translation and transcription processes in genetic regulatory networks. Finally, in Economics, delays may appear in trade cycles, business cycles in commodity markets when defining the right balance between supply and market information-based demand.

Delay systems belong to the class of infinite-dimensional systems and there exist several ways to represent their dynamics. Functional Differential Equations (FDEs) sometimes called delay differential equations (DDEs) or differential-difference equations are, by now, a classical framework for studying the qualitative and quantitative effects induced by the delays on the systems' dynamics. Throughout this chapter, we will adopt such a model representation. For a good introduction to the theory of FDEs, we refer to Bellman and Cooke (1963), Hale and Verduyn Lunel (1993).

As pointed out in the open literature (see, e.g., Sipahi et al. 2011 and the references therein), understanding the way the delay may affect systems' dynamics is not a trivial task and we may have some dichotomic behaviors. For instance, in control, on one hand, large delays may induce instability in closed-loop even in the scalar case when controlling integrators. On the other hand, small delays in the input/output channels are useful in stabilizing oscillatory systems. There exists an abundant literature devoted to the analysis of the effects induced by the delays on the stability of DDEs and to present it in detail is out of the scope of this chapter. However, our intention is to point out some important (almost forgotten, in some cases) contributions related to the proposed methodology (i.e., *frequency-sweeping approach*), and we believe that this historical perspective is useful for a better understanding of the main ideas.

To the best of the authors' knowledge, it appears that the first complete characterization of the stability regions with respect to the system's parameters was derived by Hayes (1950) for scalar DDEs in both retarded and neutral cases. At the end of the 50s, Pinney (1958) presented a detailed analysis for scalar and second-order DDEs by using the argument principle. Under the assumption that the delay is known (and equal to one), by introducing several notions (root plateau, root cell, D-set), Pinney proposed an algorithm to compute the number of unstable roots of a quasipolynomial of low-order as a function of its coefficients. Through this procedure, the parameter-space is divided in several regions, such that each region is characterized by a constant number of unstable roots. The boundaries separating the regions correspond to the cases when the characteristic function has at least one root on the imaginary axis. Such a procedure is "close" to the so-called *D-partition* method

[1] The delays may be constant or time-varying, distributed or not over a finite or infinite time-interval, depending on the state vector or not.

developed by Neimark (1949) at the end of the 40s. For an historical perspective on the D-partition and some of the existing results in the literature, we refer to Gryazina et al. (2008).

Introduced by Lee and Hsu (1969) at the end of the 60s, the so-called τ-*partition* may be seen as the "dual" of the D-partition method. More precisely, in the case of a single and constant delay (parameter), this method allows computing the delay intervals guaranteeing that the trivial solution of the DDE is exponentially stable. As a byproduct of the analysis, for a given delay interval, one may explicitly follow how the roots of the characteristic function move with respect to the imaginary axis as a function of the delay parameter. As mentioned in the above reference, such a method has its origin in the works of Sokolov and Miasnikov in the 40s and detailed in the monograph of Popov (1962). To the best of the authors' knowledge, close to the ideas of root locus,[2] it appears that the first systematic discussion on the number of unstable roots by using the continuity of the roots with respect to the delay parameter can be found in Kashiwagi (1965), where the author introduced the notion of *stability indicative function* to count the number of unstable roots for a given delay value. Finally, for a pedagogical presentation as well as some extensions of the root locus method and classical well-known Nyquist criterion to deal with linear single-input/single-output systems with one delay in the input/output channel, we refer to Krall (1968) (see also Krall 1970 for a survey of the root-locus methods).

At the beginning of the 70s, Els'golts' and Norkin (1973) mention three tests for checking the asymptotic stability of DDEs: the amplitude-phase method (referring to Tsypkin's contributions), the D-partition method (discussed above) and the direct generalization of the Routh-Hurwitz method (mainly Çebotarev's contributions), with a more detailed discussion of the first two methods by using the argument principle as well as the Rouché's Lemma. The so-called *amplitude-phase method* proposed by Tsypkin (1946) in Control area in the 40s is at the origin at most of the existing *frequency-sweeping tests*[3] in the open literature, and its principle will be briefly presented in the forthcoming sections. More precisely, in its simplest form, Tsypkin's criterion allows concluding on the so-called *delay-independent (asymptotic) stability* of a closed-loop system, that is the stability is guaranteed for all delay values. Starting with the 80s, the development of tools and techniques in robust control allowed to reconsider some of the existing methods in the literature by interpreting the delay as an *uncertainty*, and there exists an abundant literature on the delay-independent/delay-dependent stability with a particular emphasis on the computation of the so-called *delay margin*.[4] For further discussions on such topics and

[2] The origins of root locus go back to the works of Evans at the end of the 40s (see, e.g., Evans 1950 and the references therein).

[3] To the best of the authors' knowledge, the notion of "frequency-sweeping" was formally introduced by Chen and Latchman (1995), Chen (1995) into a different methodological frame: robust analysis with respect to the delay parameter, seen as an *uncertainty*, see also Niculescu (2001).

[4] Under the assumption that the system free of delays is asymptotically stable, the delay margin is the maximal value $\tau_m > 0$ such that the asymptotic stability is guaranteed for all delays inside the interval $[0, \tau_m)$; see also Chen et al. (1995), Chen (1995).

various references, we refer to Niculescu (2001), Gu et al. (2003), Michiels and Niculescu (2014), Fridman (2014) and the references therein.

The aim of this chapter is twofold: first, to introduce a simple approach easy to understand and to apply for characterizing the exponential stability of the trivial solution of linear DDEs with respect to the delay parameter. This approach enters in the so-called τ-partition category and it is based in the construction of some appropriate *frequency-sweeping curves*. This construction will allow "translating" the behavior of the roots of the corresponding characteristic function with respect to the (delay) parameters in terms of properties of such curves. The continuity of the roots of the characteristic function with respect to the delay is the main ingredient of the approach. Although the main results are presented in the case of retarded DDEs including commensurate delays, the underlying ideas can be extended to incommensurate or to some classes of distributed delays and/or to other classes of DDEs (neutral). Several case studies as well as a few applications are briefly presented. Second, we wish emphasizing an *invariance principle* that is essential for having a complete characterization of the (exponential) stability of the trivial solution. In fact, the proposed framework allows a simpler understanding of the asymptotic behavior of multiple characteristic roots by using the properties of frequency-sweeping curves. The presentation is teaching-oriented including discussions on the main ideas of the method as well as its illustration through appropriate examples and less on the explicit proof of the results. The book written by Li et al. (2015) includes complementary material as well as the proofs of the main results presented in this chapter. Finally, it is worth mentioning that Pólya (1954)'s pattern on logical induction and analogy-based reasoning strongly influenced the authors in the presentation style adopted.

The remaining document is organized as follows: Sect. 2 includes some preliminaries and prerequisites. Next, a method based on the frequency-sweeping curves is presented in Sect. 3, followed by Sect. 4 devoted to a brief discussion on the asymptotic behavior of the critical imaginary roots at some critical delay values. The *invariance property* as well as its utility in characterizing the stability with respect to the delay are presented in Sect. 5. All these ideas and results allow proposing a unified frequency-sweeping framework for the stability analysis of DDEs with respect to the delay parameter, approach that is summarized in Sect. 6. Next, Sects. 7 and 8 present various extensions of the approach as well as some applications. Finally, a few notes and comments end the chapter.

Notations: Throughout this chapter, the following notations will be used: $\mathbb{Z}$ denotes the set of integers, $\mathbb{R}$ ($\mathbb{R}_+$) denotes the set of (positive) real numbers, $\mathbb{R}^* = \mathbb{R} \setminus \{0\}$ and $\mathbb{C}$ is the set of complex numbers. For $\lambda \in \mathbb{C}$, $\mathrm{Re}(\lambda)$ and $\mathrm{Im}(\lambda)$ denote the real part and imaginary part of λ, respectively; $\mathbb{C}_-$ and $\mathbb{C}_+$ denote the sets $\{\lambda \in \mathbb{C} : \mathrm{Re}(\lambda) < 0\}$ and $\{\lambda \in \mathbb{C} : \mathrm{Re}(\lambda) > 0\}$, respectively; $\mathrm{i}\mathbb{R}$ (with $\mathrm{i} = \sqrt{-1}$) is the imaginary axis and $\partial\mathbb{D}$ is the unit circle. For $a, b \in \mathbb{R}$, we denote $[\![a, b]\!] = [a, b] \cap \mathbb{Z}$, with the convention that $[a, b] = \emptyset$ if $a > b$. For $\gamma \in \mathbb{R}$, $\lceil \gamma \rceil$ denotes the smallest integer greater than or equal to γ. Next, $\mathbb{N}$ and $\mathbb{N}_+$ are the sets of non-negative integers and positive integers (≥ 1), respectively. For a (quasi)polynomial $a(\lambda)$ ($q(\lambda)$), $\deg(a)$ ($\deg(q)$) denotes its degree and $\sigma_s(a)$ ($\sigma_s(q)$) its spectrum.

Moreover, $\det(\cdot)$ denotes the determinant, and I the identity matrix. Finally, for a function $\phi(x, y)$, $\phi_{x^\alpha y^\beta}$ $(\alpha, \beta \in \mathbb{N})$ denotes the partial derivative $\frac{\partial^{\alpha+\beta}\phi(x,y)}{\partial x^\alpha \partial y^\beta}$.

2 Preliminaries and Prerequisites

To better fix the ideas, we recall some preliminary results and prerequisites concerning the stability of linear DDEs.

2.1 Linear Time-Delay Systems

Consider the following linear system described by the delay differential equation (DDE) of retarded type

$$\dot{x}(t) = A_0 x(t) + A_1 x(t-\tau), \tag{1}$$

under appropriate initial conditions, where $x(t) \in \mathbb{R}^r$ $(r \in \mathbb{N}_+)$ is the vector state at time t, A_0, $A_1 \in \mathbb{R}^{r\times r}$ are constant real matrices, and τ is the delay parameter, that is assumed to be positive $(\tau \in \mathbb{R}_+)$.

The corresponding characteristic function $f : \mathbb{C} \times \mathbb{R}_+ \mapsto \mathbb{C}$ is given by

$$f(\lambda, \tau) = \det\left(\lambda I - A_0 - A_1 e^{-\tau\lambda}\right), \tag{2}$$

which is a *quasipolynomial* of the form

$$f(\lambda, \tau) := a_0(\lambda) + a_1(\lambda)e^{-\tau\lambda} + \cdots + a_q(\lambda)e^{-q\tau\lambda}, \tag{3}$$

where $a_0(\lambda)$, …, $a_q(\lambda)$ $(q \in \mathbb{N}_+)$ are polynomials in λ with real coefficients and represent the so-called *coefficient functions*. It is easy to observe that the quasipolynomial (3) includes multiple delays τ_k but with the particular dependence $\tau_k = k\tau$ for all $k \in [\![0, q]\!]$. Such delays are called *commensurate*, and our main ideas are presented in such a setting. For a short discussion in the incommensurate delays case, see Sect. 7.

Using the same terminology as Bellman and Cooke (1963), a complex number $\lambda \in \mathbb{C}$ such that $f(\lambda, \tau) = 0$ is called a *characteristic root*. It is well-known that, for a $\tau > 0$, the characteristic function (2) of the DDE (1) has an *infinite number* of *characteristic roots*. A fundamental well-known result from the finite-dimensional case is still valid for DDEs (see, e.g., Bellman and Cooke 1963; Michiels and Niculescu 2014):

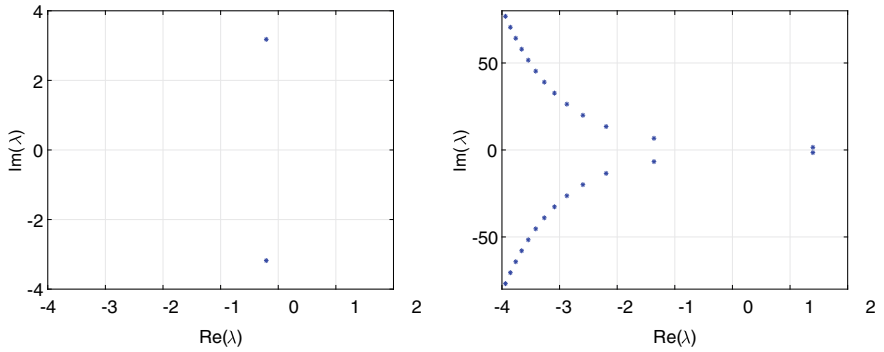

Fig. 1 Example 2.2: characteristic roots location $\mathrm{Re}(\lambda)$ versus $\mathrm{Im}(\lambda)$ for $\tau = 0.01$ (left) and $\tau = 1$ (right)

Theorem 2.1 *The trivial solution of the DDE (1) is exponentially stable if and only if all the characteristic roots of the quasipolynomial f (3) are located in the open left half-plane $\mathbb{C}_-$.*

Unfortunately, due to the infinite-dimensional nature of the system, it is not realistic to apply Theorem 2.1 directly. The following example illustrates the root distribution intuitively.

Example 2.2 Consider the following DDEs:

$$\dot{x}(t) = \begin{pmatrix} 0 & 1 \\ -1 & 1 \end{pmatrix} x(t) + \begin{pmatrix} 0 & 0 \\ -9 & -1.5 \end{pmatrix} x(t-\tau),$$

with the characteristic function $f(\lambda, \tau) = \lambda^2 - \lambda + 1 + (1.5\lambda + 9)e^{-\tau\lambda}$.

When $\tau = 0$, the system has two characteristic roots $-0.2500 \pm 3.1524\mathrm{i}$ both located in $\mathbb{C}_-$. As τ increases from 0 to $+\varepsilon$, infinitely many new characteristic roots appear at far left of the complex plane. Figure 1 (left) shows the case when $\tau = 0.01$, where the two points denote the locations of the "original" roots. Next, as τ increases, some roots move to the selected domain defined by $\mathrm{Re}(\lambda) \in [-4, 2]$ and $\mathrm{Im}(\lambda) \in [-4, 4]$. For instance, when $\tau = 1$, some roots enter in the "selected" domain and the "original" roots will leave the left-half plane and will enter in the right-half plane as shown in Fig. 1 (right). For further illustration, Fig. 2 gives the corresponding root loci w.r.t. the delay parameter.[5] □

A simple inspection of this example suggests that it will be important to understand how the behavior of the characteristic roots is affected by the delay parameter and, in particular, in the case when the delay is increased from 0 to 0_+. These issues will be addressed in the sequel.

[5] In this chapter, the root loci are numerically generated by using the DDE-BIFTOOL (Engelborghs et al. 2002; Sieber et al. 2016).

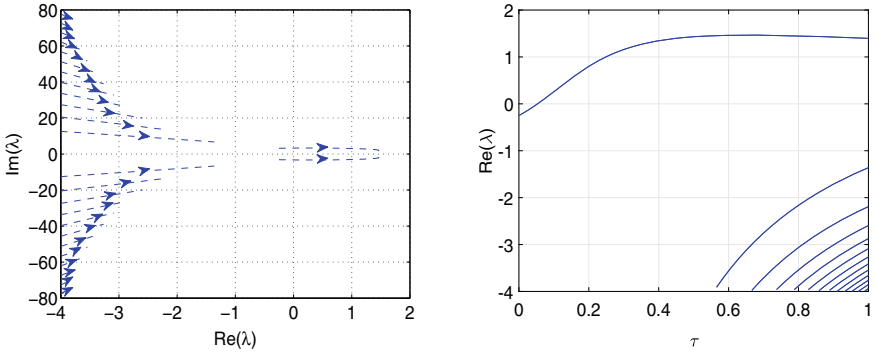

Fig. 2 Example 2.2: $\mathrm{Re}(\lambda)$ versus $\mathrm{Im}(\lambda)$ (left) and $\mathrm{Re}(\lambda)$ versus τ (right)

2.2 Characteristic Roots and Delay Parameter

In finite dimension, it has long been recognized that the roots of a polynomial are continuous functions of the coefficients as long as the leading coefficient does not vanish (see, e.g., Knopp 1996; Marden 1949). Furthermore, in the case of simple roots, these functions are also differentiable. Similar properties hold for quasipolynomials.

For the sake of simplicity, consider the simplest case $q = 1$ and assume that a_0 is a monic polynomial. Excepting the delay, assume that the set of parameters includes also the coefficients of the corresponding polynomials a_0 and a_1 and introduce the vector notation $\overrightarrow{p}$ for representing such parameters. Let $\mathcal{O}_p \subset \mathbb{R}^{n_p}$ be an open set, and assume that $\deg(a_0) > \deg(a_1)$, for all $\overrightarrow{p} \in \mathcal{O}_p$. Under these assumptions, the characteristic function (3) rewrites as $f : \mathbb{C} \times \mathcal{O}_p \times \mathbb{R}_+ \mapsto \mathbb{C}$:

$$f(\lambda, \overrightarrow{p}, \tau) := a_0(\lambda, \overrightarrow{p}) + a_1(\lambda, \overrightarrow{p})e^{-\lambda\tau}. \tag{4}$$

By using the properties of analytic functions, the quasipolynomial f given by (4) has some nice and interesting properties. For instance, the characteristic roots are isolated and only a finite number of roots lie in any compact set of the complex plane $\mathbb{C}$. Furthermore, any vertical strip of the complex plane includes at most a finite number of characteristic roots. Finally, there exists a real number γ, such that all the characteristic roots are confined to the half-plane $\mathbb{C}_\gamma$: $\{\lambda \in \mathbb{C} : \mathrm{Re}(\lambda) < \gamma\}$.[6] In conclusion, it is easy to observe that, surprisingly, despite its infinite-dimensional nature, the quasipolynomial f given by (4) has only a finite number of roots in the right-half plane $\mathbb{C}_+$. Finally, based on Rouché's lemma (see, e.g., Ahlfors 1979), we have:

Theorem 2.3 *Under the assumptions that a_0 is monic and that* $\deg(a_0) > \deg(a_1)$ *for all $\overrightarrow{p} \in \mathcal{O}_p$, let λ_0 be a characteristic root of $f(\cdot, \overrightarrow{p_0}, \tau_0)$ with multiplicity k.*

[6] For further discussions on such topics, we refer to Michiels and Niculescu (2014) and the references therein.

Then there exists a constant $\bar{\varepsilon} > 0$ *such that for all* $\varepsilon > 0$ *satisfying* $\varepsilon < \bar{\varepsilon}$, *there exists a* $\delta_\varepsilon > 0$ *such that* $f(\lambda;\ \overrightarrow{p_0} + \Delta\overrightarrow{p_0}, \tau_0 + \Delta\tau_0)$, *where* $\Delta\tau_0 \in \mathbb{R}$, $|\ \Delta\tau_0\ | < \delta_\varepsilon$, $\tau_0 + \Delta\tau_0 \geq 0$, $\Delta\overrightarrow{p_0} \in \mathbb{R}^{n_p}$, $\|\Delta\overrightarrow{p_0}\|_2 < \delta_\varepsilon$, *has exactly k zeros (multiplicity taken into account) in the disc* $\{\lambda \in \mathbb{C} :\ |\lambda - \lambda_0| < \varepsilon\}$.

Remark 2.4 This result simply states that, in the retarded case, as long as the leading coefficient of the polynomial a_0 is not vanishing and the delay is positive, the characteristic roots of the quasipolynomial (4) are continuous functions of the coefficients of the polynomials a_0 and a_1 and of the delay τ, seen as a parameter. □

For the stability analysis purposes, it is important to know where the rightmost characteristic root is located as well as the way it is affected by parameters change. To answer to such questions, introduce now the so-called *spectral abscissa function* $(\overrightarrow{p}, \tau) \in \mathcal{O}_p \times \mathbb{R}_+ \mapsto \alpha_s(\overrightarrow{p}, \tau) \in \mathbb{R}$,

$$\alpha_s(\overrightarrow{p}, \tau) := \sup\left\{\mathrm{Re}(\lambda) :\ f(\lambda, \overrightarrow{p}, \tau) = 0, \quad \overrightarrow{p} \in \mathcal{O}_p, \quad \tau \in \mathbb{R}_+\right\}.$$

As a consequence of Theorem 2.3, we have two interesting properties that will be exploited in the forthcoming sections:

(1) the function α_s always *exists*, is *bounded* and *continuous*;
(2) as the delay and/or parameters vary, the multiplicity summation of the roots of f in the open right-half plane ($\mathbb{C}_+$) can change only *if a root appears on*[7] or *crosses the imaginary axis*.

Remark 2.5 The assumption $\deg(a_0) > \deg(a_1)$ for all parameters $\overrightarrow{p} \in \mathcal{O}_p$ is essential to guarantee the continuity of the spectral abscissa function. Concerning the second property, an elementary proof for general second-order DDEs of retarded type ($\deg(a_0)$=2 and $\deg(a_1) = 1$) can be found in Cooke and Grossman (1982). □

Remark 2.6 As expected, the ideas above still hold in the commensurate delays case ($\tau_i = i\tau$ for $i \in [\![1, r]\!]$ and $\tau \in \mathbb{R}_+$ in (3)). For incommensurate delays, by introducing an appropriate notion of *delay rays* $\left\{r\overrightarrow{\tau} : r \in \mathbb{R}_+\right\}$, Datko (1978) proved that the continuity of the spectral abscissa holds with respect to one parameter, that is $r \in \mathbb{R}_+$. □

Remark 2.7 To construct the stability charts in the scalar and second-order linear DDEs in the case when $\tau = 1$, Pinney (1958) introduced the notion of (x_r, k_r)-*root plateau set*, that is the set of parameters for which the characteristic function f has k_r and only k_r roots "λ_i", $i \in [\![0, k_r]\!]$, with $\mathrm{Re}(\lambda_i) > x_r$. Thus, in the limit cases, $(0, 0)$-root plateau set covers the *stability regions*, and the minimal value of x_r of the $(x_r, 0)$-root plateau is the *spectral abscissa* notion introduced above. □

[7] Such a case may occur in the case of neutral DDEs or if the coefficients of the quasipolynomials depend on the delay parameters.

Remark 2.8 ("Small" delays: retarded DDEs) Consider now the case when the only parameter is the delay and assume that it is sufficiently small: $\tau = \varepsilon > 0$. Under the assumption that $a_1 \neq 0$, the use of Rouché's Theorem allows to conclude that the finite characteristic roots of $f(\cdot, \varepsilon)$ can be made arbitrarily close to the finite roots of $f(\cdot, 0)$ and there exists an infinite number of roots whose real parts approach negatively infinite.[8] In particular, if the system free of delays has no roots on the imaginary axis, when increasing the delay from 0 to 0_+, although the system changes its character from finite- to infinite-dimensional, the stability/instability of the delay-free system is preserved for sufficiently small delays. □

Consider now (4) and assume that the leading coefficient of the polynomial a_1 is not vanishing for all $(\overrightarrow{p}, \tau) \in \mathcal{O}_p \times \mathbb{R}_+$. The property mentioned above (Remark 2.8) does not necessarily hold in all the cases, and there are two particular situations of interest: (i) *neutral* case ($\deg(a_0) = \deg(a_1)$) and (ii) *delay-dependent coefficients* of the polynomials a_0 and a_1.

Remark 2.9 ("Small" delays: neutral DDEs) Although the individual characteristic roots behave continuously with respect to the system's parameters (see Michiels and Niculescu 2014), the spectral abscissa function is, in general, *not continuous*. Recall that a_0 is a monic polynomial, $\deg(a_0) = \deg(a_1)$, and denote by a_{1,m_0} the leading coefficient of the polynomial a_1 and assume that $a_{1,m_0} \in \mathcal{O}_0$, where $\mathcal{O}_0$ is an open set not including the origin ($0 \notin \mathcal{O}_0$). With these notations, we introduce the delay-difference equation: $y(t) + a_{1,m_0} y(t-\tau) = 0$ associated to the neutral DDE. The corresponding characteristic function $f_D : \mathbb{C} \times \mathcal{O}_0 \times \mathbb{R}_+ \mapsto \mathbb{C}$ writes as:

$$f_D(\lambda, a_{1,m_0}, \tau) = 1 + a_{1,m_0} e^{-\lambda\tau}.$$

As discussed in Michiels and Niculescu (2014), the delay-difference equation above and the original neutral DDE are related by an interesting property. More precisely, a necessary condition for the exponential stability of the trivial solution of the neutral DDE is the exponential stability of the trivial solution of the corresponding delay-difference equation. Now,

(i) if $|a_{1,m_0}| < 1$,[9] we have a similar property to the one valid in the retarded DDEs. More precisely, as the delay and/or parameters vary, the multiplicity summation of the roots of the characteristic function f in the open right-half plane ($\mathbb{C}_+$) can change only *if a root appears on* or *crosses* the *imaginary axis*.
(ii) if $|a_{1,m_0}| > 1$, then increasing the delay from 0 to 0_+ generates instability even in the case when the system free of delay is stable.

For further discussions on such topics, we refer to Hale and Verduyn Lunel (1993). Finally, Sect. 7 includes a few illustrative examples. □

[8] For a simple and elementary proof, we refer to Shaughnessy and Kashiwagi (1969).

[9] It simply guarantees the exponential stability of the trivial solution of the corresponding delay-difference equation.

Remark 2.10 ("Small" delays: delay-dependent coefficients) Such a case may appear in control engineering when the controller includes the derivative of a signal that is not necessarily available for measurement. For instance, in the case of classical proportional-derivative (PD) controllers, the derivative action can be implemented by using a (standard) Euler delay-difference approximation scheme. The corresponding closed-loop system may be *improperly-posed* in the sense that the implementation scheme may lead to instability for infinitesimal delay values in constructing the delay-difference approximation even if the initial PD-controller stabilizes the original system. Such a case is illustrated in Mendéz-Barrios et al. (2022), where it was shown that if the relative degree of the system is one,[10] then the derivative gain may be at the origin of such a lack of continuity.[11] For further discussions on DDEs with delay-dependent coefficients, we refer to Chi et al. (2018a, b) and the references therein. □

By taking into account all the observations and comments above, it appears that the stability analysis of DDEs whose characteristic function is given by f in (4) can be reduced to the following three steps:

(a) detecting all the characteristic roots "iω_c" (of f) located on the imaginary axis (i$\mathbb{R}$). Such roots are called *critical (characteristic) imaginary roots*. The delays associated to a critical "iω_c" are called *critical delays* and we may have an infinite number of critical delays for the same imaginary root. Finally, a pair (λ, τ) is called a *critical pair* if λ is a critical imaginary root and τ corresponds to a critical delay;
(b) understanding and characterizing the behavior of the characteristic roots located on i$\mathbb{R}$ with respect to the parameters' change;
(c) counting the roots crossing from $\mathbb{C}_-$ to $\mathbb{C}_+$ and vice versa by taking into account the root multiplicity.

Due to the infinite-dimensional nature of the system, it is clear that the steps (a)–(c) are not trivial even in the case when we consider one parameter - the *delay*. When the delay $\tau \equiv 0$, the characteristic roots location problem reduces to the analysis of the spectrum location of a polynomial. Next, in the simplest case when the system free of delay has not roots located on i$\mathbb{R}$, increasing the delay from 0 to 0_+ will conserve the distribution of the roots located on $\mathbb{C}_+$ as long as, there are no roots "crossing" the imaginary axis. Assume further that the system free of delays is exponentially stable. In such a situation, when increasing the delays, the stability property holds as long as there are no characteristic roots "arriving" on the imaginary axis from $\mathbb{C}_-$. These intuitive ideas are at the origin of a lot of theoretical developments in the open literature as briefly explained in the sequel.

For a better understanding of the main ideas of the so-called τ*-partition method* and related *frequency-sweeping tests,* consider now the (strictly proper) linear time-

[10] The relative degree is defined by $\deg(a_0) - \deg(a_1)$.

[11] More precisely, in this configuration (i.e., improperly-posed approximation), a characteristic root appears on the real axis in $\mathbb{C}_+$ from $+\infty$ when the delay is increased from 0 to 0_+.

invariant (LTI) single-input/single-output (SISO) system $\Sigma(A, b, c^T)$ with the state-space representation:

$$\Sigma : \quad \begin{cases} \dot{x}(t) = Ax(t) + bu(t) \\ y(t) = c^T x(t), \end{cases}$$

where the transfer function $H_{yu}(\lambda)$ of Σ writes as $H_{yu}(\lambda) = a_1(\lambda)/a_0(\lambda)$, for some appropriate real polynomials a_i, $i \in [\![0, 1]\!]$, whose coefficients are given by the "entries" (A, b, c^T) of Σ. Assume now that Σ is controlled by the feedback law $u(t) = -ky(t - \tau)$ with $k \in \mathcal{O}_0 \subset \mathbb{R}^*$. Under the assumption that k and τ are the *parameters* then the stability of the system in closed-loop reduces to the analysis of the location of the spectrum of the quasipolynomial $f(\cdot, k, \tau)$ given by $f(\lambda, k, \tau) := a_0(\lambda) + ka_1(\lambda)e^{-\lambda\tau}$.

For the sake of brevity, assume that a_0 and a_1 are coprime. If the gain is $k = 1$, f simply rewrites as $f(\lambda; \tau) := a_0(\lambda) + a_1(\lambda)e^{-\lambda\tau}$. Surprisingly, if

$$|a_1(\mathrm{i}\omega)| < |a_0(\mathrm{i}\omega)|, \tag{5}$$

for all $\omega \in \mathbb{R}$, then $\sigma_s(f) \cap \mathrm{i}\mathbb{R} = \emptyset$. By using Theorem 2.3, it is easy to observe that the characteristic roots of f can not migrate from $\mathbb{C}_-$ to $\mathbb{C}_+$ or vice-versa if τ is increased from 0 to $+\infty$. Such a system is called *hyperbolic* and it has an interesting property: *the location of the spectrum of the polynomial $a_0 + a_1$ will define the stability/instability of the system for all delays $\tau \in \mathbb{R}_+$*. For a deeper discussion on such topics, see, e.g., Niculescu (2001) (commensurate delays) and Hale et al. (1985) (more general setting).

If $0 \in \sigma_s(f(\cdot, 0))$, then $f(0, \tau) = 0$, $\forall \tau \in \mathbb{R}_+$. Thus, the origin is an *invariant root*.[12] Now, if $0 \notin \sigma_s(f(\cdot, 0))$, checking (5) for $\forall \omega \in \mathbb{R}_+^*$ is sufficient to guarantee system's hyperbolicity. Assume now that $\sigma_s(f(\cdot, 0)) \subset \mathbb{C}_-$. As observed by Tsypkin (1946), the closed-loop system is *delay-independently stable* if and only if the condition (5) holds for all $\omega \in \mathbb{R}_+^*$. It can be simply checked from the plot of z_1, where the mapping $\omega \mapsto z_1(\omega) := -a_0(\mathrm{i}\omega)/a_1(\mathrm{i}\omega)$, for $\omega \in \mathbb{R}_+^*$ defines the simplest *frequency sweeping curve*.

Example 2.11 (*Scalar case*) Consider the following DDE:

$$\dot{x}(t) = -ax(t) - bx(t - \tau),$$

where $a, b \in \mathbb{R}$. The characteristic function is given by $f(\lambda, \tau) = a_0(\lambda) + a_1(\lambda)e^{-\tau\lambda}$ with $a_0(\lambda) = \lambda + a$ and $a_1(\lambda) = b$. It is easy to see that:

$$\sup_{\omega \in \mathbb{R}_+^*} \frac{|a_1(\mathrm{i}\omega)|}{|a_0(\mathrm{i}\omega)|} = \sup_{\omega \in \mathbb{R}_+^*} \frac{|b|}{\sqrt{\omega^2 + a^2}} = \frac{|b|}{|a|},$$

[12] The common roots a_0 and a_1 on $\mathrm{i}\mathbb{R}$ are also invariant roots w.r.t. τ.

and thus if $|a| > |b|$, the system is *hyperbolic*. Consider now the case $|a| = |b|$. If $b = -a$ and $b \neq 0$, then f has a double root at the origin and the hyperbolicity is lost. Furthermore, the root at the origin is invariant with respect to the delay. Now, if $a = b \neq 0$, the system is still hyperbolic.

Based on the remarks above, if $b \in \mathbb{R}^*$ and $|a| \geq |b|$, we have that the system is *stable (unstable) independent* of the *delay* if and only if $a + b > 0$ ($a + b < 0$). Finally, it is worth mentioning that in the delay-independent instability case, the characteristic function has one (and only one) unstable real root moving on the positive real axis as long as τ varies. □

Consider now the case when the system above is *not hyperbolic*. Then there exists at least one value $\omega_c \in \mathbb{R}$, such that $f(\mathrm{i}\omega_c, \tau) = 0$ for some critical delay $\tau = \tau_c \in \mathbb{R}_+$. The real "$\omega_c$" is called *crossing frequency*, and the collection of all "ω_c" defines the *crossing set*:

$$\Omega_c := \{\omega \in \mathbb{R} : \ |a_0(\mathrm{i}\omega)| = |a_1(\mathrm{i}\omega)|\}.$$

At this stage, there are two important remarks:

(i) first, $\mathrm{card}(\Omega_c)$ is *finite*, and its computation reduces to the computation of the positive roots of an appropriate polynomial;

(ii) second, the knowledge of a crossing frequency $\omega_{i,c} \in \Omega_c$ allows to compute the minimal critical delay value $\tau^*_{i,c} \in \mathbb{R}_+$[13] generating the set of *critical (crossing) delays*

$$\mathcal{T}(\omega_{i,c}) := \left\{\tau^*_{i,c} + \frac{2k\pi}{\omega_c} \geq 0, \quad k \in \mathbb{Z}\right\}.$$

Indeed, if we formally denote $z = e^{-\mathrm{i}\omega\tau}$, then $f(\mathrm{i}\omega, \tau) = a_0(\mathrm{i}\omega) + a_1(\mathrm{i}\omega)e^{-\mathrm{i}\omega\tau}$ can be interpreted as a two-variate polynomial $f_a(\omega, z) = a_0(\mathrm{i}\omega) + a_1(\mathrm{i}\omega)z$ with z on the unit circle of the complex plane.[14] Thus, the "quantity" (if it exists) $z = -a_0(\mathrm{i}\omega)/a_1(\mathrm{i}\omega)$ may lead to a solution of f_a at some frequency ω_c if $|a_1(\mathrm{i}\omega_c)| = |a_0(\mathrm{i}\omega_c)|$, condition naturally related to the definition of the crossing (frequency) set above. For a deeper discussion of the remarks (i)–(ii) above, we refer to Michiels and Niculescu (2014).

Under the assumption of a simple characteristic root $\omega_0 \in \Omega_c$ for some delay $\tau_0 \in \mathcal{T}(\omega_0)$, Cooke and Grossman (1982) discussed the behavior of the characteristic root $\mathrm{i}\omega_0$ for values close to τ_0 by using the "quantity" $s_c := \mathrm{sgn}(\mathrm{Re}(d\lambda/d\tau))$ evaluated a $\lambda = \mathrm{i}\omega_0$ and $\tau = \tau_0$. Such an idea was further refined in Cooke and van den Driessche (1986) and largely used in the open literature during the last 30 years. More precisely, if the characteristic root located on the imaginary axis moves towards instability (stability), we will have a *stability switch* (*reversal*).[15] Surprisingly, in the case of

[13] Such a value always exists and it may be 0.

[14] It is easy to see the way the roots of f and f_a are linked. For instance, for any pair $(\mathrm{i}\omega_s, \tau_s) \in \mathbb{R}^*_+ \times \mathbb{R}^*_+$ satisfying $f(\mathrm{i}\omega_s, \tau_s) = 0$, $f_a(\omega_s, z_s) = 0$, where $z_s = e^{-\mathrm{i}\omega_s}$, etc.

[15] To the best of the authors' knowledge, during the 70s, the notions of *(stability) switches/reversals* appear in Cooke's publications.

simple imaginary roots, the "quantity" s_c above does not include any information on the delay parameter. In fact, the derivative of the function $g_a : \mathbb{R} \mapsto \mathbb{R}$ defined by $g_a(\omega) := |a_0(\mathrm{i}\omega)|^2 - |a_1(\mathrm{i}\omega)|^2$ evaluated at the crossing frequency $\omega = \omega_c$ indicates the crossing type: *switch* (*reversal*) if $g'(\omega_c) > 0$ (< 0).

2.3 Stability Problem and the Delay Parameter

Following the notation used in the literature (see, e.g., Lee and Hsu 1969; Olgac and Sipahi 2002), denote by $NU(\tau_0) \in \mathbb{N}$ the number of the characteristic roots located in $\mathbb{C}_+$ for the delay $\tau = \tau_0$. According to Theorem 2.1, the (linear) system is asymptotically stable for a delay value $\tau = \tau_0$, if and only if there are no characteristic roots located on the imaginary axis and $NU(\tau_0) = 0$. In the commensurate delays case, our objective is to obtain its exhaustive stability set for the delay parameter τ,[16] which is referred to as the *complete stability problem*. Based on the root continuity property mentioned in the previous paragraphs, the complete stability analysis can be fulfilled in two steps by solving two problems:

Problem 1: *How to exhaustively detect the critical imaginary roots and the corresponding critical delays?*

For a critical pair $(\lambda_\alpha, \tau_{\alpha,k})$, denote by $n \in \mathbb{N}_+$ the multiplicity of λ_α at $\tau_{\alpha,k}$. Clearly, a critical imaginary root is called a *simple (multiple) critical imaginary root* if the corresponding index $n = 1$ ($n > 1$). In other words, the index n simply implies that for $\lambda = \lambda_\alpha$ and $\tau = \tau_{\alpha,k}$,

$$f_{\lambda^0} = \cdots = f_{\lambda^{n-1}} = 0,\ f_{\lambda^n} \neq 0.$$

Next, introduce the index $g \in \mathbb{N}_+$ at $(\lambda_\alpha, \tau_{\alpha,k})$, by which we may *artificially* treat $\tau_{\alpha,k}$ as a g-multiple root for $f(\lambda, \tau) = 0$ when $\lambda = \lambda_\alpha$, having the property that when $\lambda = \lambda_\alpha$ and $\tau = \tau_{\alpha,k}$,

$$f_{\tau^0} = \cdots = f_{\tau^{g-1}} = 0,\ f_{\tau^g} \neq 0.$$

Remark 2.12 Unlike for the critical imaginary roots, the analytic computation for the other characteristic roots is generally very difficult. □

It is relatively simple to solve Problem 1 and various effective methods are available in the literature. In Sect. 3, a method based on the *frequency-sweeping curves* is discussed. Once Problem 1 is solved, we have to analyze the variation of a critical imaginary root as τ increases near the corresponding critical delay (value), called the *asymptotic behavior* of a critical imaginary root.

Problem 2: *How to analyze the asymptotic behavior of the critical imaginary roots w.r.t. the corresponding critical delays?*

[16] I.e., the whole set for $\tau \geq 0$ such that $NU(\tau) = 0$ excluding the possible critical points.

Remark 2.13 Owing to the conjugate symmetry of the spectrum, it suffices to consider only the critical imaginary roots with non-negative imaginary parts. □

Remark 2.14 The critical delays divide the positive τ-axis into infinitely many subintervals and within each subinterval $NU(\tau)$ is constant. Solving *Problem 2* allows monitoring $NU(\tau)$ as τ increases. For instance, consider a subinterval $\tau \in (\tau', \tau'')$ where τ' and τ'' are two positive critical delays such that there are no other critical delays inside this subinterval. If the value of $NU(\tau' - \varepsilon)$ is known and the asymptotic behavior of the critical imaginary roots at $\tau = \tau'$ is properly studied, we may precisely know the value of $NU(\tau' + \varepsilon)$. According to the root continuity argument, for any $\tau \in (\tau', \tau'')$, $NU(\tau) = NU(\tau' + \varepsilon)$. □

Problem 2 is rather involved, and is moreover divided into two sub-problems, as follows:

Problem 2.1: *How to analyze the asymptotic behavior of a critical imaginary root at a critical delay?*

To such an end, introduce some further notations. Suppose that (α, β) (with $\beta > 0$) is a critical pair with the index n. Near this critical pair, there exist n (characteristic) roots $\lambda_i(\tau)$ (counted with multiplicities) continuous w.r.t. τ satisfying $\alpha = \lambda_i(\beta), i = 1, \ldots, n$. Under some perturbation ε $(-\varepsilon)$ on β, the n roots are expressed by $\lambda_i(\beta + \varepsilon)$ $(\lambda_i(\beta - \varepsilon))$, $i = 1, \ldots, n$. Denote the number of unstable roots among $\lambda_1(\beta + \varepsilon), \ldots, \lambda_n(\beta + \varepsilon)$ $(\lambda_1(\beta - \varepsilon), \ldots, \lambda_n(\beta - \varepsilon))$ by $NU_\alpha(\beta^+)$ $(NU_\alpha(\beta^-))$. With these notations, we define:

$$\Delta NU_\alpha(\beta) \triangleq NU_\alpha(\beta^+) - NU_\alpha(\beta^-)$$

Here, $\Delta NU_\alpha(\beta)$ stands for the change of $NU(\tau)$ caused by the variation of the critical imaginary root $\lambda = \alpha$ as τ increases from $\beta - \varepsilon$ to $\beta + \varepsilon$.

Remark 2.15 The function NU introduced above is similar to the so-called *stability indicative function* introduced in the 60s by Kashiwagi (1965). To the best of the authors' knowledge, under the assumption of simple characteristic imaginary roots, the first systematic discussion on the number of unstable roots by using the continuity of the roots with respect to the delay can be found in Kashiwagi's works. □

Remark 2.16 If the system (1) free of delays has original critical imaginary roots $\lambda_\alpha = \mathrm{i}\omega_\alpha$, then $\tau_{\alpha,0} = 0$. In this case, the asymptotic behavior of the critical pair $(\lambda_\alpha, \tau_{\alpha,0})$ refers to how the original critical imaginary root λ_α varies as τ increases from 0. This information is necessary for computing $NU(+\varepsilon)$ (as it will be discussed in Theorem 6.1). □

The asymptotic behavior of a critical imaginary root at a critical delay can be properly derived if the associated Puiseux series[17] can be obtained (see, for instance, Sect. 4 below). As a critical imaginary root has an infinite number of critical delays

[17] For an elementary introduction to Puiseux series, we refer to Casas-Alvero (2000).

(see Remark 3.5 below), we need to solve the second sub-problem of *Problem 2* described as follows:

Problem 2.2: *How to analyze the asymptotic behavior of a critical imaginary root w.r.t. all the infinitely many positive critical delays?*

To solve this problem, the *invariance property* is essential (see Sect. 5 below).

3 Frequency-Sweeping Curves

We start this section by proposing the procedure to generate the *frequency-sweeping curves*. First, the characteristic function $f(\lambda, \tau)$ can be transformed by letting $z = e^{-\tau\lambda}$ into a *two-variate (auxiliary) polynomial*:

$$p_a(\lambda, z) = \sum_{i=0}^{q} a_i(\lambda) z^i.$$

Frequency-Sweeping Curves: sweep $\omega \geq 0$ and for each $\lambda = \mathrm{i}\omega$ we have q values of z such that $p(\mathrm{i}\omega, z) = 0$ (denoted by $z_1(\mathrm{i}\omega), \ldots, z_q(\mathrm{i}\omega)$). Thus, we obtain q *frequency-sweeping curves* $\Gamma_i(\omega)$: $|z_i(\mathrm{i}\omega)|$ versus ω, $i \in [\![1, q]\!]$.

Denote by $\Im_1$ the line parallel to the abscissa axis with ordinate 1. If $(\lambda_\alpha, \tau_{\alpha,k})$ is a *critical pair* with index g, then g frequency-sweeping curves intersect $\Im_1$ at $\omega = \omega_\alpha$ and the frequency ω_α is called a *critical frequency*.

Such a simple construction shows that *Problem 1* can be effectively solved by appropriately using the frequency-sweeping curves.

Remark 3.1 For each given ω, $p(\mathrm{i}\omega, z) = 0$ is a polynomial equation of z. It can be (numerically) solved by using the MATLAB command `roots`. □

Remark 3.2 Consider now the case when some curves $\Gamma_i(\omega)$ intersect $\Im_1$ at $\omega = 0$. We may have two situations: $z = 1$ and $z \neq 1$. In the first case, we have an invariant root at the origin (for all $\tau \in \mathbb{R}_+$). In the second case, $\lambda = 0$ is not a characteristic root and this point should be ignored. □

Remark 3.3 As expected, if no critical imaginary roots are detected from the frequency-sweeping curves, the system is *hyperbolic* and the property holds independently of the delay value. □

Example 3.4 Consider again the scalar DDE in Example 2.11. One can easily obtain the same conclusions by observing the frequency-sweeping curves. First, the system is asymptotically stable when $\tau = 0$ under the condition $a + b > 0$. Second, the frequency-sweeping curve does not intersect the line $\Im_1$ for any $\tau > 0$ under the condition $a \geq |b|$. It is worth noting that, the frequency-sweeping curve intersects the line $\Im_1$ at $\omega = 0$ (with the corresponding $z = -1$) if $a = b > 0$. However, as discussed in Remark 3.2, $\lambda = 0$ is not a critical imaginary root. For illustration,

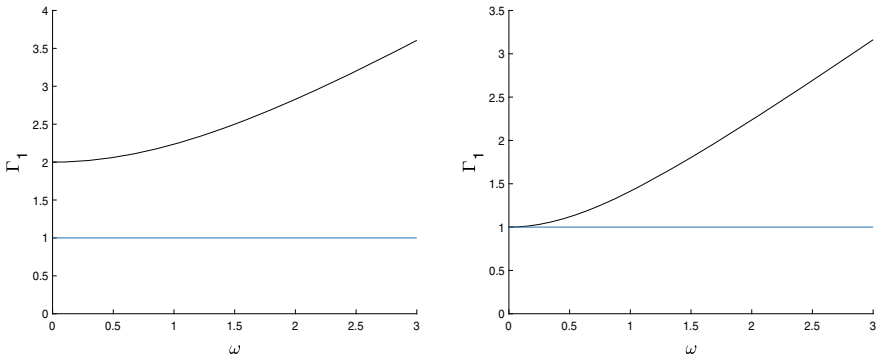

Fig. 3 Example 3.4: frequency-sweeping curves Γ_1 versus ω for $b = 1$; left: $a = 2$ and right: $a = 1$

the frequency-sweeping curves in the *delay-independent stability* cases are given respectively in Fig. 3 (left: strong; right: weak). □

Consider now that the system is *not hyperbolic*. In this case, without any loss of generality, suppose there are "u" critical pairs for $p(\lambda, z) = 0$: $(\lambda_0 = \mathrm{i}\omega_0, z_0)$, $(\lambda_1 = \mathrm{i}\omega_1, z_1), \ldots, (\lambda_{u-1} = \mathrm{i}\omega_{u-1}, z_{u-1})$ where $\omega_0 \leq \omega_1 \leq \cdots \leq \omega_{u-1}$. Notice that two critical pairs may share the same critical imaginary root. Once all the critical pairs $(\lambda_\alpha, z_\alpha)$, $\alpha = 0, \ldots, u-1$, are found, all the critical pairs (λ, τ) can be obtained. For instance, for each critical imaginary root λ_α, the corresponding critical delays are given by $\tau_{\alpha,k} \stackrel{\Delta}{=} \tau_{\alpha,0} + \frac{2k\pi}{\omega_\alpha}, k \in \mathbb{N}$, where $\tau_{\alpha,0} \stackrel{\Delta}{=} \min\{\tau \geq 0 : e^{-\tau\lambda_\alpha} = z_\alpha\}$. Thus, the pairs $(\lambda_\alpha, \tau_{\alpha,k})$, $k \in \mathbb{N}$ define a set of critical pairs associated to $(\lambda_\alpha, z_\alpha)$.

Remark 3.5 A critical imaginary root λ_α is *invariant* with respect to the *delay shift* $\frac{2\pi}{\omega_\alpha}$.[18] However, the multiplicity of a critical imaginary root is not necessarily conserved by the delay shift. □

Example 3.6 Consider the system (Example 5.11 in Gu et al. 2003)

$$\dot{x}(t) = \begin{pmatrix} 0 & 1 \\ -2 & 0.1 \end{pmatrix} x(t) + \begin{pmatrix} 0 & 0 \\ 1 & 0 \end{pmatrix} x(t-\tau),$$

for which $f(\lambda, \tau) = \lambda^2 - 0.1\lambda + 2 - e^{-\tau\lambda}$ and $p_a(\lambda, z) = -z + \lambda^2 - 0.1\lambda + 2$. The frequency-sweeping curve can be easily generated by using MATLAB.[19] For instance, in MATLAB environment, for each given ω, we assign its value to a variable `w`. The solution of $z_1(\mathrm{i}\omega)$ for $p(\mathrm{i}\omega, z) = 0$ can be obtained by using the command `roots([-1,(w* i)^ 2-0.1*w*i+2])`.

[18] More precisely, if λ_α is a critical imaginary root for $\tau = \tau_{\alpha,0}$, then the system has a critical imaginary root λ_α for all $\tau = \tau_{\alpha,0} + k\frac{2\pi}{\omega_\alpha}, k \in \mathbb{N}$.

[19] Or other software for scientific computation.

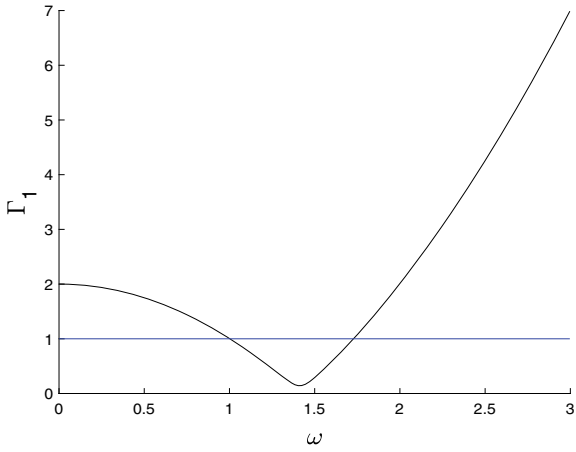

Fig. 4 Example 3.6: frequency-sweeping curve Γ_1 versus ω

The frequency-sweeping curve is depicted in Fig. 4. Two critical pairs (λ, z) for $p_a(\lambda, z) = 0$ are found from the frequency-sweeping curve: $(\lambda_0 = 1.0025\mathrm{i}, z_0 = 0.9950 - 0.1003\mathrm{i})$ and $(\lambda_1 = 1.7277\mathrm{i}, z_1 = -0.9850 - 0.1728\mathrm{i})$. For the first critical pair, we calculate the corresponding critical delays such that $e^{-\tau\lambda_0} = z_0 = e^{-(0.1004+2k\pi)\mathrm{i}}$. More precisely, one gets: $\tau_{0,k} = 0.1002 + \frac{2k\pi}{1.0025}$, $k \in \mathbb{N}$. Similarly, for the second critical pair, the associated critical delays can be computed straightforwardly from the condition: $e^{-\tau\lambda_1} = z_1 = e^{-(2.9680+2k\pi)\mathrm{i}}$. We have that $\tau_{1,k} = 1.7178 + \frac{2k\pi}{1.7277}$, $k \in \mathbb{N}$. Thus, the τ-axis is divided into intervals: $[0, 0.1002)$, $(0.1002, 1.7178)$, $(1.7178, 5.3546)$, $(5.3546, 6.3676)$, …, and $NU(\cdot)$ is constant in each such intervals. □

4 Asymptotic Behavior of a Critical Imaginary Root at a Critical Delay

As $f(\lambda, \tau)$ (3) is a quasipolynomial, it is analytical w.r.t. the variables λ and τ. Thus, in a small neighborhood of a critical pair $(\lambda_\alpha, \tau_{\alpha,k})$, the characteristic function $f(\lambda, \tau)$ can be expanded as a convergent power series of the form:

$$f(\lambda,\tau) = f(\lambda_\alpha,\tau_{\alpha,k}) + (f_\lambda\Delta\lambda + f_\tau\Delta\tau) + \frac{f_{\lambda\lambda}(\Delta\lambda)^2+2f_{\lambda\tau}\Delta\lambda\Delta\tau+f_{\tau\tau}(\Delta\tau)^2}{2!} + \frac{f_{\lambda^3}(\Delta\lambda)^3+3f_{\lambda^2\tau}(\Delta\lambda)^2\Delta\tau+3f_{\lambda\tau^2}\Delta\lambda(\Delta\tau)^2+f_{\tau^3}(\Delta\tau)^3}{3!} + \cdots, \tag{6}$$

where $\lambda = \lambda_\alpha + \Delta\lambda$ and $\tau = \tau_{\alpha,k} + \Delta\tau$. The expression (6) is a standard two-variable Taylor expansion of $f(\lambda, \tau)$. Next, we may reformulate (6) in a more convenient form. Since $f(\lambda, \tau) = f(\lambda_\alpha, \tau_{\alpha,k}) = 0$, we have:

$$0 = (f_\lambda \Delta\lambda + f_\tau \Delta\tau) + \frac{f_{\lambda\lambda}(\Delta\lambda)^2 + 2f_{\lambda\tau}\Delta\lambda\Delta\tau + f_{\tau\tau}(\Delta\tau)^2}{2!} + \frac{f_{\lambda^3}(\Delta\lambda)^3 + 3f_{\lambda^2\tau}(\Delta\lambda)^2\Delta\tau + 3f_{\lambda\tau^2}\Delta\lambda(\Delta\tau)^2 + f_{\tau^3}(\Delta\tau)^3}{3!} + \cdots. \tag{7}$$

Recall the definition of the index n: $f_\lambda = \cdots = f_{\lambda^{n-1}} = 0$ and $f_{\lambda^n} \neq 0$. As a result, from the right-hand side of (7), for a critical pair $(\lambda_\alpha, \tau_{\alpha,k})$, we now obtain a series expression $F_{(\lambda_\alpha,\tau_{\alpha,k})}(\Delta\lambda, \Delta\tau)$ describing the relation between $\Delta\lambda$ and $\Delta\tau$ as follows:

$$F_{(\lambda_\alpha,\tau_{\alpha,k})}(\Delta\lambda, \Delta\tau) = \sum_{i=n}^{\infty} L_{i0}(\Delta\lambda)^i + \sum_{i=0}^{\infty}(\Delta\lambda)^i \sum_{l=1}^{\infty} L_{il}(\Delta\tau)^l = 0, \tag{8}$$

where $L_{il} = \frac{f_{\lambda^i\tau^l}}{(i+l)!}\binom{i+l}{i}$.[20] In addition, in view of the index g, we have that $L_{01} = \cdots = L_{0(g-1)} = 0$ and $L_{0g} \neq 0$. From the root loci, it is easy to observe that for a $\Delta\tau$, $\Delta\lambda$ must have n solutions (multiplicity taken into account) satisfying $F_{(\lambda_\alpha,\tau_{\alpha,k})}(\Delta\lambda, \Delta\tau) = 0$ and $\Delta\lambda \to 0$ as $\Delta\tau \to 0$:

Theorem 4.1 *Consider the DDE (1) and assume $\lambda_\alpha \neq 0$ is an n-multiple imaginary root for $\tau = \tau_{\alpha,k}$. If τ is perturbed at $\tau_{\alpha,k}$ by $\Delta\tau$, the variation $\Delta\lambda$ of λ at λ_α corresponds to n Puiseux series solutions with respect to $\Delta\tau$. Any Puiseux series solution converges in a neighborhood of $(\Delta\lambda = 0, \Delta\tau = 0)$.*

Algorithm 1 (Puiseux series computation)

Step 0: Let $\alpha_0 = 0$ and $\beta_0 = g$.

Step 1: Define $\mu = \max\{\frac{\beta_0-\beta}{\alpha-\alpha_0} > 0 : L_{\alpha\beta} \neq 0, \alpha > \alpha_0, \beta < \beta_0\}$, where the coefficients $L_{\alpha\beta}$ are defined in (8).

Step 2: If there exists a μ, go to Step 3. Otherwise, skip to Step 5.

Step 3: Collect all the non-zero $L_{\alpha\beta}$ satisfying $\frac{\beta_0-\beta}{\alpha-\alpha_0} = \mu$ to form a set

$$\left\{ L_{\alpha_1\beta_1}(\Delta\lambda)^{\alpha_1}(\Delta\tau)^{\beta_1},\ L_{\alpha_2\beta_2}(\Delta\lambda)^{\alpha_2}(\Delta\tau)^{\beta_2},\ \ldots \right\},$$

with the order $\alpha_1 > \alpha_2 > \ldots$ We find a set of Puiseux series

$$\Delta\lambda = \widetilde{C}_{\mu,l}(\Delta\tau)^\mu + o((\Delta\tau)^\mu),\ l = 1, \ldots, \alpha_1 - \alpha_0,$$

where the coefficients $\widetilde{C}_{\mu,l}$ are the solutions of the polynomial equation

$$L_{\alpha_1\beta_1}C^{\alpha_1-\alpha_0} + L_{\alpha_2\beta_2}C^{\alpha_2-\alpha_0} + \cdots + L_{\alpha_0\beta_0} = 0.$$

Step 4: Let $\alpha_0 = \alpha_1$, $\beta_0 = \beta_1$ and return to Step 1.

Step 5: The algorithm stops.

Theorem 4.2 *For an n-multiple non-zero critical imaginary root of the DDE (1), all the Puiseux series can be obtained by Algorithm 1.*

[20] Here, $\binom{i+l}{i}$ denotes the number of i-combinations from a set of $i + l$ elements.

Remark 4.3 It is known that a simple critical imaginary root's asymptotic behavior corresponds to a Taylor series and we may treat them as a specific type of Puiseux series. In addition, the Puiseux series for a multiple critical imaginary root may include a Taylor series (in the case of more than one conjugacy class), see e.g., Examples 4.3 and 4.4 in Li et al. (2015). □

Remark 4.4 In general, when $\Delta\tau = \pm\varepsilon$, the first-order terms of the Puiseux series do not contain purely imaginary numbers, and are sufficient for the asymptotic behavior analysis. However, there exists a few cases, called *degenerate*, when such a property does not hold and, to conclude, higher order terms are necessary. In this case, we may still invoke Algorithm 1 in an iterative manner to obtain them. For a deeper discussion, we refer to Sect. 4.3 of Li et al. (2015). □

For an n-multiple critical imaginary root, we may invoke n *independent* Puiseux series. Unfortunately, such expressions are not always simple to use. However, they can be expressed in a more compact form if we introduce the concept of *conjugacy class*. Roughly speaking, for n Puiseux series belonging to one conjugacy class, one expression of Puiseux series with polydromy order n will be sufficient to describe all of them (see, e.g., Sect. 4.4 of Li et al. (2015) for further details).

Consider the critical pair $(\lambda_\alpha, \tau_{\alpha,k})$ with $\tau_{\alpha,k} > 0$. Then $\Delta NU_{\lambda_\alpha}(\tau_{\alpha,k})$ can be accurately calculated by means of the Puiseux series. More precisely, we substitute $\Delta\tau = +\varepsilon$ ($\Delta\tau = -\varepsilon$) into the corresponding Puiseux series, and the value of $\Delta NU_{\lambda_\alpha}(\tau_{\alpha,k})$ can be obtained by comparing the numbers of the values of the Puiseux series in $\mathbb{C}_+$ when $\Delta\tau = +\varepsilon$ ($\Delta\tau = -\varepsilon$).

Example 4.5 Consider a DDE with the characteristic function $f(\lambda, \tau) = e^{-\tau\lambda} + \frac{3\pi}{8}\lambda^5 - \frac{\pi^2}{8}\lambda^4 + \frac{5\pi}{4}\lambda^3 - \frac{\pi^2}{4}\lambda^2 + \frac{7\pi}{8}\lambda - \frac{\pi^2}{8} + 1$. For $\tau = \pi$, $\lambda = \mathrm{i}$ is a triple critical imaginary root with $g = 1$. By invoking Algorithm 1, we have three expressions of the Puiseux series $\Delta\lambda = (0.55 + 0.09\mathrm{i})(\Delta\tau)^{\frac{1}{3}} + o((\Delta\tau)^{\frac{1}{3}})$, $\Delta\lambda = (-0.36 + 0.43\mathrm{i})(\Delta\tau)^{\frac{1}{3}} + o((\Delta\tau)^{\frac{1}{3}})$, and $\Delta\lambda = (-0.20 - 0.53\mathrm{i})(\Delta\tau)^{\frac{1}{3}} + o((\Delta\tau)^{\frac{1}{3}})$. These three expressions correspond to the same conjugacy class. Therefore, any one among them is sufficient to fully express the asymptotic behavior of the triple critical imaginary root. For instance, we choose the expression $\Delta\lambda = (0.55 + 0.09\mathrm{i})(\Delta\tau)^{\frac{1}{3}} + o((\Delta\tau)^{\frac{1}{3}})$.

The variation of the triple critical imaginary root as the delay increases from π to $\pi + \varepsilon$ ($\pi - \varepsilon$ to π) can be deduced by substituting the three values of $(+\varepsilon)^{\frac{1}{3}}$ ($(-\varepsilon)^{\frac{1}{3}}$) into $(\Delta\tau)^{\frac{1}{3}}$ for this expression. One may notice that the value sets of the Puiseux series by the substitution of the values of $(+\varepsilon)^{\frac{1}{3}}$ and $(-\varepsilon)^{\frac{1}{3}}$ do not change if we choose the other two expressions of the Puiseux series. As a result, we see that the number of the characteristic roots located in $\mathbb{C}_+$ decreases by 1 due to the asymptotic behavior of the triple critical imaginary root, that is, $\Delta NU_{\mathrm{i}}(\pi) = -1$ (see, for instance, the root loci in Fig. 5). □

To summarize, we can now properly solve *Problem 2.1*.

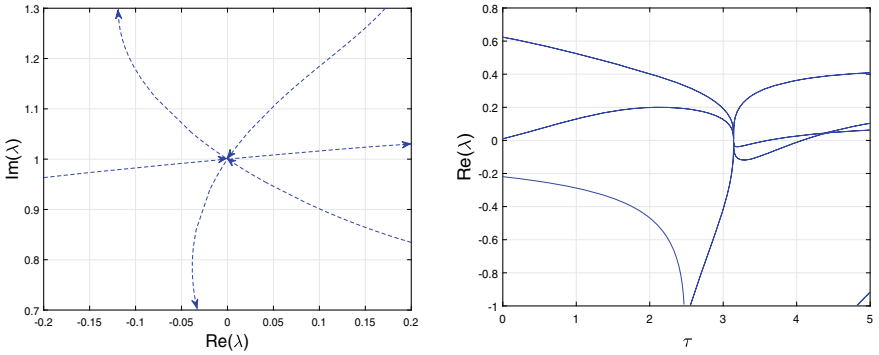

Fig. 5 Example 4.5: root loci $\mathrm{Re}(\lambda)$ versus $\mathrm{Im}(\lambda)$ and $\mathrm{Re}(\lambda)$ versus τ

5 Invariance Property of Asymptotic Behavior

In the sequel, we introduce some necessary notations concerning the asymptotic behavior of frequency-sweeping curves. For further properties and deeper discussions, we refer to Chap. 8 of Li et al. (2015).

Under the assumption $\lambda_\alpha \neq 0$, suppose that $\left\{(\lambda_\alpha, \tau_{\alpha,k}), k \in \mathbb{N}\right\}$ is a set of critical pairs with the index g. It is important to mention that g is a constant w.r.t. different k (see Property 1.2 of Li et al. 2015). Then there must exist g *frequency-sweeping curves* such that $z_i(\mathrm{i}\omega_\alpha) = z_\alpha = e^{-\tau_{\alpha,0}\lambda_\alpha}$ intersecting $\Im_1$ when $\omega = \omega_\alpha$. Among such g frequency-sweeping curves, when $\omega = \omega_\alpha + \varepsilon$ ($\omega = \omega_\alpha - \varepsilon$), we denote the number of the frequency-sweeping curves above the line $\Im_1$ by $NF_{z_\alpha}(\omega_\alpha + \varepsilon)$ ($NF_{z_\alpha}(\omega_\alpha - \varepsilon)$). Introduce now a new notation $\Delta NF_{z_\alpha}(\omega_\alpha)$ as

$$\Delta NF_{z_\alpha}(\omega_\alpha) \triangleq NF_{z_\alpha}(\omega_\alpha + \varepsilon) - NF_{z_\alpha}(\omega_\alpha - \varepsilon).$$

Such a "quantity" describes the asymptotic behavior of the frequency-sweeping curves at the critical frequency $\omega = \omega_\alpha$.

Theorem 5.1 *For a critical imaginary root λ_α of the DDEs (1), it always holds that $\Delta NU_{\lambda_\alpha}(\tau_{\alpha,k})$ is a constant $\Delta NF_{z_\alpha}(\omega_\alpha)$ for all $\tau_{\alpha,k} > 0$.*

The contribution of the above Theorem 5.1 is two-fold:

(i) First, it provides a simple method (observing the frequency-sweeping curves) to compute $\Delta NU_{\lambda_\alpha}(\tau_{\alpha,k})$, without invoking the Puiseux series; in other words, the change of $\Delta NU_{\lambda_\alpha}(\tau_{\alpha,k})$ as the delay is increased from $\tau^-_{\alpha,k}$ to $\tau^+_{\alpha,k}$ can be expressed in terms of changes of frequency-sweeping curves w.r.t. the line $\Im_1$.

(ii) Second, an interesting *invariance property* is claimed: for a critical imaginary root λ_α, since $\Delta NF_{z_\alpha}(\omega_\alpha)$ is invariant w.r.t. the delay parameter, the same property holds for $\Delta NU_{\lambda_\alpha}(\tau_{\alpha,k})$ for all $\tau_{\alpha,k} > 0$. Such a property is helpful to overcome the peculiarity that a critical imaginary root corresponds to infinitely many critical delays.

Remark 5.2 By using different arguments, the invariance property was addressed by Olgac and Sipahi (2002) (simple critical roots on imaginary axis: $n = 1$) and by Jarlebring and Michiels (2010) (case $n = 2$, $g = 1$). □

Example 5.3 Consider a DDE with the characteristic function $f(\lambda, \tau) = \sum_{i=0}^{4} a_i(\lambda)e^{-i\tau\lambda}$ where $a_0(\lambda) = \frac{15}{8}\pi^2\lambda^6 + (\frac{11}{4}\pi - \frac{15}{8}\pi^2)\lambda^4 + \frac{9}{2}\pi\lambda^3 + (1 + \frac{1}{2}\pi - \frac{75}{8}\pi^2)\lambda^2 + (3 + \frac{9}{2}\pi)\lambda + 1 - \frac{9}{4}\pi - \frac{45}{8}\pi^2$, $a_1(\lambda) = \frac{5}{4}\pi\lambda^5 + \frac{11}{2}\pi\lambda^4 + (1 + \frac{7}{2}\pi)\lambda^3 + (\pi + 7)\lambda^2 + (11 + \frac{9}{4}\pi)\lambda + 4 - \frac{9}{2}\pi$, $a_2(\lambda) = \frac{5}{4}\pi\lambda^5 + \frac{11}{4}\pi\lambda^4 + (3 - \pi)\lambda^3 + (13 + \frac{1}{2}\pi)\lambda^2 + (15 - \frac{9}{4}\pi)\lambda + 6 - \frac{9}{4}\pi$, $a_3(\lambda) = 3\lambda^3 + 9\lambda^2 + 9\lambda + 4$, and $a_4(\lambda) = \lambda^3 + 2\lambda^2 + 2\lambda + 1$.

We study the asymptotic behavior of critical pairs (i, $(2k + 1)\pi$), with $g = 2$. The frequency-sweeping curves are given in Fig. 6. According to Theorem 5.1, it is easy to see from Fig. 6 that $\Delta NU_{\mathrm{i}}((2k + 1)\pi) = 0$ for all $k \in \mathbb{N}$. In fact, the asymptotic behavior of critical pairs (i, $(2k + 1)\pi$) is complex. The multiplicity n of the critical root $\lambda = \mathrm{i}$ is 2, 3, 4, 2, when τ is π, 3π, 5π, 7π, respectively. The Puiseux series, all degenerate, are:

$$\begin{cases} \Delta\lambda = 0.1592\mathrm{i}\Delta\tau + (0.5371 - 0.3138\mathrm{i})(\Delta\tau)^2 + o((\Delta\tau)^2), \\ \Delta\lambda = 0.0796\mathrm{i}\Delta\tau + 0.0063\mathrm{i}(\Delta\tau)^2 + 0.0421\mathrm{i}(\Delta\tau)^3 \\ \quad +(0.0362 + 0.0137\mathrm{i})(\Delta\tau)^4 + o((\Delta\tau)^4), \end{cases}$$

$$\begin{cases} \Delta\lambda = (0.0385 + 0.0698\mathrm{i})(\Delta\tau)^{\frac{1}{2}} + o((\Delta\tau)^{\frac{1}{2}}), \\ \Delta\lambda = 0.1592\mathrm{i}\Delta\tau + 0.0253\mathrm{i}(\Delta\tau)^2 + 0.6696\mathrm{i}(\Delta\tau)^3 \\ \quad +(1.1585 + 0.4376\mathrm{i})(\Delta\tau)^4 + o((\Delta\tau)^4), \end{cases}$$

$$\begin{cases} \Delta\lambda = -0.1592\mathrm{i}\Delta\tau + (-05371 + 03644\mathrm{i})(\Delta\tau)^2 + o((\Delta\tau)^2), \\ \Delta\lambda = -0.0988\mathrm{i}(\Delta\tau)^{\frac{1}{3}} + (-00356 + 00028\mathrm{i})(\Delta\tau)^{\frac{2}{3}} + o((\Delta\tau)^{\frac{2}{3}}), \end{cases}$$

$$\begin{cases} \Delta\lambda = -0.0796\mathrm{i}\Delta\tau + (-0.0671 + 0.0487\mathrm{i})(\Delta\tau)^2 + o((\Delta\tau)^2), \\ \Delta\lambda = -0.1592\mathrm{i}\Delta\tau + 0.0253\mathrm{i}(\Delta\tau)^2 + 0.6615\mathrm{i}(\Delta\tau)^3 \\ \quad +(-1.1585 - 0.4363\mathrm{i})(\Delta\tau)^4 + o((\Delta\tau)^4), \end{cases}$$

for $k = 0, 1, 2$, and 3, respectively. The above Puiseux series are consistent with the analysis by Theorem 5.1. Moreover, Theorem 5.1 significantly reduces the computation burden for asymptotic behavior analysis, as the Puiseux series for this system are rather involved.[21] □

Thus, *Problem 2.2* is appropriately solved.

[21] For instance, in our case, for each k, the Puiseux series has multiple conjugacy classes; next, for each k, the Puiseux series involves many degenerate terms, and finally, the structure of Puiseux series is variable w.r.t. different k.

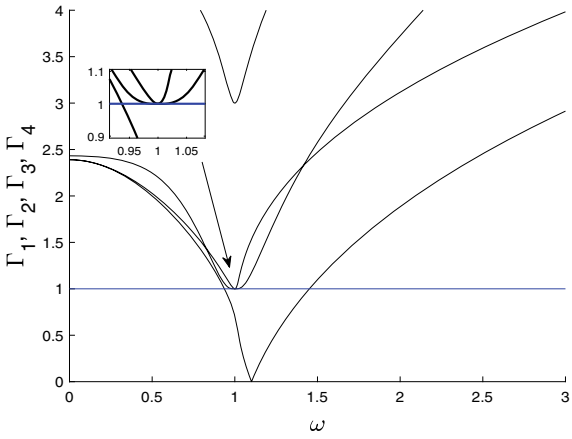

Fig. 6 Example 5.3: frequency-sweeping curves $\Gamma_1, \Gamma_2, \Gamma_3, \Gamma_4$ versus ω

6 A Unified Frequency-Sweeping Approach for Complete Stability Problem

With the results above, we can now systematically solve our *problem*.

6.1 Computation of $NU(+\varepsilon)$

As a first step, we keep track[22] of $NU(\tau)$ from $\tau = +\varepsilon$.

Theorem 6.1 *If the system (1) has no critical imaginary roots when $\tau = 0$, $NU(+\varepsilon) = NU(0)$. Otherwise, $NU(+\varepsilon) - NU(0)$ equals to the number of the values in $\mathbb{C}_+$ of the Puiseux series for all the corresponding critical imaginary roots when $\tau = 0$ with $\Delta\tau = +\varepsilon$.*

Example 6.2 Consider the DDE with the characteristic function $f(\lambda, \tau) = e^{-3\tau\lambda} - 3e^{-2\tau\lambda} + 3e^{-\tau\lambda} + \lambda^4 + 2\lambda^2$. It is easy to see that $f(\lambda, 0)$ has four characteristic roots. More precisely, $\lambda = \mathrm{i}$ ($\lambda = -\mathrm{i}$) is a double critical imaginary root. We may have the Puiseux series for the critical pair (i, 0):

$$\Delta\lambda = (0.3536 + 0.3536\mathrm{i})(\Delta\tau)^{\frac{3}{2}} + o((\Delta\tau)^{\frac{3}{2}}). \tag{9}$$

Substituting $\Delta\tau = +\varepsilon$ into (9) indicates that as τ increases from 0, the double root i splits into two branches towards $\mathbb{C}_-$ and $\mathbb{C}_+$ respectively, as seen in the root loci given in Fig. 7. Thus, by using the conjugate symmetry property, $NU(+\varepsilon) = +2$. □

[22] Since some DDEs may have critical imaginary roots when $\tau = 0$, one needs to consider a sufficiently "small" delay value $\varepsilon > 0$.

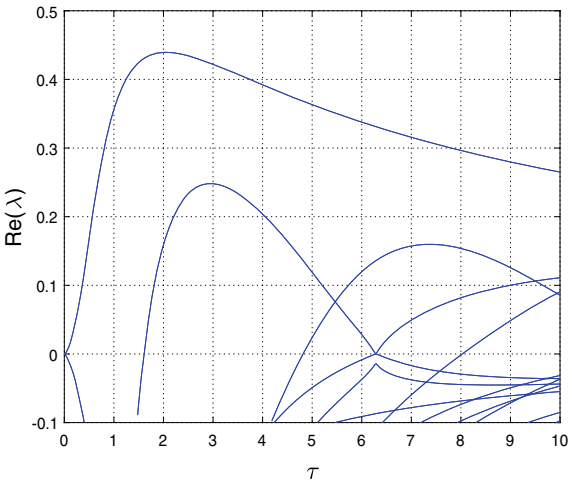

Fig. 7 Example 6.2: Re(λ) versus τ

6.2 Explicit $NU(\tau)$ Expression

The invariance property allows concluding with the following:

Theorem 6.3 *For any $\tau > 0$ which is not a critical delay, $NU(\tau)$ for the DDE (1) can be explicitly expressed as*

$$NU(\tau) = NU(+\varepsilon) + \sum_{\alpha=0}^{u-1} NU_\alpha(\tau),$$

where

$$NU_\alpha(\tau) = \begin{cases} 0, \tau < \tau_{\alpha,0}, \\ 2U_{\lambda_\alpha}\left\lceil \frac{\tau-\tau_{\alpha,0}}{2\pi/\omega_\alpha} \right\rceil, \tau > \tau_{\alpha,0}, \end{cases} if\ \tau_{\alpha,0} \neq 0,$$

$$NU_\alpha(\tau) = \begin{cases} 0, \tau < \tau_{\alpha,1}, \\ 2U_{\lambda_\alpha}\left\lceil \frac{\tau-\tau_{\alpha,1}}{2\pi/\omega_\alpha} \right\rceil, \tau > \tau_{\alpha,1}, \end{cases} if\ \tau_{\alpha,0} = 0.$$

6.3 Further Classification

With the explicit $NU(\tau)$ expression, we may accurately study the stability for any finitely long τ-interval. However, in order to thoroughly solve the complete stability problem, we need to understand the way $NU(\tau)$ changes when $\tau \to \infty$. To such an end, we introduce the following notions: a critical frequency ω_α is called a *crossing*

(touching) frequency for a frequency-sweeping curve $\Gamma_i(\omega)$, if $\Gamma_i(\omega)$ crosses (touches without crossing) the line $\Im_1$ as ω increases near ω_α. We have the following:

Theorem 6.4 *If the frequency-sweeping curves have a crossing frequency, there exists some delay value τ^* such that the time-delay system (1) is unstable for all $\tau > \tau^*$ and $\lim_{\tau\to\infty} NU(\tau) = \infty$.*

Theorem 6.5 *The DDE (1) must fall in the following three types:*

(i) Type 1: Crossing frequencies exist and $\lim_{\tau\to\infty} NU(\tau) = \infty$.
(ii) Type 2: Crossing and touching frequencies do not exist and $NU(\tau) = NU(0)$ for all $\tau > 0$.
(iii) Type 3: Crossing frequencies do not exist but touching frequencies exist and, with the exception of critical delays, $NU(\tau)$ is a constant for all $\tau \geq 0$.

Remark 6.6 A DDE of Type 2 is hyperbolic. Furthermore, if $NU(0) = 0$, it is *stable independent* of the *delay*. Discussions on other cases can be found in Sect. 9.1 of Li et al. (2015). □

6.4 Procedure for Complete Stability Analysis

We now present a unified approach for studying our stability problem:

Step 1: Generate the frequency-sweeping curves, through which we can detect all the critical imaginary roots and the corresponding critical delays.

Step 2: For each critical imaginary root λ_α, we may choose any positive critical delay $\tau_{\alpha,k}$ to compute $\Delta NU_{\lambda_\alpha}(\tau_{\alpha,k})$. Alternatively, according to Theorem 5.1, we may directly have from the frequency-sweeping curves that $\Delta NU_{\lambda_\alpha}(\tau_{\alpha,k}) = \Delta NF_{z_\alpha}(\omega_\alpha)$.

Step 3: Compute $NU(+\varepsilon)$ (by Theorem 6.1).

Step 4: Obtain the explicit expression of $NU(\tau)$ as stated in Theorem 6.3 and have a "$NU(\tau)$ versus τ" plot.

The DDE (1) is asymptotically stable for all delay intervals satisfying the condition $NU(\tau) = 0$. In addition, according to Theorem 6.5, the behavior when $\tau \to \infty$ is known.

Example 6.7 Consider again the system in Example 5.3. When $\tau = 0$ there are three characteristic roots located in $\mathbb{C}_+$ and no characteristic roots located in the imaginary axis. According to Theorem 6.1, $NU(+\varepsilon) = NU(0) = 3$. The frequency-sweeping curves are given in Fig. 6. Theorem 6.3 allows deriving $NU(\tau)$ expression. The variation of $NU(\tau)$ is shown in Fig. 8. As crossing frequencies exist, in light of Theorem 6.4, $NU(\tau) = \infty$ as $\tau \to \infty$. To resume, the system is *unstable independent of the delay*, but without being hyperbolic. □

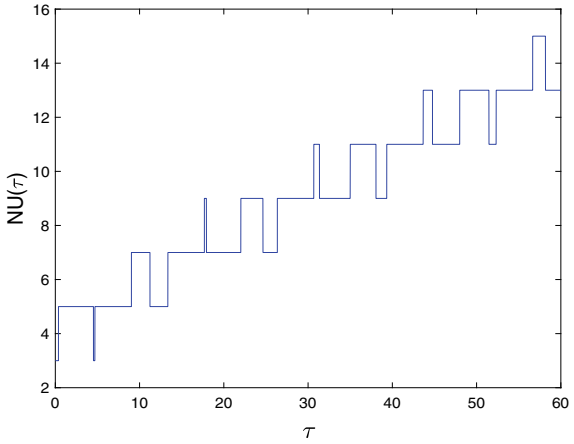

Fig. 8 Example 6.7: $NU(\tau)$ versus τ plot

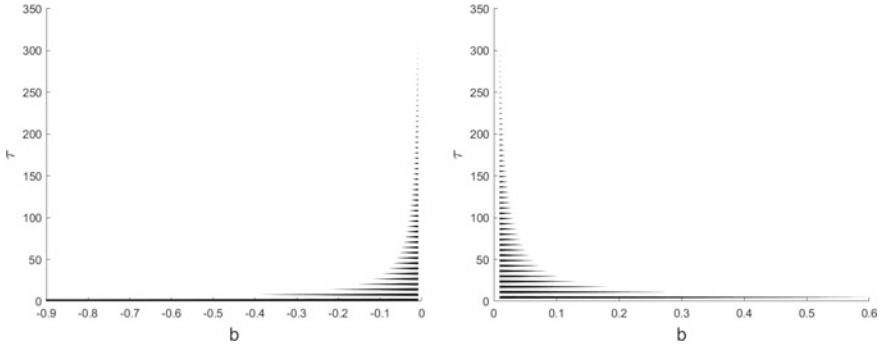

Fig. 9 Example 6.8: stability regions in (b, τ) parameter space

Example 6.8 Consider the DDE with the characteristic function

$$f(\lambda, \tau) = \lambda^2 + a^2 + be^{-\tau\lambda}, \quad a > 0.$$

It is easy to see that the system is asymptotically stable if and only if one of the following cases occurs:

(i) $-a^2 < b < 0$ and τ lies in the intervals $(\frac{2k\pi}{\sqrt{a^2+b}}, \frac{(2k+1)\pi}{\sqrt{a^2-b}})$ for all $k \in \mathbb{N}$ such that $\frac{2k\pi}{\sqrt{a^2+b}} < \frac{(2k+1)\pi}{\sqrt{a^2-b}}$;

(ii) $a^2 > b > 0$ and τ lies in the intervals $(\frac{(2k+1)\pi}{\sqrt{a^2-b}}, \frac{(2k+2)\pi}{\sqrt{a^2+b}})$ for all $k \in \mathbb{N}$ such that $\frac{(2k+1)\pi}{\sqrt{a^2-b}} < \frac{(2k+2)\pi}{\sqrt{a^2+b}}$.

For illustration of the cases (i)–(ii), take $a = 1$. The corresponding stability regions are depicted in Fig. 9 (left) and (right), respectively. □

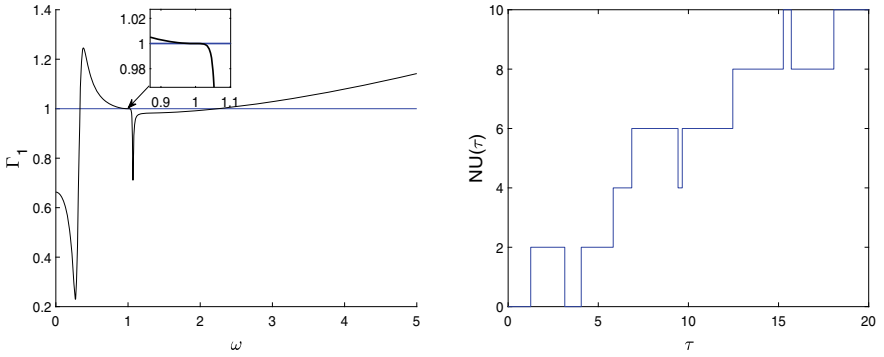

Fig. 10 Example 6.9: frequency-sweeping curve Γ_1 versus ω and $NU(\tau)$ versus τ plot

Example 6.9 [Stability reversals: further insights] Consider the time-delay system $\dot{x}(t) = A_0x(t) + A_1x(t-\tau)$ with

$$A_0 = \begin{pmatrix} 0 & 1 & \cdots & 0 \\ \vdots & \vdots & \ddots & \vdots \\ 0 & 0 & \cdots & 1 \\ \alpha_0 & \alpha_1 & \cdots & \alpha_4 \end{pmatrix}, A_1 = \begin{pmatrix} 0 & 0 & \cdots & 0 \\ \vdots & \vdots & \ddots & \vdots \\ 0 & 0 & \cdots & 0 \\ \beta_0 & \beta_1 & \cdots & \beta_4 \end{pmatrix},$$

where $\alpha_0 = \frac{\pi}{2} - \frac{\pi^2}{8} - 1$, $\alpha_1 = -2 + \frac{\pi}{2}$, $\alpha_2 = -\frac{\pi^2}{4} + \pi - 10$, $\alpha_3 = -3 + \frac{\pi}{2}$, $\alpha_4 = -\frac{\pi^2}{8} + \frac{\pi}{2} - 8$, $\beta_0 = -1$, $\beta_1 = -1$, $\beta_2 = -10$, $\beta_3 = -1$, and $\beta_4 = -8$. The characteristic function is $f(\lambda, \tau) = \lambda^5 - \sum_{\ell=0}^{4} \alpha_\ell \lambda^\ell - (\sum_{\ell=0}^{4} \beta_\ell \lambda^\ell) e^{-\tau\lambda}$. In this case, the frequency-sweeping curve is shown in Fig. 10 (left). First, we observe that three sets of critical pairs are detected: $(0.3340\mathrm{i}, 5.8296 + \frac{2k\pi}{0.3340})$, $(\mathrm{i}, (2k+1)\pi)$, and $(2.2421\mathrm{i}, 1.2525 + \frac{2k\pi}{2.2421})$. Second, when $\tau = 0$, all the characteristic roots are located in $\mathbb{C}_-$ and, according to Theorem 6.1, $NU(+\varepsilon) = NU(0) = 0$. Then, according to Theorem 6.3, we have $NU(\tau) = \sum_{\alpha=0}^{2} NU_\alpha(\tau)$, with:

$$NU_0(\tau) = \begin{cases} 0, \tau < \tau_3, \\ 2U_{0.3340\mathrm{i}} \left\lceil \frac{\tau - 5.8296}{18.8125} \right\rceil, \tau > \tau_3, \end{cases}$$

$$NU_1(\tau) = \begin{cases} 0, \tau < \tau_2, \\ 2U_{\mathrm{i}} \left\lceil \frac{\tau - \pi}{2\pi} \right\rceil, \tau > \tau_2, \end{cases} \quad NU_2(\tau) = \begin{cases} 0, \tau < \tau_1, \\ 2U_{2.2421\mathrm{i}} \left\lceil \frac{\tau - 1.2525}{2.8024} \right\rceil, \tau > \tau_1. \end{cases}$$

where $\tau_1 = 1.2525$, $\tau_2 = \pi$ and $\tau_3 = 5.8296$. In view of Theorem 5.1, the values for $U_{0.3340\mathrm{i}}$, U_{i}, and $U_{2.2421\mathrm{i}}$ are $+1$, -1, and $+1$, respectively. The variation of $NU(\tau)$ is shown in Fig. 10 (right). The system has two and only *two stability intervals* of τ: $[0, 1.2525)$ and $(\pi, 4.0549)$.

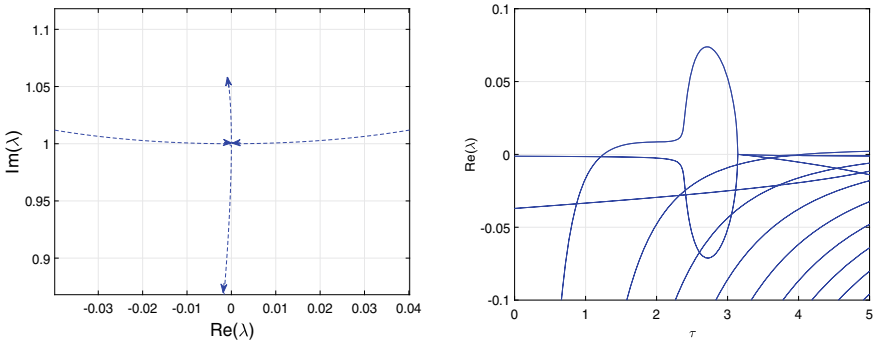

Fig. 11 Example 6.9: Re(λ) versus Im(λ) and Re(λ) versus τ

One can observe an interesting phenomenon. The asymptotic behavior of the critical pair ($\lambda = \mathrm{i}, \tau = \pi$) with the indices[23] $n = 2$ and $g = 1$ corresponds to the Puiseux series:

$$\Delta\lambda = 0.1468\mathrm{i}(\Delta\tau)^{\frac{1}{2}} + (-0.0033 - 0.1473\mathrm{i})(\Delta\tau)^{\frac{2}{2}} + o((\Delta\tau)^{\frac{2}{2}}).$$

In such a case, as τ increases from $\pi - \varepsilon$ to π two root loci[24] collide on the imaginary axis $\mathrm{i}\mathbb{R}$ and thereby a double critical imaginary root $\lambda = \mathrm{i}$ appears. As τ further increases from π to $\pi + \varepsilon$ the double root $\lambda = \mathrm{i}$ splits into two root loci, both towards the left-half plane $\mathbb{C}_-$. Meanwhile, there are no other characteristic roots in $\mathbb{C}_+$ when $\tau = \pi - \varepsilon$, and hence the system *regains asymptotic stability* at $\tau = \pi + \varepsilon$. Thus, as τ increases near π, the appearance of the double critical imaginary root i brings a *stability reversal*. In order to verify the above results, the "Re(λ) versus Im(λ)" plot near ($\lambda = \mathrm{i}, \tau = \pi$) and the "Re($\lambda$) versus τ" plot are given in Fig. 11 (left) and (right), respectively. More relevant results as well as a finer characterization of stability reversals can be found in Li et al. (2019a). □

7 Further Extensions of the Frequency-Sweeping Approach

The DDE (1) under consideration in the previous sections are all of *retarded* type. In the sequel, we address some extensions of the proposed methodology. In particular, we consider two classes: neutral delay differential equations (NDDE) and distributed delay differential equations (DDDEs) with uniform distributions.

[23] The critical root $\lambda = \mathrm{i}$ is a double critical imaginary root at $\tau = \pi$.

[24] In our case, one characteristic root is located in the right-half plane $\mathbb{C}_+$ and the other in the left-half plane $\mathbb{C}_-$.

7.1 Neutral Delay Differential Equations

Consider the following DDE of *neutral* type

$$\dot{x}(t) = Ax(t) + Bx(t-\tau) + C\dot{x}(t-\tau), \tag{10}$$

where $A \in \mathbb{R}^{r\times r}$, $B \in \mathbb{R}^{r\times r}$, and $C \in \mathbb{R}^{r\times r}$, $C \neq 0$ are constant matrices. The characteristic function of system (10) is given by

$$f_N(\lambda,\tau) = \det(\lambda I - A - Be^{-\tau\lambda} - \lambda Ce^{-\tau\lambda}),$$

which is a quasipolynomial of the form

$$f_N(\lambda,\tau) = a_0(\lambda) + a_1(\lambda)e^{-\tau\lambda} + \cdots + a_q(\lambda)e^{-q\tau\lambda}, \tag{11}$$

where $a_i(\lambda)$, $i \in [\![0,q]\!]$ are polynomials in λ with real coefficients. As mentioned in the Preliminaries, compared to the retarded DDEs (1), the stability of the trivial solution of the neutral DDEs (10) has an additional *necessary* condition: the stability of the neutral delay-difference equation

$$x(t) - Cx(t-\tau) = 0. \tag{12}$$

The other issues for studying the complete stability problem are similar[25] and can be directly addressed by using the frequency-sweeping approach. For a comprehensive introduction to the spectral properties of linear neutral DDEs, one may refer to Gu (2012) (see also Michiels and Niculescu 2014).

Lemma 7.1 *The trivial solution of the neutral delay-difference equation (12) is exponentially stable for any positive τ if and only if*

$$\rho(C) < 1.$$

Theorem 7.2 *The trivial solution of the neutral delay-difference equation (12) is exponentially stable if and only if all the frequency-sweeping curves are above the line $\Im_1$ as $\omega \to \infty$.*

Example 7.3 Consider the NDDEs of Example case 2 in Olgac and Sipahi (2004), i.e., the system (10) with matrices:

$$A = \begin{pmatrix} 0 & 1 & -1 & 0 \\ -3.346 & -2.715 & 2.075 & -2.007 \\ -4 & 0 & 2 & 0 \\ -3 & 0 & 0 & 6 \end{pmatrix}, B = \begin{pmatrix} -1 & 2 & 2 & -1 \\ 3 & 3 & -2 & 0 \\ 1 & 2 & -1 & 1 \\ 2 & 3 & 1 & -3 \end{pmatrix},$$

[25] Both the characteristic functions (3) and (11) are standard quasipolynomials.

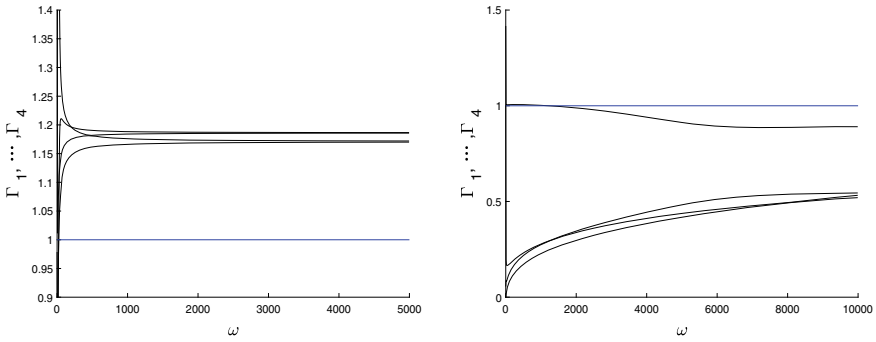

Fig. 12 Examples 7.3 and 7.4: frequency-sweeping curves $\Gamma_1, \ldots, \Gamma_4$ versus ω

$$C = \begin{pmatrix} 0.2 & -0.1 & 0.5 & -0.1 \\ -0.3 & 0.09 & -0.15 & -0.027 \\ -3.333 & 0.1 & 0.2 & 1 \\ -1 & 2 & 0.5 & 1 \end{pmatrix}.$$

The four eigenvalues of C are $0.0881 \pm 0.8494\mathrm{i}$ and $0.6569 \pm 0.5284\mathrm{i}$. Hence, $\rho(C) < 1$. This result can be directly obtained from the frequency-sweeping curves shown in Fig. 12 (left), based on Theorem 7.2. We see that as $\omega \to \infty$, $|z_i(\mathrm{i}\omega)| > 1$, $i = 1, \ldots, 4$. □

Example 7.4 Consider the NDDEs of Example b2 in Sipahi and Olgac (2003), i.e., the system (10) with matrices:

$$A = \begin{pmatrix} 12 & 10 & -6 & 14 \\ 7 & 8 & 11 & 9 \\ -5 & 7 & 3 & 3 \\ 6 & 2 & 3 & 4 \end{pmatrix}, B = \begin{pmatrix} -169 & -276.85 & -445.76 & -675.75 \\ -11 & -46 & -61 & -83 \\ 249 & 360.05 & 1070.43 & 1431.02 \\ 81.65 & 158.32 & 127.61 & 230.85 \end{pmatrix},$$

$$C = \begin{pmatrix} -4 & 12 & 3 & 1 \\ 0 & 1 & -2 & 6 \\ 12 & -8 & 4 & 2 \\ 1.47 & -10.09 & -4.33 & 0.03 \end{pmatrix}.$$

The four eigenvalues of C are $0.2816 \pm 1.3641\mathrm{i}$, -1.3469, and 1.8138. Hence, $\rho(C) > 1$. In this case, from the frequency-sweeping curves, Fig. 12 (right), we observe that as $\omega \to \infty$, $|z_i(\mathrm{i}\omega)| < 1$, $i \in [\![1, 4]\!]$, result consistent with Theorem 7.2. □

Example 7.5 Consider the following first-order NDDE (Fu et al. 2006):

$$\dot{x}(t) + \beta\dot{x}(t-\tau) = -ax(t) - bx(t-\tau),$$

where[26] $|\beta| < 1$. The characteristic function is $f_N(\lambda, \tau) = \lambda + a + (\beta\lambda + b)e^{-\tau\lambda}$. When $\tau = 0$, $\lambda = -\frac{a+b}{1+\beta}$. Thus, $NU(0) = 0$ ($NU(0) = 1$) if $a + b > 0$ ($a + b < 0$) while there exists an invariant characteristic root at the origin ($\lambda = 0$) if $a + b = 0$. As $z = -\frac{\lambda+a}{\beta\lambda+b}$, we have the following possible cases:

(i) If $|b| > |a|$, the frequency-sweeping curve intersects the line $\Im_1$ at one and only one critical frequency (there is one and only one critical imaginary root λ_0 with the critical delays $\tau_{0,k}$). More precisely, we have: (i.1) if $a + b < 0$, the NDDE is unstable for all $\tau \geq 0$, and (i.2) if $a + b > 0$, there is one and only one stability τ-interval: $[0, \tau_{0,0})$.

(ii) If $|b| < |a|$, the frequency-sweeping curve does not intersect the line $\Im_1$ (there is no critical imaginary root). Thus, the system is *hyperbolic*, *delay-independent stable* (*unstable*) if $a + b > 0$ ($a + b < 0$).

If $a = b \neq 0$, it is easy to observe that the frequency-sweeping curve intersects the line $\Im_1$ at $\omega = 0$. However, since $z = -1$, $\lambda = 0$ is not a critical imaginary root. In such a case, similarly to the case (ii) above, the NFDDE is *delay-independent stable* (*unstable*) if $a = b > 0$ ($a = b < 0$). □.

7.2 Distributed Delay Differential Equations with Uniform Distribution

For the retarded- and neutral-type DDEs discussed in the previous sections, the characteristic functions $f(\lambda, \tau)$ given by (3) include polynomials $a_i(\lambda)$, with $i \in [\![0, q]\!]$, (called *coefficient functions*), and are *"standard" quasipolynomials*. It is worth mentioning that the methodology developed above works for larger classes of coefficient functions. For instance, if we assume that the coefficient functions $a_i(\lambda)$, $i \in [\![0, q]\!]$ of $f(\lambda, \tau)$ given by (3) *are only required to be analytic in* $i\mathbb{R}\backslash\{0\}$, we are able to cover a number of epidemiological models described by integro-differential equations including delays in their representation. In the sequel, a characteristic function (3) with this relaxed condition is called *general quasipolynomial*. Due to the particular way the frequency-sweeping approach makes use of the coefficient functions, it can also be applied to general quasipolynomials. More precisely, we have the following result.

Theorem 7.6 *For a critical imaginary root λ_α of the characteristic equation $f(\lambda, \tau) = 0$ where $f(\lambda, \tau)$ is a general quasipolynomial, $\Delta NU_{\lambda_\alpha}(\tau_{\alpha,k})$ is a constant $\Delta NF_{z_\alpha}(\omega_\alpha)$ for all $\tau_{\alpha,k} > 0$.*

[26] The stability of the trivial solution of the neutral delay-difference equation is guaranteed. It is worth mentioning that the case $\beta = 0$ corresponds to the retarded DDE and it was addressed in the previous section.

To show the effectiveness of the invariance property mentioned above, consider the following Distributed Delay Differential Equation (DDDE):

$$\dot{x}(t) = A_0 x(t) + A_1 \int_{-\infty}^{t} \kappa(t-\theta) x(\theta) d\theta, \tag{13}$$

where $\kappa(\theta)$ is an appropriate kernel function. Assume that $\kappa(\cdot)$ is a *uniform-distribution* described by:

$$\kappa(\theta) = \begin{cases} \frac{1}{d_1+d_2}, & \text{if } \tau - d_1 < \theta < \tau + d_2, \\ 0, & \text{otherwise}, \end{cases} \tag{14}$$

where $\tau \geq d_1 \geq 0$ and $d_2 \geq 0$. The characteristic function rewrites as:

$$f(\lambda, \tau) = \det(\lambda I - A_0 - A_1 \frac{e^{-(\tau-d_1)\lambda} - e^{-(\tau+d_2)\lambda}}{(d_1+d_2)\lambda}), \quad \lambda \neq 0.$$

Example 7.7 Consider the DDDE (13) with

$$A_0 = \begin{pmatrix} 0 & 1 \\ -\frac{\pi^4+3\pi^2-4}{\pi^2(\pi^2+1)} & \frac{2\pi}{\pi^2+1} \end{pmatrix}, A_1 = \begin{pmatrix} 1 & 0 \\ \frac{\pi^2+4}{\pi(\pi^2+1)} & \frac{-1}{\pi^2+1} \end{pmatrix}.$$

Let $\kappa(\theta)$ be the uniform distribution (14) with $d_1 = d_2 = \frac{\pi}{2}$. Then the characteristic function is a general quasipolynomial $f(\lambda, \tau) = a_0(\lambda) + a_1(\lambda)e^{-\tau\lambda} + a_2(\lambda)e^{-2\tau\lambda}$, with the coefficient functions $a_0(\lambda) = \lambda^2 - \frac{4}{\pi^2} - \frac{2\pi\lambda-6}{\pi^2+1} + 1$, $a_1(\lambda) = \frac{(e^{-\frac{\pi\lambda}{2}} - e^{\frac{\pi\lambda}{2}})(\pi^3\lambda-\pi^2+4)}{\pi^2\lambda(\pi^2+1)}$, and $a_2(\lambda) = -\frac{(e^{-\frac{\pi\lambda}{2}} - e^{\frac{\pi\lambda}{2}})^2}{\pi^2\lambda^2(\pi^2+1)}$. At $\tau = (2k+1)\pi, \lambda = \mathrm{i}$ is a critical imaginary root: $\lambda = \mathrm{i}$ is double at $\tau = \pi$ while it is simple at all $\tau = (2k+1)\pi$, $k \in \mathbb{N}_+$. According to Theorem 7.6, we have that $\Delta NU_{\mathrm{i}}((2k+1)\pi) = \Delta NF_{-1}(1)$ for all $k \in \mathbb{N}$, where $\Delta NF_{-1}(1) = 0$ as observed from the frequency-sweeping curves shown in Fig. 13. Next, we verify the above result by invoking the Puiseux series for critical pairs $(\mathrm{i}, (2k+1)\pi)$, $k \in [\![0, 2]\!]$:

$$\begin{aligned} &\Delta\lambda = (0.2290 + 0.2930\mathrm{i})(\Delta\tau)^{\frac{1}{2}} + o((\Delta\tau)^{\frac{1}{2}}), k = 0, \\ &\Delta\lambda = -0.1592\mathrm{i}\Delta\tau + (-0.0283 + 0.0324\mathrm{i})(\Delta\tau)^2 + o((\Delta\tau)^2), \ k = 1, \\ &\Delta\lambda = -0.0796\mathrm{i}\Delta\tau + (-0.0035 + 0.0072\mathrm{i})(\Delta\tau)^2 + o((\Delta\tau)^2), \ k = 2, \end{aligned}$$

and thus, we arrive at the same conclusion. □

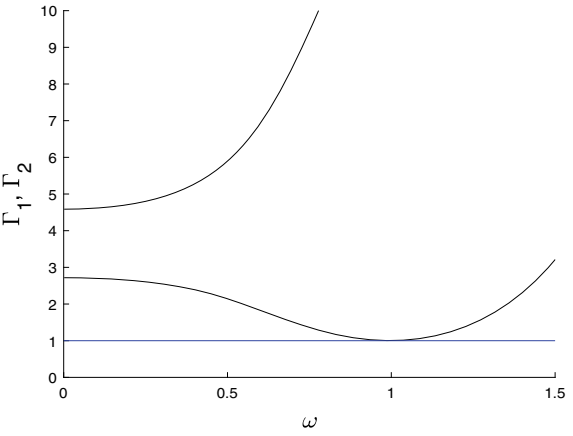

Fig. 13 Example 7.7: frequency-sweeping curves Γ_1, Γ_2 versus ω

7.3 Delay Differential Equations with Multiple Incommensurate Delays

Consider the following DDEs:

$$\dot{x}(t) = A_0 x(t) + \sum_{\ell=1}^{q} A_\ell x(t - \tau_\ell), \tag{15}$$

where $\tau_\ell \geq 0\,(\ell \in [\![1, q]\!])$ are *independent* delays. The characteristic function for (15) is $f(\lambda, \overrightarrow{\tau}) = \det(\lambda I - A_0 - \sum_{\ell=1}^{q} A_\ell e^{-\tau_\ell \lambda})$, and we are interested to characterize the stability regions in the *delay-parameter space*.

A straightforward idea is to extend the mathematical results from the single delay case to multiple delays. However, such an extension is not trivial. As in the commensurate delays case, the core of the approach is the *invariance property*. To address the problem, we may proceed "indirectly" by fixing $(q-1)$ delays and leaving the remaining delay as a "free" parameter. Thus, for any combination $\overrightarrow{\tau}^\sharp$, we may accurately compute $NU(\overrightarrow{\tau}^\sharp)$ by using several times the frequency-sweeping tests in appropriate manner. Schematically speaking, suppose that $\tau_k = \tau_{k,0}$ for all $k \in [\![1, q]\!] \backslash \{i\}$ are fixed and τ_i is the "free" parameter for some $i \in [\![1, q]\!]$. Then the corresponding characteristic function can be rewritten in the form $f(\lambda, \tau_i)$ given by (3) where the coefficient functions $a_h(\lambda)$ $(h \in [\![1, q]\!])$ can be seen as q-multivariate polynomials of λ and $(q-1)$ variables $z_k = e^{-\tau_{k,0}\lambda}$, with $k \in [\![1, q]\!] \backslash \{i\}$, for which we can apply the frequency-sweeping approach.

Example 7.8 Consider a DDE including two delays τ_1 and τ_2, with the characteristic function $f(\lambda, \tau_1, \tau_2) = \frac{1}{\pi^2} + 2 + (1 - \frac{3}{\pi})\lambda + \lambda^2 + ((\frac{2}{\pi^2} + 3) + (3 - \frac{4}{\pi})\lambda)e^{-\tau_1\lambda} + ((\frac{1}{\pi^2} + 3) + (3 - \frac{1}{\pi})\lambda)e^{-\tau_2\lambda} + (1 + \lambda)e^{-(\tau_1+\tau_2)\lambda}$. Suppose $\tau_2 = 2\pi$ is fixed and τ_1 is the free delay parameter denoted by τ. Then f can be expressed by the

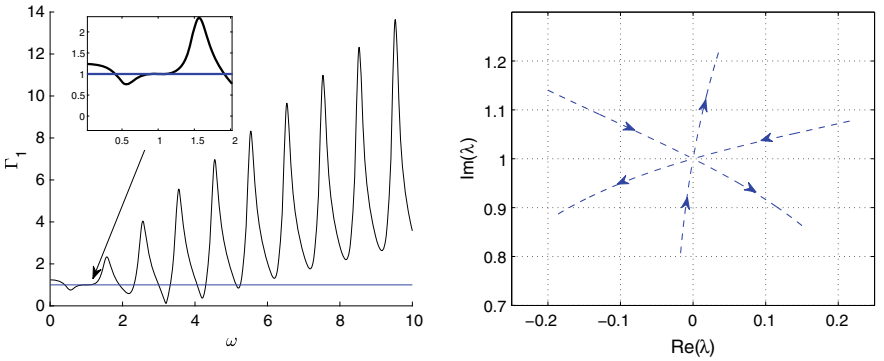

Fig. 14 Example 7.8: frequency-sweeping curve Γ_1 versus ω and $\mathrm{Re}(\lambda)$ versus $\mathrm{Im}(\lambda)$

general quasipolynomial $f(\lambda,\tau)=a_0(\lambda)+a_1(\lambda)e^{-\tau\lambda}$ with the coefficient functions $a_0(\lambda)=\frac{1}{\pi^2}+2+(1-\frac{3}{\pi})\lambda+\lambda^2+((\frac{1}{\pi^2}+3)+(3-\frac{1}{\pi})\lambda)e^{-2\pi\lambda}$ and $a_1(\lambda)=((\frac{2}{\pi^2}+3)+(3-\frac{4}{\pi})\lambda)+(1+\lambda)e^{-2\pi\lambda}$. At $\tau=\pi$, $\lambda=\mathrm{i}$ is a triple critical root.[27] According to Theorem 7.6, $\Delta NU_{\mathrm{i}}((2k+1)\pi)=\Delta NF_{-1}(1)=+1$ for all $k\in\mathbb{N}$, where $\Delta NF_{-1}(1)$ is obtained from the frequency-sweeping curve (Fig. 14 (left)). To verify the result, the Puiseux series for critical pairs $(\mathrm{i},(2k+1)\pi)$, $k\in[\![0,2]\!]$ write as:

$$\begin{aligned}
\Delta\lambda &= (0.3801-0.2846\mathrm{i})(\Delta\tau)^{\frac{1}{3}}+o((\Delta\tau)^{\frac{1}{3}}),\ k=0,\\
\Delta\lambda &= -0.1592\mathrm{i}\Delta\tau+0.0253\mathrm{i}(\Delta\tau)^2+(0.0021-0.0096\mathrm{i})(\Delta\tau)^3\\
&\quad +o((\Delta\tau)^3),\ k=1,\\
\Delta\lambda &= -0.0796\mathrm{i}\Delta\tau+0.0063\mathrm{i}(\Delta\tau)^2+(0.0001-0.0009\mathrm{i})(\Delta\tau)^3\\
&\quad +o((\Delta\tau)^3),\ k=2.
\end{aligned}$$

To further illustrate the asymptotic behavior of the triple root i, the root loci near the critical pair (i,π) is depicted in Fig. 14 (right). □

8 Applications

In this section, we present two case studies from Life Sciences: neural networks and Lotka-Volterra systems.

[27] It is worth mentioning that $\lambda=\mathrm{i}$ is simple at all $\tau=(2k+1)\pi$, $k\in\mathbb{N}_+$.

8.1 Neural Network Dynamical Systems

To illustrate our approach for the stability analysis of neural networks with delays, we present an example borrowed from Li et al. (2018b). Consider the Bidirectional Associative Memory (BAM) neural network given by:

$$\begin{cases} \dot{x}_1(t) = -\mu_1 x_1(t) + \sum_{i=1}^{4} c_{i1} f_i(x_i(t-\tau_2)), \\ \dot{y}_{k-1}(t) = -\mu_k y_{k-1}(t) + c_{1k} f_k(x_1(t-\tau_1)), \quad k \in [\![2,4]\!]. \end{cases} \tag{16}$$

where $x_1(t)$ and $y_1(t)$, $y_2(t)$, $y_3(t)$ denote respectively the state of the neurons in the I-layer and the K-layer. The functions f_i, called *activation functions*, are assumed to be $\mathcal{C}^1$-differentiable, such that $f_i(0) = 0$, for $i \in [\![1,4]\!]$. The signal transmission delay from the I-layer to the K-layer is τ_1 while the delay from the K-layer to the I-layer is τ_2. Next, $c_{ki} \in \mathbb{R}$ ($k, i \in [\![1,4]\!]$) are the connection weights through the neurons in two layers and $\mu_i \in \mathbb{R}_+$ ($i \in [\![1,4]\!]$) describe the stability of internal neuron process.

By letting $u_1(t) = x_1(t-\tau_1)$, $u_k(t) = y_{k-1}(t)$, $k \in [\![2,4]\!]$ and $\tau = \tau_1 + \tau_2$, the BAM neural network (16) rewrites as follows:

$$\begin{cases} \dot{u}_1(t) = -\mu_1 u_1(t) + \sum_{i=1}^{4} c_{i1} f_i(u_i(t-\tau)), \\ \dot{u}_k(t) = -\mu_k u_k(t) + c_{1k} f_k(u_1(t)), \quad k \in [\![2,4]\!]. \end{cases} \tag{17}$$

The linearization of the model (17) at the origin writes as:

$$\begin{cases} \dot{u}_1(t) = -\mu_1 u_1(t) + \sum_{i=1}^{4} \alpha_{i1} u_i(t-\tau), \\ \dot{u}_k(t) = -\mu_k u_k(t) + \alpha_{1k} u_1(t), \quad k \in [\![2,4]\!], \end{cases}$$

where $\alpha_{ik} = c_{ik} f_k'(0)$, $i, k \in [\![1,4]\!]$, and with the characteristic function:

$$f(\lambda,\tau) = \det \begin{pmatrix} \lambda+\mu_1 & -\alpha_{21}e^{-\tau\lambda} & -\alpha_{31}e^{-\tau\lambda} & -\alpha_{41}e^{-\tau\lambda} \\ -\alpha_{12} & \lambda+\mu_2 & 0 & 0 \\ -\alpha_{13} & 0 & \lambda+\mu_3 & 0 \\ -\alpha_{14} & 0 & 0 & \lambda+\mu_4 \end{pmatrix}.$$

This characteristic function is a quasipolynomial $a_0(\lambda) + a_1(\lambda)e^{-\tau\lambda}$, where

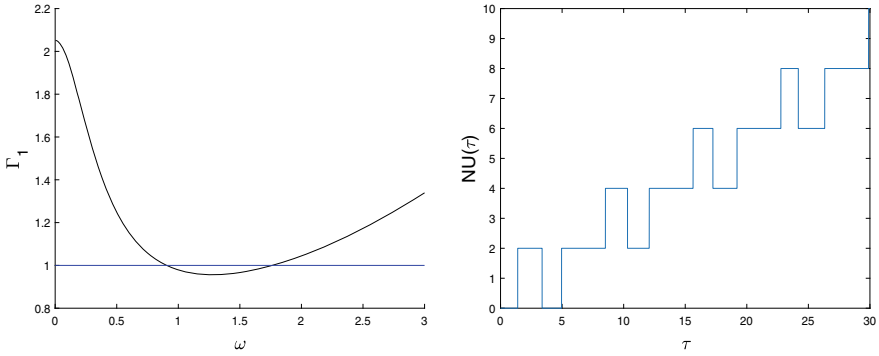

Fig. 15 BAM example: frequency-sweeping curve Γ_1 versus ω and $NU(\tau)$ versus τ plot

$$
\begin{aligned}
a_0(\lambda) &= \lambda^4 + (\mu_1+\mu_2+\mu_3+\mu_4)\lambda^3 + (\mu_1\mu_2+\mu_3\mu_4+\mu_1\mu_3+\mu_1\mu_4)\lambda^2 \\
&\quad +(\mu_2\mu_3+\mu_2\mu_4)\lambda^2 + (\mu_1\mu_2\mu_3+\mu_1\mu_2\mu_4+\mu_1\mu_3\mu_4+\mu_2\mu_3\mu_4)\lambda + \mu_1\mu_2\mu_3\mu_4, \\
a_1(\lambda) &= -(\alpha_{12}\alpha_{21}+\alpha_{13}\alpha_{31}+\alpha_{14}\alpha_{41})\lambda^2 \\
&\quad -(\alpha_{12}\alpha_{21}\mu_3+\alpha_{12}\alpha_{21}\mu_4+\alpha_{13}\alpha_{31}\mu_2+\alpha_{13}\alpha_{31}\mu_4+\alpha_{14}\alpha_{41}\mu_2+\alpha_{14}\alpha_{41}\mu_3)\lambda \\
&\qquad -(\alpha_{12}\alpha_{21}\mu_3\mu_4+\alpha_{13}\alpha_{31}\mu_2\mu_4+\alpha_{14}\alpha_{41}\mu_2\mu_3).
\end{aligned}
$$

Under the assumption that the activation functions are hyperbolic tangent functions,[28] and with choice of the coefficients as: $\mu_1 = 2.46, \mu_2 = 4.5769, \mu_3 = 0.8561, \mu_4 = 0.9669, \alpha_{12} = 4.6621, \alpha_{13} = -0.3896, \alpha_{14} = 2.3488, \alpha_{21} = -4.1320, \alpha_{31} = -2.8466, \alpha_{41} = 0.7057$, we study the local stability of the origin equilibrium. The frequency-sweeping curve is shown in Fig. 15 (left). We see that the frequency-sweeping curve intersects the line $\Im_1$ at $\omega_0 = 0.9059$ and $\omega_1 = 1.7637$. As ω increases, the frequency-sweeping curve crosses the line $\Im_1$ from above to below (from below to above) at ω_0 (ω_1). In this case, two critical imaginary roots are detected: $\lambda_0 = 0.9059\mathrm{i}$ (critical delays $\tau_{0,k} = 3.3768 + 6.9355k$) and $\lambda_1 = 1.7637\mathrm{i}$ (critical delays $\tau_{1,k} = 1.3947 + 3.5624k$). According to Theorem 5.1, $\Delta NU_{\lambda_0}(\tau_{0,k}) = -1$ and $\Delta NU_{\lambda_1}(\tau_{1,k}) = +1$ for all $k \in \mathbb{N}$. By applying Theorem 6.3, we have the expression of $NU(\tau)$, as plotted in Fig. 15 (right). Thus, the origin is locally asymptotically stable if $\tau \in [0, 1.3947) \cup (3.3768, 4.9571)$.

8.2 *Lotka-Volterra Systems*

To further illustrate the proposed approach, consider a Lotka-Volterra system with delays borrowed from Li et al. (2018a). More precisely, consider the three-species Lotka-Volterra system described by the DDEs

[28] In this case, $f_i(\cdot) = \tanh(\cdot)$, $i \in [\![1, 4]\!]$ verifying $f_i(0) = 0$ and $f_i'(0) = 1$, $i \in [\![1, 4]\!]$.

$$\begin{cases} \dot{x}_1(t) = x_1(t)(a_{10} + a_{11}x_1(t) + a_{12}x_2(t)), \\ \dot{x}_2(t) = x_2(t)(a_{20} + a_{21}x_1(t) + a_{23}x_3(t-\tau_{23})), \\ \dot{x}_3(t) = x_3(t)(a_{30} + a_{32}x_2(t-\tau_{32})), \end{cases} \tag{18}$$

This system (18) may model a three-species food chain dynamics, where $x_1(t)$, $x_2(t)$, and $x_3(t)$ denote the population densities at time t of the lowest-level prey, the mid-level predator, and the top predator, respectively. It is assumed that the top predator species needs time τ_{23} to possess the ability of predation and captures only the adult mid-level predator species with maturation time τ_{32}. The unique positive equilibrium (x_1^*, x_2^*, x_3^*) is:

$$x_1^* = \frac{a_{10}a_{32} - a_{30}a_{12}}{-a_{11}a_{32}}, x_2^* = \frac{-a_{30}}{a_{32}}, x_3^* = \frac{a_{10}a_{32}a_{21} - a_{30}a_{12}a_{21} - a_{20}a_{11}a_{32}}{a_{11}a_{32}a_{23}}.$$

Let $u_i(t) = x_i(t) - x_i^*$, $i \in [\![1, 3]\!]$. Then, we can rewrite (18) as

$$\begin{cases} \dot{u}_1(t) = (u_1(t) + x_1^*)(a_{11}u_1(t) + a_{12}u_2(t)), \\ \dot{u}_2(t) = (u_2(t) + x_2^*)(a_{21}u_1(t) + a_{23}u_3(t-\tau_{23})), \\ \dot{u}_3(t) = (u_3(t) + x_3^*)a_{32}u_2(t-\tau_{32}). \end{cases} \tag{19}$$

The linearized system of (19) at the origin (0, 0, 0) is

$$\begin{cases} \dot{u}_1(t) = a_{11}x_1^*u_1(t) + a_{12}x_1^*u_2(t), \\ \dot{u}_2(t) = a_{21}x_2^*u_1(t) + a_{23}x_2^*u_3(t-\tau_{23}), \\ \dot{u}_3(t) = a_{32}x_3^*u_2(t-\tau_{32}). \end{cases} \tag{20}$$

The characteristic function for the linear system (20) is

$$f(\lambda, \tau) = \lambda^3 - a_{11}x_1^*\lambda^2 - a_{12}a_{21}x_1^*x_2^*\lambda + (a_{11}a_{23}a_{32}x_1^*x_2^*x_3^* - a_{23}a_{32}x_2^*x_3^*\lambda)e^{-\tau\lambda},$$

where $\tau = \tau_{23} + \tau_{32}$. Let $a_{10} = 0.7915$, $a_{11} = -0.1358$, $a_{12} = -0.9557$, $a_{20} = -0.8337$, $a_{21} = 0.9089$, $a_{23} = -0.6429$, $a_{30} = -0.5726$, $a_{32} = 0.9322$. The unique positive equilibrium is ($x_1^* = 1.5056$, $x_2^* = 0.6142$, $x_3^* = 0.8318$). We analyze the local asymptotic stability. For the linearized system at the positive equilibrium, the characteristic function writes as:

$$f(\lambda, \tau) = \lambda^3 + 0.2045\lambda^2 + 0.8033\lambda + (0.3062\lambda + 0.0626)e^{-\tau\lambda}. \tag{21}$$

For $\tau = 0$, there are three characteristic roots (all in $\mathbb{C}_-$): -0.0738 ± 1.0468i and -0.0569. The frequency-sweeping curve is generated as shown in Fig. 16 (left). It is easy to observe that there are three critical imaginary roots 0.0854i (with the critical delays $22.8187 + 73.7657k$), 0.7221i (with the critical delays $3.3005 + 8.7014k$), and 1.0179i (with the critical delays $0.5218 + 6.1724k$), $k \in \mathbb{N}$. Next, simple computations lead to $\Delta NU_{0.0854\text{i}}(22.8187 + 73.7657k) = +1$, $\Delta NU_{0.7221\text{i}}(3.3005 + 8.7014k) = -1$, and $\Delta NU_{1.0179\text{i}}(0.5218 + 6.1724k) = +1$,

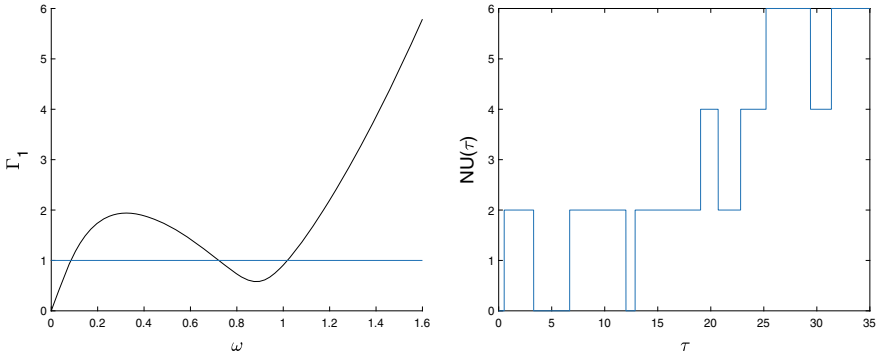

Fig. 16 Lotka-Volterra DDE: Frequency-sweeping curve Γ_1 versus ω and $NU(\tau)$ versus τ plot

for all $k \in \mathbb{N}$. Finally, the "$NU(\tau)$ versus τ" plot is depicted in Fig. 16 (right). In conclusion, all the characteristic roots of (21) are located in $\mathbb{C}_-$ if and only if $\tau \in [0, 0.5218) \cup (3.3005, 6.6942) \cup (12.0019, 12.8666)$ and, thus, we have more than one stability delay interval guaranteeing the local asymptotic stability of the original system.

9 Notes and Comments

This chapter addressed the effects induced by the delay parameter on the (exponential) stability of linear dynamical systems represented by delay differential equations. To perform such an analysis, the authors proposed a user-friendly *frequency-sweeping framework*, and the stability problem was reformulated in terms of properties of some appropriate frequency-sweeping curves. Illustrative examples and two applications from Life Sciences show the effectiveness of the method.

The main results of this chapter devoted to single (or commensurate) linear delay systems have been reported in Li et al. (2015) (see also Li et al. 2014, 2017). For a deeper discussion of the properties of the *spectral abscissa function*, the reader is referred to Michiels and Niculescu (2014) and the references therein. Next, an extension of the frequency-sweeping approach applied to the incommensurate delay case was presented in Li et al. (2019b). Finally, a guided tour of existing methods to analyze multiple characteristic roots (including the frequency-sweeping approach) can be found in Niculescu et al. (2021).

References

Ahlfors, L. V. (1979). *Complex analysis*. McGraw-Hill.

Bellman, R., & Cooke, K. L. (1963). *Differential-difference equations*. New York: Academic Press.
Casas-Alvero, E. (2000). *Singularities of plane curves*. London Mathematical Society Lecture Note Series. Cambridge University Press. https://doi.org/10.1017/CBO9780511569326.
Chen, J. (1995). On computing the maximal delay intervals for stability of linear delay systems. *IEEE Transactions on Automatic Control, 40*(6), 1087–1093.
Chen, J., & Latchman, H. A. (1995). Frequency sweeping tests for stability independent of delay. *IEEE Transactions on Automatic Control, 40*(9), 1640–1645.
Chen, J., Gu, G., & Nett, C. A. (1995). A new method for computing delay margins for stability of linear delay systems. *Systems and Control Letters, 26*, 107–117.
Chi, J., Gu, K., Niculescu, S. I., & Boussaada, I. (2018a). Stability analysis of systems with delay-dependent coefficients: An overview. *IEEE Access, 6*, 27392–27407.
Chi, J., Gu, K., Niculescu, S. I., & Boussaada, I. (2018b). Stability analysis of a more general class of systems with delay-dependent coefficients. *IEEE Transactions on Automatic Control, 64*(5), 1989–1998.
Cooke, K. L., & Grossman, Z. (1982). Discrete delay, distributed delay and stability switches. *Journal of Mathematical Analysis and Applications, 86*, 592–627.
Cooke, K. L., & van den Driessche, P. (1986). On zeroes of some transcendental equations. *Funkcialaj Ekvacioj, 29*(1), 77–90.
Datko, R. (1978). A procedure for determination of the exponential stability of certain differential-difference equations. *Quarterly of Applied Mathematics, 36*, 279–292.
Els'golts', L. E., & Norkin, S. B. (1973). *Introduction to the theory and application of the theory of differential equations with deviating argument*. New York, New York: Academic Press.
Engelborghs, K., Luzyanina, T., & Roose, D. (2002). Numerical bifurcation analysis of delay differential equations using DDE-BIFTOOL. *ACM Transactions on Mathematical Software, 28*(1), 1–21.
Evans, W. E. (1950). Control system synthesis by root locus method. *AIEE Transactions, 69*, 66–69.
Fridman, E. (2014). *Introduction to time-delay systems: Analysis and control*. Boston: Birkhauser.
Fu, P., Niculescu, S.-I., & Chen, J. (2006). Stability of linear neutral time-delay systems: Exact conditions via matrix pencil solutions. *IEEE Transactions on Automatic Control, 51*(6), 1063–1069.
Gryazina, E. N., Polyak, B. T., & Tremba, A. A. (2008). D-decomposition technique state-of-the-art. *Automation and Remote Control, 69*, 1991–2026.
Gu, K. (2012). A review of some subtleties of practical relevance for time-delay systems of neutral type. *ISRN Applied Mathematics*, pp. 1–46.
Gu, K., Kharitonov, V. L., & Chen, J. (2003). *Stability of time-delay systems*. Boston: Birkhäuser.
Hale, J. K., & Verduyn Lunel, S. M. (1993). *Introduction to functional differential equations*. Applied Mathematics Sciences (Vol. 99). New York: Springer.
Hale, J. K., Infante, E. F., & Tsen, F.-S.P. (1985). Stability in linear delay equations. *Journal of Mathematical Analysis and Applications, 105*(2), 533–555.
Hayes, N. D. (1950). Roots of the transcendental equation associated with a certain difference-differential equation. *Journal of the London Mathematical Society, s1–25*(3), 226–232. ISSN 1469-7750.
Jarlebring, E., & Michiels, W. (2010). Invariance properties in the root sensitivity of time-delay systems with double imaginary roots. *Automatica, 46*(6), 1112–1115.
Kashiwagi, Y. (1965). *Stability of linear systems with time-delay*. Ph.D. thesis, Stanford University.
Knopp, K. (1996). *Theory of Functions, Parts I and II*. Mineola, NY: Dover.
Krall, A. M. (1968). *Stability techniques for continuous linear systems*. New York: Gordon and Breach.
Krall, A. M. (1970). The root locus method: A survey. *SIAM Review, 12*(1), 64–72.
Lee, M. S., & Hsu, C. S. (1969). On the τ-decomposition method of stability analysis for retarded dynamical systems. *SIAM Journal on Control, 7*(2), 242–259.
Li, X., Liu, J.-C., Li, X.-G., Niculescu, S.-I., & Çela, A. (2019a). Reversals in stability of linear time-delay systems: A finer characterization. *Automatica*, page Article 108479.

Li, X.-G., Niculescu, S.-I., Çela, A., Wang, H.-H., & Cai, T.-Y. (2014). Invariance properties for a class of quasipolynomials. *Automatica, 50*, 890–895.

Li, X.-G., Niculescu, S.-I., & Çela, A. (2015). *Analytic curve frequency-sweeping stability tests for systems with commensurate delays*. Springer.

Li, X.-G., Niculescu, S.-I., Çela, A., Zhang, L., & Li, X. (2017). A frequency-sweeping framework for stability analysis of time-delay systems. *IEEE Transactions on Automatic Control, 62*, 3701–3716.

Li, X.-G., Chen, J.-X., Niculescu, S.-I., & Çela, A. (2018a). New insights in stability analysis of delayed Lotka-Volterra systems. *Journal of The Franklin Institute, 355*(17), 8683–8697.

Li, X.-G., Chen, J.-X., & Zhang, Y. (2018b). Complete stability analysis with respect to delay for neural networks. *IEEE Transactions on Neural Networks and Learning, 29*(10), 4672–4682.

Li, X.-G., Niculescu, S.-I., & Çela, A. (2019). An iterative frequency-sweeping approach for stability analysis of linear systems with delays. *IMA Journal of Mathematical Control I, 36*, 379–398.

Marden, M. (1949). *The geometry of the zeros of a polynomial in the complex plane*. Providence, RI: American Mathematical Society.

Mendéz-Barrios, C.-F., Niculescu, S.-I., Martínez-González, A., Ramírez, A. (2022) Characterizing some improperly-posed problems in PD-control. *International Journal of Robust and Nonlinear Control* (to appear).

Michiels, W., & Niculescu, S.-I. (2014). *Stability, Control, and Computation for Time-Delay Systems. An Eigenvalue-Based Approach (2nd Edition)*. SIAM.

Neimark, J. (1949). D-subdivisions and spaces of quasi-polynomials. *Prikl. Mat. Meh., 13*(4), 349–380.

Niculescu, S.-I. (2001). *Delay Effects on Stability. A Robust Control Approach*. Springer.

Niculescu, S.-I., Boussaada, I., Li, X.-G., Mazanti, G., & Mendez-Barrios, C.-F. (2021). Stability, delays and multiple characteristic roots. A guided tour. In *Proceedings of the 16th IFAC Workshop on Time-Delay Systems*.

Olgac, N., & Sipahi, R. (2002). An exact method for the stability analysis of time-delayed linear time-invariant (LTI) systems. *IEEE Transactions on Automatic Control, 47*(5), 793–797.

Olgac, N., & Sipahi, R. (2004). A practical method for analyzing the stability of neutral type LTI-time delayed systems. *Automatica, 40*(5), 847–853.

Pinney, E. (1958). *Ordinary difference-differential equations*. Univ. California Press.

Pólya, G. (1954). *Mathematics and plausible reasoning*. Princeton: Princeton University Press.

Popov, E. P. (1962). *The dynamics of automatic control systems*. New York, USA: Pergamon Press.

Shaughnessy, J. D., & Kashiwagi, Y. (1969). The determination of a stability indicative function for linear systems with multiple delays. Technical Report TR R-301, NASA, Washington D. C., USA.

Sieber, J., Engelborghs, K., Luzyanina, T., Samaey, G., Roose, D. (2016). Dde-biftool manual - bifurcation analysis of delay differential equations.

Sipahi, R., & Olgac, N. (2003). Degenerate cases in using the direct method. *ASME Journal of Dynamic Systems, Measurement, and Control, 125*(2), 194–201.

Sipahi, R., Niculescu, S., Abdallah, C., Michiels, W., & Gu, K. (2011). Stability and stabilization of systems with time delay. *IEEE Control Systems Magazine, 31*(1), 38–65.

Tsypkin, Ya. . Z. (1946). The systems with delayed feedback. *Avtomathika i Telemecanique, 7*, 107–129.

Counting Characteristic Roots of Linear Delay Differential Equations. Part II: From Argument Principle to Rightmost Root Assignment Methods

Silviu-Iulian Niculescu and Islam Boussaada

Abstract This chapter briefly presents some "user-friendly" methods and techniques (frequency-domain approaches) for the analysis and control of linear dynamical systems in presence of delays. The presentation is as simple as possible, focusing more on the main intuitive (algebraic, geometric) ideas to develop theoretical results, and their potential use in practical applications. To fix better the ideas, scalar and second-order examples are largely discussed. Next, a particular attention will be paid to the existing links between the maximal allowable multiplicity of the characteristic roots and the spectral abscissa of the dynamical system. The underlying property—*multiplicity induced dominancy*— will be particularly useful in constructing low-complexity controllers by *partial pole placement*. Such an idea is particularly exploited in vibration control.

1 Introduction

Propagation, transport and heredity represent some of the typical phenomena of physical, biochemical processes and properties of living organisms that can be modeled by using *delays* in their mathematical representation. Understanding the ways the delays and the other parameters may affect the models' dynamics is a problem of recurring interest during the last decades. This chapter completes the contribution by Niculescu et al. (2023) (same volume) devoted to the stability analysis of linear dynamical time-delay systems described by Delay Differential Equations (DDEs) in frequency-domain. More precisely, we will present different (frequency-domain) techniques to count the characteristic roots located in the right complex half-plane

S.-I. Niculescu (✉)
University Paris-Saclay, CNRS, CentraleSupélec, Laboratory of Signals and Systems (L2S), Inria-Saclay "DISCO" team, Gif-sur-Yvette, France
e-mail: silviu.niculescu@l2s.centralesupelec.fr

I. Boussaada
Institut Polytechnique des Sciences Avancées, Ivry-sur-Seine, France

D. Breda (ed.), *Controlling Delayed Dynamics*, CISM International Centre for Mechanical Sciences 604, https://doi.org/10.1007/978-3-031-01129-0_6

with particular emphasis on the *Pólya-Szegö results*[1] and the so-called *multiplicity induced dominancy* and its potential applications in control engineering.

In the 30s, the development of feedback amplifiers is at the origin of most of frequency-response methods in control engineering and signal processing. In this frame, Nyquist (1932) proposed a graphical method for the analysis of Single-Input/Single-Output (SISO) Linear Time-Invariant (LTI) systems to determine the (asymptotic) stability of the closed-loop system based on the transfer function of the open-loop system. Due to its simplicity, such a method became extremely popular, and it is at the origin of most of the *graphical (stability) approaches* and *tests* in frequency-domain in the open literature, see, for instance, MacFarlane (1979) and the references therein. It should be mentioned that the Cauchy's argument principle is a simple and elegant way to prove Nyquist criterion. However, inspired by some ideas about the propagation of sinusoidal signals through the systems, Nyquist came up with a different proof. It should be mentioned that the seminal work of Tsypkin (1946) includes an extension of the Nyquist criterion in the case of dynamical systems with input delay and the proof is based on the Cauchy's argument principle.

In the 50s-70s, except for some natural extensions of Nyquist diagrams to delay dynamical systems, the Mikhailov criterion[2] has been the source of further developments (see, for instance, the discussion in Barker (1979) and the references therein). For some connections between Mikhailov and Nyquist tests applied to delay systems we mention the almost forgotten paper by Chen and Tsay (1976). Other graphical criteria include the well-known *root-locus methods*[3] and the Satche's diagrams (see, e.g. Satche, 1949), where the latter can be interpreted as a variant of the Nyquist criterion, sometimes called the dual root-locus methods. For a pedagogical presentation as well as some extensions of the root locus methods and Nyquist criterion to deal with dynamical systems including one delay in the input/output channel, we refer to Krall (1968). Finally, for an historical perspective on the frequency-response methods in control area, we refer to MacFarlane (1979).

At the end of the 70s, using the Cauchy's argument principle, Stépán (1979) proposed a simple criterion to count the unstable roots of a linear DDE. The simplicity of the method has been illustrated in Stépán (1989) by constructing stability charts for several examples from mechanical engineering and represented by DDEs. The underlying idea has been extended by Hassard (1997) to also cover some cases where multiple characteristic roots exist on the imaginary axis. This method is briefly discussed in Sect. 2 and applied to a second-order DDE including a single delay.

Exploration of some earlier ideas present, e.g., in Pinney (1958) and the seminal work Hayes (1950) demonstrated that the spectral values of systems of DDEs reaching their maximal possible multiplicity tend to be dominant, in what has come to be known as the *Multiplicity Induced Dominancy* (MID) property. The MID property turns out to open some interesting perspectives in designing low-complexity feed-

[1] More precisely, the estimation of the upper bound of the number of the characteristic roots of exponential polynomials located on a horizontal strip.

[2] Based on the same Cauchy's argument principle.

[3] Whose origins date back to the work of Evans in the late 1950s, Evans (1950), MacFarlane (1979).

back control laws for delay systems. Since these seminal works, many research efforts have been devoted to the characterization of the classes of systems for which such a property is valid and to its exploration in applications to stabilize delay systems. This chapter addresses some of the most recent results in this direction.

To the best of the authors' knowledge, it should be mentioned that most general result involving the MID property so far is that of Boussaada et al. (2022), which shows that the MID property holds for retarded and neutral DDEs of an arbitrary order with a single delay and highlights the potential of applicability of such a property in the design of control feedback laws by using a partial pole placement methodology. Such results are obtained by exploring links[4] between spectra of systems of DDEs and roots of a family of confluent hypergeometric functions, known as *Kummer functions*.

The contributions of the chapter are fourfold. First, our intention is to complete the presentation of Niculescu et al. (2021) by introducing other frequency-domain methods useful to count the number of unstable characteristic roots. Second, we wish to shed some light on various methods, techniques and ideas developed by the authors of this contribution to deal with the case of multiple characteristic roots and, in particular, the so-called MID property. Finally, we are interested to emphasize the way that such a property can be applied to some control problems and, more precisely, in vibration control.

The chapter is organized as follows: some preliminary results and prerequisites are introduced in Sect. 2. Section 3 is devoted to the characterization of the multiplicity of the characteristic roots in terms of structured matrices. Next, Section 4 introduces the MID property and gives some insights on the resulting rightmost spectral value assignment on comprehensive examples, opening perspectives in control design. A parametric characterization of the MID property in the case of a second-order linear DDE is provided in Sect. 5. Next, the effect of the maximal multiplicity of a spectral value on the distribution of the remaining spectrum is discussed in Sect. 6, where some interesting links with *Kummer hypergeometric functions* are emphasized. A software dedicated to the ensuing partial pole placement, called P3δ is described in Sect. 7. Section 8 illustrates the use of the proposed control strategy in the active damping of vibrations occurring in a flexible mechanical structure. Some notes and comments end the chapter.

Notations. In this chapter, we use the following standard notations[5]: $\mathbb{Z}$ ($\mathbb{N}$) denote the set of (non negative) integers, $\mathbb{R}$ ($\mathbb{C}$) denotes the set of real (complex) numbers. Next, $\mathbb{R}_+$ ($\mathbb{R}_-$) denotes the set of strictly positive (negative) real numbers and $\mathbb{R}^* = \mathbb{R} \setminus \{0\}$. For a given complex number λ, $\Re(\lambda)$ ($\Im(\lambda)$) denote its real (imaginary) part. The open left (right) complex half-plane is the set $\mathbb{C}_-$ ($\mathbb{C}_+$) defined by $\mathbb{C}_- = \{\lambda \in \mathbb{C} \,|\, \Re(\lambda) < 0\}$ ($\mathbb{C}_+ = \{\lambda \in \mathbb{C} \,|\, \Re(s) > 0\}$). For a given complex number λ the modulus is defined by $|\lambda| = \sqrt{\Re(\lambda)^2 + \Im(\lambda)^2}$. For a given discrete set χ, card(χ) denotes the number of elements of χ. The symbol sgn des-

[4] Such links have been previously highlighted in Mazanti et al. (2021a) for a particular class of systems and then generalized in Boussaada et al. (2022).

[5] It should be mentioned that, for reading facility, some specific notations are introduced later on.

ignates the sign of a real valued function f at a given argument. Given two vectors $u = (u_1, \ldots, u_n)^T \in \mathbb{R}^n$ and $v = (v_1, \ldots, v_m)^T \in \mathbb{R}^m$ we adopt the notation: $(u/v) = (u_1, \ldots, u_n, v_1, \ldots, v_m)^T$. For a set $\mathbb{K}$ of complex numbers, denote by $\mathcal{M}_{m,n}(\mathbb{K})$ ($\mathcal{M}_n(\mathbb{K})$) the set of $m \times n$ ($n \times n$) matrices with coefficients in $\mathbb{K}$. Given matrices $M_1 \in \mathcal{M}_{m,n_1}(\mathbb{R})$ and $M_2 \in \mathcal{M}_{m,n_2}(\mathbb{R})$ the notation $[M_1\, M_2]$ designates the matrix obtained by concatenation. Next, for a vector $u \in \mathbb{R}^n$, $\|u\|_2$ denotes its 2-norm and for a matrix $A \in \mathcal{M}_n(\mathbb{R})$, its 2-norm is defined by: $\|A\|_2 = \sup_{u \neq 0} \|Au\|_2 / \|u\|_2$. Given $k, n \in \mathbb{N}$ with $k \leq n$, the binomial coefficient $\binom{n}{k}$ is defined as $\binom{n}{k} = \frac{n!}{k!(n-k)!}$ and this notation is extended to $k, n \in \mathbb{Z}$ by setting $\binom{n}{k} = 0$ when $n < 0$, $k < 0$, or $k > n$. For $\alpha \in \mathbb{C}$ and $k \in \mathbb{N}$, $(\alpha)_k$ is the *Pochhammer symbol* for the *ascending factorial*, defined inductively as $(\alpha)_0 = 1$ and $(\alpha)_{k+1} = (\alpha + k)(\alpha)_k$. Finally, $\deg(P)$ denotes the degree of $P \in \mathbb{R}[x]$.

2 Preliminaries and Prerequisites

Let $\Omega \subset \mathbb{R}^{n_p}$ be an open set and consider two matrix functions $A_0, A_1 : \Omega \mapsto \mathcal{M}_n(\mathbb{R})$, $\overrightarrow{p} \in \Omega \mapsto A_j(\overrightarrow{p})$ $(j = 0, 1)$, that are assumed to be sufficiently smooth. With these notations, consider a dynamical system described by a DDE of retarded type with a single delay of the form:

$$\dot{\xi} = A_0(\overrightarrow{p})\xi(t) + A_1(\overrightarrow{p})\xi(t - \tau), \tag{1}$$

where $\xi = (\xi_1, \ldots, \xi_n)^T \in \mathbb{R}^n$ and $(\overrightarrow{p}, \tau) \in \Omega \times \mathbb{R}_+$ denote the state-vector and the *system's parameters*, respectively. Assume further that, for a fixed delay value $\tau \in \mathbb{R}_+$, for almost all $\overrightarrow{p} \in \Omega$, under appropriate initial conditions,[6] the system above is properly defined.[7]

It is well known that the asymptotic behavior of the solutions of (1) is determined from the location of the spectrum[8] χ of the characteristic matrix function[9] and defined by $\mathbb{M} : \mathbb{C} \times \Omega \times \mathbb{R}_+ \mapsto \mathbb{C}^{n \times n}$ with

$$\mathbb{M}(\lambda, \overrightarrow{p}, \tau) = \lambda\, I - A_0(\overrightarrow{p}) - A_1(\overrightarrow{p})\, e^{-\tau\lambda}. \tag{2}$$

Furthermore, these eigenvalues are the roots of the associated characteristic function which is the quasipolynomial $Q : \mathbb{C} \times \Omega \times \mathbb{R}_+^* \to \mathbb{C}$

$$Q(\lambda, \overrightarrow{p}, \tau) = \det \mathbb{M}(\lambda, \overrightarrow{p}, \tau). \tag{3}$$

---

[6] Belonging to the Banach space of continuous functions $\mathcal{C}([-\tau, 0], \mathbb{R}^n)$.

[7] In terms of existence of solutions for the corresponding Cauchy problem.

[8] That is the set of eigenvalues of the corresponding characteristic matrix function.

[9] Depending on the parameters $\overrightarrow{p}$ and τ.

Define now the sets $\chi_+, \chi_0, \chi_- \subset \chi$ as follows: $\chi_+ = \{\lambda \in \mathbb{C},\ Q(\lambda, \overrightarrow{p}, \tau) = 0, \Re(\lambda) > 0\}$, $\chi_- = \{\lambda \in \mathbb{C},\ Q(\lambda, \overrightarrow{p}, \tau) = 0,\ \Re(\lambda) < 0\}$ and $\chi_0 = \{\lambda \in \mathbb{C},\ Q(\lambda, \overrightarrow{p}, \tau) = 0,\ \Re(\lambda) = 0\}$ which give a partition of the spectrum χ of the DDE (1) with respect to the imaginary axis. More precisely, the spectrum χ can be divided into $\chi = \chi_+ \cup \chi_0 \cup \chi_-$. This chapter focuses on the computation of $\text{card}(\chi_+)$, that is the number of unstable characteristic roots. If the only parameter of interest is the delay τ, than $Q(\lambda, \overrightarrow{p}, \tau)$ simply rewrites as $Q(\lambda, \tau)$ and (1) becomes:

$$\dot{\xi} = A_0\xi(t) + A_1\xi(t-\tau), \tag{4}$$

with A_0, A_1 constant real valued matrices in $\mathcal{M}_n(\mathbb{R})$. The proof of the proposition below is given in Michiels and Niculescu (2007).

Proposition 1 *If λ is a characteristic root of system (4), then it satisfies*

$$|\lambda| \leq \|A_0 + A_1\, e^{-\tau\lambda}\|_2. \tag{5}$$

The inequality (5) combined with the triangular inequality provides a generic *envelope curve* around the characteristic roots corresponding to the DDE (1), see for instance Mori and Kokame (1989) for further insights on spectral envelopes for DDEs with a single delay.

As in the previous chapter by Niculescu et al. (2023), most of the examples considered in the sequel are represented by a particular class of quasipolynomial functions given by:

$$Q(\lambda, \overrightarrow{p}, \tau) = P_0(\lambda, \overrightarrow{p}) + P_1(\lambda, \overrightarrow{p})\, e^{-\lambda\tau},$$

where $\deg(P_0) > \deg(P_1)$, and a particular attention will be paid to scalar and second-order DDEs. Notice that some generic result on the location of associated spectral values for arbitrary polynomials P_0 and P_1 satisfying the condition $\deg(P_0) \geq \deg(P_1)$ can be found in Boese (1998); see also Michiels and Niculescu (2007). Furthermore, in most of the cases, the parameter vector $\overrightarrow{p}$ is explicitly defined by the coefficients of the polynomials P_0 and P_1, assumed to be independent one another.

In the following paragraphs, we present a characterization of the admissible/maximal spectral values' multiplicities[10] and describe their effect on the stability of the trivial solution as well as the corresponding exponential decay rate, see for instance Mori et al. (1982). As a byproduct of the approach, the main steps of an algorithmic procedure are proposed. We think that such an idea can be extended to more general quasipolynomials.

[10] It should be noted that, even in the simple case of second-order linear DDEs of retarded type, the corresponding 5 parameters induce a large computational effort to perform such an analysis.

2.1 On Integration Contours for Quasipolynomials Corresponding to DDEs of Retarded Type

Cauchy's argument principle is a basic complex analysis property[11] widely used in the stability analysis of LTI dynamical systems, see for instance Marden (1949); Ahlfors (1979). Roughly speaking, it relates the difference between the number of zeros and poles of a meromorphic function f in a simply connected domain $\mathcal{D} \subset \mathbb{C}$ to a contour integral of the function's logarithmic derivative on the boundary $\partial\mathcal{D}$; note that, this is also equal to the winding number of the curve $\partial\mathcal{D}$ with respect to f.

Theorem 1 (Ahlfors 1979) *Let $\mathcal{D}$ be a simply connected region with boundary Γ (piecewise smooth and oriented anti-colockwise). Let f be a meromorphic function in an open set containing the closure $\overline{\mathcal{D}}$ with poles $p_1, \ldots, p_l$ and zeros $z_1, \ldots, z_m$ counted according to their multiplicity, none of which belonging to the closed curve Γ. Then*

$$\frac{1}{2i\pi}\oint_{\Gamma}\frac{f'(s)}{f(s)}\,\mathrm{d}s = \mathcal{Z} - \mathcal{P},$$

where $\mathcal{Z}$ and $\mathcal{P}$ designate respectively the number of zeros and the number of poles of f enclosed by Γ.

In particular, note that if f is a holomorphic function[12] and Γ is a closed piecewise C^1 curve then

$$\frac{1}{2i\pi}\oint_{\Gamma}\frac{f'(s)}{f(s)}\,\mathrm{d}s = \mathcal{Z}.$$

Moreover, standard contours like the modified *Bromwich* contour are often used to explore the asymptotic stability of dynamical systems' solutions, as it allows to count the zeros with $\Re(s) > 0$ (see, e.g., Fig. 1). Other contours can be chosen based on the inherent properties of the considered characteristic function (Fig. 2).

Practically, owing to Proposition 1, a generic supremum bound for the real and imaginary parts of the roots of function (30) is established. Then, one may define an integration contour $\Gamma = \cup_{k=1}^{l} g_k$ which is not passing through zeros of Q and is taken as a counterclockwise closed curve. Hence, the contour integral over Γ is defined as the sum of the integrals over the directed smooth curves that make up Γ, as illustrated in Fig. 2.

Since we are concerned with zeros of quasipolynomials,[13] the following result[14] is a direct consequence of the argument principle applied to such functions.

Theorem 2 (Bellman and Cooke 1963) *If f is an analytic function inside and on a closed contour Γ, and is not zero on Γ, then the number of zeros (counting their*

[11] The reader may find the proof of this theorem in any standard textbook on the theory of analytic functions.

[12] In our case, we deal with quasipolynomial functions.

[13] Quasipolynomials are analytic functions.

[14] Called also *the argument variation.*

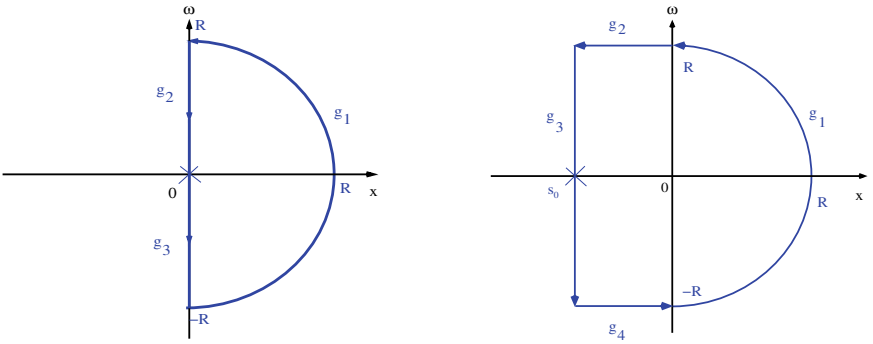

Fig. 1 LTI dynamical system; generic contours for applying the argument principle to investigate qualitative properties. (Left) Standard Bromwich contour usually adopted for asymptotic stability investigation; (Right) a contour often used to investigate $\omega-$stability or the dominancy of a given root. Figures are borrowed from Boussaada et al. (2020)

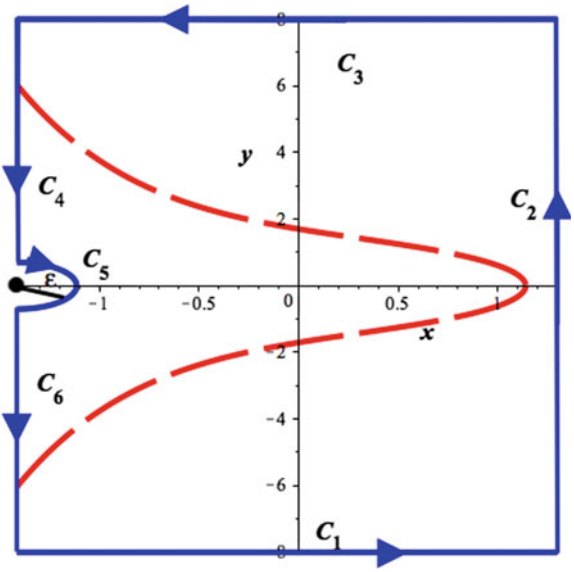

Fig. 2 Solid blue curve: simplified contour used in Boussaada and Niculescu (2018) for applying the argument principle to investigate the dominancy of multiple roots; dashed red curve: generic spectrum envelope given by Proposition 1 for the quasipolynomial $Q(\lambda, \overrightarrow{p}, \tau) = \lambda + a_0 + a_1 e^{-\lambda\tau}$ under conditions $\lambda_0 = -\frac{a_0\tau+1}{\tau}$ and $a_1 = \frac{e^{\lambda_0\tau}}{\tau}$ with $a_0 = \tau = 1$. The figure is borrowed from Boussaada et al. (2020)

respective multiplicities) of f within Γ is equal to $1/2\pi$ times the variation of the argument of $f(s)$ as s moves once around Γ in the counterclockwise sense.

Example 1 Consider the scalar DDE:

$$\dot{\xi}(t) + a\,\xi(t) + b\,\xi(t-\tau) = 0, \tag{6}$$

where $\overrightarrow{p} = (a,\ b)^T$ and τ are such that $\tau > 0$ and $0 < b < a$. To study the asymptotic stability of the trivial solution of (6), one investigates the distribution of zeros of the characteristic function given by:

$$Q(\lambda, \overrightarrow{p}, \tau) = \lambda + a + b\, e^{-\lambda \tau}. \tag{7}$$

To apply the argument principle, consider the standard Bromwich contour illustrated in Fig. 1. First, it is easy to observe that Q does not admit imaginary roots. Indeed, by assuming $Q(\mathrm{i}\,\omega, \overrightarrow{p}, \tau) = 0$, one gets:

$$\begin{cases} a = -b\, \cos(\omega\, \tau) \\ \omega = b\, \sin(\omega\, \tau), \end{cases} \tag{8}$$

where the first condition in (8) is inconsistent since $a > b$. Next, as emphasized in Proposition 1, in $\mathbb{C}_+$, the spectrum is finitely bounded by an appropriate envelope, so that Q does not admit zeros on the semi-circle C_R when $R \to \infty$. Furthermore, since, in $\mathbb{C}_+$, the zeros of $Q(\lambda, \overrightarrow{p}, \tau)$ coincides with the ones of $Q(\lambda, \overrightarrow{p}, \tau)/(\lambda + a) = 1 - \tilde{Q}(\lambda, \overrightarrow{p}, \tau)$ where $\tilde{Q}(\lambda, \overrightarrow{p}, \tau) = -\frac{b\, e^{-\lambda \tau}}{\lambda + a}$, then one may investigate the values of λ for which $\tilde{Q}(\lambda, \overrightarrow{p}, \tau) = 1$. Notice that the limiting position as $R \to \infty$ of the contour Γ under the mapping $\tilde{Q}(\lambda, \overrightarrow{p}, \tau)$ is called the *amplitude-phase characteristic*, see for instance El'sgol'ts and Norkin (1973).

To apply the argument principle or equivalently the argument variation on $\tilde{Q}(\lambda, \overrightarrow{p}, \tau)$, one needs to calculate the number of circuits of the amplitude-phase characteristic around the point $\lambda = 1$ (rather than $\lambda = 0$). Note also that under the mapping $\tilde{Q}(\lambda, \overrightarrow{p}, \tau)$, the semi-circle C_R when $R \to \infty$ reduces to a point. So that, one needs only to inspect the mapping $\tilde{Q}(\lambda, \overrightarrow{p}, \tau)$ through the imaginary axis traversed in the negative direction. When $R \to \infty$ the limiting characteristic of $\tilde{Q}(\lambda, \overrightarrow{p}, \tau)$ is nothing but the rational transformation $-b/(\lambda + a)$, which transforms the imaginary axis into the circle of center $\lambda = -b/2a$ and radius b/a. Since $a, b > 0$, then the mapping $\tilde{Q}(\lambda, \overrightarrow{p}, \tau)$ does not make any circuit around $\lambda = 1$, so that Q has no zeros in $\mathbb{C}_+$.

Another way to obtain the same conclusion of Example 1 is to employ the Rouché's Lemma.

Theorem 3 (Marden 1949) *If f and g are analytic function inside a simple closed Jordan curve Γ and if they are continuous on Γ with*

$$|f(\lambda)| < |g(\lambda)|,$$

then the function $f + g$ has the same number of zeros of g inside Γ.

Let us revisit Example 1 by applying Rouché's Lemma. To do so, let us define the functions $g(\lambda) = \lambda + a$ and $f(\lambda) = b\, e^{-\lambda \tau}$. Since $0 < b < a$, the condition of Rouché's Lemma are satisfied on the contour Γ defined as the standard Bromwich contour presented in Fig. 1, that is

$$|b\, e^{-\lambda \tau}| < |\lambda + a|.$$

Hence, Q defined by (7) does not admit any roots in $\mathbb{C}_+$.

When a given quasipolynomial function corresponding to a DDE of retarded type has no roots on the imaginary axis, then the seminal Stépán's work Stépán (1979) gives a new formalism and an easy procedure to characterize the exact number of unstable roots, that is the roots located in χ_+, see also Stépán (1989, Theorems 2.15–2.16). The proof of such a result is mainly based on the argument principle. Motivated by a potential application in bifurcation theory, the main theorem from Hassard (1997)[15] relaxes the assumption $\mathrm{card}(\chi_0) = 0$. Thus, it emphasizes the link between $\mathrm{card}(\chi_+)$ and $\mathrm{card}(\chi_0)$, both taking into account the multiplicity.

Theorem 4 (Hassard 1997, p. 223) *Consider the quasipolynomial function Q defined by*

$$Q(\lambda, \overrightarrow{\tau}) = P_0(\lambda) + \sum_{k=1}^{N} P_k(\lambda)\, e^{-\tau_k \lambda}.$$

with $\overrightarrow{\tau} = (\tau_1, \ldots, \tau_N)^T$. Let $\rho_1, \ldots, \rho_r$ be the positive roots of $\mathcal{R}(y, \overrightarrow{\tau}) = \Re(\mathrm{i}^n\, Q(\mathrm{i}\, y, \overrightarrow{\tau}))$, counted by their multiplicities and ordered so that $0 < \rho_1 \leq \ldots \leq \rho_r$. For each $j = 1, \ldots, r$ there exist τ_j such that $Q(\mathrm{i}\,\rho_j, \tau_j) = 0$, assume that the multiplicity of $\mathrm{i}\rho_j$ as a zero of $Q(\lambda, \overrightarrow{\tau})$ is the same as the multiplicity of ρ_j as a root of $\mathcal{R}(y, \overrightarrow{\tau})$. Then $\mathrm{card}(\chi_+)$ is given by the formula:

$$\mathrm{card}(\chi_+) = \frac{n - \mathrm{card}(\chi_0)}{2} + \frac{(-1)^r}{2}\,\mathrm{sgn}\ \mathcal{S}^{(\mu)}(0, \tau) + \sum_{j=1}^{r} \mathrm{sgn}\ \mathcal{S}(\rho_j, \tau_j),$$

where μ designates the multiplicity of the zero spectral value of $Q(\lambda, \overrightarrow{\tau}) = 0$ and $\mathcal{S}(y, \overrightarrow{\tau}) = \Im(\mathrm{i}^{-n} Q(iy, \overrightarrow{\tau}))$. Furthermore, $\mathrm{card}(\chi_+)$ is odd (respectively, even) if $Q^{(\mu)}(0, \overrightarrow{\tau}) < 0$ ($Q^{(\mu)}(0, \overrightarrow{\tau}) > 0$). If $\mathcal{R}(y, \overrightarrow{\tau}) = 0$ has no positive zeros (in y), set $r = 0$ and omit the summation term in the expression of $\mathrm{card}(\chi_+)$. If $s = 0$ is not a root of the characteristic equation, set $\mu = 0$ and interpret $\mathcal{S}^{(0)}(0, \overrightarrow{\tau})$ as $\mathcal{S}(0, \overrightarrow{\tau})$ and $Q^{(0)}(0, \overrightarrow{\tau})$ as $Q(0, \overrightarrow{\tau})$.

In order to illustrate the above result, we count the number of unstable roots of the following quasipolynomial with single delay and delay-dependent coefficients:

$$Q(\lambda, \tau) = \lambda^2 - \frac{4\,\lambda}{\tau} + \frac{6}{\tau^2} - \left(\frac{6}{\tau^2} + \frac{2\,\lambda}{\tau}\right) \mathrm{e}^{-\lambda\tau}. \tag{9}$$

Notice that (9) admits a characteristic root at the origin with multiplicity four.

Characterizing imaginary roots of the quasipolynomial.

In order to apply the argument principle on the standard Bromwich contour, allowing to count the roots of the quasipolynomial (9) in $\mathbb{C}_+$, a *deflation* which eliminates the roots on the imaginary axis is required. To do so, we first investigate nonzero imaginary roots of (9). Assuming that there exists $\omega > 0$ such that $\lambda = \mathrm{i}\omega$

[15] Which is strongly inspired from Stépán's result.

is a root of (9), we define $\mathcal{R}(\omega) = \Re(\mathrm{i}^{-2}Q(\mathrm{i}\omega,\tau))$ and $\mathcal{S}(\omega) = \Im(\mathrm{i}^{-2}Q(\mathrm{i}\omega,\tau))$, so that

$$\begin{cases} \mathcal{R}(\omega) = 6\,\dfrac{\cos(\omega\,\tau)}{\tau^2} + 2\,\dfrac{\omega\,\sin(\omega\,\tau)}{\tau} + \omega^2 - \dfrac{6}{\tau^2}, \\ \mathcal{S}(\omega) = 2\,\dfrac{\omega\,\cos(\omega\,\tau)}{\tau} - 6\,\dfrac{\sin(\omega\,\tau)}{\tau^2} + 4\,\dfrac{\omega}{\tau}. \end{cases} \tag{10}$$

As a consequence, for any $\lambda = \mathrm{i}\omega$, root of (9), we have $\mathcal{R}(\omega) = \mathcal{S}(\omega) = 0$. Then, some algebraic manipulations allow to eliminate the trigonometric functions as follows:

$$\begin{cases} \cos(\omega\,\tau) = -\dfrac{1}{2}\,\dfrac{7\,\omega^2\tau^2 - 18}{\omega^2\tau^2 + 9}, \\ \sin(\omega\,\tau) = -\dfrac{1}{2}\,\dfrac{\omega\,\tau\,\left(\omega^2\tau^2 - 18\right)}{\omega^2\tau^2 + 9}. \end{cases}$$

Using the standard trigonometric identity $\cos^2(\omega\,\tau) + \sin^2(\omega\,\tau) = 1$, one obtains exclusively 0 and the non-vanishing solutions $\omega = \pm\frac{3\mathrm{i}}{\tau}$, which are discarded since we are dealing with positive frequencies. By using the notations from the Theorem above where $\mathrm{card}(\chi_0)$ stands for the number of imaginary roots of (9) and κ designate the multiplicity of 0. In our case, $\mathrm{card}(\chi_0) = \kappa = 4$. Hence, the deflated function which is integrated on the Bromwich contour $\mathcal{B}$ is given by

$$\hat{Q}(\lambda,\tau) = \frac{Q(\lambda,\tau)}{\lambda^4},$$

It has the same nontrivial zeros encircled by $\mathcal{B}$ as the quasipolynomial Q.

Characterizing ω_k the positive roots of $\mathcal{R}$ and exploring $\mathrm{sgn}(\mathcal{S}(\omega_k))$. Consider now the positive roots of $\mathcal{R}$. If $\omega > 0$ is a root of the first transcendental function of (10), then

$$6\,\frac{\cos(\omega\,\tau)}{\tau^2} + 2\,\frac{\omega\,\sin(\omega\,\tau)}{\tau} + \omega^2 - \frac{6}{\tau^2} = 0.$$

Multiplying the last equation by τ^2 reduces the problem to the search of zeros of an univariate function:

$$F(\rho) = 6\,\cos(\rho) + 2\,\rho\,\sin(\rho) + \rho^2 - 6 \quad (\rho = \omega\,\tau).$$

Interestingly, the function F admits a unique solution $\rho^\star \in \left(\pi, \frac{3\pi}{2}\right)$ which is equivalent to state that, for a given positive delay $\tau^\star$, there exists a unique frequency $\omega^\star \in \mathbb{R}_+$ such that $\rho^\star = \omega^\star\,\tau^\star$ and $\mathcal{R}(\omega^\star,\tau^\star) = 0$.

By similarity, define $G(\rho) = \tau^2\,\mathcal{S}(\omega)$. Then,

$$G(\rho) = 2\,\rho(2 + \cos(\rho)) - 6\,\sin(\rho)$$

which is positive in the interval $(\pi, 2\pi)$ since $\sin(\rho) < 0$. In particular, $G(\rho^\star, \tau^\star) > 0$ and thus $\mathcal{S}(\omega^\star) > 0$.

Counting the number of roots dominating zero. We are able now to compute the number of unstable roots of (9) based on the computation of the argument variation. As a matter of fact, combining all the above collected information on the behavior of both the real $\mathcal{R}$ and the imaginary $\mathcal{S}$ parts of the quasipolynomial function (9), we apply directly the theorem above. Namely, $\mathcal{Z}$ designates the number of roots dominating 0:

$$\mathcal{Z} = \frac{n - \text{card}(\chi_0)}{2} + \frac{1}{2}(-1)^r \text{ sgn } \mathcal{S}^{(\kappa)}(0) + \sum_{j=1}^{r}(-1)^{j-1} \text{ sgn } \mathcal{S}(\omega_j), \qquad (11)$$

where n is the order of the system, κ is the multiplicity of 0 as a root of (9), K is the total number of roots of (9) on the imaginary axis and r is the number of positive real roots of $\mathcal{R}$. In our case, $n = 2$, $\kappa = \text{card}(\chi_0) = 4$, $r = 1$ and $\mathcal{S}^{(4)}(\omega) = 2\sin(\omega\tau)\tau^2 + 2\omega\cos(\omega\tau)\tau^3$ which vanishes at $\omega = 0$. As a result, we easily obtain that $\mathcal{Z} = 0$ owing to formula (11). Hence, the dominancy of 0 as a root of (9) is established; that is no roots with positive real part exist for the quasipolynomial Q.

2.2 Pólya-Szegö Theorem: Counting Quasipolynomial Roots

The following result was first introduced and claimed in the problems collection published in 1925 by G. Pólya and G. Szegö. In the fourth edition of their book,[16] the authors emphasize that the proof was obtained by N. Obreschkoff in 1928 using the argument principle, see Obreschkoff (1928). Such a result gives a bound for the number of quasipolynomial's roots in any horizontal strip. As a consequence, a bound for the number of quasipolynomial's real roots can be easily deduced.

Proposition 2 (Pólya and Szegő 1972, p. 144) *Let $\tau_1, \ldots, \tau_N$ denote real numbers such that $\tau_1 < \tau_2 < \cdots < \tau_N$, and $d_1, \ldots, d_N$ positive integers satisfying $d_1 \geq 1$, $d_2 \geq 1, \ldots, d_N \geq 1$ and define D such that $D = d_1 + d_2 + \cdots + d_N - N$.*

Let $f_{i,j}(\lambda)$ the function $f_{i,j}(\lambda) = \lambda^{j-1} e^{\tau_i \lambda}$, for $1 \leq j \leq d_i$ and $1 \leq i \leq N$. For α, β two real numbers, let $\sharp_{PS}$ be the number of zeros of the complex valued function

$$f(\lambda) = \sum_{1 \leq i \leq N, 1 \leq j \leq d_i} c_{i,j} \, f_{i,j}(\lambda)$$

[16] More precisely, Pólya and G. Szegö (1972, Problem 206.2, p. 144 and p. 347).

contained in the horizontal strip $\{\lambda \in \mathbb{C}, \alpha \leq \Im(\lambda) \leq \beta\}$. *Assuming that*

$$\sum_{1\leq k\leq d_1} |c_{1,k}| > 0, \ \ldots, \ \sum_{1\leq k\leq d_N} |c_{N,k}| > 0,$$

then

$$\frac{(\tau_N - \tau_1)\ (\beta - \alpha)}{2\,\pi} - D + 1 \leq \sharp_{PS} \leq \frac{(\tau_N - \tau_1)\ (\beta - \alpha)}{2\,\pi} + D + N - 1.$$

Setting $\alpha = \beta = 0$, the above Proposition allows to $\sharp_{PS} \leq D + N - 1$ where D stands for the sum of the degrees of the polynomials involved in the quasipolynomial function f and N designates the associated number of polynomials. As explained in the sequel, in the case of complete polynomials, this gives a sharp bound.

3 Characterizing Multiplicity Using Structured Matrices

Matrices arising from a wide range of problems in mathematics and engineering typically display a characteristic structure. Exploiting such a structure is the mean to the design of efficient algorithms, see for instance Bini and Boito (2010). The discussion below is a crossroad between the investigation of a class of such structured matrices originally involved in *multivariate interpolation problems*[17] and the estimation of the upper bound for the codimension of *spectral values* of linear DDEs (which are the zeros of the corresponding *characteristic quasipolynomial*). The aim of this section is threefold: firstly, it emphasizes the link between the above two quoted issues. Secondly, it shows that the codimension of the zero as well as purely imaginary spectral values of a given DDE are characterized by some algebraic properties of an appropriate *functional Birkhoff matrix*. Finally, it shows the effectiveness of the proposed constructive approach by exploring the generic settings as well as investigating some specific but significant sparsity patterns. In both cases, symbolic algorithms for LU-factorization are presented for some novel classes of Birkhoff matrices. It is worth mentioning that such an attempt can be exploited for further classes of Birkhoff matrices and should be of interest in some linear algebra problems involving structured matrices as well as in applications including polynomial interpolation. The proofs of the results presented in this section can be found in Boussaada and Niculescu (2016a, b).

3.1 Singularity Codimension May Exceed the Model Order:Bogdanov-Takens Singularity

Consider first a simple scalar DDE with one delay representing a biological model discussed in Cooke (1979) describing the dynamics of disease propagation. Namely,

[17] Namely, the well-known *Birkhoff interpolation problem*.

the infected host population $x(t)$ is governed by:

$$\dot{x}(t) + a_0\, x(t) + a_1\, x(t-\tau) - a_1\, x(t-\tau)\, x(t) = 0,$$

where $a_1 > 0$ designates the contact rate between infected and uninfected populations and it is assumed that the infection of the host recovery proceeds exponentially at a rate $-a_0 > 0$; see also Ruan (2006) for more insights on the modeling and stability results. The linearized system is given by

$$\dot{x}(t) + a_0\, x(t) + a_1\, x(t-\tau) = 0, \tag{12}$$

where $\overrightarrow{p} = (a_0, a_1)^T$ with $(a_0, a_1, \tau) \in \mathbb{R}^2 \times \mathbb{R}_+$, then the associated characteristic (transcendental) function Q becomes

$$Q(\lambda, \overrightarrow{p}, \tau) = \lambda + a_0 + a_1\, e^{-\lambda\tau}. \tag{13}$$

Zero is a spectral value for (12) if, and only if, Q vanishes at zero which is equivalent to $a_0 + a_1 = 0$. The computations of the first derivatives of (13) with respect to λ give:

$$Q'(\lambda, \overrightarrow{p}, \tau) = 1 - \tau\, a_1\, e^{-\lambda\tau},$$
$$Q''(\lambda, \overrightarrow{p}, \tau) = \tau^2\, a_1\, e^{-\lambda\tau}.$$

If additionally $a_1 \neq 0$, then the codimension of the zero spectral value is at most two[18] since the algebraic multiplicity 2 is ensured for $\tau^* = 1/a_1 > 0$, $a_0 = -a_1$ and $Q''(0, \overrightarrow{p^\star}, \tau^\star) \neq 0$. It should be mentioned that Q includes 3 parameters $(a_0,\ a_1,\ \tau)$ and the codimension cannot exceed 2. It is easy to observe that the Pólya-Szegö bound $\sharp_{PS} = 2$ if if one chooses[19] $\alpha = \beta = 0$.

3.2 *Codimension Counting: A Vandermonde/Birkhoff-Based Framework*

Consider now that the DDE (4) includes N discrete (constant) delays where the vector $\zeta = (\zeta_1, \ldots, \zeta_n) \in \mathbb{R}^n$ denotes the state-vector, then the DDE reads

$$\dot{\zeta} = \sum_{k=0}^{N} A_k \zeta(t - \tau_k), \tag{14}$$

[18] Bogdanov-Takens singularity corresponds to equilibrium point admitting a double spectral value at zero for which corresponds a single eigenvector. Near a Bogdanov-Takens singularity a codimension 2 bifurcation may occur in two dimensional parameters space.

[19] Indeed, in this case, we have $N = 2$, $\tau_1 = 0,\ \tau_2 = \tau$ and $d_1 = 1,\ d_2 = 0$.

where τ_k, $k = 1, \ldots, N$ are strictly increasing positive constant delays such that $\tau_0 = 0$ and $\overrightarrow{\tau} = (\tau_1, \ldots, \tau_N)^T$, and $A_k \in \mathcal{M}_n(\mathbb{R})$ for $k = 0, \ldots, N$. In this case, the characteristic function of system (14) reads

$$\hat{Q}(\lambda, \overrightarrow{p}, \overrightarrow{\tau}) = \det\left(\lambda\, I - A_0 - \sum_{k=1}^{N} A_k\, e^{-\tau_k \lambda}\right), \tag{15}$$

where $\overrightarrow{p}$ denotes the entries of the matrices A_k, for $k = 0, \ldots, N$. For a given delay vector $\overrightarrow{\tau}$ and vector parameter $\overrightarrow{p}$, the corresponding spectrum χ can be split into $\chi = \chi_+ \cup \chi_0 \cup \chi_-$ where $\chi_+ = \{\lambda \in \mathbb{C},\ \hat{Q}(\lambda, \overrightarrow{p}, \overrightarrow{\tau}) = 0,\ \Re(\lambda) > 0\}$, $\chi_- = \{\lambda \in \mathbb{C},\ \hat{Q}(\lambda, \overrightarrow{p}, \overrightarrow{\tau}) = 0,\ \Re(\lambda) < 0\}$ and $\chi_0 = \{\lambda \in \mathbb{C},\ \hat{Q}(\lambda, \overrightarrow{p}, \overrightarrow{\tau}) = 0,\ \Re(\lambda) = 0\}$.

Let us start by setting a new parameterization for the quasipolynomial function (15) of the DDE (14) and defining some useful notations adopted through this section. Some straightforward computations give the following formal expression of the quasipolynomial function (15)

$$\hat{Q}(\lambda, \overrightarrow{p}, \overrightarrow{\tau}) = P_0(\lambda, \overrightarrow{p}) + \sum_{M^k \in S_{N,n}} P_{M^k}(\lambda, \overrightarrow{p})\, e^{\sigma_{M^k}\, \lambda}, \tag{16}$$

where $\sigma_{M^k} = -M^k\, \overrightarrow{\tau}$ and $S_{N,n}$ is the set of all the possible row vectors $M^k = (M_1^k, \ldots, M_N^k)$ belonging to $\{1, \ldots, n\}^N$ such that $1 \leq M_1^k + \ldots + M_N^k \leq n$. Furthermore, by running the index from 1 to the cardinality $\tilde{N}_{N,n} := \mathrm{card}(S_{N,n})$, (16) can be written in the following compact form:

$$\hat{Q}(\lambda, \overrightarrow{p}, \overrightarrow{\tau}) = P_0(\lambda, \overrightarrow{p}) + \sum_{k=1}^{\tilde{N}_{N,n}} \overrightarrow{p}_k(\lambda, \overrightarrow{p})\, e^{\sigma_k\, \lambda}. \tag{17}$$

For instance,

$$S_{3,2} = \big\{(1,0,0), (0,1,0), (0,0,1), (2,0,0), (1,1,0), (1,0,1), (0,2,0), (0,1,1), (0,0,2)\big\}$$

is ordered first by increasing sums $(\sum_{i=1}^{N} M_i^k)$ then by lexicographical order. In this case, one has $M^2 = (0,1,0)$ and $\tilde{N}_{3,2} = 9$. A generic property of DDEs (14) allows considering p_0 as a monic polynomial of degree n in λ and the polynomials P_{M^k} satisfying $\deg(P_{M^k}) = n - \sum_{s=1}^{N} M_s^k \leq (n-1)\ \forall M^k \in S_{N,n}$. In the sequel, $p_0(\cdot, \overrightarrow{p})$ will be called the *delay-free polynomial* and the quasipolynomial function $\lambda \mapsto \sum_{k=1}^{\tilde{N}_{N,n}} P_{M^k}(\lambda, \overrightarrow{p})\, e^{\sigma_k\, \lambda}$ will be called the *transcendental part of the quasipolynomial*.

Next, define $a_{j,k}$ as the coefficient of the monomial λ^k for the polynomial P_{M^j}, $1 \leq j \leq \tilde{N}_{N,n}$, and denote $P_{M^0} = P_0$. Thus, $a_{0,n} = 1$ and $a_{j,k} = 0\ \forall k \geq d_j = n -$

$\sum_{s=1}^{N} M_s^j$. Here, $d_j - 1$ is nothing but the degree of P_{M^j}. Furthermore, we denote by $a_0 = (a_{0,0},\ a_{0,1},\ \ldots,\ a_{0,n-1})^T$ the vector of the coefficients of the delay-free polynomial and by $a_j = (a_{j,0},\ a_{j,1},\ \ldots,\ a_{j,d_j-1})^T$ the vector of the coefficients of the polynomial associated to the auxiliary delay σ_j for $1 \leq j \leq \tilde{N}_{N,n}$. Next, set the delay auxiliary vector $\sigma = (\sigma_1,\ \sigma_2,\ \ldots,\ \sigma_{\tilde{N}_{N,n}})$ and $a = (a_1 / a_2 / \cdots / a_{\tilde{N}_{N,n}})^T$.

This leads to a new parameterization of the quasipolynomial $\hat{Q}(\lambda, \overrightarrow{p}, \overrightarrow{\tau}) = Q(\lambda, \overrightarrow{a}, \overrightarrow{\tau})$. Finally, let us denote by $Q^{(k)}$ the k-th derivative of Q with respect to the variable λ. We say that zero is an eigenvalue of algebraic multiplicity $m \geq 1$ for (14) at $\overrightarrow{a} = \overrightarrow{a}_*$ and $\overrightarrow{\tau} = \overrightarrow{\tau}_*$ if $Q(0, \overrightarrow{a}_*, \overrightarrow{\tau}_*) = Q^{(k)}(0, \overrightarrow{a}_*, \overrightarrow{\tau}_*) = 0$ for all $k = 1, \ldots, m-1$ and $Q^{(m)}(0, \overrightarrow{a}_*, \overrightarrow{\tau}_*) \neq 0$. We assume also in what follows that $\sigma_k \neq \sigma_{k'}$ for any $k \neq k'$ where $k, k' \in S_{N,n}$. Indeed, if for some value of the delay vector $\overrightarrow{\tau}$ there exists some $k \neq k'$ such that $\sigma_k = \sigma_{k'}$, then the number of auxiliary delays and the number of polynomials is reduced by considering a new family of polynomials $\tilde{P}$ satisfying $\tilde{P}_{M^k} = P_{M^k} + P_{M^{k'}}$. In the sequel, $D_q = \sum_{k=0}^{\tilde{N}_{N,n}} \deg(P_{M^k}) + \tilde{N}_{N,n} - 1$ will designate *the degree* of the transcendental part of the quasipolynomial[20] .

Now, to characterize the structure of a given quasipolynomial function one needs to introduce a vector $\mathcal{V}$, called *incidence vector*, vector that reproduces the data on the vanishing components of the vector $\overrightarrow{a}$ defined above. Thus, $\mathcal{V}$ is a sparsity patterns indicator for the transcendental part of the quasipolynomial. To do so, we finally introduce the symbol $\star$ to indicate the vanishing of a given coefficient of the transcendental part of the quasipolynomial. To illustrate the above notions, consider the following quasipolynomial function

$$\begin{aligned} Q(\lambda, \overrightarrow{a}, \overrightarrow{\tau}) = P_0(\lambda, \overrightarrow{a}) + \left(a_{1,0,0,0} + a_{1,0,0,1}\lambda\right) e^{-\lambda\tau_1} \\ + a_{0,1,0,2}\lambda^2 e^{-\lambda\tau_2} + a_{0,0,1,1}\lambda e^{-\lambda\tau_3}. \end{aligned} \tag{18}$$

In this case, $\sigma_{i,j,k} = -(i\ j\ k) \cdot \overrightarrow{\tau}$ where $i, j, k = 0, 1$. More precisely, $\sigma_{1,0,0} = -\tau_1$, etc. According to the above considerations, $\deg(P_0) = n \geq 3$, and the transcendental part of (18) is characterized by the incidence vector

$$\mathcal{V} = (x_1, x_1, \star, \star, x_2, \star, x_3).$$

Namely, the first two components of $\mathcal{V}$ indicate that P_{M^1} is a *complete* polynomial with $\deg(P_{M^1}) = 1$, the three components $\star, \star, x_2$, indicate that $a_{0,1,0,0} = a_{0,1,0,1} = 0$ and P_{M^2} is *lacunary* with $\deg(P_{M^2}) = 2$ and $\star, x_3$ indicate that $a_{0,0,1,0} = 0$ and P_{M^3} is lacunary with $\deg(P_{M^3}) = 1$.

In the spirit of the definition of *functional confluent Vandermonde matrices* introduced by Ha and Gibson (1980), the *functional Birkhoff matrices* are defined as follows:

[20] In other words, the sum of the degrees of the polynomials involved in the quasi-polynomial plus the number of polynomials involved minus one is called the degree of a given quasi-polynomial. Further discussions on such a notion can be found in Wielonsky (2001).

Definition 1 The square *functional Birkhoff matrix* Υ is associated to a sufficiently regular real function $\varpi : \mathbb{R} \mapsto \mathbb{R}$ and an incidence matrix $\mathcal{E}$ (or equivalently an incidence vector $\mathcal{V}$) and is defined by concatenation

$$\Upsilon = [\Upsilon^1 \, \Upsilon^2 \, \dots \, \Upsilon^M] \in \mathcal{M}_\delta(\mathbb{R}),$$

where

$$\Upsilon^i = [\kappa^{(k_{i_1})}(x_i) \; \kappa^{(k_{i_2})}(x_i) \; \dots \; \kappa^{(k_{i_{d_i}})}(x_i)],$$

such that $k_{i_l} \geq 0$ for all $(i, l) \in \{1, \dots, M\} \times \{1, \dots, d_i\}$ and $\sum_{i=1}^{M} d_i = \delta$ with

$$\kappa(x_i) = \varpi(x_i)[1 \; \dots \; x_i^{\delta-1}]^T, \quad \text{for} \quad 1 \leq i \leq M.$$

Remark 1 In the sequel, if $n = \deg(P_0)$ let $\eta = n + 1$. Then, we consider $\varpi(x_i) = x_i^\eta$. By analogy to the Birkhoff interpolation problem, the non degeneracy of the matrices Υ will be a fundamental assumption for investigating the codimension of the zero spectral values for DDEs.

Remark 2 When $\eta = 0$, the matrix Υ is nothing else but the standard Birkhoff matrix and thus $\varpi(x_i) = 1$. If, in addition, $\mathcal{V}$ does not contain $\star$'s then we recover the confluent Vandermonde matrix (Ha and Gibson, 1980). The particular case $d_i = 1$ for $i = 1, \dots, M$ corresponds to the standard Vandermonde matrix and, in this case, $M = \delta$ since Υ is assumed to be a square matrix.

Thanks to this formalism based on functional Birkhoff matrices initially presented in Boussaada and Niculescu (2016a), one is able to characterize the codimension of imaginary spectral values of DDEs of retarded type.

3.3 Codimension of Zero Singularities of DDEs

The next result gives a bound for the zero spectral value, bound that takes into account the system structure. However, it should be noted that the proof is constructive and it exploits the existing links between the multiplicity of the zero singularity and Birkhoff matrices, see, for instance, Boussaada and Niculescu (2016a). Additionally, it gives the values of the system parameters guaranteeing an admissible multiplicity for the zero spectral value. Finally, the result holds even when the delay associated polynomials are sparse.

Proposition 3 *The following assertions hold:*

(i) The multiplicity of the zero root for the generic quasipolynomial function (17) *cannot be larger than* $\sharp_{PS} = D + \tilde{N}_{N,n}$*, where* D *is the sum of degrees of the polynomials involved in the quasipolynomial and* $\tilde{N}_{N,n} + 1$ *is the number of the associated polynomials. Moreover, such a bound is reached if, and only if, the parameters of* (17) *satisfy simultaneously:*

$$a_{0,k} = -\sum_{i \in S_{N,n}} \left(a_{i,k} + \sum_{l=0}^{k-1} \frac{a_{i,l} {\sigma_i}^{k-l}}{(k-l)!} \right), \quad 0 \leq k \leq \sharp_{PS} - 1. \tag{19}$$

(ii) Consider a quasipolynomial function (17) *containing at least one incomplete polynomial for which we associate an incidence vector* $\mathcal{V}_{\tilde{\mathcal{E}}}$. *When the associated functional Birkhoff matrix* $\Upsilon_{\tilde{\mathcal{E}}}$ *is nonsingular, then the multiplicity of the zero root for the quasipolynomial function* (17) *cannot be larger than n plus the number of nonzero coefficients of the polynomial family* $(P_{M^k})_{M^k \in S_{N,n}}$.

Remark 3 In the generic case, the Pólya-Szegö bound $\sharp_{PS}$ is completely recovered by the first assertion of Proposition 3. But, its advantage consists in providing the parameter values ensuring any admissible multiplicity of the zero singularity. The proof of Proposition 3 provides a constructive linear algebra alternative for identifying such a bound.

Remark 4 Obviously, the number of non-zero coefficients of a given quasi-polynomial function is bounded by its degree plus its number of polynomials. Thus, the bound proposed in Proposition 3 (ii) is sharper than $\sharp_{PS}$, even in the generic case, that is all the parameters of the quasipolynomial are left free, these two bounds are equal. Indeed, in the generic case, that is when the number of the left free parameters is maximal, the Pólya-Szegö bound $\sharp_{PS} = D + \tilde{N}_{N,n} = n + D_q + \tilde{N}_{N,n}$ which is nothing else than n plus the number of parameters of the polynomial family $(P_{M^k})_{M^k \in S_{N,n}}$.

Remark 5 When the matrix $\Upsilon_{\tilde{\mathcal{E}}}$ is singular, one keeps the generic Pólya-Szegö bound $\sharp_{PS}$.

Remark 6 The above proposition can be interpreted as follows. Under the hypothesis:

$$Q(\mathrm{i}\omega) = 0 \Rightarrow \omega = 0 \tag{H}$$

(that is, all the imaginary roots are located at the origin), the dimension of the projected state on the center manifold associated with zero singularity for Eq. (17) is less or equal to its number of nonzero coefficients minus one. Indeed, under (H), the codimension of the zero spectral value is equal to the dimension of the state on the center manifold since, in general, the dimension of the state on the center manifold is nothing but the sum of the dimensions of the generalized eigenspaces associated with the spectral values having a zero real part.

Remark 7 For a given quasipolynomial function, the multiplicity of real roots may reach the Polya-Szegö bound, see Boussaada et al. (2014); Boussaada and Niculescu (2014). However, the multiplicity of an imaginary crossing root may exceed the dimension of the delay-free system but never reach the Polya-Szegö bound, see, e.g., Boussaada and Niculescu (2016b).

4 Multiple Induced Dominancy and Partial Pole Assignment: Comprehensive Examples

In this section, we focus on three case studies. The first one corresponds to the simplest DDE by which one can exhibit and explain in a comprehensive way the stability induced when forcing some particular spectral value to be multiple. The second, which apparently illustrates the limitation of such a property, gives an in-depth insight into the conditions of application of such a property. The last example concerns the stabilization of a second-order oscillator controlled by a delayed-output feedback. An appropriate choice of the gain and of the delay (seen as a parameter of the system) allows assigning a dominant characteristic root in $\mathbb{C}$ with multiplicity 3.

4.1 Exponential Decay Rate of a Scalar DDE with a Single Delay

Let us revisit the scalar DDE with one delay given in (6):

$$\dot{\xi}(t) + a\,\xi(t) + b\,\xi(t-\tau) = 0, \tag{20}$$

where $b > 0$, . It was shown in Boussaada et al. (2016) that for a given positive delay, Eq. (20) admits a double spectral value at $\lambda = \lambda_0$ if, and only if,

$$\lambda_0 = -\frac{a\tau + 1}{\tau} \quad \text{and} \quad b = \frac{\mathrm{e}^{\lambda_0 \tau}}{\tau}. \tag{21}$$

In addition, it was emphasized that λ_0 is the rightmost root, and that if $\lambda_0 < 0$ then the zero solution of system (20) is asymptotically stable. Now, recall that $\lambda = \lambda_0$ is a spectral value of (20) if, and only if, λ_0 is a root of the characteristic function:

$$Q(\lambda, \overrightarrow{p}, \tau) = \lambda + a + b\,e^{-\lambda\tau}. \tag{22}$$

The main ingredient of the dominancy proof of λ_0 is an integral equation which cannot be satisfied for any spectral value λ with $\Re(\lambda) > \lambda_0$. Namely, it was shown that if b satisfies (21), then the characteristic function reads:

$$Q(\lambda, \overrightarrow{p}, \tau) = (\lambda - \lambda_0)\left(1 - \int_0^1 e^{-\tau(\lambda-\lambda_0)t}\,\mathrm{d}t\right). \tag{23}$$

As a matter of fact, if $\lambda_1 = \zeta + \mathrm{i}\eta \neq \lambda_0$ is a root of (23) then λ_1 is a root of its second factor. Hence, we obtain

$$1 = \int_0^1 e^{-\tau(\zeta-\lambda_0)t}\,\mathrm{d}t.$$

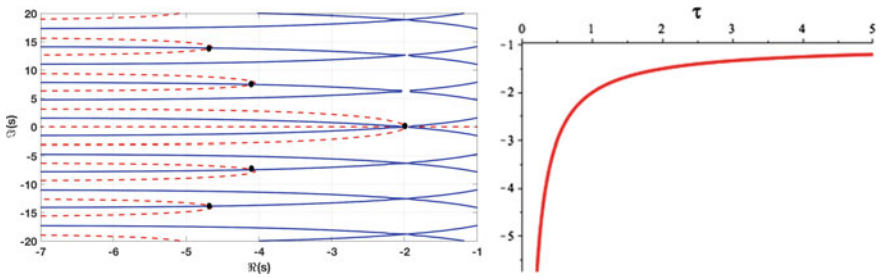

Fig. 3 (Left) Distribution of the spectrum corresponding to Eq. (22) and conditions (21) for $a = \tau = 1$ and $b = e^{-2}$. The roots' distribution is illustrated using the QPmR toolbox from Vyhlídal and Zitek (2009). (Right) Rightmost root corresponding to Eq. (22) and conditions (21) as a function of the delay τ for $a = 1$ and $b = \frac{e^{-(\tau+1)}}{\tau}$. Figures are borrowed from Boussaada et al. (2020)

But, $e^{-\tau(\zeta-\lambda_0)t} < 1$ for $\zeta - \lambda_0 > 0$ and $0 < t < 1$, thereby exhibiting the dominancy of λ_0.

Remark 8 The rightmost root λ_0 corresponding to equation (22), where system (21) is satisfied, varies in the interval $\lambda_0 \in (-\infty, -a)$. Figure 3 illustrates the behavior of the rightmost root with respect to the variation of τ.

4.2 Multiple Spectral Values for DDEs Systems are Not Necessarily Dominant

The problem of stabilization of a chain of integrators is considered in Niculescu and Michiels (2004) where a single integrator can be stabilized by a single delay state-feedback. Indeed, a positive gain guarantees the closed-loop stability of the system free of delay, and, by continuity, there exists a (sufficiently small) delay in the output preserving the stability of the closed-loop system. However, the situation is completely different for a chain of integrators of order n when $n > 1$. For instance, consider the time-delay system characterized by the following quasipolynomial function:

$$Q(\lambda, \alpha, \tau) = \lambda^2 + \alpha e^{-\tau\lambda}. \tag{24}$$

It can be checked that the maximal admissible multiplicity is 2 and it can be attained if, and only if,

$$\alpha = -4\frac{e^{-2}}{\tau^2}, \ \lambda = -\frac{2}{\tau}. \tag{25}$$

However, the main result from Niculescu and Michiels (2004) asserts that either n distinct delays or a proportional+delay compensator with $n - 1$ distinct delays are sufficient to stabilize a chain including n integrators. In Kharitonov et al. (2005), a

like assertion is shown to be also necessary to stabilize the chain of n integrators. Hence, in our case, either 2 distinct delays or a proportional+delay are necessary and sufficient to stabilize the double integrator. In conclusion, there exists at least a spectral value for (24) with a positive real part. As a result, $\lambda_0 = -\frac{2}{\tau}$, while being a multiple root, it is not dominant. Indeed, consider (24)–(25) with $\tau = 1$, that is

$$Q(\lambda, \alpha, \tau)|_{\tau=1} = \lambda^2 - 4e^{-(\lambda+2)}. \tag{26}$$

As illustrated in Fig. 4, the dominancy property is lost since $\lambda_1 \approx 0.557$ is a root of (26). This is justified by the sparsity (the vanishing of some coefficients of the corresponding P_0 polynomial) of (26).

4.3 *Stabilizing an Oscillator Via a Delayed Output-Feedback*

Consider the stability of the trivial solution corresponding to the control system

$$\begin{cases} \ddot{\xi}(t) + c_1\dot{\xi}(t) + c_0\xi(t) = u(t), \\ \phi(t) = \gamma\,\xi(t), \end{cases}$$

where $\phi(t)$ is the system output and $u(t) = \frac{\beta}{\gamma}\,\xi(t-\tau)$ is the control law, which amounts to studying the roots of the quasipolynomial function

$$Q(\lambda, \overrightarrow{p}, \tau) = \lambda^2 + a_1\lambda + a_0 + \beta\, e^{-\tau\lambda}.$$

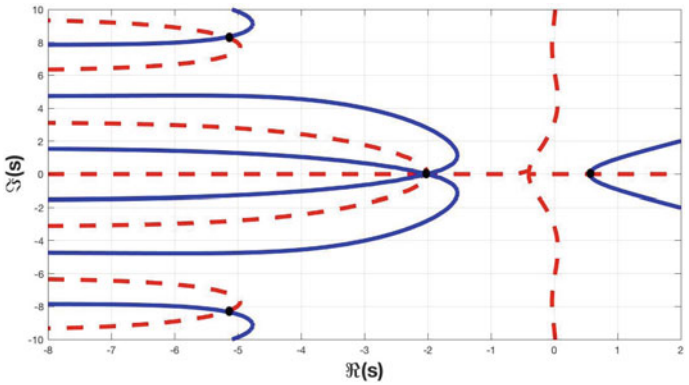

Fig. 4 Sparsity-induced loss of dominancy for the multiple spectral value. Each intersection between the solid blue/dashed red curves corresponds to a spectral value of (26). For $\tau = 1$, the dominancy of $\lambda_1 \approx 0.557$ with respect to the double root at $\lambda_0 = -2$ is illustrated. The roots' distribution is illustrated using the QPmR toolbox from Vyhlídal and Zitek (2009). The figure is borrowed from Boussaada et al. (2020)

Using the standard linear change of variables $\lambda \to \frac{c_1 \lambda}{2}$, one obtains the normalized characteristic function

$$\tilde{Q}(\lambda, \overrightarrow{p}, \tau) = \lambda^2 + 2\lambda + a_0 + \alpha e^{-\lambda \tilde{\tau}} \tag{27}$$

where $\alpha = \frac{4}{c_1^2}\beta$, $\tilde{\tau} = \frac{c_1}{2}\tau$ and $a_0 = 4\frac{c_0}{c_1^2}$. If $\alpha = 0$, the spectral abscissa is minimized at $a_0 = 1$ which corresponds to the rightmost root located at $\lambda_0 = -1$, see for instance Kirillov and Overton (2013). By exploiting the delay effect, the following proposition proved in Boussaada et al. (2018) asserts that the solution's decay rate can be further improved by decreasing the corresponding rightmost root. Assume that $a_0 > 1$, then we have:

Theorem 5 (Boussaada et al. 2018) *The following properties hold:*

(i) The multiplicity of any given root of the quasipolynomial (27) *is bounded by* 3.

(ii) The quasipolynomial (27) *admits a real spectral value at* $s_0 = -1 - \frac{1}{\tilde{\tau}}$ *with algebraic multiplicity* 3 *if, and only if,*

$$\tilde{\tau} = \sqrt{\frac{1}{a_0 - 1}} \text{ with } \alpha = -\frac{2\, e^{-(1+\tilde{\tau})}}{\tilde{\tau}^2}. \tag{28}$$

(iii) If equations (28) *are satisfied then* $s = s_0$ *is the rightmost root of* (27).

Remark 9 If equalities (28) are satisfied then the trivial solution of the second-order equation $\ddot{\xi}(t) + 2\dot{\xi}(t) + a_0\,\xi(t) = \alpha\,\xi(t - \tilde{\tau})$ is asymptotically stable with $\xi(t) \approx e^{s_0 t}$.

5 Parametric MID for Second-Order Systems

Second-order linear systems capture the dynamic behavior of many natural phenomena and have found numerous applications in a variety of fields, such as vibration and structural analysis. Stabilization of solutions to such a reduced order model represents a standard test bench to approve new paradigms and methodologies in control design.

The problem we consider in the sequel is the characterization of the admissible multiplicities of spectral values and their effect on stability of the DDE

$$\ddot{\xi}(t) + a_1\dot{\xi}(t) + a_0\xi(t) + \alpha_0\,\xi(t - \tau) + \alpha_1\dot{\xi}(t - \tau) = 0$$

It should be mentioned that such a system depicts several unexpected properties and in particular, for each choice of the coefficients, the delay parameter induces a

stabilizing/destabilizing behavior. In other words, increasing the delay value may be beneficial for the system's dynamics.[21]

>From a control theory viewpoint, the aim is to construct an appropriate delayed-state-feedback controller given by $u(t) = -\alpha_0\,\xi(t-\tau) - \alpha_1\dot{\xi}(t-\tau)$ able to stabilize the following dynamical system:

$$\ddot{\xi}(t) + a_1\dot{\xi}(t) + a_0\xi(t) = u(t). \tag{29}$$

In frequency-domain, the latter generic control problem yields the following characteristic quasipolynomial function:

$$Q(\lambda, \overrightarrow{p}, \tau) = P_0(\lambda) + P_1(\lambda)\, e^{-\tau\lambda} \tag{30}$$

where $P_0(\lambda) = \lambda^2 + a_1\lambda + a_0$ and $P_1(\lambda) = \alpha_1\,\lambda + \alpha_0$.

>From an algebraic geometry viewpoint, it is consistent to set up such a control problem via the discriminant of the characteristic polynomial related to the open-loop (uncontrolled) equation. Namely, the complex/real nature of the roots of the polynomial $P_0(\lambda)$ has a strong effect on the characterization of the controller's gains and delay enabling a desired fast stabilization using the MID property. In the sequel, it shall be emphasized that the *discriminant* of P_0 ($\Delta = a_1^2 - 4a_0$) defines an efficient and necessary criterion to exhibit the potential applicability and the limitations of the MID methodology, and our analysis splits following the sign of the discriminant Δ. The following results were presented in Boussaada et al. (2020).

5.1 Open-Loop Systems with One Oscillating Mode

One oscillating mode as solution of the uncontrolled equation (two conjugate complex roots) corresponds, from a purely algebraic viewpoint, to a characteristic polynomial with a strictly negative discriminant Δ. In such a case, the following theorem gives a bound for quasipolynomial root's multiplicity and provides the explicit MID-based controller's gains and delay.

Theorem 6 *Consider the quasipolynomial* (30)*. Then, the following assertions hold:*

(i) the multiplicity of any given root of the quasipolynomial (30) *is bounded by* 4*, and this can only be achieved on the real axis and under negativity of* Δ*.*

(ii) the quasipolynomial (30) *admits a real spectral value at* $\lambda = \lambda_0$ *with algebraic multiplicity* 4 *if, and only if,*

$$\lambda_0 = -\frac{a_1 + \sqrt{-2\,\Delta}}{2},$$

[21] Such a property does not hold for scalar systems with one delay, for which increasing the delay leads to instability, see for instance Walton and Marshall (1987), Niculescu et al. (2010).

and the system's parameters satisfy

$$\tau = 2\sqrt{-\frac{2}{\Delta}},\ \alpha_0 = \frac{\left(5\,\Delta - a_1\sqrt{-2\,\Delta}\right)}{4}\,e^{s_0\tau},\ \alpha_1 = -\frac{\sqrt{-2\,\Delta}}{2}\,e^{s_0\,\tau}. \quad (31)$$

(iii) if (31) *is satisfied, then* $\lambda = \lambda_0$ *is the spectral abscissa corresponding to* (30).
(iv) if (31) *is satisfied then the trivial solution of the closed-loop system* (29) *is asymptotically stable if, and only if, either* $\left(a_1 \geq 0 \text{ and } a_0 > \frac{a_1^2}{4}\right)$ *or* $\left(a_1 < 0 \text{ and } a_0 > \frac{3\,a_1^2}{8}\right)$.

5.2 Open-Loop Systems with Non Oscillating Modes

Consider now the case where the uncontrolled equation admits two real spectral values. As expected, under such a configuration, the MID based-design cannot be applied by exploiting the maximal multiplicity which is equal to 4, see Theorem 6. The following theorem gives a bound for the quasipolynomial roots' multiplicity in the case when $\Delta \geq 0$. In addition, it explicitly provides the MID-based controller's gains and delay by exploiting a lower multiplicity.

Theorem 7 *Consider the quasipolynomial* (30). *Then the following assertions hold:*

(i) if the discriminant $\Delta \geq 0$, *then the multiplicity of any given root of the quasipolynomial* (30) *is bounded by* 3.
(ii) for an arbitrary positive delay τ, *the quasipolynomial* (30) *admits a real spectral value at* $\lambda = \lambda_\pm$ *with algebraic multiplicity* 3 *if, and only if,*

$$\lambda_\pm = \frac{-\tau\,a_1 - 4 \pm \sqrt{8 + \tau^2\Delta}}{2\,\tau},$$

and the system parameters satisfy:

$$\begin{cases} \alpha_0 = \left(a_1\lambda_\pm + \dfrac{{a_1}^2}{2} - \dfrac{\Delta}{2} + \dfrac{6\,a_1 + 10\,\lambda_\pm}{\tau} + \dfrac{6}{\tau^2}\right) e^{\lambda_\pm\tau}, \\ 1 = \left(2\,\lambda_0 + a_1 + \dfrac{2}{\tau}\right) e^{\lambda_\pm\tau}. \end{cases}$$

(iii) if $(\star_+)$ *(respectively* $(\star_-)$*) is satisfied, then* $\lambda = \lambda_+$ *is the spectral abscissa corresponding to* (30) *(respectively* λ_- *cannot be the spectral abscissa corresponding to* (30)*). Furthermore, for an arbitrary delay* τ *the multiple spectral value at* λ_- *is always dominated by a single real root* λ_0.
(iv) if $(\star_+)$ *is satisfied then the trivial solution is asymptotically stable if, and only if,* τ *satisfies the following conditions*

$$\begin{cases} \tau \in (0, \tau_-) \ \ when \ \ a_0 < 0, \\ or \\ \in (0, \tau_-) \cup (\tau_+, \infty) \ \ when \ \ a_0 > 0 \ and \ a_1 < 0, \end{cases}$$

where $\tau_\pm = \frac{-a_1 \pm \sqrt{\Delta + 2a_0}}{a_0}$.

Remark 10 The second and third assertions of Theorem 7 hold also for negative discriminant $-\frac{8}{\tau^2} < \Delta < 0$. Moreover, when $\Delta = -\frac{8}{\tau^2}$ the triple root at $\lambda_\pm$ becomes the quadruple root prescribed in Theorem 6.

6 The Generic MID Property

Some works have shown that, for some classes of dynamical systems represented by DDEs of retarded type, a real root of maximal multiplicity is necessarily the rightmost root. Such a property is called *Generic MID*, or GMID for short. This link between maximal multiplicity and dominance has been suggested in Pinney (1958) after the study of some simple, low-order cases, but without any attempt to address the general case. Recently, a more general result on the GMID property from Mazanti et al. (2021a) for generic retarded DDEs of order n with delayed (polynomial) "term" of order $n-1$, which relies on links between quasipolynomials with a real root of maximal multiplicity and the *Kummer's confluent hypergeometric function* in terms of the location of the characteristic roots. The GMID property was also extended to neutral DDEs of orders 1 and 2 in Ma et al. (2020); Benarab et al. (2020); Mazanti et al. (2021b), as well as to the case of complex conjugate roots of maximal multiplicity in Mazanti et al. (2020).

6.1 Degenerate Hypergeometric Functions

Let $a, b \in \mathbb{C}$ and assume that b is not a nonpositive integer. The *Kummer's confluent hypergeometric function* $M(a, b, \cdot) : \mathbb{C} \to \mathbb{C}$ is the entire function defined for $\lambda \in \mathbb{C}$ by the series

$$M(a, b, \lambda) = \sum_{k=0}^{\infty} \frac{(a)_k}{(b)_k} \frac{\lambda^k}{k!}. \tag{32}$$

Furthermore, the series in (32) converges for every $\lambda \in \mathbb{C}$. As presented in Buchholz (1969); Erdélyi et al. (1981); Olver et al. (2010), the function $M(a, b, \cdot)$ satisfies *Kummer's differential equation*

$$\lambda \frac{\partial^2 M}{\partial \lambda^2}(a, b, \lambda) + (b - \lambda)\frac{\partial M}{\partial \lambda}(a, b, \lambda) - aM(a, b, \lambda) = 0. \tag{33}$$

Other solutions of (33) are usually also called Kummer's confluent hypergeometric functions, but they are not used in this chapter. Note that the Kummer's confluent hypergeometric function M admits an integral representation, which can be found, for instance, in Buchholz (1969); Erdélyi et al. (1981); Olver et al. (2010). Namely, let $a, b \in \mathbb{C}$ and assume that $\Re(b) > \Re(a) > 0$. Then

$$M(a, b, \lambda) = \frac{\Gamma(b)}{\Gamma(a)\Gamma(b-a)} \int_0^1 e^{\lambda t} t^{a-1}(1-t)^{b-a-1}\, \mathrm{d}t,$$

where Γ denotes the Gamma function.

The main result on confluent hypergeometric functions used in Mazanti et al. (2021a) to prove the GMID property is the following one on the location of the roots of some particular functions. It was proved in Wynn (1973) by using a continued fraction expansion of the ratio of two such functions.

Proposition 4 *Let $a \in \mathbb{R}$ be such that $a > -\frac{1}{2}$.*

1. *If $\lambda \in \mathbb{C}$ is such that $M(a, 2a+1, \lambda) = 0$, then $\Re(\lambda) > 0$.*
2. *If $\lambda \in \mathbb{C}$ is such that $M(a+1, 2a+1, \lambda) = 0$, then $\Re(\lambda) < 0$.*

6.2 Spectral Values of Maximal Multiplicity are Dominant

Consider the quasipolynomial function $Q : \mathbb{C} \to \mathbb{C}$ defined for $\lambda \in \mathbb{C}$ by

$$Q(\lambda, \tau) = \lambda^n + \sum_{k=0}^{n-1} a_k \lambda^k + e^{-\lambda\tau} \sum_{k=0}^{n-1} \alpha_k \lambda^k. \tag{34}$$

The following result proved in Mazanti et al. (2021a) is the following characterization of real roots of maximal multiplicity of Q, their dominance and the corresponding consequences for the stability of the trivial solution of

$$y^{(n)}(t) + \sum_{k=0}^{n-1} a_k y^{(k)}(t) + \sum_{k=0}^{n-1} \alpha_k y^{(k)}(t-\tau) = 0, \tag{35}$$

Theorem 8 (Mazanti et al. 2021a) *Consider (34) and let $\lambda_0 \in \mathbb{R}$.*

1. *The number λ_0 is a root of multiplicity $2n$ of Q if and only if, for every $k = 0, \ldots, N-1$,*

$$\begin{cases} a_k = \binom{n}{k}(-\lambda_0)^{n-k} + (-1)^{n-k} n! \sum_{j=k}^{n-1} \binom{j}{k} \binom{2n-j-1}{n-1} \frac{\lambda_0^{j-k}}{j!\tau^{n-j}}, \\ \quad = (-1)^{n-1} e^{\lambda_0 \tau} \sum_{j=k}^{n-1} \frac{(-1)^{j-k}(2n-j-1)!}{k!(j-k)!(n-j-1)!} \frac{\lambda_0^{j-k}}{\tau^{n-j}}. \end{cases} \tag{36}$$

2. *If* (36) *is satisfied, then* λ_0 *is a strictly dominant root of* Q.
3. *If* (36) *is satisfied, then the trivial solution of* (35) *is exponentially stable if and only if* $a_{n-1} > -\frac{n^2}{\tau}$.

7 Software: Partial Pole Placement via Delay Action

Based on the recent results by the authors on the MID property for DDEs, a Python software for the parametric design of stabilizing feedback laws with time-delays, called "Partial Pole Placement via Delay Action" (P3δ[22] for short), has been developed. P3δ also implements other features, which are detailed in Boussaada et al. (2022). In the sequel, we revisit the problem of damping solutions of the standard oscillator by using a delayed feedback, and the proposed results are illustrated by using P3δ:

$$\ddot{\zeta}(t) + 2\,\xi\,\omega_0\,\dot{\zeta}(t) + \omega_0^2\,\zeta(t) = c(t)$$

where $\omega_0 > 0$ and $0 < \xi < 1$ stand respectively for the oscillator natural frequency and the damping factor. Consider now the controller c as a *proportional-derivative* delayed-controller:

$$c(t) = -b_0\,\zeta(t-\tau) - b_1\,\dot{\zeta}(t-\tau).$$

Thus, the closed-loop characteristic function is given by:

$$Q(\lambda, \overrightarrow{p}, \tau) = \lambda^2 + 2\,\xi\,\omega_0\,\lambda + {\omega_0}^2 + (b_0 + b_1\,\lambda)\,\mathrm{e}^{-\tau\,\lambda}.$$

Assume the natural frequency $\omega_0 = 1$ and the damping factor $\xi = 1/2$, which corresponds to an open-loop plant with a complex-conjugate pair $\lambda_{OL}^{\pm} = -1/2 \pm \mathrm{i}\sqrt{3}/2$. Then, the closed-loop plant corresponds to the following characteristic quasipolynomial

$$Q(\lambda, \overrightarrow{p}, \tau) = \lambda^2 + \lambda + 1 + (b_0 + b_1\,\lambda)\,\mathrm{e}^{-\tau\,\lambda}. \tag{37}$$

Forcing the existence of a triple spectral value suggests that

$$\lambda_{CL}^{\pm} = -1/2 - 2\,\tau^{-1} \pm 1/2\,\tau^{-1}\sqrt{-3\,\tau^2 + 8} \tag{38}$$

[22] The software is freely available for download on https://cutt.ly/p3delta, where installation instructions, video demonstrations, and the user guide are also available.

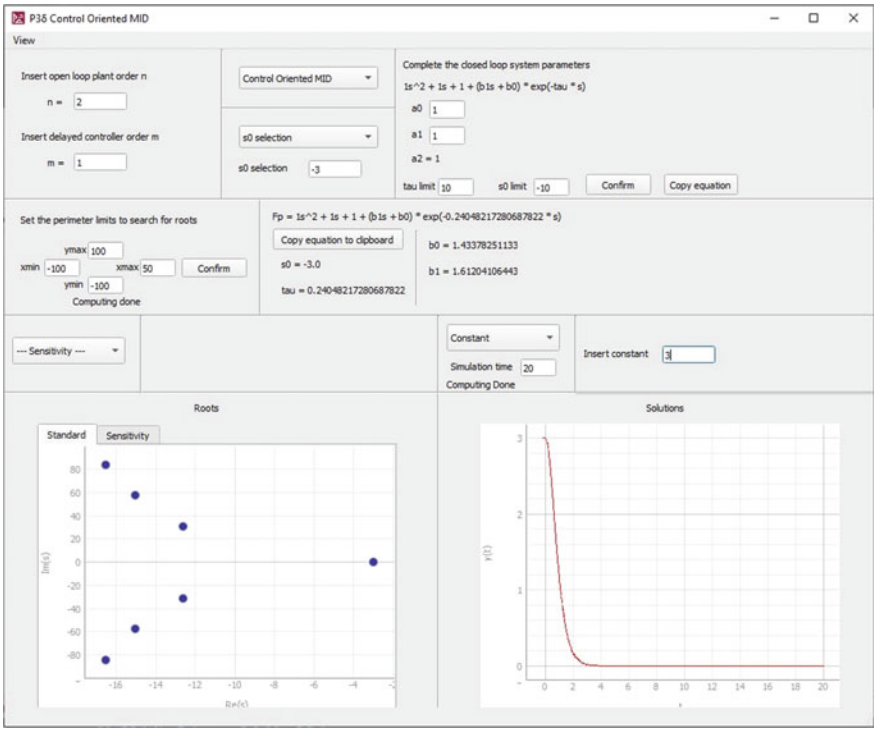

Fig. 5 P3δ interface exhibiting the design of a stabilizing delayed PD controller in the case of the characteristic function (37). (Left) Illustration of the roots location in the case $\tau = \tau^* \approx 0.24$ which by using (38) corresponds to $\lambda_{CL}^{+} = -3$. (Right) Closed-loop response corresponding to the history function $\varphi(t) = 3$ for all $t \in [-\tau^*, 0]$

are the only admissible roots. As a matter of fact, those triple spectral values are defined if, and only if, the controller's gains are such that:

$$\begin{aligned} b_0 &= \frac{\left(6 + \left(2 + \lambda_{CL}^{\pm}\right)\tau^2 + \left(10\,\lambda_{CL}^{\pm} + 6\right)\tau\right) \mathrm{e}^{\lambda_{CL}^{\pm}\tau}}{\tau^2}, \\ b_1 &= \frac{\mathrm{e}^{\lambda_{CL}^{\pm}\tau}\left(2\,\lambda_{CL}^{\pm}\tau + \tau + 2\right)}{\tau}. \end{aligned} \tag{39}$$

It follows that if (39) is satisfied and the triple root at λ_{CL}^{+} is selected then the spectral abscissa corresponds to λ_{CL}^{+} as illustrated in Fig. 5.

Notice that the assignment of the triple root $\lambda = \lambda_{CL}^{+}$ is possible only in the admissibility region $\lambda \in (-\infty,\ \lambda_M]$ which corresponds necessarily to $\tau \in (0, \tau_M]$ where $\tau_M = 2/3\sqrt{6}$ and $\lambda_M = -1/2\,(1 + \sqrt{3})$, see for instance Boussaada et al. (2020). This fact is illustrated in Fig. 6.

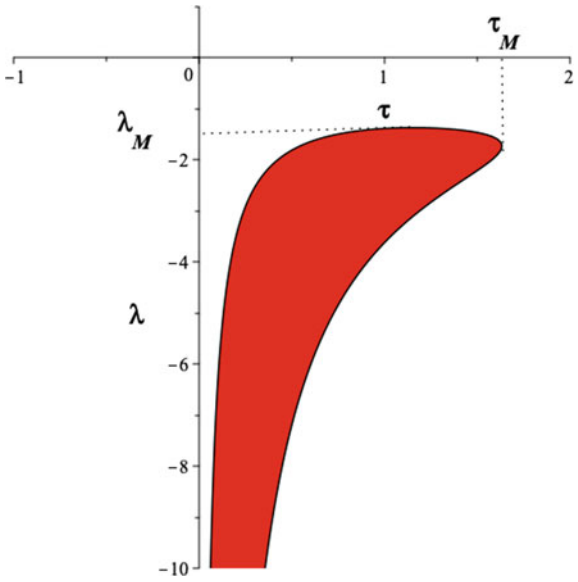

Fig. 6 MID stabilizability region defined by $(-\infty,\ \lambda_M]$, in which the assignment of a triple negative dominant root of (37) is possible, where in such a case λ_M corresponds to the lowest (in absolute value) assignable decay rate

8 Active Vibration Control in a Mechanical Flexible Structure

The problem of active vibration damping of thin mechanical structures is a topic that has received a great attention by the control community since several years (see, for instance, Tliba 2011 and the references therein), especially when actuators and sensors are based on piezoelectric materials. For deformable mechanical structures, piezoelectric materials are used as strain sensors or strain actuators. Many works have concerned the vibration control problem of the "*Euler-Bernoulli beam*" equipped with one rectangular piezoelectric actuator and sometime, another one, identical and collocated, but used as sensor. See for example Chen et al. (2004); Banks et al. (2002) where one edge of the beam is clamped whereas the other remains free. Other works dealt with the problem of vibration control for laminated rectangular plates Kögl and Bucalem (2005) or complex plate like structures Tliba et al. (2005).

8.1 Modeling of the Vibrating Beam

Consider now the flexible structure depicted in Fig. 7. It is an aluminium-based beam, embedded in a mobile support. The mobile support is subjected to an acceleration,

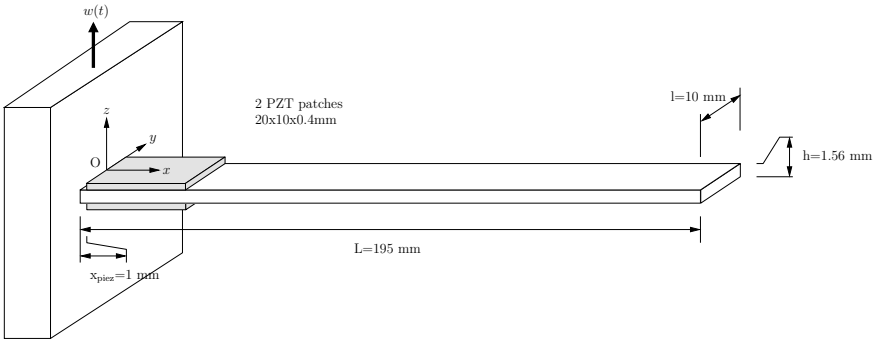

Fig. 7 Sketch of the piezo-actuated flexible beam, clamped at one edge. The figure is taken from Boussaada et al. (2017)

denoted by w in the sequel, and it is moving along the z axis. This flexible beam is equipped with two piezoelectric patches made with *lead zirconate titanate (also called PZT)*. One of them is used as an actuator and the other works as a sensor. These patches are supposed to be rigidly bounded on the beam, one on each side, located at the clamped edge. The whole device is called thereafter as a *piezo-actuated beam*. It can be deformed by the application of a voltage, denoted by u, across the actuator. The sensor delivers an electrical voltage which corresponds to a measure, denoted by y, of the local deformation under the piezoelectric patch.

Very often, this equipped mechanical structure is partly described by the in-plane Euler-Bernoulli Partial Differential Equation (PDE) that suffers from the lack of precision in describing the electro-mechanical interactions between the passive structure and the piezoelectric components. Indeed, these latter are often withdrawn in the computation of the eigenfrequencies (Tliba, 2004) of the whole structure. Nevertheless, such a structure obeys to fundamental equations of continuum mechanics in 3D space (Gérardin and Rixen, 1997), involving computations of gradient of displacement vector and divergence operator applied to strength tensor. When completed with Neumann and Dirichlet boundary conditions, the fundamental equations give several PDEs that are coupled, thus hardly or impossible to solve analytically. Then, for controller design purposes, one naturally turns toward numerical methods in order to get the input-to-output dynamical models (Komzsik, 2005).

Using Finite Element Modeling (FEM), one obtains the LTI system described by the following ordinary differential equations:

$$\mathbb{M}_{qq}\ddot{q}(t) + \mathbb{D}_{qq}\dot{q}(t) + \mathbb{K}_{qq}q(t) = \mathbb{M}_{qw}w(t) - \mathbb{K}_{qu}u(t) \tag{40}$$

$$y(t) = \mathbb{K}_{qy}q(t) \tag{41}$$

$$z(t) = \mathbb{F}_{zw}w(t) - \mathbb{F}_{zu}u(t) - \mathbb{F}_{zq}q(t) - \mathbb{F}_{zv}\dot{q}(t) \tag{42}$$

where $w(t) \in \mathbb{R}$ is the absolute acceleration (m/s^2) of the movable support along axis z, $z(t) \in \mathbb{R}$ is the relative acceleration (m/s^2) of the free end, derived from the

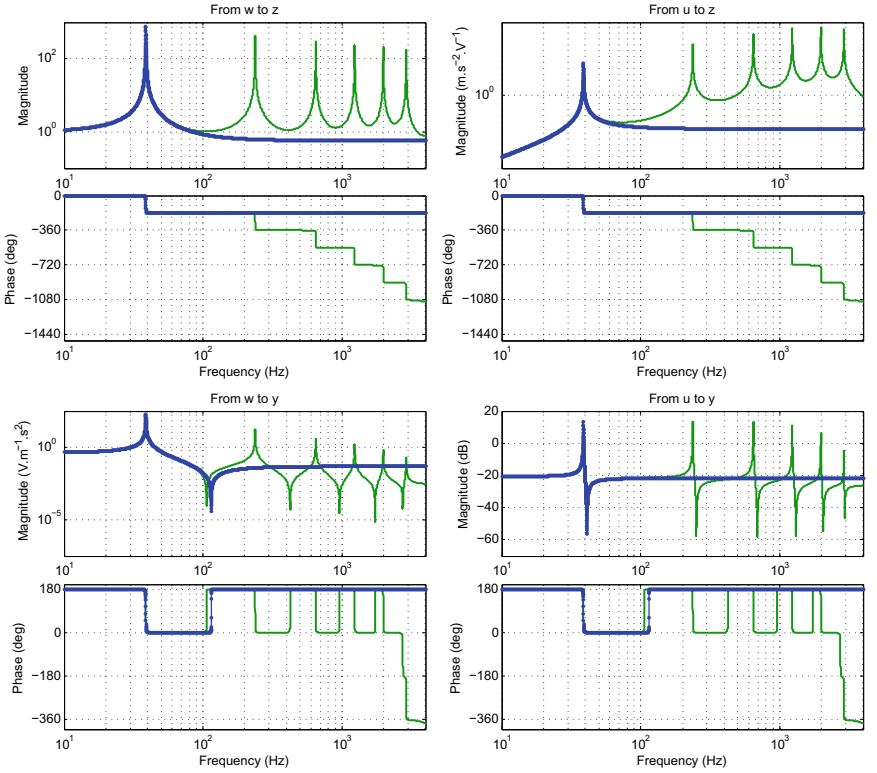

Fig. 8 Frequency responses of the analysis (-) and reduced order (.-) models. The figure is borrowed from Boussaada et al. (2017)

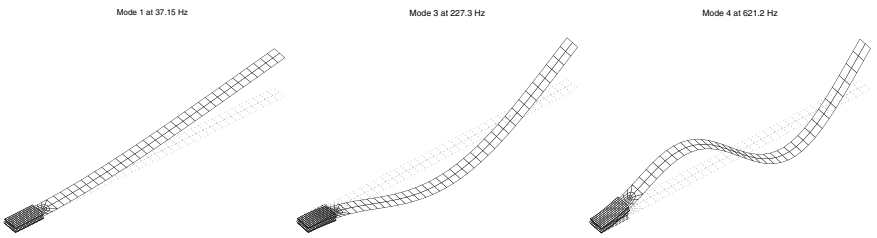

Fig. 9 First three controllable and observable modes. The figure is borrowed from Boussaada et al. (2017)

equations of motion, $u(t) \in \mathbb{R}$ is the piezoelectric voltage (V) across the actuator (control signal), $y(t) \in \mathbb{R}$ is the piezoelectric sensor voltage (V) across the sensor (measured output signal $y(t)$). Moreover, the terms $\mathbb{M}_{qq}$, $\mathbb{D}_{qq}$, $\mathbb{M}_{qw}$, $\mathbb{K}_{qq}$, $\mathbb{K}_{qu}$, $\mathbb{K}_{qy}$, $\mathbb{F}_{zw}$, $\mathbb{F}_{zu}$, $\mathbb{F}_{zq}$ and $\mathbb{F}_{zv}$ are all matrices derived from the assembly step of the FEM such that the obtained approximation is with several thousands degrees of freedom.

After producing a FEM, a modal analysis is performed to the undamped motion Eq. (40). It consists in finding the eigenstructure of $\mathbb{M}_{qq}\ddot{q}(t) + \mathbb{K}_{qq}q(t) = 0$, and using the eigenvalues and eigenvectors as a new basis allowing the description of (40)–(42) into a new system of ODEs, still linear but decoupled, involving a new state vector, called vector of modes. The advantage of this form is that it allows to build a model in state-space form devoted to analysis, (43) below, having its order sufficiently small to describe the dynamical behavior within a low-frequency bandwidth. Furthermore, a reduced-order system, devoted to the controller synthesis step, is also available and differs from the analysis one by the presence of direct feedthrough terms between the outputs $\{z, y\}$ and the inputs $\{w, u\}$. Further details can be found in Boussaada et al. (2018). The frequency responses for the analysis and the reduced-order models are shown in Fig. 8 and the shapes of the first three bending modes in Fig. 9.

$$\left\{\begin{array}{rcl} \dot{x}_p(t) &=& A_p x_p(t) \;+\; B_{p,w} w(t) \;+\; B_{p,u} u(t) \\ z(t) &=& C_{p,z} x_p(t) \;(+\; D_{p,zw} w(t) \;+\; D_{p,zu} u(t)\big) \\ y(t) &=& C_{p,y} x_p(t) \;(+\; D_{p,yw} w(t) \;+\; D_{p,yu} u(t)\big) \end{array}\right. \tag{43}$$

It is worth mentioning that the piezo-actuated beam is a SISO LTI system. In the sequel, we shall use the transfer function based model, derived from (43) by applying to it Laplace transform, given by

$$\left\{\begin{array}{l} z(\lambda) \;\; = \dfrac{N_{wz}(\lambda)}{\psi(\lambda)} w(\lambda) + \dfrac{N_{uz}(\lambda)}{\psi(\lambda)} u(\lambda) \\ y(\lambda) = \dfrac{N_{wy}(\lambda)}{\psi(\lambda)} w(\lambda) + \dfrac{N_{uy}(\lambda)}{\psi(\lambda)} u(\lambda), \end{array}\right.$$

where λ denotes the Laplace variable. By considering the first vibration mode, one gets the following numerical data for the reduced order model

$$\begin{aligned} N_{wz}(\lambda) &= -1.572\,\lambda^2 - 0.767\,\lambda + 0.114, \\ N_{uz}(\lambda) &= 0.040\,\lambda^2 + 0.019\,\lambda - 0.002, \\ N_{wy}(\lambda) &= -0.047\,\lambda^2 - 0.023\,\lambda - 24664.720, \\ \psi(\lambda) &= \lambda^2 + 0.487\,\lambda + 59495.866, \\ N_{uy}(\lambda) &= 0.082\,\lambda^2 + 0.040\,\lambda + 5472.410. \end{aligned}$$

An interesting control objective would be to damp the peak of resonance of the first bending mode, by using an *output feedback controller*, without affecting the vibrating modes that were neglected in the reduced order model. The result presented in the next section as well as its proof can be found in Boussaada et al. (2017), see also Boussaada et al. (2018).

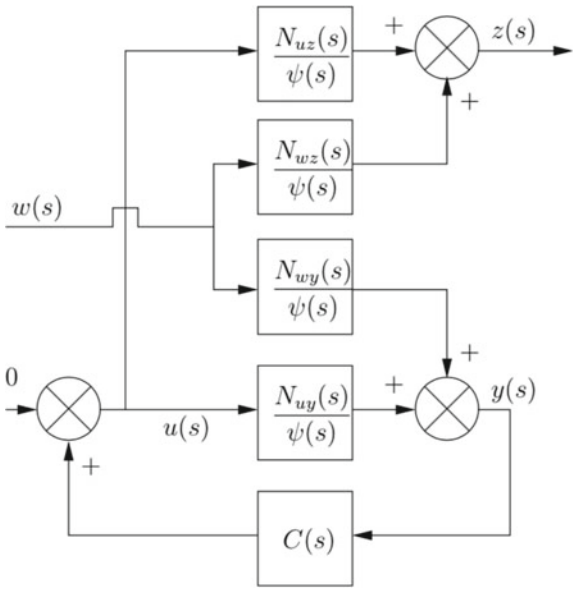

Fig. 10 Feedback control structure. The figure is borrowed from Boussaada et al. (2017)

8.2 Vibration Damping

Consider now the piezo-actuated system inserted in the typical output feedback control structure of Fig. 10, with a zero-reference signal and an input disturbance w corresponding to a rectangular impulse signal. The control problem consists in damping the vibrations due to the first mode when the mobile support is subjected to a shock-like disturbance. We define the output feedback control law $u(\lambda) = C(\lambda, \overrightarrow{p}, \tau)\, y(\lambda)$ involving the following reduced-complexity controller given in Laplace domain by

$$C(\lambda, \overrightarrow{p}, \tau) = \frac{N(\lambda, \overrightarrow{p}, \tau)}{D(\lambda, \overrightarrow{p}, \tau)} \tag{44}$$

where $N(\lambda, \overrightarrow{p}, \tau) = n_0 + n_{r_0} e^{-\tau\lambda}$ and $D(\lambda, \overrightarrow{p}, \tau) = d_0 + d_{r_0} e^{-\tau\lambda}$ and $\mathbf{p} = (n_0, n_{r0}, d_0, d_{r0})$. By applying the inverse Laplace transform, it can be easily shown that this control law writes in time-domain as:

$$u(t) = -\frac{d_{r_0}}{d_0} u(t-\tau) + \frac{n_0}{d_0} y(t) - \frac{n_{r_0}}{d_0} y(t-\tau),$$

which is an output feedback control law based on proportional actions plus delayed proportional actions. For the sake of clarity, by omitting the variable λ in the polynomials, the closed loop relation between the disturbance w and the controlled output z is given by:

$$z(\lambda) = \frac{N_{wz}\,\psi\,D + \left(N_{uz}\,N_{wy} - N_{wz}\,N_{uy}\right)\,N}{\psi\left(\psi\,D - N_{uy}\,N\right)}w(\lambda). \tag{45}$$

It can be proven that ψ divide the polynomial $\left(N_{uz}\,N_{wy} - N_{wz}\,N_{uy}\right)$ so that it can be removed from the numerator and the denominator. In this last case, let $R(\lambda)$ be the polynomial satisfying $N_{uz}(\lambda)\,N_{wy}(\lambda) - N_{wz}(\lambda)\,N_{uy}(\lambda) = R(\lambda)\,\psi(\lambda)$. Then (45) becomes

$$z(\lambda) = \frac{N_{wz}\,D + R\,N}{\psi\,D - N_{uy}\,N}w(\lambda).$$

Consider now the characteristic function

$$Q(\lambda, \overrightarrow{p}, \tau) = \psi(\lambda)\,D(\lambda, \overrightarrow{p}, \tau) - N_{uy}(\lambda)\,N(\lambda, \overrightarrow{p}, \tau).$$

By applying the MID property and the ensuing procedure, one can assign λ_0 as a rightmost root of multiplicity equal to 3 such that $\lambda_0 \simeq -192.359$. Notice that in such a case the numerical values for the parameters of the controller in (44) are given by:

$$n_0 \simeq 39.793,\ n_{r_0} \simeq 48.034,\ d_0 \simeq 4.281,\ d_{r_0} \simeq 3.961,\ \tau \simeq 0.005.$$

Notice that such a choice for the controller's gains guarantees that the closed-loop characteristic equation is of retarded type. To show the efficiency of the proposed reduced-complexity controller, we propose to compare, in Fig. 11, the time responses

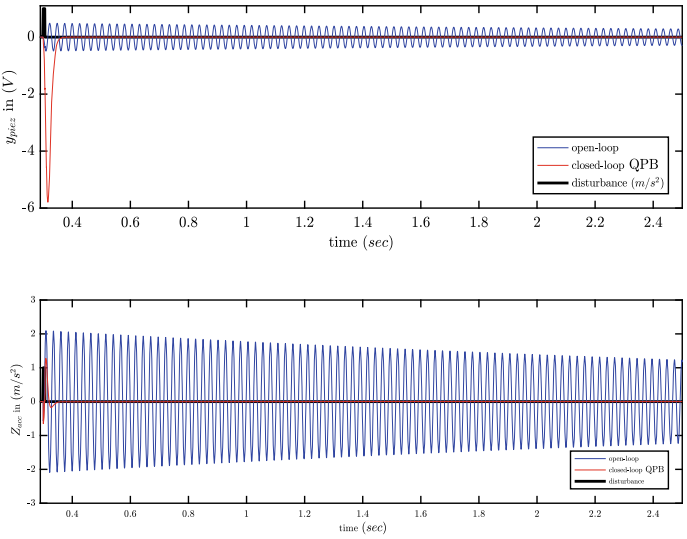

Fig. 11 Time responses of the measured output y (Top) and of the controlled output z (Bottom)

of both output signals in open-loop (blue) and in closed-loop (red) when the disturbance w is a rectangular impulse (black), say like a shock. We also put the time response of the control signal u that exhibits a peak of magnitude roughly equal to $-60\ V$ which is reasonable for this application.

9 Notes and Comments

In studying the exponential stability of the trivial solution of linear DDEs of retarded type, this chapter addressed several frequency-domain techniques to count the roots of the corresponding characteristic functions in the complex right half-plane with a particular emphasis on the MID property and its potential application in control engineering. Illustrative examples and one application in vibration control show the effectiveness of the method. The main results of this chapter have been reported in Boussaada and Niculescu (2016a) (characterizing the codimension of the zero singularity) Mazanti et al. (2021a) (characterizing the generic MID characterization for DDEs of retarded type with a single delay) and Boussaada et al. (2017) (application in vibration control). It should be noted that a guided tour of existing methods to analyze multiple characteristic roots (including the MID property mentioned in this chapter) can be found in Niculescu et al. (2021).

Acknowledgements This work is supported by a public grant overseen by the French National Research Agency (ANR) as part of the "Investissement d'Avenir" program, through the iCODE project funded by the IDEX Paris-Saclay, ANR-11-IDEX-0003-02. The authors warmly thank their collaborators Tamas Insperger (BME, Budapest), Guilherme Mazanti (L2S, University Paris-Saclay) and Sami Tliba (L2S, University Paris-Saclay).

References

Ahlfors, L. V. (1979). *Complex analysis*. McGraw-Hill, Inc.

Balogh, T., Boussaada, I., Insperger, T., & Niculescu, S. -I. (2022). Conditions for stabilizability of time-delay systems with real-rooted plant. *The International Journal of Robust and Nonlinear Control,* (to appear).

Banks, H. T., del Rosario, R. C. H., & Tran, H. T. (2002). Proper orthogonal decomposition-based control of transverse beam vibrations: Experimental implementation. *IEEE Transactions on Control Systems Technology, 10*(5), 717–726.

Barker, L. K. (1979). Mikhailov stability criterion for time-delayed systems. Technical Memorandum TM-78803, NASA, Washington D.C., USA.

Bellman, R., & Cooke, K. (1963). *Differential-difference equations*. New York: Academic Press.

Benarab, A., Boussaada, I., Trabelsi, K., Mazanti, G., & Bonnet, C. (2020). The MID property for a second-order neutral time-delay differential equation. In *Proceedings of the 24th International Conference on System Theory, Control and Computing*, pp. 202–207.

Bini, D. A., & Boito, P. (2010). A fast algorithm for approximate polynomial GCD based on structured matrix computations. In D. A. Bini et al., (Ed.), *Numerical methods for structured matrices and applications* (Vol. 199, pp. 155–173) OT. Birkhäuser Basel.

Boese, F. G. (1998). Stability with respect to the delay: On a paper of K. L. Cooke and P. van den Driessche. *Journal of Mathematical Analysis and Applications,228*(2), 293–321.

Boussaada, I., & Niculescu, S. -I. (2014). Computing the codimension of the singularity at the origin for delay systems: The missing link with Birkhoff incidence matrices. *Proceedings of the 21st International Symposium on Mathematical Theory of Networks and Systems*, pp. 1–8.

Boussaada, I., & Niculescu, S.-I. (2016a). Characterizing the codimension of zero singularities for time-delay systems. *Acta Applicandae Mathematicae, 145*(1), 47–88.

Boussaada, I., & Niculescu, S. I. (2016b). Tracking the algebraic multiplicity of crossing imaginary roots for generic quasipolynomials: A Vandermonde-based approach. *IEEE Transactions on Automatic Control, 61,* 1601–1606.

Boussaada, I., & Niculescu, S.-I. (2018). On the dominancy of multiple spectral values for time-delay systems with applications. *IFAC-PapersOnLine, 51*(14), 55–60.

Boussaada, I., Mazanti, G., Niculescu, S. I., Huynh, J., Sim, F., & Thomas, M. (2022). Partial pole placement via delay action: A Python software for delayed feedback stabilizing design.

Boussaada, I., Irofti, D. A., & Niculescu, S. I. (2014). Computing the codimension of the singularity at the origin for time-delay systems in the regular case: A Vandermonde-based approach. In *Proceedings of the 13th European Control Conference*, pp. 1–6.

Boussaada, I., Unal, H. U., & Niculescu, S. I. (2016). Multiplicity and stable varieties of time-delay systems: A missing link. In *Proceedings of the 22nd International Symposium on Mathematical Theory of Networks and Systems*, pp. 1–6.

Boussaada, I., Niculescu, S.-I., Tliba, S., & Vyhlídal, T. (2017). On the coalescence of spectral values and its effect on the stability of time-delay systems: Application to active vibration control. *Procedia IUTAM, 22,* 75–82.

Boussaada, I., Tliba, S., Niculescu, S. I., Ünal, H. U., & Vyhlídal, T. (2018). Further remarks on the effect of multiple spectral values on the dynamics of time-delay systems: Application to the control of a mechanical system. *Linear Algebra Application, 542*, 589–604.

Boussaada, I., Niculescu, S. I., El-Ati, A., Pérez-Ramos, R., & Trabelsi, K. (2020). Multiplicity-induced-dominancy in parametric second-order delay differential equations: Analysis and application in control design. *ESAIM: COCV, 26*, 57.

Boussaada, I., Mazanti, G., & Niculescu, S. I. (2022). The generic multiplicity-induced-dominancy property from retarded to neutral delay-differential equations: When delay-systems characteristics meet the zeros of Kummer functions. *Comptes Rendus de Mathématique*. https://hal.archives-ouvertes.fr/hal-03298718.

Buchholz, H. (1969). *The confluent hypergeometric function with special emphasis on its applications*. Translated from the German by H. Lichtblau and K. Wetzel. Springer Tracts in Natural Philosophy (Vol. 15). Springer New York Inc., New York.

Chen, C. F., & Tsay, Y. T. (1976). A general frequency stability criterion for multi-input-output, lumped and distributed-parameter systems. *International Journal of Control, 23*(3), 341–359.

Chen, W., Buehler, M., Parker, G., & Bettig, B. (2004). Optimal sensor design and control of piezoelectric laminate beams. *IEEE Transactions on Control Systems Technology, 12*(1), 148–155.

Cooke, K. L. (1979). Stability analysis for a vector disease model. *Rocky Mountain Journal of Mathematics, 9,* 31–42.

El'sgol'ts, L. E., & Norkin, S. B. (1973). *Introduction to the theory and application of differential equations with deviating arguments*. Academic Press.

Erdélyi, A., Magnus, W., Oberhettinger, F., & Tricomi, F. (1981). *Higher transcendental functions* (Vol. I). Melbourne, USA: Robert E. Krieger Publishing Co.

Evans, W. E. (1950). Control system synthesis by root locus method. *AIEE Transactions, 69,* 66–69.

Gérardin, M., & Rixen, D. (1997). *Mechanical vibrations: Theory and application to structural dynamics* (2nd ed.). Wiley.

Ha, T. T., & Gibson, J. A. (1980). A note on the determinant of a functional confluent Vandermonde matrix and controllability. *Linear Algebra and its Applications, 30,* 69–75.

Hassard, B. D. (1997). Counting roots of the characteristic equation for linear delay-differential systems. *Journal of Differential Equations, 136*(2), 222–235.

Hayes, N. D. (1950). Roots of the transcendental equation associated with a certain difference-differential equation. *The Journal of the London Mathematical Society, s1–25*(3), 226–232.

Kharitonov, V. L., Niculescu, S.-I., Moreno, J., & Michiels, W. (2005). Static output feedback stabilization: Necessary conditions for multiple delay controllers. *IEEE Transactions on Automatic Control, 50*(1), 82–86.

Kirillov, O., & Overton, M. (2013). Robust stability at the swallowtail singularity. *Frontiers in Physics, 1,* 24.

Komzsik, L. (2005). *What every engineer should know about computational techniques of finite element analysis*. Taylor & Francis Group, NW, FL: CRC Press.

Krall, A. M. (1968). *Stability techniques for continuous linear systems*. New York: Gordon and Breach.

Kögl, M., & Bucalem, M. L. (2005). Analysis of smart laminates using piezoelectric MITC plate and shell elements. *Computers & Structures, 83,* 1153–1163.

Ma, D., Boussaada, I., Bonnet, C., Niculescu, S. I., & Chen, J. (2020). Multiplicity-Induced-Dominancy extended to neutral delay equations: Towards a systematic PID tuning based on Rightmost root assignment. In *Proceedings of the 2020 American Control Conference*, Denver, USA.

MacFarlane, A. F. G. (1979). *Frequency-response methods in control systems*. New York: IEEE Press.

Marden, M. (1949). *Geometry of polynomials*. AMS: Providence.

Mazanti, G., Boussaada, I., Niculescu, S. I., & Vyhlídal, T. (2020). Spectral dominance of complex roots for single-delay linear equations. In *Proceedings of the 21st IFAC World Congress*, IFAC-PapersOnLine, Berlin, Germany.

Mazanti, G., Boussaada, I., & Niculescu, S. -I. (2021a). Multiplicity-induced-dominancy for delay-differential equations of retarded type. *The Journal of Differential Equations,286*, 84–118.

Mazanti, G., Boussaada, I., Niculescu, S. I., & Chitour, Y. (2021b) Effects of roots of maximal multiplicity on the stability of some classes of delay differential-algebraic systems: The lossless propagation case. In *Proceedings of the 24th International Symposium on Mathematical Theory of Networks and Systems (MTNS 2021)* (Vol. 54. pp. 764–769). IFAC-PapersOnLine. Cambridge, UK.

Michiels, W., & Niculescu, S. -I. (2007). *Stability and stabilization of time-delay systems* (Vol. 12) Advances in design and control. SIAM.

Mori, T., & Kokame, H. (1989). Stability of $\dot{x}(t) = Ax(t) + Bx(t-\tau)$. *IEEE Transactions on Automatic Control, 34,* 460–462.

Mori, T., Fukuma, N., & Kuwahara, M. (1982). On an estimate of the decay rate for stable linear delay systems. *International Journal of Control, 36*(1), 95–97.

Niculescu, S.-I., & Michiels, W. (2004). Stabilizing a chain of integrators using multiple delays. *IEEE Transactions on Automatic Control, 49*(5), 802–807.

S-Niculescu, S. I., Michiels, W., Gu, K., & Abdallah, C. T. (2010). *Delay effects on output feedback control of dynamical systems* (pp. 63–84). Springer Berlin.

Niculescu, S. I., Boussaada, I., Li, X. G., Mazanti, G., & Méndez-Barrios, C. -F. (2021). Stability, delays and multiple characteristic roots in dynamical systems: A guided tour. In *Proceedings of the 16th IFAC Workshop Time Delay Systems* (Vol. 54, pp. 222–239), IFAC-PapersOnLine. Guangzhou, China.

Niculescu, S. -I., Li, X. -G., & Çela, A. (2023). Counting characteristic roots of linear delay-differential equations. Part I: frequency-sweeping stability tests and applications. In D. Breda (Ed.), *Controlling Delayed Dynamics: Advances in Theory, Methods and Applications, CISM Lecture Notes* (pp. 117–156). Wien-New York: Springer.

Nyquist, H. (1932). Regeneration theory. *Bell System Technical Journal, 11*(1), 126–147.

Obreschkoff, N. (1928). Nullstellen linearer kombinationen von exponentialfunktionen. *Jahresbericht der Deutschen Mathematiker-Vereinigung, 37*, 81–84.

Olver, F. W. J., Lozier, D. W., Boisvert, R. F., & Clark, C. W. (Eds.). *NIST handbook of mathematical functions*. Cambridge: Cambridge University Press.

Pinney, E. (1958). *Ordinary difference-differential equations*. Berkeley: University California Press.

G. Pólya, G., & Szegő, G. (1972). *Problems and theorems in analysis* (Vol. I) Integral calculus, theory of functions. Springer, New York.

Ruan, S. (2006). Delay differential equations in single species dynamics. In *Delay Differential Equations and Applications* (pp. 477–517). Springer.

Satche, M. (1949). Discussions on "stability of linear oscillating systems with constant time lag." *Journal of Applied Mechanics, Transactions ASME,16*(4), 419–420.

Stépán, G. (1979). *On the stability of linear differential equations with delay* (pp. 971–984). Colloquia Mathematica Societas Janos Bolyai: In Qualitative Theory of Differential Equations.

Stépán, G. (1989). *Retarded dynamical systems: Stability and characteristic functions*. London: Longman Scientific.

Tliba, S. (2004). *Contrôle actif des vibrations dans des structures mécaniques minces instrumentés de transducteurs piézoélectriques (in French)*. Ph.D. Thesis, ENS Cachan, France.

Tliba, S. (2011). Control of a vibrating axisymmetric membrane using piezoelectric transducers. In *Proceedings of the 18th IFAC World Congress* (pp. 7713 (6 p.)), Milano, Italy.

Tliba, S., Abou-Kandil, H., & Prieur, C. (2005). Active vibration damping of a smart flexible structure using piezoelectric transducers: $\mathcal{H}_\infty$ design and experimental results. In *Proceedings of the 16th IFAC World Congress*, Prague.

Tsypkin, Y. Z. (1946). Stability of systems with delayed feedback. *Avtomathika i Telemech, 7,* 107–129.

Vyhlídal, T., & Zitek, P. (2009). Mapping based algorithm for large-scale computation of quasi-polynomial zeros. *IEEE Transactions on Automatic Control, 54*(1), 171–177.

Walton, K., & Marshall, J. E. (1987). Direct method for TDS stability analysis. *EE Proceedings D—Control Theory and Applications, 134*(2), 101–107.

Wielonsky, F. (2001). A Rolle's theorem for real exponential polynomials in the complex domain. *Journal de Mathématiques Pures et Appliquées, 4,* 389–408.

Wynn, P. (1973). On the zeros of certain confluent hypergeometric functions. *Proceedings of the American Mathematical Society, 40,* 173–182.

Bifurcation Analysis of Systems With Delays: Methods and Their Use in Applications

Bernd Krauskopf and Jan Sieber

Abstract This chapter presents a dynamical systems point of view of the study of systems with delays. The focus is on how advanced tools from bifurcation theory, as implemented for example in the package DDE-BIFTOOL, can be applied to the study of delay differential equations (DDEs) arising in applications, including those that feature state-dependent delays. We discuss the present capabilities of the most recent release of DDE-BIFTOOL. They include the numerical continuation of steady states, periodic orbits and their bifurcations of codimension one, as well as the detection of certain bifurcations of codimension two and the calculation of their normal forms. Two longer case studies, of a conceptual DDE model for the El Niño phenomenon and of a prototypical scalar DDE with two state-dependent feedback terms, demonstrate what kind of insights can be obtained in this way.

We are very grateful to Dimitri Breda for organizing the school *Controlling Delayed Dynamics: Advances in Theory, Methods and Applications* at the International Centre for Mechanical Sciences (CISM) in November 2019 in Udine, and we thank CISM for providing location, management and support. A big thank you also to the other presenters, Tamás Insperger, Wim Michiels, Silviu Niculescu, Sjoerd Verduyn Lunel and of course Dimitri himself, and to all participants for making the school such an enjoyable and engaging event. As this volume shows, the school achieved its goal of providing an up-to-date snapshot of the field. A lot of credit goes again to Dimitri for pulling this volume together in the very challenging time of a global pandemic.

The work reviewed in this chapter is the result of collaborations with colleagues and friends over quite a number of years. In particular, we would like to acknowledge the contributions of Renato Calleja, Henk Dijstra, Tony Humphries, Andrew Keane and Claire Postlethwaite to the two case studies presented here. Moreover, we thank Elsevier, the Society for Industrial and Applied Mathematics, and The Royal Society for permission to reproduce figures and accompanying text passages from our previously published work. The research of BK was supported by Royal Society Te Apārangi Marsden Fund grant #19-UOA-223; and that of JS by EPSRC Grant No. EP/N023544/1 and by EU Project TiPES (European Union's Horizon 2020 research and innovation programme under grant agreement number 820970).

B. Krauskopf (✉)
Department of Mathematics, University of Auckland, Auckland, New Zealand
e-mail: B.Krauskopf@auckland.ac.nz

J. Sieber
College of Engineering, Mathematics and Physical Sciences, University of Exeter, Exeter, United Kingdom
e-mail: J.Sieber@exeter.ac.uk

D. Breda (ed.), *Controlling Delayed Dynamics*, CISM International Centre for Mechanical Sciences 604, https://doi.org/10.1007/978-3-031-01129-0_7

1 Introduction

Systems with delays arising in applications come in many different forms. From a general perspective a DDE is an ordinary differential equation (ODE) with a number of terms that feature delays. When the delays are zero, or parameters multiplying such terms are zero, then the DDE reduces to the underlying ODE, that is, a finite-dimensional dynamical system. When delays are present, on the other hand, one is dealing with an actual DDE and, hence, with an infinite-dimensional dynamical system. As for ODEs, the task is to determine the possible dynamics of a given DDE as a function of its parameters. In other words, what is called for is a bifurcation analysis of the DDE that unveils the division of parameter space into regions of different behavior. In spite of this difference in the dimension of the phase space, the bifurcation theory of DDEs is effectively that of ODEs in the sense that the same bifurcations of equilibria and periodic orbits arise in both cases. The complicating issue is that equilibria, periodic orbits and their bifurcations of a given DDE "live" in an infinite-dimensional space. As is the case for ODEs, this requires specialized numerical tools for finding and tracking invariant objects and their bifurcations.

As we will demonstrate, such advanced tools are available today. We focus here on the capabilities as implemented in the package DDE-BIFTOOL—a Matlab/octave (MATLAB 2018; Eaton et al. 2017) compatible library for performing numerical bifurcation analysis of DDEs of different types. DDE-BIFTOOL uses a numerical continuation approach, originally implemented by Engelborghs et al. (2000b), Engelborghs et al. (2001), Samaey et al. (2002), and is currently accessible and maintained at sourceforge.net/projects/ddebiftool (Sieber et al. 2015). Its capabilities are a subset of those of commonly used tools for ODEs and maps, such as AUTO (Doedel et al. 1999; Doedel 2007), MATCONT (Dhooge et al. 2003; Govaerts 2000) or COCO (Dankowicz and Schilder 2013). The bifurcation analysis tool `knut` offers an alternative, stand-alone implementation (in C++) of many of the methods used in DDE-BIFTOOL; see Roose and Szalai (2007).

In contrast to the tools for ODEs, the package DDE-BIFTOOL permits differential equations with a finite number of discrete delays in their arguments. More precisely, it considers differential equations of the form

$$\begin{aligned} M x'(t) = f(x(t), x(t-\tau_1), \ldots, x(t-\tau_d), p), \quad \text{where} \\ M \in \mathbb{R}^{n\times n} \quad \text{and} \quad f : \mathbb{R}^{n\times(d+1)} \times \mathbb{R}^{n_p} \to \mathbb{R}^n, \end{aligned} \tag{1}$$

which is a DDE with $d+1$ delays (where $\tau_0 = 0$ is included in the list of discrete delays). Further, there are n_p system parameters $p \in \mathbb{R}^{n_p}$. We call the space $\mathbb{R}^n$, in which $x(t)$ lives, the *physical space* for (1) (not to be confused with the infinite-dimensional phase space of the DDE as defined below). The matrix M on the left-hand side is most commonly (and by default) equal to the identity matrix, which corresponds to the case of 'standard' DDEs. Different choices of M are used to define other types of DDEs, including equations that are neutral (featuring delayed

derivatives), are of differential algebraic form, or are of mixed type with both delayed and advances terms.

DDE-BIFTOOL distinguishes two types of DDEs, depending on the nature of the discrete delays $\tau_1, \ldots, \tau_d$: DDEs with *constant* delays and DDEs with *state-dependent* delays. In the case of constant-delay DDEs the delays $\tau_1, \ldots, \tau_d$ need to be part of the vector p of system parameters. As part of the setup, the user has to specify the list of d indices of p that correspond to the delays $\tau_1, \ldots, \tau_d$. Alternatively, when dealing with state-dependent delays one may specify the delays $\tau_1, \ldots, \tau_d$ as functions of current or delayed states of x. More precisely, the user has to specify the number d of delays and the functions

$$\begin{aligned} \tau_j^f &: \mathbb{R}^{n\times j} \times \mathbb{R}^{n_p} \to \mathbb{R} && \text{for } j = 1, \ldots, d, \text{ where then} \\ \tau_j &= \tau_j^f(x^0, \ldots, x^{j-1}, p) && \text{for } j = 1, \ldots, d, \text{ with} \qquad (2) \\ x^0 &= x(t), \quad x^j = x(t - \tau_j) && \text{for } j = 1, \ldots, d, \text{ such that} \\ x'(t) &= f(x^0, \ldots, x^d, p). && \qquad (3) \end{aligned}$$

This way of defining the system permits the user to specify that the delay τ_j depends on the instantaneous state $x(t)$, the delayed states $x(t - \tau_1), \ldots, x(t - \tau_{j-1})$ and the parameter p. For example, for $d = 2$ permitted systems are of the form

$$x'(t) = f(x(t), x(t - \tau_1(x(t), p)), x(t - \tau_2(x(t), x(t - \tau_1(x(t), p)), p)), p).$$

Hence, the recursive definition (2)–(3) permits arbitrary levels of nesting of delays.

We focus here on 'standard' DDEs with constant and state-dependent delays. We first briefly discuss their relevant properties as dynamical systems. Subsequently, we present the tasks of bifurcation analysis and then discuss how they are performed and set up in practice in DDE-BIFTOOL; here, we use a constant-delay DDE for the inverted pendulum with delayed control as the illustrating example throughout. We further illustrate the overall capabilities with two longer case studies: (1) a conceptual DDE model for the El Niño Southern Oscillation (ENSO) system with negative delayed feedback and periodic forcing, where the delay is initially constant and then state dependent; and (2) a prototypical scalar DDE with two state-dependent feedback terms that features only trivial dynamics in the absence of state dependence.

2 DDEs as Dynamical Systems

While DDEs with discrete delays are the most common type of DDEs considered for practical implementation of numerical methods, the underlying mathematical theory does not distinguish between discrete and, e.g., distributed delays. The general theory permits general functionals on the right-hand side, of the form

$$\tilde{f} : C^0([-\tau_{\max}, 0]; \mathbb{R}^n) \times \mathbb{R}^{n_p} \to \mathbb{R}^n.$$

Here $C^k([-\tau_{\max}, 0]; \mathbb{R}^n)$ (or C^k for short) is the space of k times continuously differentiable functions—the *history segments*—on the interval $[-\tau_{\max}, 0]$, where $\tau_{\max}$ is an upper bound for the delays; in particular, C^0 is the space of continuous functions on $[-\tau_{\max}, 0]$ with values in $\mathbb{R}^n$. The general DDE (also called a functional differential equation, FDE) then has the form

$$x'(t) = \tilde{f}(x_t, p), \tag{4}$$

for the standard case that M in (1) is the identity matrix. One looks for solutions $x(t) \in \mathbb{R}^n$ with $t \in [-\tau_{\max}, t_{\text{end}}]$ of (4), and the solution x_t with subscript t is the current history segment in C^0, that is,

$$\begin{aligned} x_t : [-\tau_{\max}, 0] &\to \mathbb{R}^n \\ \theta &\mapsto x(t + \theta). \end{aligned}$$

For the DDE (1) with discrete delays the functional $\tilde{f}$ has the form

$$\tilde{f}(x, p) = f(x(0), x(-\tau_1), \ldots, x(-\tau_d), p)$$

for $x \in C^0$. In case the delays are state dependent, the τ_j are defined as described by (2) when setting $t = 0$.

2.1 General Theory for DDEs With Constant Delays

For DDEs with constant delays the textbooks by Hale and Verduyn Lunel (1993) and Diekmann et al. (1995) develop the necessary theory that permits one to consider DDEs of the general type (4) (and, hence, (1)) as regular dynamical systems on the phase space C^0 of continuous functions over the (maximal) delay interval; these DDEs are referred to as abstract ODEs by Diekmann et al. (1995). For $t = 0$ one has to provide an initial history segment $\phi \in C^0$, and then at each time $t \geq 0$ the current state is the function x_t, which is also in C^0; in particular, $x_0 = \phi$. The textbooks show that the map

$$\begin{aligned} X : [0, \infty) \times C^0 &\to C^0 \\ (t, \phi) &\mapsto x_t \,, \end{aligned}$$

which maps time t and initial value ϕ to the history segment x_t at time t of the solution of the DDE, is as regular with respect to its argument ϕ as the right-hand side $\tilde{f}$ of (1) is with respect to its first argument. For example, if $\phi \mapsto \tilde{f}(\phi, p)$ is ℓ times continuously differentiable, then so is $\phi \mapsto X(t; \phi)$. Consequently, the general

theory transfers many results of the bifurcation theory for ODEs to the case of DDEs with constant delays. In particular, the solution map X is eventually compact, which implies that local center manifolds in equilibria and periodic orbits of DDEs are finite-dimensional and as regular as the right-hand side $\tilde{f}$. Therefore, the local bifurcation theory of DDEs with a finite number of constant delays is identical to the local bifurcation theory of ODEs.

2.2 General Theory for DDEs With State-Dependent Delays

For DDEs with state-dependent delays the claim that their local bifurcation theory is identical to the theory of ODEs is not fully resolved. A review of well established results and an exposition of the obstacles that one initially faces are described in the review by Hartung et al. (2006). Even assuming that the state-dependent delays are always bounded within an interval $[0, \tau_{\max}]$, the space of continuous C^0 is not a suitable phase space, since no local uniqueness of solutions to initial-value problems can be guaranteed. The difficulty lies in the fact that for state-dependent delays the functional $\tilde{f} : C^0 \to \mathbb{R}^n$ in the right-hand side of the DDE is *not* continuously differentiable (or locally Lipschitz continuous), even if all coefficients f and τ_j^f are smooth. In fact, for general DDEs of the form (4) the assumption that $\tilde{f}$ is continuously differentiable with respect to its first argument is not satisfied when the delays are state dependent. The assumption of regularity of $\phi \mapsto \tilde{f}(\phi, p)$ being satisfied could be considered as the general property underlying and, hence, defining the constant-delay case of the theory.

Walther (2003) observes that functionals $\tilde{f}$ involving state-dependent delays satisfy a weaker regularity condition, which could be called mild differentiability. For these types of functionals Walther (2003) proves that for history segments ϕ within the manifold of *compatible* initial conditions, defined as

$$\phi \in C^1_{\text{comp}} := \left\{ \phi \in C^1 : \phi'(0) = \tilde{f}(\phi) \right\},$$

a unique solution $X(t; \phi)$ of the DDE exists and is also in C^1_{comp}. Moreover, for each time $t \geq 0$, the solution map

$$\begin{aligned} X : C^1_{\text{comp}} &\to C^1_{\text{comp}} \\ \phi &\mapsto X(t; \phi) \end{aligned} \tag{5}$$

is continuously differentiable once, which means that X meets the conditions for basic stability theory. For example, the principle of linearized stability holds for equilibria and periodic orbits (Skubachevskii and Walther 2006; Mallet-Paret and Nussbaum 2011b). Moreover, local center manifolds exist, are finite-dimensional and are continuously differentiable once (Stumpf 2011).

The results for the solution map X cannot be generalized to higher degrees of continuous differentiability; hence, X is not sufficiently regular to support all aspects of local bifurcation theory. However, there exist some results on higher-order differentiability for DDEs with state-dependent delays. First, solutions of periodic boundary-value problems for state-dependent delays can be reduced to finite-dimensional algebraic systems of equations that are as regular as the coefficients, such as f and τ_j^f in (2) and (3). Thus, all computations performed during numerical bifurcation analysis of equilibria, periodic orbits or their local bifurcations can be performed as expected and depend smoothly on their data. This includes the standard tasks of continuation of solutions using Newton iterations and pseudo-arclength continuation, or branching off at singularities. Similarly, all computations performed during normal form analysis are feasible (Sieber 2012, 2017). Furthermore, Krisztin (2006) checked that the techniques used for obtaining $\ell > 1$ times differentiable local unstable manifolds of equilibria (Krisztin 2003) are also applicable to local center manifolds of equilibria.

Thus, the results by Krisztin (2006) strongly suggest that local center manifolds in DDEs with state-dependent delays are differentiable as often as the coefficients f and τ_j^f, even though the solution map X of (5) is not. For this reason, while this is not fully resolved, the local bifurcation theory of DDEs with state-dependent delays is still expected to be identical to the theory for ODEs. Indeed, this claim is supported by all theoretical results this far, as well as by numerical investigations such as the one presented in Sect. 5.

3 Capabilities of DDE-BIFTOOL Demonstrated for the Controlled Inverted Pendulum

The general theory of Sect. 2 implies that numerical bifurcation analysis should allow one to perform a range of tasks for equations of type (1), similar to those arising in the bifurcation analysis of ODEs. More specifically, the local bifurcations of (standard) DDEs with both constant and state-dependent delays are the same as those one finds in ODEs and can, hence, be found in standard textbooks such as Guckenheimer and Holmes (1983), Govaerts (2000), Kuznetsov (2013). We do not present or review here this extensive theory but rather focus on the typical tasks required for the bifurcation analysis of a given DDE (or ODE), which include:

1. continuation of equilibria in a single system parameter;
2. linear stability analysis at equilibrium points, that is, finding the (leading) eigenvalues of their linearization;
3. detection of codimension-one bifurcations of equilibria and their continuation as curves in two system parameters; in generic systems, these are the saddle-node (or fold) bifurcation and the Hopf bifurcation, while in the presence of additional (symmetry) properties they include the transcritical bifurcation and the pitchfork bifurcation;

4. detection of codimension-two bifurcations of equilibria; in generic systems, these include the saddle-node Hopf, Hopf-Hopf, cusp and degenerate Hopf bifurcations;
5. normal form analysis of generic codimension-one and codimension-two bifurcations of equilibria; this includes, for example, computing the Lyapunov coefficient for the Hopf bifurcation, which determines whether the bifurcation is supercritical or subcritical, and branching off to secondary solution or bifurcation branches;
6. continuation of periodic orbits in a single system parameter (with automatic adjustment of the period);
7. linear stability analysis of periodic orbits, that is, determining their (leading) Floquet multipliers;
8. detection of codimension-one bifurcations of periodic orbits and their continuation as curves in two system parameters; in generic systems, these are the saddle-node (or fold) bifurcation of periodic orbits, the period-doubling bifurcation and the torus (or Neimark-Sacker) bifurcation;
9. identification and continuation of connecting orbits between equilibria in a suitable number of system parameters (depending on the dimensions of the respective stable and unstable eigenspaces of the involved equilibria);
10. computation of unstable manifolds of equilibria and periodic orbits with a single unstable direction to find, for example, certain invariant tori and global bifurcations.

Continuation tasks require formulating an algebraic system of equations of the form

$$G(y) = 0, \quad \text{where } G : \mathrm{dom}(G) \to \mathrm{range}(G) \tag{6}$$

is differentiable and the nullspace $\ker G'(y)$ is one-dimensional in solutions $y \in \mathrm{dom}\, G$. For the contination of equilibria and their bifurcations we will have $\mathrm{dom}(G) = \mathbb{R}^{N+1}$ and $\mathrm{range}(G) = \mathbb{R}^N$ for some problem dependent $N \in \mathbb{N}$. For the continuation of periodic orbits and their bifurcations G will map between infinite-dimensional spaces. In these cases a discretized problem $G_\mathrm{d} : \mathbb{R}^{N+1} \to \mathbb{R}^N$ has to be constructed, where N depends on the number of mesh points, and may be increased to improve accuracy. Solution loci of system (6) are generically curves (branches), which are tracked by the continuation algorithm (Doedel et al. 1999). Within DDE-BIFTOOL, the user specifies two points near each other on the respective curve of interest; the (pseudo-arclength) continuation algorithm generates a predictor by extrapolating the secant through the (last) two points on the curve and then uses Newton iteration to correct the prediction and, hence, find the next point along the curve; this predictor-corrector step is repeated until a sufficient piece of the curve defined by (6) has been computed.

Stability computation tasks for DDEs require the creation of a matrix eigenvalue problem of an approximating, sufficiently large system of ODEs. Normal form analysis for equilibrium bifurcations in DDE-BIFTOOL computes explicit normal form coefficients for codimension-one and codimension-two bifurcations, which deter-

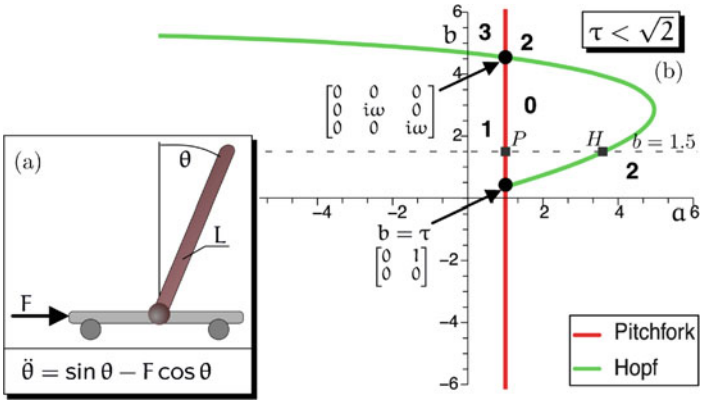

Fig. 1 Sketch of an inverted pendulum on a cart subject to a control force F with its equation in rescaled time units $\sqrt{L/g}$ (**a**), and the linear stability chart in the (a, b)-plane for PD control $F(t) = a\theta(t-\tau) + b\theta'(t-\tau)$ and delay $\tau = \sqrt{2}/4$ (**b**)

mine the dynamics close to the bifurcation according to the textbook by Kuznetsov (2013). The normal form analysis is also used to construct predictors for starting the continuation of secondary solution branches that emerge from the respective bifurcation.

3.1 DDE Model of the Controlled Inverted Pendulum

We will proceed to explain how these different tasks are performed by DDE-BIFTOOL. To demonstrate how this works in practice, we will use throughout this section the example of a simple DDE model for balancing an inverted pendulum with delayed feedback, described by Sieber and Krauskopf (2004a), Sieber and Krauskopf (2004b),

$$\theta''(t) = \sin\theta(t) - F(t)\cos(t), \text{ where } F(t) = a\theta(t-\tau) + b\theta'(t-\tau). \quad (7)$$

The dependent variable $\theta(t)$ is the angle by which the (approximately mass-less) pendulum deviates from the upright position. The term $F(t)$ is the feedback force exerted by moving the base of the pendulum, such as the cart sketched in Fig. 1a, to achieve upright balancing. In (7), the feedback is of proportional-plus-derivative type, where the correcting force depends linearly on the angle θ and on the angular velocity θ'; one speaks of PD control. Time in (7) is in units of the intrinsic time scale $\sqrt{g/L}$ of the pendulum, where L is the length of the pendulum and g is the gravitational acceleration. The delay τ models a reaction delay relative to the intrinsic time scale of the pendulum; hence, varying the delay is similar to changing the length of the pendulum, where a shorter pendulum corresponds to a longer delay after scaling.

Rewriting (7) as a first-order system gives

$$\begin{aligned} x_1'(t) &= x_2(t), \\ x_2'(t) &= \sin x_1(t) - \cos x_1(t)\,[a x_1(t-\tau) + b x_2(t-\tau)]\,. \end{aligned} \tag{8}$$

Hence, the physical space for $x(t) = (x_1(t), x_2(t))$ is $\mathbb{R}^2$, the parameter space for $p = (p_1, p_2, p_3) = (a, b, \tau)$ is $\mathbb{R}^3$, and the right-hand side f is

$$f(x^0, x^1, p) = \begin{bmatrix} x_2^0 \\ \sin x_1^0 - \cos x_1^0 \left(p_1 x_1^1 + p_2 x_2^1\right) \end{bmatrix} \tag{9}$$

in the formulation (1) of DDE-BIFTOOL, where M is the identity in $\mathbb{R}^2$. We remark that, even though the right-hand side f does not depend on τ, the delay τ must be included in the parameter vector p (as p_3) for f.

We observe that the right-hand side f has the reflection symmetry

$$f(-x^0, -x^1, p) = -f(x^0, x^1, p).$$

Therefore, system (8) has two types of solutions: symmetric solutions, which are invariant under this reflection symmetry, and symmetrically related pairs of non-symmetric solutions. As we will see later on, distinguishing the two types is of practical relevance because the control force $F(t)$ is applied by adjusting the position of the pendulum at its base, that is, by pushing the cart on which it is mounted in Fig. 1a. For non-symmetric solutions the average of $F(t)$ is non-zero, which implies that the cart accelerates away in one direction; in particular, the cart position, which we refer to as $\delta(t)$ in Fig. 2 below, is unbounded. For symmetric solutions, on the other hand, the long-term average of the force $F(t)$ on the cart is zero, which means that the cart position $\delta(t)$ may be bounded. Thus, only symmetric solutions correspond to successful balancing of the pendulum. Mathematically, the reflection symmetry introduces non-generic symmetry-breaking bifurcations, including pitchfork bifurcations, which require special treatment within DDE-BIFTOOL.

3.2 Continuation of Branches of Equilibria

The continuation of equilibria for DDEs is identical to that for ODEs: equilibria x_{eq} of $x'(t) = f(x(t), x(t-\tau_1), \ldots, x(t-\tau_d), p)$ are given by the nonlinear equation

$$G_{\mathrm{eq}}(y_{\mathrm{eq}}) = f(x_{\mathrm{eq}}, \ldots, x_{\mathrm{eq}}, p) = 0,$$

which is of the general form (6) where the dimension $N = n$ is the dimension of the physical space. One typically chooses the unknowns $y_{\mathrm{eq}} = (x_{\mathrm{eq}}, p_i)$ for continuation of equilibria in one of the system parameters p_i.

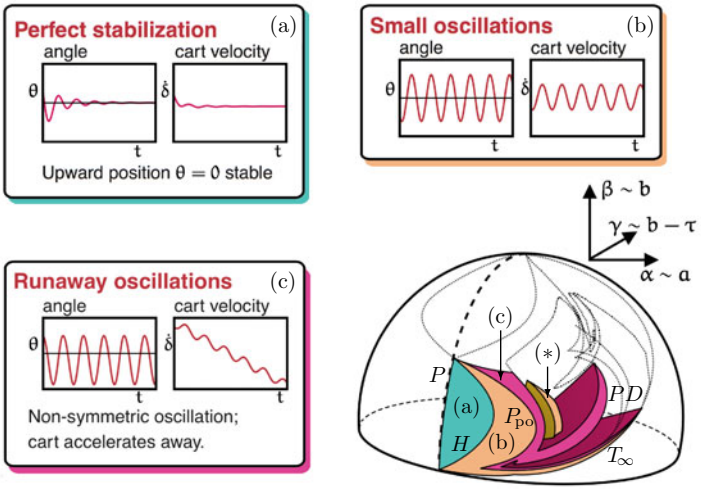

Fig. 2 Bifurcation diagram of the controlled inverted pendulum (8) on an ellipsoid around the triple-zero point, with regions of equilibrium stabilization (**a**), small oscillations (**b**) and runaway oscillations (**c**) of the pendulum. The bounded chaotic dynamics in the area labelled $(*)$ is shown separately in Fig. 3b. Curves of codimension-one bifurcations on the ellipse include those of pitchfork bifurcation P, Hopf bifurcation H, pitchfork bifurcation of periodic orbits P_{po}, period doubling PD, and connecting orbits T_∞. Here, $r = 1/2$ in the definition (12) of the ellipse

The pendulum problem (8) has the upright position $x = (0, 0)$ as its reflection-invariant trivial equilibrium solution. Figure 1b shows the line (dashed) for fixed $b = 1.5$ and varying a in the (a, b)-plane for $\tau = \sqrt{2}/4$, which corresponds to the single-parameter family of trivial equilibria $(0, 0, a)$.

3.3 *Linear Stability Analysis of Equilibria*

The natural next step is the computation of the linear stability for each equilibrium (x_{eq}, p) along the computed branch, which is determined by the stability of the DDE, linearized in the equilibrium (including $\tau_0 = 0$ into our list of discrete delays),

$$M x'(t) = \sum_{j=0}^{d} A_j x(t - \tau_j), \text{ where } \quad A_j = \frac{\partial f}{\partial x^j}(x_{\mathrm{eq}}, \ldots, x_{\mathrm{eq}}, p) \in \mathbb{R}^{n \times n}. \quad (10)$$

The stability of the origin for the linear DDE (10) is determined by the real parts of the spectrum of its infinitesimal generator $\mathcal{A}$, defined by

$$[\mathcal{A}x](\theta) = x'(\theta) \quad \text{with domain}$$
$$D(\mathcal{A}) = \left\{ x \in C^1 : Mx'(0) = \sum_{i=0}^{d} A_i x(-\tau_i) \right\}.$$

The eigenvalue problem $\lambda x = \mathcal{A}x$ in the infinite-dimensional space $D(\mathcal{A})$ is equivalent to the n-dimensional eigenvalue problem for the characteristic matrix $\Delta(\lambda) \in \mathbb{R}^{n\times n}$,

$$\Delta(\lambda)v = 0, \quad \text{where} \qquad \Delta(\lambda) = \lambda M - \sum_{i=0}^{d} A_i \exp(-\lambda\tau_i) \tag{11}$$

(Kaashoek and Verduyn Lunel, 1992). The problem of finding the right-most eigenvalues λ of $\mathcal{A}$ (or Δ) is fundamentally different from an ODE stability problem, since typically $\mathcal{A}$ has infinitely many eigenvalues. However, for the most common case where M is the identity, the infinitesimal generator $\mathcal{A}$ has at most finitely many eigenvalues to the right of any vertical line in the complex plane. For its linear stability analysis DDE-BIFTOOL does not solve $\det \Delta(\lambda) = 0$, but instead discretizes the eigenvalue problem $\lambda x = \mathcal{A}x$ to obtain an eigenvalue problem for a pair of large matrices. The approach by Breda et al. (2005) (see also Breda, 2023) is to discretize the ODE boundary-value problem

$$x'(\theta) = \lambda x(\theta), \qquad Mx'(0) = \sum_{i=0}^{d} A_i x(-\tau_i),$$

on the interval $[-\tau_{\max}, 0]$ with an mth-order pseudospectral approximation (e.g., Chebyshev polynomials) for $x : [-\tau_{\max}, 0] \to \mathbb{C}^n$ to obtain a matrix eigenvalue problem of dimension $(m+1)n$. Engelborghs and Roose (2002) discretize (10) by using a linear multistep ODE solver with a small time step $h = \tau_{\max}/m$ and express the condition that the approximate solution after a single time step, x_h, satisfies $x_h = \mu x_0$ on the uniform grid with step h on $[-\tau_{\max}, 0]$. This is also an eigenvalue problem for large matrices in μ, from which the eigenvalues λ are obtained by the relation $\lambda = (\log \mu)/h$. Both options are available in DDE-BIFTOOL, which automatically refines the discretization if the desired right-most eigenvalues are not accurate up to a specified tolerance.

For the pendulum model's upright equilibrium $x = (0, 0)$ the characteristic matrix $\Delta(\lambda)$ has the form

$$\Delta(\lambda) = \begin{bmatrix} \lambda & -1 \\ a\mathrm{e}^{-\lambda\tau} - 1 & \lambda + b\mathrm{e}^{-\lambda\tau} \end{bmatrix}.$$

When increasing a from 0 for $b = 1.5$ and $\tau = \sqrt{2}/4$, one detects a change of linear stability at the points P and H in Fig. 1b. At the point P (where $a = 1$) a real eigenvalue crosses the imaginary axis from the right to the left half of the complex plane. At this point P, the trivial equilibrium gains linear stability (under increasing a)

in a subcritical pitchfork bifurcation (owing to the reflection symmetry), and a family of non-symmetric equilibria of the form $(x_1, x_2, a) = (x_1, 0, (\sin x_1)/(x_1 \cos x_1))$ branches off. At the point H (at $a \approx 3.6$), the linear DDE has a pair of complex eigenvalues $\pm \mathrm{i}\omega \approx \pm 0.6\mathrm{i}\pi$ (crossing from left to right for increasing a) such that the upright equilibrium destabilizes in a Hopf bifurcation. Consequently, for $b = 1.5$ and $\tau = \sqrt{2}/4$ the upright position of the pendulum is linearly stable when $a \in (1, 3.6)$; that is, between the points P and H in Fig. 1b.

3.4 *Continuation of Codimension-One Bifurcations of Equilibria*

Once a bifurcation of an equilibrium (which will typically be of codimension one) has been detected one may either branch off to follow another branch (of equilibria or periodic orbits), or continue the bifurcation itself in additional parameters—as a curve in two chosen system parameters when it is indeed of codimension one. DDE-BIFTOOL supports continuation of the generic codimension-one bifurcations, the saddle-node (or fold) and the Hopf bifurcation (Engelborghs and Roose 1999). The continuation is implemented for nonlinear systems that extend the nonlinear equation $G_{\mathrm{eq}}(y_{\mathrm{eq}}) = 0$ with the eigenvalue problem (11) for the critical eigenvalue. For the fold of equilibria the eigenvalue λ is 0 such that the unknowns are $y_{\mathrm{feq}} = (x_{\mathrm{feq}}, v_{\mathrm{feq}}, p_i, p_j) \in \mathbb{R}^{2n+2}$ (with two free parameters p_i and p_j). For the Hopf bifurcation the frequency ω_H is unknown and the eigenvector v_H is complex such that we have the unknowns $y_H = (x_H, v_H, \omega_H, p_i, p_j) \in \mathbb{R}^{3n+3}$ (counting the complex vector v_H as two real vectors of length n). The nonlinear equations for the fold and Hopf bifurcations are

$$G_{\mathrm{feq}}(y_{\mathrm{feq}}) = \begin{bmatrix} f(x_{\mathrm{feq}}, \ldots, x_{\mathrm{feq}}, p) \\ \Delta(x_{\mathrm{feq}}, p; 0) v_{\mathrm{feq}} \\ v_{\mathrm{feq}}^T v_{\mathrm{feq}} - 1 \end{bmatrix} \quad \text{and} \quad G_H(y_H) = \begin{bmatrix} f(x_H, \ldots, x_H, p) \\ \Delta(x_H, p; \mathrm{i}\omega_H) v_H \\ v_{\mathrm{ref}}^T v_H - 1 \end{bmatrix},$$

which are in $\mathbb{R}^{2n+1}$ and $\mathbb{R}^{3n+2}$, respectively; here the base points (x_{feq}, p) and (x_H, p) are included as arguments of the characteristic matrix Δ (since the matrices A_i in (11) depend on them). The scale of the complex eigenvector $v_H \in \mathbb{C}^n$ is fixed with the help of a reference vector $v_{\mathrm{ref}} \in \mathbb{C}^n$ and one complex equation (i.e., two real equations).

For the balancing pendulum model, the point H is on a curve of Hopf bifurcations, which can be continued in two parameters. The resulting curve in the (a, b)-plane is shown in green in Fig. 1b. The eigenvalue zero bifurcation at the point P is not a fold, but a pitchfork bifurcation due to the equilibrium's invariance under the reflection symmetry. Thus, the equation $G_{\mathrm{feq}}(y_{\mathrm{feq}}) = 0$ is singular. An experimental feature of DDE-BIFTOOL permits the user to add constraints enforcing the symmetry of the equilibrium to make the extended nonlinear system regular (for example,

$x_{\text{feq},1} = 0$ for the inverted pendulum); see also Sect. 3.10. For system (8) the pitchfork bifurcation is at $a = 1$ for any b and τ, and this curve P is shown in red in Fig. 1b.

Along these two curves of codimension-one bifurcations one encounters degenerate points. At $\omega_H = 0$ the Hopf bifurcation meets the pitchfork bifurcation in a special point where the linearization has a zero eigenvalue of algebraic multiplicity 2; this point lies at $b = \tau$ and $a = 1$ in Fig. 1b. For small τ the Hopf bifurcation curve emerges to the right of the line of pitchfork bifurcations before it bends back to cross this line again at $b \approx 4.5$; at this point there is a pitchfork-Hopf bifurcation, where the linearization has an eigenvalue 0 and an imaginary eigenvalue pair $\pm \mathrm{i}\omega_H$.

The Hopf bifurcation curve and the pitchfork bifurcation line bound the region in Fig. 1b where the upright position $x = (0, 0)$ is linearly stable; this is indicated with the label 0, which refers to the number of unstable eigenvalues. Bosschaert et al. (2020) implemented normal form analysis for generic equilibrium bifurcations of codimension one or two. Their analysis produces normal form coefficients permitting us to branch off toward secondary codimension-one branches from codimension-two bifurcation points. The expressions rely on genericity conditions that are violated at the pitchfork bifurcation (due to the reflection symmetry), such that the routines provided by Bosschaert et al. (2020) cannot be applied to the double-zero and pitchfork-Hopf interaction points we found for the inverted pendulum DDE (8). However, the criticality of the Hopf bifurcation along the branch of Hopf bifurcation can be determined by computing the Lyapunov coefficient ℓ_1 with the routines from Bosschaert et al. (2020). The coefficient is negative everywhere, meaning that the Hopf bifurcation is supercritical. From this information the shown numbers of unstable eigenvalues of the upright equilibrium $x = (0, 0)$ in the other regions of Fig. 1b can be determined.

3.5 *Codimension-Three Singularity of the Inverted Pendulum*

The region of stability shown in Fig. 1b shrinks to the single point $(a_*, b_*) = (1, \sqrt{2})$ at the critical delay $\tau_* = \sqrt{2}$, at which the upright equilibirum $x = (0, 0)$ has a linearization with a zero eigenvalue of multiplicity 3. Hence, the critical delay τ_* is the largest possible delay for which the delayed PD control can stabilize the upright position. In Sieber and Krauskopf (2004a), Sieber and Krauskopf (2004b) we performed an analysis of the bifurcation structure in the neighborhood of this singularity. Its results are shown in Fig. 2 for parameters on an ellipsoid around the singular point $(a_*, b_*, \tau_*) = (1, \sqrt{2}, \sqrt{2})$ of codimension three. The ellipsoid is parametrized in the new coordinates (α, β, γ), which are related to the original coordinates via

$$\begin{aligned} a &= a_* + r^6\alpha, & b &= b_* + r^2\frac{\tau_*}{3}\beta, & \tau &= b + r^4\frac{\tau_*}{3}\gamma, \\ \alpha &= \sin(\varphi\pi/2), & \beta &= \cos(\varphi\pi/2)\cos(2\pi\psi), & \gamma &= \cos(\varphi\pi/2)\sin(2\pi\psi), \end{aligned} \tag{12}$$

where the radius-type scaling parameter r determines the size of the ellipsoid. The unit sphere in the rescaled (α, β, γ)-space is then parametrized by the two polar coordinate angles $(\varphi, \psi) \in [0, 1] \times [0, 1]$, yielding the representation in Fig. 2.

The viewpoint of the sphere in (α, β, γ)-space is chosen in Fig. 2 with a focus on the region of stability of the upright pendulum, labeled (a) and bounded by the curves P of pitchfork bifurcation and H of Hopf bifurcation, as well as on nearby regions with more complicated dynamics of the controlled inverted pendulum. Note from panel (a) of Fig. 2 that successful stabilization of the upright position involves convergence of the position θ as well as of the velocity $\dot{\delta}$ of the cart. As we discuss next, finding additional behavior of the system beyond stabilization requires the continuation of periodic orbits and their bifurcations.

3.6 *Continuation of Periodic Orbits*

A periodic orbit $x(t)$ with $x(t) = x(t - T)$ for some fixed period $T > 0$ and all times t is given as the solution of a periodic DDE boundary-value problem (BVP). Hence, obtaining the nonlinear problem $G_{\text{po}}(y_{\text{po}}) = 0$ for the computation and continuation of periodic orbits requires a discretization of a periodic BVP. As is common, we rescale the period to the interval $[0, 1]$ and use the variable $s = t/T$ for the rescaled time (and recall the convention that $\tau_0 = 0$) to obtain

$$\text{DDE:} \quad M x_{\text{po}}{}'(s) = T f\left(x_{\text{po}}\left(s - \frac{\tau_0}{T}\right)_{[0,1)}, \ldots, x_{\text{po}}\left(s - \frac{\tau_d}{T}\right)_{[0,1)}, p\right), \tag{13}$$

$$\text{BC:} \quad x_{\text{po}}(0) = x_{\text{po}}(1), \tag{14}$$

$$\text{PC:} \quad 0 = \int_0^1 x'_{\text{ref}}(s)^T x_{\text{po}}(s) \mathrm{d}s \tag{15}$$

for the unknowns $x_{\text{po}}(\cdot) \in C^1([0, 1]; \mathbb{R}^n)$, $T \in (0, \infty)$ and a single system parameter p. In (13) we use the notation $x_{\text{po}}(s)_{[0,1)}$ for the 'wrapped' evaluation of $x_{\text{po}}(s)$, that is, $(s)_{[0,1)} = (s - \text{floor}(s))$ (and, hence, $x_{\text{po}}(s)_{[0,1)} = x_{\text{po}}(s - \text{floor}(s))$), where $\text{floor}(s)$ is the largest integer less than or equal to s. Thus, $(s)_{[0,1)}$ is always in $[0, 1)$ and the *boundary condition* (BC) (14) simply expresses the periodicity of the solution. In the original time, the periodic orbit is then $t \mapsto x_{\text{po}}(t/T)_{[0,1)}$. A *phase condition* (PC) is required to select a unique and isolated solution of the overall BVP that represents the periodic orbit. This is the case because, if $x_{\text{po}}(\cdot)_{[0,1)}$ is a solution of (13)–(14), then so is $x_{\text{po}}(\cdot + c)_{[0,1)}$ for any $c \in [0, 1)$. We use here the integral phase condition (15), which fixes the free phase of the present solution x_{po} by minimizing the integral distance $\int_0^1 (x_{\text{ref}}(s) - x_{\text{po}}(s))^T (x_{\text{ref}}(s) - x_{\text{po}}(s)) \mathrm{d}s$ to a periodic reference solution x_{ref}; see Doedel (2007) for more details on phase conditions. We may write the infinite-dimensional nonlinear problem (13)–(15) in the form (6) as

$$G_{\text{po}}(y_{\text{po}}) = 0, \quad \text{where } y_{\text{po}} = (x_{\text{po}}(\cdot), T, p_i) \in C^1([0, 1]; \mathbb{R}^n) \times \mathbb{R} \times \mathbb{R}.$$

Engelborghs et al. (2000a) and Engelborghs and Doedel (2002) constructed a fixed-degree piecewise polynomial collocation discretization for (13)–(15). The discretization stores the approximate solution $x_{\mathrm{po}}(\cdot)$ on a mesh s_{e} of N_T subintervals in polynomial pieces of degree κ, in the form of a vector $x_{\mathrm{po,d}} \in \mathbb{R}^{n(\kappa N_T+1)}$. The discretized residual at an arbitrary point $s \in [0, 1]$ has the form

$$G_{\mathrm{DE,d}}(x_{\mathrm{po,d}}, T, p; s) =$$
$$ME^{(1)}(s)x_{\mathrm{po,d}} - Tf\left(E^{(0)}\left(s - \frac{\tau_0}{T}\right)_{[0,1)} x_{\mathrm{po,d}}, \ldots, E^{(0)}\left(s - \frac{\tau_d}{T}\right)_{[0,1)} x_{\mathrm{po,d}}, p\right).$$

The matrices $E^{(\ell)}(s)$ are $n \times (n(\kappa N_T + 1))$ interpolation (for $\ell = 0$) and differentiation (for $\ell > 0$) matrices, such that $x(s) = E^{(0)}(s)x_{\mathrm{po,d}}$ and $x^{(\ell)}(s) = E^{(\ell)}(s)x_{\mathrm{po,d}}$ for all piecewise polynomials x defined on the mesh s_{e}. The overall discretized periodic DDE BVP (13)–(15) has the form

$$G_{\mathrm{po,d}}(y_{\mathrm{po,d}}) = \begin{bmatrix} \left(G_{\mathrm{DE,d}}(x_{\mathrm{po,d}}, T, p; s_{\mathrm{c},j})\right)_{j=1}^{\kappa N_T} \\ \left[E^{(0)}(0) - E^{(0)}(1)\right] x_{\mathrm{po,d}} \\ \int_0^1 (E^{(1)}(s)x_{\mathrm{ref,d}})^T E^{(0)}(s)x_{\mathrm{po,d}} \mathrm{d}s \end{bmatrix}, \tag{16}$$

where $(s_{\mathrm{c},j})_{j=1}^{\kappa N_T}$ is a suitably chosen collocation mesh. The variable $y_{\mathrm{po,d}} = (x_{\mathrm{po,d}}, T, p_i)$ has dimension $N = n(\kappa N_T + 1) + 2$ and $G_{\mathrm{po},d}(y_{\mathrm{po,d}})$ has $n\kappa N_T + n + 1$ components. The matrix $E^{(0)}(\cdot)$ provides a natural embedding such that the function

$$x_{\mathrm{po,e}}(\cdot) : t \mapsto x_{\mathrm{po,e}}(t) = E^{(0)}(t/T)_{[0,1)}x_{\mathrm{po,d}} \tag{17}$$

is a piecewise polynomial approximation of the periodic orbit. The integral in the final component of $G_{\mathrm{po,d}}$ (the phase condition) can be computed exactly as $x_{\mathrm{ref,d}}^T W_c\, x_{\mathrm{po,d}}$ with precomputed quadrature weights W_{c}; here the discretized reference solution $x_{\mathrm{ref,d}}$ is generally chosen as the discretized periodic orbit computed at the last continuation step. While the definitions for $G_{\mathrm{po,d}}$ look identical for constant and state-dependent delays, the τ_j in the definition of $G_{\mathrm{DE,d}}$ are functions of s and $(x_{\mathrm{po,d}}, T, p)$ if they depend on the state. Convergence of the discretization for constant delays has only been proven recently by Andó and Breda (2020). Convergence proofs in earlier papers treated the variables T and τ_j as given constants, because considering (for example) the period T as an unknown creates analytical difficulties similar to those when considering state-dependent delays.

The above description agrees with the current implementation in DDE-BIFTOOL, generalizing the original construction by Engelborghs et al. (2000a) and Engelborghs and Doedel (2002) by separating the construction of the matrices $E^{(\ell)}(\cdot)$ from the construction of the nonlinear problem. Since different discretization methods enter only through different interpolation matrices $E^{(\ell)}$, different choices of discretization can be made depending on the matrix M. The mesh adaptation is based on the same error estimate and error equidistribution as those in AUTO (Doedel et al. 1999).

For the inverted pendulum model (8), the periodic orbits that emerge from the Hopf bifurcations can be computed as solutions of $G_{\mathrm{po,d}}(y_{\mathrm{po,d}}) = 0$ with $G_{\mathrm{po,d}}(y_{\mathrm{po,d}})$ given by (16), for example, with the angle ϕ as the continuation parameter p_i. These periodic orbits have the spatio-temporal symmetry $x_{\mathrm{po}}(t + T/2) = -x_{\mathrm{po}}(t)$, and a typical time profile is shown in Fig. 2b. The symmetric periodic orbits lose their stability in a symmetry breaking pitchfork bifurcation of periodic orbits, labelled P_{po} in Fig. 2; see Sects. 3.7 and 3.8 for the linear stability analysis of periodic orbits. Moreover, a branch of symmetric periodic orbits terminates when the period T (which is part of the variable y_{po} and its discretization $y_{\mathrm{po},d}$ along the solution branch) goes to infinity; at this point the periodic orbits approach a symmetric heteroclinic connection between the two non-symmetric saddle equilibria, the locus of which is labeled T_∞ in Fig. 2. Together the curves P_{po} and T_∞ bound the region of stable symmetric periodic orbits, which is labeled (b) in Fig. 2. This type of periodic orbit can be interpreted as partial stabilization of the inverted pendulum: while the upright pendulum equilibrium is no longer stable, nevertheless, the periodic motion of the pendulum as well as the velocity of the cart are bounded and initially (close to the curve H) quite small.

3.7 *Linear Stability Analysis for Periodic Orbits*

Linearizing around a solution $(x_{\mathrm{po}}(\cdot), T, p)$ of (13)–(15) yields a linear DDE with time-periodic coefficient matrices $s \mapsto A_j(s)$ and (if the delays are state-dependent) time periodic delays $s \mapsto \tau_j(s)$ of period 1. The eigenvalue problem involves a Floquet multiplier $\mu \in \mathbb{C}$ and an eigenfunction $x_{\mathrm{ev}} : [-\tau_{\max}/T, 0] \mapsto \mathbb{C}^n$, satisfying

$$0 = M x_{\mathrm{ev}}{}'(s) - \sum_{j=0}^{d} A_j(s) x_{\mathrm{ev}}\left(s - \frac{\tau_j(s)}{T}\right) \qquad \text{if } s \in (0, 1], \tag{18}$$

$$\mu x_{\mathrm{ev}}(s) = x_{\mathrm{ev}}(s + 1) \qquad \text{if } s \in [-\tau_{\max}/T, 0] \tag{19}$$

(note the absence of wrapping). Here, for state-dependent delays with $\tau_0 = 0$, $\tau_j = \tau_j^f(x^0, \ldots, x^{j-1}, p)$, $X^0 = I_n$, $x^j = x_{\mathrm{po}}(s - \tau_j/T)_{[0,1)}$, and $x'^j = x_{\mathrm{po}}{}'(s - \tau_j/T)_{[0,1)}$ for $j = 0, \ldots, d$ we have

$$A_j(s) = T \frac{\partial f}{\partial x^j}(x^0, \ldots, x^d, p) X^j \quad \text{and} \tag{20}$$

$$X^j = I_n - \frac{x'^j}{T} \sum_{\ell=0}^{j-1} \frac{\partial \tau_j^f}{\partial x^\ell}(x^0, \ldots, x^{j-1}, p) X^\ell.$$

In practice, the arguments of $\partial f/\partial x^j$ have to be evaluated for the approximate periodic orbit defined by (17), that is, $x^j = x_{\mathrm{po,e}}(s - \tau_j/T)_{[0,1)}$ and $x'^j = x'_{\mathrm{po,e}}(s - \tau_j/T)_{[0,1)}$.

Szalai et al. (2006) and Sieber and Szalai (2011) showed that the eigenvalue problem (18)–(19) is equivalent to a finite-dimensional eigenvalue problem $\Delta(\mu)v = 0$, where the dimension of the characteristic matrix $\Delta(\mu)$ may be larger than n but is bounded for bounded T and $\tau_{\max}$. Yanchuk et al. (2019) constructed a characteristic matrix for the case $d = 1$ of a single delay τ_1, which can be large but keeps $T - \tau_1$ bounded (a common scenario for pulse-type periodic solutions in systems with a single large delay).

Extending the mesh s_e from the interval $[0, 1]$ to the interval $[-\tau_{\max}/T, 1]$, a piecewise polynomial x of degree κ on $[-\tau_{\max}/T, 1]$ is now stored in a vector $x_{\mathrm{ev,d}}$ of size $n(\kappa(N_T + N_{\tau_{\max}}) + 1)$. With the help of the interpolation and differentiation matrices $E^{(\ell)}(\cdot)$ on the extended mesh s_e, we define the $n \times (n(\kappa(N_T + N_{\tau_{\max}}) + 1))$ coefficient matrix for the discretized residual of the linear DDE (18) at an arbitrary time $s \in (0, 1]$

$$A_{\mathrm{DE,d}}(s) = ME^{(1)}(s) - \sum_{j=0}^{d} A_j(s)E^{(0)}\left(s - \frac{\tau_j(s)}{T}\right).$$

Then the discretized eigenvalue problem is a $(N_1 + N_2)$-dimensional generalized matrix eigenvalue problem with $(N_1, N_2) = (n(\kappa N_{\tau_{\max}} + 1), n\kappa N_T)$ of the form (Borgioli et al. 2020)

$$Ax_{\mathrm{ev,d}} = \mu B x_{\mathrm{ev,d}}, \text{ with } A = \begin{bmatrix} (A_{\mathrm{DE,d}}(s_{c,j}))_{j=1}^{\kappa N_T} \\ 0_{N_1 \times N_2} \;\; I_{N_1 \times N_1} \end{bmatrix}$$
$$\text{and } B = \begin{bmatrix} 0_{N_2 \times (N_1+N_2)} \\ I_{N_1 \times N_1} \;\; 0_{N_1 \times N_2} \end{bmatrix}.$$

In the definition for A we may use the same collocation mesh s_c as for the computation of the periodic orbit x. The interpolation matrix $E^{(0)}$ provides a natural embedding such that $x_{\mathrm{ev,e}} : t \mapsto E^{(0)}(t/T)x_{\mathrm{ev,d}}$ is an approximate Floquet eigenfunction corresponding to a Floquet multiplier μ, where $x_{\mathrm{ev,d}}$ is the eigenvector of size $(N_1 + N_2)$ from the discrete matrix eigenvalue problem. The dimension of the matrix eigenvalue problem can be reduced to an explicit $N_1 \times N_1$ eigenvalue problem by using the first N_2 equations (where μ does not show up) to eliminate the components $((x_{\mathrm{ev,d}})_j)_{j=N_1+1}^{N_1+N_2}$. This corresponds to solving the discretized monodromy problem for the linear DDE (18), and works whenever the initial-value problem is well-posed. Yanchuk et al. (2019) observed that an adaptive mesh s_e that has been adapted for a good approximation of the periodic orbit $x_{\mathrm{po}}(t)$ may give poor approximations $x_{\mathrm{ev,e}}$ for the Floquet eigenfunctions $x_{\mathrm{ev}}(t)$ even for multipliers with $|\mu| \approx 1$. The eigenfunction $x_{\mathrm{ev}}(t)$ may have rapid oscillations where $x_{\mathrm{po}}(t)$ is approximately constant. This is common when the delay τ and the period T are relatively large and x_{po} is pulse-like (Yanchuk et al. 2019).

3.8 Continuation of Codimension-One Bifurcations of Periodic Orbits

For generic local bifurcations of periodic orbits DDE-BIFTOOL implements fully extended defining systems (Govaerts 2000) by appending the variational problem. The extended system is formulated in the infinite-dimensional space in a manner that it has again the form (13)–(15) of a periodic DDE BVP with additional free parameters and integral constraints. For the continuation of folds of periodic orbits, we consider the infinite-dimensional nonlinear problem $G_{\mathrm{po}}(y_{\mathrm{po}}) = 0$ where $y_{\mathrm{po}} = (x_{\mathrm{po}}(\cdot), T, p_i, p_j)$ (thus, adding one free parameter), and append its variational problem, such that we have

$$\begin{aligned} G_{\mathrm{fpo}}(y_{\mathrm{fpo}}) &= G_{\mathrm{fpo}}(x_{\mathrm{po}}(\cdot), T, p, x_{\mathrm{v}}(\cdot), T_v) \\ &= \begin{bmatrix} G_{\mathrm{po}}(x_{\mathrm{po}}(\cdot), T, p) \\ \partial_{x_{\mathrm{po}}} G_{\mathrm{po}}(y_{\mathrm{po}}) x_{\mathrm{v}} + \partial_T G_{\mathrm{po}}(y_{\mathrm{po}}) T_{\mathrm{v}} \\ \int_0^1 x_{\mathrm{v}}(s)^T x_{\mathrm{v}}(s) \mathrm{d}s + {T_{\mathrm{v}}}^2 - 1 \end{bmatrix}. \end{aligned}$$

Here, $p = (p_i, p_j)$ and the additional variational variables $y_{\mathrm{v}} = (x_{\mathrm{v}}(\cdot), T_{\mathrm{v}}) \in C^1([0, 1]; \mathbb{R}^n) \times \mathbb{R}$ have the same format as $(x_{\mathrm{po}}(\cdot), T)$. Thus, $G_{\mathrm{fpo}}(y_{\mathrm{fpo}})$ has the same format as (13)–(15): it consists of a periodic BVP of dimension $2n$ (for $(x_{\mathrm{po}}(\cdot), x_{\mathrm{v}}(\cdot))$) with 3 scalar integral conditions such that DDE-BIFTOOL uses the discretization $G_{\mathrm{po,d}}$ on this extended problem. The discretized problem has the overall dimension $N = 2n(\kappa N_T + 1) + 4$.

For the pitchfork bifurcation of periodic orbits found in the bifurcation diagram of the controlled inverted pendulum this system is singular. However, an experimental feature of DDE-BIFTOOL lets the user append conditions that enforce a spatio-temporal symmetry of x_{po}, such that the system becomes regular (for example, for the reflection symmetry $\int_0^1 (x_{\mathrm{po}})_1(s)\mathrm{d}s = 0$); the bifurcation curve P_{po} in Fig. 2 was computed in this way. Notice from Fig. 2c that the bifurcating asymmetric periodic orbit in the corresponding region represents oscillations around a value of θ that is not zero; in particular, the velocity $\dot{\delta}$ of the cart decreases (or increases). Hence, this type of periodic orbit no longer satisfies the condition for generalized stability of the controlled inverted pendulum.

For the continuation of period doubling and torus bifurcations we append the equation for the critical eigenfunction in periodic form: if $x_{\mathrm{ev}}(s + 1) = \mu x_{\mathrm{ev}}(s)$ and $|\mu| = 1$, we may write $\mu = \exp(\mathrm{i}\pi\omega_{\mathrm{v}})$, where $\pi\omega_{\mathrm{v}}$ is the rotation number, and introduce $x_{\mathrm{v}}(s) = \exp(-\mathrm{i}\pi\omega_{\mathrm{v}} s) x_{\mathrm{ev}}(s)$. Then the defining system for torus and period doubling bifurcations appends to (16) the equations

$$x_{\mathrm{v}}{}'(s) = -\mathrm{i}\pi\omega_{\mathrm{v}} x_{\mathrm{v}}(s) + \sum_{j=0}^{d} A_j(s) x_{\mathrm{v}}(s - \tau_j(s)/T) \exp(-\mathrm{i}\pi\omega_{\mathrm{v}}\tau_j(s)/T), \quad (21)$$

$$0 = \int_0^1 x_{\mathrm{v,ref}}(s)^T x_{\mathrm{v}}(s)\mathrm{d}s - 1, \quad (22)$$

where the A_j are as defined by (20) in the section on linear stability of periodic orbits. Equation (22) has two real components (or one complex component). It fixes the length and phase of the complex Floquet vector x_{v}, depending on a reference function $x_{\mathrm{v,ref}}$. Thus, the defining system $G_{\mathrm{tor}}(y_{\mathrm{tor}}) = 0$ for the torus bifurcation consists of $G_{\mathrm{po}}(y_{\mathrm{po}}) = 0$ defined by (16) together with (21)–(22) for the (extended) input vector variables $y_{\mathrm{tor}} = (y_{\mathrm{po}}, x_{\mathrm{v}}(\cdot), \omega_{\mathrm{v}}) = (x_{\mathrm{po}}(\cdot), T, p_i, p_j, x_{\mathrm{v}}(\cdot), \omega_{\mathrm{v}})$. Again, the solutions are both represented by discretization vectors $x_{\mathrm{po,d}}$ and $x_{\mathrm{v,d}}$ such that the overall dimension of y_{tor} is $N = 3n(\kappa N_T + 1) + 5$. For the period doubling bifurcation the unknown rotation number $\pi\omega_{\mathrm{v}}$ equals π (such that $\omega_{\mathrm{v}} = 1$).

Apart from these generic codimension-one local bifurcation of periodic orbits, DDE-BIFTOOL is able to detect and continue connecting orbits between equilibria by means of a defining system $G_{\mathrm{con}}(y_{\mathrm{con}})$ implemented by Samaey et al. (2002). As for the variable y_{po} for periodic orbits, the formulation is that of a DDE BVP and the variable y_{con} contains (discretized) orbit segments and an unknown integration time (which is, however, no longer a period). Moreover, y_{con} also contains variables associated with the locations of the equilibria and their linearizations, because the setup uses projection boundary conditions to approximate the connecting orbit by an orbit segment with a finite integration time (Beyn 1990). The DDE BVP $G_{\mathrm{con}}(y_{\mathrm{con}}) = 0$ can be used to detect connecting orbits and continue them in a parameter plane when they are of codimension one; however, the present implementation is restricted to the constant-delay case. An alternative method for computing connecting orbits that arise as limits of periodic orbits, such as homoclinic orbits, is to continue a branch of periodic orbits until the period T is very high, indicating that the parameter is close to the locus of connecting orbits. The continuation of periodic orbits with a fixed, sufficiently high period in two system parameters is then an approximation of the sought locus of connections.

This latter approach was used for finding the curve T_∞ for the controlled inverted pendulum in Fig. 2 as the locus of symmetric periodic orbits of large period. Moreover, we found that for ϕ approaching the curve T_∞ the branch of symmetric periodic orbits has an infinite sequence of pitchfork and fold bifurcations when the heteroclinic connection is approached; this is the case because the dominant eigenvalues of the linearizations at the non-symmetric saddle equilibria satisfy the (saddle-quantity) condition for a complicated (or chaotic) Shilnikov bifurcation (Kuznetsov 2013). The non-symmetric periodic orbits branching off at these pitchfork bifurcations encounter period doublings for larger ϕ and then also approach a connecting orbit, namely a non-symmetric homoclinic connection to a single non-symmetric equilibrium. The curve PD in Figure 2, bounding the dark red region, is the first of these period doubling bifurcations and it has been computed with the defining system $G_{\mathrm{tor}}(y_{\mathrm{tor}}) = 0$ as defined above.

3.9 *Symmetric and Non-Symmetric Chaos in the Pendulum*

The repeated period doublings of the non-symmetric oscillations in Fig. 2 suggest that there is a region where oscillations can be chaotic. We expect this to occur inside the wedges formed by the first period doubling curve PD, and a region with chaotic oscillations is indeed readily identified inside the largest wedge by numerical simulations. As is shown in row (a) of Fig. 3, initially, these chaotic oscillations of (8) are non-symmetric and they do not correspond to successful balancing, because they feature run-away acceleration of the cart balancing the pendulum; see Fig. 3a3. However, further inside the chaotic region, inside the subregion labelled $(*)$ in Fig. 2, the two symmetrically related non-symmetric chaotic attractors collide near a homoclinic tangency of the symmetric saddle periodic orbit. As a result, symmetric chaotic oscillations are possible, as is shown in row (b) of Fig. 3. For these symmetric chaotic oscillations of position x_1 and velocity x_2 of the pendulum, the cart performs a chaotic walk around its zero velocity; see Fig. 3b3. Therefore, this type of symmetric chaotic attractor represents a quite extreme form of generalized stabilization of the inverted pendulum. The homoclinic tangency of the saddle periodic orbit can be approximated by computing the unstable manifold of the symmetric saddle orbit and checking if it returns to the symmetric saddle orbit in a way that is tangent to the stable linear subspace of the symmetric saddle orbit. A brief description of computations of unstable manifolds of periodic orbits is given as part of the case study in Chap. 5; see Sieber and Krauskopf (2004b) for further details of the overall dynamics of the DDE model (8) of the PD controlled inverted pendulum.

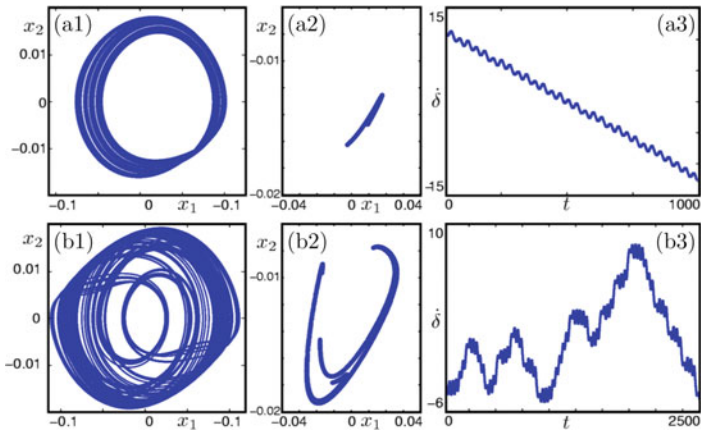

Fig. 3 Chaotic runaway motion (**a**) and chaotic bounded motion (**b**) of the controlled inverted pendulum DDE; here, panels (**a1**) and (**b1**) show the trajectory and (**a2**) and (**b2**) the Poincaré map in projection onto the (x_1, x_2)-plane, while (**a3**) and (**b3**) show the time evolution of the velocity $\dot{\delta}$ of the cart. From Sieber and Krauskopf (2004b) © 2004 Elsevier; reproduced with permission

3.10 Some Experimental Features of DDE-BIFTOOL

We finish the description of the capabilities of DDE-BIFTOOL by mentioning briefly some features that are still experimental.

Problems with discrete symmetry. Similar to the reflection symmetry of the pendulum model (9), systems with discrete symmetries (for example where $Rf(x^0, \ldots, x^d, p) = f(Rx^0, \ldots, Rx^d, p)$ for some root R of the identity matrix) have additional degeneracies when symmetry breaking occurs. The user can add additional constraints enforcing the symmetry, and request that the defining system automatically appends dummy variables to create regular continuation problems for symmetry-breaking bifurcations. This feature has been used to find the curve P_{po} of pitchfork bifurcation of periodic orbits of (8) on the ellipse in parameter space shown in Fig. 2.

Problems with rotational symmetry. A common feature of problems with delays in optics is that they have rotational symmetry, in the simplest case with a single free rotation. That is, the right-hand side f satisfies $\exp(At)f(x^0, \ldots, x^d, p) = f(\exp(At)x^0, \ldots, \exp(At)x^d, p)$ for a fixed anti-symmetric matrix $A \in \mathbb{R}^{n\times n}$ (that is, $A^T = -A$), and arbitrary $t \in \mathbb{R}$ and $x^0, \ldots, x^d \in \mathbb{R}^n$. In this case one is interested in tracking (i) any rotating wave, which is a periodic solution of the form $x(t) = \exp(A\omega t)x_{\mathrm{eq}}$, as a relative equilibrium, that is, as x_{eq}; and (ii) any modulated rotating wave, which is a quasi-periodic solution of the form $x(t) = \exp(A\omega t)x_{\mathrm{po}}(t)$ where x_{po} has period T, as a relative periodic orbit, that is, as x_{po}.

Typical examples are the DDE models for semiconductor lasers with optical feedback from mirrors or with delayed optical coupling, which are invariant under rotation of the complex electric field (Pieroux et al. 2001; Haegeman et al. 2002; Krauskopf et al. 2000; Krauskopf 2005). In fact, the wish to perform the bifurcation analysis of this type of laser system provided considerable motivation for the early development of DDE-BIFTOOL. In order to select unique solutions in the presence of this rotational symmetry, the phase of the electric field was pushed into an additional parameter, which was then set to a specific, fixed value to implement a phase condition. Generalizing this approach, DDE-BIFTOOL provides a wrapper around the defining systems in Sects. 3.2, 3.4, 3.6 and 3.8 that introduces the mean rotation frequency ω as an additional free parameter and adds an additional phase condition.

Interface with COCO. DDE-BIFTOOL can only continue curves of invariant objects and their bifurcations, that is, it computes one-dimensional solution manifolds of the respective defining system. The package COCO, on the other hand, has implemented algorithms for multi-parameter continuation by means of growing atlases of solution manifolds of arbitrary dimension, which is based on the original algorithm by Henderson (2002); see Dankowicz and Schilder (2013) for more details. An interface is available that feeds the defining systems implemented in DDE-BIFTOOL into COCO's more general continuation algorithm, and provides constructors to start such a multi-parameter continuation.

3.11 DDE-BIFTOOL Formulation for Other Types of DDEs

The capabilities we just reviewed, which allow DDE-BIFTOOL to perform the various tasks required for bifurcation analysis, can be applied to standard DDEs with constant or state-dependent delays. The latter requires the user to specify the state-dependence in the form (2); how this is done in practice is demonstrated in Sect. 4 for a conceptual DDE model of the ENSO system and in Sect. 5 for a scalar DDE with two state-dependent delays.

Moreover, DDE-BIFTOOL can be used for the study of DDEs beyond the standard form, whose formulation requires that the matix M in (1) is not the identity matrix. Permitting the matrix M to be singular drastically expands the class of DDE one can consider. In particular, the general form (1) used by DDE-BIFTOOL includes the following types of DDEs.

Neutral Equations (NDDEs). Neutral DDEs feature delayed derivatives, and this case can be formulated in the framework of (1) by a suitable choice of M. As an example, including an acceleration dependence into the feedback term F in (7) changes the governing equations for the deviation $\theta(t)$ of the pendulum angle from the upright position to

$$\theta''(t) = \sin\theta(t) - \cos\theta(t)[a\theta(t-\tau) + b\theta'(t-\tau) + c\theta''(t-\tau)],$$

where c is an additional control gain (Sieber and Krauskopf 2005; Insperger et al. 2013). This can be formulated within (1) for $x(t) = (\theta(t), \theta'(t), \theta''(t)) \in \mathbb{R}^3$ and $p = (a, b, c, \tau) \in \mathbb{R}^4$ by setting $M = \mathrm{diag}(1, 1, 0)$ and

$$f(x^0, x^1, p) = \begin{bmatrix} x_2^0 \\ x_3^0 \\ \sin x_1^0 - \cos x_1^0 \left[p_1 x_1^1 + p_2 x_2^1 + p_3 x_3^1\right] - x_3^0 \end{bmatrix}.$$

Differential Algebraic Equations (DAEs). In a number of applications one encounters algebraic constraints on the variables of a DDE, leading to a system of DAEs with delays. For example, one may define a state-dependent delay implicitly, as is

done in the position control problem with echo location measurements discussed by Walther (2002)

$$y'(t) = k\left[y_{\text{ref}} - \frac{c}{2}s(t-\tau_0)\right], \text{ where } cs(t) = y(t) + y(t-s(t)).$$

Here $y(t)$ is the position to be kept at target y_{ref} by feedback control. The other state, $s(t)$, is the travel time of an echo location signal sent from position $y(t-s(t))$ with speed c to y_{ref} and reflected back to $y(t)$ to estimate the current position offset as $cs(t)/2$. The constant delay τ_0 is a reaction delay in the application of the feedback control with target position y_{ref} (similar to the delay in the pendulum feedback in (7), where the reference position is the upright angle 0). Here $x(t) = (y(t), s(t)) \in \mathbb{R}^2$ and $p = (y_{\text{ref}}, k, c, \tau_0) \in R^4$. This can be formulated by setting $M = \text{diag}(1, 0)$, $d = 2$ and

$$\begin{aligned} \tau_1^f(x^0, p) &= p_4, \\ \tau_2^f(x^0, x^1, p) &= x_2^0, \end{aligned} \quad \text{and} \quad f(x^0, x^1, x^2, p) = \begin{bmatrix} p_2\left(p_1 - \frac{p_3}{2}x_1^2\right) \\ p_3 x_2^0 - x_0^2 - x_2^2 \end{bmatrix}.$$

Forward-Backward/Mixed-Type Equations. Even when all delays are positive in (1), the possibility of adding algebraic equations permits one to introduce both negative and positive delays. These types of equations do not describe well-posed initial-value problems but may occur when modeling traveling waves or periodic wave trains on a space-discrete lattice (Abell et al. 2005). For example, a wave in a discrete linear diffusion equation traveling with speed $1/\tau$ satisfies $u'(t) = \Delta[u(t+\tau) + u(t-\tau) - 2u(t)]$. This could be formulated by setting $M = \text{diag}(1, 0)$, $p = (\Delta, \tau) \in \mathbb{R}^2$, and

$$f(x^0, x^1, p) = \begin{bmatrix} p_1[x_1^1 + x_2^0 - 2x_1^0] \\ x_1^0 - x_2^1 \end{bmatrix},$$

such that $x(t) \in \mathbb{R}^2$ and $u(t) = x_1(t)$.

Experimental Nature of Computations for DDEs Beyond the Standard Form. While the types of problems above can be formulated for input in DDE-BIFTOOL by using a singular matrix M in (1), we stress that any subsequent computations of invariant objects and their bifurcation must be considered as being of an experimental nature. Namely, the accuracy of the results obtained by the different numerical computations we described for standard DDEs is not always guaranteed. See Barton et al. (2006) for an analysis of convergence properties for neutral DDEs and note that forward-backward problems and delayed DAEs with index higher than 1 are yet untested.

4 An ENSO DDE Model With State Dependence

Feedback loops are crucial ingredients in the dynamics of climate systems, where they arise due to the interactions between various subsystems, including distinct bodies of water, the atmosphere, land and ice masses; see, for example, Bar-Eli and Field (1998), Dijkstra (2008), Dijkstra (2013), Kaper and Engler (2013), Keane et al. (2017), Simonnet et al. (2009) as entry points to the literature. Such feedback loops are subject to inherent time delays, mainly as a result of the time it takes to transport mass or energy across the globe and/or throughout the atmosphere, or due to delayed reactions of subsystems to changing conditions. Whenever the time delays of feedback loops in climate systems are large compared to the forcing time scales under consideration, explicit modeling of the delay makes sense in conceptual models. As a specific example of immediate human and wider mathematical interest, we consider the El Niño phenomenon—a large increase of the sea surface temperature in the eastern equatorial Pacific Ocean that occurs about every 3–7 years. This oceanic phenomenon is associated with an atmospheric component, the Southern Oscillation, and they are jointly known as El Niño Southern Oscillation (ENSO) variability (Dijkstra 2008; Graham and White 1988; Kaper and Engler 2013; Tziperman et al. 1998; Zaliapin and Ghil 2010). Large peaks in the sea surface temperature of the eastern Pacific Ocean near the coast off Peru represent El Niño events, the warm phase of ENSO, while large drops represent the cool phase known as La Niña.

El Niño events have major consequences world-wide, yet they remain notoriously hard to predict even with sophisticated global climate models (Barnston et al. 2012). An important aspect of ENSO is that El Niño events tend to occur at the same time of year, always around Christmas. This suggests locking to the seasonal cycle (with a period of 1 year), which represents the characteristic forcing time scale of the ENSO system. Feedback mechanisms in ENSO arise naturally from ocean-atmosphere coupling processes in the eastern and central equatorial Pacific Ocean, and they have delay times of many months due to the time it takes waves to propagate across the Pacific Ocean.

In light of the overall complexity of climate systems, conceptual models have much to offer in terms of elucidating underlying mechanisms behind observed dynamics. Conceptual DDE models for ENSO (and some other climate phenomena) have been developed by Bar-Eli and Field (1998), Dijkstra (2013), Falkena et al. (2019), Ghil et al. (2008), Kaper and Engler (2013), Tziperman et al. (1994), Tziperman et al. (1998), Zaliapin and Ghil (2010) to provide insights into the interplay between delayed feedback loops and different types of external forcing. Such DDE ENSO models constitute a significant model reduction, compared to the full description of atmospheric and oceanic dynamics and interaction, including their velocity and temperature fields. Since the feedback loops and their delay times are explicit parts of the DDE model, their roles for observed system behavior can be investigated readily. Generally, the delays that arise in such models are estimated, from quantities such as average wave speeds and distances, and taken to be constant.

4.1 The Delayed Action Oscillator Paradigm

We consider here an ENSO DDE model that follows the prominent delayed action oscillator (DAO) paradigm that was first introduced by Suarez and Schopf (1988). There exist a number of models based on the DAO paradigm; for example, see Suarez and Schopf (1988), Battisti and Hirst (1989), Tziperman et al. (1994), Tziperman et al. (1998). The DDE model introduced by Ghil et al. (2008) is one of the simplest in that it focuses on the interaction between the negative delayed feedback and additive seasonal forcing. Its ingredients are illustrated in Fig. 4. The main quantity of interest for the DAO is the depth of the thermocline, which is the thin and distinct layer in the ocean that separates deeper cold waters from shallower warm surface water. The thermocline is deeper in the West and shallower in the East, and this is represented by the tilted bottom plane of Fig. 4. The variable $h(t)$ denotes the deviation of the thermocline depth from the long-term thermocline mean in the eastern equatorial Pacific, off the coast of Peru. A positive value of h corresponds to a larger layer of warm water and, hence, an increased sea-surface temperature (SST) in the eastern Pacific, while negative h means a decreased SST. In other words, the variable h can be seen as a proxy for SST. We are concerned here with the main negative feedback loop: off the equator, a negative anomalous thermocline depth signal is carried to the western boundary of the ocean via so-called Rossby waves, which are reflected as Kelvin waves. The oceanic waves of the negative feedback are the green arrows in Fig. 4, and they carry the shallow thermocline perturbation back to the eastern boundary of the ocean, which is a process that takes on the order of 8 months. There

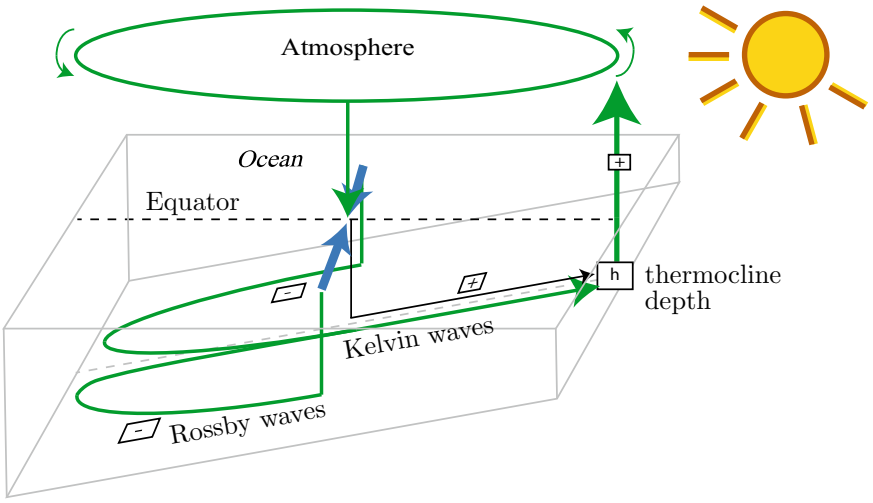

Fig. 4 Schematic of the negative feedback loop of the thermocline h at the eastern Pacific Ocean due to energy transport via Rossby and Kelvin wave from the central ocean-atmosphere interaction zone

is also a positive feedback of h with a shorter delay of only about a month. It is represented by the black arrow in Fig. 4 and arises from the fact that a warm SST anomaly slows down the easterly trade winds, leading to westerly wind anomalies that deepen the thermocline; see, for example, Dijkstra (2013), Keane et al. (2017), Keane et al. (2019) for more details.

4.2 The GZT Model

As was done by Ghil et al. (2008), we now consider only the above-mentioned negative feedback loop and the seasonal cycle, with the goal of demonstrating that their interplay is sufficient to produce rich dynamical behavior that is relevant to ENSO. The effects of including the positive feedback loop into this model are studied in detail in Keane et al. (2016). The model from Ghil et al. (2008), which we refer to as the GZT model from now on, takes the form

$$h'(t) = -b \tanh[\kappa h(t-\tau)] + c\cos(2\pi t). \tag{23}$$

Here, τ is the delay time of the negative feedback loop with amplification factor b, which is further characterized by the coupling parameter κ; note that κ is the slope at 0 of the tanh-function and see Münnich et al. (1991) for a justification for this simple type of ocean-atmosphere coupling. Throughout, we fix the parameters b and κ to the values $b = 1$ and $\kappa = 11$ that were used and justified in previous investigations of the ENSO phenomenon (Ghil et al. 2008; Zaliapin and Ghil 2010). In (23) the periodic forcing of strength c enters as an additive term. Alternatively, one may shift the period-1 response to the origin such that the seasonal forcing is parametric, as was considered in a simple DDE ENSO model by Tziperman et al. (1998), Krauskopf and Sieber (2014). We remark that simple conceptual ENSO DDEs such as the GZT model are of wider interest because they are rather prototypical: DDE models of much the same structure can also be found in control theory and machining; see, for example, Just et al. (2007), Milton et al. (2009), Purewal et al. (2014), Stépán (1989).

A key feature of system (23) is the periodic forcing term with its explicit dependence on time t; hence, this DDE is non-autonomous. Since DDE-BIFTOOL is designed for autonomous DDEs, we transform (23) into autonomous form by introducing an artificial stable oscillation that generates the periodic forcing. For any periodically forced DDE (or ODE) this can be achieved with the Hopf normal form for a stable periodic orbit of radius 1; it can be written in complex form as

$$\dot{z}(t) = (1 + \omega i)z(t) - z(t)|z(t)|^2, \tag{24}$$

and we set $\omega = 2\pi$ to have the required forcing period of 1 (year). This two-dimensional system then drives (23) in its rewritten form

$$\dot{h}(t) = -b \tanh\left[\kappa h(t-\tau)\right] + c\ \mathrm{Re}(z(t)). \tag{25}$$

The equivalent autonomous system (25) with (24) is readily implemented in DDE-BIFTOOL with physical state $x(t) = (h(t), \mathrm{Re}(z(t)), \mathrm{Im}(z(t))) \in \mathbb{R}^3$, parameter vector $p = (p_1, p_2, p_3, p_4) = (b, c, \kappa, \tau) \in \mathbb{R}^4$ (such that $\tau = p_4$), and right-hand side

$$f(x^0, x^1, p) = \begin{bmatrix} -p_1 \tanh[p_3 x_1^1] + p_2 x_2^0 \\ x_2^0 - 2\pi x_3^0 - x_2^0((x_2^0)^2 + (x_3^0)^2) \\ x_3^0 + 2\pi x_2^0 - x_3^0((x_2^0)^2 + (x_3^0)^2) \end{bmatrix}. \tag{26}$$

Figure 5 presents five stable solutions of (23) as obtained by numerical integration with the Euler method from initial conditions $h \equiv 0$ and/or $h \equiv 1$ after transients have settled down. Shown are the respective time series of h in panels (a1)–(e1), which are intuitive in the context of ENSO system since the variable h is a proxy for the SST: maxima and minima of h represent El Niño and La Niña events, respectively. Panels (a2)–(e2) of Fig. 5 are projections of the corresponding attractors onto the $(h(t-\tau), h(t))$-plane.

For zero seasonal forcing $c = 0$ there is an attracting periodic solution; see row (a) of Fig. 5. Its zigzag-like shape and period of $T = 4\tau$ years is due to the fact that the slope κ is quite large at $\kappa = 11$, so that the tanh-function is rather close to a discontinuous switching function. In the context of ENSO, this stable periodic orbit corresponds to an El Niño event exactly every 4.8 years as driven by the delay time of $\tau = 1.2$ years. On the other hand, when the periodic forcing is large compared to the negative feedback one finds a periodic solution that is quite close to sinusoidal with a period $T = 1$ year; an example is shown in row (b) of Fig. 5. The observed dynamics is clearly dominated by the seasonal forcing, meaning that the SST varies exactly with the seasonal cycle.

The interesting case is that of an interplay between negative feedback and the seasonal cycle when b and c are of the same order. In this regime one may find dynamics on invariant tori, which may be locked or quasiperiodic. Row (c) of Fig. 5 shows a stable locked periodic solution; in fact, it coexists with the seasonally driven periodic solution in row (b). Another example of multi-stability are the stable solutions shown in rows (d) and (e). The projection onto the $(h(t-\tau), h(t))$-plane in panel (d2) clearly shows that there is an attracting torus with dynamics that is quasiperiodic (or periodic with a very high period); the attractor in row (e), on the other hand, is clearly periodic and likely a locked solution on a different torus. Notice the difference in amplitude between the respective coexisting stable solutions in rows (b) and (c) and in rows (d) and (e), respectively. An interpretation of the locked periodic solutions in row (c) and (e) would be a build-up of the maxima of the SST from year to year until a global maximum, interpreted as an El Niño event, is reached and the SST decreases until a global minimum, interpreted as La Niña event, is reached and the process repeats.

Figure 6 shows two maximum maps in the (c, τ)-plane of (23), together with curves of saddle-node bifurcations of periodic orbits SL, period-doubling bifurcations PD, and torus bifurcations T. Two-parameter maximum maps, which plot for each point of a grid in parameter space the maximum of a sufficiently long time series after transients have settled down, have been considered as a convenient way

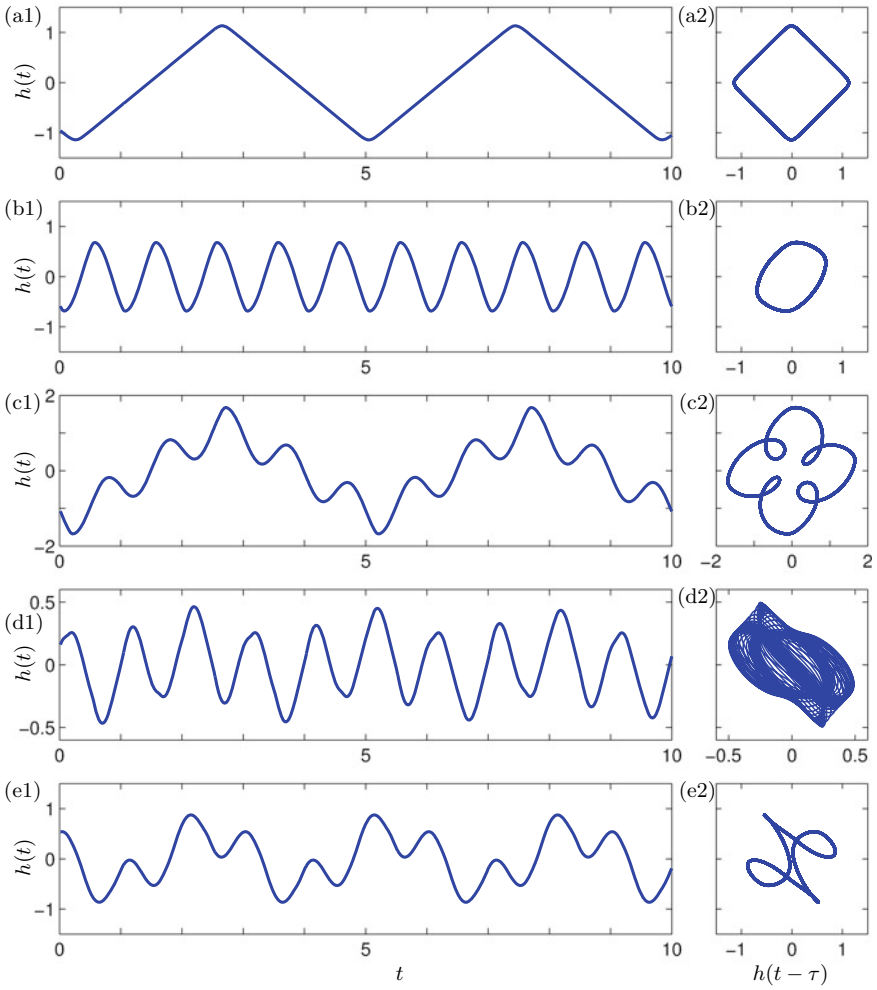

Fig. 5 Stable solutions of (23), shown as time series in panels (**a1**)–(**e1**) and as projections onto the $(h(t-\tau), h(t))$-plane in panels (**a2**)–(**e2**); throughout $b = 1$, $\kappa = 11$ and $\tau = 1.2$, $c = 0$ for (**a**), $\tau = 1.2$, $c = 3$ for (**b**) and (**c**), and $\tau = 0.62$, $c = 3$ for (**d**) and (**e**). From Keane et al. (2015) © 2015 Society for Industrial and Applied Mathematics; reproduced with permission

of obtaining an overview of the overall dynamics (Ghil et al. 2008; Keane et al. 2015). We show two maximum maps in two panels of Fig. 6 in a greyscale where, for each row of fixed delay τ, the parameter c is swept up or down in small steps as is indicated by the arrows; here the respective previous solution is used as the initial history for the next value of c. In this way, hysteresis loops in c are detected and regions of multistability are identified as regions in the (c, τ)-plane where the two maximum maps do not agree.

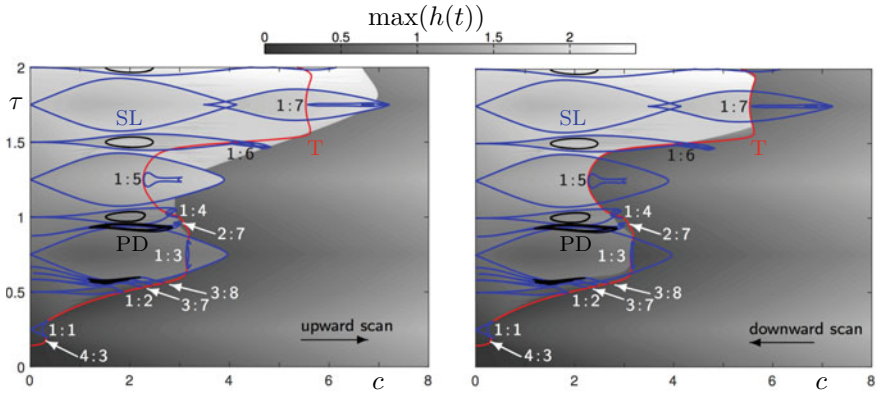

Fig. 6 Maximum maps and bifurcation set of (23) in the (c, τ)-plane with curves of saddle-node bifurcations of periodic orbits (SL), period-doubling (PD) and torus bifurcations (T), and labelled lower resonance tongues. From Keane et al. (2015) © 2015 Society for Industrial and Applied Mathematics; reproduced with permission

The bifurcation curves in Fig. 6 explain features of the two maximum maps. In particular, the curves SL of saddle-node bifurcations of periodic orbits delineate the elongated shapes. In fact, they bound resonance tongues that emerge from the line $c = 0$ of zero forcing and from the curve T of torus bifurcations, namely at points of $p:q$ resonance, some of which are labelled. In the regions bounded by respective curves SL one finds stable frequency locked solutions of the fixed frequency ratio $p:q$; compare with Fig. 5c, e. The curve T lies near the (roughly diagonal) boundary along which one finds sudden jumps of the maxima. Notice that this boundary is different for increasing c versus decreasing c in two panels of Fig. 6, showing that the curve T is associated with regions of multistability. As is discussed by Keane and Krauskopf (2018), this involves folding resonance tongues and the break-up of invariant tori in what are known as Chenciner bubbles. Overall, Fig. 6 confirms that for sufficiently large c solutions are dominated by the seasonal forcing, while there is an interplay between the forcing and the delayed feedback for lower values of c, specifically, to the left of the torus bifurcation curve T, where one finds dynamics on invariant tori.

We focus here on the existence of chaotic dynamics caused by this interplay, because it has been suggested that irregular locked motion of (23) captures important aspects of ENSO (Ghil et al. 2008; Zaliapin and Ghil 2010). Regions where such dynamics may occur are those in Fig. 6 that are bounded by curves PD of period-doubling bifurcations, which are found inside some of the shown resonance tongues. This is a known feature that occurs when resonance tongues overlap and the corresponding tori lose their normal hyperbolicity and break up; see, for example, Broer et al. (1998), Kuznetsov (2013). To identify where chaotic dynamics can be found, Fig. 7 shows the bifurcation curves in the (c, τ)-plane overlaid on a map of the maximal Lyapunov exponent, as computed for an upsweep of c with the algorithm

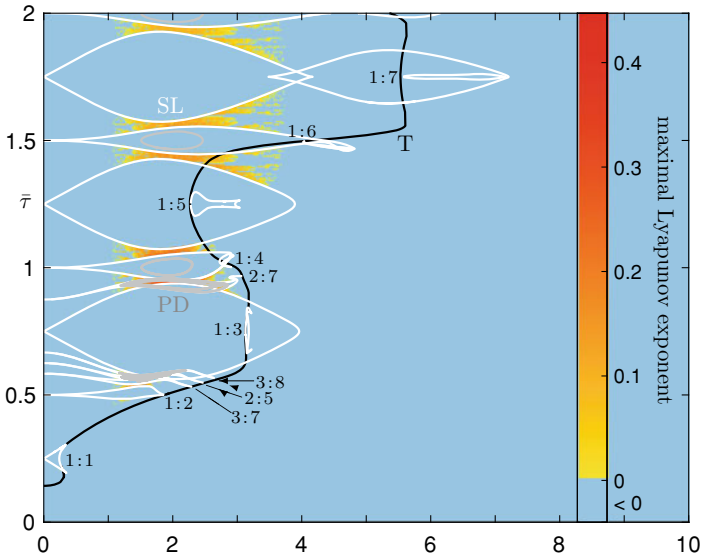

Fig. 7 Bifurcation set and maximal Lyapunov exponent of solutions in the (c, τ)-plane of (23) [corresponding to that of (28) with $\eta_c = 0$ and $\eta_e = 0$]. From Keane et al. (2019) © 2019 The Royal Society; reproduced with permission

for DDEs from Farmer (1982). It shows that a positive maximal Lyapunov exponent indicating chaotic dynamics is generally associated with period-doubling cascades and can be found only in small regions of the parameter plane. Note that some of these regions of positive maximal Lyapunov exponents can be found where no curves of period-doublings are shown; indeed, there exist infinitely many higher-order resonance tongues in between those we have shown, and they are expected to overlap. As demonstrated for a related DDE model by Keane et al. (2016), regions of chaotic dynamics may also be entered via intermittent transitions that are characterized by the sudden appearance of chaos at a saddle-node bifurcation (Pomeau and Manneville 1980). The conclusion to be drawn from Fig. 7 is that chaotic dynamics of (23) can be found, but only for quite specific and small ranges of c and τ. As we will show next, state dependence of the feedback loop changes this picture considerably.

4.3 State Dependence Due to Upwelling and Ocean Adjustment

It is important to recognize that taking a constant value for any delay in a DDE model is a modeling assumption that must be justified. The assumption of delays being constant is well justified in certain applications, such as machining (Insperger and Stépán 2000) and laser dynamics (Kane and Shore 2005). On the other hand,

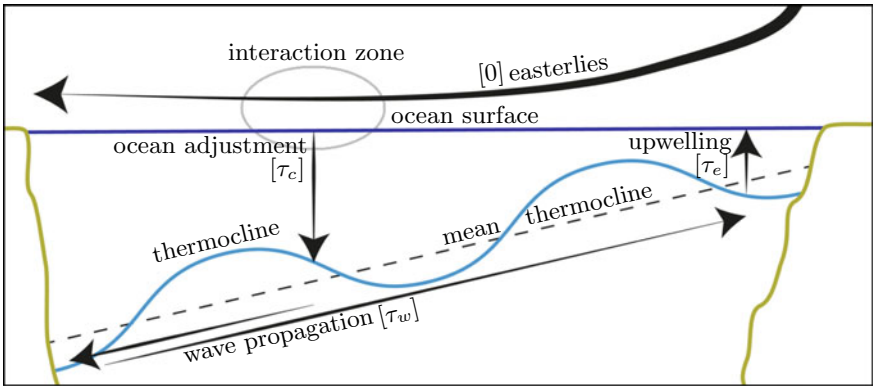

Fig. 8 Ocean adjustment and upwelling as sources of state-dependence in the ocean-atmosphere interaction in the central and eastern equatorial Pacific Ocean. From Keane et al. (2019) © 2019 The Royal Society; reproduced with permission

delays in many applications, and certainly in climate modeling, are definitely not constant. While the delays in conceptual DDE climate models have generally been taken to be constant (Keane et al. 2017), there are many reasons to suspect that this is not actually the case. Generally, the delay times will depend on the state of the system itself, which leads to DDE models with state-dependent delays. The main questions that need to be addressed from a more general modeling perspective are:

(1) When does state dependence arise from physical processes and what mathematical forms does it take?
(2) Does state dependence of delays have a significant effect on the observed dynamics of the respective DDE model?

Specifically for the GZT model (23), a non-constant delay in the negative feedback loop arises from the physics of the coupling of the ocean surface with the thermocline below. Figure 8 illustrates the heuristic argument for considering two terms with state dependence in the overall negative delay loop of ENSO, which are not described by and go beyond the original DAO mechanism; more details can be found in Keane et al. (2019). The horizontal direction represents longitude along the equator between the basin boundaries of the Pacific Ocean and the vertical direction represents depth below the ocean surface with the atmosphere above. The thermocline is sketched as a deviation from its mean, which is about 50 m deep in the East and 150 metres deep in the central equatorial Pacific Ocean. The black arrows represent the four components of the negative feedback loop. A positive perturbation in the thermocline depth $h(t)$ in the eastern equatorial Pacific increases the SST after an upwelling process with associated delay time τ_e. The easterly winds forming the atmospheric component that transports such a perturbation to the interaction zone in the central Pacific Ocean are considered fast and are modelled as instanteaneous (as is the case in all DAO models). The interaction zone is reasonably localized, and it is simplified to a point

in mathematical derivations of DAO models (Cane et al. 1990; Jin 1997). There is then a delay τ_c due to the coupling process known as ocean adjustment of the SST influencing the thermocline, which depends on the current thermocline depth $h(t)$. As in the GZT model without state dependence, Rossby waves then carry the signal to the western basin boundary and are reflected as Kelvin waves, which carry the signal back to the East with an associated delay time τ_w, which we assume here is constant. The total delay time associated with the negative feedback loop is therefore

$$\tau = \tau_e + \tau_c + \tau_w.$$

Here τ_e and τ_c are state dependent, that is, depend on the thermocline depth h. To determine their functional form we summarize briefly the modeling exercise in Keane et al. (2019), where more details can be found. It is convenient to define the constant part of the delay τ (with respect to the mean thermocline depth) as

$$\bar{\tau} = \bar{\tau}_e + \bar{\tau}_c + \tau_w.$$

Here $\bar{\tau}_e$ is the constant time it takes the signal to travel from the mean thermocline depth to the surface, and $\bar{\tau}_c$ is the constant time of the ocean adjustment at the central Pacific associated with the mean thermocline depth. From a correlation analysis of observational SST and thermocline depth data (Zelle et al. 2004) one concludes that the two constant delay times $\bar{\tau}_e$ and $\bar{\tau}_c$ for the long-term average of the thermocline are 2 weeks and 4 months, respectively, which gives the values $\bar{\tau}_e = 2/52$ and $\bar{\tau}_c = 4/12$ (in years) that we use from now on. Moreover, based on oceanic wave speeds calculated from TOPEX/POSEIDON satellite data in Boulanger and Menkes (1995), Chelton and Schlax (1996), realistic values of τ_w lie between 5.2 and 7.2 months, that is, in the range $[0.43, 0.6]$ when scaled to years. Hence, one obtains the estimated range $[0.80, 0.97]$ for the constant part $\bar{\tau}$ of the overall delay.

The upwelling delay can be modelled by

$$\tau_e = \bar{\tau}_e + \eta_e h(t - \bar{\tau}), \tag{27}$$

where η_e is the inverse of the upwelling speed. Note that the state-dependent term is itself subject to a delay because the thermocline depth signal that ultimately returns to the eastern equatorial Pacific at time t began its journey at the thermocline one feedback cycle ago; in (27) this implicitly defined state dependence is resolved by considering the first-order approximation given by the constant part $\bar{\tau}$. Maximum deviations in the thermocline depth in the eastern equatorial Pacific Ocean are about 50 metres (Harrison and Vecchi 2001) and it follows, with time measures in years, that the nominal value of the inverse upwelling speed is $\eta_e \approx 2/52 \approx 0.04$.

The dependence of the delay time τ_c due to mass transport between ocean surface and the thermocline can be modelled by

$$\tau_c = \bar{\tau}_c + \eta_c h(t),$$

where η_c is the ocean-adjustment speed. Since the maximum deviations in thermocline depth in the central equatorial Pacific Ocean of 150 metres corresponds to about one third of its mean depth, we obtain similarly the nominal value $\eta_c \approx (4/3)/12 \approx 0.11$ (in units of years per meter).

4.4 The GZT Model With Upwelling and Ocean Adjustment

The resulting state-dependent GZT ENSO DDE model we consider in what follows is given by (23) with the overall state-dependent delay

$$\tau(h) = \bar{\tau} + \eta_e h(t - \bar{\tau}) + \eta_c h(t), \tag{28}$$

which has the additional parameters η_e and η_c that allow us to 'switch on' the two types of state dependence. Clearly, for $\eta_e = \eta_c = 0$ this model reduces to the constant-delay GZT DDE. When implementing the state-dependent delay in DDE-BIFTOOL, the expression for the right-hand side is very similar to that given in (26), but the parameter vector is changed to $p = (p_1, \ldots, p_6) = (b, c, \kappa, \bar{\tau}, \eta_c, \eta_e) \in \mathbb{R}^6$, the number of delays is specified as $d = 2$, and the delays are given as functions:

$$\begin{aligned}
\tau_1^f(x^0, p) &= p_4, \\
\tau_2^f(x^0, x^1, p) &= p_4 + p_5 x_1^0 + p_6 x_1^1, \\
f(x^0, x^1, x^2, p) &= \begin{bmatrix} -p_1 \tanh[p_3 x_1^2] + p_2 x_2^0 \\ x_2^0 - 2\pi x_3^0 - x_2^0((x_2^0)^2 + (x_3^0)^2) \\ x_3^0 + 2\pi x_2^0 - x_3^0((x_2^0)^2 + (x_3^0)^2) \end{bmatrix}.
\end{aligned}$$

Note that the delayed argument appearing in f is now x_1^2, instead of x_1^1 as was the case in (26). The question is what effects the two types of state dependence have on the observed dynamics as represented by the bifurcation set in the $(c, \bar{\tau})$-plane. This was considered by Keane et al. (2019) for ranges of η_e and η_c up to $\eta_e = 0.08$ and $\eta_c = 0.22$, that is, twice their nominal values. It turns out that, within the ranges of the parameters considered, state dependence of τ_e alone has a negligible effect on the bifurcation set. State dependence of τ_c, on the other hand, has a significant impact on the bifurcation set in the $(c, \bar{\tau})$-plane, featuring considerably increased and more overlapping resonance regions. Surprisingly, for $0 < \tau_c$, state dependence of τ_e does have a definite influence on the bifurcation set, namely that of increasing the observed complexity even further.

As an example of the effect of both types of state dependence, Fig. 9 shows the bifurcation set and maximal Lyapunov exponent of solutions in the $(c, \bar{\tau})$-plane of (23) with (28) for the case where the upwelling η_e and the ocean adjustment η_c are at the maximum of their considered ranges at $\eta_e = 0.08$ and $\eta_c = 0.22$, respectively. As for $\eta_e = \eta_c = 0$ in Fig. 7, shown in Fig. 9 are curves SL, PD and T of saddle-

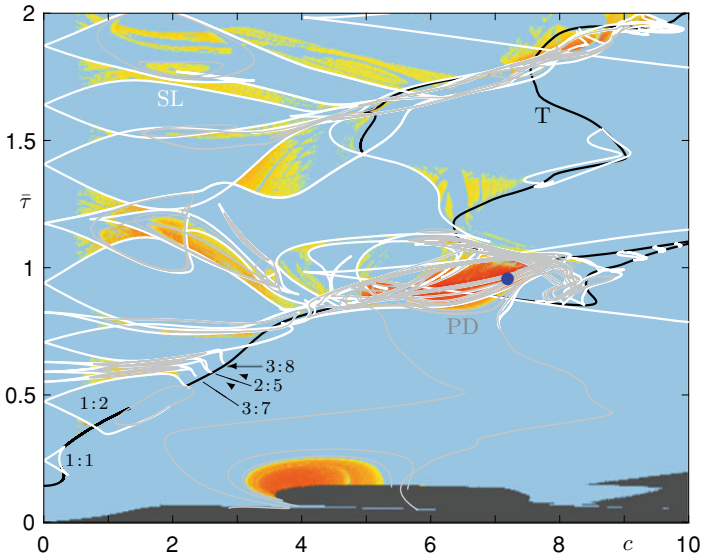

Fig. 9 Bifurcation set and maximal Lyapunov exponent of solutions in the $(c, \bar{\tau})$-plane of (23) with (28) for $\eta_e = 0.08$ and $\eta_c = 0.22$; see Fig. 7 for the color map. The dot indicates the parameter point for the time series in Fig. 10. From Keane et al. (2019) © 2019 The Royal Society; reproduced with permission

node of periodic orbits, period-doubling and torus bifurcations, respectively. They were computed with DDE-BIFTOOL, thus, demonstrating that such computations can be performed readily also for DDEs that feature state dependence. The maximal Lyapunov exponent of solutions was computed again for an upsweep of c with the algorithm for DDEs from Farmer (1982). Note that in the dark grey region for low values of $\bar{\tau}$ the delay becomes negative during the integration, so that a sufficiently long time series to determine the Lyapunov exponent cannot be found. Similarly, some curves of period-doubling bifurcations stop in this region because the delay becomes negative along the respective periodic orbit during the continuation.

Comparing Fig. 9 with Fig. 7 clearly drives home the point that state dependence has a large effect on the bifurcation set and, hence, on the observable dynamics of the GZT model (23). In Fig. 9 the bifurcation set now extends substantially further into the region of large forcing c: the curve T of torus bifurcation has moved, as have resonance regions associated with it. In particular, there is now a cluster of overlapping resonance regions near $\bar{\tau} = 1$, that is, in the physically relevant range of the $(c, \bar{\tau})$-plane. Notice that this cluster is associated with large positive Lyapunov exponents. More generally, state dependence results here in considerably more and larger regions where chaotic dynamics can be found. Interestingly, there is also a large region of chaotic dynamics for very low values of $\bar{\tau}$, near the boundary where the delay becomes negative.

Clearly, introducing a physically motivated state-dependent delay time changes the overall observed dynamics of the GZT model. We finish by demonstrating that this model modification leads to dynamics that represents realistic aspects of the ENSO system, more so than those found in the absence of state dependence. Namely, in the constant delay case, irregular (chaotic) behavior could only be found for small pockets of the $(c, \bar{\tau})$-plane and, as such, could not be considered a prominent feature of the model behavior. In the presence of state dependence due to upwelling and ocean adjustment, on the other hand, this type of behavior is more prominent, especially in the physically relevant cluster of period-doublings near $\bar{\tau} = 1$. The blue dot in this cluster indicates the parameter point $(c, \bar{\tau}) = (7.2, 0.95)$, and Fig. 10 shows the corresponding times series and power spectra in direct comparison with those for the measured Nino3 index. This data is the spatially averaged SST over 5°N–5°S and 150°W–90°W as derived from the Optimum Interpolation SST V2 data by the National Oceanic and Atmospheric Administration in Boulder, Colorado. The Nino3 time series, which was linearly detrended, is shown in Fig. 10a1. Prominent in the time series data is the strong annual forcing, which is represented by the large peak at 1 year in the power spectrum in panel (a2), which was calculated by using the Welch method with windows of length 15 years and overlapping across 12 years. Moreover, the Nino3 time series shows characteristic larger maxima, that is, El Niño events, about every 3–7 years, which give rise to the distinct but broad peak in the power spectrum that is centred near the frequency of about $1/3.5$ years. Indeed, there is clearly a high degree of variability in the timing of larger maxima and, as we checked, they tend to be seasonally locked. As row (b) of Fig. 10 shows, time series and power spectrum of the thermocline deviation h of the GZT model (23) with delays given by (28) and $\eta_e = 0.08$ and $\eta_c = 0.22$ at $(c, \bar{\tau}) = (7.2, 0.95)$ also possess these important characteristics of ENSO. The solution from which the time series is derived evolves on a chaotic attractor that lies at the intersection of several resonance tongues. The times series in panel (b1) clearly lacks certain aspects of the data in panel (a1), and it is not obvious how exactly the thermocline deviation h as described by the rather simple conceptual GZT model translates to an observable such as Nino3. Nevertheless, the time series of h features irregularity in the form of relatively large peaks that occur every 2–7 years, with a similar broad peak centered near the frequency of about $1/2.5$ years as well as seasonal locking, which is very robust with respect to the choice of parameters. The number and distribution of large maxima, on the other hand, depends on where the parameters point is chosen to lie in the regions of overlapping $p:q$ resonance tongues. Moreover, the relative strengths between the peaks in the power spectrum, representing both seasonal and El Niño time scales can be influenced by the choice of the seasonal forcing strength c. Overall, we conclude that solutions with fundamental ENSO characteristics can be found in appropriate regions of parameter space of the state-dependent GZT model as considered here.

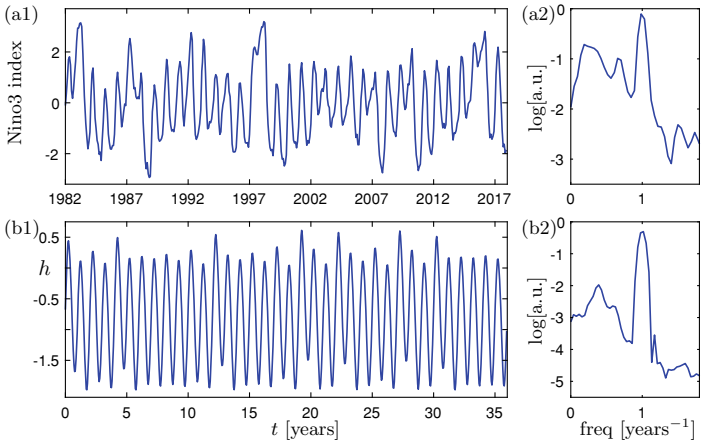

Fig. 10 Time series of the Nino3 index (**a1**) obtained from the observational data set NOAA Optimum Interpolation SST V2 (Jan. 1982–Dec. 2017) by linear detrending and the corresponding power spectrum (**a2**); and times series (**b1**) and corresponding power spectrum (**b2**) for the attractor of (23) with (28) for $\eta_e = 0.08$ and $\eta_c = 0.22$ at the parameter point $(c, \bar{\tau}) = (7.2, 0.95)$ indicated in Fig. 9. Data for row (**a**) is provided by the Physical Sciences Division, Earth System Research Laboratory, NOAA, Boulder, Colorado. From Keane et al. (2019) © 2019 The Royal Society; reproduced with permission

5 Resonance Phenomena in a Scalar DDE With Two State-Dependent Delays

The previous section demonstrated that state dependence of delays can have a serious impact on the observed dynamics of a given DDE. On the other hand, the GZT model for ENSO features complicated dynamics already when the delays are constant. As we will discuss now, state dependence of delays alone can create complicated nonlinear dynamics, even when the constant-delay DDE has only trivial, linear dynamics. This surprising result was obtained in Calleja et al. (2017) for the scalar DDE

$$u'(t) = -\gamma u(t) - \kappa_1 u(t - a_1 - c_1 u(t)) - \kappa_2 u(t - a_2 - c_2 u(t)). \tag{29}$$

Here, $0 < \gamma$ is the linear decay rate and $0 \le \kappa_1, \kappa_2$ are the strengths of the two negative feedback loops with the constant delay times $0 < a_1, a_2$ and linear state dependence of strengths $0 \le c_1, c_2$. For $\kappa_1 = \kappa_2 = 0$, this system is simply a linear scalar equation whose solutions decay exponentially to the origin with rate $0 < \gamma$. For $0 < \kappa_1, \kappa_2$, on the other hand, (29) is a DDE with two negative feedback loops. For $c_1 = c_2 = 0$ this DDE is linear with the two fixed delays a_1 and a_2 and all trajectories of (29) decay to the origin or blow up to infinity, depending on the values of γ, κ_1 and κ_2; see Bellman and Cooke (1963), Hale (1977), Hale and Verduyn Lunel (1993). In other words, the dynamics of the system without state dependence in the delay terms is indeed trivial.

The situation is very different with state dependence, that is, for $0 < c_1, c_2$, in which case (29) may show a wide range of behaviors. The two-delay state-dependent DDE (29) was introduced by Humphries et al. (2012). It is a generalisation of the single-delay state-dependent DDE, corresponding to setting $\kappa_2 = 0$, which was first introduced in a singularly perturbed form as an example problem in Mallet-Paret et al. (1994) and considered extensively in Mallet-Paret and Nussbaum (2011a). A singularly perturbed version of the two-delay state-dependent DDE (29) was studied by Humphries et al. (2016) and Kozyreff and Erneux (2013). Specifically, solutions near the singular Hopf bifurcations were considered by Kozyreff and Erneux (2013), while large amplitude singular solutions are constructed and studied by Humphries et al. (2016). We report here on the work by Calleja et al. (2017) and consider (29) for $a_1 < a_2$ without loss of generality. It was shown by Humphries et al. (2012) that the state-dependent delays can never become advanced when $\kappa_2 < \gamma$, which we assume from now on. Hence, for any Lipschitz continuous initial condition the initial value problem given by (29) has a unique solution. Moreover, Humphries et al. (2012) showed that state dependence of the delay terms changes the dynamics in an essential way. In particular, although it is only linear, the state dependence of the delays for $0 < c_1, c_2$ is responsible for nonlinearity in the system, and the dynamics of the DDE (29) is no longer linear. Given that it has two feedback loops, the system is, colloquially speaking, potentially at least as complicated as two coupled damped nonlinear oscillators.

This realization was the starting point of the extensive bifurcation analysis of the two delay state-dependent DDE (29) by Calleja et al. (2017), where more details can be found. The first step is to bring (29) into the form required by DDE-BIFTOOL. To this end, one has to specify the number of delays, $d = 2$, and define

$$\begin{aligned} \tau_1^f(x^0, p) &= a_1 + c_1 x^0, \\ \tau_2^f(x^0, x^1, p) &= a_2 + c_2 x^0, \\ f(x^0, x^1, x^2, p) &= -\gamma x^0 - \kappa_1 x^1 - \kappa_2 x^2. \end{aligned}$$

Note that here the physical space is one-dimensional since $x(t) \in \mathbb{R}^1$, $M = 1$ and the parameter vector is $p = (p_1, \ldots, p_7) = (\gamma, \kappa_1, \kappa_2, a_1, a_2, c_1, c_2) \in \mathbb{R}^7$.

5.1 *Hopf-Hopf Bifurcation as an Organizing Center*

We focus here on resonance phenomena associated with a point HH_1, where a Hopf-Hopf bifurcation occurs. As in Humphries et al. (2012), Calleja et al. (2017), we fix the parameters of (29) to $\gamma = 4.75$, $a_1 = 1.3$, $a_2 = 6$, and $c_1 = c_2 = 1$. Thus, parameters κ_1 and κ_2 are bifurcation parameters, where we restrict to $\kappa_2 \in (0, 4.75)$ so that indeed $\kappa_2 < \gamma$. The bifurcation diagram of (29) in the (κ_1, κ_2)-plane is shown in Fig. 11; here row (a) focuses on the immediate vicinity of the point HH_1, while

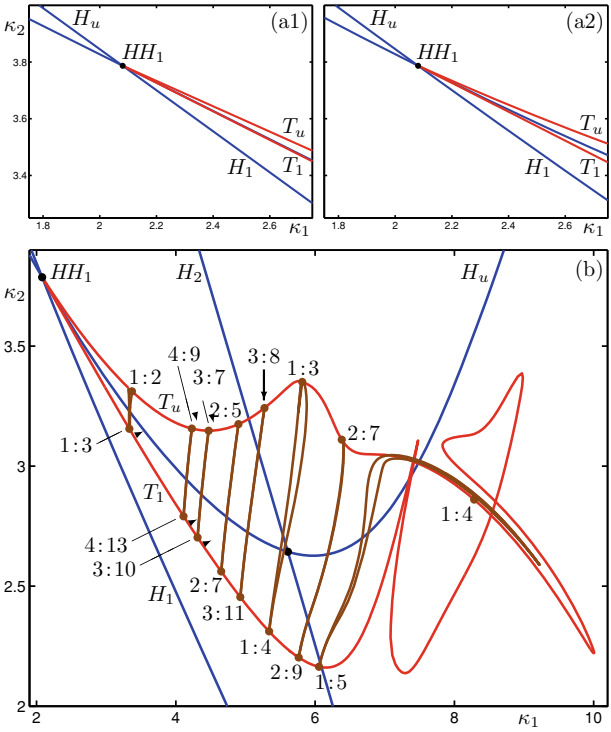

Fig. 11 Local torus bifurcation curves T_1 and T_u of (29) emerging from a Hopf-Hopf bifurcation point HH_1 at the intersection of curves H_1 and H_u, as computed from the normal form (**a1**) and by numerical continuation (**a2**). The bifurcation diagram in the (κ_1, κ_2)-plane (**b**) shows resonance tongues connecting different points of resonance on T_1 and T_u, which are actually part of a single closed curve of torus bifurcation. From Calleja et al. (2017) © 2017 Society for Industrial and Applied Mathematics; reproduced with permission

panel (b) shows the relevant bifurcation set associated with HH_1 over a wider range of κ_1 and κ_2.

An important contribution of Calleja et al. (2017) is the computation of the third-order normal form of the state-dependent DDE in the form of an ordinary differential equation (ODE) on the center manifold near Hopf-Hopf points; see, for example, Guckenheimer and Holmes (1983), Kuznetsov (2013) for the respective ODE normal forms. This is achieved by expanding the state dependence to derive a DDE with terms up to a given order and with only constant delays. This constant-delay DDE can then be reduced to the required four-dimensional ODE normal form with standard techniques; see Bélair and Campbell (1994), Guo and Wu (2013), Wage (2014). Computation with DDE-BIFTOOL shows that the point HH_1 lies at $(\kappa_1, \kappa_2) = (2.08092, 3.78680)$ where the Hopf bifurcation curves H_1 and H_u intersect; it features a double pair of purely complex conjugate eigenvalues with frequencies (imaginary parts) $\omega_1 = 2.48710$ and $\omega_2 = 1.58215$. The normal form

computation at this Hopf-Hopf point, details of which can be found in Calleja et al. (2017), shows that HH_1 is subcase III of what is referred to as the simple case in Kuznetsov (2013). This means that there are two curves of torus (or Neimark-Sacker) bifurcations emerging from the codimension-two Hopf-Hopf point. When the normal form coordinates are transformed back into the (κ_1, κ_2)-plane, one obtains the bifurcation diagram shown in Fig. 11a1, featuring the curves H_1 and H_u and the torus bifurcation curves T_1 and T_u. Note that all curves are straight lines, whose slopes are determined by the respective normal form coefficient. The bifurcation diagram in Fig. 11a2 shows the same bifurcation curves H_1, H_u, T_1 and T_u but now computed for (29) by continuation with DDE-BIFTOOL. Note that these curves are no longer straight lines. Comparison with panel (a1) shows that the nature, order and slopes of the respective bifurcation curves is indeed as determined by the normal form computation, which strongly supports the correctness of the expansion method used to derive the Hopf-Hopf normal form of the full state-dependent DDE (29). This approach has been extended by Sieber (2017) to all codimension-two bifurcations of steady-states that are defined by conditions on the linearization. Hence, normal form calculations for these codimension-two bifurcations, which had been incorporated into the capabilities of the package DDE-BIFTOOL for constant-delay DDEs by Wage (2014), are now also available for state-dependent DDEs; see Sieber et al. (2015).

Figure 11b shows that the local curves T_1 and T_u, when continued beyond a neighborhood of the Hopf-Hopf point HH_1, actually form a single curve in the (κ_1, κ_2)-plane. As expected from theory, along the branches T_1 and T_u of torus bifurcations one finds points of $p:q$ resonance, which we include for $q \leq 13$. At each such point the Floquet multiplier is a rational multiple of 2π and a resonance tongue emerges where the dynamics on the torus is $p:q$ locked. For parameter points that do not lie in a resonance tongue the rotation number is an irrational multiple α of 2π and the dynamics of the torus is quasiperiodic. In either case, the bifurcating torus is normally hyperbolic, and hence smooth, near the respective torus bifurcation. Each resonance region is bounded locally near the point of $p:q$ resonance by a pair of saddle-node bifurcations of periodic orbit. Tori with fixed irrational rotation number α, on the other hand, lie on smooth curves that connect to the point on the torus bifurcation curve with the corresponding Floquet multiplier. Also shown in Fig. 11b are the bounding curves of saddle-node bifurcations for the resonance points with $q \leq 13$. They have been found by identifying, by means of numerical integration, stable locked periodic orbits near the respective branch of torus bifurcation; this is possible because the tori bifurcating from T_1 and T_u are actually attracting (which is in agreement with the normal form calculation). The subsequent continuation of these with DDE-BIFTOOL in κ_1 identifies the pair of saddle-node bifurcations, at two specific values of κ_2, that form the boundary of the resonance tongue. Once these two points of saddle-node bifurcations of periodic orbits have been found, they can be continued in both κ_1 and κ_2 towards the curves T_1 and T_u to obtain the respective curves shown in the (κ_1, κ_2)-plane. Note that the gap between the two bounding curves of the $p:q$ resonance tongue becomes smaller for increasing q.

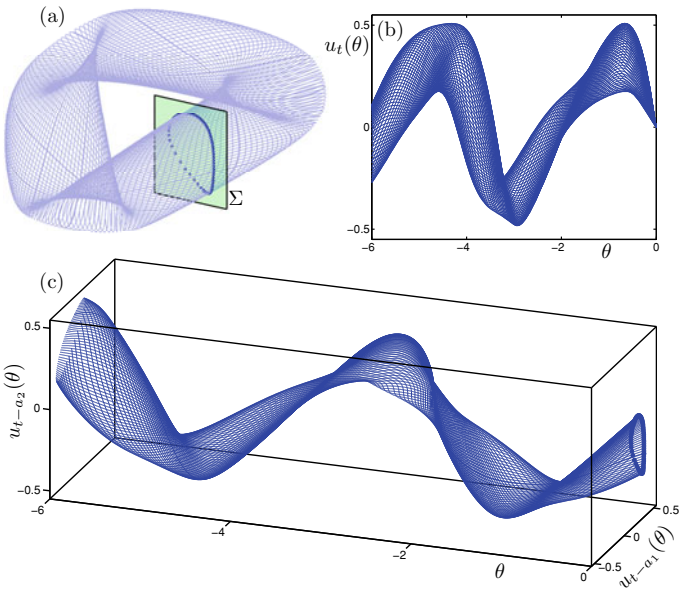

Fig. 12 Normally hyperbolic quasiperiodic torus of (29) for $\kappa_1 = 4.44$ and $\kappa_2 = 3.0$ in projection onto $(u(t), u(t-a_1), u(t-a_2))$-space (**a**), represented by a single trajectory (light blue) together with the Poincaré trace (blue dots) on the (projected) section Σ (green); also shown are the corresponding function segments represented by $u_t(\theta)$ (**b**) and by $(u_{t-a_1}(\theta), u_{t-a_2}(\theta))$ (**c**). From Calleja et al. (2017) © 2017 Society for Industrial and Applied Mathematics; reproduced with permission

5.2 *Finding and Representing Smooth Invariant Tori*

As we show now, invariant tori of DDEs can also be computed, including when the delay is state dependent; see Krauskopf and Green (2003), Green et al. (2003), Calleja et al. (2017). This is quite straightforward for an attracting quasiperiodic torus, because it is densely filled by any trajectory on it. Such a trajectory can be obtained readily by numerical integration from an initial condition sufficiently near the torus, after transients have settled down. Such a torus is a smooth two-dimensional submanifold that lives in the infinite-dimensional phase space C of the DDE. Therefore, the question is how to represent it via a suitable low-dimensional projection. Figure 12 shows with the example of the smooth attracting quasiperiodic torus of (29) for $\kappa_1 = 4.44$ and $\kappa_2 = 3.0$ how this can be achieved. Panel (a) shows the computed long trajectory on the torus in the natural and convenient projection onto the three-dimensional $(u(t), u(t-a_1), u(t-a_2))$-space of (29). Also shown is the intersection set of the trajectory on the torus with the shown section Σ, which forms a smooth invariant curve as is expected for a quasiperiodic torus.

Note that the representation of the torus in Fig. 12a looks very much like a two-dimensional smooth torus in a three-dimensional phase space of an ODE, with an associated image of the dynamics of the Poincaré map in the two-dimensional section

Σ. However, it is important to recognize that this image is a projection from the infinite-dimensional phase space C. In particular, it is an interesting question how best to define a Poincaré map for a DDE. In general terms, given a section Σ of codimension one in the phase space C that is transverse in some region of interest to the (semi)flow Φ^t generated by the DDE, the (local) Poincaré map P is defined as

$$\begin{aligned} P_\Sigma : \ \Sigma &\to \Sigma, \\ q &\mapsto \Phi^{t_q}(q)\,, \end{aligned}$$

where $t_q > 0$ is the return time to Σ. The main issue from a practical perspective is how to define the section Σ. When the DDE has a physical space $\mathbb{R}^n$ of sufficient dimension (at least three), then it is convenient to consider a codimension-one section $\Sigma \subset \mathbb{R}^n$; requiring that the headpoint $q(0)$ of the point q lies in Σ induces a codimension-one section in the infinite dimensional phase space C, which we also refer to as Σ for simplicity; see Krauskopf and Green (2003). Moreover, there is a natural projection onto $\mathbb{R}^n$ and just considering the headpoints in the section $\Sigma \subset \mathbb{R}^n$ gives what we refer to as the finite-dimensional Poincaré trace of the dynamics. Unfortunately, this approach is not workable for (29) because it is a scalar DDE and, moreover, state dependent. Instead, we make use of the fact that all periodic and quasi-periodic orbits repeatedly cross $\{u = 0\} \subset \mathbb{R}$ when the parameters are all positive as considered here; therefore, it is natural to use this condition for defining the Poincaré section as

$$\Sigma = \{q \in C : q(0) = 0\}. \tag{30}$$

Clearly, the section Σ is infinite dimensional itself, and the local Poincaré map P_Σ on Σ is defined as the map that takes a downward transversal crossing of zero (where $q(0) = 0$ with $q'(0) < 0$) to the next such crossing. The Poincaré trace in the $u(t - a_1), u(t - a_2))$-plane, which is the projection of the infinite-dimensional Σ from (30), is obtained from the projection onto $(u(t), u(t - a_1), u(t - a_2))$-space simply by also requiring that $u(t) = 0$. This projected section, which we again refer to as Σ for convenience, is shown in Fig. 12a.

The underlying projection onto $(u(t), u(t - a_1), u(t - a_2))$-space generalizes an idea of Mackey and Glass (1977), who were the first to project solutions of DDEs into finite dimensions by plotting values of $u(t - \tau)$ against $u(t)$ for a single-delay DDE. Defining the section Σ for (29) by $q(0) = 0$ has the advantage that the two delays are exactly a_1 and a_2, that is, constant. Figure 12b, c illustrates this by showing the function segments of all the points that generate the Poincaré trace on Σ; they are represented by $u_t(\theta)$ in panel (b) and by $(u_{t-a_1}(\theta), u_{t-a_2}(\theta))$ in panel (c), both as functions of the argument θ, which runs over the interval $[-6, 0]$ since $a_1 = a_2 = 6$. In particular, Fig. 12c clearly shows the "history tails" over the time interval $[-6, 0]$ associated with headpoints that form the trace in (the two-dimensional projection of) Σ (given by $\theta = 0$); see also Krauskopf and Green (2003).

Figure 13 shows an example of an attracting smooth invariant torus with locked dynamics; namely this example for $\kappa_1 = 5.405$ and $\kappa_2 = 2.45$ is from the 1:4 reso-

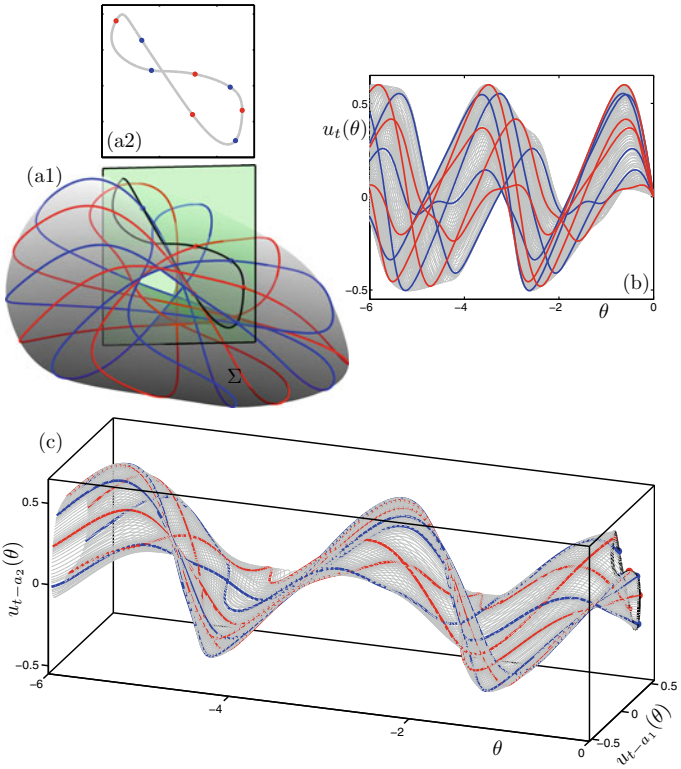

Fig. 13 Normally hyperbolic 1:4 phase-locked torus of (29) for $\kappa_1 = 5.405$ and $\kappa_2 = 2.45$ in projection onto $(u(t), u(t-a_1), u(t-a_2))$-space (**a1**), represented by the stable periodic orbit (blue), the saddle periodic orbit (red), and its unstable manifold (grey curves), together with the Poincaré trace on the (projected) section Σ (green) (**a2**); also shown are the corresponding function segments represented by $u_t(\theta)$ (**b**) and by $(u_{t-a_1}(\theta), u_{t-a_2}(\theta))$ (**c**). From Calleja et al. (2017) © 2017 Society for Industrial and Applied Mathematics; reproduced with permission

nance tongue. Hence, there are a stable periodic orbit and a saddle periodic periodic orbit that both form a 1:4 torus knot. The presentation is as for the quasi-periodic torus in Fig. 12. Panel (a1) of Fig. 13 shows the shows the torus rendered as a surface in projection onto $(u(t), u(t-a_1), u(t-a_2))$-space, together with the (projection of the) section Σ. The Poincaré trace in the $(u(t-a_1), u(t-a_2))$-plane, that is, the intersection set of the torus with Σ, is shown on its own in panel (a2). The associated function segments or history tails are shown in Fig. 13c, d as represented by $u_t(\theta)$ and by $(u_{t-a_1}(\theta), u_{t-a_2}(\theta))$, respectively, for $\theta \in [-6, 0]$. The locked dynamics on the torus as represented in Fig. 13a is again very reminiscent of what one would expect to find for a torus of a three-dimensional ODE: its two-dimensional Poincaré trace in panel (a2) clearly shows a single smooth curve with four points of a stable period-four orbit and four points of an unstable period-four orbit; see Fig. 13a2. Notice that

the invariant curve has a point of self-intersection; this is due to projection and a reminder that we are dealing with a DDE with an infinite-dimensional phase space.

As opposed to the case of a quasiperiodic torus, a torus with locked dynamics cannot be found by numerical integration alone. Indeed, any initial condition will, after transients have settled down, trace out only the attracting periodic orbit. The torus on which it lies can be computed as follows. Continuation of the stable periodic orbit in the parameter κ_1 gives, after a fold or saddle-node bifurcation of periodic orbits, the coexisting saddle periodic orbit for the initial value of $\kappa_1 = 5.405$. As theory predicts, this saddle peridic orbit has one unstable Floquet multiplier and, hence, one unstable eigenfunction, which we extracted from the DDE-BIFTOOL data; see also Green et al. (2003). We then used the eigenfunction to define two initial functions in the local unstable manifold of the periodic orbit, one on each side of and sufficiently close to the saddle periodic orbit. Trajectory segments that lie on the unstable manifold were then found with numerical integration from initial functions along the unstable eigenfunction; a selection of them is shown in Fig. 13b, c. The torus was rendered as a surface in $(u(t), u(t-a_1), u(t-a_2))$-space in panel (a1) and as an invariant curve in the $(u(t-a_1), u(t-a_2))$-plane in panel (a2) by ordering a suitable selection of trajectory segments from the Poincaré section back to itself.

5.3 *Locked Nonsmooth Invariant Tori*

As was already mentioned in Sect. 5.1, any computed pair of saddle-node bifurcation curves shown in Fig. 11b emerges at a resonance point on the torus bifurcation curve T_u and connects to a point of resonance on the torus bifurcation curve T_1 (or vice versa). More generally, this is evidence for the observation that, near the Hopf-Hopf point HH_1, any $p:q$ resonance point on the upper branch T_u is connected by a pair of saddle-node bifurcation curves with a $p:(p+q)$ resonance point on the lower branch T_1. In the region of locked dynamics bounded by such a pair one, hence, finds $p:q$ locked dynamics on a smooth invariant torus near T_u and $p:(p+q)$ locked dynamics on a smooth invariant torus near T_1. Since a $p:q$ torus knot and a $p:(p+q)$ torus knot cannot exist on one and the same smooth torus for topological reasons, the torus inside the respective resonance tongue cannot be smooth throughout in the transition inside the tongue from the $p:q$ to the $p:(p+q)$ resonance point (or vice versa). On the other hand, without the requirement that the periodic orbit lies on an invariant two-dimensional torus, it is possible to transform a periodic orbit with q loops into one with $(p+q)$ loops; in other words, there is indeed no topological obstruction for the bounding curves of saddle-node bifurcations of periodic orbits to connect in the way we found in Fig. 11b.

Figure 14 shows that it is possible to perform computations that show how an invariant locked torus of a DDE loses its smoothness and bifurcates further. The key idea here is to compute the one-dimensional unstable manifold in the Poincaré trace that is associated with a saddle-periodic orbit with a single unstable Floquet multiplier. In other words, the approach we used to compute the smooth 1:4 phase-

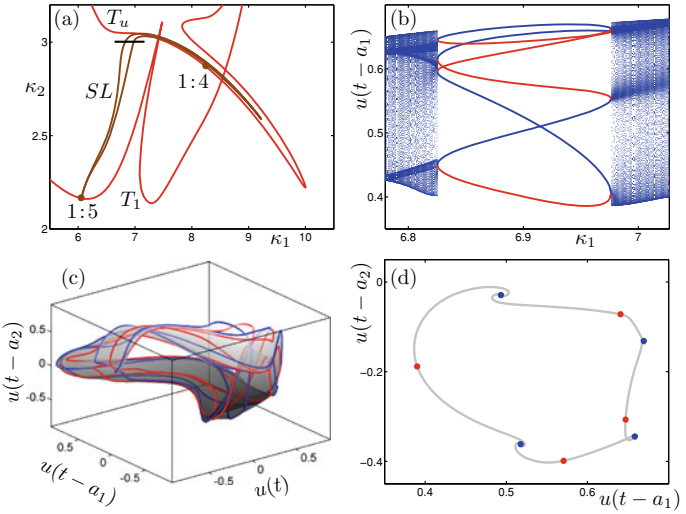

Fig. 14 The resonance tongue in the (κ_1, κ_2)-plane of (29) that connects the 1:4 resonance on T_u with the 1:5 resonance on T_1 (**a**); the one-parameter bifurcation diagram in κ_1 for fixed $\kappa_2 = 3.0$ (**b**) showing the values of $u(t - a_1)$ of the Poincaré traces of stable (blue) and saddle (red) periodic orbits (red) inside the resonance tongue, and of other solutions on tori outside the resonance tongue; the 1:4 phase-locked torus-like object (grey) for $\kappa_1 = 6.93$ with the stable and saddle periodic orbits in projection onto $(u(t), u(t - a_1), u(t - a_2))$-space (**c**); and its Poincaré trace in the $(u(t - a_1), u(t - a_2))$-plane (**d**). From Calleja et al. (2017) © 2017 Society for Industrial and Applied Mathematics; reproduced with permission

locked torus in Fig. 13 also works when the torus is no longer smooth; the only requirement is that the saddle-periodic orbit still exists and has a single unstable Floquet multiplier; see also Krauskopf and Green (2003), Green et al. (2003), Calleja et al. (2017), Keane and Krauskopf (2018). Panel (a) of Fig. 14 shows the resonance tongue in the (κ_1, κ_2)-plane that connects the 1:4 resonance on T_u with the 1:5 resonance on T_1. The line segment at $\kappa_2 = 3.0$ indicates the κ_1-range of the one-parameter bifurcation diagram shown in panel (b). Specifically, shown is the value of $u(t - a_1)$ when $u(t) = 0$, that is, the first component of the $(u(t - a_1), u(t - a_1))$-plane of the Poincaré trace. Inside the resonance tongue we find 1:4 locking: there are four branches of the stable periodic orbit and four branches of the saddle periodic orbit, which meet and disappear in saddle-node bifurcations; these branches were found with DDE-BIFTOOL by continuation in κ_1, and this computation also confirms that the saddle periodic orbit has a single unstable Floquet multiplier throughout the κ_1-range of the resonance tongue when $\kappa_2 = 3.0$. Outside the resonance tongue we find quasi-periodic dynamics or dynamics of very high period; it was identified by numerical integration and is represented by many points in the Poincaré trace whose $u(t - a_1)$-values effectively fill out intervals.

Panels (c) and (d) of Fig. 14 show the result of computing the unstable manifold of the saddle periodic orbit for $\kappa_1 = 6.93$ with the approach from Sect. 5.2. While this

is hard to see in the projection onto $(u(t), u(t-a_1), u(t-a_1))$-space in Fig. 14c, the Poincaré trace in the $(u(t-a_1), u(t-a_1))$-plane in panel (d) clearly shows that the one-dimensional unstable manifold of the saddle periodic orbit now spirals around the stable periodic orbit. This means that the stable periodic orbit has two dominant Floquet multipliers that are complex conjugate, which is confirmed by the computation of the Floquet multipliers during the continuation of the periodic orbits with DDE-BIFTOOL. The attracting periodic orbit on the torus developing a pair of complex conjugate Floquet multiplier is a mechanism for the loss of normal hyperbolicity of an invariant torus that is known from ODE theory (Aronson et al. 1982). As Fig. 14c, d shows, there is still a continuous two-dimensional torus, formed by the closure of this unstable manifold, but this torus is indeed no longer smooth.

Further bifurcations may occur that change the nature of the invariant set in the Poincaré trace, including homoclinic and heteroclinic tangencies of unstable manifold of saddle periodic orbits. This happens, for example, when the 1 : 4 resonance tongue is crossed again at $\kappa_2 = 3.0$ for larger values of κ_1; see Calleja et al. (2017) for the details. Other examples where such global bifurcations in DDEs have been identified via unstable manifold computations are the transition to chaos in a laser with phase-conjugate feedback in Krauskopf and Green (2003), Green et al. (2003) and the break-up of a torus in the GZT model of Sect. 4.2 due to the transition through a bifurcation structure known as a Chenciner bubble in Keane and Krauskopf (2018).

6 Conclusions and Outlook

The case studies of the GZT ENSO model and of the DDE with two state-dependent delays we presented show that core tasks of numerical bifurcation analysis can be performed for DDEs with finitely many discrete delays, even when the delays are state dependent. More specifically, the routines that are implemented within the package DDE-BIFTOOL include the detection and continuation of equilibria, periodic orbits and their bifurcations of codimension one, of codimension-one connecting orbits between equilibria, as well as the computation of normal forms of bifurcations of equilibria up to including codimension two. This suite of tools puts the present capabilities practically at the same level that is available for ODEs. In other words, the numerical bifurcation analysis of DDEs, whether they arise in applications or in a theory context, is now perfectly feasible.

One area where the capabilities for DDEs still lag behind that for ODEs is the computation of normal forms for bifurcation of periodic orbits. The approach to normal form analysis designed by Dhooge et al. (2003) for MATCONT and extended by Bosschaert et al. (2020) to equilibria of DDEs with constant delays is, in principle, applicable also to periodic orbits and their bifurcations. However, there remain some technical difficulties. For example, in case delays are bifurcation parameters or are state dependent, the computation of normal form coefficients may involve the computation of high-order time derivatives of the piecewise polynomials representing the solution.

We considered here chiefly DDEs in standard form with a finite number of discrete delays. For this class the discussed tools for the numerical bifurcation analysis are on very firm ground theoretically when the delays are constant. On the other hand, some present capabilities of the numerical methods and the software assume properties of the underlying DDE that have not yet been proven rigorously when the delays are state dependent. For example, convergence of the collocation schemes used for the representing periodic orbits has been proved for standard DDE with constant delays, but remains an open question when the delays are part of the unknowns or state-dependent. Case studies such as the ones presented here clearly suggest that collocation 'works well' also in such wider circumstances; moreover, the techniques introduced by Andó and Breda (2020) look promising as a tool for proving this. Similarly and as we also demonstrated, associated normal form calculations appear to be working perfectly fine when delays are state dependent and are in agreement with the results of numerical bifurcation analysis. Yet the proof that the suggested expansion of the state dependence gives the correct normal form is still outstanding—owing to the fact that regularity results for local center manifolds in DDEs with state-dependent delays are strictly speaking still open. In spite of these technical difficulties, we would argue that the tools we presented can be used with considerable confidence also for DDEs with discrete state-dependent delays.

The methods as implemented in DDE-BIFTOOL actually permit the bifurcation analysis of systems from a far larger class of problems, including neutral DDEs (with constant or state-dependent delays), differential algebraic equations with delay, possibly of higher index, and advanced-delayed systems. We explained briefly how these types of systems can be defined within the framework of the software, so that the different tasks of bifurcation theory can be performed also for such DDEs that are not in standard form (with a non-identity matrix multiplying the left-hand side). However, rigorous regularity results (such as the existence of smooth local center manifolds or branches of periodic orbits) and numerical convergence statements are not available yet for many of these problems. Therefore, when attempting a numerical bifurcation analysis in this wider context it is presently the responsibility of the user to experiment and test for convergence a-posteriori.

Finally, we hope that this review may encourage the use of numerical tools from bifurcation theory in the study of systems with delays in different application contexts. In particular, we would like to stress again that these tools are available and reliable not only when the delays are constant, but also for the case that delays are state dependent. Hence, there is no need to approximate state-dependent delays with constant delays. This message is important from a practical perspective because state dependence may be responsible for layers of additional dynamics. Indeed, as we have demonstrated, in some situations it may even generate all of the nontrivial dynamics. Case studies of specific DDEs beyond the standard form would also be very interesting and are encouraged. While this is more challenging in terms of ensuring that the results stand up to scrutiny, such investigations have a role in guiding the further development of theory and methods—in much the same way as case studies of standard DDEs with constant and state-dependent delays have helped us get to where we are now.

References

Abell, K. A., Elmer, C. E., Humphries, A. R., & Van Vleck, E. S. (2005). Computation of mixed type functional differential boundary value problems. *SIAM Journal on Applied Dynamical Systems, 4*(3), 755–781.

Andó, A., & Breda, D. (2020). Convergence analysis of collocation methods for computing periodic solutions of retarded functional differential equations. *SIAM Journal on Numerical Analysis, 58*(5), 3010–3039.

Aronson, D. G., Chory, M. A., Hall, G. R., & McGehee, R. P. (1982). Bifurcations from an invariant circle for two-parameter families of maps of the plane: A computer-assisted study. *Communications in Mathematical Physics, 83*(3), 303–354.

Bar-Eli, K., & Field, R. J. (1998). Earth-average temperature: A time delay approach. *Journal of Geophysical Research: Atmospheres, 103*(D20), 25949–25956.

Barnston, A. G., Tippett, M. K., L'Heureux, M. L., Li, S., & DeWitt, D. G. (2012). Skill of real-time seasonal ENSO model predictions during 2002–11: Is our capability increasing? *Bulletin of the American Meteorological Society, 93*(5), 631–651.

Barton, D. A. W., Krauskopf, B., & Wilson, R. E. (2006). Collocation schemes for periodic solutions of neutral delay differential equations. *Journal of Difference Equations and Applications, 12*(11), 1087–1101.

Battisti, D. S., & Hirst, A. C. (1989). Interannual variability in a tropical atmosphere-ocean model: Influence of the basic state, ocean geometry and nonlinearity. *Journal of the Atmospheric Sciences, 46*(12), 1687–1712.

Bélair, J., & Campbell, S. A. (1994). Stability and bifurcations of equilibria in a multiple-delayed differential equation. *SIAM Journal on Applied Mathematics, 54*(5), 1402–1424.

Bellman, R. E., & Cooke, K. L. (1963). *Differential-difference equations*. Academic.

Beyn, W. (1990). The numerical computation of connecting orbits in dynamical systems. *IMA Journal of Numerical Analysis, 3*, 379–405.

Borgioli, F., Hajdu, D., Insperger, T., Stépán, G., & Michiels, W. (2020). Pseudospectral method for assessing stability robustness for linear time-periodic delayed dynamical systems. *International Journal for Numerical Methods in Engineering, 121*(16), 3505–3528.

Bosschaert, M. M., Janssens, S. G., & Kuznetsov, Yu. A. (2020). Switching to nonhyperbolic cycles from codimension two bifurcations of equilibria of delay differential equations. *SIAM Journal on Applied Dynamical Systems, 19*(1), 252–303.

Boulanger, J.-P., & Menkes, C. (1995). Propagation and reflection of long equatorial waves in the Pacific Ocean during the 1992–1993 El Niño. *Journal of Geophysical Research: Oceans, 100*(C12), 25041–25059.

Breda, D. (2023). Pseudospectral methods for the stability analysis of delay equations. Part I: the infinitesimal generator approach. methods and applications. In D. Breda (Ed.), *Controlling Delayed Dynamics: Advances in Theory, CISM Lecture Notes* (pp. 65–94). Wien-New York: Springer.

Breda, D., Maset, S., & Vermiglio, R. (2005). Pseudospectral differencing methods for characteristic roots of delay differential equations. *SIAM Journal on Scientific Computing, 27*(2), 482–495.

Broer, H., Simó, C., & Tatjer, J. C. (1998). Towards global models near homoclinic tangencies of dissipative diffeomorphisms. *Nonlinearity, 11*(3), 667.

Calleja, R. C., Humphries, A. R., & Krauskopf, B. (2017). Resonance phenomena in a scalar delay differential equation with two state-dependent delays. *SIAM Journal on Applied Dynamical Systems, 16*(3), 1474–1513.

Cane, M. A., Münnich, M., & Zebiak, S. F. (1990). A study of self-excited oscillations of the tropical ocean-atmosphere system. Part I: Linear analysis. *Journal of the Atmospheric Sciences*, *47*(13), 1562–1577.

Chelton, D. B., & Schlax, M. G. (1996). Global observations of oceanic Rossby waves. *Science, 272*(5259), 234–238.

Dankowicz, H., & Schilder, F. (2013). *Recipes for Continuation*. Computer Science and Engineering. SIAM. COCO download: http://sourceforge.net/projects/cocotools.

Dhooge, A., Govaerts, W. J. F., & Kuznetsov, Yu. A. (2003). MatCont: a Matlab package for numerical bifurcation analysis of ODEs. *ACM Transactions on Mathematical Software, 29*(2), 141–164. https://sourceforge.net/projects/matcont/.

Diekmann, O., van Gils, S., Verduyn Lunel, S. M., & Walther, H.-O. (1995). *Delay Equations*, *Applied Mathematical Sciences* (Vol. 10). Springer.

Dijkstra, H. A. (2008). *Dynamical oceanography*. Springer Science & Business Media.

Dijkstra, H. A. (2013). *Nonlinear climate dynamics*. Cambridge University Press.

Doedel, E. J. (2007). Lecture notes on numerical analysis of nonlinear equations. In B. Krauskopf, H. M. Osinga, & J. Galán-Vioque (Eds.), *Numerical continuation methods for dynamical systems: Path following and boundary value problems* (pp. 1–49). Dordrecht: Springer.

Doedel, E. J., Champneys, A. R., Fairgrieve, T. F., Kuznetsov, Y. A., Sandstede, B., Wang, X. (1999). *AUTO97: Continuation and bifurcation software for ordinary differential equations*. http://indy.cs.concordia.ca/auto/.

Eaton, J. W., Bateman, D., Hauberg, S., & Wehbring, R. (2017). *GNU Octave version 4.2.1 manual: a high-level interactive language for numerical computations*. https://www.gnu.org/software/octave/doc/v4.2.1/.

Engelborghs, K., & Doedel, E. J. (2002). Stability of piecewise polynomial collocation for computing periodic solutions of delay differential equations. *Numerische Mathematik, 91*(4), 627–648.

Engelborghs, K., & Roose, D. (1999). Numerical computation of stability and detection of Hopf bifurcations of steady state solutions of delay differential equations. *Advances in Computational Mathematics, 10*(3–4), 271–289.

Engelborghs, K., & Roose, D. (2002). On stability of LMS methods and characteristic roots of delay differential equations. *SIAM Journal on Numerical Analysis, 40*(2), 629–650.

Engelborghs, K., Luzyanina, T., in 't Hout, K. J., & Roose, D. (2000a). Collocation methods for the computation of periodic solutions of delay differential equations. *SIAM Journal on Scientific Computing, 22*, 1593–1609.

Engelborghs, K., Luzyanina, T., & Samaey, G. (2000b). DDE-BIFTOOL: a Matlab package for bifurcation analysis of delay differential equations. Report TW 305, Katholieke Universiteit Leuven.

Engelborghs, K., Luzyanina, T., & Samaey, G. (2001). DDE-BIFTOOL v.2.00: a Matlab package for bifurcation analysis of delay differential equations. Report TW 330, Katholieke Universiteit Leuven.

Falkena, S. K. J., Quinn, C., Sieber, J., Frank, J., & Dijkstra, H. A. (2019). Derivation of delay equation climate models using the Mori-Zwanzig formalism. *Proceedings of the Royal Society A, 475*(2227).

Farmer, J. D. (1982). Chaotic attractors of an infinite-dimensional dynamical system. *Physica D, 4*(3), 366–393.

Ghil, M., Zaliapin, I., & Thompson, S. (2008). A delay differential model of ENSO variability: Parametric instability and the distribution of extremes. *Nonlinear Processes in Geophysics, 15*(3), 417–433.

Govaerts, W. J. F. (2000). *Numerical methods for bifurcations of dynamical equilibria*. Miscellaneous titles in applied mathematics series. SIAM.

Graham, N. E., & White, W. B. (1988). The El Niño cycle: A natural oscillator of the Pacific ocean-atmosphere system. *Science, 240*, 1293–1302.

Green, K., Krauskopf, B., & Engelborghs, K. (2003). One-dimensional unstable eigenfunction and manifold computations in delay differential equations. *Journal of Computational Physics, 197*(1), 86–98.

Guckenheimer, J., & Holmes, P. (1983). *Nonlinear oscillations, dynamical systems, and bifurcations of vector fields*. Springer.

Guo, S., & Wu, J. (2013). *Bifurcation theory of functional differential equations*. Applied mathematical sciences. Springer.

Haegeman, B., Engelborghs, K., Roose, D., Pieroux, D., & Erneux, T. (2002). Stability and rupture of bifurcation bridges in semiconductor lasers subject to optical feedback. *Physical Review E, 66*, 046216.

Hale, J. K. (1977). *Theory of functional differential equations*. Applied mathematical sciences. Springer.

Hale, J. K., & Verduyn Lunel, S. M. (1993). *introduction to functional differential equations*. Applied mathematical sciences. Springer.

Harrison, D. E., & Vecchi, G. A. (2001). El Niño and La Niña equatorial Pacific thermocline depth and sea surface temperature anomalies, 1986–98. *Geophysical Research Letters, 28*(6), 1051–1054.

Hartung, F., Krisztin, T., Walther, H.-O., & Wu, J. (2006). Functional differential equations with state-dependent delays: theory and applications. In P. Drábek, A. Cañada, & A. Fonda (Eds.), *Handbook of differential equations: ordinary differential equations* (Vol. 3, Chap. 5, pp. 435–545). North-Holland.

Henderson, M. E. (2002). Multiple parameter continuation: Computing implicitly defined k-manifolds. *International Journal of Bifurcation and Chaos, 12*(03), 451–476.

Humphries, A. R., DeMasi, O. A., Magpantay, F. M. G., & Upham, F. (2012). Dynamics of a delay differential equation with multiple state-dependent delays. *Discrete and Continuous Dynamical Systems, 32*(8), 2701–2727.

Humphries, A. R., Bernucci, D. A., Calleja, R., Homayounfar, N., & Snarski, M. (2016). Periodic solutions of a singularly perturbed delay differential equation with two state-dependent delays. *Journal of Dynamics and Differential Equations, 8*, 1215–1263.

Insperger, T., & Stépán, G. (2000). Stability of the milling process. *Periodica Polytechnica Mechanical Engineering, 44*(1), 47–57.

Insperger, T., Milton, J., & Stépán, G. (2013). Acceleration feedback improves balancing against reflex delay. *Journal of the Royal Society Interface, 10*(79), 20120763.

Jin, F.-F. (1997). An equatorial ocean recharge paradigm for ENSO. Part II: A stripped-down coupled model. *Journal of the Atmospheric Sciences, 54*(7), 830–847.

Just, W., Fiedler, B., Georgi, M., Flunkert, V., Hövel, P., & Schöll, E. (2007). Beyond the odd number limitation: A bifurcation analysis of time-delayed feedback control. *Physical Review E, 76*, 026210.

Kaashoek, M. A., & Verduyn Lunel, S. M. (1992). Characteristic matrices and spectral properties of evolutionary systems. *Transactions of the American Mathematical Society, 334*(2), 479–517.

Kane, D. M., & Shore., K. A. (2005). *Unlocking dynamical diversity: Optical feedback effects on semiconductor lasers*. Wiley.

Kaper, H., & Engler, H. (2013). *Mathematics and climate*. SIAM.

Keane, A., & Krauskopf, B. (2018). Chenciner bubbles and torus break-up in a periodically forced delay differential equation. *Nonlinearity, 31*(6), R165.

Keane, A., Krauskopf, B., & Postlethwaite, C. M. (2015). Delayed feedback versus seasonal forcing: Resonance phenomena in an El Niño Southern Oscillation model. *SIAM Journal on Applied Dynamical Systems, 14*(3), 1229–1257.

Keane, A., Krauskopf, B., & Postlethwaite, C. M. (2016). Investigating irregular behavior in a model for the El Niño Southern Oscillation with positive and negative delayed feedback. *SIAM Journal on Applied Dynamical Systems, 15*(3), 1656–1689.

Keane, A., Krauskopf, B., & Postlethwaite, C. M. (2017). Climate models with delay differential equations. *Chaos, 27*(11), 114309.

Keane, A., Krauskopf, B., & Dijkstra, H. A. (2019). The effect of state dependence in a delay differential equation model for the El Niño Southern Oscillation. *Philosophical Transactions of the Royal Society A, 377*(2153), 2153.

Kozyreff, G., & Erneux, T. (2013). Singular Hopf bifurcation in a differential equation with large state-dependent delay. *Procedings of the Royal Society A, 470*(2162).

Krauskopf, B. (2005). Bifurcation analysis of lasers with delay. In D. M. Kane & K. A. Shore (Eds.) *Unlocking dynamical diversity: Optical feedback effects on semiconductor lasers* (Chap. 5, pp. 147–183). Wiley, Hoboken, NJ, USA.

Krauskopf, B., & Green, K. (2003). Computing unstable manifolds of periodic orbits in delay differential equations. *Journal of Computational Physics, 186*(1), 230–249.

Krauskopf, B., & Sieber, J. (2014). Bifurcation analysis of delay-induced resonances of the El-Niño Southern Oscillation. *Procedings of the Royal Society A, 470*(2169), 20140348.

Krauskopf, B., Van Tartwijk, G. H. M., & Gray, G. R. (2000). Symmetry properties of lasers subject to optical feedback. *Optics Communications, 177*(1–6), 347–353.

Krisztin, T. (2003). A local unstable manifold for differential equations with state-dependent delay. *Discrete and Continuous Dynamical Systems, 9*(4), 993–1028.

Krisztin, T. (2006). Smooth center manifolds for differential equations with state-dependent delay. In *AIMS Conference Poitiers*.

Kuznetsov, Yu. A. (2013). *Elements of applied bifurcation theory*. Springer Science & Business Media.

Mackey, M. C., & Glass, L. (1977). Oscillation and chaos in physiological control systems. *Science, 197*(4300), 287–289.

Mallet-Paret, J., & Nussbaum, R. D. (2011). Superstability and rigorous asymptotics in singularly perturbed state-dependent delay-differential equations. *Journal of Differential Equations, 250*, 4037–4084.

Mallet-Paret, J., & Nussbaum, R. D. (2011). Stability of periodic solutions of state-dependent delay-differential equations. *Journal of Differential Equations, 250*(11), 4085–4103.

Mallet-Paret, J., Nussbaum, R. D., & Paraskevopoulos, P. (1994). Periodic solutions for functional differential equations with multiple state-dependent time lags. *Topological Methods in Nonlinear Analysis, 3*, 101–162.

MATLAB (2018). *version 9.5.0.944444 (R2018b)*. The MathWorks Inc., Natick, Massachusetts.

Milton, J., Townsend, J. L., King, M. A., & Ohira, T. (1891). Balancing with positive feedback: The case for discontinuous control. *Philosophical Transactions of the Royal Society A, 367*, 2009.

Münnich, M., Cane, M. A., & Zebiak, S. E. (1991). A study of self-excited oscillations of the tropical ocean-atmosphere system. Part II: Nonlinear cases. *Journal of the Atmospheric Sciences, 48*(10), 1238–1248.

Pieroux, D., Erneux, T., Haegeman, B., Engelborghs, K., & Roose, D. (2001). Bridges of periodic solutions and tori in semiconductor lasers subject to delay. *Physics Letters, 87*, 193901.

Pomeau, Y., & Manneville, P. (1980). Intermittent transition to turbulence in dissipative dynamical systems. *Communications in Mathematical Physics, 74*(2), 189–197.

Purewal, A. S., Postlethwaite, C. M., & Krauskopf, B. (2014). A global bifurcation analysis of the subcritical Hopf normal form subject to Pyragas time-delayed feedback control. *SIAM Journal on Applied Dynamical Systems, 13*(4), 1879–1915.

Roose, D., & Szalai, R. (2007). Continuation and bifurcation analysis of delay differential equations. In B. Krauskopf, H. M. Osinga, & J. Galán-Vioque (Eds.), *Numerical continuation methods for dynamical systems: Path following and boundary value problems* (pp. 359–399). Dordrecht: Springer.

Samaey, G., Engelborghs, K., & Roose, D. (2002). Numerical computation of connecting orbits in delay differential equations. *Numerical Algorithms, 30*, 335–352.

Sieber, J. (2012). Finding periodic orbits in state-dependent delay differential equations as roots of algebraic equations. *Discrete & Continuous Dynamical Systems-A, 32*(8), 2607–2651. updated with corrections on arXiv:1010.2391.

Sieber, J. (2017). Local bifurcations in differential equations with state-dependent delay. *Chaos, 27*(11), 114326.

Sieber, J., & Krauskopf, B. (2004). Bifurcation analysis of an inverted pendulum with delayed feedback control near a triple-zero eigenvalue singularity. *Nonlinearity, 17*(1), 85–103.

Sieber, J., & Krauskopf, B. (2004). Complex balancing motions of an inverted pendulum subject to delayed feedback control. *Physica D, 197*(3–4), 332–345.

Sieber, J., & Krauskopf, B. (2005). Extending the permissible control loop latency for the controlled inverted pendulum. *Dynamical Systems, 20*(1), 189–199.
Sieber, J., & Szalai, R. (2011). Characteristic matrices for linear periodic delay differential equations. *SIAM Journal on Applied Dynamical Systems, 10*(1), 129–147.
Sieber, J., Engelborghs, K., Luzyanina, T., Samaey, G., & Roose, D. (2015). DDE-BIFTOOL manual — bifurcation analysis of delay differential equations. arXiv preprint arXiv:1406.7144, 2015. download: https://sourceforge.net/projects/ddebiftool.
Simonnet, E., Dijkstra, H. A., & Ghil, M. (2009). Bifurcation analysis of ocean, atmosphere, and climate models. In *Handbook of numerical analysis* (Vol. 14, pp. 187–229). Elsevier.
Skubachevskii, A. L., & Walther, H.-O. (2006). On the Floquet multipliers of periodic solutions to nonlinear functional differential equations. *Journal of Dynamics and Differential Equations, 18*, 257–355.
Stépán, G. (1989) *Retarded dynamical systems: Stability and characteristic functions*. Longman Scientific and Technical.
Stumpf, E. (2011). The existence and C^1-smoothness of local center-unstable manifolds for differential equations with state-dependent delay. *Rostocker Mathematisches Kolloquium, 66*, 3–44.
Suarez, M. J., & Schopf, P. S. (1988). A delayed action oscillator for ENSO. *Journal of the Atmospheric Sciences, 45*(21), 3283–3287.
Szalai, R., Stépán, G., & Hogan, S. J. (2006). Continuation of bifurcations in periodic delay differential equations using characteristic matrices. *SIAM Journal on Scientific Computing, 28*(4), 1301–1317.
Tziperman, E., Stone, L., Cane, M. A., & Jarosh, H. (1994). El Niño chaos: Overlapping of resonances between the seasonal cycle and the Pacific ocean-atmosphere oscillator. *Science, 264*, 72–74.
Tziperman, E., Cane, M. A., Zebiak, S. E., Xue, Y., & Blumenthal, B. (1998). Locking of El Niño's peak time to the end of the calendar year in the delayed oscillator picture of ENSO. *Journal of Climate, 11*(9), 2191–2199.
Wage, B. (2014). Normal form computations for delay differential equations in DDE-BIFTOOL. *Masters thesis, Universiteit Utrecht*.
Walther, H.-O. (2002). Stable periodic motion of a system with state-dependent delay. *Differential and Integral Equations, 15*, 923–944.
Walther, H.-O. (2003). The solution manifold and C^1-smoothness for differential equations with state-dependent delay. *Journal of Differential Equations, 195*(1), 46–65.
Yanchuk, S., Ruschel, S., Sieber, J., & Wolfrum, M. (2019). Temporal dissipative solitons in time-delay feedback systems. *Physical Review Letters, 123*(5), 053901.
Zaliapin, I., & Ghil, M. (2010). A delay differential model of ENSO variability - Part 2: Phase locking, multiple solutions and dynamics of extrema. *Nonlinear Processes in Geophysics, 17*(2), 123–135.
Zelle, H., Appeldoorn, G., Burgers, G., & van Oldenborgh, G. J. (2004). The relationship between sea surface temperature and thermocline depth in the eastern equatorial Pacific. *Journal of Physical Oceanography, 34*(3), 643–655.

Design of Structured Controllers for Linear Time-Delay Systems

Wim Michiels

Abstract We present an overview of control design methods for linear time-delay systems, which are grounded in matrix theory and numerical linear algebra techniques, such as eigenvalue computations, solving Lyapunov matrix equations, eigenvalue perturbation theory and eigenvalue optimization. The methods are particularly suitable for the design of structured controllers, as they rely on a direct optimization of stability, robustness and performance indicators as a function of controller or design parameters. Several illustrations complete the presentation.

1 Introduction

We consider the system

$$\begin{cases} \dot{x}(t) = A_0 x(t) + \sum_{i=1}^{m} A_i x(t-\tau_i) + B\zeta(t), \\ \eta(t) = Cx(t) + D\zeta(t-\tau_0), \end{cases} \tag{1}$$

where $x(t) \in \mathbb{C}^n$ is the state variable at time t, $\zeta(t) \in \mathbb{C}^{n_\zeta}$ is the input and $\eta(t) \in \mathbb{C}^{n_\eta}$ is the output at time t, and τ_i, $i = 0, \ldots, m$, represent time-delays. We assume that the state delays are ordered such that $0 < \tau_1 < \cdots < \tau_m$. The input is not assumed to be delayed, yet input-output delays can be taken into account in the models addressed in Sect. 5.

It is well known that the solutions of (1), with $\zeta \equiv 0$, satisfy a spectrum determined growth property, in the sense that their asymptotic behavior and stability properties

This work was supported by the project C14/17/072 of the KU Leuven Research Council, by the project G092721N of the Research Foundation-Flanders (FWO - Vlaanderen), and by the project UCoCoS, funded by the European Unions Horizon 2020 research and innovation programme under the Marie Sklodowska-Curie Grant Agreement No 675080.

W. Michiels (✉)
Department of Computer Science, KU Leuven, Heverlee, Belgium
e-mail: Wim.Michiels@cs.kuleuven.be

D. Breda (ed.), *Controlling Delayed Dynamics*, CISM International Centre for Mechanical Sciences 604, https://doi.org/10.1007/978-3-031-01129-0_8

are determined by the location of the characteristic roots, see Hale and Verduyn Lunel (1993), compare also with Breda (2023). The latter appear among the solutions of the nonlinear eigenvalue problem

$$\left(\lambda I - A_0 - \sum_{i=1}^{m} A_i e^{-\lambda \tau_i}\right) v = 0, \ v \in \mathbb{C}^n, \ v \neq 0. \tag{2}$$

For example the null solution of (1), with zero input, is exponentially stable if and only if all its characteristic roots are confined to the open left half plane (Niculescu 2001; Gu et al. 2003). In such a case, we call system (1) internally exponentially stable.

As a common approach in the domain of robust control, we assume that input ζ and output η are defined in such a way that performance and robustness requirements for the system can be expressed in terms of norms of the associated transfer function $G : \mathbb{C} \to \mathbb{C}^{n_\eta \times n_\zeta}$,

$$G(\lambda) := C \left(\lambda I - A_0 - \sum_{i=1}^{m} A_i e^{-\lambda \tau_i}\right)^{-1} B + D e^{-\lambda \tau_0}, \tag{3}$$

which corresponds to the Laplace transform of the impulse response h of the system. Important measures are the $\mathcal{H}_2$ and $\mathcal{H}_\infty$ norm of the input-output map of the system (Zhou et al. 1995). For an internally exponentially stable system, the $\mathcal{H}_2$ norm is defined as

$$\|G\|_{\mathcal{H}_2} := \sqrt{\int_0^\infty \operatorname{tr}\left(h(t)^H h(t)\right) \mathrm{d}t},$$

which, by Parseval's relation, can also be expressed as

$$\|G\|_{\mathcal{H}_2} = \sqrt{\frac{1}{2\pi} \int_{-\infty}^{\infty} \operatorname{tr}\left(G(\mathrm{i}\omega)^H G(\mathrm{i}\omega)\right) \mathrm{d}\omega}. \tag{4}$$

The $\mathcal{H}_2$ norm is particularly suitable to quantify the effects of additive perturbations to the differential equation on the deviation from the equilibrium, as it can be interpreted as the trace of the covariance matrix of the output, when the system input consists of white noise. The $\mathcal{H}_\infty$ norm, on its turn, is equal to the peak gain of the transfer function in the closed right half plane. Once again under assumption of internal exponential stability, it can be defined by the expression

$$\|G\|_{\mathcal{H}_\infty} := \sup_{\omega \in \mathbb{R}} \sigma_1(G(\mathrm{i}\omega)),$$

where $\sigma_1(\cdot)$ denotes the largest singular value. In the time-domain the $\mathcal{H}_\infty$ norm can be interpreted as the induced $\mathcal{L}_2$-norm from input ζ to output η, when considered

as functions on the interval $[0, \infty)$, that is $\|G\|_{\mathcal{H}_\infty} = \max_{u \not\equiv 0} \frac{\|y\|_{\mathcal{L}_2}}{\|u\|_{\mathcal{L}_2}}$, emphasizing its role in assessing the disturbance rejection of a dynamical system. In addition, many robustness criteria for stability against perturbations to system model (1) can be expressed in terms of the reciprocal of the $\mathcal{H}_\infty$ norm of an appropriately defined transfer function. For example, considering complex valued perturbations δA_i on matrices A_i, $i = 0, \ldots, m$, in (1), whose size is measured by

$$\|(\delta A_0, \ldots, \delta A_m)\|_{\text{glob}} := \left\| \begin{bmatrix} w_0 \|\delta A_0\|_2 \\ \vdots \\ w_m \|\delta A_m\|_2 \end{bmatrix} \right\|_\infty,$$

where numbers $w_i \in \mathbb{R}_0^+ \cup \{\infty\}$[1] are weights associated to the different matrix perturbations, the associated stability radius

$$r_{\mathbb{C}}(\|\cdot\|_{\text{glob}}) := \inf \Big\{ \|(\delta A_0, \ldots, \delta A_m)\|_{\text{glob}} : \ \delta A_i \in \mathbb{C}^{n\times n}, 0 \le i \le m, \text{ and } \dot{x}(t) = (A_0 + \delta A_0)x(t) + \textstyle\sum_{i=1}^m (A_i + \delta A_i)x(t - \tau_i)) \text{ is not exponentially stable} \Big\}$$

can be expressed as

$$r_{\mathbb{C}}(\|\cdot\|_{\text{glob}}) = \left\{ \left\| \left(\mathrm{i}\omega I - A_0 - \sum_{i=1}^m A_i e^{-\mathrm{i}\omega\tau_i} \right)^{-1} \right\|_{\mathcal{H}_\infty} \sum_{i=0}^m \frac{1}{w_i} \right\}^{-1},$$

see Michiels and Niculescu (2014). It should be noticed that

$$\|(\delta A_0, \ldots, \delta A_m)\|_{\text{glob}} < 1 \ \Leftrightarrow \ \|\delta A_i\|_2 < \frac{1}{w_i}, 0 \le i \le m.$$

The above result can be extended by exploiting structured, real valued perturbations, see, e.g., Borgioli and Michiels (2020), Borgioli et al. (2019), where the $\mathcal{H}_\infty$ framework is generalized to the μ-framework (Zhou et al. 1995). We note that Borgioli et al. (2019) also considers bounded perturbations on the delays. Finally, the system norms can also be used in the context of structure preserving model reduction. Denoting by $\tilde{G}$ the transfer function of a reduced model for (1) of the form

$$\hat{G}(\mathrm{i}\omega) = \hat{C} \left(\lambda I - \sum_{i=0}^m \hat{A}_i e^{-\lambda\tau_i} \right)^{-1} \hat{B} + D e^{-\lambda\tau_0}, \quad \hat{A}_i \in \mathbb{C}^{k\times k}, \ i = 0, \ldots, m,$$

assuming n large and $k \ll n$, the matrices of the reduced model could be determined by minimizing

$$\|G - \tilde{G}\|_{\mathcal{H}_2}, \text{ or } \|G - \tilde{G}\|_{\mathcal{H}_\infty},$$

[1] $\mathbb{R}_0^+$ denotes the set of strictly positive real numbers.

see Gomez et al. (2019), Pontes Duff et al. (2018). Here we can express the mismatch between the transfer functions in the form of a standard transfer function, namely

$$G(\mathrm{i}\omega) - \hat{G}(\mathrm{i}\omega) = [C \ -\hat{C}] \times \left(\mathrm{i}\omega \begin{bmatrix} I_n & 0 \\ 0 & I_k \end{bmatrix} - \sum_{i=0}^{m} \begin{bmatrix} A_i & 0 \\ 0 & \hat{A}_i \end{bmatrix} e^{-\mathrm{i}\omega\tau_i} \right)^{-1} \begin{bmatrix} B \\ \hat{B} \end{bmatrix},$$

enabling tools for optimizing system or controller parameters.

The structure of the chapter is as follows. In Sect. 2 we present some numerical methods for the computation of the rightmost characteristic roots of (1) and for the computation of the $\mathcal{H}_2$ and $\mathcal{H}_\infty$ norm of transfer function (3). These analysis tools are at the basis of the controller synthesis methods discussed in Sect. 3. There we assume that the system matrices in (1) depend on a finite number of parameters, which may originate from the parametrization of a controller (hence, system (1) may correspond already to the so-called *closed-loop* system). The stabilization problem and the optimization of the $\mathcal{H}_2$ and $\mathcal{H}_\infty$ norm of (3) are addressed. The approach is inspired by controller synthesis methods for finite-dimensional linear time-invariant systems which rely on eigenvalue optimization, as for instance implemented in the package HIFOO (Burke et al. 2006). These methods have proven very useful for synthesis problems where the controller is constrained or its order (dimension) is smaller than the dimension of the plant. They are particularly powerful for time-delay systems, because any design problem involving the determination of a finite number of parameters can be interpreted as a reduced-order control design problem due to the infinite dimension of the system, and they constitute an important component of the established eigenvalue based framework for time-delay systems (Michiels and Niculescu 2014; Michiels 2019). In Sect. 4 we illustrate the flexibility of the approach in two complementary directions, by incorporating pole location constraints in the stabilization procedure, and by synthesizing a proportional-retarded controller optimizing the $\mathcal{H}_2$ norm of the system, respectively. In Sect. 5 we briefly address extensions of the approach towards delay differential algebraic equation models, which can also describe systems of neutral type. Finally, in Sect. 6 we present some concluding remarks.

2 Solving Analysis Problems

We start with the reformulation of (1) as an infinite-dimensional linear system in a standard state space representation, based on Curtain and Zwart (1995), because the interplay between the two representations has played an important role in the development of computational tools. Consider the Hilbert space $X := \mathbb{C}^n \times \mathcal{L}_2([-\tau_m, 0], \mathbb{C}^n)$, equipped with the inner product

$$< (y_0, y_1), (z_0, z_1) >_X = < y_0, z_0 >_{\mathbb{C}^n} + < y_1, z_1 >_{\mathcal{L}_2},$$

and denote by $AC([-\tau_m, 0], \mathbb{C}^n)$ the space of absolutely continuous functions from $[-\tau_m, 0]$ to $\mathbb{C}^n$. Let $\mathcal{A} : X \to X$ be the derivative operator defined by

$$\mathcal{D}(\mathcal{A}) := \{z = (z_0, z_1) \in X : z_1 \in AC([-\tau_m, 0], \mathbb{C}^n),\ z_0 = z_1(0)\},$$
$$\mathcal{A}z = \left(A_0 z_0 + \sum_{i=1}^{m} A_i z_1(-\tau_i)\right), \quad z \in \mathcal{D}(\mathcal{A}),$$

and let the operators $\mathcal{B} : \mathbb{C}^{n_\zeta} \to X$ and $\mathcal{C} : X \to \mathbb{C}^{n_\eta}$ be given by

$$\begin{array}{ll} \mathcal{B}\zeta := (B\zeta, 0), & \zeta \in \mathbb{C}^{n_\zeta}, \\ \mathcal{C}z := Cz_0, & z = (z_0, z_1) \in X. \end{array}$$

We can now rewrite system (1) as

$$\begin{cases} \dot{\Xi}(t) = \mathcal{A}\Xi(t) + \mathcal{B}\zeta(t), \\ \eta(t) \ = \mathcal{C}\Xi(t) + D\zeta(t - \tau_0), \end{cases} \tag{5}$$

where $\Xi(t) \in \mathcal{D}(A) \subset X$. The relation between corresponding solutions of (5) and (1) is given by $\Xi_0(t) = x(t)$ and $\Xi_1(t)(\theta) \equiv x(t + \theta)$ for $\theta \in [-\tau_m, 0]$.

2.1 Computation of Characteristic Roots and the Spectral Abscissa

The spectral properties of the operator $\mathcal{A}$ in (5) are described in detail in Michiels and Niculescu (2014, Chap. 1). The operator only has a point spectrum. Hence, its spectrum, $\sigma(\mathcal{A})$, is fully determined by the eigenvalue problem

$$\mathcal{A}\, z = \lambda z,\ z \in X,\ z \neq 0. \tag{6}$$

The connections with the characteristic roots are as follows. The characteristic roots are the eigenvalues of operator $\mathcal{A}$. Moreover, if $\lambda \in \sigma(\mathcal{A})$, then the corresponding eigenfunction takes the form

$$z(\theta) = ve^{\lambda\theta}, \theta \in [-\tau_m, 0], \tag{7}$$

where $v \in \mathbb{C}^n$ and the pair (λ, v) satisfies (2). Conversely, if a pair (λ, v) satisfies (2), then (7) is an eigenfunction of $\mathcal{A}$ corresponding to the eigenvalue λ. From the equivalent representation of (1) as (5), we conclude that the characteristic roots can be equivalently expressed as

1. the solutions of the finite-dimensional nonlinear eigenvalue problem (2);
2. the solutions of the infinite-dimensional linear eigenvalue problem (6).

This dual viewpoint lies at the basis of available tools to compute the rightmost characteristic roots. On the one hand, discretizing (6) and solving the resulting standard eigenvalue problems allows to obtain global information, for example, estimates of *all* characteristic roots in a given compact set or in a given right half plane. On the other hand, the (finitely many) nonlinear equations (2) allow us to make *local corrections* on characteristic root approximations up to the desired accuracy, e.g., using Newton's method or inverse residual iteration.

There are several possibilities to discretize eigenvalue problem (6). Given a positive integer N and a mesh Ω_N of $N+1$ distinct points in the interval $[-\tau_m, 0]$,

$$\Omega_N = \{\theta_{N,i},\ i = 1, \ldots, N+1\}, \tag{8}$$

with

$$-\tau_m \leq \theta_{N,1} < \ldots < \theta_{N,N} < \theta_{N,N+1} = 0,$$

a spectral discretization as in Breda et al. (2005) (see also Breda 2023) leads for example to the eigenvalue problem

$$\mathcal{A}_N \mathbf{x}_N = \lambda \mathbf{x}_N, \mathbf{x}_N \in \mathbb{C}^{n(N+1)}, \mathbf{x}_N \neq 0, \tag{9}$$

where

$$\mathcal{A}_N = \begin{bmatrix} d_{1,1} & \ldots & d_{1,N+1} \\ \vdots & & \vdots \\ d_{N,1} & \ldots & d_{N,N+1} \\ a_1 & \ldots & a_{N+1} \end{bmatrix} \in \mathbb{R}^{n(N+1)\times n(N+1)} \tag{10}$$

and

$$\begin{aligned} d_{i,k} &= l'_{N,k}(\theta_{N,i}) I_n, && i = 1, \ldots, N, k = 1, \ldots, N+1, \\ a_k &= A_0 l_{N,k}(0) + \sum_{i=1}^{m} A_i l_{N,k}(-\tau_i), && k = 1, \ldots, N+1. \end{aligned}$$

The functions $l_{N,k}$ represent the Lagrange polynomials relative to the mesh Ω_N, i.e. polynomials of degree N such that, $l_{N,k}(\theta_{N,i}) = 1$ if $i = k$ and $l_{N,k}(\theta_{N,i}) = 0$ if $i \neq k$, In Breda et al. (2005) it is proven that spectral accuracy on the individual characteristic root approximations (approximation error $O(N^{-N})$) is obtained with a mesh consisting of (scaled and shifted) Chebyshev extremal points, that is,

$$\theta_{N,i} = -\cos \frac{\pi(i-1)}{N},\ i = 1, \ldots, N+1.$$

The discretization of (6) into (9) lays at the basis of the software tool TRACE-DDE (Breda et al. 2009). The stability routine for equilibria of the package DDE-BIFTOOL (Engelborghs et al. 2002; Sieber et al. 2016) exploits the dual representation of the

eigenvalue problem, since it is based on discretizing the solution operator of (5), whose infinitesimal generator is $\mathcal{A}$, using a spline collocation approach, followed by Newton corrections on (2). For a pseudospectral collocation approach to discretize the solution operator see Breda (2023).

Both aforementioned tools rely on computing all eigenvalues of the discretized system, which restricts the size of the problem from a computational point of view. In Jarlebring et al. (2010) an iterative method is proposed for computing selected eigenvalues of large-scale systems. This method has an interpretation as Arnoldi's method (see, e.g.,Saad 1992) in a function setting, applied to the inverse of the infinite-dimensional operator $\mathcal{A}$, which is characterized in the following proposition.

Proposition 2.1 *The inverse of $\mathcal{A} : X \to X$ exists if and only if matrix $A_0 + \sum_{i=1}^{m} A_i$ is nonsingular. Moreover, it can be explicitly expressed as*

$$\begin{aligned} \mathcal{D}(\mathcal{A}^{-1}) &= X \\ \left(\mathcal{A}^{-1}\,\phi\right)(\theta) &= \left(C(\phi), \int_0^{\theta} \phi_1(s)\,\mathrm{d}s + C(\phi), \theta \in [-\tau_m, 0)\right), \quad \phi \in \mathcal{D}(\mathcal{A}^{-1}), \end{aligned}$$

where

$$C(\phi) = \left(A_0 + \sum_{i=1}^{m} A_i\right)^{-1} \left[\phi_0 - \sum_{i=1}^{m} A_i \int_0^{-\tau_i} \phi_1(s)\,\mathrm{d}s\right]. \tag{11}$$

We note that all information about the system is concentrated in the integration constant (11). To get some insight in the method of Jarlebring et al. (2010), let us apply first the power method to $\mathcal{A}^{-1}$ for scalar system

$$\dot{x}(t) = -2x(t) + \frac{1}{3}x(t - \log 3),$$

whose smallest characteristic root is equal to -1. Starting with the constant initial function $\phi \equiv 1$, the iterations result in polynomials of increasing degree

$$\begin{aligned} &1. \\ &1. - 1.21993t \\ &1. - 1.03416t + .630804t^2 \\ &1. - .999697t + .516927t^2 - .210204t^3 \\ &1. - .998615t + .499156t^2 - .172070t^3 + 0.0524783t^4 \\ &1. - .999733t + .499174t^2 - .166341t^3 + 0.0430061t^4 - 0.0104929t^5 \\ &1. - 1.00000t + .499869t^2 - .166392t^3 + 0.0415855t^4 - 0.00860127t^5 + 0.00174882t^6, \end{aligned}$$

in which one easily recognizes an approximation of the Taylor series of function $\exp(-t)$, the eigenfunction of $\mathcal{A}$ corresponding to eigenvalue $\lambda = -1$, which is closest to the origin. In order to compute multiple eigenvalue approximations, the power method can be replaced by Arnoldi's method, furnishing the basis of the Infinite Arnoldi method (Jarlebring et al. 2010), or by a Rational Krylov method, laying the basis of the dynamic variants of the algorithm proposed in Güttel et al. (2014). As features of interest, these methods do not explicitly rely on a discretization

of the delay equation, while all operations are still performed on vectors and matrices (of finite dimension), in addition to their ability to exploit sparsity of the coefficient matrices.

We note that also methods for generic nonlinear eigenvalue problems can be used for computing characteristic roots, see for instance the CORK framework described in Van Beeumen et al. (2015) and the software package NEP-PACK (Jarlebring et al. 2018).

2.2 Computation of $\mathcal{H}_\infty$ Norms

For systems without delay, level set methods are standard methods for computing $\mathcal{H}_\infty$ norms and related problems, see, e.g., Boyd and Balakrishnan (1990), Bruinsma and Steinbuch (1990) and the references therein. These methods originate from the property that all the intersections of the singular value curves, corresponding to the transfer function, and a constant function (the level) can be directly computed from the solutions of a structured eigenvalue problem. This property enables a fast two-directional search for the dominant peak in the singular value plot.

In Michiels and Gumussoy (2010) an extension of this approach for computing the $\mathcal{H}_\infty$ norm of transfer function (3) is described. The theoretical foundation is contained in the following proposition from Michiels and Gumussoy (2010, Lemma 2.1 and Proposition 2.2).

Proposition 2.2 *Let $\xi > 0$ be such that the matrix $D_\xi := D^T D - \xi^2 I$ is non-singular. For $\omega \geq 0$, matrix $G(i\omega)$ in (3) has a singular value equal to ξ if and only if $\lambda = i\omega$ is a solution of the equation*

$$\det H(\lambda; \xi) = 0, \tag{12}$$

where

$$H(\lambda; \xi) := \lambda I - M_0 - \sum_{i=1}^{m} \left(M_i e^{-\lambda \tau_i} + M_{-i} e^{\lambda \tau_i} \right) - \left(N_1 e^{-\lambda \tau_0} + N_{-1} e^{\lambda \tau_0} \right),$$

with

$$M_0 := \begin{bmatrix} A_0 & -B D_\xi^{-1} B^T \\ -C^T C + C^T D D_\xi^{-1} D^T C & -A_0^T \end{bmatrix},$$
$$M_i := \begin{bmatrix} A_i & 0 \\ 0 & 0 \end{bmatrix}, \; M_{-i} := \begin{bmatrix} 0 & 0 \\ 0 & -A_i^T \end{bmatrix}, \; 1 \leq i \leq m,$$
$$N_1 := \begin{bmatrix} 0 & 0 \\ 0 & C^T D D_\xi^{-1} B^T \end{bmatrix}, \; N_{-1} := \begin{bmatrix} -B D_\xi^{-1} D^T C & 0 \\ 0 & 0 \end{bmatrix}.$$

Moreover, (12) holds if and only if λ is an eigenvalue of the operator $\mathcal{L}_\xi$, defined by

$$\mathcal{D}(\mathcal{L}_\xi) := \Big\{\phi \in Z : \ \phi'(0) = M_0\phi(0) + \sum_{i=1}^{m} (M_i\phi(-\tau_i) + M_{-i}\phi(\tau_i)) + N_1\phi(-\tau_0) + N_{-1}\phi(\tau_0)\Big\}$$

$$\mathcal{L}_\xi\, \phi := \phi', \quad \phi \in \mathcal{D}(\mathcal{L}_\xi),$$

where $Z := AC([-\tau_m, \tau_m], \mathbb{C}^{2n})$.

According to Proposition 2.2, the intersections of the constant function $\mathbb{R} \ni \omega \mapsto \xi$, with level $\xi > 0$ prescribed, and the curves

$$\mathbb{R} \ni \omega \mapsto \sigma_i(G(\mathrm{i}\omega)), \ 1 \le i \le \min(n_\zeta, n_\eta),$$

where $\sigma_i(\cdot)$ denotes the ith singular value, can be found by computing the solutions on the imaginary axis of either

1. the finite-dimensional nonlinear eigenvalue problem,

$$H(\lambda; \xi)v = 0, v \in \mathbb{C}^{2n}, \ v \neq 0, \text{ or} \tag{13}$$

2. the infinite-dimensional linear eigenvalue problem

$$\mathcal{L}_\xi\phi = \lambda\phi, \phi \in Z, \phi \neq 0.$$

These two characterizations are similar to the representations of characteristic roots as eigenvalues. As a consequence, the methods outlined in Sect. 2.1 can be adapted accordingly.

The method presented in Michiels and Gumussoy (2010) for computing the $\mathcal{H}_\infty$ norm of (3) relies on a two-directional search in a modification of the singular value plot, induced by a spectral discretization of operator $\mathcal{L}_\xi$, followed by a local correction of the peak value up to the desired accuracy. The latter is based on the nonlinear equation (13), supplemented with a local optimality condition. The main steps are sketched in Fig. 1.

Finally, a closely related problem is the computation of the pseudospectral abscissa, for which we refer to Gumussoy and Michiels (2010) and the references therein.

2.3 Computation of $\mathcal{H}_2$ Norms

We assume that (1) is internally exponentially stable and, in addition, that matrix D is equal to zero. Under these conditions the $\mathcal{H}_2$ norm of G is finite and it satisfies (4). We present two different approaches for its computation, which once again stem

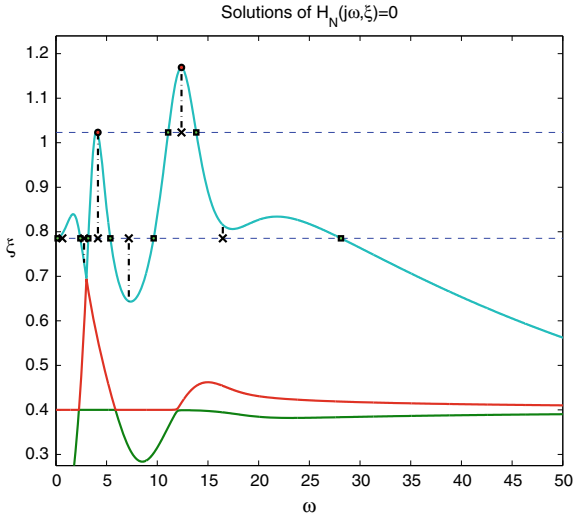

Fig. 1 Principles of the method in Michiels and Gumussoy (2010). Function H_N is an approximation of H, induced by a spectral discretization of $\mathcal{L}_\xi$ on a mesh consisting of $2N+1$ points over the interval $[-\tau_m, \tau_m]$. In the first step the peak value is found for a fixed value of N by the iterative algorithm of Bruinsma and Steinbuch (1990): for a given level ξ all intersections with the approximate singular value curves are computed (squares). In the geometric midpoints of these intersections (crosses) a vertical search for intersections is performed. The maximum value of ξ over all the intersections gives rise to the new value of the level. In the second step, the effect of the discretization is removed by a local corrector based on nonlinear eigenvalue problem (13) (circles)

from the two descriptions of the time-delay system, by the functional differential equation (1) and by the abstract linear equation (5), respectively.

The first approach makes use of so-called delay-Lyapunov equations, introduced in the context of constructing complete-type Lyapunov-Krasovskii functionals for stability assessment (see for instance Kharitonov and Plischke 2006). The following result is a special case of Jarlebring et al. (2011, Theorem 1).

Theorem 1 *Assume that (1) is internally exponentially stable and $D = 0$. Then the $\mathcal{H}_2$ norm of transfer function (3) satisfies*

$$\begin{aligned} \|G\|_{\mathcal{H}_2} &= \mathrm{tr}(B^T U(0) B), \\ &= \mathrm{tr}(C V(0) C^T), \end{aligned}$$

where U, V are the unique solutions of the delay Lyapunov equation

$$\begin{cases} U'(t) = U(t)A_0 + \sum_{k=1}^{m} U(t-\tau_k)A_k, \quad t \in [0, \tau_1], \\ U(-t) = U^T(t), \\ -C^TC = U(0)A_0 + A_0^T U(0) + \sum_{k=1}^{m} \left(U^T(\tau_k)A_k + A_k^T U(\tau_k)\right), \end{cases} \tag{14}$$

and the dual delay Lyapunov equation

$$\begin{cases} V'(t) = V(t)A_0^T + \sum_{k=1}^{m} V(t-\tau_k)A_k^T, \ t \in [0, \tau_{\max}], \\ V(-t) = V^T(t), \\ -BB^T = V(0)A_0^T + A_0V(0) + \sum_{k=1}^{m} \left(V^T(\tau_k)A_k^T + A_kV(\tau_k)\right). \end{cases} \tag{15}$$

The underlying idea in the proof is that the solutions of (14)–(15), as well as the $\mathcal{H}_2$ norm, can be expressed in terms of the *fundamental solution* of the delay equation (see, e.g., Kharitonov and Plischke 2006; Jarlebring et al. 2011).

Theorem 1 opens the possibility to compute $\mathcal{H}_2$ norms by solving delay Lyapunov equations numerically. An approach based on spectral collocation on a Chebyshev mesh is presented in Jarlebring et al. (2011). This approach is generally applicable, but the convergence rate of the approximation (as a function of the number of mesh points) depends on the smoothness properties of the solution, which are on their turn determined by the interdependence of the delays (see Sect. 4 of the reference for a complete characterization). It is also shown that, in the case of commensurate delay values, an analytic solution of (14)–(15) can be obtained, which leads to an *explicit* expression for the $\mathcal{H}_2$ norm involving only matrices of finite dimension.

The second approach is based on discretizing (5). A spectral discretization on the mesh (8) leads us to the linear system

$$\begin{cases} \dot{\mathbf{x}}_N(t) = \mathcal{A}_N\mathbf{x}_N(t) + \mathcal{B}_N\zeta(t), \\ \eta(t) \quad = \mathcal{C}_N\mathbf{x}_N(t), \end{cases} \tag{16}$$

where $\mathcal{A}_N$ is given by (10) and

$$\mathcal{B}_N = [0 \ \cdots \ 0 \ I]^T \otimes B, \mathcal{C}_N = [0 \ \cdots \ 0 \ I] \otimes C.$$

From the fact that (16) is a standard linear time-invariant system we can approximately compute

$$\begin{aligned} \|G\|_{\mathcal{H}_2} \approx \|G_N\|_{\mathcal{H}_2} &= \operatorname{tr}(\mathcal{B}^T Q_N \mathcal{B}_N) \\ &= \operatorname{tr}(\mathcal{C}_N P_N \mathcal{C}^T), \end{aligned}$$

where G_N is the transfer function of (16) and the pair (P_N, Q_N) satisfies (see, e.g., Zhou et al. 1995),

$$\begin{aligned} \mathcal{A}_N P_N + P_N \mathcal{A}_N^T &= -\mathcal{B}_N \mathcal{B}_N^T, \\ \mathcal{A}_N^T Q_N + Q_N \mathcal{A}_N &= -\mathcal{C}_N^T \mathcal{C}_N. \end{aligned} \tag{17}$$

In Vanbiervliet et al. (2011) it has been shown that the approximation error satisfies

$$\|G\|_{\mathcal{H}_2} - \|G_N\|_{\mathcal{H}_2} = \mathcal{O}(N^{-3}), \ N \to \infty,$$

while arguments are provided why fairly accurate results are expected for a moderate value of N already.

Although the second approach is essentially a "discretize first" approach, it is amendable for most control problems because, unlike the delay Lyapunov equation approach of Jarlebring et al. (2011), it does not involve an explicit vectorization of matrix equations (which squares the dimensions of the problem), and because derivatives of the $\mathcal{H}_2$ norm with respect to the elements of the system matrices in (3) can easily be obtained as a by-product of solving (17), see Vanbiervliet et al. (2011).

Finally, for large-scale problems involving sparse coefficient matrices, a discretization-free method has been proposed in Michiels and Zhou (2019), which is related to the infinite Arnoldi method discussed at the end of Sect. 2.1.

3 Making the Leap From Analysis to Synthesis

In what follows we assume that the system matrices in (1) smoothly depend on a finite number of parameters $p = (p_1, \ldots, p_{n_p}) \in \mathbb{R}^{n_p}$. Making the dependence explicit in the notations leads us to system

$$\begin{cases} \dot{x}(t) = A_0(p)x(t) + \sum_{i=1}^{m} A_i(p)x(t-\tau_i) + B(p)\zeta(t), \\ \eta(t) = C(p)x(t) + D(p)\zeta(t-\tau_0). \end{cases} \tag{18}$$

In many control design problems the *closed-loop* system can be brought into the form (18), where the parameters p have an interpretation in terms of a parametrization of the controller, while ζ and η appear as external inputs and outputs, used in the description of performance and robustness specifications. We note that both static and dynamic controllers can be addressed in this framework. It is also possible to impose additional structure on the controller, such as a proportional-integral-derivative (PID) structure, or to impose a sparsity pattern, enabling the design of decentralized and distributed controllers (Dileep et al. 2018).

Because time-delay systems constitute a class of infinite-dimensional systems, illustrated by representation (5) and by the typical presence of infinitely many characteristic roots, *any* control design problem involving the determination of a finite number of parameters can be interpreted as a reduced-order controller synthesis

problem. This explains to a large extent the difficulties and limitations in controlling time-delay systems (Niculescu 2001; Sipahi et al. 2011; Michiels 2019).

The proposed control synthesis methods are based on a direct optimization of appropriately defined cost functions as a function of the parameters p.

3.1 Stabilization

In order to impose internal exponential stability of the null solution of (18), it is necessary to find values of p for which the spectral abscissa

$$c(p) := \sup_{\lambda \in \mathbb{C}} \left\{ \Re(\lambda) : \det \left(\lambda I - A_0(p) - \sum_{i=1}^{m} A_i(p) e^{-\lambda \tau_i} \right) = 0 \right\}$$

is strictly negative. The approach of Vanbiervliet et al. (2008) is based on minimizing the function

$$p \to c(p). \tag{19}$$

Function (19) is in general non convex. It may be not everywhere differentiable, even not everywhere Lipschitz continuous. A lack of differentiability may occur when there are more than one *active* characteristic roots, i.e., a characteristic roots whose real part equals the spectral abscissa. A lack of Lipschitz continuity may occur when an active characteristic roots is multiple and non-semisimple. On the contrary, the spectral abscissa function is differentiable at points where there is only one active characteristic root with multiplicity one. If this is the case with probability one when randomly sampling parameter values, the spectral abscissa is smooth almost everywhere (Vanbiervliet et al. 2008).

The properties of function (19) preclude the use of standard optimization methods, developed for smooth problems. Instead we propose the Broyden-Fletcher-Goldfarb-Shanno (BFGS) algorithm with weak Wolfe line search, whose favorable properties for nonsmooth problems have been reported in Lewis and Overton (2009), with refinements using the gradient sampling algorithm (Burke et al. 2005). This combination of algorithms has been implemented in the MATLAB code HANSO (Overton 2009). The code only requires the evaluation of the objective function, as well as its derivatives with respect to parameters, *whenever* it is differentiable.

The value of the spectral abscissa can be obtained by computing the rightmost characteristic roots, using the methods described in Sect. 2.1. If there is only one active characteristic root λ_a with multiplicity one, the spectral abscissa is differentiable and we can express

$$\frac{\partial c}{\partial p_k}(p) = \Re \left(\frac{w^H \left(\frac{\partial A_0}{\partial p_k}(p) + \sum_{i=1}^{m} \frac{\partial A_i}{\partial p_k}(p) e^{-\lambda_a \tau_i} \right) v}{w^H \left(I + \sum_{i=1}^{m} A_i(p) \tau_i e^{-\lambda_a \tau_i} \right) v} \right)$$

for $k = 1, \ldots, n_p,$, where w and v are the left and right eigenvector corresponding to eigenvalue λ_a.

3.2 Optimizing $\mathcal{H}_\infty$ and $\mathcal{H}_2$ Norms

The properties of the function

$$p \mapsto \|G(\cdot;\, p)\|_{\mathcal{H}_\infty}, \tag{20}$$

where $G(\lambda;\, p)$ is the transfer function of (18), are very similar to the spectral abscissa function. In particular, function (20) is in general not convex, not everywhere differentiable, but it is smooth almost everywhere. Consequently, the methods described in Sect. 3.1 can also be applied to (20). For almost all p derivatives exist and they can be computed from the sensitivity of an individual singular value of $G(\mathrm{i}\omega;\, p)$ with respect to p, for a fixed value of ω, see Gumussoy and Michiels (2011). Unlike objective function (20), function

$$p \mapsto \|G(\cdot;\, p)\|_{\mathcal{H}_2}, \tag{21}$$

is smooth whenever it is finite, which allows an embedding in a derivative based optimization framework. Derivatives of (21) can be obtained either by constructing the *variational equation* corresponding to (14), as worked out in Gomez et al. (2019), or, in a discretize-first setting, from the solutions of the two Lyapunov matrix equations in (17), see Vanbiervliet et al. (2011).

The minimization problems of (20) and (21) contain an implicit constraint, $c(p) < 0$, because the norms are only finite if the system is internally exponentially stable. This leads us to a two-stage approach: if the initial values of the parameters are not stabilizing, then the overall procedure contains a preliminary stabilization phase, using the methods of Sect. 3.1. For the next phase, the actual minimization of (20)–(21), the line-search mechanism in BFGS and the gradient sampling algorithm are adapted in order to discard trial steps or samples outside the feasible set, defined by the implicit constraint (Gumussoy and Michiels 2011).

Instead of directly optimizing the spectral abscissa as in Sect. 3.1, which requires methods for nonsmooth optimization problems, it is also possible to optimize a smooth relaxation of the spectral abscissa function, proposed in Vanbiervliet et al. (2009b), Gomez and Michiels (2019b), which is defined in terms of a relaxed $\mathcal{H}_2$ criterion. In this way stability optimization can also be performed within a derivative based framework. Moreover, an adaptation of the approach makes it possible to solve $\mathcal{H}_2$ optimization problems without the explicit need for a preliminary stabilization phase (Vanbiervliet et al. 2009a).

4 Case Studies

In this section we illustrate the flexibility of the presented control design approach. With the first example from Michiels et al. (2010), we show how to incorporate pole location constraints in the stabilization procedure. The additional flexibility consists of assigning a finite number of characteristic roots, smaller or equal than the number of controller parameters, and using the remaining degrees of freedom to optimize the real part of the rightmost non-assigned characteristic root. With the second example from Gomez et al. (2019), we illustrate the design of a proportional-retarded controller, thereby optimizing a cost function expressed in terms of the $\mathcal{H}_2$ norm and using a delay as a controller parameter.

Example 4.1 Many design criteria for linear control systems, such as the settling time, damping and amount of overshoot, can be translated into a desired location of the rightmost characteristic roots. The characteristic matrix of (18) is given by

$$\Delta(\lambda;\, p) := \lambda I - A_0(p) - \sum_{i=1}^{m} A_i(p) e^{-\lambda \tau_i}.$$

Assigning a real characteristic root to the location r results into the following constraint on the parameter values,

$$\det\left(\Delta(r;\, p)\right) = 0. \tag{22}$$

Similarly, assigning a complex conjugate pair of characteristic roots, $r \pm sj$, results in the constraints

$$\Re\left(\det\left(\Delta(r \pm sj;\, p)\right)\right) = 0;\ \ \Im\left(\det\left(\Delta(r \pm sj;\, p)\right)\right) = 0. \tag{23}$$

If matrix Δ depends in an affine way on p and if the condition

$$\operatorname{rank}\left(\left[\frac{\partial \Delta}{\partial p_1}(\lambda;\, p)\ \cdots\ \frac{\partial \Delta}{\partial p_{n_p}}(\lambda;\, p)\right]\right) = 1,\ \ \forall \lambda \in \mathbb{C}, \tag{24}$$

is satisfied, then the constraints (22)–(23) are affine in p. Hence, assigning k characteristic roots, with $k \leq n_p$, can be expressed by constraints of the form

$$Sp = R, \tag{25}$$

where $S \in \mathbb{R}^{k \times n_p}$ and $R \in \mathbb{R}^{k \times 1}$. It is important to note that the rank condition (24) is satisfied for problems where the closed-loop characteristic matrix results from control through a single input.

In article Michiels et al. (2010) it is shown how the constraints (25) on the parameters can be eliminated. Subsequently, the optimization problem

$$\min_{p\in\mathbb{R}^{n_p},\ Sp=R} \bar{c}(p) \tag{26}$$

is addressed, where

$$\bar{c}(p) := \sup_{\lambda\in\mathbb{C}} \left\{ \Re(\lambda) : \frac{\det\left(\lambda I - A_0(p) - \sum_{i=1}^{m} A_i(p)e^{-\lambda\tau_i}\right)}{\Pi_{i=1}^{k}(\lambda-\lambda_i)} = 0 \right\} \tag{27}$$

and $\{\lambda_1, \ldots, \lambda_k\}$ are the assigned characteristic roots. Problem (26) is a modification of the spectral abscissa minimization problem discussed in Sect. 3.1. Since the assigned roots are specified by the designer, the value of (27) can be obtained by computing the rightmost characteristic roots and removing the assigned ones, which are invariant over the (reduced) controller parameter space.

Let us now consider the solution of problem (26) for the model of an experimental heat transfer set-up at the Czech Technical University in Prague, comprehensively described in Vyhlídal et al. (2009). The model consists of 10 delay differential equations. The addition of an integrator, to achieve a zero steady state error of one of the controlled state variables with respect to a prescribed set-point, eventually results in equations of the form

$$\dot{x}(t) = A_0 x(t) + \sum_{i=1}^{5} A_i x(t-\tau_i) + Bu(t-\tau_6), \tag{28}$$

with $x(t) \in \mathbb{R}^{11\times 11}$ and $u(t) \in \mathbb{R}$. We refer to Vyhlídal et al. (2009) for the corresponding matrices and delay values. In Fig. 2 we show the rightmost characteristic roots of the open-loop system. For the control law

$$u(t) = \sum_{i=1}^{11} p_i x_i(t),$$

the solutions of optimization problem (26) are presented in Table 1. The setting SN1 corresponds to the (unconstrained) minimization of the spectral abscissa (19). The other settings correspond to assigning one real characteristic root (SN2), one pair of complex conjugate characteristic roots (SN3) and, finally, two real roots and two complex conjugate roots (SN4). The assigned characteristic roots were chosen to the right of the minimum of the spectral abscissa function, because these root were intended to become the rightmost roots after solving (26). Their positions were optimized to achieve a properly damped set-point response and disturbance rejection (Michiels et al. 2010). The optimized characteristic root locations are shown in Fig. 3 for settings SN1 and SN4.

Example 4.2 We consider a second-order, oscillatory system of the form

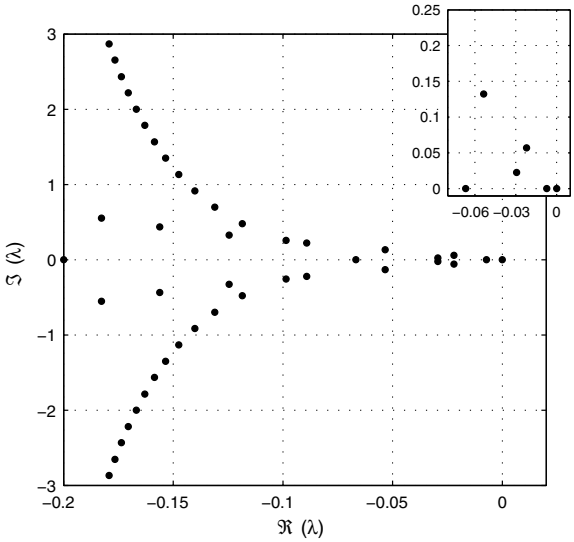

Fig. 2 Rightmost characteristic roots of the open-loop system (28)

Table 1 Controller parameters corresponding to the solution of (26), see the main text for more details

SN	1	2	3	4
λ_i	- - - -	-0.01	$-0.02 \pm 0.02i$	$-0.02, -0.03$ $-0.03 \pm 0.03i$
$\min \bar{c}$	-0.0565	-0.0629	-0.0659	-0.0736
p_1	-5.4349	-0.0732	-4.1420	-0.3521
p_2	3.5879	8.1865	5.9345	8.6190
p_3	-1.4411	-1.2503	-2.3820	-4.8822
p_4	-3.7043	-7.1472	-7.9449	-17.2747
p_5	24.616	32.8003	27.8585	35.1494
p_6	-2.1778	4.4977	0.4490	-1.3188
p_7	9.6924	10.3140	8.4887	6.0338
p_8	-4.5121	-2.6572	-0.2605	5.4190
p_9	-14.631	-21.6711	-20.5152	-24.6596
p_{10}	11.351	4.1244	5.4531	2.3754
p_{11}	-0.7562	-0.2749	-0.3635	-0.1360

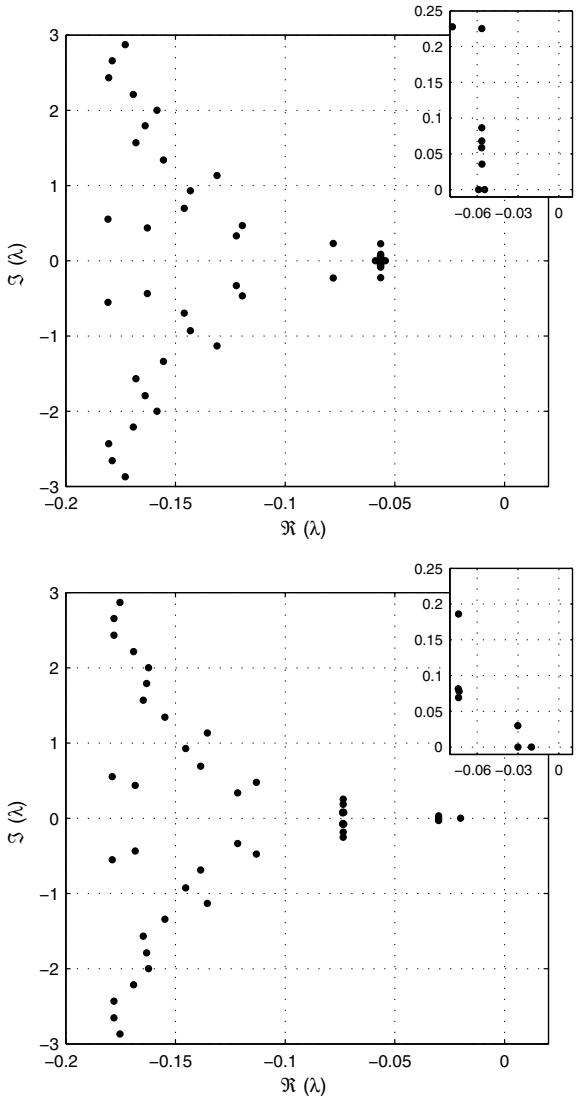

Fig. 3 Rightmost characteristic roots corresponding to the solution of (26), for settings SN1 and SN4 in Table 1

$$\begin{aligned} \dot{x}(t) &= Ax(t) + B(u(t) + \zeta(t)) \\ y(t) &= Cx(t), \\ \eta(t) &= Cx(t), \end{aligned} \tag{29}$$

with matrices

$$A = \begin{bmatrix} 0 & 1 \\ -\nu^2 & -2\delta\nu \end{bmatrix}, \; B = \begin{bmatrix} 0 \\ b \end{bmatrix}, \; C = \begin{bmatrix} 1 & 0 \end{bmatrix},$$

where ν is the natural frequency, δ is the damping factor, and b is the input gain. We introduce a Proportional-Retarded (PR) controller of the form

$$u(t) = -k_p y(t) + k_r y(t - \tau_1), \tag{30}$$

where we consider k_r and τ_1 as parameters. This class of controllers, where the delay is a design parameter, has been studied in recent works (see, for instance, Villafuerte et al. 2013). As a main motivation from an application perspective, controller (30) mimics the behavior of a proportional-derivative (PD) controller, without the need to explicitly differentiate the output, which might amplify sensor noise considerably. The closed-loop system, formed by coupling (29) with (30), is given by

$$\begin{aligned} \dot{x}(t) =& \begin{bmatrix} 0 & 1 \\ -\nu^2 - bk_p & -2\delta\nu \end{bmatrix} x(t) + \begin{bmatrix} 0 & 0 \\ bk_r & 0 \end{bmatrix} x(t - \tau_1) + \begin{bmatrix} 0 \\ b \end{bmatrix} \zeta(t) \\ \eta(t) =& Cx(t). \end{aligned} \tag{31}$$

In order to bring this system model in the form of (18), we perform a transformation of time. Setting $\bar{x}(\bar{t}) = x(t)$, with $t = \tau_1 \bar{t}$, we arrive at

$$\begin{aligned} \dot{\bar{x}}(\bar{t}) =& \begin{bmatrix} 0 & \tau_1 \\ -\nu^2\tau_1 - bk_p\tau_1 & -2\delta\nu\tau_1 \end{bmatrix} \bar{x}(\bar{t}) + \begin{bmatrix} 0 & 0 \\ bk_r\tau_1 & 0 \end{bmatrix} \bar{x}(\bar{t} - 1) \\ &+ \begin{bmatrix} 0 \\ b\tau_1 \end{bmatrix} \zeta(\tau_1 \bar{t}) \\ \eta(\tau_1 \bar{t}) =& C\bar{x}(\bar{t}). \end{aligned} \tag{32}$$

The relation between the $\mathcal{H}_2$ norm of systems (31) and (32) is given as follows:

$$\|G\|_{\mathcal{H}_2}^2 = \frac{1}{\tau_1} \|\bar{G}\|_{\mathcal{H}_2}^2, \tag{33}$$

where $\bar{G}$ is the transfer function of the time-scaled system (32). We use this equality in order to minimize $\|G\|_{\mathcal{H}_2}^2$. We set the following numerical values, corresponding to the model of a DC servomechanism in Villafuerte et al. (2013),

$$\nu = 17.6,\ \delta = 0.0128,\ b = 31,\ k_p = 22.57,$$

and take as parameter vector $p = [p_1\ p_2]$, with $p_1 = \tau_1$ and $p_2 = k_r\tau_1$. From (33), the gradient of $\|G\|_{\mathcal{H}_2}^2$ with respect to p can be expressed as

$$\nabla \|G\|_{\mathcal{H}_2}^2 = \frac{1}{p_1} \begin{bmatrix} \dfrac{\partial \|\bar{G}\|_{\mathcal{H}_2}^2}{\partial p_1} - \dfrac{\|\bar{G}\|_{\mathcal{H}_2}^2}{p_1} \\ \dfrac{\partial \|\bar{G}\|_{\mathcal{H}_2}^2}{\partial p_2} \end{bmatrix}.$$

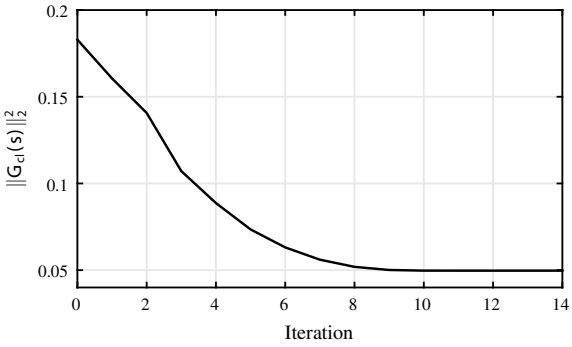

Fig. 4 Values of $\|G\|_{\mathcal{H}_2}^2$ at every iteration, corresponding to Example 4.2

The values of the delay and the gain obtained by minimization of the $\mathcal{H}_2$ norm of system (31), with initial parameters $p = [0.03\ 0.09]$, are given by $\tau_1 = 0.05187$ and $k_r = 17.9643$, while the achieved value of $\|G\|_{\mathcal{H}_2}^2$ is 0.0497. Figure 4 shows the value of the $\mathcal{H}_2$ norm of system (31) at every iteration of the optimization of function (33).

5 Equations of Neutral Type and Delay Differential Algebraic Equations

In this section we consider delay differential algebraic equation (DDAE) models of the form

$$\begin{cases} E\dot{x}(t) = A_0 x(t) + \sum_{i=1}^{m} A_i x(t-\tau_i) + B\zeta(t), \\ \eta(t) = Cx(t), \end{cases} \tag{34}$$

where leading matrix E is singular, $x(t) \in \mathbb{C}^n, \zeta(t) \in \mathbb{C}^{n_\zeta}$, $\eta(t) \in \mathbb{C}^{n_\eta}$ are the (pseudo)state, input and output at time t, and $0 < \tau < \cdots < \tau_m$ represent the time-delays. With the following examples we illustrate the generality of model (34).

Example 5.1 Consider the feedback interconnection of system

$$\begin{cases} \dot{x}(t) = Ax(t) + B_1 u(t) + B_2 \zeta(t), \\ y(t) = Cx(t) + D_1 u(t), \\ \eta(t) = Fx(t), \end{cases}$$

and controller

$$u(t) = Ky(t-\tau).$$

For $\tau = 0$, it is possible to eliminate the output and the controller equation, which results in the closed-loop system

$$\begin{cases} \dot{x}(t) = Ax(t) + B_1K(I - D_1K)^{-1}Cx(t) + B_2\zeta(t), \\ \eta(t) = Fx(t). \end{cases} \tag{35}$$

This approach is for instance taken in the software package HIFOO (Burke et al. 2006). If $\tau \neq 0$, then the elimination is not possible any more. However, if we let $X = [x^T\ u^T\ y^T]^T$ we can describe the system by the equations

$$\begin{cases} \begin{bmatrix} I & 0 & 0 \\ 0 & 0 & 0 \\ 0 & 0 & 0 \end{bmatrix} \dot{X}(t) = \begin{bmatrix} A & B_1 & 0 \\ C & D_1 & -I \\ 0 & I & 0 \end{bmatrix} X(t) - \begin{bmatrix} 0 & 0 & 0 \\ 0 & 0 & 0 \\ 0 & 0 & K \end{bmatrix} X(t-\tau) + \begin{bmatrix} B_2 \\ 0 \\ 0 \end{bmatrix} \zeta(t), \\ \eta(t) = \begin{bmatrix} F & 0 & 0 \end{bmatrix} X(t), \end{cases}$$

which are of the form (34). Furthermore, the dependence of the matrices of the closed-loop system on the controller gain K is still linear, unlike in (35).

Example 5.2 The presence of a direct feedthrough term from ζ to η, as in

$$\begin{cases} \dot{x}(t) = A_0x(t) + A_1x(t-\tau) + B\zeta(t), \\ \eta(t) = Fx(t) + D_2\zeta(t), \end{cases} \tag{36}$$

can be avoided by introducing a slack variable. If we let $X = [x^T\ \gamma^T]^T$, where γ is the slack variable, we can bring (36) in the form (34):

$$\begin{cases} \begin{bmatrix} I & 0 \\ 0 & 0 \end{bmatrix} \dot{X}(t) = \begin{bmatrix} A_0 & 0 \\ 0 & -I \end{bmatrix} X(t) + \begin{bmatrix} A_1 & 0 \\ 0 & 0 \end{bmatrix} X(t-\tau) + \begin{bmatrix} B \\ I \end{bmatrix} \zeta(t), \\ \eta(t) = [F\ D_2]\, X(t). \end{cases}$$

In a similar fashion the feedthrough term $Du(t - \tau_0)$ in (1) can be eliminated.

Example 5.3 The following system with input delay and input dynamics,

$$\begin{cases} \dot{x}(t) = Ax(t) + B_1\zeta(t) + B_2\zeta(t-\tau), \\ \eta(t) = Cx(t), \end{cases}$$

can also be brought into standard form (34), again by using a slack variable. Setting $X = [x^T\ \gamma^T]^T$, with (pseudo)state variable γ representing a copy of the input, we can express

$$\begin{cases} \dot{X}(t) = \begin{bmatrix} A & B_1 \\ 0 & -I \end{bmatrix} X(t) + \begin{bmatrix} 0 & B_2 \\ 0 & 0 \end{bmatrix} X(t-\tau) + \begin{bmatrix} 0 \\ I \end{bmatrix} \zeta(t), \\ \eta(t) = [C\ \ 0]\, X(t). \end{cases}$$

In a similar way we can handle multiple delays in the output.

Example 5.4 Neutral type systems can be considered as well. The following neutral equation

$$\frac{\mathrm{d}}{\mathrm{d}t}\left(x(t)+\sum_{i=1}^{m} G_i x(t-\tau_i)\right)=\sum_{i=0}^{m} H_i x(t-\tau_i)$$

can for instance be rewritten as

$$\begin{cases} \dot{\gamma}(t) = \displaystyle\sum_{i=0}^{m} H_i x(t-\tau_i), \\ 0 \;\; = -\gamma(t)+x(t)+\displaystyle\sum_{i=1}^{m} G_i x(t-\tau_i). \end{cases} \tag{37}$$

Clearly (37) is of the form (34), with (pseudo)state $[\gamma(t)^T \; x(t)^T]^T$.

It should be noted that DDAE models are particularly suitable for the (automated) modeling and description of interconnected systems, where the differential equations stem from a systematic description of the subsystems or components, while the algebraic and delay difference equations model their interconnections. As a final illustration, the feedback interconnection of any retarded type time-delay system and controller with the following state-space representations,

$$\begin{cases} \dot{x}_G(t) = \displaystyle\sum_{i=0}^{m_a} A^i x_G(t-\tau_i^a) + \sum_{i=0}^{m_{b_1}} B_1^i \zeta(t-\tau_i^{b_1}) + \sum_{i=0}^{m_{b_2}} B_2^i u(t-\tau_i^{b_2}) \\ \eta(t) = \displaystyle\sum_{i=0}^{m_{c_1}} C_1^i x_G(t-\tau_i^{c_1}) + \sum_{i=0}^{m_{d_{11}}} D_{11}^i \zeta(t-\tau_i^{d_{11}}) + \sum_{i=0}^{m_{d_{12}}} D_{12}^i u(t-\tau_i^{d_{12}}) \\ y(t) = \displaystyle\sum_{i=0}^{m_{c_2}} C_2^i x_G(t-\tau_i^{c_2}) + \sum_{i=0}^{m_{d_{21}}} D_{21}^i \zeta(t-\tau_i^{d_{21}}) + \sum_{i=0}^{m_{d_{22}}} D_{22}^i u(t-\tau_i^{d_{22}}) \end{cases} \tag{38}$$

and

$$\begin{cases} \dot{x}_K(t) = \displaystyle\sum_{i=0}^{m_{a_k}} A_K^i x_K(t-\tau_i^{a_k}) + \sum_{i=0}^{m_{b_k}} B_K^i y(t-\tau_i^{b_k}) \\ u(t) = \displaystyle\sum_{i=0}^{m_{c_k}} C_K^i x_K(t-\tau_i^{c_k}) + \sum_{i=0}^{m_{d_k}} D_K^i u(t-\tau_i^{d_k}), \end{cases} \tag{39}$$

can be written in the form of (34) by combining the techniques illustrated with the previous examples. More precisely, the transformation consists of the elimination of input dynamics, output dynamics, and non-trivial feedthrough terms.

The price to pay for the generality of model (34) is the increase of the dimension of the system, n, compared to classical DDE models, which may affect the efficiency of the numerical methods. However, this is a minor problem in most of the applications, because the delay difference equations or algebraic constraints are related to inputs and outputs, and for large-scale problems the number of inputs and outputs are usually much smaller than the number of state variables. Another consequence of the generality is that assumptions for well-posedness are necessary (in the next

subsection we will introduce such an assumption). To illustrate the necessity, the DDAE

$$\begin{aligned} \dot{x}_1(t) &= x_1(t) + x_2(t-\tau_1) \\ 0 &= -x_2(t-\tau_2) + x_1(t-\tau_3) \end{aligned}$$

is not causal if $\tau_2 > \tau_1 + \tau_3$, following from the underlying delay differential equation $\dot{x}_1(t) = x_1(t) + x_1(t-\tau_1-\tau_3+\tau_2)$.

5.1 Preliminaries and Assumptions

Let matrix E in (34) satisfy

$$\operatorname{rank}(E) = n - \nu,$$

with $1 \leq \nu < n$, and let the columns of matrix $U \in \mathbb{R}^{n\times\nu}$, respectively $V \in \mathbb{R}^{n\times\nu}$, be a (minimal) basis for the right, respectively left nullspace of E, which implies

$$U^T E = 0, \;\; EV = 0.$$

Furthermore we define $U^\perp$ and $V^\perp$ as $n \times (n-\nu)$ matrices whose columns span the orthogonal complement of the column spaces of U and V. Throughout the remainder of the chapter we make the following assumption.

Assumption 5.5 Matrix $U^T A_0 V$ is nonsingular.

Assumption 5.5 implies that the differentiation index of (34) is one, corresponding to a system of semi-explicit DDAEs. It is satisfied for all the examples discussed before. The equations (34) can now be explicitly separated into coupled delay differential and delay difference equations. The pre-multiplication of (34) with matrix

$$\begin{bmatrix} U^{\perp T} \\ -(U^T A_0 V)^{-1} U^T \end{bmatrix}$$

and the substitution

$$x = \begin{bmatrix} V^\perp & V \end{bmatrix} \begin{bmatrix} x_1 \\ x_2 \end{bmatrix},$$

with $x_1(t) \in \mathbb{R}^{n-\nu}$ and $x_2(t) \in \mathbb{R}^\nu$, result in the coupled equations

$$\left\{ \begin{aligned} E^{(11)}\dot{x}_1(t) &= \sum_{i=0}^{m} A_i^{(11)} x_1(t-\tau_i) + \sum_{i=0}^{m} A_i^{(12)} x_2(t-\tau_i) + B_1\zeta(t), \\ x_2(t) &= \sum_{i=0}^{m} A_i^{(21)} x_1(t-\tau_i) + \sum_{i=1}^{m} A_i^{(22)} x_2(t-\tau_i) + B_2\zeta(t), \\ \eta(t) &= C_1 x_1(t) + C_2 x_2(t), \end{aligned} \right. \tag{40}$$

where we have $\tau_0 = 0$,

$$E^{(11)} = U^{\perp T} E V^{\perp},\ A_i^{(11)} = U^{\perp T} A_i V^{\perp},\ A_i^{(12)} = U^{\perp T} A_i V,$$

$$\begin{aligned} A_i^{(21)} &= -(U^T A_0 V)^{-1} U^T A_i V^{\perp},\ i = 0, \ldots, m, \\ A_i^{(22)} &= -(U^T A_0 V)^{-1} U^T A_i V, \quad i = 1, \ldots, m, \end{aligned}$$

and

$$B_1 = U^{\perp T} B,\ B_2 = -(U^T A_0 V)^{-1} U^T B,\ C_1 = C V^{\perp},\ C_2 = C V.$$

In (40) matrix $E^{(11)}$ is invertible, following from

$$\operatorname{rank}(E^{(11)}) = \operatorname{rank}\left(\left[U^{\perp}\ U\right]^T E \left[V^{\perp}\ V\right]\right) = \operatorname{rank}(E) = n - \nu.$$

We consider initial functions φ for Eq. (34) that belong to the set $AC\left([-\tau_m, 0], \mathbb{C}^n\right)$ and call them consistent if the corresponding initial value problem at $t = 0$ has at least one solution (Du et al. 2013). A function $x(t; \varphi)$ is called a (classical) solution if it is absolutely continuous, it satisfies (34) almost everywhere on $[0, \infty)$, and $x(\theta; \varphi) = \varphi(\theta)$ for $\theta \in [-\tau_m, 0]$, where φ is a consistent initial function. For a continuously differentiable input function, the space of consistent initial functions for (34) is given by

$$\mathcal{X} := \left\{ \begin{array}{l} \varphi \in AC\left([-\tau_m, 0], \mathbb{C}^n\right) : \\ \qquad U^T A_0 \varphi(0) + \displaystyle\sum_{i=1}^{m} U^T A_i \varphi(-\tau_i) + U^T B \zeta(0) = 0 \end{array} \right\},$$

which corresponds to the set of initial conditions for which the second equation in (40) is satisfied at $t = 0$. Moreover, for every initial function belonging to $\mathcal{X}$, a forward solution is uniquely defined (Ha and Mehrmann 2012; Du et al. 2013; Fridman 2002). We say that system (34), with zero input, is (internally) exponentially stable if there exist constants $\gamma > 0$ and $\sigma > 0$ such that for every initial condition $\varphi \in \mathcal{X}$, the emanating solution satisfies

$$\|x(t; \varphi)\|_2 \leq \gamma e^{-\sigma t} \left(\sup_{\theta \in [-\tau_m, 0]} \|\varphi(\theta)\|_2 \right),\ \forall t \geq 0.$$

5.2 *Spectral Properties and Stability*

We summarize the main theoretical results from Michiels (2011), addressing the stability of the null solution of (34) for $\zeta \equiv 0$.

Exponential Stability. Stability conditions can still be expressed in terms of the position of the characteristic roots, satisfying

$$\det \Delta(\lambda) = 0,$$

where $\Delta : \mathbb{C} \to \mathbb{C}^{n\times n}$ is the characteristic matrix,

$$\Delta(\lambda) := \lambda E - A_0 - \sum_{i=1}^{m} A_i e^{-\lambda\tau_i}.$$

In particular, we have the following result.

Proposition 5.6 *The null solution of (34) is internally exponentially stable if and only if $c < 0$, where c is the* spectral abscissa*:*

$$c := \sup\{\Re(\lambda) : \det \Delta(\lambda) = 0\}.$$

Continuity of the Spectral Abscissa and Strong Stability. We discuss the dependence of the spectral abscissa of (34) on the delay parameters $\vec{\tau} := (\tau_1, \ldots, \tau_m)$. In general the function

$$\vec{\tau} \in (\mathbb{R}_0^+)^m \mapsto c(\vec{\tau}) \tag{41}$$

is not everywhere continuous, as we shall illustrate with an example later on. In fact the lack of continuity carries over from the spectral properties of delay difference equations (see, e.g., Avellar and Hale 1980; Michiels et al. 2002, 2009). Therefore, we first outline properties of the function

$$\vec{\tau} \in (\mathbb{R}_0^+)^m \mapsto c_D(\vec{\tau}) := \sup\{\Re(\lambda) : \det \Delta_D(\lambda; \vec{\tau}) = 0\}, \tag{42}$$

with

$$\Delta_D(\lambda; \vec{\tau}) := -I + \sum_{i=1}^{m} A_i^{(22)} e^{-\lambda\tau_i}. \tag{43}$$

Note that (43) can be interpreted as the characteristic matrix of the delay difference equation

$$x_2(t) = \sum_{i=1}^{m} A_i^{(22)} x_2(t - \tau_i), \tag{44}$$

which is associated with the neutral equation.

The property that function (42) may not be continuous led in Michiels and Vyhlídal (2005) to the smallest upper bound, which is '*insensitive*' to small delay changes. Letting

$$\mathcal{B}(\vec{\tau}, \epsilon) := \{\vec{\theta} \in (\mathbb{R}^+)^m : \|\vec{\theta} - \vec{\tau}\|_2 < \epsilon\}, \tag{45}$$

we can define the robust spectral abscissa c_D of the delay difference equation (44) as follows.

Definition 5.7 For $\vec{\tau} \in (\mathbb{R}_0^+)^m$, let $C_D(\vec{\tau}) \in \mathbb{R}$ be defined as

$$C_D(\vec{\tau}) := \lim_{\epsilon \to 0+} c_D^{\epsilon}(\vec{\tau}),$$

where

$$c_D^{\epsilon}(\vec{\tau}) := \sup \{c_D(\vec{\tau}_\epsilon) : \vec{\tau}_\epsilon \in \mathcal{B}(\vec{\tau}, \epsilon)\}.$$

Several properties of this upper bound on c_D are listed below (see (Michiels 2011, Sect. 3) for an overview).

Proposition 5.8 *The following assertions hold:*

1. *function*
$$\vec{\tau} \in (\mathbb{R}_0^+)^m \mapsto C_D(\vec{\tau})$$
is continuous;
2. *for every $\vec{\tau} \in (\mathbb{R}_0^+)^m$, the quantity $C_D(\vec{\tau})$ is equal to the unique zero of the strictly decreasing function*
$$\chi \in \mathbb{R} \to f(\chi; \vec{\tau}) - 1,$$
where $f : \mathbb{R} \to \mathbb{R}^+$ is defined by
$$f(\chi; \vec{\tau}) := \max_{\vec{\theta} \in [0,\ 2\pi]^m} \rho \left(\sum_{k=1}^{m} A_k^{(22)} e^{-\chi \tau_k} e^{i\theta_k} \right) \tag{46}$$
and $\rho(\cdot)$ denotes the spectral radius;
3. *$C_D(\vec{\tau}) = c_D(\vec{\tau})$ for rationally independent delays*[2]
4. *for all $\vec{\tau}_1, \vec{\tau}_2 \in (\mathbb{R}_0^+)^m$, we have*
$$\text{sign}\,(C_D(\vec{\tau}_1)) = \text{sign}\,(C_D(\vec{\tau}_2)) =: \Sigma;$$
5. *condition $\Sigma < 0$ (> 0) holds if and only if $\gamma_0 < 1$ (> 1) holds, where*
$$\gamma_0 := \max_{\vec{\theta} \in [0,\ 2\pi]^m} \rho \left(\sum_{k=1}^{m} A_k^{(22)} e^{i\theta_k} \right). \tag{47}$$

We now come back to DDAE (34) and, in particular, the properties of its spectral abscissa function (41). The following two technical lemmas establish connections between the characteristic roots of (34) and the zeros of (43).

[2] The m components of $\vec{\tau} = (\tau_1, \ldots, \tau_m)$ are rationally independent if and only if $\sum_{k=1}^{m} n_k \tau_k = 0,\ n_k \in \mathbb{Z}$ implies $n_k = 0, \forall k = 1, \ldots, m$.

Lemma 5.9 *If c_D is finite, then there exists a sequence $\{\lambda_k\}_{k\geq 1}$ of characteristic roots of (34) satisfying*

$$\lim_{k\to\infty} \Re(\lambda_k) = c_D, \ \lim_{k\to\infty} \Im(\lambda_k) = +\infty.$$

Lemma 5.10 *For every $\epsilon > 0$ the number of characteristic roots of (34) in the half plane*

$$\{\lambda \in \mathbb{C} : \Re(\lambda) \geq C_D(\vec{\tau}) + \epsilon\}$$

is finite.

The lack of continuity of the spectral abscissa function (41) leads us again to an upper bound that takes into account the effect of small delay perturbations.

Definition 5.11 For $\vec{\tau} \in (\mathbb{R}_0^+)^m$, let the *robust spectral abscissa* $C(\vec{\tau})$ of (34) be defined as

$$C(\vec{\tau}) := \lim_{\epsilon\to 0+} c^\epsilon(\vec{\tau}), \tag{48}$$

where

$$c^\epsilon(\vec{\tau}) := \sup\{c(\vec{\tau}_\epsilon) : \vec{\tau}_\epsilon \in \mathcal{B}(\vec{\tau}, \epsilon)\}.$$

The following characterization of the robust spectral abscissa (48) constitutes the main theoretical result of this section.

Proposition 5.12 *The following assertions hold:*

1. *the function*
$$\vec{\tau} \in (\mathbb{R}_0^+)^m \mapsto C(\vec{\tau})$$
is continuous;
2. *for every $\vec{\tau} \in (\mathbb{R}_0^+)^m$, we have*
$$C(\vec{\tau}) = \max(C_D(\vec{\tau}), c(\vec{\tau})).$$

In line with the sensitivity of the spectral abscissa with respect to infinitesimal delay perturbations, which has been resolved by considering the robust spectral abscissa (48) instead, we define the notion of strong stability.[3]

Definition 5.13 The null solution of (34), with zero input, is strongly stable if there exists a number $\hat{\tau} > 0$ such that the null solution of

$$E\dot{x}(t) = A_0 + \sum_{k=1}^{m} A_k x(t - (\tau_k + \delta\tau_k))$$

[3] This terminology is borrowed from the theory of neutral delay differential equations (Hale and Verduyn Lunel 2002; Michiels and Vyhlídal 2005).

is exponentially stable for all $\delta\vec{\tau} \in (\mathbb{R}^+)^m$ satisfying $\|\delta\vec{\tau}\|_2 < \hat{\tau}$ and $\tau_k + \delta\tau_k \geq 0,\ k = 1, \ldots, m$.

The following result provides necessary and sufficient conditions for strong stability.

Theorem 5.14 *The null solution of (34) is strongly stable if and only if* $C(\vec{\tau}) < 0$, *or, equivalently,* $c(\vec{\tau}) < 0$ *and* $\gamma_0 < 1$, *where* γ_0 *is defined by (47).*

Finally we note, that both the spectral abscissa and the robust spectral abscissa of (34) are continuous functions of the elements of the system matrices.

5.3 Robust Stabilization by Eigenvalue Optimization

As in Sect. 3, we assume that the system matrices smoothly depend on control or design parameters $p \in \mathbb{R}^{n_p}$, which is made explicit in the description

$$E\dot{x}(t) = A_0(p)x(t) + \sum_{i=1}^{m} A_i(p)x(t - \tau_i). \tag{49}$$

For example, in the feedback interconnection (38)–(39) parameter vector p may arise from a parameterization of matrices $(A_K^i,\ B_K^i,\ C_K^i,\ D_K^i)$.

To impose exponential stability of the null solution of (49), it is necessary to find values of p for which the spectral abscissa is strictly negative. If the achieved stability is required to be *robust against small delay perturbations*, this requirement must be strengthened to the negativeness of the robust spectral abscissa. This brings us to the optimization problem

$$\min_p C(\vec{\tau};\, p). \tag{50}$$

Strongly stabilizing values of p exist if the objective function can be made strictly negative. By Theorem 5.14 the latter can be evaluated as

$$C(\vec{\tau};\, p) = \max(c(\vec{\tau};\, p), C_D(\vec{\tau};\, p)). \tag{51}$$

An alternative approach consists of solving the constrained optimization problem

$$\inf_p c(\vec{\tau};\, p),\ \text{subject to}\ \gamma_0(p) < \gamma, \tag{52}$$

with $\gamma < 1$. If the objective function is strictly negative, then the satisfaction of the constraint implies strong stability. Problem (52) can be solved using the barrier method proposed in Vyhlídal et al. (2010), which is inspired by interior point algorithms, see, e.g., Boyd and Vandenberghe (2004). The first step consists of finding a feasible point, i.e., a set of values for p satisfying the constraint. If the feasible set is

nonempty, such a point can be found by solving

$$\min_p \gamma_0(p). \tag{53}$$

Once a feasible point $p = p_0$ has been obtained, one can solve in the next step the unconstrained optimization problem

$$\min_p \; c(p) - r \log(\gamma - \gamma_0(p)), \tag{54}$$

where $r > 0$ is a small number and γ satisfies

$$\gamma_0(p) < \gamma \leq 1.$$

The second term in (54), the barrier, assures that the feasible set cannot be left when the objective function is decreased in a quasi-continuous way (because the objective function will go to infinity when $\gamma_0 \to \gamma$). If (54) is repeatedly solved for decreasing values of r and with the previous solution as a starting value, a solution of (52) is obtained.

For optimization problem (50) and for subproblems (53) and (54), which are in general not everywhere differentiable but smooth a.e., we use once again the code HANSO (Overton 2009). Note in particular that the switching between the arguments of the maximum operator in (51) is treated in the same way as the switching between individual characteristic root paths when optimizing only the spectral abscissa. The overall algorithm only requires the evaluation of the objective function, as well as its derivatives with respect to the controller parameters, *whenever* it is differentiable. The spectral abscissa can be computed using a spectral discretization, directly extending the approach of Sect. 2.1, followed by Newton corrections. The quantities C_D and γ_0 can be computed using the characterizations in Theorem 5.8, where the (global) maximization problems in (46) and (47) are solved by discretizing the domain $[0,\ 2\pi]^{m-1}$, followed by local corrections. In all cases derivatives with respect to p can be obtained from derivatives of individual eigenvalues or singular values. For more details and expressions we refer to Michiels (2011).

5.4 Examples

We first illustrate the design of a strongly stabilizing controller. Subsequently, we show how the computation of zeros of transfer function (3) can be recast in the computation of characteristic roots of an associated DDAE.

Example 5.15 We consider the system with input delay from Vanbiervliet et al. (2008),

$$\dot{x}(t) = Ax(t) + Bu(t-\tau), \quad y(t) = x(t), \tag{55}$$

where

$$A = \begin{bmatrix} -0.08 & -0.03 & 0.2 \\ 0.2 & -0.04 & -0.005 \\ -0.06 & 0.2 & -0.07 \end{bmatrix}, \quad B = \begin{bmatrix} -0.1 \\ -0.2 \\ 0.1 \end{bmatrix}, \quad \tau = 5. \tag{56}$$

The uncontrolled system is unstable, with spectral abscissa equal to 0.108. We design a stabilizing static controller

$$u(t) = Ky(t), \tag{57}$$

as well as a dynamic controller of the form

$$\begin{cases} \dot{x}_c(t) = A_c x_c(t) + B_c y(t), \\ u(t) \ = C_c x_c(t) + D_c y(t), \quad x_c(t) \in \mathbb{R}^{n_c}, \end{cases} \tag{58}$$

using the approach of Sect. 5.3. More precisely we treat (55) and (57), respectively (55) and (58), as a system of DDAEs, with (pseudo)state $[x^T \ u^T \ y^T]^T$, respectively $[x^T \ x_c^T \ u^T \ y^T]^T$, while we set $p = \text{vec}\, K$, respectively

$$p = \text{vec} \begin{bmatrix} A_c & B_c \\ C_c & D_c \end{bmatrix}.$$

Since the transfer function from u to y in (55) is strictly proper, the robust spectral abscissa equals the spectral abscissa, and optimization problems (50) and (52) reduce to the (unconstrained) minimization of the spectral abscissa. The resulting optimized spectrum is displayed in Fig. 5 for the static controller and for a dynamic controller of order $n_c = 2$. Note that the additional degrees of freedom in the dynamic controller lead to a further reduction of the spectral abscissa.

Next we assume that the measured output of system (55) is instead given by

$$\tilde{y}(t) = x(t) + \begin{bmatrix} 3 \\ 4 \\ 1 \end{bmatrix} u(t - 2.5) + \begin{bmatrix} 2/5 \\ -2/5 \\ -2/5 \end{bmatrix} u(t - 5), \tag{59}$$

for which we design a static controller,

$$u(t) = D_c \tilde{y}(t).$$

As a main difference with the previous example, there are two non-trivial feedthrough terms in the system model, which are both delayed. By a combination of this model and the control law, the closed loop system is no longer of retarded type. Solving optimization problem (50) leads us to

$$C = -0.0309, \quad D_c = [0.0409 \ \ 0.0612 \ \ 0.3837]. \tag{60}$$

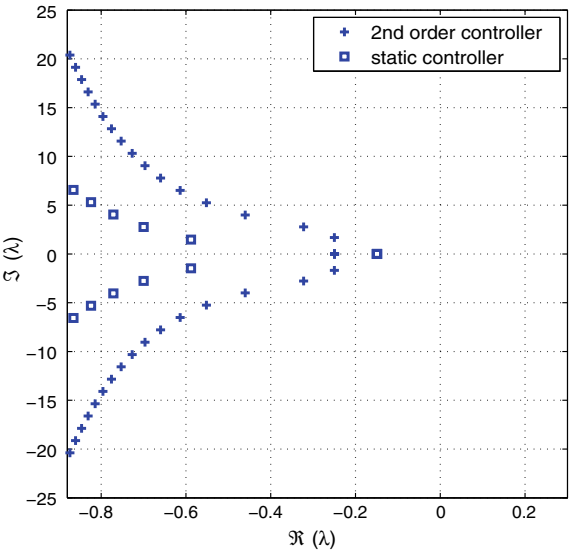

Fig. 5 Characteristic roots of controlled system (55)–(56), corresponding to a minimum of the spectral abscissa function, for static controller (57) (boxes) and for dynamic controller (58) of order two (pluses)

The computed rightmost characteristic roots of the closed-loop system are given by

$$\begin{aligned}\lambda_1 &= -0.0309,\\ \lambda_{2,3} &= -0.0309 \pm 0.0001\mathrm{i},\\ \lambda_{4,5} &= -0.3336 \pm 2.3789\mathrm{i},\\ \lambda_{6,7} &= -0.3499 \pm 4.8863\mathrm{i}.\end{aligned}$$

They indicate that the optimum is characterized by a rightmost characteristic root of multiplicity three, which must be non-semisimple because of the use of a single control input. Note that due to the high sensitivity of such roots (Michiels et al. 2017), a very accurate replication using an a-posteriori spectrum computation is not possible.

The presence of three rightmost roots (counting multiplicity) may sound counter-intuitive because the number of degrees of freedom in the controller is also three. The explanation is that we are in a situation where $C_D \geq c$. In fact, the optimum of (50) is characterized by an equality between C_D and the spectral abscissa c. Hence, in the optimum we have four conflicting objectives: the three eigenvalues constituting the multiple root, and the behavior of high frequency characteristic roots, captured by quantity C_D. In the left panel of Fig. 6 we show the rightmost characteristic roots corresponding to the minimum of the robust spectral abscissa (60). The dotted line corresponds to $\Re(\lambda) = c_D$, the dashed line to $\Re(\lambda) = C_D$. In order to illustrate that we indeed have $c = C_D$, we depict in the right panel of Fig. 6 the rightmost characteristic roots after perturbing the delay value 2.5 in (59) to 2.51.

When we solve instead the constrained optimization problem (52) with the default parameters $r = 10^{-3}$ and $\gamma = 1 - 10^{-3}$ in the relaxation (54), we arrive at the

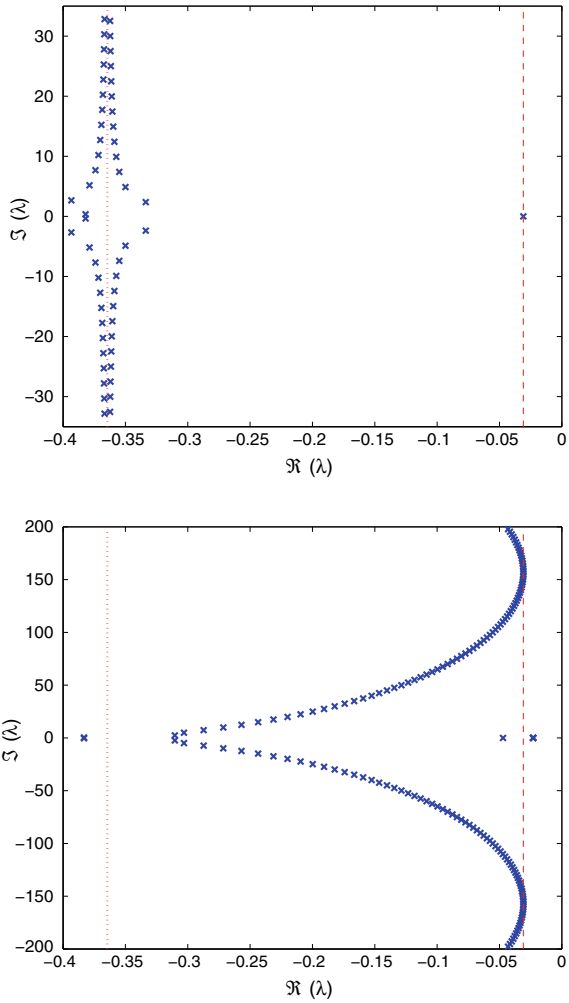

Fig. 6 (Top) Characteristic roots corresponding to the minimum of the robust spectral abscissa of the second example (55) and (59), using a static controller. The rightmost characteristic roots, $\lambda \approx -0.0309$, has multiplicity three. (Bottom) Effect on the characteristic roots of a perturbation of the delays (2.5, 5) in (59) to (2.51, 5)

controller gain $D_c = [0.0249\ 0.1076\ 0.3173]$. Compared to (60), where we had $C = c = C_D$, a further reduction of the spectral abscissa to $c = -0.0345$ has been achieved, at the price of an increased value of C_D (equal to -0.00602). This is expected because the constraint $\gamma_0 < 1$ imposes robustness of stability, yet no bound on the exponential decay rate of the solutions.

Example 5.16 A transmission zero of system (1) is a number $z_0 \in \mathbb{C}$ such that $G(z_0) = 0$. In the time-domain the meaning is as follows. If an exponentially stable system is excited by signal

$$\zeta(t) = \underline{\zeta} e^{z_0 t}, \tag{61}$$

then the stationary response in the output η is identically zero, for any $\underline{\zeta} \in \mathbb{C}^{n_\zeta}$. This interpretation is at the basis of the computation of transmission zeros. Due to the separation principle in the frequency domain, the stationary response to excitation (61) takes the form

$$x(t) = \underline{x}e^{z_0 t}, \ \eta(t) = \underline{\eta}e^{z_0 t}.$$

Substituting these functions in (1) and requiring that $\eta \equiv 0$ brings us to

$$\begin{bmatrix} z_0 I - A_0 - \sum_{i=1}^{m} A_i e^{-z_0 \tau_i} & -B \\ C & De^{-z_0 \tau_{m+1}} \end{bmatrix} \begin{bmatrix} \underline{x} \\ \underline{\zeta} \end{bmatrix} e^{z_0 t} = 0.$$

The 2-by-2 block matrix in the left-hand side can be interpreted as the characteristic matrix of a DDAE, and, accordingly, its characteristic roots are the transmission zeros. The extension to model (34) is straightforward.

Transmission zeros play a central role in applications related to vibration control. Signal shapers and vibration absorbers are tuned in such a way that the transfer function from the location where undesired vibrations enter the system to the location where vibrations need to be annihilated, has transmission zeros at the dominant frequencies. For the design and implementation of novel classes of signal shapers and vibration absorbers that explicitly use delays as controller parameters, and for the use of DDAE models to describe the overall system, we refer to Pilbauer (2017) and the references therein.

5.5 *Note on the Strong $\mathcal{H}_2$ and $\mathcal{H}_\infty$ Norm*

Similarly to the spectral abscissa, the $\mathcal{H}_2$ and $\mathcal{H}_\infty$ system norms of DDAEs suffer from a fragility problem, in the sense of being potentially sensitive to infinitesimal delay perturbations. The latter cannot be excluded from an application point of view. Before we analyze the problem and present robustified measures, we introduce some notation and motivating examples. We denote by $\hat{G}$ the transfer function of (34),

$$\hat{G}(\lambda) := C \left(\lambda E - A_0 - \sum_{i=1}^{m} A_i e^{-\lambda \tau_i} \right)^{-1} B.$$

We also introduce the corresponding *asymptotic transfer function* $\hat{G}_a$,

$$\hat{G}_a(s) := C_2 \left(I - \sum_{i=1}^{m} A_i^{(22)} e^{-\lambda \tau_i} \right)^{-1} B_2.$$

It can be interpreted as the transfer function of delay difference equation

$$\begin{cases} x_2(t) = \sum_{i=1}^{m} A_i^{(22)} x_2(t-\tau_i) + B_2\zeta(t), \\ \eta(t) = C_2 x_2(t), \end{cases} \tag{62}$$

obtained by setting $x_1 = 0$ in the second equation of (40). It describes the asymptotic behavior of $\hat{G}(\lambda)$ for $|\lambda| \to \infty$ in the closed right half plane. The following property is proven in Gumussoy and Michiels (2011).

Proposition 5.17 *For all $\gamma > 0$, there exists a number $\Omega > 0$ such that $\left\| \hat{G}(i\omega) - \hat{G}_a(i\omega) \right\|_2 < \gamma$ for all $\omega > \Omega$.*

With the following example we illustrate that functions

$$\left(\mathbb{R}_0^+\right)^m \ni \vec{\tau} \mapsto \left\| \hat{G}(\cdot;\vec{\tau}) \right\|_{\mathcal{H}_2}, \quad \left(\mathbb{R}_0^+\right)^m \ni \vec{\tau} \mapsto \left\| \hat{G}(\cdot;\vec{\tau}) \right\|_{\mathcal{H}_\infty}$$

may not be continuous, even if the system is strongly stable, and that this phenomenon is related to the behavior of the asymptotic transfer function.

Example 5.18 We consider system (34), already in the form (40) with $m = 2$ and matrices $E^{(11)} = 1$, $A_0^{(11)} = -10$, $A_0^{(12)} = \begin{bmatrix} 1 & 1 \end{bmatrix}$, $A_0^{21} = \begin{bmatrix} 0 & 0 \end{bmatrix}^T$,

$$\left[\begin{array}{c|c} A_1^{(11)} & A_1^{(12)} \\ \hline A_1^{(21)} & A_1^{(22)} \end{array}\right] = \left[\begin{array}{c|cc} 0 & 0 & 0 \\ \hline 0 & \frac{1}{4} & 0 \\ 0 & -1 & \frac{1}{4} \end{array}\right], \quad \left[\begin{array}{c|c} A_2^{(11)} & A_2^{(12)} \\ \hline A_2^{(21)} & A_2^{(22)} \end{array}\right] = \left[\begin{array}{c|cc} 0 & 0 & 0 \\ \hline 0 & \frac{1}{8} & \frac{1}{8} \\ 0 & 1 & \frac{1}{8} \end{array}\right],$$
$$\left[\begin{array}{c} B_1 \\ \hline B_2 \end{array}\right] = \left[\begin{array}{c} 100 \\ \hline 1 \\ 0 \end{array}\right], \quad \left[\begin{array}{c|c} C_1 & C_2 \end{array}\right] = \left[\begin{array}{c|cc} 1 & 0 & 1 \end{array}\right]. \tag{63}$$

The system is exponentially stable for all delay values, and thus strongly stable. Due to its tridiagonal structure, its spectrum namely consists of eigenvalue $\lambda = -10$, supplemented with the spectrum of (62), which is confined to the open left half plane because $\gamma_0 = 0.625 < 1$.

We now analyze the system norms from input ζ to output η. In Fig. 7 we show in the left the transfer function $\hat{G}$ and in the right the asymptotic transfer function $\hat{G}_a$, evaluated on the imaginary axis, for $\lambda = \mathrm{i}\omega$. Notice their matching at large frequencies, in accordance with Proposition 5.17. For $\vec{\tau} = (1, 1)$ there is clearly no feedthrough from input to output, inducing a finite $\mathcal{H}_2$ norm. Let us now consider rationally independent delays $\vec{\tau} = (1, 1 + \pi/\upsilon)$ with $\upsilon \in \mathbb{N}$. For $\upsilon = 50$ we see that functions $\hat{G}$ and $\hat{G}_a$ do not tend to zero as $\omega \to \infty$. If υ tends to infinity, the deviation from nominal delays $(1, 1)$ tends to zero. However, the $\mathcal{H}_2$ norms of $\hat{G}$ and $\hat{G}_a$ remain unbounded, while the significant mismatch of the transfer functions and the corresponding transfer functions for the limit $\vec{\tau} = (1, 1)$ only shifts towards higher frequencies. This is visualized in the figure by comparing the cases where $\upsilon = 50$ and $\upsilon = 200$. Thus, the $\mathcal{H}_2$ norm of $\hat{G}$ is not continuous at the nominal delays $\vec{\tau} = (1, 1)$. Its $\mathcal{H}_\infty$ norm is continuous and characterized by the peak gain reached for $\omega = 0$.

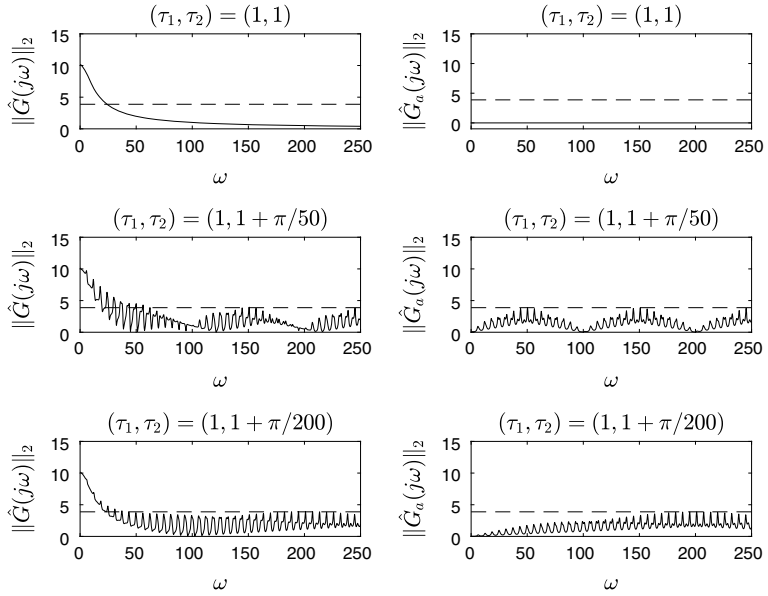

Fig. 7 Maximum singular value of the transfer function (left) and asymptotic transfer function (right) of the system in Example 5.18 as a function of $s = \mathrm{i}\omega$, for three cases: $\vec{\tau} = (1, 1)$ (top), $\vec{\tau} = (1, 1 + \pi/50)$ (middle) and $\vec{\tau} = (1, 1 + \pi/200)$ (bottom). The dashed line indicates the strong $\mathcal{H}_\infty$ norm of $\hat{G}_a$

Let us now consider other numerical values for the input matrix B, while keeping the other system matrices:

$$B = \left[\frac{B_1}{B_2}\right] = \left[\begin{array}{c} 25 \\ \hline 1 \\ 0 \end{array}\right]. \tag{64}$$

In Fig. 8 we display again the transfer functions. With the modified input matrix, not only the $\mathcal{H}_2$ norm is discontinuous at nominal delays $(1, 2)$, but also the $\mathcal{H}_\infty$ norm.

The possible discontinuity of the system norms brings us to the following robustified counter parts, which explicitly take into account infinitesimal delay perturbations.

Definition 5.19 The strong $\mathcal{H}_2$ and strong $\mathcal{H}_\infty$ norm of $\hat{G}$ are defined as

$$\begin{aligned} |||\hat{G}(\cdot; \vec{\tau})|||_{\mathcal{H}_2} &:= \lim_{\epsilon \to 0+} \sup\{\|\hat{G}(\cdot; \vec{\tau}_\epsilon)\|_{\mathcal{H}_2} : \vec{\tau}_\epsilon \in \mathcal{B}(\vec{\tau}, \epsilon)\}, \\ |||\hat{G}(\cdot; \vec{\tau})|||_{\mathcal{H}_\infty} &:= \lim_{\epsilon \to 0+} \sup\{\|\hat{G}(\cdot; \vec{\tau}_\epsilon)\|_{\mathcal{H}_\infty} : \vec{\tau}_\epsilon \in \mathcal{B}(\vec{\tau}, \epsilon)\}, \end{aligned}$$

with $\mathcal{B}$ given by (45).

The strong $\mathcal{H}_2$ and $\mathcal{H}_\infty$ norm of $\hat{G}_a$ are defined in a similar way. In order to provide mathematical characterizations of the strong norms, we first introduce matrix poly-

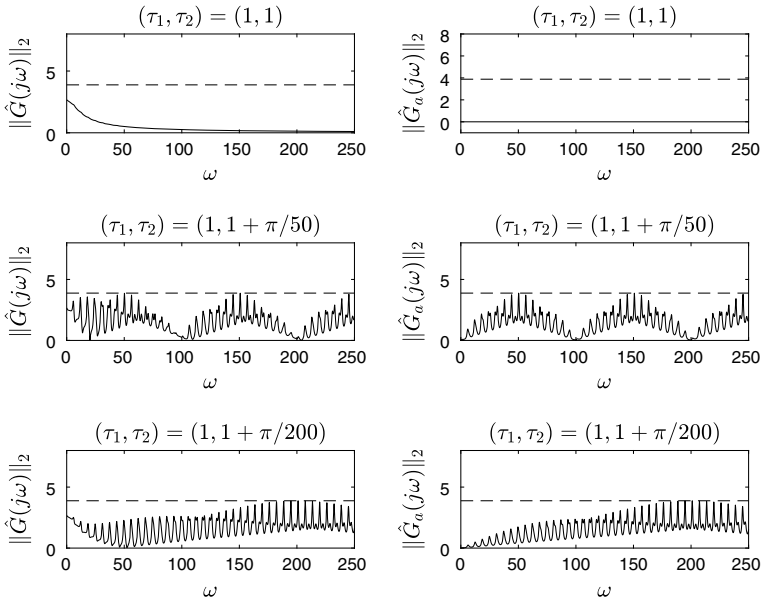

Fig. 8 Maximum singular value of the transfer function (left) and asymptotic transfer function (right) of the system in Example 5.18, with modified input matrix (64), as a function of $s = \mathrm{i}\omega$, for three cases: $\vec{\tau} = (1, 1)$ (top), $\vec{\tau} = (1, 1 + \pi/50)$ (middle) and $\vec{\tau} = (1, 1 + \pi/200)$ (bottom). The dashed line indicates the strong $\mathcal{H}_\infty$ norm of $\hat{G}_a$

nomials $P_{k_1,\ldots,k_m}$, with $k_i \in \mathbb{Z}^+$, $i = 1, \ldots, m$, which are recursively defined through the following expressions:

$$P_{0,\ldots,0} := I, \tag{65}$$

$$\begin{aligned} P_{k_1,\ldots,k_m} := {} & A_1^{(22)} P_{k_1-1,k_2,\ldots,k_m} + A_2^{(22)} P_{k_1,k_2-1,k_3,\ldots,k_m} \\ & + \ldots + \hat{A}_m^{(22)} P_{k_1,k_2,\ldots,k_{m-1},k_m-1} \end{aligned} \tag{66}$$

and

$$P_{k_1,\ldots,k_m} := 0 \text{ if any } k_i \in \mathbb{Z}^-, i = 1, \ldots, m. \tag{67}$$

For instance, for $m = 2$ and $k_1 + k_2 \leq 2$ these matrix polynomials are

$$\begin{aligned} & P_{0,0} = I, \\ & P_{1,0} = A_1^{(22)}, \ P_{0,1} = A_2^{(22)}, \\ & P_{2,0} = A_1^{(22)} A_1^{(22)}, \ P_{1,1} = A_1^{(22)} A_2^{(22)} + A_2^{(22)} A_1^{(22)}, \ P_{0,2} = A_2^{(22)} A_2^{(22)}, \end{aligned}$$

while we also have

$$P_{2,1} = A_1^{(22)} A_1^{(22)} A_2^{(22)} + A_1^{(22)} A_2^{(22)} A_1^{(22)} + A_2^{(22)} A_1^{(22)} A_1^{(22)}.$$

Hence $P_{k_1,\ldots,k_m}$ is the sum of all monomials of order k_i in matrix $A_i^{(22)}$, for all $i = 1, \ldots, m$. We can now formulate a characterization of the strong norms of the asymptotic transfer function.

Proposition 5.20 (Gomez et al. 2010, Proposition 1) *Assume that system* (34) *is strongly stable. Then its asymptotic transfer function* $\hat{G}_a$ *satisfies*

$$\| \hat{G}_a \|_{\mathcal{H}_\infty} = \max_{\vec{\theta} \in [0,\ 2\pi]^m} \left\| C_2 \left(I - \sum_{i=1}^{m} A_i^{(22)} e^{-i\theta_i} \right)^{-1} B_2 \right\|_2 . \tag{68}$$

If conditions

$$C_2 P_{k_1,\ldots,k_m} B_2 = 0, \quad \forall (k_1, \ldots, k_m) \in \left(\mathbb{Z}^+\right)^m : \sum_{i=1}^{m} k_i < mn \tag{69}$$

are satisfied, with multi-powers $P_{k_1,\ldots,k_m}$ *defined by* (65)-(67)*, then it holds that* $\|G_a\|_{\mathcal{H}_2} = 0$*. Otherwise, it holds that* $\|G_a\|_{\mathcal{H}_2} = +\infty$*.*

It is important to point out that the strong norms of the asymptotic transfer function do not depend on the delay values. We can now state the corresponding results for transfer function $\hat{G}$.

Proposition 5.21 (Gomez et al. 2010, Proposition 2) *If system* (34) *is strongly stable, then its transfer function* $\hat{G}$ *satisfies*

$$\| \hat{G}(\cdot; \vec{\tau}) \|_{\mathcal{H}_\infty} = \max \left\{ \| \hat{G}(\cdot; \vec{\tau}) \|_{\mathcal{H}_\infty}, \| \hat{G}_a \|_{\mathcal{H}_\infty} \right\} \tag{70}$$

and

$$\|\hat{G}(\cdot; \vec{\tau})\|_{\mathcal{H}_2} = \begin{cases} \| \hat{G}(\cdot; \vec{\tau}) \|_{\mathcal{H}_2} < +\infty, & \text{if (69) is satisfied,} \\ +\infty, & \text{otherwise.} \end{cases}$$

Furthermore, function $\left(\mathbb{R}_0^+\right)^m \ni \vec{\tau} \mapsto \|\hat{G}(\cdot; \vec{\tau})\|_{\mathcal{H}_\infty}$ *is continuous whenever* (34) *is strongly stable. Function* $\left(\mathbb{R}_0^+\right)^m \ni \vec{\tau} \mapsto \|\hat{G}(\cdot; \vec{\tau})\|_{\mathcal{H}_2}$ *is continuous whenever* (34) *is strongly stable and the strong* $\mathcal{H}_2$ *norm is finite.*

Example 5.22 We revisit Example 5.18 and consider nominal delay values $(\tau_1, \tau_2) = (1, 1)$. By evaluating (68) we arrive at $\|\hat{G}_a\|_{\mathcal{H}_\infty} = 3.88$, whose corresponding level sets are the dashed horizontal lines in Figs. 7 and 8. Because we have

$$C_2 A_1^{(22)} B_2 = -1, \ C_2 A_2^{(22)} B_2 = 1,$$

the conditions (69) are not satisfied, implying $\|G_a\|_{\mathcal{H}_2} = +\infty$.

For the first choice of B, as in (63), the maximum in the right-hand side of (70) is attained by the first term, hence, the strong $\mathcal{H}_\infty$ norm is reached at a finite frequency,

here $\omega = 0$. For the second choice (64), it is reached by the second term, hence, $|||\hat{G}|||_{\mathcal{H}_\infty} = |||\hat{G}_a|||_{\mathcal{H}_\infty} = 3.88$. Obviously, we have in both cases $|||G|||_{\mathcal{H}_2} = +\infty$.

The computation and subsequent optimization of the strong $\mathcal{H}_\infty$ norm as in Gumussoy and Michiels (2011) is based on expression (70), where in a first phase (68) is evaluated using a combination of gridding and local correction. Here it is important to note that the number of nonzero coefficient matrices $A_i^{(22)}$ is typically very small in applications, as they all correspond to the presence of a control loop along which high frequency modes are not damped. In the second phase, an extension of the level-set algorithm, described in Sect. 2.2 and illustrated with Fig. 1, is used to compute the nominal $\mathcal{H}_\infty$ norm, provided it is larger than $|||\hat{G}_a|||_{\mathcal{H}_\infty}$. For this, the latter norm is used as initial value for the level. Derivatives of the objective function (70) with respect to controller parameters are obtained from derivatives of corresponding active eigenvalues or singular values.

We now address the $\mathcal{H}_2$ norm computation. With several examples, including Examples 5.2 and 5.18, we illustrated that a DDAE of the form (34) may hide nontrivial feedthrough terms, hence after checking strong stability it should be determined first whether the strong $\mathcal{H}_2$ norm is finite. An important property of the necessary and sufficient condition (69), derived in Gomez et al. (2020) using a multi-dimensional generalization of the Cayley-Hamilton theorem, is that this involves checking only finitely many equalities. However, the number of equalities to check has an exponential growth as a function of the number of delays m. In response to this, it can be noted that conditions

$$\begin{aligned} CB &= 0, \\ CA_{\sigma_1} \cdots A_{\sigma_k} B &= 0, \ \forall k \in \mathbb{Z}^+, \forall \sigma_i \in \{1, \ldots, m\}, \ i = 1, \ldots, k \end{aligned} \tag{71}$$

imply that $CP_{k_1,\ldots,k_m}B = 0$ for any m-tuple $(k_1, \ldots, k_m)$, and, hence, that finiteness criterion (69) is satisfied. In Gomez et al. (2010) it is shown that checking sufficient condition (71) can be done with an algorithm having significantly better scalability properties in terms of both the dimension of the system and the number of delays. It is also shown that the satisfaction of (71) is equivalent to the existence of a simultaneous block triangularization of the matrices of delay difference equation (62). The latter is instrumental to a special regularization procedure that allows to transform DDAE (34) to a neutral equation with the same transfer matrix, without any need for differentiation of inputs or outputs. This transformation enables to compute the strong $\mathcal{H}_2$ norm using an established approach grounded in Lyapunov matrices (Jarlebring et al. 2011), thereby directly extending Theorem 1 and the related algorithms. For further reading we refer to Gomez and Michiels (2019a), Gomez et al. (2010, 2020).

6 Concluding Remarks

An eigenvalue based solution to the robust control of linear time-delay systems has been presented. Because any controller characterized by a finite number of parameters can be seen as a structured, reduced-order controller, a direct optimization approach has been taken. Its main advantages are two-fold. First, the methods are generally applicable. The extension of model (1) towards DDAE models allows to consider both retarded and neutral type stand-alone and interconnected systems, with discrete delays in states, control input, sensors outputs, and in the inputs and outputs used to describe the robustness and performance specifications. As a second advantage, the approach is not conservative in the sense that a stabilizing or optimal fixed-structure $\mathcal{H}_2 - \mathcal{H}_\infty$ controller can be computed whenever it exists, in contrast to approaches inferred from sufficient (but not necessary) conditions for a stabilizing or a guaranteed cost controller. As a price to pay for these beneficial properties, the optimization problems encountered in Sects. 3 and 5.3 are in general non-convex, hence, there is no guarantee that the computed optima found by the presented local optimization algorithms are global.

The eigenvalue based framework has recently been extended to the robust stability analysis and stabilization of linear time-periodic systems with delay (Michiels and Fenzi 2020; Borgioli et al. 2020), the $\mathcal{H}_2$ norm analysis of such systems (Michiels and Gomez 2020), and it has been applied to problems from machining (Hajdu et al. 2020). It has also been adopted to the design of prediction based controllers, see, e.g., Zhou et al. (2019) and the references therein.

Software tools for solving the analysis and synthesis problems discussed in this article, as well as a benchmark data, are available at

`http://twr.cs.kuleuven.be/research/software/delay-control/`.

They have been integrated in the software package TDS-CONTROL (Appeltans and Michiels 2022).

References

Appelmans, P., & Michiels, W. (2022). TDS-CONTROL: A MATLAB package for the analysis and controller-design of time-delay systems. In *Proceedings of the 18th IFAC Workshop on Control Applications of Optimization*, Gif-sur-Yvette, France.

Avellar, C. E., & Hale, J. K. (1980). On the zeros of exponential polynomials. *Journal of Mathematical Analysis and Applications, 73*, 434–452.

Borgioli, F., & Michiels, W. (2020). A novel method to compute the structured distance to instability for combined uncertainties on delays and system matrices. *IEEE Transactions on Automatic Control, 65*(4), 1747–1754.

Borgioli, F., Michiels, W., Lu, D., & Vandereycken, B. (2019). A globally convergent method to compute the real stability radius for time-delay systems. *Systems & Control Letters, 127*, 44–51.

Borgioli, F., Hajdu, D., Insperger, T., Stépán, G., & Michiels, W. (2020). Pseudospectral method for assessing stability robustness for linear time-periodic delayed dynamical systems. *International Journal for Numerical Methods in Engineering*.

Boyd, S., & Balakrishnan, V. (1990). A regularity result for the singular values of a transfer matrix and a quadratically convergent algorithm for computing its $\mathcal{L}_\infty$-norm. *Systems & Control Letters, 15*, 1–7.

Boyd, S., & Vandenberghe, L. (2004). *Convex optimization*. Cambridge University Press.

Breda, D. (2023). Pseudospectral Methods for the Stability Analysis of Delay Equations. Part I: the Infinitesimal Generator Approach. methods and applications. In D. Breda (Ed.) *Controlling Delayed Dynamics: Advances in Theory, Methods and Applications, CISM Lecture Notes* (pp. 65–94). Wien-New York: Springer.

Breda, D. (2023). Pseudospectral Methods for the Stability Analysis of Delay Equations. Part II: the Solution Operator Approach. methods and applications. In D. Breda (Ed.) *Controlling Delayed Dynamics: Advances in Theory, Methods and Applications, CISM Lecture Notes* (pp. 95–116). Wien-New York: Springer.

Breda, D., Maset, S., & Vermiglio, R. (2005). Pseudospectral differencing methods for characteristic roots of delay differential equations. *SIAM Journal on Scientific Computing, 27*(2), 482–495.

Breda, D., Maset, S., & Vermiglio, R. (2009). TRACE-DDE: a tool for robust analysis and characteristic equations for delay differential equations. In *Topics in time-delay systems*, *Lecture Notes in Control and Information Sciences* (Vol. 388, pp. 145–155). Springer.

Bruinsma, N. A., & Steinbuch, M. (1990). A fast algorithm to compute the $\mathcal{H}_\infty$-norm of a transfer function matrix. *Systems & Control Letters, 14*, 287–293.

Burke, J. V., Lewis, A. S., & Overton, M. L. (2005). A robust gradient sampling algorithm for nonsmooth, nonconvex optimization. *SIAM Journal on Optimization, 15*(3), 751–779.

Burke, J. V., Henrion, D., Lewis, A. S., Overton, M. L. (2006). HIFOO - a MATLAB package for fixed-order controller design and H-infinity optimization. In *Proceedings of the 5th IFAC Symposium on Robust Control Design*, Toulouse, France.

Curtain, R. F., & Zwart, H. (1995). *An introduction to infinite-dimensional linear systems theory*, *Texts in Applied Mathematics* (Vol. 21). Springer.

Dileep, D., Van Parys, R., Pipeleers, G., Hetel, L., Richard, J.-P., & Michiels, W. (2020). Design of robust decentralised controllers for MIMO plants with delays through network structure exploitation. *The International Journal of Control, 93*(10), 2275–2289.

Du, N. H., Linh, V. H., Mehrmann, V., & Thuan, D. D. (2013). Stability and robust stability of linear time-invariant delay differential-algebraic equations. *SIAM Journal on Matrix Analysis and Applications, 34*(4), 1631–1654.

Engelborghs, K., Luzyanina, T., & Roose, D. (2002). Numerical bifurcation analysis of delay differential equations using DDE-BIFTOOL. *ACM Transactions on Mathematical Software, 28*(1), 1–24.

Fridman, E. (2002). Stability of linear descriptor systems with delay: A Lyapunov-based approach. *Journal of Mathematical Analysis and Applications, 273*, 24–44.

Gomez, M. A., & Michiels, W. (2019a). Analysis and computation of the $\mathcal{H}_2$ norm of delay differential algebraic equations. *IEEE Transactions on Automatic Control, 65*(5), 2192–2199.

Gomez, M. A., & Michiels, W. (2019b). Characterization and optimization of the smoothed spectral abscissa for time-delay systems. *The International Journal of Robust and Nonlinear Control, 29*(13), 4402–4418.

Gomez, M. A., Egorov, A., Mondié, S., & Michiels, W. (2019). Optimization of the $\mathcal{H}_2$ norm for single-delay systems, with application to control design and model approximation. *IEEE Transactions on Automatic Control, 64*(2), 804–811.

Gomez, M. A., Jungers, R. M., & Michiels, W. (2020). On the m-dimensional Cayley-Hamilton theorem and its application to an algebraic decision problem inferred from the $\mathcal{H}_2$ norm analysis of delay systems. *Automatica, 113*, 108761.

Gomez, M. A., Jungers, R. M. & Michiels, W. (2010). On the strong $\mathcal{H}_2$ norm of differential algebraic systems with multiple delays: finiteness criteria, regularization and computation. *IEEE Transactions on Automatic Control*. Accepted for publication.

Gu, K., Kharitonov, V. L., & Chen, J. (2003). *Stability of time-delay systems*. Birkhauser.

Gumussoy, S., & Michiels, W. (2010). A predictor - corrector type algorithm for the pseudospectral abscissa computation of time-delay systems. *Automatica, 46*(4), 657–664.

Gumussoy, S., & Michiels, W. (2011). Fixed-order H-infinity control for interconnected systems using delay differential algebraic equations. *SIAM Journal on Control and Optimization, 49*(5), 2212–2238.

Güttel, S., Van Beeumen, R., Meerbergen, K., & Michiels, W. (2014). NLEIGS: A class of fully rational Krylov methods for nonlinear eigenvalue problems. *SIAM Journal on Scientific Computing, 36*(6), A2842–A2864.

Ha, P., & Mehrmann, V. (2012). Analysis and reformulation of linear delay differential-algebraic equations. *The Electronic Journal of Linear Algebra, 23*, 703–730.

Hajdu, D., Borgioli, F., Michiels, W., Insperger, T., & Stépán, G. (2020). Robust stability of milling operations based on pseudospectral approach. *International Journal of Machine Tools and Manufacture, 149*, 103516.

Hale, J. K., & Verduyn Lunel, S. M. (1993). *Introduction to functional differential equations*, *Applied Mathematical Sciences* (Vol. 99). Springer.

Hale, J. K., & Verduyn Lunel, S. M. (2002). Strong stabilization of neutral functional differential equations. *IMA Journal of Mathematical Control and Information, 19*, 5–23.

Jarlebring, E., Meerbergen, K., & Michiels, W. (2010). A Krylov method for the delay eigenvalue problem. *SIAM Journal on Scientific Computing, 32*(6), 3278–3300.

Jarlebring, E., Vanbiervliet, J., & Michiels, W. (2011). Characterizing and computing the $\mathcal{H}_2$ norm of time-delay systems by solving the delay Lyapunov equation. *IEEE Transactions on Automatic Control, 56*, 814–825.

Jarlebring, E., Bennedich, M., Mele, G., Ringh, E., & Upadhyaya, P. (2018). NEP-PACK: A julia package for nonlinear eigenproblems - v0.2.

Kharitonov, V., & Plischke, E. (2006). Lyapunov matrices for time-delay systems. *Systems & Control Letters, 55*(9), 697–706.

Lewis, A., & Overton, M. L. (2009). Nonsmooth optimization via BFGS. Available from `http://cs.nyu.edu/overton/papers.html`.

Michiels, W. (2019). Control of linear systems with delays (pp. 1–7). London: Springer. ISBN 978-1-4471-5102-9.

Michiels, W. (2011). Spectrum-based stability analysis and stabilisation of systems described by delay differential algebraic equations. *IET Control Theory & Applications, 5*, 1829–1842.

Michiels, W., Boussaada, I., & Niculescu, S.-I. (2017). An explicit formula for the splitting of multiple eigenvalues for nonlinear eigenvalue problems and connections with the linearization for the delay eigenvalue problem. *SIAM Journal on Matrix Analysis and Applications, 38*(2), 599–620.

Michiels, W., Engelborghs, K., Roose, D., & Dochain, D. (2002). Sensitivity to infinitesimal delays in neutral equations. *SIAM Journal on Control and Optimization, 40*(4), 1134–1158.

Michiels, W., & Fenzi, L. (2021). Spectrum-based stability analysis and stabilization of a class of time-periodic time delay systems. *SIAM Journal on Matrix Analysis and Applications, 5*(16), 1829–1842.

Michiels, W., & Gomez, M. A. (2020). On the dual linear periodic time-delay system: Spectrum and Lyapunov matrices, with application to $\mathcal{H}_2$ analysis and balancing. *The International Journal of Robust and Nonlinear Control, 30*(10), 3906–3922.

Michiels, W., & Gumussoy, S. (2010). Characterization and computation of H-infinity norms of time-delay systems. *SIAM Journal on Matrix Analysis and Applications, 31*(4), 2093–2115.

Michiels, W., & Niculescu, S.-I. (2014). *Stability and stabilization of time-delay systems. An eigenvalue based approach*, 2nd edn. SIAM.

Michiels, W., & Vyhlídal, T. (2005). An eigenvalue based approach to the robust stabilization of linear time-delay systems of neutral type. *Automatica, 41*(6), 991–998.

Michiels, W., Vyhlídal, T., & Zítek, P. (2010). Control design for time-delay systems based on quasi-direct pole placement. *Journal of Process Control, 20*(3), 337–343.

Michiels, W., Vyhlídal, T., Ziték, P., Nijmeijer, H., & Henrion, D. (2009). Strong stability of neutral equations with an arbitrary delay dependency structure. *SIAM Journal on Control and Optimization, 48*(2), 763–786.

Michiels, W., & Zhou, B. (2019). Computing delay lyapunov matrices and $\mathcal{H}_2$ norms for large-scale problems. *SIAM Journal on Matrix Analysis and Applications, 40*(3), 845–869.

Niculescu, S.-I. (2001). *Delay effects on stability. A robust control approach*, *Lecture Notes in Control and Information Sciences* (Vol. 269). Springer.

Overton, M. (2009). HANSO: a hybrid algorithm for nonsmooth optimization. `http://cs.nyu.edu/overton/software/hanso/`.

Pilbauer, D. (2017). *Spectral Methods in Vibration Suppression Control Systems with Time Delays*. Ph.D. thesis, Double Doctorate Chech Technical University in Prague - KU Leuven.

Pontes Duff, I., Poussot-Vassal, C., & Seren, C. (2018). H_2-optimal model approximation by input/output-delay structured reduced order models. *Systems & Control Letters, 117,* 60 – 67.

Saad, Y. (1992). *Numerical methods for large eigenvalue problems*. Manchester University Press.

Sieber, J., Engelborghs, K., Luzyanina, T., Samey, G., & Roose, D. (2016). DDE-BIFTOOL manual - bifurcation analysis of delay differential equations - v3.1.1.

Sipahi, R., Niculescu, S. I., Abdallah, C. T., Michiels, W., & Gu, K. (2011). Stability and stabilization of systems with time delay. *IEEE Control Systems Magazine, 31*(38–65), 3278–3300.

Van Beeumen, R., Meerbergen, K., & Michiels, W. (2015). Compact rational Krylov methods for nonlinear eigenvalue problems. *SIAM Journal on Matrix Analysis and Applications, 36*(2), 820–838.

Vanbiervliet, J., Vandereycken, B., Michiels, W., & Vandewalle, S. (2008). A nonsmooth optimization approach for the stabilization of time-delay systems. *ESAIM: Control, Optimisation and Calculus of Variations, 14*(3), 478–493.

Vanbiervliet, J., Michiels, W., & Vandewalle, S. (2009a). Smooth stabilization and optimal $\mathcal{H}_2$ design. In *Proceedings of the IFAC Workshop on Control Applications of Optimization*, Jyväskylä, Finland.

Vanbiervliet, J., Vandereycken, B., Michiels, W., Vandewalle, S., & Diehl, M. (2009). The smoothed spectral abscissa for robust stability optimization. *SIAM Journal on Optimization, 20*(1), 156–171.

Vanbiervliet, J., Michiels, W., & Jarlebring, E. (2011). Using spectral discretisation for the optimal $\mathcal{H}_2$ design of time-delay systems. *International Journal of Control, 84*(2), 228–241.

Villafuerte, R., Mondié, S., & Garrido, R. (2013). Tuning of proportional retarded controllers: Theory and experiments. *IEEE Transactions on Control Systems Technology, 21*(3), 983–990.

Vyhlídal, T., Zítek, P., & Paulů, K. (2009). Design, modelling and control of the experimental heat transfer set-up. In J. J. Loiseau et al. (Ed.), *Topics in time delay systems. analysis, algorithms, and control*, *Lecture Notes in Control and Information Sciences* (Vol. 308, pp. 303–314). Springer.

Vyhlídal, T., Michiels, W., & McGahan, P. (2010). Synthesis of strongly stable state-derivative controllers for a time-delay system using constrained non-smooth optimization. *IMA Journal of Mathematical Control and Information, 27*(4), 437–455.

Zhou, B., Liu, Q., & Michiels, W. (2019). Design of pseudo-predictor feedback for neutral-type linear systems with both state and input delays. *Automatica, 109*, 108502.

Zhou, K., Doyle, J. C., & Glover, K. (1995). *Robust and optimal control*. Prentice Hall.

A Scalable Controller Synthesis Method for the Robust Control of Networked Systems

Pieter Appeltans and Wim Michiels

Abstract This chapter discusses a scalable controller synthesis method for networked systems with a large number of identical subsystems based on the $\mathcal{H}_\infty$-norm control framework. The dynamics of the individual subsystems are described by identical linear time-invariant delay differential equations and the effect of transport and communication delay is explicitly taken into account. The presented method is based on the result that, under a particular assumption on the graph describing the interconnections between the subsystems, the $\mathcal{H}_\infty$-norm of the overall system is upper bounded by the robust $\mathcal{H}_\infty$-norm of a single subsystem with an additional uncertainty. This chapter will therefore briefly discuss a recently developed method to compute this last quantity. The resulting controller is then obtained by directly minimizing this upper bound in the controller parameters.

1 Introduction

This chapter presents a controller synthesis method for networked systems. Such networked systems consist of a large number of smaller subsystems that interact over a network. The analysis and control of these networked systems is challenging due to their large dimension and the presence of delays. These delays originate from the time needed to transfer matter, energy and information between subsystems. In this context, the traditional approach of using one global controller for the complete network is not feasible due to the high communication requirements and the poor scalability with respect to the number of subsystems. Furthermore, the assumption that all measurements are centrally available, does often not hold for networked systems. These limitations inspired local control approaches, in which each subsystem has its own local controller. Neighboring controllers can however communicate to

This work was supported by the project C14/17/072 of the KU Leuven Research Council and by the project G092721N of the Research Foundation-Flanders (FWO - Vlaanderen).

P. Appeltans · W. Michiels (✉)
Department of Computer Science, KU Leuven, Heverlee, Belgium
e-mail: Wim.Michiels@cs.kuleuven.be

D. Breda (ed.), *Controlling Delayed Dynamics*, CISM International Centre for Mechanical Sciences 604, https://doi.org/10.1007/978-3-031-01129-0_9

improve control performance. This approach of having multiple local controllers instead of one global controller fits the framework of distributed and decentralized control.

In this chapter we consider networked systems in which the dynamics of the individual subsystems are described by identical linear time-invariant delay differential equations. The resulting local controllers are identical and minimize an upper bound for the $\mathcal{H}_\infty$-norm of the overall system. This $\mathcal{H}_\infty$-norm is an important performance measure in robust control theory, see Zhou and Doyle (1998).

The computation cost of the standard algorithms for calculating the $\mathcal{H}_\infty$-norm of dynamical systems with discrete delays, such as Gumussoy and Michiels (2011), scales cubically with respect to the number of states (and hence the number of subsystems). However, for some networked systems this computation cost can be decreased significantly using the decoupling transformation presented in Massioni and Verhaegen (2009), Dileep et al. (2018b). More specifically, if the subsystems are identical and the graph describing the interconnections between the subsystems fulfills a particular assumption, then the $\mathcal{H}_\infty$-norm of the complete system is equal to the maximal $\mathcal{H}_\infty$-norm of a single parametrized subsystem where the allowable values of the parameter correspond to the eigenvalues of the adjacency matrix of the interconnection graph. Moreover, in Dileep et al. (2018a) it was suggested to consider this parameter as an uncertainty bounded to a region in the complex plane that comprises all these eigenvalues. As such, the worst-case $\mathcal{H}_\infty$-norm of this uncertain subsystem gives an upper bound for the $\mathcal{H}_\infty$-norm of the complete network. Furthermore, this worst-case $\mathcal{H}_\infty$-norm is also known as the robust $\mathcal{H}_\infty$-norm and can be computed at a cost that only depends on the dimension of an individual subsystem using the method presented in Appeltans and Michiels (2021).

For the controller synthesis, we will directly minimize the robust $\mathcal{H}_\infty$-norm of the uncertain subsystem in the controller parameters. Our method thus fits in the frequency based, direct optimization framework, used in Gumussoy and Michiels (2011), Michiels (2011), Dileep et al. (2018a), Özer and Iftar (2015). This framework allows to easily incorporate constraints on the structure of the controller, such as PID or reduced order control. In contrast, $\mathcal{H}_\infty$-controller design methods based on Riccati equations and linear matrix inequalities typically give rise to dense controllers with dimensions equal to that of the system. A notable exception is Hilhorst et al. (2015), which allows to design reduced order controllers using the aforementioned framework. Another advantage of the direct optimization approach compared to methods based on Riccati equations and linear matrix inequalities, in particular for systems with delays, is that the obtained results are less conservative. This comes however at the cost of having to solve a non-convex and non-smooth optimization problem.

The remainder of this chapter is structured as follows. First, Sect. 2 introduces the considered networked systems and details the aforementioned decoupling transformation. Next, a recently developed method to compute the robust $\mathcal{H}_\infty$-norm of uncertain linear time-invariant systems with discrete delays is discussed in Sect. 3.

Subsequently, the direct optimization approach to synthesize the controller is outlined in Sect. 4. Finally, the resulting design methodology is illustrated using an example problem in Sect. 5 and some concluding remarks are given in Sect. 6.

2 Computing the $\mathcal{H}_\infty$-norm of Networked Systems

In Sect. 2.1 we introduce the considered networked systems and the control objective. Section 2.2 presents the decoupling transformation that allows to compute an upper bound for the $\mathcal{H}_\infty$-norm of the overall system at a computation cost that does not depend on the number of subsystems.

2.1 System Description and Control Objective

In this chapter, we consider networked systems with N subsystems. The dynamics of the individual subsystems are identical and described by a state-space representation of the following form:

$$\begin{cases} \dot{x}_j(t) = \sum_{k=0}^{K} A_k\, x_j(t-\tau_k) + B_u\, u_j(t-\tau_u) + B_{u_n}\, u_j^{(n)}(t) + B_w\, w_j(t) \\ y_j(t) = C_y\ x_j(t) \\ y_j^{(n)}(t) = C_{y_n}\, x_j(t) \\ z_j(t) = C_z\ x_j(t) \qquad\qquad \text{for } j = 1, \ldots, N \end{cases} \tag{1}$$

with $x_j(t) \in \mathbb{R}^{(n)}$ the state vector of subsystem j, $u_j(t) \in \mathbb{R}^{m_c}$ its control input, $y_j(t) \in \mathbb{R}^{p_c}$ its measured output, $w_j(t) \in \mathbb{R}^m$ its performance input, $z_j(t) \in \mathbb{R}^p$ its performance output, $0 = \tau_0 < \tau_1 < \cdots < \tau_K$ discrete delays, $\tau_u \geq 0$ an input delay and A_k, B_u, B_{u_n}, B_w, C_y, C_{y_n} and C_z real-valued matrices of appropriate dimension. The input $u_j^{(n)}(t)$ and the output $y_j^{(n)}(t)$ model the interactions between the subsystems:

$$u_j^{(n)}(t) = \sum_{i=1}^{N} P_{j,i}^N\, y_i^{(n)}(t-\tau_n),$$

with $\tau_n \geq 0$ the interaction delay and $P_N = [P_{j,i}^N]_{j,i=1}^N$ the adjacency matrix of the interconnection graph of the network. More specifically, an element $P_{j,i}^N$ is non-zero if and only if the dynamics of subsystem j are influenced by subsystem i.

Each subsystem is controlled using a local controller and these local controllers are identical. Here we will consider dynamic output feedback controllers of order n_c:

$$\begin{cases} \dot{\xi}_j(t) = J_{\mathbf{p}}\, \xi_j(t) + F_{\mathbf{p}}\, y_j(t) + F_{\mathbf{p}}^{(n)}\, u_j^{(nc)}(t) \\ u_j(t) = L_{\mathbf{p}}\, \xi_j(t) + K_{\mathbf{p}}\, y_j(t) + K_{\mathbf{p}}^{(n)}\, u_j^{(nc)}(t) \end{cases} \quad \text{for } j = 1, \ldots, N \tag{2}$$

with $\xi_j(t) \in \mathbb{R}^{n_c}$ the controller state of the local controller associated with subsystem j. The matrices $J_{\mathbf{p}}$, $F_{\mathbf{p}}$, $F_{\mathbf{p}}^{(n)}$, $L_{\mathbf{p}}$, $K_{\mathbf{p}}$ and $K_{\mathbf{p}}^{(n)}$ are real-valued and of appropriated dimension. The subscript $\mathbf{p}$ is used to indicate that these matrices depend on some tunable control parameters $\mathbf{p}$. If $F_{\mathbf{p}}^{(n)} \neq 0$ and/or $K_{\mathbf{p}}^{(n)} \neq 0$, the local controllers can communicate their sensor measurements to neighboring subsystems. It is however required that the adjacency matrix of the communication graph is equal to the adjacency matrix of the interaction graph:

$$u_j^{n_c}(t) = \sum_{i=1}^{N} P_{j,i}^{N}\, y_i(t - \tau_{nc}),$$

with $\tau_{nc} \geq 0$ the communication delay.

Remark 2.1 In the remainder of this chapter we restrict our attention to controller architectures where the local controllers can only share sensor measurements. Note however that the results can be extended to architectures where the local controllers can also share their internal state.

By eliminating the control and coupling variables, we find the following state-space description for the closed-loop of the complete networked system:

$$\begin{cases} \dot{x}(t) = \sum_{k=0}^{K} (I_N \otimes A_k)\, x(t-\tau_k) + \left(I_N \otimes B_u K_{\mathbf{p}} C_y\right) x(t-\tau_u) + \\ \qquad \left(P_N \otimes B_{u_n} C_{y_n}\right) x(t-\tau_n) + \left(I_N \otimes B_u L_{\mathbf{p}}\right) \xi(t-\tau_u) + \\ \qquad \left(P_N \otimes B_u K_{\mathbf{p}}^{(n)} C_y\right) x(t-\tau_u-\tau_{nc}) + (I_N \otimes B_w)\, w(t) \\ \dot{\xi}(t) = \left(I_N \otimes J_{\mathbf{p}}\right) \xi(t) + (I_N \otimes F_{\mathbf{p}} C_y)\, x(t) + \\ \qquad \left(P_N \otimes F_{\mathbf{p}}^{(n)} C_y\right) x(t-\tau_{nc}) \\ z(t) = (I_N \otimes C_z)\, x(t) \end{cases} \tag{3}$$

with I_N the identity matrix of size N, $x(t) = [x_1(t)^T \cdots\ x_N(t)^T]^T$ the combined state, $\xi(t) = [\xi_1(t)^T \cdots\ \xi_N(t)^T]^T$ the combined controller state, $w(t) = [w_1(t)^T \cdots\ w_N(t)^T]^T$ the combined performance input, $z(t) = [z_1(t)^T \cdots\ z_N(t)^T]^T$ the combined performance output and $\otimes$ the Kronecker product. The corresponding transfer function from w to z is equal to:

$$T(s; \mathbf{p}, N) = \left(I_N \otimes \begin{bmatrix} C_z & 0 \end{bmatrix}\right) \left(I_{N(n+n_c)} s - I_N \otimes Q_{\mathbf{p}}(s) - P_N \otimes R_{\mathbf{p}}(s)\right)^{-1} \times \left(I_N \otimes \begin{bmatrix} B_w \\ 0 \end{bmatrix}\right) \tag{4}$$

with

$$Q_{\mathbf{p}}(s) = \begin{bmatrix} A_0 & 0 \\ F_{\mathbf{p}} C_y & J_{\mathbf{p}} \end{bmatrix} + \sum_{k=1}^{K} \begin{bmatrix} A_k & 0 \\ 0 & 0 \end{bmatrix} e^{-s\tau_k} + \begin{bmatrix} B_u K_{\mathbf{p}} C_y & B_u L_{\mathbf{p}} \\ 0 & 0 \end{bmatrix} e^{-s\tau_u}$$

and

$$R_{\mathbf{p}}(s) = \begin{bmatrix} B_{u_n} C_{y_n} & 0 \\ 0 & 0 \end{bmatrix} e^{-s\tau_n} + \begin{bmatrix} B_u K_{\mathbf{p}}^{(n)} C_y & 0 \\ 0 & 0 \end{bmatrix} e^{-s(\tau_u + \tau_{nc})} + \begin{bmatrix} 0 & 0 \\ F_{\mathbf{p}}^{(n)} C_y & 0 \end{bmatrix} e^{-s\tau_{nc}}.$$

If system (3) is exponentially stable, the $\mathcal{H}_\infty$-norm of (4) equals:

$$\|T(\cdot; \mathbf{p}, N)\|_{\mathcal{H}_\infty} = \max_{\omega \in \mathbb{R}^+} \sigma_1\big(T(\jmath\omega; \mathbf{p}, N)\big)$$

with $\sigma_1(\cdot)$ the largest singular value of its matrix argument (Gumussoy and Michiels, 2011). Here we recall that the $\mathcal{H}_\infty$-norm is an important performance measure in robust control theory, used to asses the disturbance rejection of a dynamical system as it gives the worst-case energy gain of the system with respect to energy-bounded noise signals:

$$\|T(\cdot; \mathbf{p}, N)\|_{\mathcal{H}_\infty} = \max_{w \in L_m^2} \frac{\|z\|_{L_p^2}}{\|w\|_{L_m^2}},$$

with $\|w\|_{L_m^2} := \sqrt{\int_0^{+\infty} \|w(t)\|_2^2 \, \mathrm{d}t}$, $L_m^2 := \{w : [0, +\infty) \mapsto \mathbb{R}^m \text{ such that } \|w\|_{L_m^2}^2 < +\infty\}$, $\|w(t)\|_2$ the Euclidean norm, and $\|z\|_{L_p^2}$ and L_p^2 defined analogously (Zhou and Doyle 1998).

2.2 Upper Bound for the H-Infinity Norm

In this subsection we show that under the following assumption on P_N, there exists a decoupling transformation that allows to compute an upper bound for the $\mathcal{H}_\infty$-norm of (4) at a computation cost that does not depend on the number of subsystems.

Assumption 1 The matrix P_N has real-valued eigenvalues confined to an interval $[a, b]$ and is diagonalizable by a unitary matrix V_N, i.e.,

$$V_N{}^H P_N V_N = \Lambda_N$$

with $\Lambda_N = \mathrm{diag}(\lambda_1, \lambda_2, \ldots, \lambda_N)$ and $\lambda_j \in [a, b]$ for $j = 1, \ldots, N$.

If we apply the following change of variables to the states, the controller states, the performance input and the performance output of system (3)

$$\begin{aligned}\bar{x}(t) &:= (V_N{}^H \otimes I_n)\ x(t)\\ \bar{\xi}(t) &:= (V_N{}^H \otimes I_{n_c})\ \xi(t)\\ \bar{w}(t) &:= (V_N{}^H \otimes I_m)\ w(t)\\ \bar{z}(t) &:= (V_N{}^H \otimes I_p)\ z(t)\end{aligned}$$

we obtain

$$\begin{cases}\dot{\bar{x}}(t) = \sum_{k=0}^{K}(I_N \otimes A_k)\,\bar{x}(t-\tau_k) + (I_N \otimes B_u K_{\mathbf{p}} C_y)\,\bar{x}(t-\tau_u) + \\ \qquad (\Lambda_N \otimes B_{u_n} C_{y_n})\,\bar{x}(t-\tau_n) + \left(I_N \otimes B_u L_{\mathbf{p}}\right)\bar{\xi}(t-\tau_u) + \\ \qquad (\Lambda_N \otimes B_u K_{\mathbf{p}}^{(n)} C_y)\,\bar{x}(t-\tau_u-\tau_{nc}) + (I_N \otimes B_w)\,\bar{w}(t) \\ \dot{\bar{\xi}}(t) = \left(I_N \otimes J_{\mathbf{p}}\right)\bar{\xi}(t) + \left(I_N \otimes F_{\mathbf{p}} C_y\right)\bar{x}(t) + \\ \qquad \left(\Lambda_N \otimes F_{\mathbf{p}}^{(n)} C_y\right)\bar{x}(t-\tau_{nc}) \\ \bar{z}(t) = (I_N \otimes C_z)\,\bar{x}(t).\end{cases} \tag{5}$$

Notice that all matrices in (5) are block diagonal and hence the behavior of this transformed system is fully characterized by its N independent subsystems. This leads to the following theorem.

Theorem 2.2 *For a networked system of form* (3) *whose adjacency matrix fulfills Assumption 1, it holds that*

$$\|T(\cdot;\mathbf{p},N)\|_{\mathcal{H}_\infty} = \|\bar{T}_{\bar{w}\bar{z}}(\cdot;\mathbf{p},N)\|_{\mathcal{H}_\infty} = \max_{\lambda\in\{\lambda_1,\ldots,\lambda_N\}} \|\hat{T}_{\hat{w}\hat{z}}(\cdot;\mathbf{p},\lambda)\|_{\mathcal{H}_\infty}$$

with $\bar{T}_{\bar{w}\bar{z}}(\cdot;\mathbf{p},N)$ *the transfer function from* $\bar{w}$ *to* $\bar{z}$ *of system* (5) *and* $\hat{T}_{\hat{w}\hat{z}}(\cdot;\mathbf{p},\lambda)$ *the transfer function from* $\hat{w}$ *to* $\hat{z}$ *of the following system parameterized in* λ*:*

$$\begin{cases}\dot{\hat{x}}(t) = \sum_{k=0}^{K} A_k\,\hat{x}(t-\tau_k) + B_u K_{\mathbf{p}} C_y\,\hat{x}(t-\tau_u) + \lambda B_{u_n} C_{y_n}\,\hat{x}(t-\tau_n) \\ \qquad +\lambda B_u K_{\mathbf{p}}^{(n)} C_y\,\hat{x}(t-\tau_u-\tau_{nc}) + B_u L_{\mathbf{p}}\,\hat{\xi}(t-\tau_u) + B_w\,\hat{w}(t) \\ \dot{\hat{\xi}}(t) = J_{\mathbf{p}}\,\hat{\xi}(t) + F_{\mathbf{p}} C_y\,\hat{x}(t) + \lambda F_{\mathbf{p}}^{(n)} C_y\,\hat{x}(t-\tau_{nc}) \\ \hat{z}(t) = C_z\,\hat{x}(t).\end{cases} \tag{6}$$

Proof The provided proof is added for self-containedness and is similar to the ones given in Massioni and Verhaegen (2009); Dileep et al. (2018b). We refer to these papers for more details.
The relation between $T(\jmath\omega;\mathbf{p},N)$ and $\bar{T}_{\bar{w}\bar{z}}(\jmath\omega;\mathbf{p},N)$ is given by

$$T(\jmath\omega;\mathbf{p},N) = \left(V_N \otimes I_p\right)\ \bar{T}_{\bar{w}\bar{z}}(\jmath\omega;N)\ \left(V_N{}^H \otimes I_m\right).$$

Because $(V_N \otimes I_p)$ and $(V_N{}^H \otimes I_m)$ are unitary matrices if follows that,

$$\sigma_1\big(T(\jmath\omega;\mathbf{p},N)\big) = \sigma_1\Big(\big(V_N\otimes I_p\big)\ \bar{T}_{\bar{w}\bar{z}}(\jmath\omega;\mathbf{p},N)\ \big({V_N}^H\otimes I_m\big)\Big)$$
$$= \sigma_1\left(\bar{T}_{\bar{w}\bar{z}}(\jmath\omega;\mathbf{p},N)\right).$$

The second equality follows from the fact that

$$\bar{T}_{\bar{w}\bar{z}}(\jmath\omega;\mathbf{p},N) = \text{blkdiag}_{j=1,\ldots,N}\left(\hat{T}_{\hat{w}\hat{z}}(\jmath\omega;\mathbf{p},\lambda_j)\right),$$

and hence

$$\sigma_1\left(\bar{T}_{\bar{w}\bar{z}}(\jmath\omega;\mathbf{p},N)\right) = \max_{\lambda\in\{\lambda_1,\ldots,\lambda_N\}}\sigma_1\big(\hat{T}_{\hat{w}\hat{z}}(\jmath\omega;\mathbf{p},\lambda)\big),$$

which concludes the proof. □

Note that system (6) corresponds to a single subsystem in (3) where the network connections are replaced by a parameter. By treating λ in (6) as an uncertainty confined to the interval $[a,\ b]$, the robust $\mathcal{H}_\infty$-norm associated with (6), which is defined as the maximal value of the $\mathcal{H}_\infty$-norm over all instances of the uncertain parameter,

$$\|\hat{T}_{\hat{w}\hat{z}}(\cdot;\mathbf{p},\cdot)\|_{\mathcal{H}_\infty}^{[a,\,b]} = \max_{\lambda\in[a,\,b]}\|\hat{T}_{\hat{w}\hat{z}}(\cdot;\mathbf{p},\lambda)\|_{\mathcal{H}_\infty}, \tag{7}$$

can be used as an upper bound for the $\mathcal{H}_\infty$-norm of (3), as stated in the following corollary.

Corollary 2.3 *The $\mathcal{H}_\infty$-norm of a networked system of form (3) whose adjacency matrix fulfills Assumption 1, is upper bounded by the robust $\mathcal{H}_\infty$-norm of $\hat{T}_{\hat{w}\hat{z}}(\cdot;\mathbf{p},\lambda)$, with λ an uncertain parameter confined to $[a,\ b]$:*

$$\|T(\cdot;\mathbf{p},N)\|_{\mathcal{H}_\infty} \le \|\hat{T}_{\hat{w}\hat{z}}(\cdot;\mathbf{p},\cdot)\|_{\mathcal{H}_\infty}^{[a,\,b]}.$$

Furthermore, if Assumption 1 holds with a and b independent of N, then $\|\hat{T}_{\hat{w}\hat{z}}(\cdot;\mathbf{p},\cdot)\|_{\mathcal{H}_\infty}^{[a,\,b]}$ is also an upper bound for the supremum of $\|T(\cdot;\mathbf{p},N)\|_{\mathcal{H}_\infty}$ over the number of subsystems:

$$\sup_{N=1,\ldots,+\infty}\|T(\cdot;\mathbf{p},N)\|_{\mathcal{H}_\infty} \le \|\hat{T}_{\hat{w}\hat{z}}(\cdot;\mathbf{p},\lambda)\|_{\mathcal{H}_\infty}^{[a,\,b]}.$$

If, furthermore, the (Hausdorff) distance between $[a,\ b]$ and $\bigcup_{N=1}^{+\infty}\{\lambda\in\mathbb{C}:\det(I_N\lambda - P_N)=0\}$ goes to zero then

$$\sup_{N=1,\ldots,+\infty}\|T(\cdot;\mathbf{p},N)\|_{\mathcal{H}_\infty} = \|\hat{T}_{\hat{w}\hat{z}}(\cdot;\mathbf{p},\lambda)\|_{\mathcal{H}_\infty}^{[a,\,b]}.$$

Example 2.4 To illustrate the applicability of this result, we consider the following adjacency matrices:

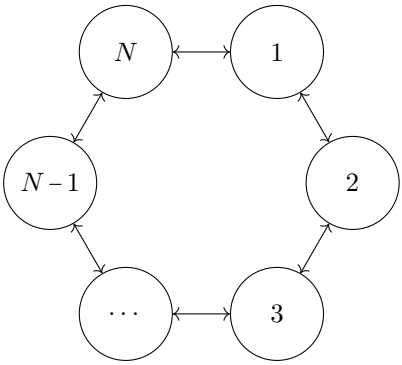

Fig. 1 Bidirectional ring topology

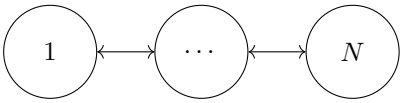

Fig. 2 Bidirectional line topology

$$P_N^{\text{ring}} = \begin{bmatrix} 0 & 0.5 & & & 0.5 \\ 0.5 & 0 & 0.5 & & \\ & 0.5 & 0 & 0.5 & \\ & & \ddots & \ddots & \ddots \\ & & & 0.5 & 0 & 0.5 \\ 0.5 & & & & 0.5 & 0 \end{bmatrix} \text{ and } P_N^{\text{line}} = \begin{bmatrix} 0 & 0.5 & & & \\ 0.5 & 0 & 0.5 & & \\ & 0.5 & 0 & 0.5 & \\ & & \ddots & \ddots & \ddots \\ & & & 0.5 & 0 & 0.5 \\ & & & & 0.5 & 0 \end{bmatrix}.$$

The first adjacency matrix, P_N^{ring}, corresponds to a bidirectional ring topology, see Fig. 1; the second one corresponds to a bidirectional line topology, see Fig. 2. The eigenvalues of these adjacency matrices are $\left\{\cos\left(\frac{2\pi(j-1)}{N}\right)\right\}_{j=1}^{\lfloor\frac{N+2}{2}\rfloor}$ and $\left\{\cos\left(\frac{j\pi}{N+1}\right)\right\}_{j=1}^{N}$, respectively. The eigenvalues of both matrices are thus confined to the interval $[a,\ b] = [-1,\ 1]$ for all $N > 1$. As both adjacency matrices are symmetric and hence unitary diagonalizable, we can apply Corollary 2.3 to compute an upper bound for the $\mathcal{H}_\infty$-norm of (4) that holds for all $N > 1$ at a computation cost that only depends on the dimension of a single subsystem. Furthermore, this upper bound is the same for both topologies.

3 Computing the Robust $\mathcal{H}_\infty$-norm

This section introduces a numerical algorithm to efficiently compute the robust $\mathcal{H}_\infty$-norm of an uncertain linear time-invariant system with discrete delays:

$$\begin{cases} \dot{x}(t) = \sum_{r=0}^{R} (H_r + \lambda\, G_r)\ x(t - \tau_r) + B_w\ w(t) \\ z(t) = C_z x(t) \end{cases} \tag{8}$$

with $x(t) \in \mathbb{R}^{(n)}$ the state, $w(t) \in \mathbb{R}^m$ the performance input, $z(t) \in \mathbb{R}^p$ the performance output, $0 = \tau_0 < \tau_1 < \cdots < \tau_R$ discrete delays, H_r, G_r, B_w and C_z real-valued matrices of appropriate dimension and λ a real-valued, scalar parameter addressed as an uncertainty confined to the interval $[a,\ b]$. Note that system (6) fits this form.

Under the assumption that system (8) is internally exponentially stable for all $\lambda \in [a,\ b]$, its (asymptotic) input-output behavior for each allowable value of λ is described in the Laplace domain by the following transfer function:

$$T(s; \lambda) = C_z \Big(I_n s - \sum_{r=0}^{R} (H_r + \lambda G_r)\ e^{-s\tau_r} \Big)^{-1} B_w,$$

and the associated robust $\mathcal{H}_\infty$-norm is equal to

$$\|T(\cdot; \cdot)\|_{\mathcal{H}_\infty}^{[a,\,b]} = \max_{\lambda \in [a,\,b]} \|T(\cdot; \lambda)\|_{\mathcal{H}_\infty} = \max_{\substack{\lambda \in [a,\,b] \\ \omega \in \mathbb{R}^+}} \sigma_1\big(T(\jmath\omega; \lambda)\big).$$

In Appeltans and Michiels (2021) a novel numerical algorithm to compute the robust $\mathcal{H}_\infty$-norm of an uncertain time-delay system is presented. This algorithm is based on the relation between the robust $\mathcal{H}_\infty$-norm and the robust stability radius of an "uncertain" characteristic matrix. This relation is illustrated in Sect. 3.1. The resulting algorithm is given in Sect. 3.2.

3.1 Relation With the Robust Stability Radius

Consider the following "uncertain" characteristic matrix

$$M(s; \lambda, \Delta) := I_n s - \sum_{r=0}^{R} (H_r + \lambda G_r)\ e^{-s\tau_r} - B_w \Delta C_z, \tag{9}$$

with H_r, G_r, B_w, C_z, τ_r and λ as defined above, I_n the identity matrix of size n and $\Delta \in \mathbb{C}^{m \times p}$ a complex-valued uncertainty with $\|\Delta\|_2 \leq \varepsilon$ and $\varepsilon \geq 0$. Note that this uncertain characteristic matrix has two uncertainties: a scalar λ which is real-valued and bounded to the interval $[a,\ b]$ and an $m \times p$ matrix Δ which is complex-valued and bounded in spectral norm by ε, or in other words $\Delta \in \mathcal{B}_{\|\cdot\|_2 \leq \varepsilon}^{\mathbb{C}^{m \times p}}$ with

$$\mathcal{B}_{\|\cdot\|_2 \leq \varepsilon}^{\mathbb{C}^{m \times p}} := \left\{ \Delta \in \mathbb{C}^{m \times p} : \|\Delta\|_2 \leq \varepsilon \right\}.$$

Next, we define three important concepts related to this uncertain characteristic matrix. The spectral value set of this uncertain characteristic matrix is defined as

$$\Lambda_{\varepsilon}^{[a,\,b]} := \bigcup_{\lambda \in [a,\,b]} \bigcup_{\Delta \in \mathcal{B}_{\|\cdot\|_2 \leq \varepsilon}^{\mathbb{C}^{m \times p}}} \{s \in \mathbb{C} : \det\left(M(s; \lambda, \Delta)\right) = 0\},$$

i.e., the union of the characteristic roots of $M(\cdot; \lambda, \Delta)$ over all $\lambda \in [a, b]$ and $\Delta \in \mathcal{B}_{\|\cdot\|_2 \leq \varepsilon}^{\mathbb{C}^{m \times p}}$. Note that this spectral value set is symmetric with respect to the real axis. The pseudo-spectral abscissa is defined as the real part of the rightmost point, i.e., the point with the largest real part, in this spectral value set,

$$\alpha_{\varepsilon}^{[a,\,b]} := \max\left\{\Re\left(s\right) : s \in \Lambda_{\varepsilon}^{[a,\,b]}\right\}.$$

Finally, the robust stability radius is defined as the smallest ε for which this pseudo-spectral abscissa becomes non-negative,

$$r_{[a,\,b]} := \min\left\{\varepsilon \in [0, +\infty) : \alpha_{\varepsilon}^{[a,\,b]} \geq 0\right\}. \tag{10}$$

Furthermore, because $\alpha_{\varepsilon}^{[a,\,b]}$ is a continuous function of ε (this can be shown using a similar argument as in Borgioli and Michiels Borgioli and Michiels (2020, Section IV), the transition to a non-negative pseudo-spectral abscissa is characterized by an ε for which $\alpha_{\varepsilon}^{[a,\,b]}$ equals zero. This means that the robust stability radius can also be defined as the smallest ε for which the spectral value set touches the imaginary axis:

$$r_{[a,\,b]} = \min\left\{\varepsilon \in [0, +\infty) : \exists\, \omega \in \mathbb{R}^{+} \text{ such that } \jmath\omega \in \Lambda_{\varepsilon}^{[a,\,b]}\right\}. \tag{11}$$

The following example illustrates these three concepts in more detail.

Example 3.1 Consider the following uncertain characteristic matrix:

$$\begin{bmatrix} 1 & 0 \\ 0 & 1 \end{bmatrix} s - \left(\begin{bmatrix} -5 & 3 \\ 2 & -6 \end{bmatrix} + \lambda \begin{bmatrix} 2 & 2 \\ -2 & -1 \end{bmatrix}\right) - \left(\begin{bmatrix} -3 & -1 \\ 0 & 2 \end{bmatrix} + \lambda \begin{bmatrix} 1 & 1 \\ -1 & 1 \end{bmatrix}\right) e^{-s} - \begin{bmatrix} 1 \\ -3 \end{bmatrix} \Delta \begin{bmatrix} 2 & 5 \end{bmatrix}. \tag{12}$$

Figure 3 shows the part of the spectral value set in the region $[-0.5, -0.2] \times \jmath[2.1, 2.7]$ for $[a,\ b]$ equal to $[-1,\ 1]$ and several values of ε. For $\varepsilon = 0$, only the real-valued uncertainty λ plays a role and the viewed part of the spectral value set is a curve. For nonzero ε, also the complex-valued uncertainty Δ affects the characteristic matrix and the viewed part of the spectral value set becomes a region in the complex plane which grows as ε increases. Figure 4 shows the pseudo-spectral abscissa $\alpha_{\varepsilon}^{[a,\,b]}$ in function of ε. We find that $r_{[-1,1]} = 0.22491$. Finally, Figure 5 shows the part of the associated spectral value set in the region $[-3, 0.3] \times \jmath[-10, 10]$. One sees that the spectral value set touches the imaginary axis at the origin ($\omega = 0$).

We are now ready to state the relation between the robust $\mathcal{H}_{\infty}$-norm associated with uncertain system (8) and the robust stability radius of (9).

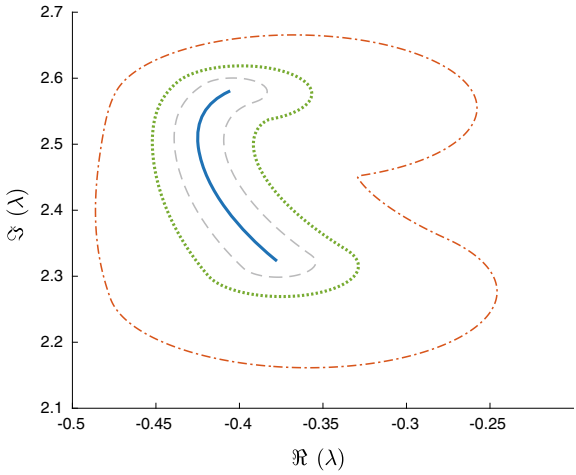

Fig. 3 The part of the spectral value set of (12) in the region $[-0.5, -0.2] \times \jmath[2.1, 2.7]$ for $[a,\ b]$ equal to $[-1,\ 1]$ and ε equal to 0 (full line), 0.05 (dashed line), 0.1 (dotted line) and 2/9 (dash dotted line)

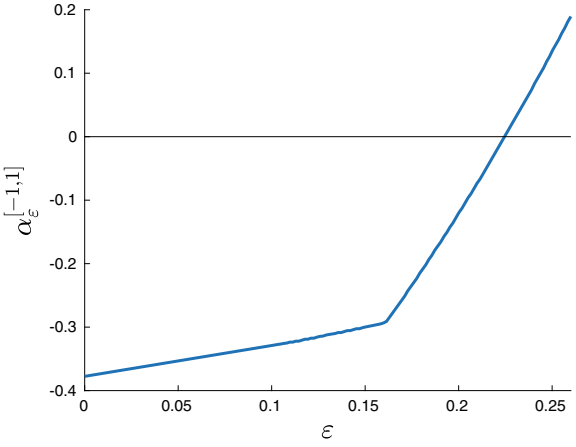

Fig. 4 The pseudo-spectral abscissa of (12) for $[a,\ b]$ equal to $[-1,\ 1]$ in function of ε

Theorem 3.2 *If uncertain system* (8) *is internally exponentially stable for all* $\lambda \in [a,\ b]$*, its associated robust* $\mathcal{H}_\infty$*-norm is equal to the reciprocal of the robust stability radius of* (9).

Proof The following proof is a simplification of the result in Appeltans and Michiels (2021).
A complex number $\jmath\omega$ lies in $\Lambda_{\varepsilon}^{[a,\,b]}$ if and only if there exist $\lambda \in [a,\ b]$ and $\Delta \in \mathcal{B}_{\|\cdot\|_2 \le \varepsilon}^{\mathbb{C}^{m\times p}}$ such that

$$\det\left(M(\jmath\omega;\,\lambda,\,\Delta)\right) = \det\left(I_n\,\jmath\omega - \textstyle\sum_{r=0}^{R}(H_r + \lambda\, G_r)e^{-\jmath\omega\tau_r} - B_w\Delta C_z\right) = 0.$$

Because we required that (8) is internally exponentially stable for all $\lambda \in [a,\ b]$, this is equivalent to

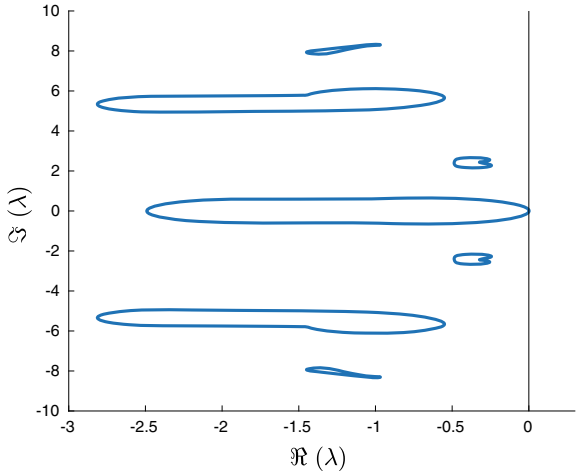

Fig. 5 The part of the spectral value set of (12) in $[-3, 0.3] \times \jmath[-10, 10]$ for $[a, b]$ equal to $[-1, 1]$ and $\varepsilon = 0.22491$

$$\det\left(I_n - \left(I_n \jmath\omega - \sum_{r=0}^{R}(H_r + \lambda G_r)e^{-\jmath\omega\tau_r}\right)^{-1} B_w \Delta C_z\right) = 0.$$

By the Weinstein-Aronszajn identity, this last equality can be rewritten as

$$\begin{aligned}\det\left(I - C_z\left(I\jmath\omega - \sum_{r=0}^{R}(H_r + \lambda G_r)e^{-\jmath\omega\tau_r}\right)^{-1} B_w \Delta\right) &= \det\left(I - T(\jmath\omega;\lambda)\Delta\right)\\ &= 0.\end{aligned}$$

The characterization of the robust stability radius in (11) can thus be rewritten as

$$r_{[a,b]} = \min_{\omega\in\mathbb{R}^+} \min_{\lambda\in[a,b]} \min_{\Delta\in\mathbb{C}^{m\times p}} \left\{\|\Delta\|_2 : \det\left(I - T(\jmath\omega;\lambda)\Delta\right) = 0\right\}.$$

Using $\min_{\Delta\in\mathbb{C}^{m\times p}}\{\|\Delta\|_2 : \det(I - M\Delta) = 0\} = \sigma_1(M)^{-1}$ from Packard and Doyle (1993) one finds that

$$\begin{aligned} r_{[a,b]} &= \min_{\substack{\lambda\in[a,b]\\ \omega\in\mathbb{R}^+}} \left(\sigma_1\left(T(\jmath\omega;\lambda)\right)\right)^{-1}\\ &= \left(\max_{\substack{\lambda\in[a,b]\\ \omega\in\mathbb{R}^+}} \sigma_1\left(T(\jmath\omega;\lambda)\right)\right)^{-1} = \left(\|T(\cdot;\cdot)\|_{\mathcal{H}_\infty}^{[a,b]}\right)^{-1}, \end{aligned}$$

which concludes the proof. □

Remark 3.3 The presented relation can be generalized to systems with uncertainties on the delays, multiple uncertainties and other uncertainty structures, such as full block and diagonal uncertainties. Also systems with delays and uncertainties in the

input, output and direct feed-through terms can be considered. For more information, see Appeltans and Michiels (2021).

3.2 Numerical Algorithm

This subsection presents a numerical algorithm to compute the robust stability radius. Once this quantity is found, the robust $\mathcal{H}_\infty$-norm associated with (8) follows immediately from Theorem 3.2.

By (10), the robust stability radius is the zero-crossing of the function $\mathbb{R}^+ \ni \varepsilon \mapsto \alpha_\varepsilon^{[a,\,b]}$. This zero-crossing can be found using the Newton-Bisection method, see Press et al. (1996, Chap. 9.4) for a reference implementation. This root finding method requires the evaluation of both $\alpha_\varepsilon^{[a,\,b]}$ and its derivative with respect to ε for given ε (whenever this derivative exists). The quantity $\alpha_\varepsilon^{[a,\,b]}$ can be computed using the method presented in Appeltans and Michiels (2021), which notes that $\alpha_\varepsilon^{[a,\,b]}$ is the solution of the following optimization problem:

$$\begin{array}{ll} \max\limits_{s,\,\lambda,\,\Delta} & \Re\,(s)\,, \\ \text{subject to} & \det\big(M(s;\,\lambda,\,\Delta)\big) = 0, \\ & \lambda \in [a,\,b], \\ & \Delta \in \mathcal{B}^{\mathbb{C}^{m\times p}}_{\|\cdot\|_2 \le \varepsilon}. \end{array} \tag{13}$$

Furthermore, the following proposition shows that there exists a Δ of rank one and norm ε associated with local optima of this optimization problem. This result will allow us to reduce the search space for Δ to the space of matrices of rank one and spectral norm ε. We will denote this space as $\mathcal{B}^{\mathbb{C}^{m\times p}}_{\|\cdot\|_2=\varepsilon,\,\mathrm{rank}=1}$.

Lemma 1 *Let $s^\star \notin \Lambda_0^{[a,\,b]}$ be a local rightmost point of $\Lambda_\varepsilon^{[a,\,b]}$, then there exist $\lambda^\star \in [a,\,b]$ and $\Delta^\star = \varepsilon u v^H$ with $u \in \mathbb{C}^m$, $v \in \mathbb{C}^p$ and $\|u\|_2 = \|v\|_2 = 1$ such that* $\det\,(M(s^\star;\,\lambda^\star,\,\Delta^\star)) = 0$.

Proof Firstly, using similar ideas as in the proof of Theorem 3.2 one can show that

$$\Lambda_\varepsilon^{[a,\,b]} = \Lambda_0^{[a,\,b]} \cup \left\{ s \in \mathbb{C} \setminus \Lambda_0^{[a,\,b]} : \max_{\lambda \in [a,\,b]} \sigma_1\,(T(s;\,\lambda)) \ge \varepsilon^{-1} \right\}.$$

Because $s^\star \notin \Lambda_0^{[a,\,b]}$ and $s^\star$ is a rightmost point of of $\Lambda_\varepsilon^{[a,\,b]}$, $s^\star$ must lie on the boundary of $\left\{ s \in \mathbb{C} \setminus \Lambda_0^{[a,\,b]} : \max_{\lambda\in[a,\,b]} \sigma_1\,(T(s;\,\lambda)) \ge \varepsilon^{-1} \right\}$. Hence, it holds that there exists a $\lambda^\star \in [a,\,b]$ such that $\sigma_1\,(T(s^\star;\,\lambda^\star)) = \varepsilon^{-1}$.
Secondly, it can easily be verified that $\det\left(I - T(s^\star;\,\lambda^\star)(\varepsilon \nu \upsilon^H)\right) = 0$ for υ and ν the left and right normalized singular vectors associated with $\sigma_1\big(T(s^\star;\,\lambda^\star)\big)$. Following the derivation in the first part of the proof of Theorem 3.2 in the opposite direction one finds $\det\left(M\left(s^\star;\,\lambda^\star,\,\varepsilon\nu\upsilon^H\right)\right) = 0$. □

Constrained optimization problem (13) is solved using a projected gradient flow method. The idea of this approach is to define a flow in the space of permissible variables along which the objective function monotonically increases and whose attractive stationary points are (local) optimizers of the optimization problem. These stationary points can be found by choosing initial parameters and discretizing the resulting path till convergence to a stationary point using Euler's forward method. The step size is chosen such that the objective function monotonically increases along the discretized path. For more details on the usage of these methods for the computation of extreme points of spectral value sets we refer to Borgioli and Michiels (2020), Guglielmi and Lubich (2011), Guglielmi and Lubich (2013).

In our case we are thus looking for a path $[0, +\infty) \ni \theta \mapsto (\lambda(\theta), \Delta(\theta)) \in [a,\ b] \times \mathcal{B}^{\mathbb{C}^{m\times p}}_{\|\cdot\|_2=\varepsilon,\,\mathrm{rank}=1}$ such that the function

$$\theta \mapsto \max\{\Re(s) : \det\left(M\big(s;\, \lambda(\theta),\, \Delta(\theta)\big)\right) = 0\}$$

is monotonically increasing and such that the (local) optimizers of (13) appear as attractive stationary points. Furthermore, to improve computational performance we employ an explicit decomposition of $\Delta(\theta)$ as $\varepsilon u(\theta)v(\theta)^H$ inspired by Guglielmi and Lubich (2011). Here we consider the following flow where $\dot{u}$, $\dot{v}$ and $\dot{\lambda}$ denote the derivatives of u, v and λ with respect to θ and where the dependency of $u(\theta)$, $v(\theta)$ and $\lambda(\theta)$ on θ is omitted for notational convenience:

$$\begin{cases} \dot{u} = \frac{\varepsilon}{\xi(\theta)}\left(\left(I - uu^H\right) B_w^T \varphi(\theta)\psi(\theta)^H C_z^T v + \frac{1}{2}\Im\left(u^H B_w^T \varphi(\theta)\psi(\theta)^H C_z^T v\right) u\right) \\ \dot{v} = \frac{\varepsilon}{\xi(\theta)}\left(\left(I - vv^H\right) C_z\, \psi(\theta)\varphi(\theta)^H B_w u + \frac{1}{2}\Im\left(v^H C_z\, \psi(\theta)\varphi(\theta)^H B_w u\right) v\right) \\ \dot{\lambda} = \begin{cases} 0 & \lambda = b \text{ and } \left(\sum_{r=0}^{R} \Re\left(\varphi(\theta)^H G_r \psi(\theta) e^{-s(\theta)\tau_k}\right)\right) > 0 \\ 0 & \lambda = a \text{ and } \left(\sum_{r=0}^{R} \Re\left(\varphi(\theta)^H G_r \psi(\theta) e^{-s(\theta)\tau_k}\right)\right) < 0 \\ \frac{1}{\xi(\theta)} \sum_{r=0}^{R} \Re\left(\varphi(\theta)^H G_r \psi(\theta) e^{-s(\theta)\tau_k}\right) & \text{otherwise} \end{cases} \end{cases} \tag{14}$$

with $s(\theta)$ the rightmost characteristic root of $M\big(s;\, \lambda(\theta), \varepsilon u(\theta)v(\theta)^H\big)$, and $\varphi(\theta)$ and $\psi(\theta)$ the associated left and right eigenvectors, normalized such that

$$\xi(\theta) = \varphi(\theta)^H \left(I + \sum_{r=0}^{R} \left(H_r + \lambda(\theta) G_r\right) \tau_r e^{-s(\theta)\tau_r}\right) \psi(\theta) > 0.$$

These paths are a combination of the paths presented in Borgioli and Michiels (2020) (computing the pseudo-spectral abscissa for real-valued Frobenius norm bounded uncertainties) and Guglielmi and Lubich (2011) (computing the pseudo-spectral abscissa for complex-valued spectral norm bounded uncertainties). The fulfillment of the constraints, the monotonic increase of the objective function and the (local) optimality of stationary points follows from these works. To conclude, we give some intuition behind (14): the right-hand side can be interpreted as a projection

of the gradient of the objective function on the tangent space of the feasible set. This projection step is needed to ensure that the variables remain within the feasible set.

The algorithm for numerically solving (13) is summarized in Algorithm 1, where $s_R\big(M(s;\lambda,\varepsilon uv^H)\big)$ gives the rightmost characteristic root of $M(s;\lambda,\varepsilon uv^H)$ and $\dot{u}_k$, $\dot{v}_k$ and $\dot{\lambda}_k$ correspond to the right-hand side of (14) evaluated at u_k, v_k and λ_k.

Algorithm 1 Discretization algorithm to solve (13).

$k \leftarrow 0$ and choose initial λ_0, u_0, v_0
$s_{-1} \leftarrow -\infty$ and $s_0 \leftarrow s_R\left(M\big(s;\lambda_0,\varepsilon u_0 v_0^H\big)\right)$
while $|s_k - s_{k-1}| > \text{tol} \cdot \frac{|s_k+s_{k-1}|}{2}$ **do**
  Find h such that $\Re\Big(s_R\left(M\big(s;\lambda_k+h\dot{\lambda}_k,\varepsilon(u_k+h\dot{u}_k)(v_k+h\dot{v}_k)^H\big)\right)\Big) \geq$
    $\Re\Big(s_R\big(M(s;\lambda_k,\varepsilon u_k v_k^H)\big)\Big)$
  if No $h > tol_h$ is found **then** stop.
  else
    $\lambda_{k+1} \leftarrow \lambda_k + h\dot{\lambda}_k$; $\lambda_{k+1} \leftarrow \max\{a, \min\{\lambda_{k+1}, b\}\}$;
    $u_{k+1} \leftarrow u_k + h\dot{u}_k$; $u_{k+1} \leftarrow \frac{u_{k+1}}{\|u_{k+1}\|_2}$;
    $v_{k+1} \leftarrow v_k + h\dot{v}_k$; $v_{k+1} \leftarrow \frac{v_{k+1}}{\|v_{k+1}\|_2}$;
    $s_{k+1} \leftarrow s_R\left(M\big(s;\lambda_{k+1},\varepsilon u_{k+1}v_{k+1}^H\big)\right)$;
    $k \leftarrow k+1$;
  end if
end while

Remark 3.4 To compute the rightmost characteristic root, we use the algorithm presented in Wu and Michiels (2012). This algorithm exploits the relation between a nonlinear delay eigenvalue problem and the linear eigenvalue problem corresponding to the solution operator of the associated delay differential equation. More precisely, this method uses a spectral discretization of the solution operator to approximate the characteristic roots. These roots are subsequently refined by applying Newton corrections based on the original non-linear eigenvalue problem formulation. This methods is however restricted to small problems. For large sparse matrices one could use iterative methods such as Jarlebring et al. (2010), Güttel et al. (2014) to compute the rightmost characteristic roots.

Once $\alpha_\varepsilon^{[a,b]}$ is computed, its derivative with respect to ε can be computed almost everywhere as shown in the following proposition.

Proposition 3.5 *Let $\lambda^\star$ and $\Delta^\star = \varepsilon u^\star v^{\star H}$ be the unique optimizers of (13) and assume that the rightmost characteristic root of $M(s;\lambda^\star,\Delta^\star)$ is simple, then*

$$\frac{d\alpha_\varepsilon^{[a,b]}}{d\varepsilon} = \frac{\Re\left(\varphi^{\star H} B_w u^\star v^{\star H} C_z \psi^\star\right)}{\varphi^{\star H}\left(I + \sum_{r=0}^{R}\left(A_k + \lambda^\star G_r\right)\tau_r e^{-\tau_r s^\star}\right)\psi^\star},$$

with $s^\star$ the rightmost characteristic root of $M(s; \lambda^\star, \Delta^\star)$ and $\phi^\star$ and $\psi^\star$ its corresponding left and right eigenvectors, normalized such that the denominator is real and positive.

Proof Similar as in Borgioli and Michiels (2020, Theorem 2).

4 A Scalable H-Infinity Controller Synthesis Method

In this section we will describe a controller synthesis method for networked systems of form (3) whose associated adjacency matrix fulfills Assumption 1. The idea behind the presented method is to find a suitable controller by directly minimizing (7) in the controller parameters $\mathbf{p}$. Or in other words, we look for controller parameters $\mathbf{p}^\star$ that fulfill

$$\mathbf{p}^\star \in \arg\min_{\mathbf{p}} \|\hat{T}_{\hat{w}\hat{z}}(\cdot; \mathbf{p}, \cdot)\|_{\mathcal{H}_\infty}^{[a,b]}. \tag{15}$$

Note however that $\|\hat{T}_{\hat{w}\hat{z}}(\cdot; \mathbf{p}, \cdot)\|_{\mathcal{H}_\infty}^{[a,b]}$ is only an upper bound for the actual $\mathcal{H}_\infty$-norm of (4). The resulting control parameters will therefore in most cases not minimize the actual $\mathcal{H}_\infty$-norm of the system, but this methodology has the advantage that its computation cost does not depend on the number of subsystems. Furthermore, if Assumption 1 remains valid with a and b independent of the number of subsystems, then the resulting controller guarantees a level of disturbance rejection even if the number of subsystems is unknown.

The minimization of (15) is however not trivial, as the robust $\mathcal{H}_\infty$-norm may be a non-smooth and non-convex function of the controller parameters even if the controller matrices are analytic functions of the controller parameters. This precludes the usage of standard optimization methods. Therefore, we will use HANSO (Overton 2009), which implements a combination of BFGS with weak Wolfe line search and gradient sampling. Furthermore, to decrease the chance of ending up at a local optimum we will restart the optimization algorithm from several initial points. The optimization procedure requires the evaluation of both the objective function and its derivative with respect to the control parameters whenever this derivative exists. To evaluate the objective function, we use the method presented in Sect. 3. The derivative with respect to the control parameters follows from the following proposition.

Proposition 4.1 *If there exists a unique pair*

$$(\omega^\star, \lambda^\star) \in \operatorname*{argmax}_{\lambda \in [a,b],\ \omega \in \mathbb{R}^+} \sigma_1\left(T(\jmath\omega; \mathbf{p}, \lambda)\right)$$

and if $\sigma_1\left(T(\jmath\omega^\star; \mathbf{p}, \lambda^\star)\right)$ is simple, then the function $\mathbf{p} \mapsto \|\hat{T}_{\hat{w}\hat{z}}(\cdot; \mathbf{p}, \cdot)\|_{\mathcal{H}_\infty}^{[a,b]}$ is differentiable at $\mathbf{p}$, with

$$\frac{\mathrm{d}}{\mathrm{d}\mathbf{p}}\|T(\cdot;\mathbf{p},\cdot)\|_{\mathcal{H}_\infty}^{[a,\,b]} = \Re\left(u^H\left(\frac{\partial}{\partial\mathbf{p}}T(\jmath\omega^\star;\mathbf{p},\lambda^\star)\right)v\right),$$

in which u and v are the normalized left and right singular vectors associated with $\sigma_1\big(T(\jmath\omega^\star;\mathbf{p},\lambda^\star)\big)$, respectively.

Finally, to start the optimization process we need initial controller parameters $\mathbf{p}$ for which the system is internally exponentially stable for all $\lambda \in [a,\ b]$. To find such a starting point, we use the method presented in Dileep et al. (2018a).

5 Example

In this example we consider a networked system that consists of N frictionless carts that are interconnected using identical springs and that each balance an inverted pendulum. Furthermore, the first and the last cart are connected to the wall using additional (but identical) springs. This set-up is illustrated in Fig. 6 for N equal to 3. The dynamics of an individual cart-pendulum subsystem are governed by the following non-linear delay differential equations

$$\begin{cases} (M+m)\ddot{d}_j(t) + ml\cos\big(\theta_j(t)\big)\ddot{\theta}_j(t) - ml\sin\big(\theta_j(t)\big)\big(\dot{\theta}_j(t)\big)^2 + \\ k\big(d_j(t)-d_{j+1}(t)\big) + k\big(d_j(t)-d_{j-1}(t)\big) - u_j(t-\tau_u) - w_{j,1}(t) = 0 \\ l\ddot{\theta}_j(t) - g\sin\big(\theta_j(t)\big) + \ddot{d}_j(t)\cos\big(\theta_j(t)\big) - w_{j,2}(t) = 0 \end{cases}$$

for $j = 1, \ldots, N$ and M the mass of the individual carts, m the mass of the pendulum's bob which is connected to the cart using a massless rod of length l, k the spring constant, u_j a controllable force that acts on the cart with an input delay τ_u, $w_{j,1}$ and $w_{j,2}$ external disturbances, θ_j the angular displacement of the pendulum of cart j, d_j the horizontal displacement of the jth cart's centre of mass with respect to its equilibrium position and $d_0 = d_{N+1} = 0$. By a linearization around the equilibrium

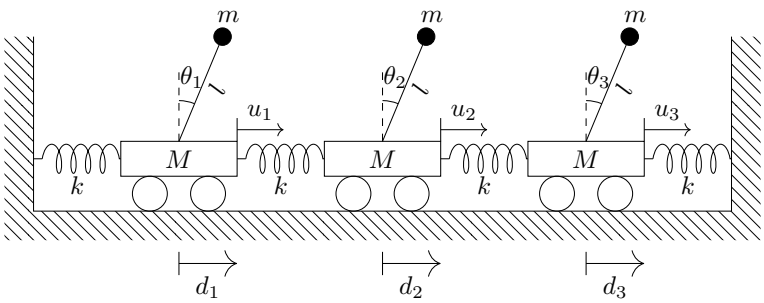

Fig. 6 Schematic representation of the considered set-up for $N = 3$

point $(d_j, \dot{d}_j, \theta_j, \dot{\theta}_j) = (0, 0, 0, 0)$ for $j = 1, \ldots, N$ and choosing $\begin{bmatrix} d_j(t) & \theta_j(t) \end{bmatrix}^T$ as both measured and performance output, we obtain the following linear state-space model of form (1):

$$\begin{aligned} \dot{x}_j(t) = &\begin{bmatrix} 0 & 1 & 0 & 0 \\ -\frac{2k}{M} & 0 & -\frac{mg}{M} & 0 \\ 0 & 0 & 0 & 1 \\ \frac{2k}{Ml} & 0 & \frac{g}{l} + \frac{mg}{Ml} & 0 \end{bmatrix} x_j(t) + \begin{bmatrix} 0 \\ \frac{1}{M} \\ 0 \\ \frac{-1}{Ml} \end{bmatrix} u_j(t - \tau_u) + \begin{bmatrix} 0 \\ \frac{k}{M} \\ 0 \\ \frac{-k}{Ml} \end{bmatrix} u_j^{(n)}(t) + \\ &\begin{bmatrix} 0 & 0 \\ \frac{1}{M} & \frac{-m}{M} \\ 0 & 0 \\ \frac{-1}{Ml} & \frac{1}{l} + \frac{m}{Ml} \end{bmatrix} w_j(t) \end{aligned} \tag{16}$$

$$y_j(t) = \begin{bmatrix} 1 & 0 & 0 & 0 \\ 0 & 0 & 1 & 0 \end{bmatrix} x_j(t), \quad y_j^{(n)}(t) = \begin{bmatrix} 2 & 0 & 0 & 0 \end{bmatrix} x_j(t), \quad z_j(t) = \begin{bmatrix} 1 & 0 & 0 & 0 \\ 0 & 0 & 1 & 0 \end{bmatrix} x_j(t)$$

with,

$$u_j^{(n)}(t) = \sum_{i=1}^{N} P_{j,i}^N \, y_i^{(n)}(t),$$

and

$$P_N = P_N^{\text{line}} = \begin{bmatrix} 0 & 0.5 & & & \\ 0.5 & 0 & 0.5 & & \\ & \ddots & \ddots & \ddots & \\ & & 0.5 & 0 & 0.5 \\ & & & 0.5 & 0 \end{bmatrix}.$$

The input signal u_j is generated using a controller of form (2) with n_c equal to 2. Furthermore, we will allow communication between the controllers of neighboring subsystems and as control parameters $\mathbf{p}$ we choose the elements of the control matrices.

As mentioned in Example 2.4, the eigenvalues of P_N^{line} are restricted to the interval $[-1, 1]$ for all $N > 1$. It thus follows from Corollary 2.3 that the robust $\mathcal{H}_\infty$-norm of a parametrized subsystem of form (6) with λ an uncertainty bounded to $[-1, 1]$, forms an upper bound for the $\mathcal{H}_\infty$-norm of the overall network that holds independent of N. Furthermore, this upper bound can be computed efficiently using the method presented in Sect. 3.

For the following parameter values: $M = 1\,\text{kg}, m = 0.05\,\text{kg}, k = 1\,\text{N/m}, l = 1\,\text{m}$, $g = 9.8\,\text{m/s}^2$, $\tau_u = 0.1\,\text{s}$ and $\tau_{u_{nc}} = 0.2\,\text{s}$, we apply the procedure of Chap. 4 to find the controller parameters that minimize this upper bound. The obtained controller matrices (rounded to four digits accuracy) are:

Table 1 The $\mathcal{H}_\infty$-norm (rounded to 6 digits accuracy) of the closed loop networked system for several N and the computation time required by the algorithm described in Gumussoy and Michiels (2011) to compute these values

N	3	5	10	15
$\|T(\cdot; \mathbf{p}^\star, N)\|_{\mathcal{H}_\infty}$	0.512228	0.512239	0.512246	0.512247
Computation time (s)	17.39	91.56	806.3	2961

$$
\begin{aligned}
J_{\mathbf{p}^\star} &= \begin{bmatrix} -67.92 & -313.2 \\ -52.15 & -306.8 \end{bmatrix} & F_{\mathbf{p}^\star} &= \begin{bmatrix} -407.4 & 1139 \\ 141.8 & 1519 \end{bmatrix} \\
F^{(n)}_{\mathbf{p}^\star} &= \begin{bmatrix} -33.74 & -112.6 \\ -91.45 & -147.9 \end{bmatrix} & L_{\mathbf{p}^\star} &= \begin{bmatrix} -143.3 & -834.4 \end{bmatrix} \\
K_{\mathbf{p}^\star} &= \begin{bmatrix} 349.9 & 4172 \end{bmatrix} & K^{(n)}_{\mathbf{p}^\star} &= \begin{bmatrix} -246.5 & -406.9 \end{bmatrix},
\end{aligned} \tag{17}
$$

in which the subscript $\mathbf{p}^\star$ is used to indicate that these matrices correspond to the minimizing control parameters. The corresponding upper bound for the $\mathcal{H}_\infty$-norm equals 0.512249 (rounded to 6 digits). Table 1 gives the actual $\mathcal{H}_\infty$-norm of the closed loop system with controller matrices (17) for several N. We observe that these values lie close to the computed upper bound. This table also gives the time required by the algorithm described in Gumussoy and Michiels (2011) to compute these values. As expected, the computation time grows roughly cubically with respect to N. For comparison, the computation time of the robust $\mathcal{H}_\infty$-norm of the associated uncertain subsystem equals 75.70 s. For system with large number of subsystems it is thus beneficiary to minimize this upper bound instead of the actual $\mathcal{H}_\infty$-norm.

Next, we will examine the disturbance rejection of the closed loop system for N equal to 20. We simulate the system for $t \in [0, 10]$ where both the state and the controller state are equal to 0 for $t < 0$, and each performance input is low pass filtered ($\omega_{cutoff} = 6\pi$) Gaussian white noise which is scaled after filtering to have a root mean square energy of 0.1. Figure 7 shows the performance inputs and outputs of the 10th subsystem. We observe that the noise is well attenuated. The root mean square energy of $z_{10,1}$ and $z_{10,2}$ are equal to 0.03610 and 0.02094, respectively.

As explained in Corollary 2.3, the robust $\mathcal{H}_\infty$-norm of an associated uncertain subsystem of form (6) was used as upper bound for the actual $\mathcal{H}_\infty$-norm of the networked system. Figure 8 shows the "worst-case gain function" of this associated uncertain subsystem:

$$
\omega \mapsto \max_{\lambda \in [-1,\, 1]} \sigma_1 \left(\hat{T}_{\hat{w}\hat{z}}(\jmath\omega; \mathbf{p}^\star, \lambda) \right) \tag{18}
$$

for $\omega \in [10^{-1}, 10^2]$. The robust $\mathcal{H}_\infty$-norm, which is equal to the maximal value of this worst-case gain function, is indicated with a dashed line. We observe that the worst-case gain function is flat and almost equal to the robust $\mathcal{H}_\infty$-norm for $\omega \in [0, 10]$. This phenomenon is typical for the direct optimization framework.

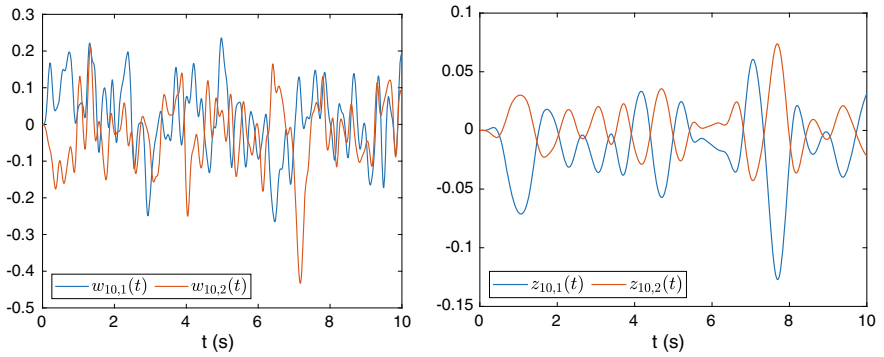

Fig. 7 Simulation of the performance inputs (left) and outputs (right) of the 10th subsystem for $t \in [0, 10]$ of the closed loop system (16)–(17) for $N = 20$. The state and the controller state are equal to zero for $t < 0$. Each performance input is low pass filtered ($\omega_{cutoff} = 6\pi$) Gaussian white noise, scaled after filtering to have a root mean square energy of 0.1

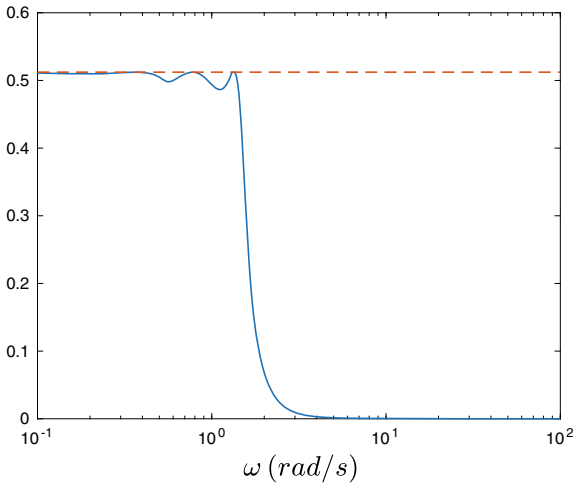

Fig. 8 The worst-case gain function of the associated uncertain subsystem as defined in (18) for $\omega \in [10^{-1}, 10^{2}]$. The robust $\mathcal{H}_\infty$-norm, $\|\hat{T}_{\hat{w}\hat{z}}(\cdot; \mathbf{p}^\star, \cdot)\|_{\mathcal{H}_\infty}^{[-1,1]}$, is indicated with a dashed line

6 Conclusion

In this chapter we introduced a scalable controller synthesis method for networked systems with identical subsystems and an interconnection topology that fulfills Assumption 1. Using the decoupling transformation of Sect. 2 we arrived at an upper bound for the $\mathcal{H}_\infty$-norm which can be computed at a cost that does not depend on the number of subsystems. This upper bound was the robust $\mathcal{H}_\infty$-norm of a single subsystem with an additional scalar uncertainty. Subsequently an algorithm to compute this robust $\mathcal{H}_\infty$-norm was discussed in Sect. 3. Finally, Sect. 4 showed how a controller that minimizes this upper bound can be synthesized using the direct optimization framework.

To conclude, we note that the presented method can be extended to more general identical subsystems, e.g., subsystems with direct feed-through terms. For such systems, however, the $\mathcal{H}_\infty$-norm is sensitive to infinitesimal delay changes and the strong $\mathcal{H}_\infty$-norm is a more appropriate performance measure (Gumussoy and Michiels, 2011). Furthermore, as in Sect. 2, one can show that the strong $\mathcal{H}_\infty$-norm of the overall system is upper bounded by the robust strong $\mathcal{H}_\infty$-norm of a single uncertain subsystem. This robust strong $\mathcal{H}_\infty$-norm can be computed using the method presented in Appeltans and Michiels (2021).

References

Appeltans, P., & Michiels, W. (2021). A pseudo-spectrum based characterization of the robust strong H-infinity norm of time-delay systems with real-valued and structured uncertainties. *The IMA Journal of Mathematical Control I., 38*(1), 267–296.

Borgioli, F., & Michiels, W. (2020). A novel method to compute the structured distance to instability for combined uncertainties on delays and system matrices. *IEEE Transactions on Automatic Control, 65*(4), 1747–1754.

Dileep, D., Borgioli, F., Hetel, L., Richard, J. P., & Michiels, W. (2018). A scalable design method for stabilising decentralised controllers for networks of delay-coupled systems. *IFAC-PapersOnLine, 51*(33), 68–73.

Dileep, D., Van Parys, R., Pipeleers, G., Hetel, L., Richard, J. P., & Michiels, W. (2018). *Design of robust decentralised controllers for MIMO plants with delays through network structure exploitation*. Control: Int. J.

Guglielmi, N., & Lubich, C. (2011). Differential equations for roaming pseudospectra: Paths to extremal points and boundary tracking. *SIAM Journal on Numerical Analysis, 49*(3), 1194–1209.

Guglielmi, N., & Lubich, C. (2013). Low-rank dynamics for computing extremal points of real pseudospectra. *SIAM Journal on Matrix Analysis and Applications, 34*(1), 40–66.

Gumussoy, S., & Michiels, W. (2011). Fixed-order H-Infinity control for interconnected systems using delay differential algebraic equations. *SIAM Journal on Control and Optimization, 49*(5), 2212–2238.

Güttel, S., Van Beeumen, R., Meerbergen, K., & Michiels, W. (2014). NLEIGS: A Class of fully rational Krylov methods for nonlinear eigenvalue problems. *SIAM Journal on Scientific Computing, 36*(6), A2842–A2864.

Hilhorst, G., Pipeleers, G., Michiels, W., & Swevers, J. (2015). Sufficient LMI conditions for reduced-order multi-objective H 2 / H ∞ control of LTI systems. *European Journal of Control, 23,* 17–25.

Jarlebring, E., Meerbergen, K., & Michiels, W. (2010). A Krylov method for the delay eigenvalue problem. *SIAM Journal on Scientific Computing, 32*(6), 3278–3300.

Massioni, P., & Verhaegen, M. (2009). Distributed control for identical dynamically coupled systems: A decomposition approach. *IEEE Transactions on Automatic Control, 54*(1), 124–135.

Michiels, W. (2011). Spectrum-based stability analysis and stabilisation of systems described by delay differential algebraic equations. *IET Control Theory & Applications, 5*(16), 1829–1842.

Overton, M. L. (2009). HANSO: Hybrid Algorithm for Non-Smooth Optimization. https://cs.nyu.edu/overton/software/hanso/.

Özer, S. M., & Iftar, A. (2015). Decentralized controller design for time-delay systems by optimization. *IFAC-PapersOnLine, 28*(12), 462–467.

Packard, A., & Doyle, J. C. (1993). The complex structured singular value. *Automatica, 29*(1), 71–109.

Press, W. H., Teukolsky, S. A., & Vetterling, W. T. (1996). *Numerical recipes in Fortran 77: The art of scientific computing* (2nd ed.). Cambridge: Cambridge University Press.

Wu, Z., & Michiels, W. (2012). Reliably computing all characteristic roots of delay differential equations in a given right half plane using a spectral method. *The Journal of Computational and Applied Mathematics, 236*(9), 2499–2514.

Zhou, K., & Doyle, J. C. (1998). *Essentials of robust control*. Upper Saddle River, NJ: Prentice hall. ISBN 978-0135258330.

Regenerative Machine Tool Vibrations

Tamás Insperger and Gabor Stépán

Abstract Two basic models of machine tool vibrations are presented. First, a simple model of orthogonal turning process is discussed where material is removed from the rotating workpiece by a tool. Vibrations of the tool are copied on the workpiece's surface and, after one revolution, the tool cuts this wavy surface. This phenomenon is called surface regeneration and the equations governing the vibrations are delay differential equations where the time delay is equal to the rotation period of the workpiece. Then, the mechanical model of milling operation is presented. Here the surface regeneration effect is combined by the parametric forcing of the entering and exiting cutting teeth. The governing equation is hence a time-periodic delay differential equation where the time delay and the principal period are both equal to the tooth passing period. Stability diagrams in the plane of the technological parameters are constructed for both turning and milling operations.

1 Introduction

Machine tool vibration or machine tool chatter is known as a large amplitude vibration between the tool and the workpiece during machining typically involving intermittent loss of contact of the tool and the workpiece. These vibrations are accompanied with a high-frequency noise during machining (chatter noise) and are copied on the workpiece surface resulted in chatter marks (see Fig. 1). Machine tool chatter decreases the lifetime of the tool and results in a poor surface quality, therefore its prediction is of high importance in manufacturing engineering.

The research reported in this paper and carried out at BME has been supported by the Hungarian National Research, Development and Innovation Office (NKFI-K-132477 and NKFI-KKP-133846), by the NRDI Fund (TKP2020 IES,Grant No. BME-IE-MIFM and TKP2020 NC, Grant No. BME-NC) based on the charter of bolster issued by the NRDI Office under the auspices of the Ministry for Innovation and Technology.

T. Insperger (✉) · G. Stépán
Department of Applied Mechanics, Budapest University of Technology and Economics, Budapest, Hungary
e-mail: insperger@mm.bme.hu

D. Breda (ed.), *Controlling Delayed Dynamics*, CISM International Centre for Mechanical Sciences 604, https://doi.org/10.1007/978-3-031-01129-0_10

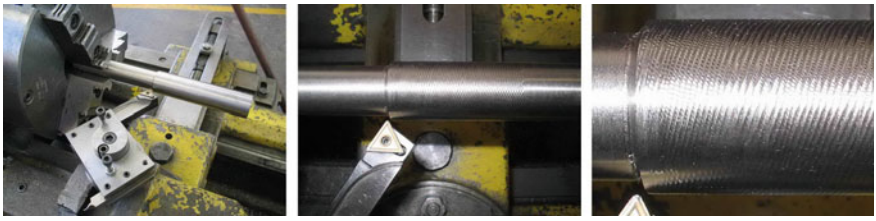

Fig. 1 Chattermarks caused by the vibrating tool (photo by Roland Horvath)

The history of machine tool chatter goes back to a century, when Taylor (1907) described machine tool chatter as the "most obscure and delicate of all problems facing the machinist." After the extensive work of Tobias and Tlusty (Tobias and Fishwick, 1958; Tobias, 1965; Tlusty et al., 1962), the so-called regenerative effect became the most commonly accepted explanation for machine tool chatter. This effect is related to the cutting-force variation due to the wavy workpiece surface cut one revolution ago. Stability properties of the machining process are depicted by the so-called stability lobe diagrams, which plot the maximum stable axial depths of cut versus the spindle speed. These diagrams provide a guide to the machinist to select the optimal technological parameters in order to achieve maximum material removal rate without chatter. Although there exist many sophisticated methods to optimize manufacturing processes, machine tool chatter is still an existing problem in manufacturing centers.

This chapter gives an overview on the main mechanism of regenerative machine tool chatter in turning and milling processes. First, the mechanical model of regenerative vibrations in turning operations is given, the governing equation, which is a Delay Differential Equation (DDE) with constant coefficients, is derived, the stability analysis is performed and the stability lobe diagrams are constructed. Second, the mechanical model of milling operations is considered, which are described by DDEs with time-periodic coefficients. Stability analysis of milling operations is determined by the semidiscretization method (Insperger and Stépán, 2011).

2 Turning Operations

The basis of regenerative cutting models is that either the tool, or the workpiece or both are flexible and the chip thickness varies due the relative vibrations of the tool and the workpiece. The tool cuts the surface that was formed in the previous cut, and the chip thickness is determined by the current and a previous position of the tool/workpiece. The time delay between two succeeding cuts is equal to the period of the workpiece rotation for turning (or the tooth-passing period for milling). The simplest model to describe regenerative machine tool vibrations is the orthogonal turning process.

2.1 Mechanical Model

Fig. 2 shows the chip removal process in an orthogonal turning operation for an ideally rigid tool and for a compliant tool. In the latter case, the tool experiences bending vibrations and leaves a wavy surface behind. The system can be modeled as a two-degrees-of-freedom oscillator excited by the cutting force, as shown in Fig. 3. If there is no dynamic coupling between the x and y directions, then the governing equation can be given as

$$m\ddot{x}(t) + c_x\dot{x}(t) + k_x x(t) = F_x(t) \ ,$$
$$m\ddot{y}(t) + c_y\dot{y}(t) + k_y y(t) = F_y(t) \ ,$$

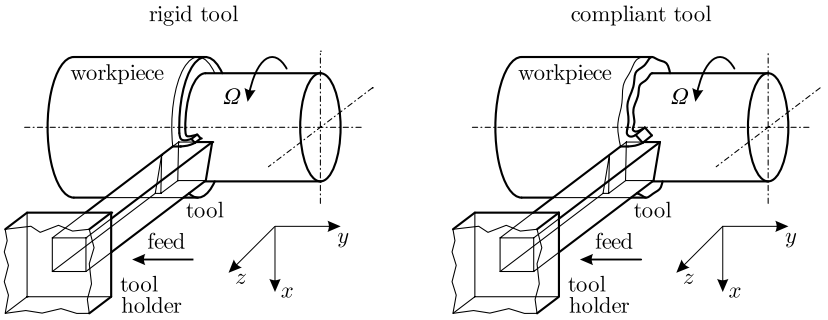

Fig. 2 Chip removal in orthogonal turning processes in the case of an ideally rigid tool (left) and real compliant tool (right)

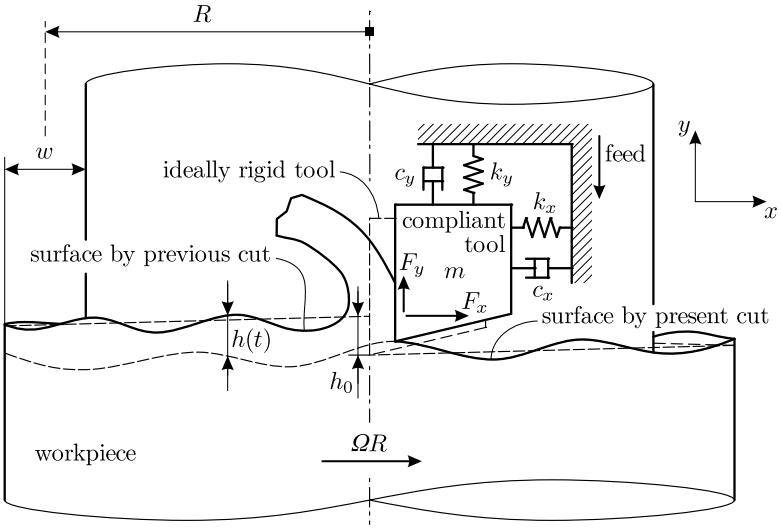

Fig. 3 Surface regeneration in an orthogonal turning process

where m, c_x, c_y, k_x, and k_y are the modal mass and the damping and stiffness parameters in the x and y directions, respectively. The cutting force is given in the form

$$F_x(t) = K_x\, w\, h^q(t)\ , \tag{1}$$

$$F_y(t) = K_y\, w\, h^q(t)\ , \tag{2}$$

where K_x and K_y are the cutting-force parameters in the tangential (x) and the normal (y) directions, w is the depth of cut (also known as the width of cut or the chip width in cases of orthogonal cutting), $h(t)$ is the instantaneous chip thickness, and q is the cutting-force exponent. In this model, it is assumed that the tool never leaves the workpiece, that is, $h(t) > 0$ during the cutting process.

If the tool were rigid, then the chip thickness would be constant $h(t) \equiv h_0$, which is just equal to the feed per revolution. However, in reality, the tool experiences vibrations that are recorded on the workpiece, and after one revolution, the tool cuts this wavy surface. The chip thickness h is determined by the feed motion, by the current tool position and by an earlier position of the tool. The time delay τ between the present and the previous cut is determined by the equation

$$\frac{R2\pi\Omega\tau}{60} = 2R\pi + x(t) - x(t-\tau)\ ,$$

where Ω is the spindle speed given in [rpm] and R is the radius of the workpiece. Since the amplitude of the vibrations is typically much smaller than the workpiece diameter (i.e., $|x(t)| \ll 2R\pi$), the regenerative time delay will be approximated by the constant

$$\tau = \frac{60}{\Omega}\ .$$

The chip thickness can be given as the combination of the feed and the present and the delayed positions of the tool in the form

$$h(t) = v_{\mathrm{f}}\tau + y(t-\tau) - y(t)\ ,$$

where v_{f} is the feed velocity. Thus, the governing equation can be written as

$$m\ddot{x}(t) + c_x\dot{x}(t) + k_x x(t) = K_x w\Big(v_{\mathrm{f}}\tau + y(t-\tau) - y(t)\Big)^q\ , \tag{3}$$

$$m\ddot{y}(t) + c_y\dot{y}(t) + k_y y(t) = K_y w\Big(v_{\mathrm{f}}\tau + y(t-\tau) - y(t)\Big)^q\ . \tag{4}$$

The substitution of the equilibrium states $x(t) \equiv \bar{x}$ and $y(t) \equiv \bar{y}$ into (3) and (4) gives the solution

$$\bar{x} = \frac{K_x w (v_\mathrm{f}\tau)^q}{k_x} \,, \tag{5}$$

$$\bar{y} = \frac{K_y w (v_\mathrm{f}\tau)^q}{k_y} \,. \tag{6}$$

This constant steady-state solution is equal to the deflection of the tool for a stationary case when the tool does not vibrate during the cutting process, but it has a constant deflection. Linearization about the equilibrium gives the variational system

$$m\ddot{\xi}(t) + c_x\dot{\xi}(t) + k_x\xi(t) = K_x w q (v_\mathrm{f}\tau)^{q-1}\Big((\eta(t-\tau) - \eta(t))\Big) \,, \tag{7}$$

$$m\ddot{\eta}(t) + c_y\dot{\eta}(t) + k_y\eta(t) = K_y w q (v_\mathrm{f}\tau)^{q-1}\Big((\eta(t-\tau) - \eta(t))\Big) \,, \tag{8}$$

where $\xi = x - \bar{x}$ and $\eta = y - \bar{y}$. Note that Eq. (7) is an Ordinary Differential Equation (ODE) forced by η, while Eq. (8) is a DDE. Consequently, the stability of the linear system is determined only by Eq. (8).

Dividing equation (8) by m gives

$$\ddot{\eta}(t) + 2\zeta\omega_\mathrm{n}\dot{\eta}(t) + \omega_\mathrm{n}^2\eta(t) = H\left(\eta(t-\tau) - \eta(t)\right) \,, \tag{9}$$

where $\omega_\mathrm{n} = \sqrt{k_y/m}$ is the natural angular frequency, $\zeta = c_y/(2m\omega_\mathrm{n})$ is the damping ratio of the tool in the y direction, and $H = K_y w q (v_\mathrm{f}\tau)^{q-1}/m$ is the specific cutting-force coefficient. Note that H is linearly proportional to the depth of cut w, which is an important technological parameter for machinists. Equation (9) is the simplest mathematical model that describes regenerative machine tool chatter.

2.2 Stability Analysis

The stability of the system can be determined by the D-subdivision method (Stépán, 1989). Substitution of the trial solution $\eta(t) = A\mathrm{e}^{\lambda t}$ into Eq. (9) or alternatively, the Laplace transformation gives the characteristic equation

$$\lambda^2 + 2\zeta\omega_\mathrm{n}\lambda + \omega_\mathrm{n}^2 + H\left(1 - \mathrm{e}^{-\lambda\tau}\right) = 0 \,.$$

Substitution of $\lambda = \gamma \pm \mathrm{i}\,\omega$ and decomposition into real and imaginary parts give

$$\mathrm{Re}: \quad \gamma^2 - \omega^2 + 2\zeta\omega_\mathrm{n}\gamma + \omega_\mathrm{n}^2 + H - H\mathrm{e}^{-\gamma\tau}\cos(\omega\tau) = 0 \,, \tag{10}$$

$$\mathrm{Im}: \quad 2\zeta\omega + 2\zeta\omega_\mathrm{n}\omega + H\mathrm{e}^{-\gamma\tau}\sin(\omega\tau) = 0 \,. \tag{11}$$

The D-curves can be obtained by substituting $\gamma = 0$:

$$\text{Re}: \quad -\omega^2 + \omega_\text{n}^2 + H - H\cos(\omega\tau) = 0\,, \tag{12}$$

$$\text{Im}: \quad 2\zeta\omega_\text{n}\omega + H\sin(\omega\tau) = 0\,. \tag{13}$$

This system of equation should be solved for H and $\Omega = 60/\tau$. First, taking the square of both sides of Eqs. (12) and (13) and summing them gives

$$\left(\omega_\text{n}^2 - \omega^2\right)^2 + 2\,H\left(\omega_\text{n}^2 - \omega^2\right) + H^2 + 4\zeta^2\omega_\text{n}^2\omega^2 = H^2\,.$$

This equation yields

$$H = \frac{\left(\omega^2 - \omega_\text{n}^2\right)^2 + 4\zeta^2\omega_\text{n}^2\omega^2}{2\left(\omega^2 - \omega_\text{n}^2\right)}\,. \tag{14}$$

Then, move the terms with H to the right side in Eqs. (12) and (13) and divide the left and right sides of the resulted equations to get

$$\frac{\omega^2 - \omega_\text{n}^2}{-2\zeta\omega_\text{n}\omega} = \frac{1 - \cos(\omega\tau)}{\sin(\omega\tau)}\,.$$

Utilize that

$$\frac{1 - \cos(\omega\tau)}{\sin(\omega\tau)} = \tan\left(\frac{1}{2}\,\omega\tau\right)\,,$$

and from here one gets

$$\tau = \frac{2}{\omega}\left(j\pi - \arctan\left(\frac{\omega^2 - \omega_\text{n}^2}{2\zeta\omega_\text{n}\omega}\right)\right)\,, \quad j = 0, 1, 2, \ldots\,, \tag{15}$$

which gives

$$\Omega = \frac{30\omega}{j\pi - \arctan\left(\dfrac{\omega^2 - \omega_\text{n}^2}{2\zeta\omega_\text{n}\omega}\right)}\,, \quad j = 0, 1, 2, \ldots\,. \tag{16}$$

The D-curves in parametric curves are given by Eqs. (14) and (16), where the parameter ω is the frequency of the arising vibrations in [rad/s]. Figure 4 shows the D-curves and the number of unstable characteristic exponents in the plane of the dimensionless specific cutting-force coefficient

$$\frac{H}{\omega_\text{n}^2} = \frac{\left(\left(\frac{\omega}{\omega_\text{n}}\right)^2 - 1\right)^2 + 4\zeta^2\left(\frac{\omega}{\omega_\text{n}}\right)^2}{2\left(\left(\frac{\omega}{\omega_\text{n}}\right)^2 - 1\right)}$$

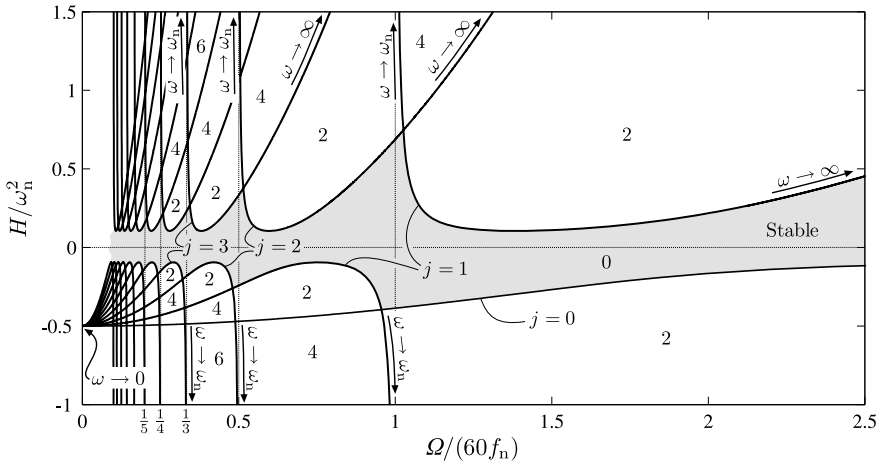

Fig. 4 Stability chart and the number of unstable characteristic exponents for (9) with $\zeta = 0.05$

and the dimensionless spindle speed $\Omega/(60 f_n)$, where $f_n = \omega_n/2\pi$ is the natural frequency of the tool in [Hz]. As can be seen, (16) and (14) give a pair of D-curves for each integer $j \geq 1$, one in the domain $H > 0$ associated with $\omega > \omega_n$ and one in the domain $H < 0$ associated with $\omega < \omega_n$. The case $j = 0$ gives a single curve in the domain $H < 0$. In the literature, these D-curves are called lobes or stability lobes. The lobes of index $j = 1$ are the rightmost ones; all the other lobes with $j \geq 2$ are located at lower spindle speeds. Each pair of lobes has a vertical asymptote at $\Omega = 60 f_n/j$ indicated by dotted lines in Fig. 4. The limits for the frequency parameter ω along the stability lobes are also presented. Frequency parameters $\omega < 0$ give D-curves in the negative spindle speed domain (not presented here).

The number of unstable characteristic exponents can be determined by the analysis of the exponent-crossing direction (also called root tendency) along the D-curves. For this analysis, one should take the partial derivative of both sides of Eqs. (10) and (11) with respect to the specific cutting force coefficient H, and then substitute $\gamma = 0$. This gives the system of equations

$$\begin{aligned} A\,\gamma' + B\,\omega' &= \cos(\omega\tau) - 1\ , \\ -B\,\gamma' + A\,\omega' &= -\sin(\omega\tau)\ , \end{aligned}$$

where γ' and ω' are the partial derivatives of γ and ω with respect to H, respectively, and

$$\begin{aligned} A &= 2\zeta\omega_n + H\tau\cos(\omega\tau)\ , \\ B &= H\tau\sin(\omega\tau) - 2\omega\ . \end{aligned}$$

From here, one gets

$$\gamma' = \frac{1}{A^2 + B^2}(A\cos(\omega\tau) - AB\sin(\omega\tau)) \ ,$$

which, after substituting A and B gives

$$\gamma' = \frac{1}{A^2 + B^2}\left(\tau\left(\omega^2 - \omega_{\rm n}^2\right) + 2\,H\zeta\omega_{\rm n}\left(\omega^2 + \omega_{\rm n}^2\right)\right) \ .$$

This implies that the sign of γ' is equal to the sign of H along the D-curves (note that $\omega < \omega_{\rm n}$ if $H < 0$ and $\omega > \omega_{\rm n}$ if $H > 0$). In the case $H = 0$, the system is a damped oscillator, which is asymptotically stable. Consequently, in the region bounded by the stability lobes (indicated by gray shading in Fig. 4), the number of unstable characteristic exponents is zero. This parameter region is associated with stable/chatter-free machining process. Note that from a practical point of view, only the domain $H > 0$ is relevant, since this corresponds to positive depth of cut values.

The stability boundaries in Fig. 4 represent Hopf bifurcation, since the characteristic exponents cross the imaginary axis with a nonzero imaginary part (i.e., $\omega \neq 0$) as we cross the stability boundaries. If the cutting forces are given in the form (1) and (2) with $q \approx 0.75$, then the stability boundaries represent subcritical Hopf bifurcations. In case of a subcritical Hopf bifurcation, an unstable periodic orbit coexists with the stable stationary cutting state that may lead to chatter even within the linear stability boundaries.

Figure 5 shows the practical region of the stability chart (i.e., for positive depths of cut) and the associated frequency ratio diagram, where $f = \omega/2\pi$ is the frequency of the arising self-excited vibrations at the stability boundaries in [Hz]. The stability lobes are usually characterized by their index: the lobe of index j is called the jth lobe. The minimum points of the lobes can be determined by differentiating (14) with respect to ω, giving

$$\frac{{\rm d}H}{{\rm d}\omega}(\omega^*) = 0 \quad \Rightarrow \quad \omega^* = \omega_{\rm n}\sqrt{2\zeta + 1} \ , \quad H_{\rm min} = H(\omega^*) = 2\zeta\omega_{\rm n}^2(1 + \zeta) \ . \quad (17)$$

For $\zeta = 0.05$ in Fig. 5, (17) gives $H_{\rm min}/\omega_{\rm n}^2 = 2\zeta(1 + \zeta) = 0.105$.

2.3 *Phase Shift Along the Stability Lobes*

Regenerative machine tool chatter is also often explained by the phase shift between the actual $\eta(t)$ and the delayed $\eta(t - \tau)$ position of the tool. The relation between the regenerative delay and the chatter frequency is

$$\tau = \frac{2\pi}{\omega}k + \frac{\varepsilon}{\omega} \ ,$$

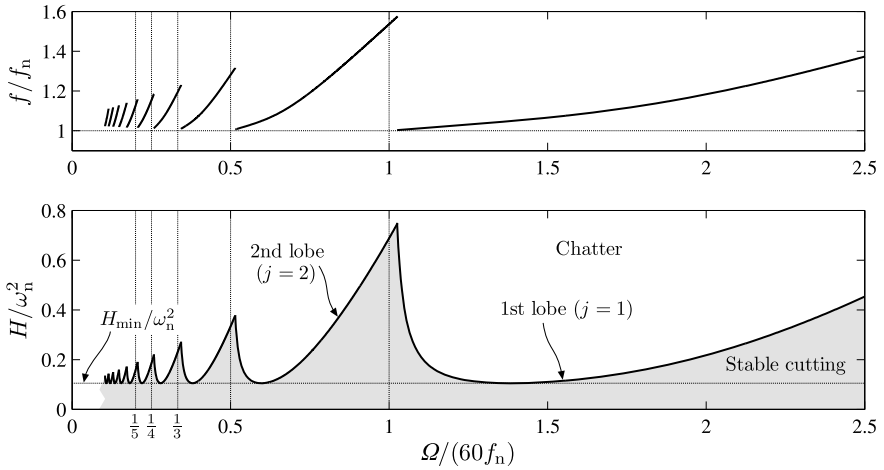

Fig. 5 Stability lobe diagram (bottom) and frequency diagram (top) for (9) with $\zeta = 0.05$

where k is the number of full oscillation completed during the period τ and $\varepsilon \in (0, 2\pi]$ is the phase shift. If $\varepsilon = 0$ (or 2π) then the tool at time instant t is in phase with the tool at time instant $t - \tau$. If $\varepsilon = \pi$ then the tool at time instant t is in antiphase with the tool at time instant $t - \tau$. Using (15), the phase shift can be given as

$$\varepsilon = \left(j - k - \frac{1}{\pi} \arctan\left(\frac{\omega^2 - \omega_n^2}{2\zeta\omega_n\omega} \right) \right) 2\pi \ ,$$

where j is the lobe number. The fact that $\omega > \omega_n$ (if $H > 0$) and $\varepsilon \in (0, 2\pi]$ implies that $j - k = 1$. That is, the number of full oscillations by the tool over a delay period is $k = j - 1$.

The value of the phase shift can be determined at specific points along the stability lobes. At the left side of the lobe of number j, where $\omega \to \omega_n$:

$$\Omega = \left. \frac{30\omega}{j\pi - \arctan\left(\dfrac{\omega^2 - \omega_n^2}{2\zeta\omega_n\omega} \right)} \right|_{\omega \to \omega_n} = \frac{1}{j} \frac{60}{2\pi} \omega_n \ ,$$

$$\varepsilon = 2\pi \left(j - k - \frac{1}{\pi} \arctan\left(\frac{\omega^2 - \omega_n^2}{2\zeta\omega_n\omega} \right) \right) \Bigg|_{\omega \to \omega_n} = 2\pi$$

(note that $j - k = 1$). This means that during one revolution of the workpiece, the tool completes $k + 1 = j$ number of full oscillations. In other words the tool at time instant t is in phase with the tool at time instant $t - \tau$.

At the right side of the lobe of number j, where $\omega \to \infty$:

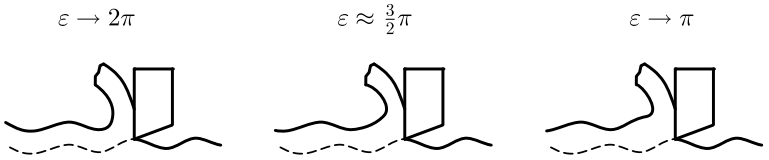

Fig. 6 Phase shift between the actual $\eta(t)$ and the delayed $\eta(t-\tau)$ position of the tool. See the variation of the chip thickness: the actual tool position is in phase (left) and in antiphase (right) with previous tool position

$$\Omega = \left.\frac{30\omega}{j\pi - \arctan\left(\dfrac{\omega^2-\omega_\mathrm{n}^2}{2\zeta\omega_\mathrm{n}\omega}\right)}\right|_{\omega\to\infty} = \infty\,,$$
$$\varepsilon = \left.2\pi\left(j-k-\frac{1}{\pi}\arctan\left(\frac{\omega^2-\omega_\mathrm{n}^2}{2\zeta\omega_\mathrm{n}\omega}\right)\right)\right|_{\omega\to\infty} = \pi\,.$$

Thus, during one revolution of the workpiece, the tool completes $k+1/2 = j-1/2$ number of full oscillations. In other words the tool at time instant t is in antiphase with the tool at time instant $t-\tau$.

At the minimum point of lobe of number j, where $\omega = \omega^* = \omega_\mathrm{n}\sqrt{2\zeta+1}$:

$$\Omega = \frac{30\omega_\mathrm{n}\sqrt{2\zeta+1}}{j\pi - \arctan\left(\dfrac{\omega_\mathrm{n}^2(2\zeta+1)-\omega_\mathrm{n}^2}{2\zeta\omega_\mathrm{n}\omega_\mathrm{n}\sqrt{2\zeta+1}}\right)} \approx \frac{1}{j-\frac{1}{4}}\,\frac{60}{2\pi}\omega_\mathrm{n}\,,$$
$$\varepsilon = \left.2\pi\left(j-k-\frac{1}{\pi}\arctan\left(\frac{\omega_\mathrm{n}^2(2\zeta+1)-\omega_\mathrm{n}^2}{2\zeta\omega_\mathrm{n}\omega_\mathrm{n}\sqrt{2\zeta+1}}\right)\right)\right|_{\omega\to\infty} = \frac{3}{2}\pi\,.$$

(Here, it was used that $\sqrt{2\zeta+1}\approx 1$ if ζ is small.) Thus, during one revolution of the workpiece, the tool completes $k+1/2 = j-1/4$ number of full oscillations.

The phase between the actual and the delayed position of the tool for different phase shifts ε is shown in Fig. 6. The oscillations of the tool over a delay period along the stability lobes are shown in Fig. 7. The number of full oscillations is increasing with the number j of the lobes.

3 Milling Operations

Compared to turning processes, regenerative machine tool chatter is an even more challenging problem for milling operations. In the case of milling, the rotation of the tool and the continuously entering and exiting cutting edges (see Fig. 8) present a parametric excitation, which, combined with the surface regeneration effect, results in a DDE with time-periodic coefficients. The first results regarding the stability

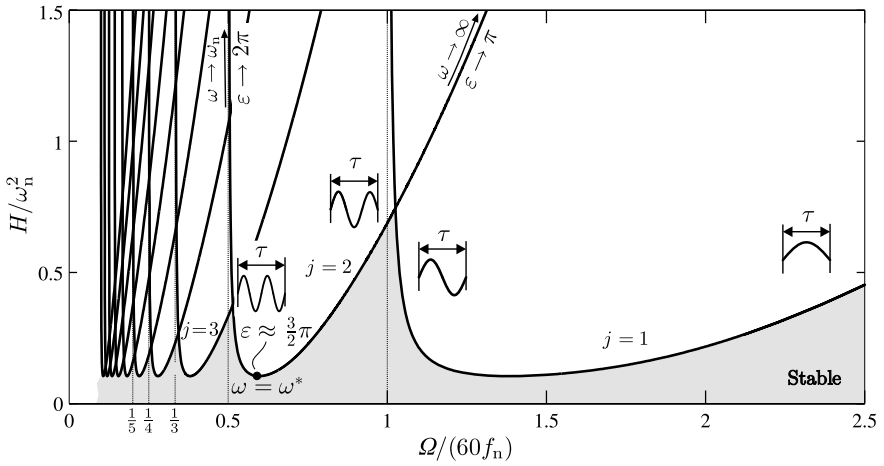

Fig. 7 Oscillations over a delay period along the stability lobes

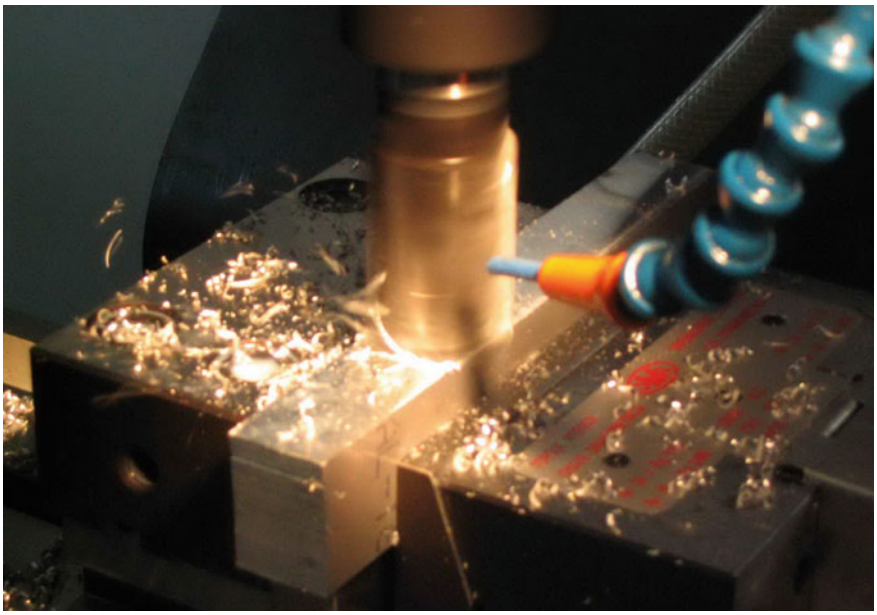

Fig. 8 Milling operation

properties of milling processes appeared in Tobias's and Tlusty's works (Tobias and Fishwick, 1958; Tobias, 1965; Tlusty et al., 1962). They considered the time-averaged cutting force instead of the time-periodic one, so their models were equivalent to a DDE with constant coefficients. These models can be used for processes with large radial immersion and large number of cutting teeth when the parametric excitation of the teeth is negligible. For small radial immersion, however, the intermittent nature of the cutting process cannot be neglected. In these cases, the extended Floquet theory should be applied for the stability analysis. A well-known technique is the multi frequency solution developed by Budak and Altintas (Altintas and Budak, 1995; Budak and Altintas, 1998; Altintas, 2012), which is a frequency-domain method based on Fourier expansion of the periodic terms and Hill's infinite determinant technique. An alternative, time-domain method is the semidiscretization method (Insperger and Stépán, 2002, 2011). In this chapter, we consider a single-degree-of-freedom model of milling operation and determine the stability properties using the semidiscretization method.

3.1 Mechanical Model

One of the simplest models of end milling is shown in Fig. 9. This model is taken from Insperger et al. (2003a). The workpiece is assumed to be flexible in the feed direction (direction x) with modal mass m, damping coefficient c, and spring stiffness k, while the tool is assumed to be rigid. The tool has N equally distributed cutting teeth with zero helix angles. The spindle speed is Ω given in [rpm]. According to Newton's law, the equation of motion reads

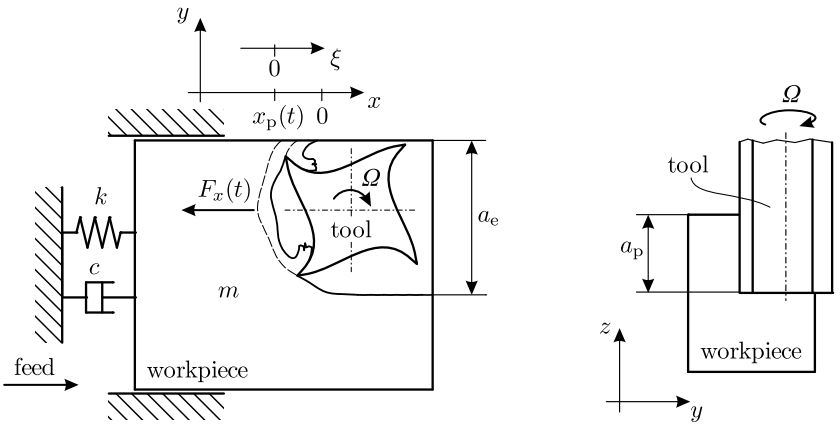

Fig. 9 Single-degree-of-freedom mechanical model of end milling process with a straight fluted tool

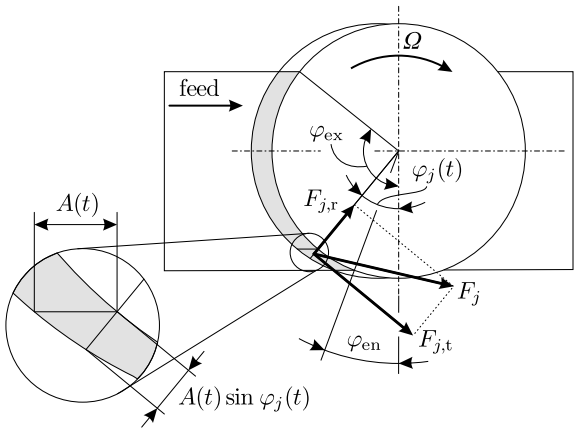

Fig. 10 Cutting-force components and chip thickness model in the milling process

$$m\ddot{x}(t) + c\dot{x}(t) + kx(t) = -F_x(t) \ , \tag{18}$$

where $F_x(t)$ is the x component of the cutting force vector acting on the tool. Let the teeth of the tool be indexed by $j = 1, 2, \ldots, N$. The geometry of the milling process and the cutting forces are shown in Fig. 10.

The tangential and radial components of the cutting force acting on tooth j read

$$F_{j,\mathrm{t}}(t) = g_j(t) K_\mathrm{t} a_\mathrm{p} h_j^q(t) \ ,$$
$$F_{j,\mathrm{r}}(t) = g_j(t) K_\mathrm{r} a_\mathrm{p} h_j^q(t) \ ,$$

where K_t and K_r are the tangential and radial cutting-force parameters, respectively, a_p is the axial depth of cut, $h_j(t)$ is the chip thickness cut by tooth j and q is the cutting-force exponent. Function $g_j(t)$ is a screen function; it is equal to 1 if tooth j is in the cut and 0 if it is not. If φ_en and φ_ex denote the angular locations where the cutting teeth enter and exit the cut, then the screen function reads

$$g_j(t) = \begin{cases} 1 & \text{if } \varphi_\mathrm{en} < (\varphi_j(t) \bmod 2\pi) < \varphi_\mathrm{ex} \ , \\ 0 & \text{otherwise,} \end{cases}$$

where

$$\varphi_j(t) = \frac{2\pi\,\Omega}{60} t + j\,\frac{2\pi}{N}$$

is the angular position of tooth j and mod is the modulo function. In the case of up-milling,

$$\varphi_\mathrm{en} = 0 \ , \qquad \varphi_\mathrm{ex} = \arccos\left(1 - \frac{2a_\mathrm{e}}{D}\right) \ ,$$

while in the case of down-milling,

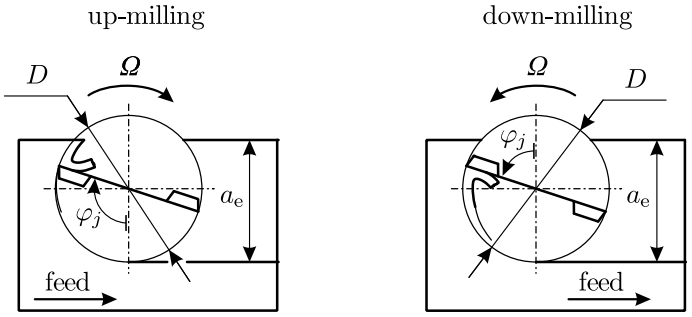

Fig. 11 Sketch of up-milling and down-milling operations

$$\varphi_{\mathrm{en}} = \arccos\left(\frac{2a_{\mathrm{e}}}{D} - 1\right) , \qquad \varphi_{\mathrm{ex}} = \pi ,$$

where a_{e} is the radial immersion and D is the diameter of the tool (see Fig. 11).

Although a constant feed f_{z} per tooth is prescribed, the actual feed $A(t)$ per tooth is not constant, since it is affected by the present and a delayed position of the workpiece in the form

$$A(t) = f_{\mathrm{z}} + x(t) - x(t-\tau) ,$$

where $\tau = 60/(N\Omega)$ [s] is the regenerative delay, which coincides with the tooth-passing period (note that the spindle speed Ω is given in [rpm]). The instantaneous chip thickness $h_j(t)$ is determined by the actual feed per tooth and the angular position of the cutting teeth. A circular approximation of the tooth path gives

$$h_j(t) = A(t)\sin\varphi_j(t) = (f_{\mathrm{z}} + x(t) - x(t-\tau))\sin\varphi_j(t) .$$

The x component of the cutting force acting on tooth j is obtained as the projection of $F_{j,\mathrm{t}}$ and $F_{j,\mathrm{r}}$ in the x direction, i.e.,

$$F_{j,x}(t) = F_{j,\mathrm{t}}(t)\cos\varphi_j(t) + F_{j,\mathrm{r}}(t)\sin\varphi_j(t) .$$

The x component of the resultant cutting force acting on the tool reads

$$F_x(t) = Q(t)\,(f_{\mathrm{z}} + x(t) - x(t-\tau))^q ,$$

where

$$Q(t) = \sum_{j=1}^{N} a_{\mathrm{p}} g_j(t)\sin^q\varphi_j(t)\left(K_{\mathrm{t}}\cos\varphi_j(t) + K_{\mathrm{r}}\sin\varphi_j(t)\right)$$

is a periodic function with period τ. Thus, the equation of motion is the following nonlinear time-periodic DDE:

$$m\ddot{x}(t) + c\dot{x}(t) + kx(t) = -Q(t)\,(f_z + x(t) - x(t-\tau))^q \ . \tag{19}$$

Assume that the motion of the workpiece can be written in the form

$$x(t) = x_p(t) + \xi(t) \ , \tag{20}$$

where $x_p(t) = x_p(t+\tau)$ is a τ-periodic function, and $\xi(t)$ is the perturbation (see Fig. 9). In fact, $x_p(t)$ is the solution for the unperturbed ideal case when no self-excited vibrations arise. Substitution of (20) into (19) yields

$$\begin{aligned} m\ddot{x}_p(t) + c\dot{x}_p(t) + kx_p(t) + m\ddot{\xi}(t) + c\dot{\xi}(t) + k\xi(t) \\ = -Q(t)\,(f_z + \xi(t) - \xi(t-\tau))^q \ . \end{aligned} \tag{21}$$

In the ideal unperturbed case, $\xi(t) \equiv 0$ and the oscillations of the workpiece are described by $x(t) = x_p(t)$. This case gives an ODE for x_p in the form

$$m\ddot{x}_p(t) + c\dot{x}_p(t) + kx_p(t) = -f_z^q\,Q(t) \ . \tag{22}$$

Since this is a linear differential equation with τ-periodic forcing, it has a τ-periodic particular solution. This proves the existence of the τ-periodic function $x_p(t)$ and verifies the decomposition (20).

For linear stability analysis, the variational system of (19) about the periodic motion $x_p(t)$ should be determined. Taylor expansion of the nonlinear terms in (21) with respect to ξ and neglecting the higher-order terms gives

$$\begin{aligned} m\ddot{x}_p(t) + c\dot{x}_p(t) + kx_p(t) + m\ddot{\xi}(t) + c\dot{\xi}(t) + k\xi(t) \\ = -f_z^q\,Q(t) - qf_z^{q-1}\,Q(t)\,(\xi(t) - \xi(t-\tau)) \ . \end{aligned} \tag{23}$$

Using (22) and (23), a linear time-periodic DDE is obtained for ξ:

$$m\ddot{\xi}(t) + c\dot{\xi}(t) + k\xi(t) = -qf_z^{q-1}\,Q(t)\,(\xi(t) - \xi(t-\tau)) \ . \tag{24}$$

Introducing the natural angular frequency $\omega_n = \sqrt{k/m}$ and the damping ratio $\zeta = c/(2m\omega_n)$, (24) can be written in the form

$$\ddot{\xi}(t) + 2\zeta\omega_n\dot{\xi}(t) + \omega_n^2\xi(t) = -HG(t)\,(\xi(t) - \xi(t-\tau)) \ , \tag{25}$$

where $H = a_p q f_z^{q-1} K_r/m$ is the specific cutting-force coefficient and

$$G(t) = \sum_{j=1}^{N} g_j(t)\sin^q\varphi_j(t)\left(\frac{K_t}{K_r}\cos\varphi_j(t) + \sin\varphi_j(t)\right)$$

is a τ-periodic function called the directional dynamic cutting-force coefficient, or simply the directional factor. If $K_r = K_y$, $a_p = w$, $f_z = v_f\tau$, and $G(t) \equiv 1$, then (25) gives the governing Eq. (9) of turning operations.

The system can be written in the first-order form

$$\dot{x}(t) = A(t)x(t) + B(t)u(t-\tau) \,, \tag{26}$$

$$u(t) = Dx(t) \,, \tag{27}$$

where

$$x(t) = \begin{pmatrix} \xi(t) \\ \dot{\xi}(t) \end{pmatrix} \,, \qquad D = \begin{pmatrix} 1 & 0 \end{pmatrix} \,,$$

$$A(t) = \begin{pmatrix} 0 & 1 \\ -\left(\omega_n^2 + HG(t)\right) & -2\zeta\omega_n \end{pmatrix} \,, \qquad B(t) = \begin{pmatrix} 0 \\ HG(t) \end{pmatrix} \,.$$

3.2 *Stability Analysis by Semidiscretization*

In this section, stability charts are determined for the system (26)–(27) using the zeroth-order semidiscretization method (Insperger and Stépán, 2002, 2011). Semidiscretization is based on the discrete time scale $t_i = ih$, $i \in \mathbb{Z}$, where the discretization step is $h = \tau/r$ and r an integer approximation parameter. The point of the semidiscretization method is that the delayed terms and the time-periodic coefficients are discretized (such as in discrete-time sampling), while all the other terms in the differential equation are unchanged. The (zeroth-order) semidiscrete approximation of the system (26)–(27) reads

$$\dot{y}(t) = A_i y(t) + B_i v(t_{i-r}) \,, \quad t \in [t_i, t_{i+1}) \,, \tag{28}$$

$$v(t_i) = Dy(t_i) \,, \tag{29}$$

where

$$A_i = \frac{1}{h}\int_{t_i}^{t_{i+1}} A(t)\,\mathrm{d}t \,, \quad B_i = \frac{1}{h}\int_{t_i}^{t_{i+1}} B(t)\,\mathrm{d}t \,.$$

Approximation of the term $u(t-\tau)$ by term $v(t_{i-r})$ with piecewise constant argument over the interval $t \in [t_i, t_{i+1})$ actually corresponds to a perturbation in the delay, since the term $v(t_{i-r})$ can also be written as $v(t-\rho(t))$, where

$$\rho(t) = rh - t_i + t \,, \qquad t \in [t_i, t_{i+1}) \,, \tag{30}$$

is a sawtooth-like time-periodic time delay shown in Fig. 12. If $r \to \infty$ and $h \to 0$ such that $rh = \tau$ remains constant, then the time-periodic time delay $\rho(t)$ tends to the constant delay τ, as shown in Fig. 12.

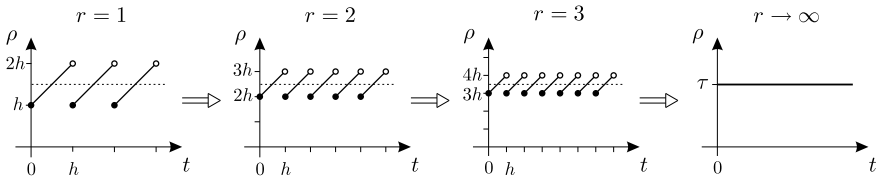

Fig. 12 Discrete-time sampling effect presented as time-periodic delay

In fact, the sampling effect introduces a periodic parametric excitation at the time delay according to (30). System (28)–(29) is still a time-periodic DDE (i.e., a DDE with time-periodic coeffcients and time-periodic point delay) with principal period τ. The stability conditions are determined by the eigenvalues of the monodromy operator, which is typically an infinite-dimensional operator in case of delayed systems (see, e.g., Breda, 2023). On the other hand, system (28)–(29) can also be considered as a series of ODEs with a piecewise constant forcing on the right-hand side, which implies that a finite-dimensional representation of the monodromy operator can be given as shown below. The approximation parameter r is related to the resolution of the delay period τ, therefore, it is called the *delay resolution*.

Solution over the interval $[t_i, t_{i+1})$ gives

$$y_{i+1} = P_i y_i + R_{i,0} v_{i-r} \ , \tag{31}$$

where

$$P_i = \mathrm{e}^{A_i h} \ ,$$
$$R_i = \int_0^h \mathrm{e}^{A_i (h-s)} \, \mathrm{d}s \ B_i \ .$$

If A_i^{-1} exists, then integration gives

$$R_i = \left(\mathrm{e}^{A_i h} - I \right) A_i^{-1} \, B_i \ ,$$

where I is the 2×2 identity matrix. Equations (31) and (29) imply the $(2+r)$-dimensional discrete map

$$z_{i+1} = G_i z_i \ , \tag{32}$$

where

$$z_i = \left(y_i \ v_{i-1} \ v_{i-2} \cdots v_{i-r} \right)^T = \left(x_i \ \dot{x}_i \ x_{i-1} \ x_{i-2} \cdots x_{i-r} \right)^T$$

is the augmented state vector and the $(2+r) \times (2+r)$ coefficient matrix reads

$$G_i = \begin{pmatrix} P_i & 0 & \cdots & 0 & R_i \\ D & 0 & \cdots & 0 & 0 \\ 0 & I & \cdots & 0 & 0 \\ \vdots & & & & \vdots \\ 0 & 0 & \cdots & I & 0 \end{pmatrix} .$$

Recalling that $\tau = rh$, r repeated applications of (32) with initial state z_0 gives the monodromy mapping

$$z_r = \Phi z_0,$$

where

$$\Phi = G_{r-1} G_{r-2} \cdots G_0$$

is a $(2 + r)$-dimensional matrix representation of the monodromy operator of system (26)–(27). In this way, Φ provides a finite-dimensional approximation of the infinite-dimensional monodromy operator of the original system (26)–(27).

The stability of the approximate system (28)–(29) can be assessed by the eigenvalue analysis of matrix Φ. If all the eigenvalues are inside the unit circle of the complex plane, then the system (28)–(29) is asymptotically stable. Since semidiscretization preserves asymptotic stability of the original system (28)–(29) (Hartung et al., 2006), the method can be used to construct approximate stability charts.

As was mentioned in Chap. 2, the critical characteristic multipliers can be located in three ways:

1. $|\mu_{1,2}| = 1$ with $\mathrm{Im}\mu_{1,2} \neq 0$ (secondary Hopf bifurcation);
2. $\mu_1 = 1$ (cyclic-fold bifurcation);
3. and $\mu_1 = -1$ (period-doubling or flip bifurcation).

It can easily be seen that the case $\mu_1 = 1$ cannot occur for (25). It is known that in the critical subspace, $\xi(t + \tau) = \mu_1 \xi(t)$ is satisfied. If $\mu_1 = 1$, then $\xi(t - \tau) = \xi(t)$, and substitution into (25) gives the damped oscillator

$$\ddot{\xi}(t) + 2\zeta\omega_\mathrm{n}\dot{\xi}(t) + \omega_\mathrm{n}^2 \xi(t) = 0 . \tag{33}$$

Since ζ and ω_n are positive, (33) is asymptotically stable; consequently, it cannot have a characteristic exponent equal to zero, i.e., it cannot have a characteristic multiplier equal to 1. This proves that cyclic-fold bifurcation cannot arise for (25).

With a different conclusion, the same idea can be applied in the case $\mu_1 = -1$. Here, $\xi(t - \tau) = -\xi(t)$, and substitution into (25) gives

$$\ddot{\xi}(t) + 2\zeta\omega_\mathrm{n}\dot{\xi}(t) + \left(\omega_\mathrm{n}^2 + 2\,HG(t)\right)\xi(t) = 0 .$$

This is an ODE with time-periodic coefficient, for which the characteristic multiplier $\mu_1 = -1$ typically arises for some parameter combination.

3.3 Chatter Frequencies in Milling Operations

The vibration frequencies arising at the boundary of stability can be determined using the critical characteristic multipliers obtained by the semidiscretization method (Insperger et al., 2003b; Mann et al., 2003). Vibrations arise when the system loses stability, i.e., when the critical characteristic multiplier satisfies $|\mu_1| = 1$. Equation (25) is periodic at the tooth-passing period τ. According to the Floquet theory, the solution corresponding to the critical characteristic multiplier μ_1 reads

$$\xi(t) = a(t)\mathrm{e}^{\lambda_1 t} + \bar{a}(t)\mathrm{e}^{\bar{\lambda}_1 t} \,, \tag{34}$$

where $a(t)$ is a τ-periodic function, bar denotes complex conjugate, and λ_1 is the critical characteristic exponent, i.e., $\mu_1 = \mathrm{e}^{\lambda_1 \tau}$. Fourier expansion of $a(t)$ and substitution of $\lambda_1 = \mathrm{i}\,\omega_1$ results in

$$\xi(t) = \sum_{j=-\infty}^{\infty} \left(C_j \mathrm{e}^{\mathrm{i}\,(\omega_1 + j2\pi/\tau)t} + \bar{C}_j \mathrm{e}^{-\mathrm{i}\,(\omega_1 + j2\pi/\tau)t} \right) \,, \tag{35}$$

where C_j and $\bar{C}_j$ are some complex coefficients. Note that $\omega_1\tau$ is equal to the phase angle describing the direction of μ_1 in the complex plane, so that $-\pi < \omega_1\tau \leq \pi$. The exponents in (35) give the angular frequency content of the vibrations. The corresponding vibration frequencies are

$$f = \pm\frac{\omega_1}{2\pi} + \frac{j}{\tau}\ [\mathrm{Hz}] \,, \qquad j = 0, \pm 1, \pm 2, \ldots \,.$$

Of course, only the positive frequencies have physical meaning.

For the secondary Hopf lobes, the critical characteristic multipliers are a complex conjugate pair in the form $\mu = \mathrm{e}^{\pm \mathrm{i}\,\omega\tau}$, and the chatter frequencies are given by

$$f_{\mathrm{H}} = \pm\frac{\omega_1}{2\pi} + j\frac{N\Omega}{60}\ [\mathrm{Hz}] \,, \quad j = 0, \pm 1, \pm 2, \ldots \,. \tag{36}$$

According to (34), the solution is given as the product of the τ-periodic function $a(t)$ and the $(2\pi/\omega_1)$-periodic function $\mathrm{e}^{\lambda_1 t} = \mathrm{e}^{\mathrm{i}\omega_1 t}$. Consequently, the resulting vibrations are quasiperiodic. In the literature, vibrations due to secondary Hopf bifurcations are often referred to as quasiperiodic chatter.

For the flip lobes, the critical characteristic multiplier is $\mu_1 = -1$, i.e., $\omega_1\tau = \pi$. The corresponding chatter frequencies are

$$f_{\mathrm{F}} = \frac{N\Omega}{120} + j\frac{N\Omega}{60}\ [\mathrm{Hz}] \,, \quad j = 0, \pm 1, \pm 2, \ldots \,. \tag{37}$$

In this case, the period of the function $e^{\lambda_1 t} = e^{i\omega_1 t} = e^{i\pi t/\tau}$ is 2τ. Consequently, the solution according to (34) is a 2τ-periodic function that explains the terminology *period doubling*: the period of the vibration is double of the tooth-passing period.

3.4 Stability Lobe Diagrams for Milling

Figure 13 shows a series of stability lobe diagrams in the plane of the dimensionless spindle speed $N\Omega/(60 f_n)$ and the dimensionless specific cutting-force coefficient H/ω_n^2 for different milling operations (note that H is linearly proportional to the axial depth of cut a_p). The corresponding frequency diagrams and the directional factor $G(t)$ are also presented. The damping ratio is $\zeta = 0.02$, the cutting-force ratio is $K_r/K_t = 0.3$, and the cutting-force exponent is $q = 0.75$. The same diagrams are also shown for turning as the special limiting case when $G(t) \equiv 1$. The technological parameters for the milling operations were determined such that the time-dependency of the directional factor $G(t)$ becomes stronger and stronger. The first case is a full-immersion milling with a 4-fluted tool. In this case the tool is always in contact with the workpiece, since two of its cutting edges are always in the cut, and the directional factor $G(t)$ is a continuous function. The other cases are all up-milling operations by a 4-fluted tool with smaller and smaller radial immersion, resulting in more and more interrupted machining. Highly interrupted machining operations can be modeled approximately by a finite-dimensional discrete map instead of infinite-dimensional DDEs such that the cutting process is considered as an impact with the cutting force impulse being proportional to the chip thickness. In this sense, Fig. 13 presents a transition between two special models of machining: the traditional time-independent DDE model of turning operation and the discrete map model of highly interrupted machining (Insperger and Stépán, 2004). Figure 13 shows that a series of extra stability lobes arises in addition to the Hopf lobes of turning as the process becomes more and more interrupted. Numerical calculation shows that along these additional lobes, a single characteristic multiplier crosses the unit circle at -1, i.e., these lobes are associated with period-doubling (flip) bifurcation. As the radial immersion decreases, the orientation of the flip lobes become vertical.

The frequency diagrams in Fig. 13 were obtained using (36) and (37). While turning operations are characterized by a well-defined single chatter frequency according to the Hopf bifurcation of autonomous systems, milling operations, being parametrically excited systems, present multiple vibration frequencies. Along the flip lobes, the basic frequency of the vibrations is equal to half of tooth-passing frequency. Along the Hopf lobes, quasiperiodic vibrations arise. It should be mentioned that flip instability is directly related to the time-periodic nature of the milling process. It occurs mostly for operations with small radial immersion when the directional factor $G(t)$ is strongly time-dependent.

Note that the frequency diagrams in Fig. 13 do not distinguish the dominant vibration frequencies. Generally, only one or two of these frequencies characterize the

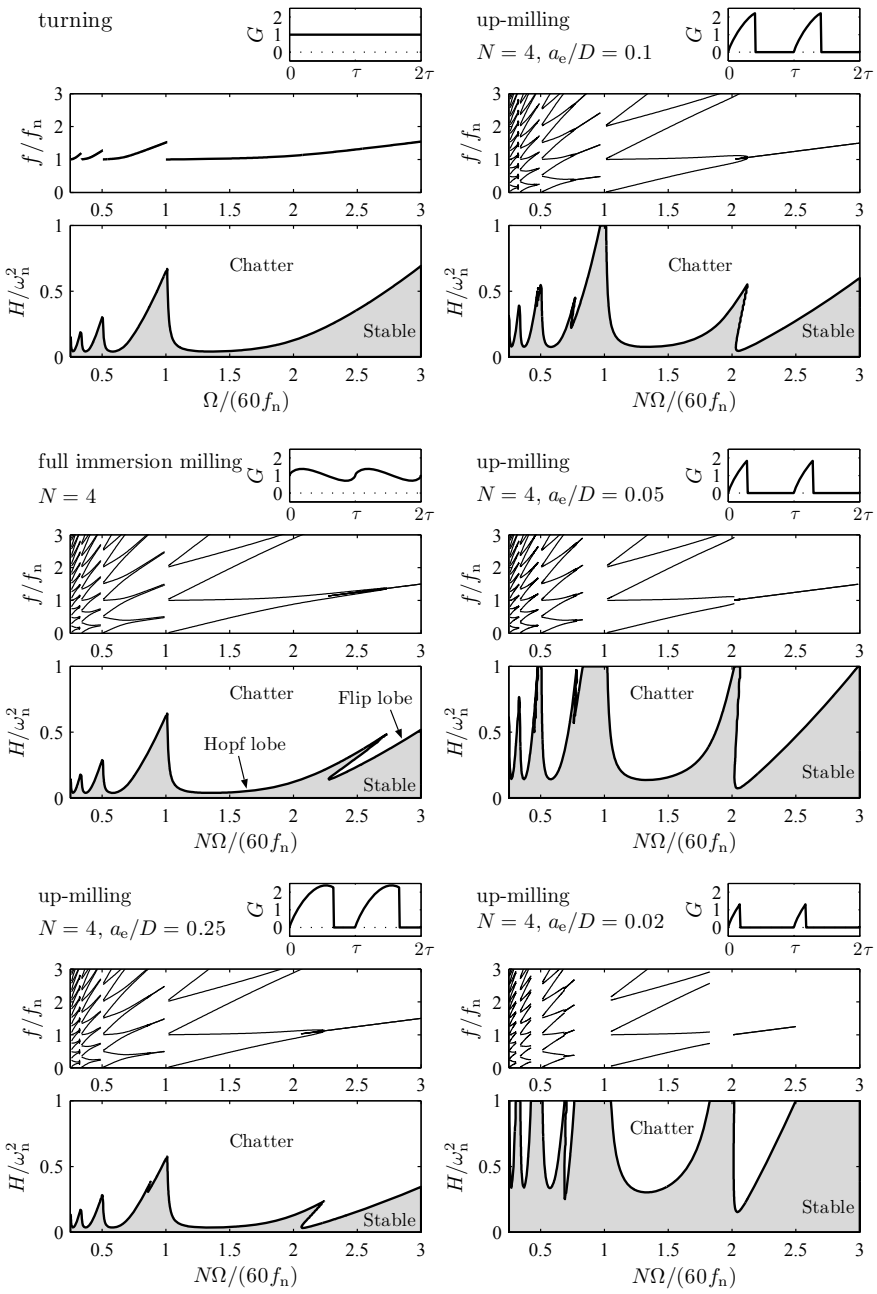

Fig. 13 Stability charts and frequency diagrams with the corresponding directional factor $G(t)$ for turning and different milling operations

chatter signal, and the other harmonics are associated with negligible amplitudes. For more details on the dominant chatter frequencies, see Dombovari et al. (2011).

Figure 14 shows a series of stability charts for different radial immersion ratios a_e/D for a 2-fluted end mill cutter. The damping ratio is $\zeta = 0.02$, the cutting-force ratio is $K_r/K_t = 0.3$, and the cutting-force exponent is $q = 0.75$. The plots give a transition of the stability charts between up-milling and down-milling. For up-milling operations, the Hopf lobes are located to the left of the flip lobes. As the radial immersion is increased, the flip lobes open and new Hopf stability boundaries appear while the original Hopf lobe shrinks to a loop-like curve (see the full-immersion case). Reducing the radial immersion at the other side of the workpiece leads to the down-milling operations (see Fig. 11). As the radial immersion is decreased, the loop-like lobe disappears, while the new Hopf lobes remain dominant. For down-milling operations, the Hopf lobes are located to the right of the flip lobes.

Figure 14 clearly shows the main differences between up- and down-milling operations with a 2-fluted cutter. As can be seen, the flip lobes are located more or less at the same spindle speed ranges, although they may vary in size for the different cases. This is not true for the Hopf lobes. For low-immersion up-milling operations, the Hopf lobes are located to the left of the flip lobes, while for down-milling, the Hopf lobes are positioned to the right of the flip lobes. The physical explanation for this special duality is the following. The flip lobes are related to the impact effects of the cutting teeth as they enter and leave the cut. These are more or less independent of the sense (up or down) of the operation. This is not the case for the Hopf lobes. As was shown in Fig. 4, the conventional stability chart of turning operations contains a part for negative depths of cut, which has no physical meaning there. In the case of milling, the cutting force is multiplied by the directional factor $G(t)$, which is mostly positive for up-milling and mostly negative for down-milling operations (see Fig. 14). The new Hopf lobes that emerge as the operation turns from up-milling to down-milling are related to the lobes in the negative depth of cut values in Fig. 4, which are dual to those in the positive region. This is the explanation for the duality in the stability properties of up- and down-milling.

In addition to the intricate transition between the up- and down-milling cases, the stability chart of (25) shows another interesting feature: the flip stability boundaries are not always open lobes, but for certain parameter combinations, they are closed curves forming unstable islands in the stability charts (Szalai and Stépán, 2006). Figure 15 shows the stability charts for an up-milling operation with radial immersion $a_e/D = 0.02$ by a 4-fluted tool for different damping-ratio parameters. It can be seen that as the damping ratio gets larger, the stability domains grow and the second flip lobe at spindle speed $N\Omega/(60 f_n) \approx 0.7$ closes and forms an unstable island within the stable domain. These unstable islands appear as a result of the parametric forcing of the milling process, and are therefore referred to as *parametrically induced flip islands*.

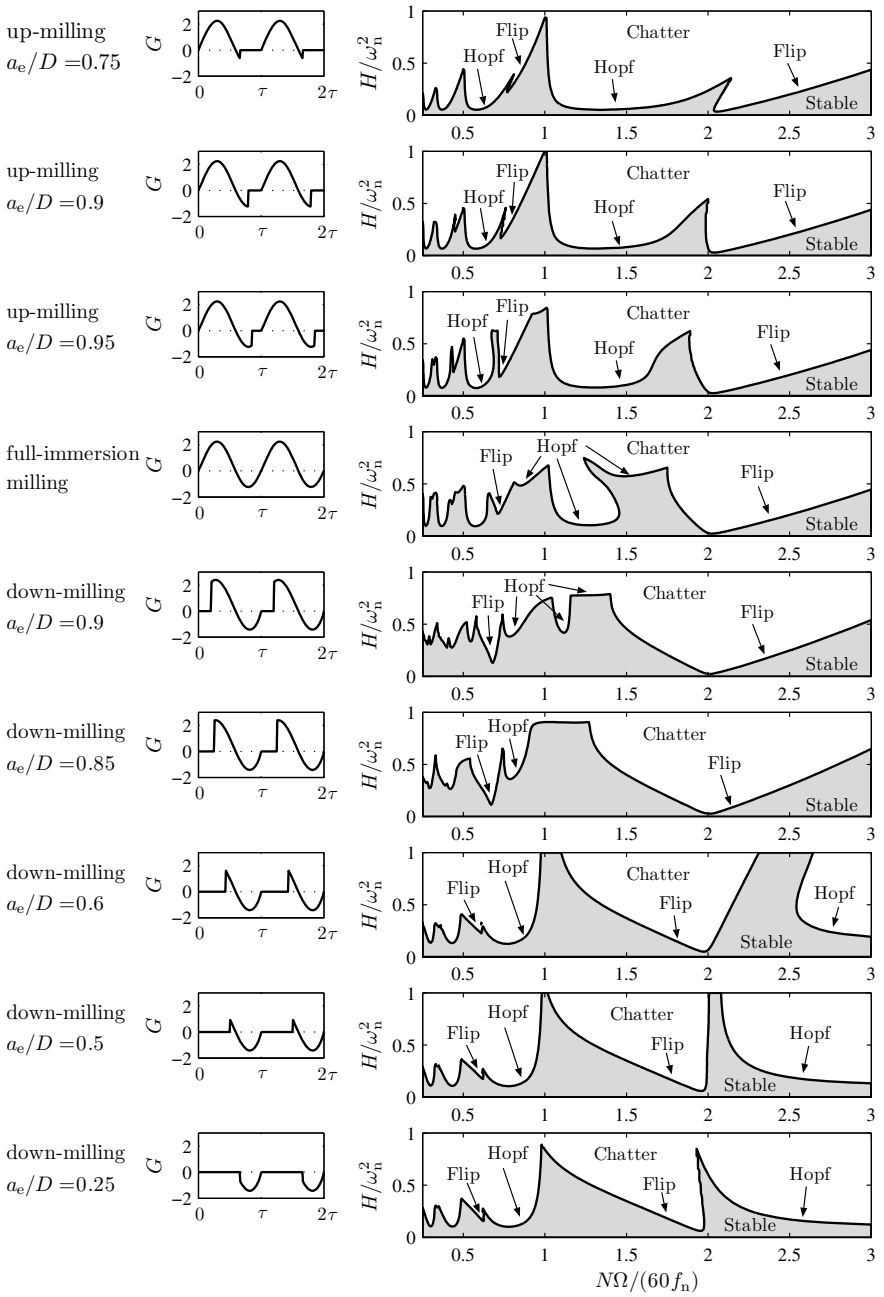

Fig. 14 Stability charts and the corresponding directional factor $G(t)$ for milling operations with different radial immersions for a 2-fluted tool ($N = 2$)

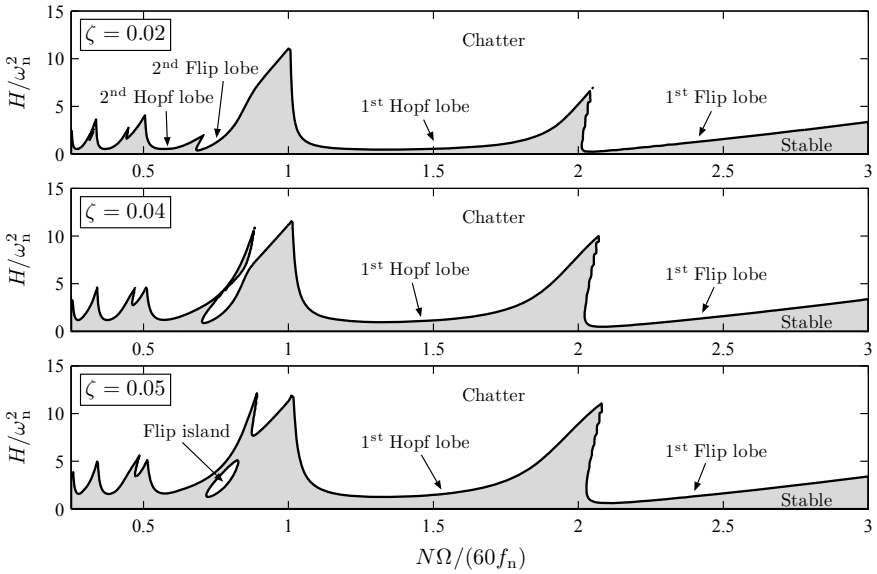

Fig. 15 Stability charts for an up-milling operation with radial immersion $a_e/D = 0.02$ by a straight fluted tool with four cutting teeth for different damping ratio parameters ζ. The cutting-force exponent is $q = 1$

3.5 Milling with Helical Tools

In the case of helical tools, the forces acting on the cutting edges change along the axial direction of the tool. In the case of large axial immersion, this effect should also be taken into account.

The single-degree-of-freedom model of end milling shown in Fig. 9 is considered now with a helical tool of uniform helix angle β. The equation of motion of the system is the same as (18), but here, the cutting-force component $F_x(t)$ should be derived in a different way due to the helical cutting edges. For this purpose, the tool is divided into elementary disks along the axial direction, as shown in Fig. 16.

The angle of twist of the cutting edge j at axial immersion z is $\psi(z) = 2z \tan\beta/D$, where D is the diameter of the tool. The relation between the helix angle β and the helix pitch l_p is $\tan\beta = D\pi/(Nl_p)$. Thus, the angular position of the cutting edges along the axial direction reads

$$\varphi_j(t,z) = \frac{2\pi\,\Omega}{60}t + j\,\frac{2\pi}{N} - z\frac{2\pi}{Nl_p}\,.$$

The elementary cutting-force components acting on tooth j at a disk element of width $\mathrm{d}z$ are

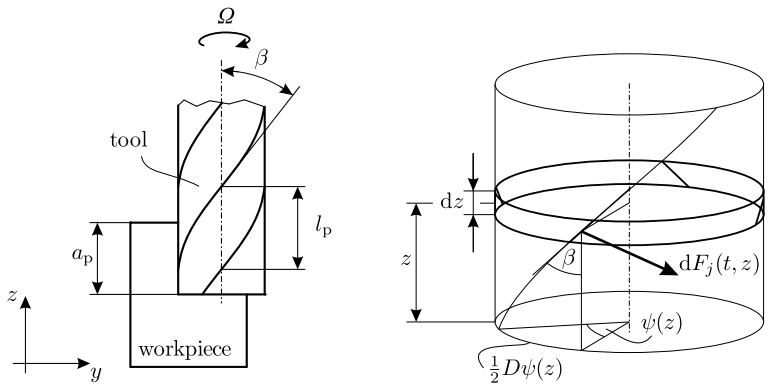

Fig. 16 Geometry of a helical tool and its division into elementary disks along the axial z direction

$$\mathrm{d}F_{j,\mathrm{t}}(t,z) = g_j(t,z)K_\mathrm{t}h^q(t,z)\mathrm{d}z \ ,$$
$$\mathrm{d}F_{j,\mathrm{r}}(t,z) = g_j(t,z)K_\mathrm{r}h^q(t,z)\mathrm{d}z \ ,$$

where K_t and K_r are the cutting-force parameters in the tangential and radial directions, respectively, $h_j(t,z)$ is the chip thickness cut by tooth j at axial immersion z, and q is the cutting-force exponent. Function $g_j(t,z)$ reads

$$g_j(t,z) = \begin{cases} 1 & \text{if } \varphi_\mathrm{en} < (\varphi_j(t,z) \bmod 2\pi) < \varphi_\mathrm{ex} \ , \\ 0 & \text{otherwise} \ , \end{cases}$$

where φ_en and φ_ex are the entrance and exit immersion angles. The instantaneous chip thickness at axial immersion z can be given as

$$h_j(t,z) = (f_\mathrm{z} + x(t) - x(t-\tau))\sin\varphi_j(t,z) \ ,$$

where f_z is the feed per tooth and $\tau = 60/(N\Omega)$ [s] is the tooth-passing period. The x component of the elementary cutting force acting on tooth j reads

$$\mathrm{d}F_{j,x}(t,z) = \mathrm{d}F_{j,\mathrm{t}}(t,z)\cos\varphi_j(t,z) + \mathrm{d}F_{j,\mathrm{r}}(t,z)\sin\varphi_j(t,z) \ ,$$

and the x component of the resultant cutting force acting on the tool is

$$F_x(t) = Q(t)\,(f_\mathrm{z} + (x(t) - x(t-\tau)))^q \ ,$$

where

$$Q(t) = \sum_{j=1}^{N} \left(\int_0^{a_\mathrm{p}} g_j(t,z) \sin^q \varphi_j(t,z) \left(K_\mathrm{t} \cos \varphi_j(t,z) + K_\mathrm{r} \sin \varphi_j(t,z) \right) \mathrm{d}z \right) .$$

The equation of motion is the nonlinear time-periodic DDE

$$m\ddot{x}(t) + c\dot{x}(t) + kx(t) = -Q(t) \left(f_\mathrm{z} + x(t) - x(t-\tau) \right)^q .$$

Linearization about the steady-state periodic solution $x_\mathrm{p}(t) = x_\mathrm{p}(t+\tau)$ gives the variational system in the form

$$\ddot{\xi}(t) + 2\zeta\omega_\mathrm{n}\dot{\xi}(t) + \omega_\mathrm{n}^2 \xi(t) = -G(t, a_\mathrm{p}) \left(\xi(t) - \xi(t-\tau) \right) , \tag{38}$$

where

$$G(t, a_\mathrm{p}) = \sum_{j=1}^{N} \left(\frac{q f_\mathrm{z}^{q-1}}{m} \int_0^{a_\mathrm{p}} g_j(t,z) \sin^q \varphi_j(t,z) \big(K_\mathrm{t} \cos \varphi_j(t,z) + K_\mathrm{r} \sin \varphi_j(t,z) \big) \mathrm{d}z \right)$$

is a particular directional factor that depends on the axial immersion a_p. Equation (38) is written in the first-order form

$$\begin{aligned} \dot{x}(t) &= A(t)x(t) + B(t)u(t-\tau) , \\ u(t) &= Dx(t) , \end{aligned}$$

with

$$x(t) = \begin{pmatrix} \xi(t) \\ \dot{\xi}(t) \end{pmatrix} , \qquad D = \begin{pmatrix} 1 & 0 \end{pmatrix} ,$$

$$A(t) = \begin{pmatrix} 0 & 1 \\ -\left(\omega_\mathrm{n}^2 + G(t, a_\mathrm{p}) \right) & -2\zeta\omega_\mathrm{n} \end{pmatrix} , \qquad B(t) = \begin{pmatrix} 0 \\ G(t, a_\mathrm{p}) \end{pmatrix} .$$

Stability charts can be determined by the semidiscretization method, as shown in Sect. 3.2.

Stability charts are presented in Fig. 17 for up-milling operations with different helix pitches.

A 4-fluted tool is considered ($N = 4$) with diameter $D = 20\,\mathrm{mm}$. The radial immersion is $a_\mathrm{e} = 2\,\mathrm{mm}$; thus, the radial immersion ratio is $a_\mathrm{e}/D = 0.1$. The cutting-force parameters are $K_\mathrm{t} = 107 \times 10^6\,\mathrm{N/m}^{1+q}$ and $K_\mathrm{r} = 40 \times 10^6\,\mathrm{N/m}^{1+q}$; the cutting-force exponent is $q = 0.75$. The feed per tooth is $f_\mathrm{z} = 0.1\,\mathrm{mm}$, for which the linearized cutting-force coefficients are $K_\mathrm{t} q f_\mathrm{z}^{q-1} = 800 \times 10^6\,\mathrm{N/m}^2$ and $K_\mathrm{r} q f_\mathrm{z}^{q-1} = 300 \times 10^6\,\mathrm{N/m}^2$. The stiffness is $k = 20 \times 10^6\,\mathrm{N/m}$, the natural frequency is $f_\mathrm{n} = \omega_\mathrm{n}/2\pi = 400\,\mathrm{Hz}$, and the damping ratio is $\zeta = 0.02$. The first panel

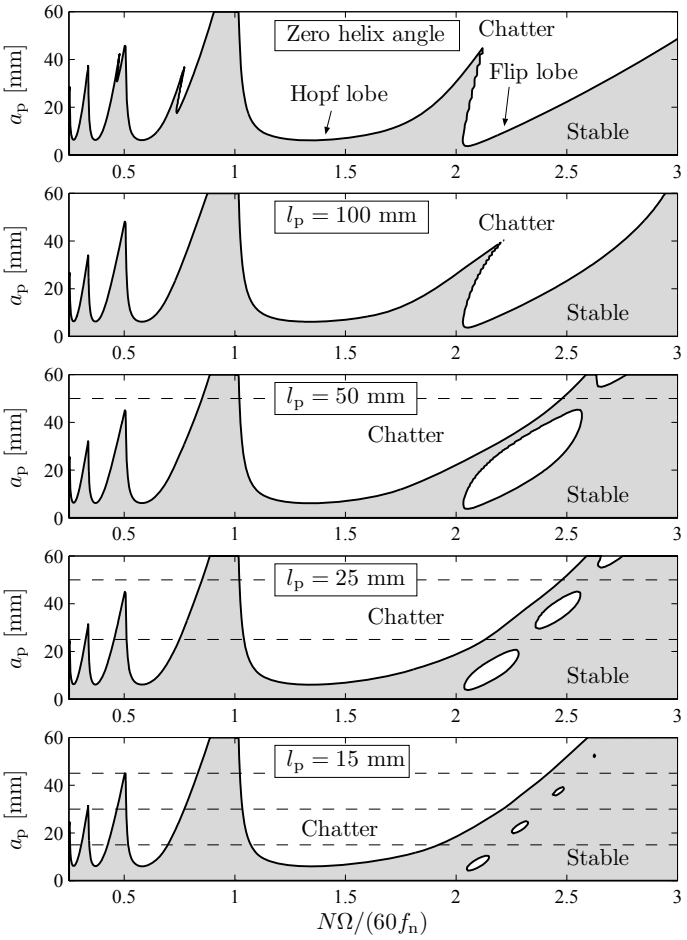

Fig. 17 Stability charts for a straight fluted tool (zero helix angle) and for helical tools with different helix pitches

shows the stability diagram for a straight fluted tool. This diagram corresponds to the case $a_e/D = 0.1$ in Fig. 13. The other panels in Fig. 17 show the stability charts for milling tools with different helix pitches. It can be seen that the flip lobes turn to closed curves forming unstable islands within the stable domain. These islands are separated by the lines where the depth of cut is equal to the multiples of the helix pitch l_p (indicated by dashed lines in Fig. 17).

The analysis of the particular directional factor $G(t, a_p)$ gives a clear explanation for the existence of these unstable islands. If the axial depth of cut is equal to a multiple of the helix pitch, that is, $a_p = jl_p$ with j being a positive integer, then $G(t, a_p)$ becomes constant in time, since the variation of the cutting forces distributed along the helical edges are balanced along the helix pitch l_p. Figure 18 shows the unstable

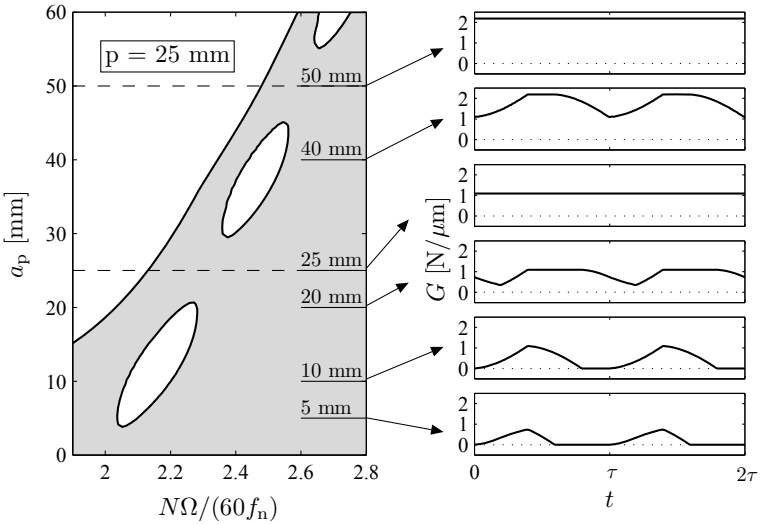

Fig. 18 Stability chart for a helical tool with $l_p = 25\,\text{mm}$ and the particular directional factor $G(t, a_p)$ for certain axial depths of cut a_p

islands for $l_p = 25\,\text{mm}$ and the plots of the particular directional factor $G(t, a_p)$ for different depths of cut a_p. For $a_p = l_p$ and $a_p = 2l_p$, $G(t, a_p)$ is constant in time. Consequently, at these parameters, the system is described by an autonomous DDE. Therefore, the only possible way for loss of stability is the Hopf bifurcation. If flip stability boundaries exist for other axial depths of cut (when $a_p \neq jl_p$, $j = 1, 2, \ldots$) then they should form bounded islands between the lines $a_p = jl_p$.

Note that these flip islands are different from the parametrically induced ones shown in Fig. 15. While the parametrically induced islands are related to the periodic nature of the machining process, the islands in Figs. 17 and 18 are related to the helical edges of the tool, and are therefore referred to as *helix-induced flip islands*.

4 Final Comments

In this chapter only some basic models were presented, which highlight the effect of the regenerative delay on the dynamic behavior of machining processes. There exist more sophisticated models in terms of the tooth path approximation (Faassen et al., 2007; Bachrathy et al, 2011; Totis et al., 2019), the cutting edge geometry (Sims et al., 2008; Dombovari and Stépán, 2012; Stépán et al., 2014; Kilic and Altintas, 2016) or the cutting force distribution on the cutting edge (Molnar et al., 2016, 2017). Models involving multiple delays and time- and state-dependent delays are discussed in Wan et al. (2011), Totis et al. (2019) and in Insperger et al. (2007), Bachrathy et al (2011), Molnar et al. (2016), respectively. For a general and detailed overview on

machine tool chatter and vibration suppression techniques, see Altintas and Weck (2004); Munoa et al. (2016).

There is a huge literature for the numerical stability analysis of milling operations, i.e., time-periodic delayed systems. The higher order semidiscretization method (Insperger et al., 2008; Insperger and Stépán, 2011), the multi frequency solution (Altintas and Budak, 1995; Budak and Altintas, 1998; Merdol and Altintas, 2004; Altintas et al., 2008; Bachrathy and Stépán, 2013), the Chebyshev collocation method (Butcher et al., 2004; Totis et al., 2014), the spectral element method (Khasawneh and Mann, 2011; Lehotzky et al., 2016, 2017) or the pseudospectral tau approximation (Lehotzky and Insperger, 2016) can be mentioned as examples. For some special models, analytical approaches can also be used, see e.g., the method in (Sims et al., 2008; Sims, 2016) for variable pitch cutters. Several methods have also been developed to robust stability analysis of machine tool chatter, which account for the uncertainties in the model parameters (Totis, 2009; Hajdu et al., 2017, 2020).

References

Altintas, Y. (2012). *Manufacturing automation: Metal cutting mechanics, machine tool vibrations, and CNC design* (2nd ed.). Cambridge University Press.

Altintas, Y., & Budak, E. (1995). Analytical prediction of stability lobes in milling. *CIRP Annals, 44,* 357–362.

Altintas, Y., & Weck, M. (2004). Chatter stability of metal cutting and grinding. *CIRP Annals-Manufacturing Technology, 3*(2), 619–642.

Altintas, Y., Stépán, G., Merdol, D., & Dombovari, Z. (2008). Chatter stability of milling in frequency and discrete time domain. *CIRP Journal of Manufacturing Science and Technology, 1,* 35–44.

Bachrathy, D., & Stépán, G. (2013). Improved prediction of stability lobes with extended multi frequency solution. *CIRP Annals-Manufacturing Technology, 62*(1), 411–414.

Bachrathy, D., Stépán, G., & Turi, J. (2011). State dependent regenerative effect in milling processes. *The Journal of Computational and Nonlinear Dynamics, 6*(4), 041002.

Breda, D. (2023). Pseudospectral methods for the stability analysis of delay equations. Part II: The solution operator approach: Methods and applications. In D. Breda (Ed.), *Controlling Delayed Dynamics: Advances in Theory, Methods and Applications, CISM Lecture Notes* (pp. 95–116). Wien-New York: Springer.

Budak, E., & Altintas, Y. (1998). Analytical prediction of chatter stability in milling—Part I: General formulation. *The Journal of Dynamic Systems, Measurement, and Control, 120,* 22–30.

Butcher, E. A., Ma, H., Bueler, E., Averina, V., & Szabo, Z. (2004). Stability of linear time-periodic delay-differential equations via Chebyshev polynomials. *International Journal for Numerical Methods in Engineering, 59*(7), 895–922.

Dombovari, Z., & Stépán, G. (2012). The effect of helix angle variation on milling stability. *The Journal of Manufacturing Science and Engineering,134*(5), 051015.

Dombovari, Z., Iglesias, A., Zatarain, M., & Insperger, T. (2011). Prediction of multiple dominant chatter frequencies in milling processes. *International Journal of Machine Tools and Manufacture, 51,* 457–464.

Faassen, R. P. H., van de Wouw, N., Nijmeijer, H., & Oosterling, J. A. J. (2007). An improved tool path model including periodic delay for chatter prediction in milling. *The Journal of Computational and Nonlinear Dynamics*, *2*(2), 167–179.

Hajdu, D., Insperger, T., & Stépán, G. (2017). Robust stability analysis of machining operations. *International Journal of Advanced Manufacturing Technology, 88*(1), 45–54.

Hajdu, D., Borgioli, F., Insperger, T., Stépán, G., & Michiels, W. (2020). Robust stability of milling operations based on pseudospectral approach. *International Journal of Machine Tools and Manufacture, 149*, 103516.

Hartung, F., Insperger, T., Stépán, G., & Turi, J. (2006). Approximate stability charts for milling processes using semi-discretization. *Applied Mathematics and Computation, 174,* 51–73.

Insperger, T., & Stépán, G. (2002). Semi-discretization method for delayed systems. *International Journal for Numerical Methods in Engineering, 55,* 503–518.

Insperger, T., & Stépán, G. (2004). Vibration frequencies in high-speed milling processes or a positive answer to Davies, Pratt, Dutterer and Burns. *Journal of Manufacturing Science and Engineering, 126*(3), 481–487.

Insperger, T., & Stépán, G. (2011). *Semi-discretization for time-delay systems*. Springer.

Insperger, T., Mann, B. P., Stépán, G., & Bayly, P. V. (2003). Stability of up-milling and down-milling, Part 1: Alternative analytical methods. *International Journal of Machine Tools and Manufacture, 43*(1), 25–34.

Insperger, T., Stépán, G., Bayly, P. V., & Mann, B. P. (2003). Multiple chatter frequencies in milling processes. *Journal of Sound and Vibration, 262*(2), 333–345.

Insperger, T., Stépán, G., & Turi, J. (2007). State-dependent delay in regenerative turning processes. *Nonlinear Dynamics, 47*(1–3), 275–283.

Insperger, T., Stépán, G., & Turi, J. (2008). On the higher-order semi-discretizations for periodic delayed systems. *Journal of Sound and Vibration, 313,* 334–341.

Khasawneh, F. A., & Mann, B. P. (2011). A spectral element approach for the stability of delay systems. *International Journal for Numerical Methods in Engineering, 87,* 566–592.

Kilic, Z. M., & Altintas, Y. (2016). Generalized mechanics and dynamics of metal cutting operations for unified simulations. *International Journal of Machine Tools and Manufacture, 104,* 1–13.

Lehotzky, D., & Insperger, T. (2016). A pseudospectral tau approximation for time delay systems and its comparison with other weighted-residual-type methods. *International Journal for Numerical Methods in Engineering, 108,* 588–613.

Lehotzky, D., Insperger, T., & Stépán, G. (2016). Extension of the spectral element method for stability analysis of time-periodic delay-differential equations with multiple and distributed delays. *Communications in Nonlinear Science and Numerical Simulation, 35,* 177–189.

Lehotzky, D., Insperger, T., Khasawneh, F., & Stépán, G. (2017). Spectral element method for stability analysis of milling processes with discontinuous time-periodicity. *International Journal of Advanced Manufacturing Technology, 89*(9), 2503–2514.

Mann, B. P., Insperger, T., Bayly, P. V., & Stépán, G. (2003). Stability of up-milling and down-milling, part 2: Experimental verification. *International Journal of Machine Tools and Manufacture, 43*(1), 35–40.

Merdol, S. D., & Altintas, Y. (2004). Multi frequency solution of chatter stability for low immersion milling. *Journal of Manufacturing Science and Engineering, 126*(3), 459–466.

Molnar, T. G., Insperger, T., & Stépán, G. (2016). State-dependent distributed-delay model of orthogonal cutting. *Nonlinear Dynamics, 84,* 1147–1156.

Molnar, T. G., Insperger, T., Bachrathy, D., & Stépán, G. (2017). Extension of process damping to milling with low radial immersion. *International Journal of Advanced Manufacturing Technology, 89*(9), 2545–2556.

Munoa, J., Beudaert, X., Dombovari, Z., Altintas, Y., Budak, E., Brecher, C., & Stépán, G. (2016). Chatter suppression techniques in metal cutting. *CIRP Annals-Manufacturing Technology, 65*(2), 785–808.

Sims, N. D. (2016). Fast chatter stability prediction for variable helix milling tools. *Proceedings of the Institution of Mechanical Engineers, Part C, 230*(1), 133–144.

Sims, N. D., Mann, B., & Huyanan, S. (2008). Analytical prediction of chatter stability for variable pitch and variable helix milling tools. *Journal of Sound and Vibration, 317*(3–5), 664–686.

Stépán, G. (1989). *Retarded dynamical systems*. Longman.

Stépán, G., Munoa, J., Insperger, T., Surico, M., Bachrathy, D., & Dombovari, Z. (2014). Cylindrical milling tools: Comparative real case study for process stability. *CIRP Annals-Manufacturing Technology, 63*(1), 385–388.

Szalai, R., & Stépán, G. (2006). Lobes and lenses in the stability chart of interrupted turning. *Journal of Computational and Nonlinear Dynamics, 1,* 205–211.

Taylor, F. W. (1907). On the art of cutting metals. *Transactions of the American Society of Mechanical Engineers, 28,* 31–350.

Tlusty, J., Polacek, A., Danek, C., & Spacek, J. (1962). *Selbsterregte Schwingungen an Werkzeugmaschinen*. VEB Verlag Technik.

Tobias, S. A. (1965). *Machine tool vibration*. Blackie.

Tobias, S. A., & Fishwick, W. (1958). Theory of regenerative machine tool chatter. *The Engineer, 199–203,* 238–239.

Totis, G. (2009). RCPM—A new method for robust chatter prediction in milling. *International Journal of Machine Tools and Manufacture, 49,* 273–284.

Totis, G., Albertelli, P., Sortino, M., & Monno, M. (2014). Efficient evaluation of process stability in milling with spindle speed variation by using the Chebyshev collocation method. *Journal of Sound and Vibration, 333,* 646–668.

Totis, G., Insperger, T., Sortino, M., & Stépán, G. (2019). Symmetry breaking in milling dynamic. *International Journal of Machine Tools and Manufacture, 139,* 37–59.

Wan, M., Wang, Y. T., Zhang, W. H., Yang, Y., & Dang, J. W. (2011). Prediction of chatter stability for multiple-delay milling system under different cutting force models. *International Journal of Machine Tools and Manufacture, 51*(4), 281–295.

Dynamics of Human Balancing

Tamás Insperger, Gabor Stépán and John Milton

Abstract Mechanical models of two human balancing tasks, quiet standing and stick balancing on the fingertip, are discussed with special attention to the reaction time delay. As in many control systems, time delay sets limitation to performance during balancing tasks. Human subjects cannot balance an arbitrarily short stick on the fingertip, because a short stick falls faster than the time needed to make a corrective motion. Also, increased reaction time delay is one of the main reasons of instability during quiet standing, which can lead to falls especially among the elderly. The governing equation of the two models are second-order delay differential equations. In this chapter, stabilizability issues are discussed in terms of the critical delay for different feedback concepts, such as proportional-derivative, proportional-derivative-acceleration and predictor feedback.

1 Introduction

Human balancing has several implications to people's everyday activities. Falling due to loss of balance is one of the most important and, at the same time, one of the most challenging problems related to human balance. Indeed, in the aging society, falls are a leading cause of accidental death and morbidity in the elderly. From the mechanical point of view, postural sway during standing, maintaining balance

The research reported in this paper and carried out at BME has been supported by the NRDI Fund (TKP2020 IES, Grant No. BME-IE-BIO and TKP2020 NC,Grant No. BME-NC) based on the charter of bolster issued by the NRDI Office under the auspices of the Ministry for Innovation and Technology (IT,SG), by the William R Kenan, Jr Charitable trust (JM) and by the Hungarian-Chinese Bilateral Scientific and Technological Cooperation Fund under Grant No. 2018-2.1.14-TET-CN-2018-00008 (IT,SG).

T. Insperger (✉) · G. Stépán
Department of Applied Mechanics, Budapest University of Technology and Economics, Budapest, Hungary
e-mail: insperger@mm.bme.hu

J. Milton
W. M. Keck Science Department, The Claremont Colleges Claremont, Claremont, CA, USA

D. Breda (ed.), *Controlling Delayed Dynamics*, CISM International Centre for Mechanical Sciences 604, https://doi.org/10.1007/978-3-031-01129-0_11

during walking or running and balancing an object on the fingertip are all similar processes in the sense that they all require stabilization of an object around an unstable equilibrium or unstable periodic motion in the gravitational field. According to the Newtonian dynamics, the stabilization process is described by second-order differential equations. An important feature of balancing tasks is the reaction time delay: the time duration between perception and action. In this chapter, we present some basic models and concepts of balancing an object around an unstable equilibrium in the presence of reaction time delay. Two balancing models are investigated: postural sway during quiet standing and stick balancing on the fingertip. Postural sway can be modeled by a pinned inverted pendulum to describe the angular oscillation of the human body in the anterior-posterior plane around the ankle joint. Stick balancing on the fingertip is associated with the pendulum-cart model.

2 Mechanical Models

Balancing tasks can be described by a set of second-order Delay Differential Equations (DDEs). One-degree-of-freedom tasks, such as ball and beam balancing (Buza et al., 2020), stick balancing (Mehta and Schaal, 2002; Insperger and Milton, 2014), quiet standing with ankle strategy (Maurer and Peterka, 2005; Asai et al., 2009) can be described by a single second-order DDE. Two-degree-of-freedom tasks, such as balancing on a balance board (Chagdes et al., 2013; Cruise et al., 2017; Molnar et al., 2017; Chumacero-Polanco and Yang, 2019) or quiet standing with ankle-hip strategy (Suzuki et al., 2012; Morasso et al., 2019) can be described by a set of two second-order DDEs. Here, we illustrate the mathematical analysis by focusing on the simplest models of quiet standing and stick balancing.

2.1 Human Postural Sway: The Pinned Inverted Pendulum Model

Postural sway refers to the movements made by the human body to maintain balance during quiet standing. It is typically monitored by having a subject stand quietly with eyes closed on a force platform. In a quiet room with eyes closed the fluctuations in the center of pressure (COP) are about 0.5 cm. This suggests that the postural sway oscillations are in the order of 0.5 deg for healthy individuals with no history of falling.

Balance is maintained by applying a torque at the ankle joint. The COP is the weighted average of all of the downward forces acting on the force platform through the soles of the feet. It depends primarily on stance width and the motor control of the position of the ankle. Postural sway results from changes in the relative positions of the COP and the center of mass (COM) during quiet standing (Winter, 2005).

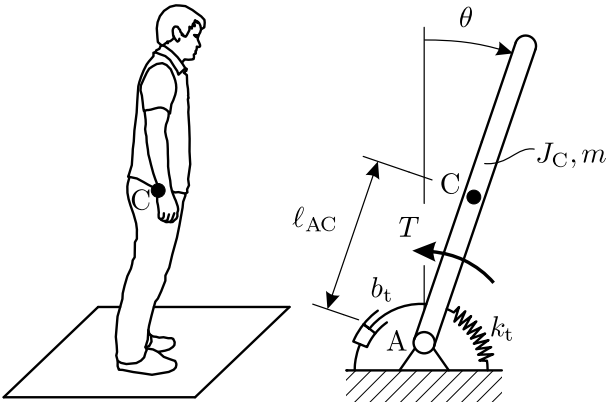

Fig. 1 Pinned pendulum model of postural sway

For example, in 1 dimension, as the COP moves to the right of the COM, the COM moves left, and vice versa. The biomechanical condition for stable quiet standing is that the COM must be located within the base of support defined by the area under and between the feet.

Figure 1 shows a pinned inverted pendulum model of quiet standing in the anterior-posterior direction. The human body is modeled as a rod of mass m pivoted on a joint A. The distance between the center of gravity C and the suspension point A is denoted by ℓ_{AC}. The equation of motion around the upright unstable equilibrium can be written in the form

$$J_A\ddot{\theta}(t) + b_t\dot{\theta} + (k_t - mg\ell_{AC})\theta(t) = -T(t)\ , \tag{1}$$

where $J_A = J_C + m\ell_{AC}^2$ is the moment of inertia of the body with respect to the normal line via the pivot point A and J_C is the moment of inertia with respect to the normal line via the center of gravity and T is the active torque exerted at the ankle.

The passive resistance of the ankle joint against falling is modeled by a torsional spring of stiffness k_t and a torsional dashpot of damping b_t (Winter et al., 1998). These elements are attributed to the foot, Achilles' tendon and aponeurosis and they cannot be neurally regulated during quiet standing. As shown by Loram and Lakie (2002), the stiffness increases slightly with ankle torque, which verifies the linear spring model. They also showed that the intrinsic mechanical stiffness of the ankle is insufficient for stability during quiet standing, and additional modulation of parallel connected calf muscle fibers is required to maintain balance. Consequently the system without the control torque $T(t)$ is unstable, since the intrinsic mechanical stiffness of the ankle alone cannot maintain stability, i.e., $k_t - mg\ell_{AC} < 0$.

Equation (1) can be written as

$$\ddot{\theta}(t) + b\dot{\theta}(t) + a\theta(t) = -f(t)\ , \tag{2}$$

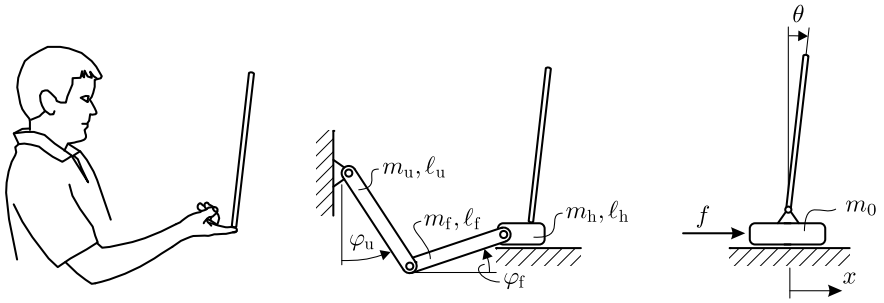

Fig. 2 Pendulum-cart model of stick balancing on the fingertip. Parameters from de Leva (1996): upper arm: $m_\mathrm{u} = 1.775\mathrm{kg}$, $\ell_\mathrm{u} = 0.2874\mathrm{m}$; forearm: $m_\mathrm{f} = 1.015\mathrm{kg}$, $\ell_\mathrm{f} = 0.2666\mathrm{m}$; hand: $m_\mathrm{h} = 0.395\mathrm{kg}$, $\ell_\mathrm{h} = 0.0821\mathrm{m}$

where

$$b = \frac{b_\mathrm{t}}{J_\mathrm{A}}\,, \quad a = \frac{k_\mathrm{t} - mg\ell_\mathrm{AC}}{J_\mathrm{A}} < 0\,, \quad f(t) = \frac{T(t)}{J_\mathrm{A}}.$$

Parameter a is referred as system parameter hereafter.

2.2 Stick Balancing: The Pendulum-Cart Model

Stick balancing at the fingertip has been investigated for over 70 years as a paradigm to explore the neural control of balance and skill acquisition (Cabrera and Milton, 2002, 2004a; Gawthrop et al., 2013; Lee et al., 2012; Milton et al., 2009, 2016; Stépán, 2009). The study of stick balancing offers a number of advantages for both the experimentalist and the modeller: (1) the movements in three dimensions can be measured with high precision using 3-D motion analysis techniques (Cabrera and Milton, 2002, 2004a); (2) the difficulty of the task can be readily manipulated by changing the length of the stick (Cabrera and Milton, 2004b; Milton et al., 2016); (3) skill level can be significantly increased with just a few days of practice (Cabrera and Milton, 2004b, 2012); and (4) virtual stick balancing tasks that involve the interaction between a human and a computer provide a way to manipulate important parameters (Cabrera et al., 2004; Kovacs et al., 2019; Mehta and Schaal, 2002; Milton et al., 2013; Patzelt et al., 2007).

A model for stick balancing at the fingertip in the AP direction is shown in Fig. 2. Since during stick balancing the position of the fingertip is continually moving the mechanical model takes the form of a pendulum-cart system. This is now a two-degree-of-freedom system, where θ is the angular position of the stick and x is the position of the cart (fingertip).

A pendulum-cart model for stick balancing at the fingertip around the upright unstable position of the stick takes the form

$$\begin{pmatrix} \frac{1}{3}m\ell^2 & \frac{1}{2}m\ell \\ \frac{1}{2}m\ell & m+m_0 \end{pmatrix}\begin{pmatrix} \ddot{\theta} \\ \ddot{x} \end{pmatrix} + \begin{pmatrix} -\frac{1}{2}mg\ell & 0 \\ 0 & 0 \end{pmatrix}\begin{pmatrix} \theta \\ x \end{pmatrix} = \begin{pmatrix} 0 \\ F(t) \end{pmatrix},$$

where m, m_0 are, respectively, the mass of the stick and cart, $\ddot{x}$ is the acceleration of the cart (fingertip) and $F(t)$ describes the neural control force. If $F(t)$ does not depend on x and on $\dot{x}$, then the term $\ddot{x}$ can be eliminated from the equation and the balancing process can be reduced to a one-degree-of-freedom model given by

$$\left(\frac{1}{3}m\ell^2 - \frac{m^2\ell^2}{4(m+m_0)}\right)\ddot{\theta} - \frac{1}{2}mg\ell\,\theta = -\frac{m\ell}{2(m+m_0)}F(t).$$

This equation can be written in the the simple form

$$\ddot{\theta}(t) + a\theta(t) = -f(t), \tag{3}$$

where

$$a = -\frac{6g}{\mu\ell}\,, \quad f(t) = \frac{6}{\mu(m+m_0)\ell}\,F(t)$$

and

$$\mu = \frac{4-3m}{(m+m_0)}.$$

Here, the parameter μ is equal to 1 when $m_0 = 0$ and $\mu \approx 4$ when $m_0 \gg m$. Note that the system parameter a is related to the time constant of the system since

$$T_\mathrm{p} = \frac{2\pi}{\sqrt{-a}} \tag{4}$$

is the period of the small amplitude oscillations of a pendulum-cart system in the hung down position.

The dynamics of the pendulum-cart system is strongly affected by the value of μ, i.e., by the relation between the mass m_0 of the cart and the mass m of the stick. In order to estimate m_0, the human arm is modeled as a slider crank mechanism shown in Fig. 2. The parameters of the mechanism are set according to the average human arm segment as listed in the figure legend. The equivalence of the slider crank mechanism and the pendulum-cart model can be established based on the equivalence of their kinetic energy (Insperger and Milton, 2017; Nagy et al., 2020). For a typical posture of the balancing arm ($\varphi_\mathrm{u} \approx 20^\circ$ and $\varphi_\mathrm{f} \approx 10^\circ$) with the given parameters, one get $m_0 = 2.5$ kg. The mass of the stick (in case of wooden stick that is mostly used in stick balancing experiments) is significantly smaller than m_0, hence $\mu = 4$ can be set for practical calculations. This gives

$$a = -\frac{3g}{2\ell}\,, \quad f(t) = \frac{6}{4(m+m_0)\ell}\,F(t)\,,$$

which actually corresponds to the parameters of a pinned inverted pendulum (Insperger and Milton, 2017).

2.3 Unifying the Two Models

One should notice that (3) is actually equivalent to (2) with $b = 0$. Hence in the following we will analyze (2) as a general governing equation for one-degree-of-freedom balancing tasks.

3 Time-Delayed Feedback Control

The type of feedback depends on the available sensory information provided by the biological sensors that detect the magnitude and time-dependent changes in the controlled variable. Here, three types of feedback are to be investigated. All of them uses different combination of the perceived angular position, velocity and acceleration and the efferent copies of the actual control commands.

3.1 Proportional-Derivative (PD) Feedback

Here the feedback depends on two state variables, the position θ and its derivative $\dot{\theta}$ measured at time $t - \tau$. The control effort in this case takes the form

$$f_{\mathrm{PD}}(t) = k_{\mathrm{p}}\theta(t-\tau) + k_{\mathrm{d}}\dot{\theta}(t-\tau) \tag{5}$$

where k_{p} and k_{d} are, respectively, the proportional and derivative gains and τ is the feedback delay. Equation (2) with (5) is an example of a retarded functional differential equation (RFDE).

Although this type of control scheme seems to be restrictive, it still has a great importance. All nonlinear feedback controllers that can be written in the form $f(t) = h(\theta(t-\tau), \dot{\theta}(t-\tau))$ can be reduced to PD feedback after linearization if the function h is smooth in both of its arguments.

3.2 Proportional-Derivative-Acceleration (PDA) Feedback

In addition to displacement and velocity the feedback may also include a term for corrective contributions related to acceleration. The corresponding control action takes the form

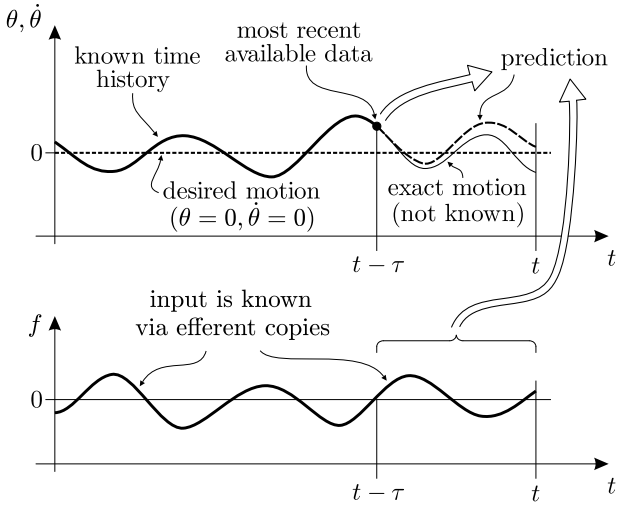

Fig. 3 Schematic representation of predictor feedback. Note that this control concept requires the knowledge of the input f over the interval $[t - \tau, t]$. In the human neural system, this is provided by the efferent copies of the actual control commands

$$f_{\mathrm{PDA}}(t) = k_{\mathrm{p}}\theta(t - \tau) + k_{\mathrm{d}}\dot{\theta}(t - \tau) + k_{\mathrm{a}}\ddot{\theta}(t - \tau) \tag{6}$$

where k_{a} is the acceleration gain. Equations (2) with (6) is an example of a neutral functional differential equation (NFDE) since the delay appears in the argument with the highest derivative. In contrast to a RFDE, the characteristic equation for a NFDE can have infinitely many roots with positive real parts. A necessary condition for stability is that $|k_{\mathrm{a}}| < 1$ (Kolmanovskii and Nosov, 1986; Stépán, 1989).

3.3 Predictor Feedback (PF)

Predictor feedback (Krstic, 2009) corresponds to an internal, or forward, model in the neuroscience literature (Kawato, 1999; Mehta and Schaal, 2002). It is often associated with finite spectrum assignment or delay compensation in the engineering control literature (Krstic, 2009; Michiels and Niculescu, 2007) and prediction using an internal model in the neuroscience literature (Kawato, 1999; Mehta and Schaal, 2002; Shadmehr et al., 2010). The optimum prediction for a system with input delay is obtained when the system equations are solved over the delay period (Kleinman, 1969; Mannitius and Olbrot, 1979).

Predictor feedback controllers suggest that rather than feeding back the delayed state, one should predict the actual state using the most recent available information on the state and the available control force history as demonstrated in Fig. 3. The corresponding control action has the form

$$f_{\mathrm{PF}}(t) = \int_0^t \eta(\theta(s-\tau_\theta), \dot{\theta}(s-\tau_\theta), f_{\mathrm{PF}}(s-\tau_f))\mathrm{d}s,$$

where η is a measurable function and τ_θ, τ_f are, respectively, the delays involved in obtaining the angle θ and feedback information f. We assume that $\tau_\theta = \tau$ and the feedback information is readily provided by the efferent copies, thus $\tau_f = 0$. The function η can be determined by the prediction given by the solution of (2). In order to describe predictor feedback, it is most convenient to write (2) in the first-order form

$$\dot{z}(t) = Az(t) + Bf_{\mathrm{PF}}(t), \tag{7}$$

where

$$z(t) = \begin{pmatrix} \theta(t) \\ \dot{\theta}(t) \end{pmatrix}, \quad A = \begin{pmatrix} 0 & 1 \\ -a & -b \end{pmatrix}, \quad B = \begin{pmatrix} 0 \\ -1 \end{pmatrix}.$$

We assume that the control effort f_{PF} is readily provided for the nervous system by the efferent copies, and matrices A and B and the delay τ are also available for the nervous system via an internal model with high accuracy as a result of a long enough learning process. The state is predicted by the solution of (7) over the interval $[t-\tau, t]$ as

$$z_{\mathrm{pred}}(t) = \mathrm{e}^{\tilde{A}\tilde{\tau}} z(t-\tau) + \int_{t-\tilde{\tau}}^t \mathrm{e}^{\tilde{A}(t-s)} \tilde{B} f_{\mathrm{PF}}(s)\mathrm{d}s\,, \tag{8}$$

where $\tilde{A}$, $\tilde{B}$ and $\tilde{\tau}$ are the estimated values of A, B and τ used by the neural internal model. Note that this prediction uses the most recent available state $z(t-\tau)$ and the control force f_{PF} issued over the interval $[t-\tau, t]$, which is readily provided by the efferent copies of motor command. The predictor feedback effort reads

$$f_{\mathrm{PF}}(t) = Kz_{\mathrm{pred}}(t),$$

with

$$K = \begin{pmatrix} k_{\mathrm{p}} & k_{\mathrm{d}} \end{pmatrix}.$$

Thus, the control action can be written as

$$f_{\mathrm{PF}}(t) = \tilde{k}_{\mathrm{p}}\theta(t-\tau) + \tilde{k}_{\mathrm{d}}\dot{\theta}(t-\tau) + \int_{t-\tilde{\tau}}^t k_{\mathrm{f}}(t-s) f_{\mathrm{PF}}(s)\mathrm{d}s,$$

where $\tilde{k}_{\mathrm{p}}$ and $\tilde{k}_{\mathrm{d}}$ are the elements of $\tilde{K} = K\mathrm{e}^{\tilde{A}\tilde{\tau}}$ and $k_{\mathrm{f}}(t-s) = K\mathrm{e}^{\tilde{A}(t-s)}\tilde{B}$.

If the prediction is perfect, i.e., $\tilde{A} = A$, $\tilde{B} = B$, $\tilde{\tau} = \tau$, the numerical calculations in (8) are performed with perfect accuracy and there are no perturbations then $z_{\mathrm{pred}}(t) = z(t)$ and the system dynamics becomes

$$\dot{z}(t) = Az(t) + BKz(t)\,, \tag{9}$$

which is equivalent to state feedback equation without any delay. Hence, the system becomes an Ordinary Differential Equation (ODE) with finite spectrum. This is why predictor feedback is called finite spectrum assignment or delay compensation in control systems theory (Mannitius and Olbrot, 1979; Krstic, 2009; Michiels and Niculescu, 2007).

3.4 PD and PDA as Predictor Feedback

It shall be mentioned that PD and PDA feedback can also be represented as a predictor feedback. In case of PD feedback, the simple control logic is used that the state does not significantly change over the delay interval, thus $\theta(t) \approx \theta(t-\tau)$ and $\dot{\theta}(t) \approx \dot{\theta}(t-\tau)$. The corresponding control action can be written as

$$\begin{aligned} f_{\mathrm{PD}}(t) &= k_{\mathrm{p}}\theta(t-\tau) + k_{\mathrm{d}}\dot{\theta}(t-\tau) \\ &= k_{\mathrm{p}} \underbrace{\left(\theta(t-\tau) + \tau\dot{\theta}(t-\tau)\right)}_{\approx\theta(t)} + \left(k_{\mathrm{d}} - k_{\mathrm{p}}\tau\right)\dot{\theta}(t-\tau). \end{aligned}$$

This is equivalent to the feedback of a linearly predicted position over the delay τ and the delayed velocity.

In case of PDA feedback, the control action can be written as

$$\begin{aligned} f_{\mathrm{PDA}}(t) &= k_{\mathrm{p}}\theta(t-\tau) + k_{\mathrm{d}}\dot{\theta}(t-\tau) + k_{\mathrm{a}}\ddot{\theta}(t-\tau) \\ &= k_{\mathrm{p}} \underbrace{\left(\theta(t-\tau) + \tau\dot{\theta}(t-\tau)\right)}_{\approx\dot{\theta}(t)} + \left(k_{\mathrm{d}} - k_{\mathrm{p}}\tau\right) \underbrace{\left(\dot{\theta}(t-\tau) + \tau\ddot{\theta}(t-\tau)\right)}_{\approx\dot{\theta}(t)} \\ &\qquad + \left(k_{\mathrm{a}} - k_{\mathrm{d}}\tau + k_{\mathrm{p}}\tau^2\right)\ddot{\theta}(t-\tau). \end{aligned}$$

When $k_{\mathrm{a}} = k_{\mathrm{d}}\tau - k_{\mathrm{p}}\tau^2$ then this is equivalent to the feedback of a linearly predicted position and linearly predicted velocity.

It can easily be seen that if the state is predicted based on its own delayed values only, and the feedback term f is not involved into the prediction, then the predicted state can be written as

$$z_{\mathrm{pred}}(t) = P(\tau)z(t-\tau)\ ,$$

where $P(\tau)$ is a matrix describing the prediction over the delay period. Feedback of the predicted state according to the linear control law $f_{\mathrm{PF}}(t) = K z_{\mathrm{pred}}(t)$ gives

$$\dot{z}(t) = Az(t) + BKP(\tau)z(t-\tau)\ .$$

This is actually equivalent to a direct delayed state feedback with control gain matrix $KP(\tau)$.

4 Stability Analysis

Here, we derive and discuss the stability properties of the inverted pendulum models subject to PD, PDA and predictor feedback in terms of the control gains, the system parameters and the feedback delay.

4.1 PD Feedback

Equations (2) with (5) define the DDE

$$\ddot{\theta}(t) + b\dot{\theta}(t) + a\theta(t) = -k_\mathrm{p}\theta(t-\tau) - k_\mathrm{d}\dot{\theta}(t-\tau)\,. \tag{10}$$

The corresponding characteristic function reads

$$D(\lambda) = \lambda^2 + b\lambda + a + k_\mathrm{p}\mathrm{e}^{-\lambda\tau} + k_\mathrm{d}\lambda\mathrm{e}^{-\lambda\tau}\,.$$

Stability analysis can be performed according to the D-subdivision method (Kolmanovskii and Nosov, 1986; Stépán, 1989). For this, we take $\lambda = \gamma + \mathrm{i}\omega$, $\omega \geq 0$, with i being the imaginary unit and set $D(\lambda) = 0$. Decomposing into real and imaginary parts, we obtain

$$\begin{aligned}\mathrm{Re}:\ & \gamma^2 - \omega^2 + b\gamma + a + k_\mathrm{p}\mathrm{e}^{-\gamma\tau}\cos(\omega\tau) + k_\mathrm{d}\gamma\mathrm{e}^{-\gamma\tau}\cos(\omega\tau) \\ & \qquad + k_\mathrm{d}\omega\mathrm{e}^{-\gamma\tau}\sin(\omega\tau) = 0 \qquad (11)\\ \mathrm{Im}:\ & 2\gamma\omega + b\omega - k_\mathrm{p}\mathrm{e}^{-\gamma\tau}\sin(\omega\tau) + k_\mathrm{d}\omega\mathrm{e}^{-\gamma\tau}\cos(\omega\tau) \\ & \qquad - k_\mathrm{d}\gamma\mathrm{e}^{-\gamma\tau}\sin(\omega\tau) = 0. \qquad (12)\end{aligned}$$

The condition for stability is that $\mathrm{Re}(\lambda) < 0$ for all λ. Thus we take $\gamma = 0$ to obtain the D-curves as

$$\begin{aligned}\text{if } \omega = 0:\quad & k_\mathrm{p} = -a, \qquad k_\mathrm{d} \in \mathbb{R}\,, && (13)\\ \text{if } \omega \neq 0:\quad & k_\mathrm{p} = (\omega^2 - a)\cos(\omega\tau) + b\omega\sin(\omega\tau)\,, && (14)\\ & k_\mathrm{d} = \frac{\omega^2 - a}{\omega}\sin(\omega\tau) - b\cos(\omega\tau)\,. && (15)\end{aligned}$$

Figure 4 shows that the inverted pendulum is stable if k_p and k_d are located within a D-shaped stability region. It should be noted that stabilization is possible only if $k_\mathrm{d} \geq -a\tau > 0$. In other words it is not possible to stabilize the inverted pendulum using only position feedback.

The D-subdivision method can be used to construct stability diagrams for autonomous DDEs. The D-curves separate the parameter space into regions where the number of unstable characteristic exponents (also called the instability degree)

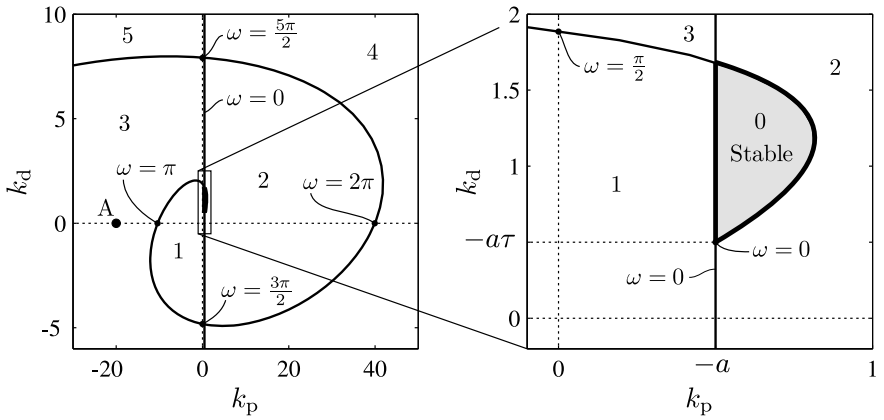

Fig. 4 Stability chart indicating the number of unstable characteristic exponents for (10) with $a = -0.5$, $b = 0$ and $\tau = 1$

are constant. Two methods are used to determine the number of unstable characteristic exponents in the individual parameters regions: (1) the exponent-crossing direction method and (2) the Stepan's formulas (Stépán, 1989).

The exponent crossing direction is the sign of the partial derivative of the real part of the characteristic exponent λ with respect to one of the system's parameters. The D-curves are given by

$$R(\omega) = 0, \quad S(\omega) = 0, \quad \omega \in [0, \infty)\,,$$

where

$$R(\omega) := \mathrm{Re}\; D(\mathrm{i}\omega), \quad S(\omega) := \mathrm{Im}\; D(\mathrm{i}\omega)\,. \tag{16}$$

When a D-curve is crossed in some direction then the number of unstable characteristic exponents changes. If the number of unstable characteristic exponents is known for at least one point in a parameter region, then it can be determined for the other regions by considering the exponent-crossing direction along the D-curves. The stable region is associated with zero unstable exponents. Thus, the stability boundaries are the D-curves that bounds the region with zero unstable characteristic exponents.

In case of (10), the D-curve given by (13) is associated with a real characteristic exponent $\lambda = 0$, $k_\mathrm{p} = -a$, and the D-curve given by (14)–(15) is associated with a complex conjugate pair of characteristic exponents of the form $\lambda = \pm\mathrm{i}\omega$. For fixed a, these curves cut the parameter space $(k_\mathrm{p}, k_\mathrm{d})$ into infinitely many regions as shown in Fig. 4. The exponent-crossing direction along the D-curve $k_\mathrm{p} = -a$ is obtained by taking the partial derivatives of (11) and (12) and substituting $\gamma = 0, \omega = 0, k_\mathrm{p} = -a$ to get

$$\frac{\partial \gamma}{\partial k_\mathrm{p}} = -\frac{1}{a\tau + k_\mathrm{d} - b}.$$

We see that this derivative is positive for $k_\mathrm{d} < b - a\tau$ and negative for $k_\mathrm{d} > b - a\tau$. If the line $k_\mathrm{p} = -a$ is crossed from left to right with $k_\mathrm{d} > b - a\tau$, then a real characteristic exponent becomes stable. If $k_\mathrm{d} < b - a\tau$, then a real exponent becomes unstable as the line $k_\mathrm{p} = -a$ is crossed from left to right. Since the choice $(k_\mathrm{p}, k_\mathrm{d}) = (0, 0)$ corresponds to an ODE with one unstable characteristic exponent, i.e., the fixed point is a saddle, the number of unstable characteristic exponents can be given for all the regions in the parameter plane $(k_\mathrm{p}, k_\mathrm{d})$ by considering the exponent-crossing directions along the D-curve $k_\mathrm{p} = -a$ (see Fig. 4).

Stepan's formulas (Stépán, 1989) provide a direct way to determine the number of unstable characteristic exponents via utilizing Cauchy's argument principle. It is only necessary to use (16) and it is not necessary to know the exponent-crossing direction. This method assumes (1) a system of n first-order, linear DDEs; (2) the past effect decays exponentially in the past; and (3) $D(\lambda)$ has no zeros on the imaginary axis. If n is even, i.e., $n = 2m$ where m is an integer, the number of unstable characteristic exponents is

$$N = m + (-1)^m \sum_{i=1}^{r} (-1)^{i+1} \mathrm{sgn} S(\rho_i) \tag{17}$$

where $\rho_1 \geq \cdots \geq \rho_r > 0$ are the positive real zeros of $R(\omega)$. If n is odd, i.e. $n = 2m + 1$, then

$$N = m + \frac{1}{2} + (-1)^m \left[\frac{1}{2} (-1)^s \mathrm{sgn} R(0) + \sum_{i=1}^{s-1} (-1)^i \mathrm{sgn} R(\sigma_i) \right],$$

where $\sigma_1 \geq \cdots \geq \sigma_s = 0$ are the nonnegative real zeros of $S(\omega)$.

To illustrate for (10), we have

$$\begin{aligned} R(\omega) &= -\omega^2 + a + k_\mathrm{p} \cos(\omega\tau) + k_\mathrm{d} \sin(\omega\tau), \quad \omega \in [0, \infty), \\ S(\omega) &= b\omega - k_\mathrm{p} \sin(\omega\tau) - k_\mathrm{d}\omega \cos(\omega\tau), \quad \omega \in [0, \infty) . \end{aligned}$$

Take $\tau = 1$, $b = 0$ and choose the point labelled A in Fig. 4, which corresponds to $a = -0.5$, $k_\mathrm{p} = -20$ and $k_\mathrm{d} = 0$. Point A is located in the parameter region that has three unstable characteristic exponents. For these parameters, $R(\omega)$ has zeros at $\rho_1 = 3.844$ and $\rho_2 = 1.750$. Using (17) we obtain $N = 3$.

4.2 PDA Feedback

Equation (2) with (6) define

$$\ddot{\theta}(t) + b\dot{\theta}(t) + a\theta(t) = -k_\mathrm{p}\theta(t - \tau) - k_\mathrm{d}\dot{\theta}(t - \tau) - k_\mathrm{a}\ddot{\theta}(t - \tau) . \tag{18}$$

This is an NFDE since the second derivative of the state variable appears both with actual and with delayed arguments. A necessary condition for stability is that the difference part $\ddot{\theta}(t) = -k_a \ddot{\theta}(t-\tau)$ has to be stable, i.e., $|k_a|$ should be less than 1 (Kolmanovskii and Nosov, 1986; Stépán, 1989; Zhang et al., 2018). If $|k_a| > 1$ then the system has infinitely many unstable characteristic exponents.

The characteristic function for (18) is

$$D(\lambda) = \lambda^2 + b\lambda + a + k_p e^{-\lambda} + k_d \lambda e^{-\lambda} + k_a \lambda^2 e^{-\lambda} .$$

We apply the D-subdivision method. Substituting $\lambda = \gamma \pm i\omega, \omega \geq 0$ into $D(\lambda) = 0$ and then decomposing into real and imaginary parts gives

$$\begin{aligned} \text{Re}: \quad & \gamma^2 - \omega^2 + b\gamma + a + k_p e^{-\gamma} \cos\omega + k_d \gamma e^{-\gamma} \cos\omega + k_d \omega e^{-\gamma} \sin\omega \\ & + k_a(\gamma^2 - \omega^2) e^{-\gamma} \cos\omega + k_a 2\gamma\omega e^{-\gamma} \sin\omega = 0 , \qquad (19) \\ \text{Im}: \quad & 2\gamma\omega + b\omega - k_p e^{-\gamma} \sin\omega + k_d \omega e^{-\gamma} \cos\omega - k_d \gamma e^{-\gamma} \sin\omega \\ & + k_a 2\gamma\omega e^{-\gamma} \cos\omega - k_a(\gamma^2 - \omega^2) e^{-\gamma} \sin\omega = 0 . \qquad (20) \end{aligned}$$

Substitution of $\gamma = 0$ into (19) and (20) gives the D-curves in the form

$$\begin{aligned} \text{if } \omega = 0 \ : \quad & k_p = -a , \quad k_d \in \mathbb{R} , \qquad (21) \\ \text{if } \omega \neq 0 \ : \quad & k_p = (\omega^2 - a)\cos\omega + b\omega \sin(\omega\tau) + k_a \omega^2 \qquad (22) \\ & k_d = \frac{\omega^2 - a}{\omega} \sin\omega - b\cos(\omega\tau) \qquad (23) \end{aligned}$$

where ω is the frequency parameter, which is equal to the imaginary part of the characteristic exponent λ, i.e., $\omega = \text{Im}(\lambda)$.

The D–curve $k_p = -a$ given by (21) is associated with a real critical characteristic exponent $\lambda = 0$, while the D–curve given by (22) is associated with a complex conjugate pair of characteristic exponents of the form $\lambda = \pm i\omega$. In fact, the parametric curve (22)–(23) defines a spiral in the plane (k_p, k_d) as shown in Fig. 5. Some specific values of the frequency parameter ω along the stability boundaries are also presented. The stable region (with zero unstable characteristic roots) is indicated by gray shading in the right (zoomed) panel in Fig. 5.

In order to determine the number of unstable characteristic exponents we need to determine the exponent crossing direction along the D-curve $k_p = -a$. Thus we take the partial derivatives of (19) and (20) with respect to k_p. Setting $\gamma = 0, \omega = 0$ and $k_p = -a$ we obtain

$$\frac{\partial\gamma}{\partial k_p} = -\frac{1}{a\tau + k_d - b},$$

which is actually the same as for PD feedback. We see that this derivative is positive for $k_d < b - a\tau$ and negative if $k_d > b - a\tau$. If $k_p = 0, k_d = 0$ with $|k_a| < 1, a < 0$ and $b = 0$ then the number of unstable characteristic exponents is 1 (see, for example,

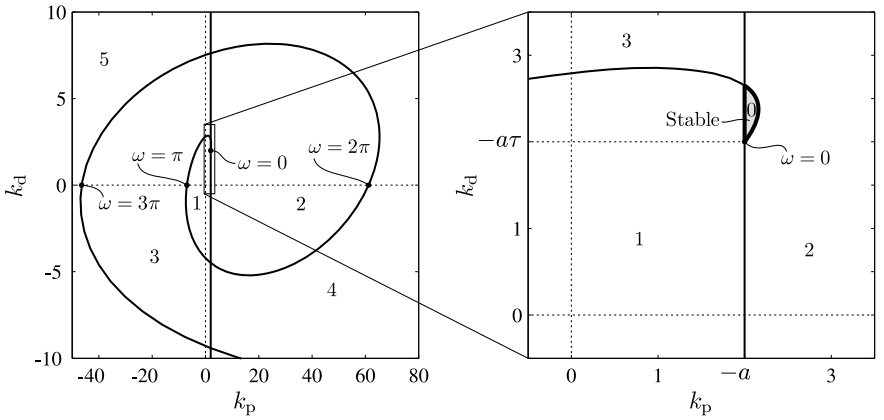

Fig. 5 Stability chart with the number of unstable characteristic exponents for (18) with $a=-2$, $b=0$, $\tau=1$ and $k_\mathrm{a}=0.5$

Fig. 3.10 on p. 64 in Stépán (1989)). Thus the number of unstable characteristic exponents can be determined for all the regions in the parameter plane $(k_\mathrm{p}, k_\mathrm{d})$ by examining the exponent-crossing directions along the D-curve $k_\mathrm{p}=-a$. It is also possible to determine the number of unstable characteristic exponents using (17).

4.3 Predictor Feedback

In case of predictor feedback with perfect delay compensation, the system is reduced to the ODE (9), which is equivalent to

$$\ddot{\theta}(t)+b\dot{\theta}(t)+a\theta(t)=-k_\mathrm{p}\theta(t)-k_\mathrm{d}\dot{\theta}(t)\ . \tag{24}$$

Hence, stability requires that $a+k_\mathrm{p}>0$ and $b+k_\mathrm{d}>0$. The corresponding stability chart is shown in Fig. 6. The stable region is infinitely large for this ideal case. In case of imperfections in the implementation of the predictor feedback due to parameter uncertainties, noise or computational limitations (e.g., discretization, quantization), the stable region becomes finite (Mondíe et al., 2002; Molnar and Insperger, 2016).

5 Critical Parameters

It is known that time delay in feedback systems is a source of unstable behaviour. Indeed, in many control applications, stabilization is not possible if the delay or some system parameters exceed a critical value. Stabilizability properties can be

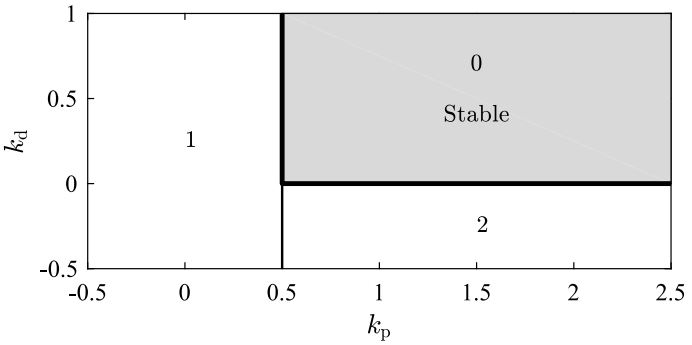

Fig. 6 Stability chart with the number of unstable characteristic exponents for the perfect predictor feedback (24) with $a = -0.5$ and $b = 0$

demonstrated on the stick balancing task. Balancing a short stick is more difficult than balancing a longer one. This is because shorter sticks fall faster than the time needed to make a corrective motion. Actually, there is a limitation in the length of the stick: even expert stick balancers cannot balance a stick of length shorter than 20 cm (Milton et al., 2016). In this section the terminology of the critical delay is discussed for PD, PDA and predictor feedback.

5.1 PD Feedback

Figure 7 shows a series of stability diagrams for (10) with $b = 0$ and $\tau = 1$. It can be seen that as the magnitude of the system parameter a decreases the stable region shrinks until it finally disappears when $a = -2$. This happens when the tangent of the parametric curve (14)–(15) at $\omega = 0$ becomes vertical. It can be shown that

$$\lim_{\omega\to 0} \frac{\mathrm{d}k_\mathrm{d}}{\mathrm{d}k_\mathrm{p}} = \lim_{\omega\to 0} \frac{\frac{\mathrm{d}k_\mathrm{d}}{\mathrm{d}\omega}}{\frac{\mathrm{d}k_\mathrm{p}}{\mathrm{d}\omega}} = \frac{6\tau + 3b\tau^2 + a\tau^3}{6 + 6b\tau + 3a\tau^2}\,.$$

The tangent is vertical if $6 + 6b\tau + 3a\tau^2 = 0$ and hence the critical system parameter is

$$a_{\mathrm{crit,PD}} = -\frac{2 + 2b\tau}{\tau^2} \tag{25}$$

If $a < a_{\mathrm{crit,PD}}$, then the fixed point of (10) is unstable for all k_p and k_d.

Alternatively, for a fixed system parameter, one can determine a critical delay as

$$\tau_{\mathrm{crit,PD}} = -\frac{1}{a}\left(b + \sqrt{b^2 - 2a}\right). \tag{26}$$

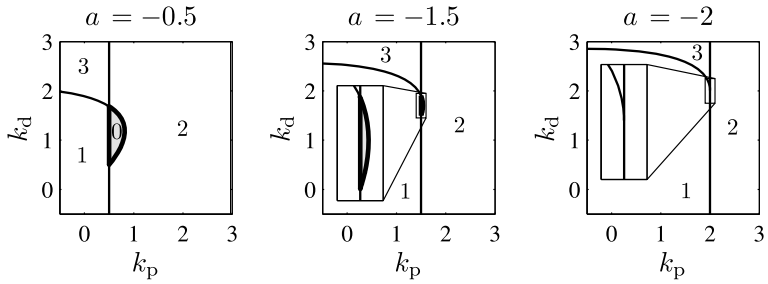

Fig. 7 Stability diagrams for (10) (PD feedback) as a function of k_p and k_d when $b = 0$ and $\tau = 1$. As a decreases, the size of the D-shaped stability region decreases until it disappears when $a = -2$

If $\tau > \tau_{\mathrm{crit,PD}}$ then the system cannot be stabilized by PD feedback.

When $b = 0$, the critical delay can be given in the elegant form

$$\tau_{\mathrm{crit,PD}}\big|_{b=0} = \sqrt{\frac{2}{-a}} = \frac{T_\mathrm{p}}{\pi\sqrt{2}},$$

where T_p is the period of the small oscillations around the hung down equilibrium given by (4) (Stépán, 2009).

5.2 PDA Feedback

Similarly to PD feedback, the stable region shrinks also for PDA feedback as the system parameter a decreases. Stabilizability conditions have been investigated previously for the case $b = 0$ (Sieber and Krauskopf, 2005; Insperger et al., 2013). Note that stability requires $|k_\mathrm{a}| < 1$. Series of stability diagrams with different system parameters a and acceleration control gain k_a for (18) with $b = 0$ and $\tau = 1$ are presented in Fig. 8. The figure shows that the intersection points along the line $k_\mathrm{p} = -a$ are more and more dense and the number of unstable characteristic exponents gets larger and larger as k_a gets closer and closer to $+1$ or -1. Note that if $k_\mathrm{a} > 1$ or $k_\mathrm{a} < -1$, then the system has infinitely many unstable characteristic exponents.

In order to determine the critical system parameter $a_{\mathrm{crit,PDA}}$, which limits the stabilizability of (18), it is necessary to analyze the D-curves (22) and (23) for different values of a and k_a. Figure 8 shows that as the system parameter a gets smaller and smaller, the region of stability shrinks and disappears when the tangent of the parametric curve (22)–(23) at $\omega = 0$ becomes vertical. This is reminiscent of the behavior we have already observed for PD feedback. A long but straightforward algebraic derivation gives

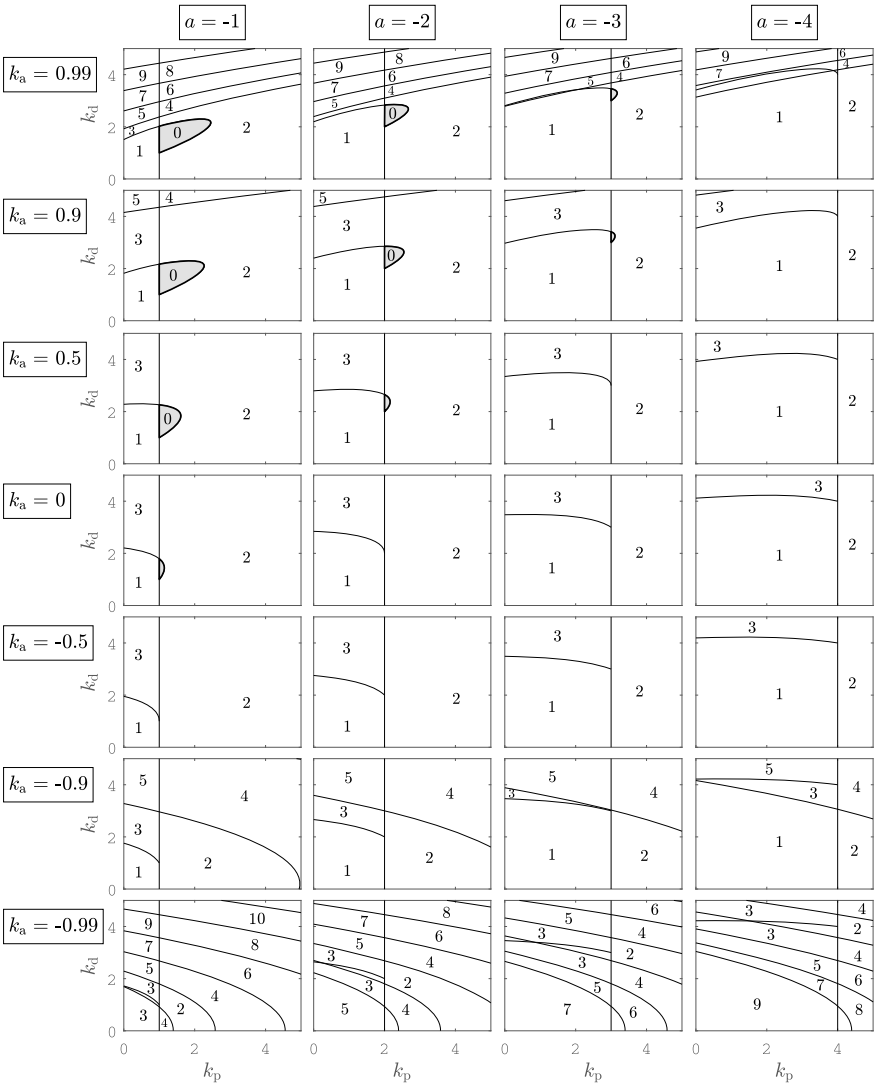

Fig. 8 D-curves and the number of unstable characteristic exponents for (18) with different system parameters a and acceleration control gains k_a for $b = 0$ and $\tau = 1$

$$\lim_{\omega\to 0}\frac{\mathrm{d}k_\mathrm{d}}{\mathrm{d}k_\mathrm{p}}=\lim_{\omega\to 0}\frac{\frac{\mathrm{d}k_\mathrm{d}}{\mathrm{d}\omega}}{\frac{\mathrm{d}k_\mathrm{p}}{\mathrm{d}\omega}}=\frac{6\tau+3b\tau^2+a\tau^3}{6+6k_\mathrm{a}+6b\tau+3a\tau^2}$$

The tangent is vertical if $6+6k_\mathrm{a}+6b\tau+3a\tau^2=0$, which gives the critical system parameter

$$a_{\mathrm{crit,PDA}}=-\frac{2+2b\tau+2k_\mathrm{a}}{\tau^2}.$$

Since there is a limitation to k_a, namely, $|k_\mathrm{a}|<1$, the actual critical system parameter can be given by setting $k_\mathrm{a}=1$, which gives

$$a_{\mathrm{crit,PDA}}=-\frac{4+2b\tau}{\tau^2}\,. \tag{27}$$

If the system parameter is fixed then the critical delay can be expressed as

$$\tau_{\mathrm{crit,PDA}}=-\frac{1}{a}\left(b+\sqrt{b^2-4a}\right).$$

If $\tau>\tau_{\mathrm{crit,PDA}}$ then the system cannot be stabilized by PDA feedback.

It should be noted that $\tau_{\mathrm{crit,PD}}>\tau_{\mathrm{crit,PDA}}$, i.e., PDA feedback allows larger feedback delay than PD feedback does. If $b=0$ then

$$\tau_{\mathrm{crit,PD}}=\sqrt{\frac{2}{-a}}\quad\text{and}\quad\tau_{\mathrm{crit,PDA}}=\sqrt{\frac{4}{-a}}=\sqrt{2}\,\tau_{\mathrm{crit,PD}}.$$

This shows that feeding back the acceleration increases the critical delay by approximately 41% compared to PD feedback when $b=0$.

5.3 PF Feedback

If the parameters of the internal model match the actual system parameters, i.e., if $\tilde{A}=A$, $\tilde{B}=B$ and $\tilde{\tau}=\tau$ in (7) and (8), then the prediction gives the exact state, i.e., $z_\mathrm{pred}(t)=z(t)$. In this case, the feedback of the predicted state eliminates the delay from the control loop and one ends up with (9), i.e., with (24). In this case the characteristic exponents can arbitrarily be assigned to any point within the complex plane by tuning the control gains in k_p and k_d. It is often stated that the goal of predictor feedback is to compensate for the effects of the time delay. If this compensation is perfect then, at least in principle, any large delay can be compensated, i.e.,

$$\tau_{\mathrm{crit,PF}}\to\infty\,.$$

The critical system parameter is

$$a_{\text{crit,PF}} \to -\infty\,.$$

If there is any mismatch between the internal model and the real system or the implementation of the predictor feedback is not perfect due to noise or computational limitations, then the critical parameter becomes finite. For instance if $\tilde{a}$ and $\tilde{\tau}$ in the internal model differs by 10% from the actual parameters a and τ then critical delay for PDA feedback becomes larger than that of the predictor feedback (Molnar and Insperger, 2016).

6 Conclusions

Limitations in the stabilization by different control concepts can be demonstrated on the stick balancing task. The governing equation is given by (3). By taking into consideration the inertia of the human arm ($\mu = 4$), the system parameter can be written as $a = -3g/(2\ell)$. From here, the critical length can be given using the expression of the critical system parameter.

In case of PD feedback, the governing equation is (10) with $b = 0$. Using (25) one get

$$\ell_{\text{crit,PD}} = \frac{3}{4} g\tau^2\,.$$

For a typical human reaction delay $\tau = 230$ ms (Milton et al., 2016), the critical length is $\ell_{\text{crit,PD}} = 39$ cm. Indeed, most unskilled subject find difficult balancing a sticks shorter than 39 cm.

In case of PDA feedback, one get (18) with $b = 0$. Equation (27) gives

$$\ell_{\text{crit,PDA}} = \frac{3}{8} g\tau^2 = \frac{1}{2}\ell_{\text{crit,PD}}.$$

Hence, acceleration feedback actually helps in the stabilization.

In case of predictor feedback with prefect prediction,

$$\ell_{\text{crit,PF}} = 0\,,$$

i.e., a stick of arbitrarily short length can be balanced.

Skilled stick balancers can balance a stick as short as ≈ 30 cm (Milton et al., 2016). This observation has been interpreted as indicating that skilled stick balancers use a predictor feedback controller whose performance is limited by the presence of a sensory dead zone.

The model of the quiet standing can directly be linked to the model of the inverted pendulum as shown in Sect. 2.1. The human body can be modelled as a homogeneous rod of height H with $J_{\text{A}} = \frac{1}{3} m H^2$ and $\ell_{\text{AC}} = \frac{1}{2} H$. Here, an important parameter is the passive stiffness k_{t}, which reduces the magnitude of the system parameter. In the

literature, the ratio $k_t/mg\ell_{AC}$ is ranging between 0.8 and 0.91 (Loram and Lakie, 2002; Asai et al., 2009). Taking the lower estimate 0.8, the system parameter becomes

$$a = \frac{k_t - mg\ell_{AC}}{J_A} = -\frac{0.2\,mg\ell_{AC}}{J_A} = -\frac{0.2\,mg\frac{1}{2}H}{\frac{1}{3}mH^2} = -\frac{3g}{10H}$$

Assuming PD feedback, (26) gives the critical delay as

$$\tau_{crit,PD} = \sqrt{\frac{2}{-a}} = \sqrt{\frac{20H}{3g}}.$$

According to this model, a toddler of height 70 cm needs faster than $\tau_{crit} = 0.69$ s reaction time to be able to stand unsupported. For an adult of height 180 cm, $\tau_{crit} = 1.1$ s. For PDA feedback this critical delay is $\tau_{crit,PDA} = 1.41\tau_{crit,PD}$, while for prefect predictor feedback $\tau_{crit,PF} \to \infty$.

It is highlighted in Sect. 3.4 that the main difference between predictor feedback and delayed state feedback is whether the feedback term f is involved into the control law or not. In human motor control, involving f into the prediction is possible through an efferent copy of corollary discharges of the motor command. Hence, predictor feedback is also a possible control mechanism for balancing tasks. The question is whether is it economically beneficial to the neural system to develop a predictor feedback control strategy? Or does the decision of employing state or predictor feedback depend on the difficulty of the task?

References

Asai, Y., Tanaka, Y., Nomura, K., Nomura, T., Casidio, M., & Morasso, P. (2009). A model of postural control in quiet standing: Robust compensation of delay-induced instability using intermittent activation of feedback control. *PLOS ONE, 4*, e6169.

Buza, G., Milton, J., Bencsik, L., & Insperger, T. (2020). Establishing metrics and control laws for the learning process: Ball and beam balancing. *Biological Cybernetics, 114,* 83–93.

Cabrera, J. L., & Milton, J. G. (2002). On-off intermittency in a human balancing task. *Physical Review Letters, 89*, 158702.

Cabrera, J. L., & Milton, J. G. (2004). Human stick balancing: Tuning Lévy flights to improve balance control. *Chaos, 14,* 691–698.

Cabrera, J. L., & Milton, J. G. (2004). Stick balancing: On-off intermittency and balance times. *Nonlinear Studies, 11,* 305–317.

Cabrera, J. L., & Milton, J. G. (2012). Stick balancing, falls and Dragon Kings. *The European Physical Journal Special Topics, 205,* 231–241.

Cabrera, J. L., Bormann, R., Eurich, C., Ohira, T., & Milton, J. G. (2004). State-dependent noise and human balance control. *Fluctuation and Noise Letters, 4,* L107–L118.

Chagdes, J. R., Rietdyk, S., Jeffrey, M. H., Howard, N. Z., & Raman, A. (2013). Dynamic stability of a human standing on a balance board. *Journal of Biomechanics, 46*(15), 2593–2602.

Chumacero-Polanco, E., & Yang, J. (2019). Basin of attraction and limit cycle oscillation amplitude of an ankle-hip model of balance on a balance board. *The Journal of Biomechanical Engineering, 141*(11), 111007.

Cruise, D. R., Chagdes, J. R., Liddy, J. J., Rietdyk, S., Haddad, J. M., Zelaznik, H. N., & Raman, A. (2017). An active balance board system with real-time control of stiffness and time-delay to assess mechanisms of postural stability. *Journal of Biomechanics, 60,* 48–56.

de Leva, P. (1996). Adjustments to zatsiorsky-seluyanov's segment inertia parameters. *Journal of Biomechanics, 19,* 1223–1230.

Gawthrop, P., Lee, K. Y., Halaki, M., & O'Dwyer, N. (2013). Human stick balancing: An intermittent control explanation. *Biological Cybernetics, 107,* 637–652.

Insperger, T., & Milton, J. (2014). Sensory uncertainty and stick balancing at the fingertip. *Biological Cybernetics, 108,* 85–101.

Insperger, T., & Milton, J. (2017). Stick balancing with feedback delay, sensory dead zone, acceleration and jerk limitation. *In Procedia IUTAM, 22,* 59–66.

Insperger, T., Milton, J., & Stépán, G. (2013). Accleration feedback improves balancing against reflex delay. *Journal of the Royal Society, Interface, 36,* 2156–2163.

Kawato, M. (1999). Internal models for motor control and trajectory planning. *Current Opinion in Neurology, 9,* 718–727.

Kleinman, D. L. (1969). Optimal control of linear systems with time-delay and observation noise. *IEEE Transactions on Automatic Control, 14,* 524–527.

Kolmanovskii, V. B., & Nosov, V. R. (1986). *Stability of functional differential equations*. Academic Press.

Kovacs, B. A., Milton, J., & Insperger, T. (2019). Virtual stick balancing: Sensorimotor uncertainties related to angular displacement and velocity. *Royal Society Open Science, 6*, 191006.

Krstic, M. (2009). *Delay compensation for nonlinear, adaptive, and PDE systems*. Birkhäuser.

Lee, K.-Y., O'Dwyer, N., Halaki, M., & Smith, R. (2012). A new paradigm for human stick balancing: A suspended not an inverted pendulum. *Experimental Brain Research, 221,* 309–328.

Loram, I. D., & Lakie, M. (2002). Direct measurement of human ankle stiffness during quiet standing: The intrinsic stiffness is insufficient for stability. *Journal of Physiology, 545,* 1041–1053.

Mannitius, A. Z., & Olbrot, A. W. (1979). Finite spectrum assignment problem for systems with delays. *IEEE Transactions on Automatic Control, AC-24*, 541–553

Maurer, C. V., & Peterka, R. J. (2005). A new interpretation of spontaneous sway measures based on a simple model of human postural control. *Journal of Neurophysiology, 93,* 189–200.

Mehta, B., & Schaal, S. (2002). Forward models in visuomotor control. *Journal of Neurophysiology, 88,* 942–953.

Michiels, W., & Niculescu, S. -I. (2007). *Stability and stabilization of time-delay systems: An eigenvalue-based approach*. SIAM Publications.

Milton, J., Cabrera, J. L., Ohira, T., Tajima, S., Tonosaki, Y., Eurich, C. W., & Campbell, S. A. (2009). The time-delayed inverted pendulum: Implications for human balance control. *Chaos, 19*, 026110.

Milton, J., Fuerte, A., Bélair, C., Lippai, J., Kamimura, A., & Ohira, T. (2013). Delayed pursuit-escape as a model for virtual stick balancing. *Nonlinear Theory and Its Applications, IEICE, 4*, 129–137.

Milton, J., Meyer, R., Zhvanetsky, M., Ridge, S., & Insperger, T. (2016). Control at stability's edge minimizes energetic costs: Expert stick balancing. *Journal of the Royal Society Interface, 13*, 20160212.

Molnar, C. A., Zelei, A., & Insperger, T. (2017). Estimation of human reaction time delay during balancing on balance board. In *2017 13th IASTED International Conference on Biomedical Engineering (BioMed), IEEE*, pp. 176–180.

Molnar, T. G., & Insperger, T. (2016). On the robust stabilizability of unstable systems with feedback delay by finite spectrum assignment. *Journal of Vibration and Control, 22*(3), 649–661.

Mondíe, S., Dambrine, M., & Santos, O. (2002). Approximation of control laws with distributed delays: A necessary condition for stability. *Kybernetika, 38,* 541–551.

Morasso, P., Cherif, A., & Zenzeri, J. (2019). Quiet standing: The single inverted pendulum model is not so bad after all. *PLOS ONE, 14*(3), e0213870.

Nagy, D. J., Bencsik, L., & Insperger, T. (2020). Experimental estimation of tactile reaction delay during stick balancing using cepstral analysis. *Mechanical Systems and Signal Processing, 138*, 106554.

Patzelt, F., Riegel, M., Ernst, U., & Pawelzik, K. (2007). Self-organized critical noise amplification in human closed loop control. *Frontiers in Computational Neuroscience, 1*, 4.

Shadmehr, R., Smith, M. A., & Krakauer, J. W. (2010). Error correction, sensory prediction, and adaptation in motor control. *Annual Review of Neuroscience, 33*, 89–108.

Sieber, J., & Krauskopf, B. (2005). Extending the permissible control loop latency for the controlled inverted pendulum. *Dynamical Systems, 20,* 189–199.

Stépán, G. (1989). *Retarded dynamical systems*. Longman.

Stépán, G. (2009). Delay effects in the human sensory system during balancing. *Philosophical Transactions of the Royal Society A, 367,* 1195–1212.

Suzuki, Y., Nomura, T., Casadio, M., & Morasso, P. (2012). Intermittent control with ankle, hip, and mixed strategies during quiet standing: A theoretical proposal based on a double inverted pendulum model. *Journal of Theoretical Biology, 310,* 55–79.

Winter, D. A. (2005). *Biomechanics and motor control of human movement* (3rd ed.). Wiley.

Winter, D. A., Patla, A. E., Prince, F., Ishac, M. G., & Gielo-Perczak, K. (1998). Stiffness control of balance in quiet standing. *Journal of Neurophysiology, 80,* 1211–1221.

Zhang, L., Stépán, G., & Insperger, T. (2018). Saturation limits the contribution of acceleration feedback to balancing against reaction delay. *Journal of the Royal Society Interface, 15*, 20170771.